VOLUME 76 APRIL 27, 1972 NUMBER 9

JPCHAx

THE JOURNAL OF PHYSICAL CHEMISTRY

PUBLISHED BIWEEKLY BY THE AMERICAN CHEMICAL SOCIETY

THE JOURNAL OF

PHYSICAL CHEMISTRY

 Published biweekly by the American Chemical Society at 20th and Northampton Sts., Easton, Pa. 18042. Second-class postage paid at Washington, D. C., and at additional mailing offices.

All manuscripts should be sent to *The Journal of Physical Chemistry,* Department of Chemistry, University of Minnesota, Minneapolis, Minn. 55455.

Additions and Corrections are published once yearly in the final issue. See Volume 75, Number 26 for the proper form.

Extensive or unusual alterations in an article after it has been set in type are made at the author's expense, and it is understood that by requesting such alterations the author agrees to defray the cost thereof.

The American Chemical Society and the Editor of *The Journal of Physical Chemistry* assume no responsibility for the statements and opinions advanced by contributors.

Correspondence regarding accepted copy, proofs, and reprints should be directed to Editorial Production Office, American Chemical Society, 20th and Northampton Sts., Easton, Pa. 18042. Manager: CHARLES R. BERTSCH. Assistant Editor: EDWARD A. BORGER.

Advertising Office: Century Communications Corporation, 142 East Avenue, Norwalk, Conn. 06851.

Business and Subscription Information

Remittances and orders for subscriptions and for single copies, notices of changes of address and new professional connections, and claims for missing numbers should be sent to the Subscription Service Department, American Chemical Society, 1155 Sixteenth St., N.W., Washington, D. C. 20036. Allow 4 weeks for changes of address. Please include an old address label with the notification.

Claims for missing numbers will not be allowed (1) if received more than sixty days from date of issue, (2) if loss was due to failure of notice of change of address to be received before the date specified in the preceding paragraph, or (3) if the reason for the claim is "missing from files."

Subscription rates (1972): members of the American Chemical Society, $20.00 for 1 year; to nonmembers, $60.00 for 1 year. Those interested in becoming members should write to the Admissions Department, American Chemical Society, 1155 Sixteenth St., N.W., Washington, D. C. 20036. Postage to Canada and countries in the Pan-American Union, $5.00; all other countries, $6.00. Single copies for current year: $3.00. Rates for back issues from Volume 56 to date are available from the Special Issues Sales Department, 1155 Sixteenth St., N.W., Washington, D. C. 20036.

This publication and the other ACS periodical publications are now available on microfilm. For information write to: MICROFILM, Special Issues Sales Department, 1155 Sixteenth St., N.W., Washington, D. C. 20036.

Notice to Authors last printed in the issue of December 23, 1971

THE JOURNAL OF

PHYSICAL CHEMISTRY

Volume 76, Number 9 April 27, 1972

JPCHAx 76(9) 1231–1388 (1972)

COMMUNICATIONS TO THE EDITOR

AUTHOR INDEX

In papers with more than one author the name of the author to whom inquiries about the paper should be addressed is marked with an asterisk in the by-line.

THE JOURNAL OF
PHYSICAL CHEMISTRY

VOLUME 76, NUMBER 9 APRIL 27, 1972

Physical Chemistry of Lipid Films at the Air–Water Interface.

I. Intermolecular Energies in Single-Component Lipid Films

by N. L. Gershfeld* and R. E. Pagano[1]

Laboratory of Physical Biology, National Institute of Arthritis and Metabolic Diseases, National Institutes of Health, U. S. Department of Health, Education, and Welfare, Bethesda, Maryland 20014 *(Received April 22, 1971)*

Publication costs assisted by the National Institutes of Health

The thermodynamic properties of the film compression process were evaluated for a series of liquid-condensed and liquid-expanded films between the condensed area, A_c, and 10^5 Å^2/molecule. At the highly expanded areas, it was demonstrated that the films approached ideal gas behavior. From a theoretical analysis, the hydrocarbon and polar group contributions to the film compression energies were separated and evaluated. It was shown that for the liquid-condensed and liquid-expanded monolayers, the hydrocarbon region is energetically similar to bulk hydrocarbon liquids. The energetic contributions from the polar region are significant. Entropies of compression of the polar groups, ΔS_c^p, evaluated for the process of compressing a lipid film from the "ideal gas" to a condensed state, suggest that characteristic changes in water structure are likely to occur in the formation of each condensed monolayer state.

Introduction

It is generally assumed that lipid films on water exist in physical states with internal pressures comparable to those for bulk states.[2] The basic correctness of this assumption is attested by the occurrence of phase transitions in lipid films,[3] the similarity of the free energy of activation of flow in surfaces with that in bulk flow,[4] and the fact that the heats of evaporation of aliphatic alcohols from monolayers on water are of the same order of magnitude as the heats of evaporation from the bulk liquid alcohol.[5] However, a quantitative evaluation of the intermolecular energies in condensed lipid films has not been obtained. In this paper we present measurements of these energies for liquid-condensed and liquid-expanded lipid films.

Evaluation of the internal energy of the lipid films has been hampered by two basic problems. First, it was essential to develop a method for measuring the very low surface pressure π in the region where the monolayer behaves as an "ideal gas";[6,7] a film balance for this purpose is described elsewhere.[8,9] Secondly, a method for treating the contribution of the aqueous phase to the film properties must be established before a complete thermodynamic model of the lipid film can be developed.

(1) Staff associate, National Institutes of Health, 1968–1970.

(2) (a) H. Devaux, *Smithsonian Inst. Annu. Rept.*, 261 (1913); (b) N. K. Adam, "The Physics and Chemistry of Surfaces," 3rd ed, Oxford University Press, London, 1941.

(3) N. K. Adam and G. Jessop, *Proc. Roy. Soc., Ser. A*, **110**, 423 (1926).

(4) W. J. Moore and H. Eyring, *J. Chem. Phys.*, **6**, 391 (1938); S. Glasstone, K. J. Laidler, and H. Eyring, "Theory of Rate Processes," 1st ed, McGraw-Hill, New York, N. Y., 1941, p 510.

(5) J. H. Brooks and A. E. Alexander, *Int. Congr. Surface Activity, 3rd*, **2**, 196 (1960).

(6) N. L. Gershfeld in "Techniques of Surface and Colloid Chemistry and Physics" Vol. 1, R. J. Good, R. R. Stromberg, and R. L. Patrick, Ed., Marcel Dekker, New York, N. Y., pp 1–39, 1972.

(7) N. L. Gershfeld, *J. Colloid Interface Sci.*, **32**, 167 (1970).

(8) N. L. Gershfeld, R. E. Pagano, W. S. Friauff, and J. Fuhrer, *Rev. Sci. Instrum.*, **41**, 1356 (1970).

(9) R. E. Pagano and N. L. Gershfeld, *J. Colloid Interface Sci.*, in press.

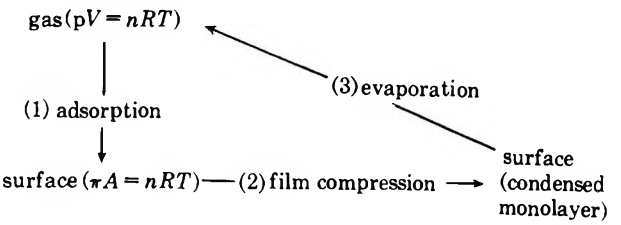

Figure 1. Cyclical process for evaluation of intermolecular energies in monomolecular films on water (see text for discussion).

In principle this last problem can be solved rigorously by the method illustrated in Figure 1. Step 1 is the process of adsorption of lipid molecules from the bulk standard gaseous state to the surface ideal gas state—where there are no lipid–lipid interactions. Defined in this way, the adsorption process involves hydration and possible changes in molecular configuration of the absorbed lipids. Step 2 is film compression—the transformation of the monolayer from the "ideal gas" to a condensed film—and involves changes in lipid–lipid interactions as well as possible changes in film hydration. Step 3 is surface evaporation—the transfer of lipid molecules from a condensed surface state to the bulk standard gas state. The energy of the surface evaporation process will contain contributions from all intermolecular energies in the condensed monolayer. With some exceptions,[5] most of the higher molecular weight lipids have vapor pressures which are too low at room temperature to be measured; thus the process of adsorption and surface evaporation will be extremely difficult to measure by present techniques. This seriously limits the ability to measure the contribution of water to the internal energy of the film.

To avoid the difficulty of measuring the water contribution by the vaporization process, we will assume, with Langmuir,[10] that the aliphatic region of the monolayer may be treated as a separate entity with bulk liquid properties. The energy of this lipid layer will be evaluated, by methods discussed later, and then by difference the energy of the polar region will be obtained. In support of this approach, it has been demonstrated from the data of Adam and Jessop[3] that the hydrocarbon and polar group contributions to the Helmholtz free energy of compression ΔF_c are indeed separable and additive.[7] To evaluate the contributions of the hydrocarbon and polar moieties, we compare ΔF_c with ΔF_c(ideal gas), *i.e.*, the work of compressing the hypothetical ideal gas film ($\pi A = kT$) under identical conditions. Thus we may write

$$\Delta F_c - \Delta F_c(\text{ideal gas}) = \Delta F_c^{p} + \Delta F_c^{h} \qquad (1)$$

where superscripts p and h refer to the polar group and hydrocarbon contributions to film compression. It follows that similar relations may be written for the heats ΔH_c and entropies ΔS_c of compression.

To extract the hydrocarbon contributions from the total energy, it is important to consider the correct functional dependence of ΔF_c^{h}, ΔH_c^{h}, and ΔS_c^{h} on n, the number of $-CH_2-$ groups in the hydrocarbon chain. For ΔF_c, it has been shown[7] that liquid-condensed and liquid-expanded films obey the relation

$$\Delta F_c^{h} = n\bar{f} \qquad (2)$$

where $\bar{f}$ is the average contribution per $-CH_2-$ to ΔF_c^{h}; $\bar{f}$ is a function of the physical state of the lipid film.

To evaluate ΔH_c^{h}, it is useful to refer to the cyclic processes in Figure 1, where it is seen that $\Delta H_c^{h} = \Delta H_v^{h} - \Delta H_{ads}^{h}$, where ΔH_v^{h} and ΔH_{ads}^{h} are the heats of evaporation and adsorption for the hydrocarbon moiety. We shall examine each of these processes separately. Huggins[11] has shown that the heats of vaporization ΔH_v^{h} of a homologous series of normal liquid hydrocarbons in bulk obey the relation

$$\Delta H_v^{h} = k_{vap} n^{2/3} \qquad (3)$$

where k_{vap} is a constant and n is the length of the hydrocarbon chain. The physical basis for this dependence is that the gas molecules form spheres with an internal energy similar to that for the liquid, but with an added hydrocarbon–air interfacial energy which is proportional to the surface area of the sphere; the latter increases as $n^{2/3}$, with increasing n. Moreover, using experimental results of heats of vaporization of hydrocarbon liquids,[12,13] Huggins confirmed this relation.[11] We assume that a relation similar in form to eq 3 is applicable to the vaporization of the hydrocarbon moiety in condensed monolayers.

In the adsorption process (step 1, Figure 1), if the hydrocarbon chain configuration is unchanged (*i.e.*, spherical), the heat content in the adsorbed state will be a function of the hydrocarbon–water interfacial energy and hence will depend on the surface area of the hydrocarbon molecule in the surface. This area and the heat will also vary as $n^{2/3}$. Thus, one would expect from this model of adsorption that ΔH_{ads}^{h} will also depend on $n^{2/3}$. Indeed, from the data of Jones and Ottewill,[14] reproduced in Table I, the relation

$$\Delta H_{ads}^{h} = k_{ads} n^{2/3} \qquad (4)$$

is obeyed, as indicated by the constancy (within a few per cent) of k_{ads} shown in Table I. Although the adsorption data are limited to only the C_5 through C_8 hydrocarbons, where nonspherical configurations may be anticipated, it has been reported that heptane and

(10) I. Langmuir, *J. Chem. Phys.*, **1**, 756 (1933); I. Langmuir, *Proc. Roy. Soc., Ser. A*, **170**, 1 (1939).

(11) H. L. Huggins, *J. Phys. Chem.*, **43**, 1083 (1939).

(12) B. H. Sage, W. N. Lacey, and J. G. Schaafsma, *Ind. Eng. Chem.*, **27**, 48 (1935).

(13) J. W. Schultz, *ibid.*, **21**, 557 (1929).

(14) D. C. Jones and R. H. Ottewill, *J. Chem. Soc.*, 4076 (1955).

Table I: Dependence of ΔH_{ads} for Normal Aliphatic Hydrocarbons on the Length of the Hydrocarbon Chain, n[a]

Compound	ΔH_{ads}^h, cal/mol	$k_{ads} = \Delta H_{ads}^h/n^{2/3}$
n-Pentane	−5146	−1760
n-Hexane	−5995	−1816
n-Heptane	−6585	−1800
n-Octane	−7324	−1831

[a] Data are from ref 14.

octane approximate a spherical configuration in the vapor as determined by gas viscosity studies.[15]

From the cyclic process in Figure 1, since both ΔH_v^h and ΔH_{ads}^h are functions of $n^{2/3}$, it follows that ΔH_c^h will be described by the relation

$$\Delta H_c^h = k_c n^{2/3} \tag{5}$$

where k_c is a constant characteristic of the compression process. To evaluate k_c, it is only necessary to measure ΔH_c for two normal aliphatic compounds, 1 and 2, which possess identical polar groups and are in the same surface physical state. Thus

$$k_c = \frac{\Delta H_c^{(1)} - \Delta H_c^{(2)}}{n_1^{2/3} - n_2^{2/3}} \tag{6}$$

Given ΔH_c^h and ΔF_{-c}^h, one can calculate ΔS_c^h from the second law. It follows that the analogous parameters for the polar group contributions may be determined from the experimental ΔF_c, ΔH_c, and ΔS_c using eq 1.

Materials and Methods

The following materials, listed with common names, were obtained from Applied Science Laboratories and used without further purification: *cis*-9-hexadecen-1-ol (palmitoleyl alcohol), *cis*-9-octadecen-1-ol (oleyl alcohol), *cis*-9-hexadecenoic acid (palmitoleic acid), *cis*-9-octadecenoic acid (oleic acid), 1-octadecanol (stearyl alcohol), *n*-hexadecanoic acid (palmitic acid), *n*-octadecanoic acid (stearic acid), octadecanoic acid methyl ester (methyl stearate), and cholesterol. Octadecylacetamide was prepared from octadecylamine by treatment with acetic anhydride followed by recrystallization from ether (mp 78.5°). All solutions were prepared in petroleum ether except for octadecylacetamide. For the latter, a 4/1 mixture of petroleum ether (bp 30–60°) and benzene was used as the spreading solvent. Solvents were passed over an activated silica gel column prior to use.

The film balance used in these studies employed a horizontal float system with end loops made of lightly paraffined nylon thread (diameter 20 μ); the sensitivity of the system is ±0.001 dyn/cm in the range 0–0.10 dyn/cm. A more complete description of the float[9] and surface pressure sensing unit[8] is presented elsewhere. Temperatures were regulated ±0.1° by circulating water through the base of the trough. Isotherms were determined point by point.

Calculations. (*A*) *Thermodynamics of Film Compression.* The Helmholtz free energy of compression ΔF_c is evaluated directly from the experimental π–A isotherms. ΔF_c represents the work required to compress the film from an ideal gas, where no intermolecular contacts occur, to some condensed state where the intermolecular contacts result in repulsive and cohesive energies characteristic of that state.[7] The free energy of compression is calculated according to the expression

$$\Delta F_c = F - F_i = -\int_{A_i}^{A_c} \pi dA \tag{7}$$

To illustrate the graphical integration of eq 7 and to define terms which are used throughout this series of papers, we present in Figure 2 a generalized π–A curve for a single-component insoluble lipid monolayer on water. We will consider three regions of the isotherm. (i) At areas less than A_c, the monolayer exists as a single homogenous condensed phase. For monolayers containing normal aliphatic chains, A_c is typically ~20, ~25, or ~40–50 Å^2/molecule, depending on whether the monolayer forms a solid film, a liquid-condensed film, or a liquid-expanded film, respectively; these terms refer to the physical state of the monolayer and are discussed at length by Harkins.[16] (ii) At areas greater than A_v, typically 1,000–5,000 Å^2/molecule, the film behaves as a nonideal two-dimensional gas, eventually approaching ideal gas behavior as the surface area of the film is increased. This area, denoted A_i in Figure 2, is of the order of 50,000 Å^2/molecule. It has been shown on theoretical grounds that the πA product in this ideal gas region should be equal to kT,[3] where k is the Boltzmann constant and T the absolute temperature. (iii) Between A_c and A_v, the surface pressure is independent of the molecular area. It has been demonstrated that in this region there exist two discrete surface phases in equilibrium, a condensed film and its two-dimensional vapor;[17] thus π_v is called the surface vapor pressure. The value of ΔF_c which we wish to determine is given by the shaded area in Figure 2.

For the studies reported in this paper, ΔF_c was evaluated by dividing the integral in eq 7 into two parts

$$\Delta F_c = -\int_{A}^{A_c} \pi dA - \int_{A_i}^{A} \pi dA \tag{8}$$

The first integral was evaluated directly from the ex-

(15) R. Melaven and E. Mack, Jr., *J. Amer. Chem. Soc.*, **54**, 888 (1932).

(16) W. D. Harkins, "The Physical Chemistry of Surface Films," Reinhold, New York, N. Y., 1952, p 131.

(17) N. K. Adam and J. B. Harding, *Proc. Roy. Soc., Ser. A*, **138**, 419 (1932).

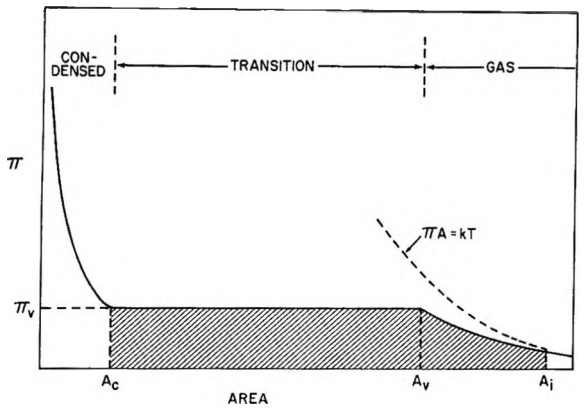

Figure 2. Schematic representation of π–A isotherm in the transition region between a condensed state, area A_c, and a gas, area A_v. The surface vapor pressure π_v, is given by the value of the horizontal line in the diagram. The magnitude of the shaded area is ΔF_c (see text) (reproduced from *J. Colloid Interface Sci.*, **32**, 167 (1970), by permission).

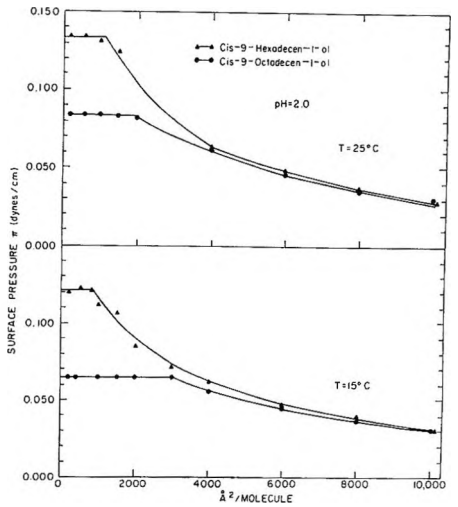

Figure 3. π–A isotherms at 25 and 15° and pH 2 for ▲ palmitoleyl alcohol (*cis*-9-hexadecen-1-ol) and (●) oleyl alcohol (*cis*-9-octadecen-1-ol).

perimental π–A isotherms from A = 10,000 Å²/molecule to area A_c. Values of A_c were taken as 50 Å²/molecule for liquid-expanded films and 25 Å²/molecule for the liquid-condensed monolayers. To evaluate the second integral, a relation (eq 9) in the form of the two-dimensional van der Waals equation of state was first fitted to the experimental data between 6000 and 10,000 Å²/molecule.

$$\left(\pi + \frac{a_s}{A^2}\right)(A - A_0) = kT \qquad (9)$$

A_0 and a_s are constants. Successive values of A_0 were selected by trial and error and a new value of a_s calculated until the equation of state fit the experimental data to ±0.001 dyn/cm. The second integral of eq 8 could then be evaluated from the integrated form of the van der Waals equation, where the upper limit of the integration was 10,000 Å²/molecule. A_i was arbitrarily chose as 100,000 Å²/molecule for all systems, where the equation of state indicated that the πA product was within a few per cent of kT.

For systems where the transition area A_v was larger than 10,000 Å²/molecule, and where π_v is low (*e.g.*, for liquid-condensed films) it was assumed that A_v is given by the ideal gas law, kT/π_v. ΔF_c was calculated according to equation 10, where A_i = 100,000 Å²/molecule.

$$\Delta F_c = \pi_v(A_v - A_c) - kT \ln (A_v/A_i) \qquad (10)$$

For palmitoleic acid, the gaseous portion of the isotherm was assumed to be identical with that measured for oleic acid. This was justified on the grounds that the isotherms in the gaseous region for the analogous alcohols were nearly identical (see Figure 3). Thus, only π_v was measured for palmitoleic acid.

The heat, ΔH_c, and entropy, ΔS_c, of compression were computed from the temperature dependence of ΔF_c using the relation $\Delta F_c = \Delta H_c - T\Delta S_c$.

(*B*) *Experimental Errors.* In calculating the experimental error, it is assumed that the error is incurred exclusively in the region between area A_c and 10,000 Å²/molecule, and that the equation of state correctly describes the isotherms beyond this point. The standard deviation for the surface pressure, σ_π, was found to be about 0.001 dyn/cm and was independent of area. The standard deviation in the Helmholtz free energy of compression, $\sigma_{\Delta F_c}$, given by $\sigma_\pi \Delta A$,[18] was about ±14 cal/mol. This value is an absolute error and is independent of the magnitude of ΔF_c. Standard deviations for the heats and entropies of compression were calculated to be 25 cal/mol and 2 eu, respectively. Thus, based on a 1-mdyn/cm error in all measurements of the surface pressure π, our errors (±S.D.) are ±14 cal/mol, ±25 cal/mol, and ±2 eu, respectively, for ΔF_c, ΔH_c, and ΔS_c.

Any errors in ΔF_c due to an error in fitting the equations of state have been ignored in the above calculations. This omission is justified for the following reasons. (i) The equation of state fits the experimental data very closely (±0.001 dyn/cm) over a large range of molecular areas (6000–10,000 Å²/molecule). (ii) Any discrepancies between actual pressures and those obtained from the equation of state must diminish as the molecular area is increased, since the πA product obtained from both the equation of state and the experimental data approaches kT with increasing areas. (iii) Estimates of the errors in ΔF_c which might result between 10,000 and 100,000 Å²/molecule were made by assuming that the true value of π was either plus or minus two standard deviations (±0.002 dynes/cm)

(18) K. Pettigrew and C. S. Patlak, private communication.

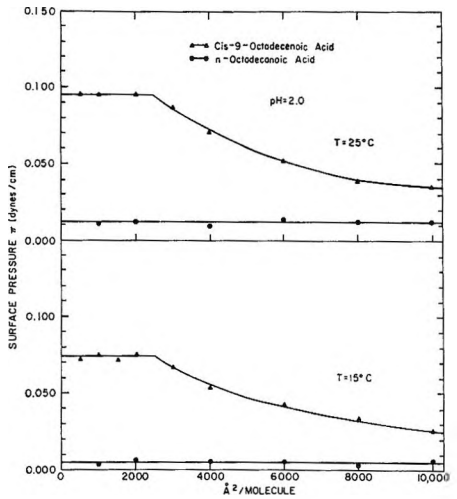

Figure 4. π–A isotherms at 25 and 15° and pH 2 for (▲) oleic acid (*cis*-9-octadecenoic acid) and (●) stearic acid (*n*-octadecanoic acid).

from the measured values of π. Using these numbers to fit eq 9, new values of the constants a_s and A_0 were calculated and a new value of ΔF_c was determined from eq 10. The results of these calculations gave an additional error of ±10 cal/mol in ΔF_c. This calculation, however, is arbitrary, where the errors are for extreme cases. Since there are good reasons (i and ii above) for assuming that the actual errors are smaller, only the *experimental* errors in the thermodynamic parameters are quoted throughout this series of papers.

Results

π–A isotherms for the pure components palmitoleyl alcohol, oleyl alcohol, oleic acid, and stearic acid at 25 and 15° and pH 2.0 are presented in Figures 3 and 4. All measurements were carried out to 10,000 Å²/molecule.

The constants a_s and A_0 used in fitting the van der Waals equation of state (eq 9) to the experimental data for the gaseous isotherms of each pure component are listed in Table II. Between 6000 and 10,000 Å²/molecule, the calculated values of the surface pressure π agreed with measured values within ±0.001 dyn/cm.

Table III lists the thermodynamic parameters for each of the pure lipid components studied, calculated according to the treatment outlined in the Calculations section of this paper. In addition, the surface vapor pressures and temperatures of each measurement are also given.

Table II: Parameters for van der Waals Equation of State

Compound	T, °K	A_0, cm² × 10¹⁶	a_s × 10²⁷, (erg cm³)/molecule²
Palmitoleyl alcohol	298	2200	21.3
	288	2200	19.2
Oleyl alcohol	298	2200	21.3
	288	2200	19.2
Oleic acid	298	2200	20.1
	288	2200	22.5

Discussion

(*A*) *Hydrocarbon Contributions to Film Compression.* In the analysis of Adam and Jessop's data, ΔF_c^h was found to be characteristic of the condensed phase.[7] In the present study, using the values of ΔF_c at 15° for the liquid-expanded films containing like polar groups, f was calculated to be −95 cal/mol of $-CH_2-$. An average value of −450 cal/mol of $-CH_2-$ was taken for the liquid-condensed films, since it was found that the data for stearyl alcohol and palmitic and stearic acids fit the plot of ΔF_c *vs.* n for the liquid-condensed films studied by Adam and Jessop.[3] Values of ΔF_c^h, ΔH_c^h, and ΔS_c^h are given in Table IV for each alcohol and acid measured in liquid-condensed and liquid-expanded states.

Values for average heats of compression per mole of $-CH_2-$ were calculated using eq 5 and 6 for each of the compounds listed in Table IV. For a given physical state there is a weak dependence on n in $\Delta H_c^h/n$, as expected for eq 5: −580 to −610 cal/mol for the liquid-expanded, and −850 to −910 cal/mol for the liquid-condensed systems.

Large negative entropies of compression for the hydrocarbon phase, ΔS_c^h, were found (−24 to −31 eu). Here it is not possible to make a distinction between the values obtained for the liquid-condensed and liquid-expanded films, since the errors in ΔS_c^h are ±3 eu.

Given the heats and entropies of compression for the hydrocarbon phase of the monolayers, we now compare them in a meaningful way to the corresponding values for bulk hydrocarbon systems. In particular, the energies involved in the combined steps 1 and 2 (Figure 1) for the monolayer are contrasted to the comparable energies for bulk hydrocarbons, namely those for vaporization and sublimation. For consistency, we define the transition process (TRANS) as proceeding from a bulk standard gas state either to a bulk hydrocarbon (solid or liquid) or to a monolayer (liquid condensed or liquid expanded). For this purpose we will compare the properties of the normal C_{15} hydrocarbon, pentadecane, with hydrocarbon properties derived for the C_{15} acids in Table IV.

ΔH_{TRANS} and ΔS_{TRANS} for the bulk C_{15} hydrocarbon were obtained from relations given by Huggins[11] and are listed in Table V.

ΔH_{TRANS} for the monolayers is given by the sum of the heats for the adsorption and compression processes (Figure 1, step 1 plus step 2). ΔH_{ads} (step 1) was calculated from eq 4, assuming $k_{ads} = -1815$ (Table I). The corresponding heat of compression (step 2) for the C_{15} hydrocarbon in a liquid-condensed or

Table III: Thermodynamic Parameters for the Film Compression Process

Compound	T, °K	$\pi_V \pm 0.001$ dyn/cm	$\Delta F_c \pm 14$ cal/mol	$\Delta H_c \pm 25$ cal/mol	$\Delta S_c \pm 2$ eu
		Liquid Expanded			
Palmitoleyl alcohol	298	0.134	2161	−283	−8
	288	0.122	2079		
Oleyl alcohol	298	0.085	1991	−1,078	−10
	288	0.065	1888		
Palmitoleic acid	301	0.149	2300	−5,750	−27
	290	0.128	2030		
Oleic acid	301	0.105			
	298	0.095	2135	−6,537	−29
	288	0.074	1844		
	286	0.070			
	276	0.053			
		Liquid Condensed			
Stearyl alcohol	298	0.010	874	−12,327	−44
	288	0.003	431		
Palmitic acid	300	0.084			
	298	0.076	2310	−14,497	−56
	288	0.031	1746		
Stearic acid	298	0.012	1272	−15,684	−57
	288	0.005	703		
Methyl stearate	298	0.036	1876	−18,239	−67
	286	0.010	1066		
Octadecylacetamide	298	0.028	1727		
	286	0.010	1124	−13,233	−50
	282.5	0.007	905		
	280.0	0.001			
Cholesterol	298	0.006	815	−14,915	−53
	288	0.002	287		

Table IV: Hydrocarbon Contributions to Film Compression at 15°

Compound	$\Delta F_c^h = n\bar{f}$, cal/mol	$\Delta H_c^h/n$, cal/mol of $-CH_2-$	ΔS_c^h, eu
	Liquid Expanded ($\bar{f} = -95$)		
$C_{15}H_{29}$-COOH	−1425	−602	−26
$C_{16}H_{31}$-OH	−1520	−607	−28
$C_{17}H_{33}$-COOH	−1615	−577	−29
$C_{18}H_{35}$-OH	−1710	−584	−31
	Liquid Condensed ($\bar{f} = -450$)		
$C_{15}H_{31}$-COOH	−6750	−908	−24
$C_{17}H_{35}$-COOH	−7650	−871	−25
$C_{18}H_{37}$-OH	−8100	−855	−25

Table V: Comparison of the Thermodynamics of Transition for Bulk and Monolayer Hydrocarbons at 15° for 1 Mole of a C_{15} Hydrocarbon ($n = 15$)

Transition process from bulk gas to	ΔH_{TRANS}, kcal/mol	ΔS_{TRANS}, eu
	Bulk[a]	
(a) Solid	−34.1	−58.6
(b) Liquid	−21.6	−32.6
	Monolayer	
(a) Solid	−24.9	
(b) Liquid condensed	−24.7	−28 ± 3
(c) Liquid expanded	−20.1	−30 ± 3

[a] Calculated from the relations given by Huggins.[11]

liquid-expanded monolayer was calculated using the values of $(\Delta H_c^h/n)$ in Table IV.

From the Sakur–Tetrode equation for the bulk vapor and the two-dimensional analog,[19] we calculated the entropy of adsorption, ΔS_{ads}, for pentadecane to be −4.4 eu. This value is based on our monolayer-gas standard state of 100,000 Å²/molecule. Entropies of compression ΔS_c^h for the C_{15} compounds were taken directly from Table IV. Entropies of transition (step 1 plus step 2, Figure 1) for the monolayer are listed in Table V for liquid-expanded and liquid-condensed states.

We have estimated ΔH_{TRANS} for the solid monolayer by using the data of Harkins, Young, and Boyd,[20] who measured the isotherms for hexadecanol and octadecanol monolayers between the liquid-condensed and the solid monolayer states as a function of temperature.

(19) C. Kemball, *Proc. Roy. Soc., Ser. A*, **187**, 73 (1946).

(20) W. D. Harkins, T. F. Young, and E. Boyd, *J. Chem. Phys.*, **8**, 954 (1940).

It was estimated that an additional heat of −10 cal/mol of $-CH_2-$ is involved in compressing the monolayer from the liquid-condensed to the solid monolayer state. Therefore, we estimate ΔH_{TRANS} for the C_{15} solid monolayer to be −25 kcal/mol (Table V).

It is clear from Table V that the heats of transition for all three monolayer states are closer to that for the bulk hydrocarbon liquid than for the solid. Moreover, the entropies of transition for the monolayers are essentially the same as for the bulk liquid. The small differences in the heats of transition suggest that the liquid-expanded film is slightly less condensed and the liquid-condensed film is slightly more condensed than the bulk liquid hydrocarbon.

Given the hydrocarbon energies, we can now calculate the polar group contributions to the film compression process.

(B) Polar Group Contributions to Film Compression. The polar group contributions to the thermodynamic parameters for film compression were calculated using eq 1. The formal relations for obtaining ΔF_c^p, ΔH_c^p, and ΔS_c^p along with the results of these calculations are given in Table VI.

Table VI: Polar Group Contributions to Film Compression at 15°

Compound	ΔF_c^p,[a] cal/mol	ΔH_c^p, cal/mol	ΔS_c^p,[b] eu
	Liquid Expanded		
$C_{16}H_{31}$–OH	−775	+9430	+35
$C_{18}H_{35}$–OH	−775	+9430	+35
$C_{15}H_{29}$–COOH	−915	+3280	+14
$C_{17}H_{33}$–COOH	−915	+3280	+14
	Liquid Condensed		
$C_{18}H_{37}$–OH	+3755	+3060	−2.5
$C_{15}H_{31}$–COOH	+3725	−880	−16.5
$C_{17}H_{35}$–COOH	+3575	−880	−15.5
$C_{17}H_{35}$–$COOCH_3$	+3945	−3430	−26.5
$C_{18}H_{37}$–$NHCOCH_3$	+3445	+2160	−8.5

[a] $\Delta F_c^p = \Delta F_c + RT \ln (A_c/A_i) - \Delta F_c^h$. [b] $\Delta S_c^p = \Delta S_c - R \ln (A_c/A_i) - \Delta S_c^h$.

Before considering the significance of ΔH_c^p and ΔS_c^p, it is important to reemphasize that these energies reflect possible changes due to altered states of film hydration, hydrogen bonding, and structure of the underlying water when the monolayer is compressed from the ideal surface gas to the condensed state. While we cannot separate these contributions rigorously, we shall attempt to establish reasonable limits by considering some physically meaningful possibilities.

Let us suppose that the process of film compression results in formation of an intermolecularly hydrogen bonded network of polar groups, as suggested by Alexander.[21,22] If we assume the formation of the H-bonded network results in the complete loss of rotational freedom for the polar group, then $\Delta S_c^p = -R \ln 4\pi = -5.1$ eu. If an icelike layer is formed in the underlying water layer, as suggested by a variety of monolayer studies,[23] then for the extreme case of the formation of 1 mol of ice, $\Delta S_c^p = \Delta S_{fusion} = -5$ eu.

Neither of these models can explain the large positive values of ΔS_c^p observed for the liquid-expanded films (Table VI). On the contrary, for the liquid-expanded films, a disordering of the polar region is suggested by the large positive values for ΔS_c^p.

For the liquid-condensed films in this study, all values of ΔS_c^p are negative, suggesting that both hydrogen bonding and the formation of an icelike layer are possible. However, for the ester, the polar group least likely to form intermolecular hydrogen bonds, we find the largest value for ΔS_c^p (−26.5 eu). In this instance, one should expect a minimum of 5 mol of ice per mole of polar group to form. The significance of the ΔS_c^p values is presently being studied in greater detail.

In conclusion, the hydrocarbon contributions in the condensed monolayer states are energetically similar to those in bulk hydrocarbon liquids (Table V). The interactions in the polar region make significant contributions to ΔH_c for the condensed monolayers. For the liquid-expanded films, the polar and hydrocarbon group contributions to ΔH_c may be of the same order of magnitude, and opposite in sign; *e.g.*, for palmitoleyl alcohol, $\Delta H_c^p = +9430$ and $\Delta H_c^h = -9030$ cal/mol. For the liquid-condensed and solid monolayers, the relative contribution of the hydrocarbon interactions to ΔH_c increase; *e.g.*, for stearic acid, $\Delta H_c^p = -880$, while $\Delta H_c^h = -15{,}400$ cal/mol.

While the contribution of the water to the surface phases cannot be evaluated absolutely from the monolayer experiments, our studies suggest that changes in the water structure are likely to occur in the formation of each monolayer state.

(21) A. E. Alexander, *Proc. Roy. Soc., Ser. A*, 179, 470, 486 (1942).
(22) G. E. Hibberd and A. E. Alexander, *J. Phys. Chem.*, 66, 1854 (1962).
(23) J. T. Davies and E. K. Rideal, "Interfacial Phenomena," Academic Press, New York, N. Y., 1961, p 369.

Physical Chemistry of Lipid Films at the Air–Water Interface. II. Binary Lipid Mixtures. The Principles Governing Miscibility of Lipids in Surfaces[1a]

by R. E. Pagano[1b] and N. L. Gershfeld*

Laboratory of Physical Biology, National Institute of Arthritis and Metabolic Diseases, National Institutes of Health, U. S. Department of Health, Education, and Welfare, Bethesda, Maryland 20014 *(Received April 22, 1971)*

Publication costs assisted by the National Institutes of Health

The surface vapor pressure–composition diagrams for a variety of binary lipid mixtures have been determined and shown, from the thermodynamics of the mixing process, to be analogous to those for bulk systems. It was observed that (a) two liquid-condensed or two liquid-expanded lipids gave ideal mixing, and (b) the mixing of a liquid-condensed with a liquid-expanded lipid gave either positive deviations from ideal behavior or phase separation (immiscibility). These results are shown to be consistent with regular solution theory, with the mixing process dominated by the hydrocarbon region of the film. Polar group interactions do not contribute significantly to the mixing process. Regular solution theory predicts that mixtures of cholesterol with either a liquid-expanded or a liquid-condensed lipid will show large positive deviations from "ideal" behavior, or phase separation. This is in agreement with the vapor pressure–composition studies. There is no evidence for specific interactions between cholesterol and neutral lipids in surface films.

Introduction

Binary lipid mixtures in monolayers at the air–water interface have been treated formally as two-dimensional solutions.[2] The great majority of the experimental studies have been in the high surface pressure π region of the π–A isotherms. However, the significance of the results of many of the binary mixture studies may be questioned on the grounds that the surface mixtures may be neither homogeneous nor at equilibrium.[3]

In part I of this series,[4] the surface vapor pressures π_v of single-component lipid films on water were measured under equilibrium conditions. In the present paper we consider the mixing of two lipid components in the region of π_v. The surface vapor pressure–composition (π_v/x) diagrams will be used for classifying the lipid mixtures analogous to bulk systems. The validity of this analogy was established by measuring the thermodynamic parameters of mixing for a two-dimensional solution. We shall demonstrate that the mixing process in the surface follows general principles of regular solution behavior as developed for bulk systems.[5]

Theoretical Section

(*A*) *Thermodynamic Studies.* The relations for obtaining the thermodynamic properties of insoluble mixed lipid films were developed analogously to the procedure first used by Goodrich.[2a] From the definition of ΔF_c given in part I (eq 7), the free energy of mixing for two lipid components may be written

$$\Delta F^M = \Delta F_c^{(12)} - x_1\Delta F_c^{(1)} - x_2\Delta F_c^{(2)} + RT(x_1 \ln x_1 + x_2 \ln x_2) \quad (1)$$

where $\Delta F_c^{(1)}$, $\Delta F_c^{(2)}$, and $\Delta F_c^{(12)}$ are the work of compression for the pure components and mixed films, and x_1 and x_2 are the mole fractions of the components in the mixture. The last term of eq 1 represents the ideal free energy of mixing. From the temperature dependence of ΔF^M and the second law, we obtain all the thermodynamic parameters for the two-dimensional solutions.

(*B*) *Miscibility Studies.* If two surface-active components are premixed in an organic solvent and then spread as a monolayer at the air–water interface, we are unable to tell by any direct measurement whether the components are truly miscible in the surface and exist as a homogenous surface phase, or whether phase separation due to limited solubility of one component in the other has occurred. Defay[6a] and, more recently, Crisp[6b] have developed the phase rule to explicitly include surfaces, and hence the phase rule may be em-

(1) (a) Presented in part at the 15th Annual Meeting of The Biophysical Society, Feb 15–18, 1971, New Orleans, La; (b) Staff Associate, National Institutes of Health, 1968–1970.

(2) (a) F. C. Goodrich, "Proceedings of 2nd International Congress on Surface Activity," Vol. 1, Butterworths, London, 1957, p 85; (b) G. L. Gaines, Jr., "Insoluble Monolayers at Liquid-Gas Interfaces," Interscience, New York, N. Y., 1966.

(3) (a) N. L. Gershfeld and R. E. Pagano, Abstracts 160th National Meeting American Chemical Soc., Sept. 1970: (b) see part III of this series, N. L. Gershfeld and R. E. Pagano, *J. Phys. Chem.*, **76**, 1244 (1972).

(4) N. L. Gershfeld and R. E. Pagano, *J. Phys. Chem.*, **76**, 1231 (1972).

(5) J. H. Hildebrand and R. L. Scott, "The Solubility of Nonelectrolytes," 3rd ed, Dover Publications, New York, N. Y., 1950;

(6) (a) R. Defay, Thesis, Brussels, 1932; see also, R. Defay, I. Prigogine, A. Bellemans, and D. H. Everett, "Surface Tension and Adsorption," Wiley, New York, N. Y., 1966, pp 74–78. (b) D. J. Crisp in "Surface Chemistry," Supplement to Research, Butterworths, London, 1949, p 17, 23.

ployed to determine the homogeneity of a multicomponent surface film. At constant temperature and external pressure, and in the absence of any externally imposed electrical potentials, the number of degrees of freedom, f, for the system will be

$$f = C^B + C^S - P^B - P^S + 1 \qquad (2)$$

where C^B is the number of components in bulk which are equilibrated throughout the system, C^S is the number of components restricted to the surface, P^B is the number of bulk phases, and P^S is the number of monolayer phases in equilibrium with each other.

In order to test the miscibility of two components in the surface, components 1 and 2 are premixed in a spreading solvent at mole fractions x_1 and x_2 and deposited at the air–water interface at a surface concentration corresponding to the two-dimensional liquid–vapor transition region (see Figure 2, part I, this series). A vapor pressure–composition (π_v/x) curve is generated by measuring the surface vapor pressure as a function of the mole fraction x. Several results are possible. (i) *Complete Miscibility.* If 1 and 2 are miscible in all proportions, then two homogeneous surface phases ($P^S = 2$) will be present in equilibrium with one another: a two-dimensional liquid with composition x_1' and x_2' in equilibrium with a two-dimensional gas of composition x_1^g and x_2^g. Since $P^B = 2$ (air, water), $C^B = 2$ (air, water), and $C^S = 2$ (components 1 and 2), eq 2 gives one degree of freedom ($f = 1$). Thus, if 1 and 2 are miscible in all proportions, the surface vapor pressure should vary continuously with the composition of the film. The completely miscible binary lipid mixtures may exhibit positive, negative, or no deviations from ideal behavior. When there is no deviation from ideal behavior, the monolayer analog of Raoult's law is obeyed. (ii) *Partial Miscibility.* If over a region of the mixing (π_v/x) curve, 1 and 2 are immiscible, then there will be three equilibrium surface phases present: two immiscible condensed surface phases of distinct and different composition x_1', x_2', and x_1'', x_2'', and a surface gas phase of composition x_1^g, x_2^g. Since $P^S = 3$, $P^B = 2$ (air, water), $C^B = 2$ (air, water), and $C^S = 2$ (1 and 2), f is calculated to be zero from the phase rule. Thus, in the range of immiscibility, π_v is invariant of the composition and the vapor pressure–composition (π_v/x) diagram must be flat over this region. (iii) *Complete Immiscibility.* In the case of complete immiscibility, the surface vapor pressure will be independent of x and equal to the sum of the vapor pressures for the pure components ($\pi_v^1 + \pi_v^2$).

Thus we see that in the monolayer it is possible to detect when mixing occurs from the vapor pressure–composition diagram.

It is important to note that the mole fraction x in each of the surface phases is not necessarily the same as that which would be calculated from the composition of the bulk spreading solution, and that in the monolayer it is impossible to analyze the composition of each surface phase directly. An indirect method must be used. Thus, if a surface concentration is chosen close to the condensed area A_c, but within the transition region (see Figure 2, part I), then the amount of the component in the vapor is small and it can be assumed that all the lipids are in the condensed phase. Similarly, if the surface concentration is chosen close to the vapor transition area A_v, but again within the transition region, then all of the lipids will be present as a two-dimensional gas.

Experimental Section

The film balance and the compounds used in the studies reported here were all described in part I of this series.[4] Spreading solutions containing mixtures of the film-forming molecules in the desired molar ratios were prepared from stock solutions of the pure components and stored at −20°.

To study the vapor pressure–composition (π_v/x) curves in the miscibility studies, aliquots of the various spreading solutions were each spread at molecular areas slightly greater than A_c: 50–100 Å^2. In the vapor pressure–composition diagrams (Figures 2, 3, and 4), the surface vapor pressure was plotted *vs.* the mole fraction calculated on the basis of the lipid composition in the spreading solution. Since these vapor pressures were determined at 50–100 Å^2/molecule, this mole fraction should be nearly equal to that for the two-dimensional liquid phase. On the assumption that the vapor molecules in the liquid–vapor transition region occupy an area A_v, we estimate a maximum error of about 2% in the mole fraction.

In the thermodynamic studies of the mixed films, the isotherms were determined point by point. A few points on the palmitoleyl alcohol + oleyl alcohol (1:1) isotherms were determined by compression and expansion of the film to verify equilibrium. The work of compression for each film was determined by graphical integration of the isotherm from area A_c (Figure 2, part I) to 10,000 Å^2/molecule, and by application of a suitable equation of state from 10,000 to 100,000 Å^2/molecule, as discussed in part I.

Results

The π–A isotherms for the pure components palmitoleyl alcohol and oleyl alcohol, and for the mixture palmitoleyl + oleyl alcohols (1:1) at 25 and 15° and pH 2.0 are given in Figure 1. We define A for the mixed film as the average area per lipid molecule in the surface; all measurements were carried out to 10,000 Å^2/molecule. The isotherms for the pure components are taken from part I of this series.[4] It should be noted that, unlike for the pure components, the liquid–vapor transition region for the mixed film is not independent of the surface concentration, but rather varies continuously with A. This finding is in accordance

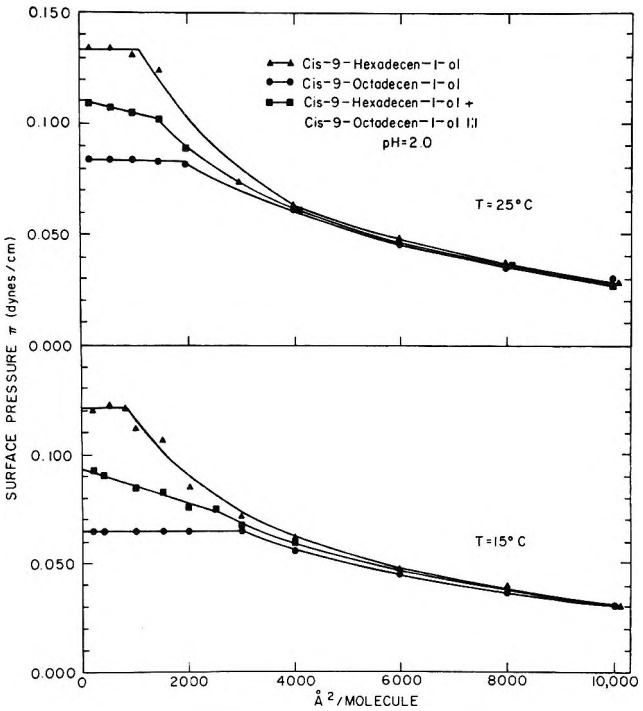

Figure 1. π–A isotherm at 25 and 15° and pH 2 for ▲ palmitoleyl alcohol (*cis*-9-hexadecen-1-ol), (●) oleyl alcohol (*cis*-9-octadecen-1-ol), and (■) palmitoleyl alcohol + oleyl alcohol (1:1).

with the phase rule (eq 2) which predicts one degree of freedom when $P^S = P^B = C^S = C^B = 2$. Thus, in the mixed films, varying A within the transition region ($A_c \leq A \leq A_v$) changes not only the proportions of the condensed and surface vapor phases present but also the composition of each phase.

The parameters a_s and A_0 used in fitting the van der Waals equation of state to the experimental data for the mixed gaseous film are presented in Table I. These parameters were used in calculating the Helmholtz free energy of compression, ΔF_c, between 10,000 and 100,000 Å²/molecule for the mixed film.

Table I: Parameters for van der Waals Equation of State for the Film Palmitoleyl Alcohol + Oleyl Alcohol (1:1)

T, °K	A_0, cm² × 10¹⁶	a_s × 10²⁷ (ergs cm²)/molecule²
298	2200	21.3
288	2200	19.2

Table II presents the Helmholtz free energy of compression for each of the pure components and the mixed film between area A_c (Figure 2, part I) and 100,000 Å²/molecule. Calculations of ΔF_c were made as described in part I of this series.[4]

The free energy, ΔF^M; heat, ΔH^M; and entropy, ΔS^M, of mixing were calculated from the experimental values of ΔF_c (Table II) using eq 1 and are tabulated in Table III.

Table II: Helmholtz Free Energy of Compression for Palmitoleyl Alcohol, Oleyl Alcohol, and a 1:1 Mixture

Monolayer	T, °K	ΔF_c[a] ± 14 cal/mol
(a) Palmitoleyl alcohol	298	2161
	288	2079
(b) Oleyl alcohol	298	1991
	288	1888
(c) Palmitoleyl alcohol + oleyl alcohol (1:1)	298	2069
	288	1977

[a] Evaluated between A_c and 100,000 Å²/molecule.

Table III: The Thermodynamic Parameters of Mixing for Equimolar Mixtures of Palmitoleyl Alcohol and Oleyl Alcohol Monolayers

	Measured	Ideal
ΔF^M, cal/mol		
T = 298°	−424 ± 24	−417
T = 288°	−410 ± 24	−403
ΔH^M, cal/mol	0 ± 41	0
ΔS^M, eu	1.4 ± 3.4	1.4

The vapor pressure-composition curves for a variety of binary lipid mixtures are presented in Figures 2–4.

Discussion

Thermodynamic Studies. To establish the correctness of treating surface mixtures analogously to bulk systems, we examined in detail the thermodynamic parameters for the mixed film palmitoleyl alcohol + oleyl alcohol (1:1). From the vapor pressure–composition diagram for this mixture (Figure 2C), one would infer that an ideal surface solution existed. From Table III, the measured ΔF^M, ΔH^M, and ΔS^M are, within experimental error, equal to the values calculated for an ideal surface solution. Thus we conclude ideal solution behavior for a system whose vapor pressure is a linear function of x over the entire range of composition.

Miscibility Studies. In this section we present the vapor pressure–composition diagrams for a large variety of binary surface solutions to elucidate the physicochemical factors which control the miscibility of two lipid components in the surface. In particular, we will examine the influence on the mixing process of the physical state of the pure components and the chemical nature of the polar group. The results, shown in Figure 2, illustrate the application of the phase rule to the miscibility problem in surfaces. The data are seen to fall naturally into three categories. (a) *Ideal Mixing.* For the pairs myristic + oleic acids, palmitoleic +

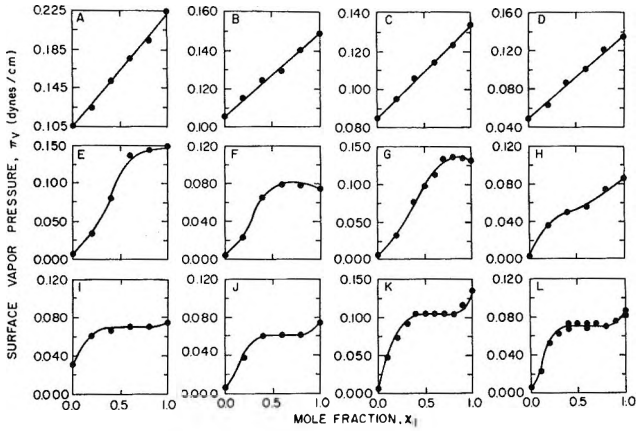

Figure 2. Vapor pressure–composition curves for (A) myristic acid + oleic acid, 27.5°, pH 2.0; (B) palmitoleic acid + oleic acid, 27.5°, pH 2.0; (C) palmitoleyl alcohol + oleyl alcohol, 25°, pH 5.8; (D) palmitoleyl alcohol + elaidyl alcohol, 25°, pH 5.8; (E) palmitoleic acid + cholesterol, 27.5°, pH 2.0; (F) oleic acid + cholesterol, 15°, pH 2.0; (G) palmitoleyl alcohol + cholesterol, 25°, pH 5.8; (H) oleyl alcohol + cholesterol, 25°, pH 5.8; (I) oleic acid + palmitic acid, 15°, pH 2.0; (J) oleic acid + stearic acid, 15°, pH 2.0; (K) palmitoleyl alcohol + stearyl alcohol, 25°, pH 5.8; (L) oleyl alcohol + stearyl alcohol, 25°, pH 5.8.

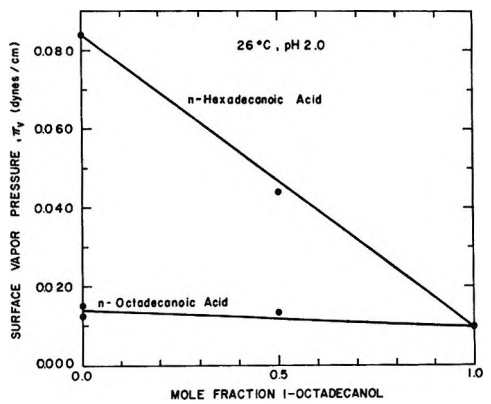

Figure 3. Vapor pressure–composition curves for palmitic acid (*n*-hexadecanoic acid) + stearyl alcohol (1-octadecanol), and stearic acid (*n*-octadecanoic acid) + stearyl alcohol.

oleic acids, palmitoleyl + oleyl alcohols, palmitoleyl + elaidyl alcohols (Figure 2A–D), and palmitic acid + stearyl alcohol, stearic acid + stearyl alcohol (Figure 3) the data points for each mixed film fall on a straight line connecting the vapor pressures of the two pure components. From the preceding thermodynamic argument we conclude that these mixtures form ideal surface solutions. It should be noted that according to the phase rule, since π_v is a monovariant function of x, the two compounds must necessarily be miscible in all proportions. (b) *Partial Miscibility.* For oleic + palmitic acids, oleic + stearic acids, palmitoleyl + stearyl alcohols, and oleyl + stearyl alcohols (Figure 2I–L), each vapor pressure–composition curve exhibits a horizontal region where π_v is independent of x_1. By the phase rule this portion of the mixing curve

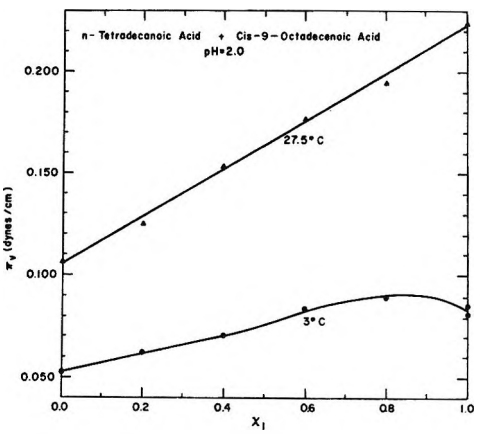

Figure 4. Vapor pressure–composition curves for myristic (*n*-tetradecanoic) + oleic (*cis*-9-octadecenoic) acids at 27.5 and 3°.

must represent a region of immiscibility, since the number of degrees of freedom is zero (equation 2). The ends of the horizontal region of the mixing curve define the composition of the two immiscible condensed surface phases or, equivalently, the limits of miscibility of the first component in the second and *vice versa*. Thus, for example, in the case of oleyl and stearyl alcohol mixtures (Figure 2L), the solubility limits in the surface are (i) 40 mol % oleyl alcohol in stearyl alcohol and (ii) 20 mol % stearyl alcohol in oleyl alcohol. It should be noted that for any mole fraction x_1 of oleyl alcohol between 0.4 and 0.8, both of these two-dimensional condensed phases coexist in equilibrium with the monolayer vapor phase. Changing x_1 between 0.4 and 0.8 changes the relative amounts of the two condensed phases present, but not their composition. (c) *Miscibility with Positive Deviations.* For mixtures of palmitoleic acid, oleic acid, palmitoleyl alcohol, or oleyl alcohol with cholesterol, positive deviations from ideal mixing were observed (Figure 2E–H). Since these mixing curves are monovariant, cholesterol is completely miscible in these surface solutions at these temperatures.

Two additional categories of the vapor pressure–composition studies which may be expected to occur but were not observed in this study are complete immiscibility and negative deviations from ideal mixing. An example of the former has been given[3] where cholesterol was observed not to mix with stearyl alcohol, stearic acid or dipalmitolyl lecithin. A preliminary vapor pressure–composition study of cholesterol–dipalmitolyl lecithin mixtures also indicates complete immiscibility for this pair.[7] Complete miscibility with negative deviations was not obtained for any binary system we have examined by the vapor pressure technique.

Application of Regular Solution Theory. To identify

(7) R. E. Pagano and N. L. Gershfeld, unpublished results.

parameters which are important in determining the two-dimensional solution properties of a mixed monolayer, we will apply regular solution theory and evaluate the "solubility parameter," introduced by Hildebrand in the study of bulk solutions.[8] The solubility parameter δ is given by the square root of the energy of vaporization per cubic centimeter

$$\delta = (E^v/V)^{1/2} \quad (3)$$

This parameter has been very useful in predicting deviations from ideal solution behavior from the properties of the pure component liquids, and in estimating the heat of mixing ΔH^M according to the theoretical expression

$$\Delta H^M = V_m(\delta_1 - \delta_2)^2\phi_1\phi_2 \quad (4)$$

where ϕ_1 and ϕ_2 are the volume fractions of components 1 and 2 (neglecting volume changes on mixing) and V_m is the volume of the mixture.

According to the theory of regular solutions, two liquids will mix ideally if they possess similar solubility parameters and molar volumes.[9] If the values of δ differ, the theory predicts positive deviations from ideal behavior. If the molar volumes differ, negative deviations from ideal mixing will be observed due to corrections in the entropy of mixing. For the systems in our study, the maximum disparity in molecular size for any given pair is less than 2, *e.g.*, cholesterol *vs.* oleyl alcohol. These differences cannot be expected to contribute significantly to the free energy of mixing.[10] Thus all deviations from ideal solution behavior should be attributable only to differences in δ.

To obtain the analogous solubility parameter for the monolayer we may replace E^v with ΔH_c, the heat of surface compression between the condensed monolayer and ideal surface vapor states (see part I). Thus, we write

$$\delta = (\Delta H_c/V)^{1/2} \quad (5)$$

where V, the molar volume of the film-forming molecules in the surface, was estimated from the bulk densities.

Values of ΔH_c or ΔH_c^h, the contribution to the heats of compression due to the hydrocarbon region alone, were used to calculate δ from eq 5. The results are given in Table IV. With the exception of myristic acid and cholesterol, ΔH_c and ΔH_c^h were taken directly from part I, Tables III and IV.[4]

For myristic acid, where the isotherm was not available, ΔH_c was estimated to be -4520 cal/mol using $\Delta H_c^h/n = -600$ cal/mol of $-CH_2-$ and $\Delta H_c^p = +3280$ for the carboxyl group in a liquid-expanded film (part I, Table VI).

Since it is not possible to measure ΔH_c^h for cholesterol, we estimated this contribution by subtracting ΔH_c^p for the hydroxyl group. This calculation is complicated by the fact that the area for the –OH group (37 Å^2) in films of cholesterol is intermediate between the liquid-condensed (22 Å^2) and liquid-expanded (45 Å^2) areas. We assumed that ΔH_c^p will be intermediate in the case of cholesterol, and used an average value of +6250 cal/mol (Part I, Table VI). Therefore, ΔH_c^h ($= \Delta H_c - \Delta H_c^p$) was calculated to be -8670 cal/mol. While this is only an approximation, the value of ΔH_c^p clearly cannot be that for the liquid-condensed monolayer because of the disparity in the molecular areas. The choice of ΔH_c^p will not significantly alter the conclusions which follow.

Table IV: Solubility Parameters, δ, of Lipid Monolayers

Compound	$\delta = (\Delta H_c/V)^{1/2}$, cal$^{1/2}$ (cm^3)$^{-1/2}$	$\delta = (\Delta H_c^h/V_h)^{1/2}$,[a] cal$^{1/2}$ (cm^3)$^{-1/2}$
Liquid Expanded		
Myristic acid	4.1	5.7
Palmitoleic acid	4.5	5.8
Oleic acid	4.5	5.7
Palmitoleyl alcohol	1.0	5.8
Oleyl alcohol	1.8	5.7
Liquid Condensed		
Cholesterol	6.4	4.9
Stearyl alcohol	6.1	6.9
Palmitic acid	7.3	7.0
Stearic acid	7.2	6.9

[a] V_h represents molar volumes for the equivalent aliphatic hydrocarbons.

Applying regular solution theory to predict the results in Figure 2, we note that when $\delta = (\Delta H_c/V)^{1/2}$ is used, inconsistencies result, *e.g.*, palmitoleyl alcohol ($\delta = 1.0$) and oleyl alcohol ($\delta = 1.8$) mix ideally, whereas one would predict positive deviations from ideal mixing. Another example of this inconsistency (Figure 3) is the mixing of stearyl alcohol ($\delta = 6.1$) with stearic acid ($\delta = 7.2$); these compounds also mix ideally.

On the other hand, if we assume that the mixing process is dominated by the hydrocarbon region of the film and use $\delta = (\Delta H_c^h/V_h)^{1/2}$, where V_h is the molar volume of the equivalent aliphatic hydrocarbon, our results are entirely consistent with regular solution theory. For example, mixtures of two liquid-condensed films (Figure 3) or two liquid-expanded films (Figure 2A–D) form ideal mixtures as predicted from their solubility parameters (Table IV). Furthermore, mixing of a liquid-condensed with a liquid-expanded film should give positive deviations or immiscibility, depending on the mixing temperature.[11] Our results again are in accord with this prediction (Figure 2E–L).

(8) Reference 5, Chapter XXIII.

(9) Reference 5, Chapters VII and VIII.

(10) Reference 5, p 116.

(11) S. Glasstone, "Textbook of Physical Chemistry," 2nd ed, Van Nostrand, Princeton, N. J., p 712.

When cholesterol is one of the components of the mixture, the same principles are obeyed. Thus, using the value of $\delta = 4.9$ for cholesterol, we would predict positive deviations or immiscibility on mixing with either a liquid-expanded or a liquid-condensed component. Indeed, these predictions are fulfilled for both the liquid-expanded films (Figure 2E–H) and liquid-condensed films.[3]

We have also examined the effect of temperature on mixing two components in a surface solution and find these results consistent with regular solution theory. We determined the temperature dependence of the vapor pressure–composition curves for oleic and myristic acids at 27.5 and 3° (Figure 4). These temperatures were chosen because it has been demonstrated that oleic acid gives a liquid-expanded film over this temperature interval,[12] while myristic acid forms a liquid-condensed film at 3° and is a liquid-expanded film at 27.5°.[13] Since each physical state has a characteristic δ (Table IV), we would predict ideal mixing at 27.5° and positive deviations or immiscibility at 3°. Our results agree with these predictions.

Other factors which might be expected to influence the mixing of lipids in surfaces are polar group interactions, the presence of double bonds, and isomer effects. Polar group interactions appear to be insignificant in the mixing of liquid-condensed films. Since the mixing of an acid and an alcohol is ideal (Figure 3), the interactions between these two groups in liquid-condensed films appears to be insignificant. Other polar group interactions can be assessed similarly. We have not observed any influence on mixing behavior due to the presence of a double bond. Thus, oleic acid mixes ideally with either a saturated (myristic, Figure 4) or unsaturated (palmitoleic, Figure 2B) fatty acid. Furthermore, we have not observed any particular effect of isomers on the properties of the mixtures. For example, *cis*-9-hexadecen-1-ol (palmitoleyl alcohol) mixes ideally with either the cis (oleyl alcohol, Figure 2C) or trans (elaidyl alcohol, Figure 2D) isomers of 9-octadecen-1-ol.

In conclusion, regular solution theory can be applied to predict qualitatively the behavior of lipid mixtures at the air–water interface. Moreover, the mixing of lipids in surfaces is dominated by interactions in the hydrocarbon region of the film. In addition, we have demonstrated that the (π_v/x) studies are consistent with mixing studies in condensed films. For the latter it is particularly important to recognize that phase separations may occur which will complicate any attempt to describe the packing of the two components in the condensed film. In view of the positive deviations from Raoult's law observed for the lipid mixtures in the surface vapor region, an increase in π (as in the condensed high-pressure region) may lead to phase separation.[14]

(12) W. D. Harkins, T. F. Young, and E. Boyd, *J. Chem. Phys.*, 8, 954 (1940).

(13) N. K. Adam, "The Physics and Chemistry of Surface Films," 3rd ed, Oxford University Press, London, 1941, p 65.

(14) G. L. Gaines, Jr., *J. Colloid Interface Sci.*, 21, 315 (1966).

Physical Chemistry of Lipid Films at the Air–Water Interface. III. The Condensing Effect of Cholesterol. A Critical Examination of Mixed-Film Studies[1a]

by N. L. Gershfeld* and R. E. Pagano[1b]

Laboratory of Physical Biology, National Institute of Arthritis and Metabolic Diseases, National Institutes of Health, U. S. Department of Health, Education, and Welfare, Bethesda, Maryland 20014 *(Received April 22, 1971)*

Publication costs assisted by the National Institutes of Health

The condensing effect reported for mixed monolayers containing cholesterol has been based on assumptions of equilibrium and homogenity in the "spread" film. The inconclusive nature of these experiments has led us to reexamine the mixing process in mixed lipid films under conditions where equilibrium and film homogeneity have been assured. Using aqueous solutions which are well stirred and saturated with respect to the lipids, the composition of the equilibrium surface film is deduced from radiotracer, surface potential, and surface pressure measurements. The surface mixtures which form are treated as two-dimensional solutions; a theoretical analysis predicting the surface tension when the lipid components mix "ideally" is presented. From these results, it is concluded that (a) in the absence of specific interactions, the liquid-condensed films (octadecanol, stearic acid, and dipalmitoyl lecithin) are immiscible with cholesterol; (b) cholesterol forms nonideal mixtures with liquid-expanded (oleic acid, oleyl alcohol, and *m*-oleyl phosphate) and gaseous (octadecyl sulfate) films. Since the assumption of film homogeneity in the spread film must be violated for at least some cholesterol–lipid mixed film systems, it is questioned whether the "condensing" effect which occurs in these systems can be meaningfully interpreted.

Introduction

The natural occurrence of lipids in cell membranes, organelles, and other biological structures has led to extensive investigations of the properties of lipid mixtures in monolayers at the air–water interface with the purpose of establishing a physicochemical basis for the stability of the lipid-containing biological structures. Using "spread films," films prepared by depositing lipid mixtures on the water surface from a volatile solvent, Leathes[2] reported for cholesterol in combination with natural lecithins that the sum of the partial molecular areas in the mixture was significantly less than the calculated sum of the molecular areas of the pure components. This "condensing" effect with cholesterol has been confirmed by other investigators.[3–6] "Expanding" effects with other lipid pairs have also been reported.[7,8]

Attempts to rationalize the condensing phenomenon of cholesterol in molecular terms have resulted in the development of two general models—one assumes that the condensing effect may be attributed to the packing of the hydrocarbon moieties in the mixed film;[3a,5] the other assumes that an association with an accompanying heat occurs between the lipid components.[9] Neither model has been established. The inconclusive nature of the experimental results with respect to the "condensing" effect has led us to reexamine the mixed lipid film experiment.

Of crucial importance to these condensing and expanding phenomena are the implicit assumptions that the spread film of mixed lipids is at equilibrium and homogeneous. Clearly, if more than one surface phase appears upon mixing cholesterol with another lipid, the calculation of the average area per film molecule would be dubious. For this reason, this paper examines the mixing of lipids in films under experimental conditions which assured that the system is at equilibrium and that only one surface phase is present. We have studied the interaction of cholesterol with other lipids for which condensing effects have been reported. In the sections which follow, the first presents the theoretical basis for our experiments; the second section

(1) (a) Presented at the 160th National Meeting of the American Chemical Society, Chicago, Ill., Sept 1970; (b) Staff Associate, National Institutes of Health, 1968–1970.

(2) J. B. Leathes, *Lancet*, **208**, 853 (1925).

(3) (a) N. K. Adam and G. Jessop, *Proc. Roy. Soc., Ser. A*, **120**, 473 (1928); (b) L. de Bernard, *Bull. Soc. Chim. Biol.*, **40**, 161 (1958).

(4) L. L. M. Van Deenen, U. M. T. Houtsmuller, G. H. De Haas, and E. Mülder, *J. Pharm. Pharmacol.*, **14**, 429 (1962).

(5) D. O. Shah and J. H. Schulman, *J. Lipid Res.*, **8**, 215 (1967).

(6) D. Chapman, N. F. Owens, M. C. Phillips, and D. A. Walker, *Biochim. Biophys. Acta*, **183**, 458 (1969).

(7) W. D. Harkins and R. T. Florence, *J. Chem. Phys.*, **6**, 847 (1938).

(8) M. C. Phillips, B. D. Ladbrooke, and D. Chapman, *Biochim. Biophys. Acta*, **196**, 35 (1970).

(9) R. A. Demel, L. L. M. Van Deenen, and B. A. Pethica, *ibid.*, **135**, 11 (1967).

describes the experimental details for assuring equilibrium and film homogeneity in films; in the last section we shall demonstrate that, for the condensing effect, at least one basic assumption may be violated, and thus interpretations of the film condensing effect may be questionable.

Theoretical Section

In this section we derive expressions for calculating the surface mole fractions of two lipid components and the surface tension when the components mix "ideally" in the surface. To avoid the experimental problems associated with spread "insoluble" films, *i.e.*, monolayer desorption, and the possible coexistence of two surface phases,[10] well-stirred aqueous solutions saturated with respect to both lipid components were studied. The phase rule[11] applied to this system indicates that at equilibrium and constant temperature and pressure, only one surface phase will exist, characterized by a single value of surface tension γ.

The following analysis of this system treats the adsorbed film of lipid molecules as an "ideal" two-dimensional solution, where the activity of component i in the surface is equal to its surface mole fraction, x_i. Moreover, we assume that no interactions occur between the lipid components in the bulk reservoir of lipids, or in the aqueous solution at equilibrium.

The mole fraction of each component in the surface is evaluated by methods developed by previous workers.[12-16] For an aqueous solution containing i lipid components each of which is at saturation, the chemical potential of the ith component in solution μ_i is written

$$\mu_i = \mu_i^0 + RT \ln a_i(\text{satd}) \quad (1)$$

where a_i(satd) is the chemical activity in the saturated solution and μ_i^0 the standard chemical potential. The chemical potential of the ith component in the surface film may be written

$$\mu_i^s = \mu_i^{s,0} + RT \ln x_i - \gamma A_i^* \quad (2)$$

here A_i^* is the molar area of i in the surface mixture of the solution whose surface tension is γ. We choose as a reference state the surface saturated with component i in the absence of other lipid components, such that $x_i = 1$; the surface tension of the solution becomes that for the saturated solution of pure component i, where $\gamma = \gamma_i$. Equation 2 then becomes

$$\mu_i^s = \mu_i^{s,0} - \gamma_i A_i \quad (3)$$

where A_i is the molar area of component i in the film and corresponds to the molar area at the equilibrium spreading pressure of component i.

At equilibrium, $\mu_i = \mu_i^s$; and from eq 1 and 2

$$RT \ln a_i(\text{satd}) = (\mu_i^{s,0} - \mu_i^0) + RT \ln x_i - \gamma A_i^* \quad (4)$$

But, from eq 1 and 3

$$RT \ln a_i(\text{satd}) = (\mu_i^{s,0} - \mu_i^0) - \gamma_i A_i \quad (5)$$

Subtracting eq 4 from 5

$$RT \ln x_i = \gamma A_i^* - \gamma_i A_i \quad (6)$$

For the lipids in our study, we shall assume without serious error that the mole fraction of water in the "lipid-continuous" monolayer is zero,[17,18] and that $A_i = A_i^*$. Writing eq 6 explicitly for lipid components 1 and 2

$$RT \ln x_1 = A_1(\gamma - \gamma_1) \quad (7a)$$

and

$$RT \ln x_2 = A_2(\gamma - \gamma_2) \quad (7b)$$

Equations 7a and 7b may be combined by eliminating γ from both equations; to the resulting equation, we introduce the identity

$$\gamma_2 - \gamma_1 = \pi_1^e - \pi_2^e \quad (8)$$

where π_i^e is the equilibrium spreading pressure of component i, defined by the relation $\pi_i^e = \gamma_w - \gamma_i$; γ_w is the surface tension of water. Combining eq 7 and 8 and the relation $x_1 + x_2 = 1$ yields

$$\frac{(1 - x_1)^{A_1/A_2}}{x_1} = e^{(\pi_2^e - \pi_1^e)A_1/RT} \quad (9)$$

Equation 9 may be solved numerically. Thus, given values for π_1^e, π_2^e, A_1, and A_2—all of which are experimentally accessible—values for the mole fractions of each component in the equilibrium "ideal" mixed film may be obtained. With these values of x_i and eq 7, the surface tension of the ideal mixed film γ(ideal) may be calculated.

In principle, there are three ways in which the cholesterol–lipid interactions in the surface will be manifested. (a) *The surface components are completely immiscible.* Since only one surface phase can be present under the conditions of this experiment, one component must be excluded from the surface. The surface composition will be exclusively that of the component with the highest equilibrium spreading pressure. (b) *The surface components are miscible and form ideal mix-*

(10) G. L. Gaines, Jr., "Insoluble Monolayers at Liquid-Gas Interfaces," Interscience, New York, N. Y., 1966.

(11) D. J. Crisp in "Surface Chemistry," Supplement to Research, Butterworths, London, 1949, pp 17, 23.

(12) J. A. V. Butler, *Proc. Roy. Soc., Ser. A*, **135**, 348 (1932).

(13) A. Schuchowitzky, *Acta Physicochim. URSS*, **19**, 176, 508 (1944).

(14) J. W. Belton and M. G. Evans, *Trans. Faraday Soc.*, **41**, 1 (1945).

(15) E. A. Guggenheim, *ibid.*, **41**, 150 (1945).

(16) J. H. Hildebrand and R. L. Scott, "The Solubility of Nonelectrolytes," 3rd ed, Dover Publications, New York, N. Y., 1950, pp 406–413.

(17) W. M. Sawyer and F. M. Fowkes, *J. Phys. Chem.*, **62**, 159 (1958).

(18) F. M. Fowkes, *ibid.*, **65**, 355 (1961).

tures in the surface. (c) *The components are miscible but form nonideal mixtures in the surface.* In our experiments, the equilibrium spreading pressures for each lipid component as well as γ for the mixtures were measured. The values calculated from equation 7, γ-(ideal), were compared with the experimental values of the mixtures, γ(meas.). In addition Γ_1, the surface excess concentration of cholesterol, was measured directly.

Experimental Section

(*A*) *Materials.* Synthetic dipalmitoyl lecithin (Sigma Chemical Co.) and oleyl alcohol, octadecanol, oleic acid, stearic acid, and cholesterol (Applied Science Laboratories) were used without further purification. Monooleyl phosphate and monooctadecyl phosphate were obtained from Hooker Chemical Co. and purified by a procedure reported earlier.[19] A pure sample of sodium octadecyl sulfate was a gift from Dr. V. Lamberti.

Each of the solvents used in this study, benzene (Matheson Coleman and Bell, Spectroquality reagent), petroleum ether (Malinckrodt, bp 30–60°), and methanol (Baker Reagent grade) was passed over a column of Florisil–silica gel to remove any surface-active contaminants. Water, freshly distilled twice from quartz glass, was used directly or, when necessary, adjusted to pH 2.0 with concentrated HCl (Baker Reagent grade).

Labeled cholesterol-4-^{14}C, obtained from New England Nuclear Corp. and Tracerlab, was isotopically diluted to give specific activities in the range 1–3 mCi/mmol.

(*B*) *Methods.* (*1*) *Preparation of Saturated Cholesterol Solutions.* To prepare the aqueous suspensions of cholesterol, the necessary weight of cholesterol to attain the desired concentration, dissolved in ethanol, was added with constant stirring to the aqueous phase. The final concentration of ethanol by volume was never more than 1–2%. We shall demonstrate that our experimental results are independent of the volume of alcohol used. The cholesterol concentration was determined using labeled cholesterol of a known specific activity. The concentrations determined isotopically, always gave slightly lower values than expected, presumably due to possible adsorption of cholesterol on the vessel walls.

(*2*) *Radiotracer Experiments.* The aqueous suspension (30 ml) containing cholesterol-4-^{14}C at a known molar concentration was poured into each of a series of petri dishes 50 cm^2 in area; each dish contained a magnetic flea for stirring. Surface excess concentrations of cholesterol, Γ_1 (moles per square centimeter), were obtained by measuring the surface radioactivity with a thin-window gas-flow GM tube which was maintained at a fixed distance above the solution surface. The general principles for determining Γ_1 with labeled compounds has been described.[20,21] All experiments were performed at room temperature (23 ± 1°). Preliminary experiments showed that in the absence of stirring the adsorption of cholesterol at the air–water surface was extremely slow. With stirring, the counting rate for the system reaches a constant value in about 1.5 days, while in the absence of stirring, we estimated that approximately 1 month would be required to reach saturation.

An estimate of the saturation concentration for cholesterol was obtained by measuring the equilibrium surface concentration of cholesterol as a function of the bulk concentration in the absence of a second lipid component. At a critical concentration, C_{satd}, (approximately 5×10^{-6} M), a saturated monolayer of cholesterol (4.5×10^{-10} mol/cm^2) is obtained in the surface. Moreover, a fivefold increase in the bulk concentration of cholesterol does not change the surface concentration. All adsorption experiments were thus carried out above this saturation concentration for cholesterol. This estimate of C_{satd} is probably high because of the probable presence of oxidation products of cholesterol due to autoxidation at the air–water surface.[22] However, autoxidation is not considered a serious difficulty in our studies, since the autoxidation of cholesterol in mixed-lipid films is almost completely inhibited.[22]

It should also be noted that since a different volume of alcohol was used to disperse the cholesterol in bulk for each concentration, and since the excess surface concentration is constant above C_{satd}, we conclude that the 1–2% ethanol used in these experiments has no effect on the adsorption process.

To study the adsorption of cholesterol in the presence of a second lipid component, the following procedure was used. For a given experiment, labeled cholesterol solution was poured into a petri dish at time zero. A monolayer of the desired component was then spread on the surface of the cholesterol solution, using a suitable spreading solvent,[10] and an excess of this component in the form of a liquid lens or crystals was added directly to the interface with a clean platinum spatula. Measurements of the surface radioactivity were made shortly after spreading of the film and again at regular intervals until the experiment was terminated. Between readings, the solutions were covered and allowed to stir or stand as desired.

(*3*) *Film Balance Experiments.* Measurements of the surface tensions for equilibrium mixed-lipid films prepared according to the above procedure were made using a modified Langmuir-type horizontal float film balance. Modifications, shown schematically in Fig-

(19) N. L. Gershfeld, *J. Phys. Chem.*, **66**, 1923 (1962).

(20) G. Aniansson and O. Lamm, *Nature (London)*, **165**, 357 (1950).

(21) D. J. Salley, A. J. Weith, Jr., A. A. Argyle, and J. K. Dixon, *Proc. Roy. Soc., Ser. A*, **203**, 42 (1950).

(22) A. M. Kamel, N. D. Weiner, and A. Felmeister, *J. Colloid Interface Sci.*, **35**, 163 (1971).

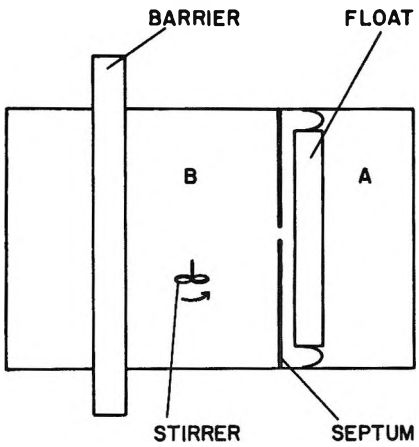

Figure 1. Schematic diagram of modified film balance (see text).

ure 1, were made to facilitate the adsorption experiments. A Teflon septum mounted on the base of the trough and immediately adjacent to the float system separates the trough into two sections, A and B. A small slot in the upper edge of the septum allowed the integrity of the surface film on side B to be maintained all the way to the float. The purpose of the septum is to limit the diffusion of soluble components from side B to A. A Teflon-coated magnetic bar was used to produce vigorous stirring of the solution in section B.

Surface potentials, ΔV, with a reproducibility of ± 10 mV were measured with a ^{226}Ra electrode and electrometer.

In a typical experiment, a saturated suspension of cholesterol in water, the equivalent of 1×10^{-5} M, was poured into the trough and sides A and B swept clean with a Teflon barrier. A film of cholesterol was spread on side A along with excess crystals. Since adsorption of cholesterol in the absence of stirring is very slow, the surface tension of the solution on side B is initially very nearly that for water, and the equilibrium spreading pressure of cholesterol was recorded. Next, on side B, a monolayer of the second component was spread and an excess added either as crystals or as a lens. By vigorously stirring side B, the system was brought to equilibrium and a final surface pressure and surface potential were recorded. At the end of the experiment, side B was swept to remove the mixed film, and the equilibrium spreading pressure for the cholesterol film on side A was again measured. This control indicated that none of the second lipid component had diffused from B to A during the experiment.

In another experiment, no second lipid component was added to side B. Following several hours of stirring, the surface tension of the solution on side B approached within 1–2 dyn that for side A (saturated surface of cholesterol); moreover, the surface potential measured on side B was that of a saturated cholesterol film. Thus, on side B a monolayer of cholesterol had adsorbed from the bulk solution to the surface in this time. After sweeping side B, the equilibrium spreading pressure of cholesterol was again measured and it was found that the surface potential had dropped to zero. This experiment substantiates the conclusion that the cholesterol films obtained by either spreading or adsorption are identical.

Equilibrium spreading pressures π^e of the pure components were obtained by the conventional method of adding the pure lipid in excess to the surface.[10]

(4) *Equilibrium Criteria.* In interpreting the results of the adsorption experiments, it is essential that the systems be at thermodynamic equilibrium. The following criteria were used to establish that equilibrium had been attained.

In the radiotracer experiments, the counts per minute (cpm) representing the equilibrium concentration of cholesterol in the surface was taken to be that value which remained constant, within experimental error, for 3–5 days prior to termination of the experiment. During this period, it could be demonstrated that this cpm value was not affected by the addition of more of the second component to the surface, or by vigorous stirring or standing of the solutions.

Equilibrium was reached in a much shorter time in the film balance (several hours) than the radiotracer experiments (several days). The difference in rates is due to less vigorous stirring in the radiotracer experiments in order to prevent accidental splashing of the isotope. In both series of experiments, all measurements were made after stirring had been interrupted.

The following criteria was used to verify equilibrium in the film balance experiments. (i) It was possible to add more of the second lipid component to side B without changing ΔV and π. (ii) The surface area of side B could be decreased or increased by 50% and, following a reequilibration of the components in the system, the original values of π and ΔV were obtained. (iii) Following stirring and equilibration, the surface potential and pressure were constant; in some cases, the systems were checked after 24 hr with no variation in these parameters.

Results and Discussion

The measurements of π_1^e, π_2^e, γ(measd), and Γ_1, where subscript 1 refers to cholesterol and 2 to the second lipid component, are summarized in Table I. ΔV_1, ΔV_2, and ΔV_m are the surface potentials of components 1, 2, and the equilibrium mixture. Also listed in Table I are A_1 and A_2 (as determine from "spread-film" experiments) and γ(ideal), calculated according to eq 7.

When cholesterol is mixed with the liquid-condensed films of octadecanol, stearic acid, or dipalmitoyl lecithin (pH 5.8), the equilibrium surface film contains only cholesterol. This is supported by the fact that Γ_1 for cholesterol equals, within our experimental error, the

Table I: Properties of Equilibrium Surface Mixtures of Cholesterol with Other Lipids; T = 23°, pH 2

Film	$\pi_2^e \pm 0.5$ dyn/cm	A_2, Å²	$\Gamma_1 \times 10^{10}$ mol/cm²	$\Delta V_2 \pm 10$ mV	ΔV_M[a] ± 10 mV	γ(measd) ± 1 dyn/cm	γ(ideal), dyn/cm
			Liquid Condensed				
Octadecanol	37.6	20	4.3 ± 0.3	+390	+400	33	23.4
Stearic acid	0.5	22	3.8 ± 0.4	+360	+400	35	30.8
Dipalmitoyl lecithin (pH 5.8)	35.9	44	4.6 ± 0.4	+470	+360	33	26.7
m-Octadecyl phosphate	40.1	22	1.4 ± 0.2	+330	+350	26	22.8
			Liquid Expanded				
Oleic acid	28.9	30	3.9 ± 0.3	+240	+620	34	30.7
Oleyl alcohol	29.0	30	2.0 ± 0.2	+230	+360	35	30.7
m-Oleyl phosphate	40.6	30	0.45 ± 0.05	+400	+485	25	23.9
			Gaseous				
Octadecyl sulfate	27.4	50	1.3 ± 0.1	−80	+220	40	30.7
			Cholesterol(saturated)				
	38.8 ± 1	37	4.5 ± 0.27	ΔV_1 = +400		33.2	

[a] When $\Delta V_M = \Delta V_1$(cholesterol), the film is pure cholesterol.

saturation value for cholesterol (4.5×10^{-10} mol/cm²) and that γ(measd) equals the surface tension for a saturated solution of cholesterol (33.2 dyn/cm). We conclude that these liquid-condensed components are immiscible with cholesterol films.

The immiscibility of cholesterol with either octadecanol or stearic acid is corroborated by the surface potentials ΔV_m which equal that for pure cholesterol (+400 mV). The smaller value of ΔV_m obtained with diplalmitoyl lecithin (+360 mV) suggests slight miscibility which was not seen in our measurement of Γ_1; however, this must be less than 6%, the error in our values of Γ_1.

Cholesterol is miscible with the liquid-condensed *m*-octadecyl phosphate, with the liquid-expanded oleyl alcohol, oleic acid, and oleyl phosphate, and with the gaseous octadecyl sulfate. These conclusions follow from the fact that Γ_1 is less than the saturation value for cholesterol. In the case of oleic acid, although Γ_1 was close to the saturation value, mixing was deduced because ΔV_m (+620 mV) was not equal to ΔV_1 (+400 mV) or ΔV_2 (+240 mV). For the remainder of these compounds, Γ_1 and ΔV_m are significantly different from the values for pure cholesterol or pure component 2.

From the data in Table I, we find that γ(measd) is always greater than γ(ideal), and we conclude that none of these lipids forms ideal surface mixtures with cholesterol. Since deviations from "ideal" mixing can often indicate the type of interactions which occur in mixtures,[16] it would be useful if $\gamma - \gamma$(ideal) can be so interpreted. However, it can be shown that $\gamma - \gamma$(ideal) can only indicate deviations in the surface film *relative* to any deviations which may occur in the equilibrium bulk solution.[16,18] To establish whether positive or negative deviations from ideal surface solutions occur, it is necessary to study the surface mixing process independent of the bulk solution. In principle, the spread-film system allows one to study the surface interactions directly. Indeed, our studies with spread-films at very low surface pressures (see part II of this series[23]) indicate that there is a continuity of the mixing behavior of lipids from the very low surface pressure to the high surface pressure region. In the low surface pressure region, we have established that lipid mixtures will form regular solutions which exhibit either large positive deviations from Raoult's law or phase separation. In the present study of the high surface pressure region, we also have observed two general types of behavior: the two lipid components are either completely immiscible where no mixing in the surface will occur at any mole fraction, or the components are at least partially miscible and form nonideal surface mixtures.

It is important to note one major distinction between the spread-film experiments and the present adsorption studies. With spread-films, the subphase is generally not saturated and, according to the phase rule, more than one surface phase can exist. In the present study we have set the experimental conditions such that only one surface phase can be present. Thus, in a two-component system where miscibility is evident, our experiment does not allow us to determine for the components which mix whether they do so in *all* proportions, since a second surface phase, should it form, would be excluded from the surface. Thus, even for the case where the adsorption experiment indicates miscibility of the surface components, the spread film may still have two coexisting surface phases.

The "condensing" effect with cholesterol has been

(23) R. E. Pagano and N. L. Gershfeld, *J. Phys. Chem.*, **76**, 1238 (1972).

studied as spread-films in the range of high surface pressures. Since the subphase is usually not saturated with respect to both lipid components, one cannot establish unequivocally whether the mixed film is homogeneous. However, in at least one system—dipalmitoyl lecithin plus cholesterol—we have demonstrated that the components are immiscible. Thus, the spread-film for which a condensing effect has been reported[5] must contain two surface phases. Therefore, the assumption of film homogeneity has been violated, and the reported condensing effect cannot be interpreted meaningfully.[24-26]

A condensing effect has also been reported for mixtures of cholesterol with oleic acid[3a] and, on the basis of less direct evidence, with octadecyl sulfate.[27] In these cases, while film miscibility is indicated by our adsorption studies, it is again important to recognize that this does not necessarily indicate complete miscibility; the second phase, if it exists, will be excluded from the surface.

In summary, we have demonstrated that the behavior of mixed-lipid films at high surface pressures is consistent with regular solution theory, where one would predict either large positive deviations from Raoult's law or phase separation. For lipid mixtures at high surface pressures, where condensing effects have been reported, phase separation has been shown to occur. While the reported condensing effect may be shown ultimately to involve a decrease in molecular areas for surface mixtures of lipids (much as the mixing of hydrocarbons in bulk results in a decrease in volume), at present the significance of this effect must remain in doubt until a more rigorous method for studying spread films in the high surface pressure region can be devised.

(24) The immiscibility of dipalmitoyl lecithin and cholesterol has also been verified in the low surface pressure region: R. E. Pagano and N. L. Gershfeld, unpublished results.

(25) Surface viscosity studies have recently been used to test for cholesterol–lecithin interactions. The significance of these studies must also be questioned on the basis that similar results were obtained with both immiscible and miscible systems.[26]

(26) P. Joos, *Chem. Phys. Lipids*, **4**, 162 (1970).

(27) M. Muramatsu and N. L. Gershfeld, *J. Phys. Chem.*, **73**, 1157 (1969).

Recoil Tritium Reactions with Hexamethyldisilane in the Gas Phase

by S. H. Daniel, G. P. Gennaro, K. M. Ranck, and Y.-N. Tang*

Department of Chemistry, Texas A&M University, College Station, Texas 77843 *(Received November 29, 1971)*

Publication costs assisted by the U. S. Atomic Energy Commission

A series of recoil tritium experiments is described with hexamethyldisilane in which hydrogen abstraction and substitution, heavy group displacement, and reaction at the Si–Si bond are observed. Effects of additives, total system pressure, and radiolysis were evaluated. Reactivities on a "per bond" basis were determined for each bond in hexamethyldisilane relative to those in neopentane. The relative order was found to be: Si–Si > C–H > C–Si > C–C. In fact, the Si–Si bond was estimated to be the most reactive single bond toward high-energy tritium yet encountered. This high reactivity is thought, on the basis of O_2 and C_2H_4 additive effects, to be due to both a low threshold energy and a high reaction cross section. Results are interpreted in terms of possible chemical effects on these high-energy reactions, such as a low bond dissociation energy.

Introduction

The importance of various chemical parameters as controlling factors in high energy atom reactions has been indicated by several recent investigations.[1-12] Bond dissociation energies have been shown to be a major determinant in both recoil tritium abstraction and substitution reactions. For the abstraction reaction, the excellent correlation between D(C–H) and HT yields of various organic compounds has been established by Rowland and coworkers.[5-9] For the substitution reaction, a correlation between D(C–X) and product yields from the T*-for-X substitution in both CH_3X and the substituted benzoic acids has been reported.[1,10,13]

(1) Y.-N. Tang, E. K. C. Lee, E. Tachikawa, and F. S. Rowland, *J. Phys. Chem.*, **75**, 1290 (1971).

(2) S. H. Daniel and Y.-N. Tang, *ibid.*, **75**, 301 (1971).

(3) F. S. Rowland, E. K. C. Lee, and Y.-N. Tang, *ibid.*, **73**, 4024 (1969).

(4) J. W. Root, *ibid.*, **73**, 3174 (1969).

(5) W. Breckenridge, J. W. Root, and F. S. Rowland, *J. Chem. Phys.*, **39**, 2374 (1963).

As for other chemical factors, a most noteworthy result is that an electron density effect was demonstrated by the correlation between NMR proton chemical shifts and the T*-for-H substitution yields in a number of alkanes and halomethanes.[1,3]

All of these observations, although not denying the possible effect of physical-geometrical parameters (*e.g.*, the rotational inertia hypothesis used for the explanation of heavy-group substitution by tritium atoms),[14-17] have positively identified the active role of certain chemical factors in hot atom reactions.

The present series of studies on recoil tritium reactions with silicon-containing compounds has been designed to search for further evidence of chemical effects in hot atom reactions by increasing or extending our working parameters.[18,19] Our previous work on trimethylfluorosilane has convincingly demonstrated the existence of a bond strength effect in the T*-for-X substitution in highly substituted silanes.[18] In the present case, we wish to examine in detail how the bond strength effect works in recoil tritium reactions with hexamethyldisilane, the major feature of this molecule being the presence of a weak Si–Si bond.[20] Furthermore, we wish to identify any possible clues for the presence of additional chemical factors, such as the use of 3d atomic orbitals.[21]

The primary products expected from reaction of recoil tritium with hexamethyldisilane are as follows

$$T^* + (CH_3)_3Si\text{–}Si(CH_3)_3 \longrightarrow HT + (CH_3)_3Si\text{–}Si(CH_3)_2CH_2 \quad (1)$$

$$T^* + (CH_3)_3Si\text{–}Si(CH_3)_3 \longrightarrow (CH_3)_3Si\text{–}Si(CH_3)_2CH_2T + H \quad (2)$$

$$T^* + (CH_3)_3Si\text{–}Si(CH_3)_3 \longrightarrow CH_3T + (CH_3)_3Si\text{–}Si(CH_3)_2 \quad (3)$$

$$T^* + (CH_3)_3Si\text{–}Si(CH_3)_3 \longrightarrow (CH_3)_3Si\text{–}SiT(CH_3)_2 + CH_3 \quad (4)$$

$$T^* + (CH_3)_3Si\text{–}Si(CH_3)_3 \longrightarrow (CH_3)_3SiT + (CH_3)_3Si \quad (5)$$

All of the expected tritiated products, with the exception of pentamethyldisilane, for which identification is tentative, are observed.

Experimental Section

General Procedure. The standard procedures used in recoil tritium reactions were followed.[19] Samples containing ^3He, hexamethyldisilane vapor, and additives were filled into Pyrex 1720 bulbs and sealed with standard high-vacuum techniques. The nuclear reaction, ^3He (n,p) ^3H, was used for the tritium production. Irradiations were carried out at the Texas A&M University Nuclear Science Center reactor with a thermal neutron flux of 1×10^{13} neutrons/(cm^2 sec) for 5 or 8 min. The tritium-labeled products were analyzed by radiogas chromatography.[22] Mass peaks were detected by a thermal conductivity detector and measured by disc integration. Measurement of radioactivity in the eluent was accomplished by gas proportional counting of the helium stream after it had been mixed with propane. There was no indication of quenching by the hexamethyldisilane.

Chemicals. Hexamethyldisilane, with a purity level of >98%, was obtained from Peninsular Chemical Co. A gas chromatographic purity check showed no detectable impurities, $(CH_3)_3SiH$ included. ^3He was obtained from Mound Laboratory, Monsanto Research Corp., and has a tritium content of less than 2×10^{-11}%.

Oxygen (Airco), CO_2 (Matheson, >99.5% purity), C_2H_4 (Matheson, >99% purity), and *neo*-C_5H_{12} (Matheson, >99% purity) were all used without further purification.

Gas Chromatographic Columns. For most of the samples, two columns were sufficient for a complete analysis, a 50-ft TTP (tri-*o*-tolyl phosphate) column at 50° for the evaluation of labeled parent and $(CH_3)_3SiT$ yields and a combination set of columns (glass beads, activated alumina, and molecular sieves) for the HT and CH_3T separation.

For ethylene-containing samples, a 50-ft TIB (triisobutylene) column at 0° was also used. This permitted separation of $(CH_3)_3SiT$ without interference from tritiated hydrocarbons.

A small radioactive peak which appears somewhat before the parent on the TTP column and whose activity is generally 1–5% of that found in the tritiated

(6) J. W. Root, W. Breckenridge, F. S. Rowland, *J. Chem. Phys.*, **43**, 3694 (1965).

(7) E. Tachikawa, Y.-N. Tang, and F. S. Rowland, *J. Amer. Chem. Soc.*, **90**, 3584 (1968).

(8) E. Tachikawa and F. S. Rowland, *ibid.*, **90**, 4767 (1968).

(9) E. Tachikawa and F. S. Rowland, *ibid.*, **91**, 559 (1969).

(10) Y.-N. Tang, Ph.D. Thesis, University of Kansas, 1964.

(11) F. Schmidt-Bleek and F. S. Rowland, *Angew. Chem.*, **76**, 901 (1964).

(12) F. S. Rowland, "Proceedings of the International School of Physics, "Enrico Fermi" Course XLIV–Molecular Beam and Reaction Kinetics," Ch. Schlier, Ed., Academic Press, New York, N. Y., 1970.

(13) R. M. White and F. S. Rowland, *J. Amer. Chem. Soc.*, **82**, 5345 (1960).

(14) R. Wolfgang, *Progr. React. Kinet.*, **3**, 97 (1965).

(15) R. Wolfgang, *Annu. Rev. Phys. Chem.*, **16**, 15 (1965).

(16) R. A. Odum and R. Wolfgang, *J. Amer. Chem. Soc.*, **83**, 4668 (1961).

(17) R. A. Odum and R. Wolfgang, *ibid.*, **85**, 1050 (1963).

(18) S. H. Daniel and Y.-N. Tang, *J. Phys. Chem.*, **73**, 4378 (1969).

(19) S. H. Daniel, Ph.D. Thesis, Texas A&M University, 1971.

(20) I. M. T. Davidson and I. L. Stephenson, *J. Chem. Soc. A*, 282 (1968).

(21) E. A. V. Ebsworth, "Volatile Silicon Compounds," MacMillan, New York, N. Y., 1963.

(22) J. K. Lee, E. K. C. Lee, B. Musgrave, Y.-N. Tang, J. W. Root, and F. S. Rowland, *Anal. Chem.*, **34**, 741 (1962).

Table I: Recoil Tritium Reactions with Hexamethyldisilane in Systems Scavenged by O_2

	Gas pressure, Torr					
$(CH_3)_3Si-Si(CH_3)_3$	20	20	25	25	25	27
^3He	20	20	26	25	25	50
O_2	26	28	66	80	100	167
$O_2/(CH_3)_6Si_2$ ratio	1.3	1.4	2.6	3.2	4.0	6.2
	Product yields[a]					
HT	100	100	100	100	100	100
CH_3T	16 ± 1	16 ± 1	18 ± 1	19 ± 1	19 ± 1	19 ± 1
$(CH_3)_3SiT$	30 ± 1	35 ± 1	20 ± 1	18 ± 1	16 ± 1	13 ± 1
$(CH_3)_3Si-Si(CH_3)_2CH_2T$	72 ± 1	67 ± 1	56 ± 1	58 ± 1	57 ± 1	54 ± 1

[a] Relative to HT as 100.

parent is probably $(CH_3)_5Si_2T$. The identification is only tentative, since no authentic sample was available for column calibration.

Results

Variation of Product Yields with Scavenger Concentration. Recoil tritium reactions with hexamethyldisilane in the presence of various amounts of oxygen as a scavenger were carried out, and the results are shown in Table I. The O_2/parent ratio ranged from 1 to 6. In this table, HT, which is normally used as a pressure-independent reference, was chosen as a comparison standard because, for well-scavenged systems, the HT yield from the abstraction of hydrogen from a reasonably strong C–H bond should not be very sensitive to the scavenger concentration. Error limits in this and subsequent tables are computed from counting statistics only, unless otherwise specified.

The data in Table I reveal that as the O_2/parent ratio goes from 1 to 6, the relative yields of $(CH_3)_3SiT$ decrease by a factor of approximately 3. However, the relative yields of all the other primary products show much less variation.

Radiolysis of Hexamethyldisilane. A small amount of trimethylsilane (<1%) is observed from the radiolysis of hexamethyldisilane. In order to verify that radiolysis during pile irradiation will not complicate our interpretations of labeled product yields, a number of O_2-scavenged samples of hexamethyldisilane were irradiated for different lengths of time.

The level of radiation damage for these samples ranged from approximately one-half to five times those observed in actual runs. The ratio of $(CH_3)_3SiT$ to $(CH_3)_3Si-Si(CH_3)_3CH_2T$ for samples with radiation damage up to those encountered for actual runs are essentially the same. This indicates that there is no significant contribution to $(CH_3)_3SiT$ yields from reactions of radiolytically produced species.

Pressure Effect in the Hexamethyldisilane Systems. In Table I, the total pressure of the system is a variable, as well as the scavenger concentration. In order to ensure that the observed variation in $(CH_3)_3SiT$ yield is due to increasing amounts of scavenger rather than increasing pressure, several samples of 1 atm total pressure with CO_2 as the pressure builder were analyzed, and the results are shown in Table II. The use of CO_2 is necessary, because hexamethyldisilane has a vapor pressure of only about 26 Torr.

Table II: Results of Recoil Tritium Reactions with Hexamethyldisilane in Systems Having a Total Pressure of 1 Atm

	Gas pressure, Torr		
$(CH_3)_3Si-Si(CH_3)_3$	26	26	26
^3He	18	20	18
O_2	22	22	23
CO_2	731	727	738
Total pressure	797	795	805
	Product yields[a]		
HT	100	100	100
CH_3T	19 ± 1	19 ± 1	20 ± 1
$(CH_3)_3SiT$	28 ± 1	26 ± 1	22 ± 1
$(CH_3)_3Si-Si(CH_3)_2CH_2T$	55 ± 1	22 ± 1	51 ± 1

[a] Relative to HT as 100.

A comparison of the results in Table II with those samples in Table I having a similar O_2/parent ratio shows that the yield of $(CH_3)_3SiT$ is rather similar. However, a comparison of these samples with the one in Table III having the same total pressure (1 atm), but filled with O_2 rather than CO_2, reveals a large difference in the $(CH_3)_3SiT$ yield.

Strictly speaking, the above-mentioned samples should not be directly compared owing to an expected difference in the reacting tritium energy spectrum.[14] However, the qualitative picture obtained obviously indicates that the vast variation in the $(CH_3)_3SiT$ yield as shown in Table I is mostly due to a scavenger concentration effect and not a pressure effect.

Table III: Variation of Product Yields with Oxygen Concentration

	Gas pressure, Torr										
$(CH_3)_3Si-Si(CH_3)_3$	25	22	20	20	25	25	25	27	27	27	27
^3He	25	20	20	20	26	25	25	50	49	49	48
O_2	0	0	26	28	66	80	100	167	473	591	720
$O_2/(CH_3)_6Si_2$ ratio	0	0	1.3	1.4	2.6	3.2	4.0	6.2	17.5	21.9	26.7
	Product yields[a]										
HT	215 ± 13	137 ± 1	139 ± 2	149 ± 2	179 ± 2	173 ± 2	176 ± 1	186 ± 1	*c*	*c*	*c*
CH_3T	26 ± 2	19 ± 1	22 ± 1	24 ± 1	31 ± 1	32 ± 1	33 ± 1	35 ± 1	*c*	*c*	*c*
$(CH_3)_3SiT$	107 ± 5[b]	114 ± 1	42 ± 1	52 ± 1	36 ± 1	31 ± 1	29 ± 1	24 ± 1	8 ± 1	11 ± 1	6 ± 1
$(CH_3)_3Si-Si(CH_3)_2CH_2T$	100	100	100	100	100	100	100	100	100	100	100

[a] Relative to $(CH_3)_3Si-Si(CH_3)_2CH_2T$ as 100. [b] The average of three samples of the same composition. [c] Not determined owing to quenching.

Table IV: Variation of Product Yields with Ethylene Concentration

	Gas pressure, Torr							
$(CH_3)_3Si-Si(CH_3)_3$	21	19	21	17	21	17	21	17
^3He	15	17	14	16	16	10	15	17
C_2H_4	16	22	45	59	93	165	369	508
$C_2H_4/(CH_3)_6Si_2$ ratio	0.76	1.2	2.1	3.5	4.4	9.7	17.6	29.9
	Product yields[a]							
HT	(205 ± 1)	165 ± 1	176 ± 1	221 ± 1	221 ± 1	(309 ± 1)	264 ± 1	368 ± 1
CH_3T		22 ± 2	21 ± 2	26 ± 2	24 ± 2		16 ± 2	18 ± 2
C_2H_3T	103 ± 1	206 ± 1	204 ± 1	360 ± 1	433 ± 1	796 ± 1	791 ± 1	1383 ± 1
$(CH_3)_3SiT$	38 ± 1	22 ± 1	26 ± 1	23 ± 1	20 ± 1	19 ± 1	12 ± 1	12 ± 1
$(CH_3)_3Si-Si(CH_3)_2CH_2T$	100	100	100	100	100	100	100	100
Specific activity ratio per bond (C=C/Si-Si)[b]	3.6	8.0	3.6	4.6	4.8	4.3	3.7	4.0

[a] Relative to $(CH_3)_3Si-Si(CH_3)_2CH_2T$ as 100. [b] $[(C_2H_3T)/P(C_2H_4)/((CH_3)_3SiT)/P((CH_3)_6Si_2)]$

Effect of Oxygen Concentration on $(CH_3)_3SiT$ Yield. An internal gas proportional counter will be quenched by a large O_2 peak[10] and, as a result, the yields of the accompanying radioactive products, such as HT and CH_3T, will therefore be erratic. Because of this, the use of the tritiated parent as a comparison standard should be more meaningful than the use of HT in covering a wide range of oxygen concentrations. Accordingly, we have listed in Table III the relative yields of products with the tritiated parent as a standard covering an O_2/parent ratio from 0 to 27. For the oxygen-free samples, hexamethyldisilane-*t* is definitely the best standard because extra HT is expected to be formed from thermal tritium reactions.

The trend of decreasing $(CH_3)_3SiT$ yield with increasing oxygen concentration is very obvious in Table III. These yields are plotted in Figure 1 as a function of the O_2/parent ratio.

Effect of Ethylene Concentration on $(CH_3)_3SiT$ yield. An experiment, parallel to the above oxygen system, was conducted with ethylene as an additive, and the results are shown in Table IV. The $(CH_3)_3SiT$ yield again decreases as the ethylene/parent ratio increases from 1 to 30. This is illustrated in Figure 2. The curves in Figures 1 and 2 are nearly identical, with the ethylene curve falling slightly below the oxygen curve in the low additive concentration region. Their basic similarity indicates that the efficiency of these two molecules to remove thermal tritium atoms is about the same.

In Table IV, the specific activity ratios per bond for C=C in ethylene and Si–Si in hexamethyldisilane have been calculated. On the average, the former is approximately *four* times more reactive than the latter toward recoil tritium for the entire ethylene/parent ratio range.

Specific Activity Ratio for the T-for-H Substitution in Hexamethyldisilane and Neopentane.* Hexamethyldisilane samples indicated in Table II were actually irradiated in a rotisserie together with four samples of neopentane of similar composition. Each of these had approximately the same amounts of parent compound, ^3He, O_2, and CO_2. The rotisserie irradiation is necessary so that each sample is exposed to the same

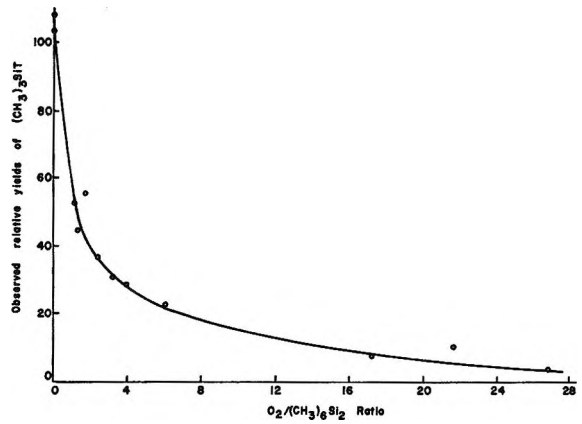

Figure 1. Dependence of the relative yields of $(CH_3)_3SiT$ on oxygen concentration.

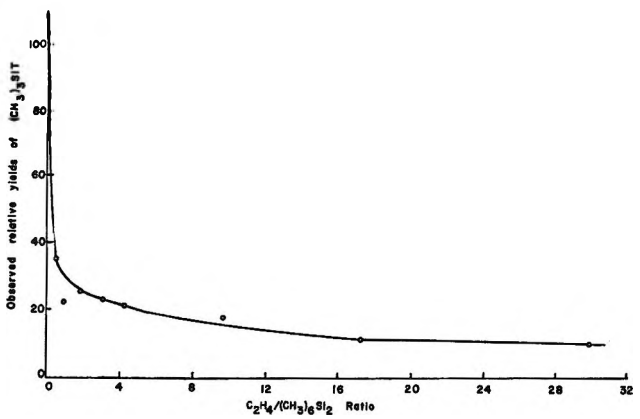

Figure 2. Dependence of the relative yields of $(CH_3)_3SiT$ on ethylene concentration.

neutron flux. This was done in order to measure the specific activity ratio for the T*-for-H substitution in these two compounds. With the ^3He mass peak area measured, the average specific activity for T*-for-H substitution in hexamethyldisilane can be evaluated on an arbitrary basis. Similarly, the same parameter can be calculated for neopentane. A comparison of the two shows that the specific activity ratio per molecule for the T*-for-H substitution is 1.57 in favor of the silane.

Discussion

Relative Reactivity of the Si–Si Bond in Hexamethyldisilane and the C–C Bond in Neopentane. In Table V, the 1.57 value for the specific activity ratio per molecule for the T*-for-H substitution in hexamethyldisilane and neopentane is used to normalize the various yields. Then, for each type of reaction, the yield per molecule is divided by the number of reaction sites in the molecule to derive the "per bond" yield.

Results indicate that the C–H bonds in both molecules have rather similar reactivities for either abstraction or substitution. The total reactivity for the Si–C bond is approximately twice that of the C–C bond in

Table V: A Comparison of the Reactivity of Hexamethyldisilane with Neopentane toward Recoil Tritium

	Products[a]			
	$(CH_3)_6Si_2$		$(CH_3)_4C$	
	Specific activity[b]			
	Per molecule	Per bond	Per molecule	Per bond
T-for-H substitution	1570 ± 10	87 ± 1	1000	83
HT	2970 ± 40	165 ± 2	1400 ± 70	116 ± 2
CH_3T	573 ± 9	96 ± 2	222 ± 16	56 ± 1
T-for-CH_3 substitution	77 ± 9	13 ± 1	19 ± 3	5 ± 1
$(CH_3)_3SiT$	752 ± 60	752 ± 60		

[a] Relative to neopentane as 1000. [b] [(Obsd activity/^3He mass peak)($P(CO_2)/P$(Parent))].

neopentane. Similar values have been observed in some of the direct methylsilane–alkane competition systems.[18]

The most significant result of this comparison, however, is that the Si–Si bond in hexamethyldisilane is about twelve times more reactive than the C–C bond in neopentane.

Low Threshold Energy and High Reaction Cross Section. Further examination of Table V reveals the qualitative order of the total reactivity of bonds in hexamethyldisilane and neopentane as

$$\text{Si–Si} > \text{C–H} > \text{C–Si} > \text{C–C}$$

This means that the Si–Si bond is probably the most reactive single bond toward recoil tritium atoms ever studied. On a per bond basis, its reactivity is two or three times greater than the sum of hydrogen abstraction and substitution reactivities at C–H bonds.

The high reactivity for the recoil tritium reactions at the Si–Si bond may be due to either a low threshold energy or a high reaction cross section, or a combination of both. The evidence for the former is an extremely high $(CH_3)_3SiT$ yield in nonscavenged samples and a very sharp drop in its yield with the addition of small amounts of oxygen or ethylene, indicating the presence of a thermal reaction with a very low reaction threshold. The indication of a high reaction cross section comes from the observation that the yield of $(CH_3)_3SiT$ is still rather high in extremely well-scavenged systems, under which conditions thermal processes supposedly are completely suppressed.

Further evidence for the low threshold energy of the Si–Si bond reaction may be extracted from the product yields observed for hexamethyldisilane–ethylene mixtures. The fact that the specific activity ratio per bond for C=C/Si—Si (Table IV) is approximately independent of the mole fraction of ethylene in these mixtures indicates that the reaction probability curves for recoil tritium reaction with C=C in ethylene and Si–Si in hexamethyldisilane are nearly parallel to each

other and lie in a similar energy range. This implies that the latter process should possess a reasonably low threshold energy, such as has been convincingly demonstrated for the reaction of recoil tritium atoms at C=C in olefins.[23]

Bond Strength Effects. Both the low threshold energy and the high reaction cross section for recoil tritium reactions at Si–Si bonds may be explained by a relatively low bond dissociation energy. This may be viewed as another example of the bond strength effect in hot atom substitution reactions.

Several values of D(Si–Si) in hexamethyldisilane have been reported in the literature. From electron impact studies, Hess, Lampe, and Sommer[24] have obtained a value as high as 86 kcal/mol. On the other hand, Connor[25] and coworkers have determined values of 58 and 49 kcal/mol by the toluene carrier technique in a flow system. Very recently, Davidson and Stephenson[20] have derived from the rate of pyrolysis of hexamethyldisilane a value of 67 ± 2 kcal/mol for D(Si–Si). They commented that (a) in the electron impact studies, the value used for the appearance potential of $(CH_3)_3Si^+$ from hexamethyldisilane was 0.7 eV too high and (b) some heterogeneous processes might have complicated the toluene carrier flow experiments. Thus, the value of 67 ± 2 kcal/mol appears to be the most reliable figure.

This low bond dissociation energy will give rise to a low activation energy for tritium atom reactions at the Si–Si bond. This in turn may be sufficient to explain the observation of both a high reaction cross section and a reaction probability curve with a low threshold.

Other Possible Contributing Factors. Physical-geometric factors, such as the large size of the silicon atoms as compared to carbon atoms, may also contribute to the relatively high reactivity of Si–Si bonds. Furthermore, the slow Si–H bending vibrational frequency may also increase the probability of Si–T bond formation as proposed by Witkin and Wolfgang.[26] However, both of these contributions should be minor because the increment in reactivity in going from the C–C bond to the C–Si bond is much smaller than that in going from the C–Si bond to the Si–Si bond. Neither of these causes can account for the extremely large increment in reactivity in the latter case.

Possible Use of Silicon 3d Orbitals. It is possible, although in no way conclusive, that the high reactivity of Si–Si bonds is due to the combination of two processes. One is an ordinary type of recoil tritium substitution reaction at the Si–Si single bond. The other is the interaction of the 3d orbitals of the silicon atom with the incoming tritium.

The former process should be similar to recoil tritium interactions at C–C bonds, but with a somewhat higher reactivity. The expected high reactivity should be primarily due to a weak Si–Si bond with certain contributions from the larger size of the silicon atom and the slower vibrational frequency of the Si–Si bond. This is actually the same process which we have discussed in the previous sections. However, this process, although expected to have a high reaction cross section, does not necessarily have a low threshold energy.

The additional 3d orbital process might be somewhat similar to the recoil tritium interactions with π bonds. The silicon atoms might employ their 3d orbitals to accommodate the incoming tritium atoms to form a certain kind of complex which decomposes to give the final product, $(CH_3)_3SiT$, by breaking the weak Si–Si bond. A similar type of d complex might have also formed in the case of recoil tritium reactions with the C–Si bond. However, since all the σ bonds in this complex, including the C–Si bonds, are reasonably strong, the d complex would break down by releasing the tritium, again giving no net observable reaction. It seems logical that the d-complex process would be fruitful only when there are some very weak bonds, such as the Si–Si bond, in the system which could be preferentially broken during the decay of the complex. Like the π-bond addition reaction, this d-orbital addition process also should possess an extremely low threshold energy, whose actual observation gives the best clue to the possible presence of such a process.

Although the present results suggest the use of 3d orbitals by silicon for recoil tritium reactions, conclusive proof of this process will require additional evidence.

Acknowledgment. This research was supported by AEC Contract No. AT-(40-1)-3898.

(23) R. Kushner and F. S. Rowland, *J. Amer. Chem. Soc.*, **91**, 1539 (1969).

(24) George G. Hess, F. W. Lampe, and L. H. Sommer, *ibid*, **87**, 5327 (1965).

(25) J. A. Connor, G. Finney, F. J. Leigh, R. N. Haszeldine, P. J. Robinson, R. D. Sedgwick, and R. F. Simmons, *Chem. Commun.*, 178 (1966).

(26) J. Witkin and R. Wolfgang, *J. Phys. Chem.*, **72**, 2631 (1968).

Chemical Effects Due to Low-Energy Electron Impact on Thin Films of Cyclohexane and *n*-Hexane at 77°K

by Toshiaki Matsushige[1] and William H. Hamill*

Department of Chemistry and the Radiation Laboratory,[2] University of Notre Dame, Notre Dame, Indiana 46556
(Received November 1, 1971)

Publication costs assisted by The U. S. Atomic Energy Commission

Films (570–840 Å) of cyclohexane and *n*-hexane at 77°K have been subjected to low-energy electron impact and the products have been analyzed. The yield of bicyclohexyl onsets at ~8.5 eV, maximizes at ~13 eV, and minimizes at ~30 eV. Of the C_{12} products from *n*-hexane only *n*-dodecane was resolved in the gas chromatogram. The onset is well below the threshold of optical absorption. Only the *n*-hexane fragment hydrocarbon products ethane, propane, *n*-butane, *n*-pentane, and their congruent olefins (in the order of decreasing yields) were measured in detail. Their yield *vs.* energy profiles were similar with onsets at ~3.5 eV, maxima at ~6.5 eV, and minima at ~7.0 eV. The results for *n*-hexane at low energy are attributed to decompositions from vibrationally excited, low-lying triplet states by direct excitation with spin exchange.

Introduction

The chemical effects of high-energy radiation tend to be indiscriminate and, with few exceptions, only the ultimate and penultimate products can be characterized and identified. A simple technique has been described to measure the chemical consequences of low-energy electron impact on simple solid molecular systems.[3] Practical considerations require a very low vapor pressure and therefore low temperature. For even modest precision in measurement of the electron energy it is essential to avoid trapping electrons in the target. Consequently, compounds which undergo dissociative electron attachment are not suitable. Since even solid alkanes and alkenes can trap electrons physically, the target should be as thin as possible to minimize this effect.

The present work is concerned with the energy dependence of the yields of bicyclohexyl from cyclohexane, and of *n*-dodecane and C_2–C_5 alkanes and alkenes from *n*-hexane, under slow electron impact.

Experimental Section

Samples of cyclohexane (Hinton's Primary Standard Grade 99.98%) and *n*-hexane (Phillip's Research Grade 99.95%) were outgassed and stored on a grease-free vacuum line. From the measured *P–V–T* of the vapor admitted to the reactor at 77°K the film thickness was ~570 Å for cyclohexane and ~840 Å for *n*-hexane.

The reactor, a 1-l. Pyrex flask, was inner-surfaced with an evaporated gold film as anode. After rough pumping (mechanical and mercury vapor diffusion pumps) the vacuum handling system, which contained only Pyrex glass, Kovar, and stainless steel, was valved off, baked out, and evacuated to 2.5×10^{-7} Torr by an ion pump. This pressure was also maintained during electron bombardment. A schematic diagram appears in Figure 1. The filament and its mounting have been described.[3]

The filament temperature was adjusted, prior to admitting each sample, to give 10^{-4} A anode current I_a ($\sim 2 \times 10^{-7}$ A/cm^2) at a selected anode voltage V_a. After admitting a sample the filament was restored to the predetermined temperature gradually over 15 min, then held there ~3 min to achieve stability before applying the anode voltage. Tests showed no evidence of pyrolysis. The anode voltage V_a (*n.b.*, for the bare anode) defines the nominal electron energy for each run and it is used throughout this work unless otherwise explicitly stated. For constant V_a, *i.e.*, a voltmeter reading, I_a decreases, mostly during the first few seconds. In the space-charge limited regime this results from a change in the potential difference, presumably due to injected electrons being trapped in the film. It is assumed that increasing V_a to restore the initial I_a compensates for this effect, and this adjustment was made as needed throughout each run to maintain constant I_a.[3] For $V_a < 10$ V the adjustment was <1 V.

Independent work with an electron gun operating on its *I–V* plateau shows that electron transmission through films of *c*-C_6H_{12} and *n*-C_6H_{14} is not space-charge limited at $\sim 2 \times 10^{-7}$ A/cm^2.[4] Consequently, the *I–V* characteristics reported previously for the bare anode[3] apply equally for coated anodes, except for a voltage shift.

It is considered perferable to describe the dependence of 100-eV product yields, *G*, in terms of onsets, rather than peaks, in the *G*(product) *vs.* *V* spectra. As a

(1) This work is based on a dissertation submitted in partial fulfillment of the requirements of the Ph.D. degree at the University of Notre Dame.

(2) The Radiation Laboratory is operated by the University of Notre Dame under contract with the Atomic Energy Commission. This is AEC Document No. COO-38-813.

(3) L. M. Hunter, T. Matsushige, and W. H. Hamill, *J. Phys. Chem.*, **74**, 1883 (1970).

(4) K. Hiraoka, work in progress at this laboratory.

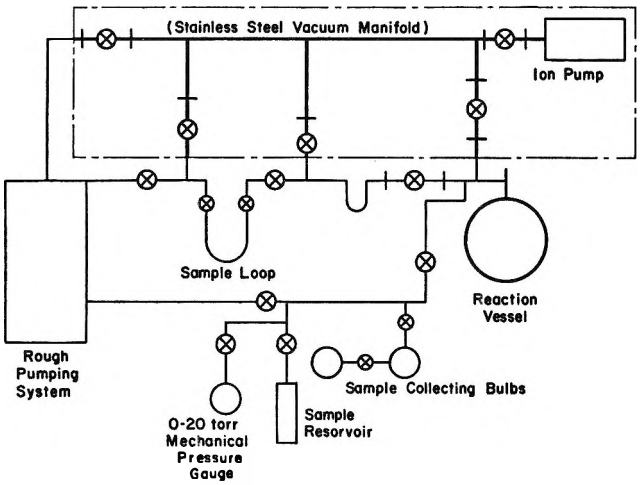

Figure 1. A schematic diagram of the apparatus used for low-energy irradiation of cyclohexane and *n*-hexane by electron impact.

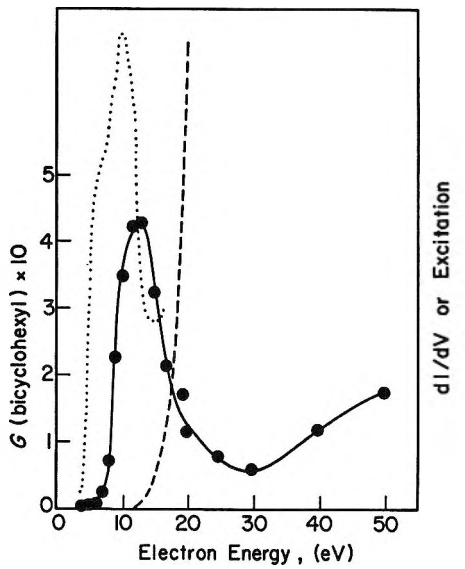

Figure 2. The electron energy profile of the 100-eV yield of bicyclohexyl from cyclohexane (●); the excitation curve for 490-nm emission (- - -), and the spectrum dI_a/dV_a *vs.* V_a (. . .) for cyclohexane.

consequence, one-half the *IR* drop along the filament (*IR* ≅ 1.5 V) and an additional Boltzmann spread will introduce a rather large low-energy shift in onsets relative to voltmeter readings. The effect of contact potentials cannot be assessed for the equipment used, but it is known that relative to a given cathode, contact potentials for several alkanes and alkenes are the same.[4]

From five to ten runs were performed at each electron energy, the average deviation of yields amounting to 15–20%. Sample collection and analysis have been described.[3]

Results

The only product from cyclohexane in the region of higher boiling compounds in the gas chromatogram (with a silicone gum rubber SE-30 column) was bicyclohexyl. Small yields of cyclohexyl–hexane and cyclohexyl–cyclohexene are produced by γ irradiation. (The yield of cyclohexene could not be measured on the same column and circumstances did not allow an additional 10^2 experiments.) The yield of bicyclohexyl was linear with dose over a considerable range at low electron energy, *e.g.*, to $\sim 10^{-21}$ eV/g. At higher electron energy the yield–dose curve fell off more rapidly. All yields are reported for the linear region.

The electron-energy profile of the yield of bicyclohexyl appears in Figure 2. By rough extrapolation from the initial steep rise the onset is ~8.5 eV. There are small yields of bicyclohexyl at low energy, amounting to 2, 2, 5, 28, and 76 in units of molecules/10^5 eV at 4, 5, 6, 7, and 8 eV. The maximum is G(bicyclohexyl) = 0.43 at 13 eV, compared to G = 1.55 for γ irradiation at 77°K.[5,6]

Of the C_{12} products produced by electron impact on thin films of *n*-hexane only *n*-dodecane could be fully resolved by gas chromatography. Although this compound contributes <10% to the combined C_{12} yield, this limited information is adequate for the present purpose since there is a nearly uniform G–V dependence for the entire group. The results, limited to the very low energy range, appear in Figure 3. The onset occurs at ~2 eV (nominal). The yield for γ irradiation at 77°K is included for comparison.

Of the alkane and alkene fragment products from *n*-hexane, only propane and propene could not be resolved while methane was not retained during recovery of the sample prior to analysis. The results for ethane and ethylene were badly scattered at 3 eV and the yields of all fragment products are small and inaccurate at 2 V, but circumstances did not permit further work. The results in Figure 4 still provide evidence for a maximum in the yield of ethane at ~3 eV in addition to that at 6 eV. The yields of ethylene (not shown) were 10–20% of the yields of ethane. The energy profiles for the combined C_3's in Figure 5 and for butane and butene in Figure 6 follow the same pattern as ethane. The profiles for pentane and pentene in Figure 5 differ only at ≥10 eV.

A brief examination of 1,3-cyclohexadiene under electron impact at 3.0, 4.0, and 4.5 eV showed that benzene was a product at each energy and the largest yield, $G(C_6H_6)$ = 0.6, occurred at 4.0 eV.

Discussion

Characteristic energy losses by electrons in solids are quantized, distinctive of the substance and independent of the incident electron energy and of the target thickness. For thin films these losses can be measured

(5) J. A. Stone, *Can. J. Chem.*, **43**, 809 (1969).
(6) A. Charlesby, *Intern. J. Radiat. Phys. Chem.*, 1, 45 (1961).

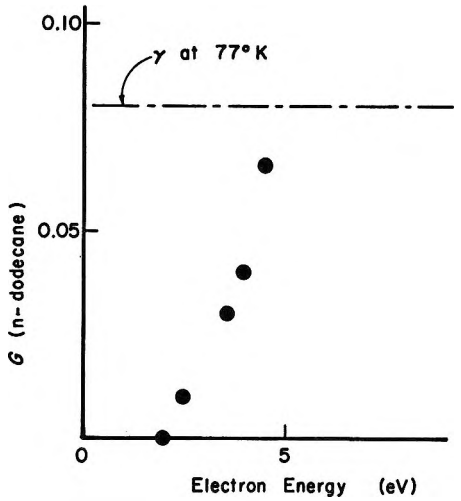

Figure 3. The electron energy profile of the 100-eV yield of *n*-dodecane from *n*-hexane. The yield of *n*-dodecane from γ irradiation at 77°K is included for comparison.

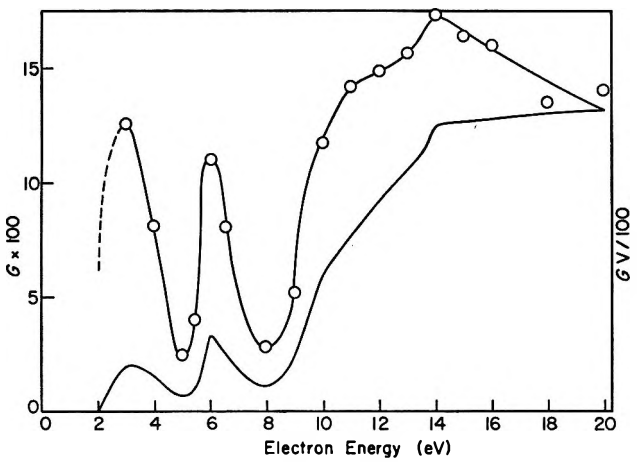

Figure 4. The electron energy profile of the 100-eV yield of ethane from *n*-hexane (O) and the corresponding dependence for $GV_a/100$ (——).

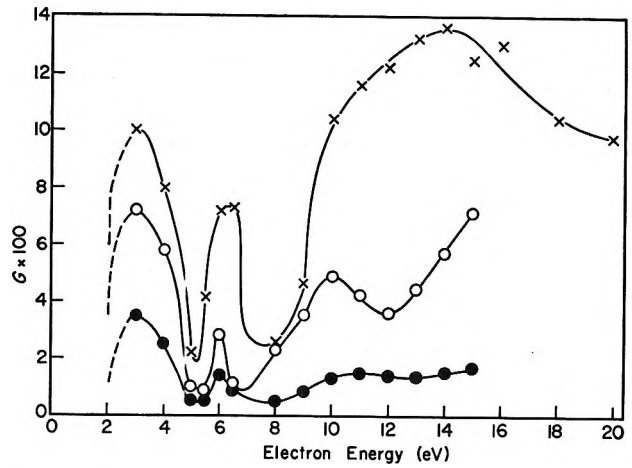

Figure 5. The electron energy profile of the 100-eV yields of combined propane and propene (×), of *n*-pentane (O), and O, *n*-pentene (●).

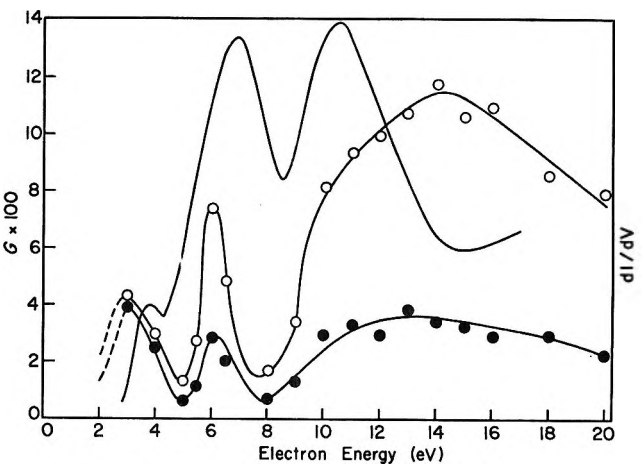

Figure 6. The electron energy profile of the 100-eV yields of *n*-butane (O) and *n*-butene-1 (●) from *n*-hexane. The upper curve (from ref 4) is dI_a/dV_a *vs.* V_a for *n*-hexane.

directly by energy analysis of backscattered electrons,[7] or indirectly from structure in curves of dI_a/dV_a *vs.* V_a.[4,8] The reliability of the method has been tested on several aromatic compounds for which optical and photoelectron spectra have been measured. For a total of 37 energy levels the methods agree within ~0.1 V, on the average.[4] Data for such electron impact measurements have been included in Figure 2 where it can be seen that they correlate in part with visual estimates of dG/dV_a *vs.* V_a. It is not possible to allow for the contact potential difference between a tungsten filament used in this work and a rhenium filament coated with lanthanum hexaboride.[4,7] It is clear, nevertheless, that there are characteristic electron energy losses to cyclohexane well below the onset of optical absorption. In cyclohexane this energy is not efficiently utilized, unlike earlier results for hexene-1[3] and present results for *n*-hexane.

The yields of bicyclohexyl from cyclohexane are very small below ~8 eV. Consequently, low-lying triplet states of cyclohexane contribute negligibly to chemical yield, although they do contribute appreciably to electron energy losses.[4]

The yield of bicyclohexyl drops rather sharply at 13 eV and the small yields of bicyclohexyl above ~20 eV may be a consequence of increasing yields of cyclohexene, but this is not supported by other work. Batten[9] has measured the formation of hydrogen from cyclohexane at 77°K under electron impact. The onset at ~7.5 eV was attributed to elimination of H and H_2 from an excited neutral, and this may correlate with the onset for bicyclohexyl formation. It appears to be unlikely that a higher onset in formation of hy-

(7) P. B. Merkel and W. H. Hamill, *J. Chem. Phys.*, **55**, 1409 (1971).
(8) L. M. Hunter, D. Lewis, and W. H. Hamill, *ibid.*, **52**, 1733 (1970).
(9) C. F. Batten, Ph.D. Thesis, University of Notre Dame, 1971.

drogen at ~18 eV can be attributed to a process producing molecular hydrogen which would compete with formation of bicyclohexyl. The low yields may be an artifact of thin films caused by the migration of excited states to the anode at which they would be quenched, but this is not indicated by related studies of luminescence.[9,10]

Under slow electron impact, thin films of cyclohexane at 77°K emit at 210, 360, and 490 nm,[10] the relative intensities being ~1, 1.5, and $>10^2$. The onset of excitation for the 490-nm band was ~12.5 eV. Although the other bands were too weak for measurement near onset, it was observed that the intensity of the 210-nm band *decreased* at >15 eV and was not detectable at 25 eV. In a rough way this follows the behavior of $G(C_{12}H_{22})$ *vs.* V and suggests that 210-nm fluorescence and cyclohexyl radicals arise from a common state, or set of states. The quantum yield for 201-nm fluorescence of cyclohexane at 298°K is 0.0035,[11] and it should not be less at 77°K. If the cross sections for excitation of the thin film states emitting at 210 nm and 490 nm are comparable, then the probability of emission at 490 nm from $\gtrsim$3-eV excited states produced by electron impact at $\gtrsim$12.5 eV may approach unity. That is, luminescence may compete effectively with chemical decomposition. The excitation curve for 490-nm luminescence,[9,10] included in Figure 2, is expressed in terms of uncorrected electron energies. The excitation curve suggests that luminescence arises from an excited state of the molecular ion. This state does not contribute appreciably to the yield of bicyclohexyl since it cannot be excited below ~12.5 eV. The final state of the electronic transition is expected to be the ground state of the molecular ion, and this cannot be a major precursor of bicyclohexyl since luminescence competes with decomposition. Recalling that 210-nm luminescence decreased as 490-nm intensity increased, it may be proposed that the 210-nm fluorescing state does not have ground-state molecular ion as a major precursor, and that it is the principal precursor of bicyclohexyl.

The cross section for excitation by electron impact typically reaches a maximum within a few volts of onset, then declines gradually. The dependence of G(bicyclohexyl) *vs.* V_a is consistent with the assumption that excited singlet states are responsible since it resembles the excitation function for a state, or narrow group of states. The onset of ionization does not compete strongly because the cross section for ground state ion is small for the first few electron volts. Finally, several excited states of the ion are available with cross sections still increasing at ~14 eV and G(singlets) falls rapidly by competition. One further assumption is that ion–electron combination produces fewer singlets than direct impact. Since triplets do not contribute to $G(C_{12}H_{22})$, and charge combination yields mostly triplets, this is plausible.

The results for *n*-hexane provide more detailed information than the preceding. The yields of all products provide evidence for energy deposition by electrons at <4 eV, *i.e.*, well below the threshold for optical excitation. There is no known mechanism whereby slow electrons can rupture C–C and C–H bonds by energy transfer to a high vibrational level of the neutral ground-state alkane. Electronic excitation must be invoked and low-lying triplet states are postulated, for which there is other evidence.[4,7,8,12]

If it is assumed that the precursor of *n*-dodecane at low energy is *n*-dodecyl, then the bond dissociation energy $D(n\text{-}C_6H_{13}\text{–H}) \cong 4.3$ eV requires an energy scale shift of ~2.3 eV in Figure 3. If the onsets of the ~6-eV peaks in Figures 4–6 are attributed to the lowest excited singlet states, then the average of the corresponding onsets at 5.2 eV must also be shifted by ~2.3 eV to match the onset of optical absorption of *n*-hexane at 7.4 eV.[13] The shift arises in part from the work function of the emitter, the bulk electron affinity of the target, and the trapped charges therein. It depends also on the arbitrary choice of a point on the I–V characteristic for the bare anode, on the IR drop in the filament, on the high-energy tail of the Boltzmann, and on the necessity of measuring onsets. Clearly, internal standards must be adopted.

Characteristic electron energy losses for *n*-hexane would provide appropriate internal standards but they could not be measured under the experimental arrangements used in this work. They have been measured[4,7,8] and, together with other work,[12] locate the lowest alkane triplet states well below the bond dissociation energies. The spectrum of dI/dV *vs.* V in Figure 6 shows these losses for slow electrons injected thermionically into a thin film of *n*-hexane at 77°K.[4,8] Consequently, in the present work the lower excited vibronic levels are not expected to give measurable products. Rather, excitation must reach a point on the first triplet potential energy surface at least as high as the asymptote along which the specified radical pair can separate in their ground states to form the observed products. Under favorable conditions the appearance potentials for these products will be equal to the corresponding bond dissociation energies along the ground state singlet surface. The two surfaces converge rapidly as the radical–radical separation increases since a singlet pair of doublets will have the same energy as a triplet pair of doublets.

It is assumed that decomposition of *n*-hexane from the lowest vibronic level of the first excited singlet state is possible and that the appearance potentials

(10) P. B. Merkel and W. H. Hamill, *J. Chem. Phys.*, **54**, 1695 (1971).
(11) F. Hirayama and S. Lipsky, *ibid.*, **51**, 3616 (1969).
(12) D. Lewis and W. H. Hamill, *ibid.*, **52**, 6348 (1970).
(13) J. W. Raymonda and W. T. Simpson, *ibid.*, **47**, 430 (1967).

at ~5.0 eV (nominal) in Figures 4–6 are characteristic of the state and not of the bond. The higher onsets at $\lesssim$8 eV (nominal) must then be shifted by 2.3 eV to $\lesssim$10.3 eV, which suggests that ionization is responsible, and quite possibly an excited state of the ion. If polarization lowers the energy required for ionization in the film, the excess energy at onset in $C_6H_{14}^{+*}$ is ~1.3 eV. This approximates the energy required for fragmentation.

The fluctuations in electron energy utilization for production of some products (Figures 4–6) cannot be reliably accounted for because there may be balancing changes in the yields of products not measured. Since the combined yield of all hydrocarbon products from γ irradiation at 77°K corresponds to 4.5 molecules of *n*-hexane decomposed per 100 eV absorbed, and only 9% appears in C_2–C_5 products,[14] such competition is quite possible. On the other hand, characteristic energy losses are markedly energy dependent and this requires some corresponding changes in G *vs.* V.

Luminescence from *n*-hexane at 77°K with λ_{max} 490 nm is excited by electron impact with an onset at ~12.5 eV.[10] The emitting state may be the highest of the first group of excited states of alkane ions.[15] Since they can be observed by mass spectrometry,[16] but at rather low abundance, luminescence may compete with unimolecular decomposition. The intensity of 490-nm luminescence is ~200 times that at 210 nm. The quantum yield for 207-nm fluorescence under rather different conditions (1470-Å excitation and 298°K) is 2×10^{-4}.[11] This suggests that the efficiency of 490-nm emission may be very small and so not compete with decomposition.

The yields of fragment products from *n*-hexane also decrease at $\gtrsim$14 eV, but not nearly as markedly as G(bicyclohexyl) in the same interval. In fact, if the electron yields are expressed as molecules of product per electron impact, *i.e.*, $GV_a/100$, then the yields are nearly constant in the interval 14–25 eV. For each of the products in Figures 4–6, the electron yields at 25 eV (not shown) are very nearly the same as those at 15–20 eV.

Taking ethane as a representative product, and considering the electron yield profile, it can be inferred that ground-state ions are not efficient precursors of product. That is, they neither decompose efficiently as ions nor upon subsequent neutralization.

The formation of C_2–C_5 products as well as *n*-dodecane below 5 eV is considered to be evidence for low-lying triplet states of *n*-hexane. This interpretation is supported by evidence from mass spectrometry for an excited state of *n*-hexane at 2.8 eV.[17] It is also consistent with 4.4-sec recombination luminescence from 3-methylpentane[18] and with slow electron energy losses for *n*-hexane, cyclohexane, and 3-methylpentane.[7,8] If the lowest potential energy surface for triplet *n*-hexane were repulsive for all molecular configurations the minimum vertical excitation energy would be rather greater than the minimum bond dissociation energy, contrary to observation. Neither would such an assumption be able to account for a slow recombination luminescence. Consequently, it is assumed that vertical excitation to a low-lying triplet potential energy surface and Franck–Condon effects may produce either a stable slow emitter or a radical pair, depending upon the vibrational excitation.

(14) L. Kevan and W. F. Libby, *J. Chem. Phys.*, **39**, 1288 (1963).

(15) K. Fueki, *J. Phys. Chem.*, **68**, 2656 (1964); J. C. Lorquet, *Advan. Mass Spectrom.*, **3**, 443 (1966).

(16) C. E. Melton and W. H. Hamill, *J. Chem. Phys.*, **41**, 546 (1964).

(17) D. Lewis and W. H. Hamill, *ibid.*, **52**, 6348 (1970).

(18) P. B. Merkel and W. H. Hamill, *ibid.*, **53**, 3414 (1970).

Role of Added Olefins and Oxygen in the Gas-Phase Radiolysis of *n*-Butane

by Noboru Fujisaki, Ikuo Fujimoto, and Yoshihiko Hatano*

Laboratory of Physical Chemistry, Tokyo Institute of Technology, Meguro-ku, Tokyo, Japan *(Received October 18, 1971)*

Publication costs borne completely by The Journal of Physical Chemistry

The addition of ethylene, propylene, and cyclopropane to *n*-butane caused a definite increase in the yields of ethane, propane, and propane, respectively, in the gas-phase radiolysis of *n*-butane containing 5 mol % oxygen. An attempt has been made to determine the extent to which these additives undergo H- and H_2-transfer reactions. Assuming the relative rates for H and H_2 transfer, $k(H)/k(H_2)$, to the propylene molecule from the *n*-butane parent ion to be 0.1, the relative rates $k(H)/k(H_2)$ for the *n*-butane parent ion–ethylene and *n*-butane parent ion–cyclopropane reaction pairs are determined, respectively, to be 0.9 and 1.8. The influence of the occurrence of H- and H_2-transfer reactions between the *n*-butane parent ion and the added ethylene or propylene on the mechanism of the hydrogen formation is also discussed. The fact that the *G* value of nitrogen from *n*-butane–1.1 mol % nitrous oxide mixtures decreased from 12 to 0 upon the addition of 2.6 mol % oxygen suggests that oxygen scavenges an electron or its equivalent as well as a thermal free radical in the gas phase.

Introduction

Thus far, an olefin such as ethylene has frequently been used as a suitable thermal hydrogen-atom scavenger in the radiolysis of saturated hydrocarbons.[1] Recently, however, mass spectrometric[2-4] and product analysis studies[5-7] have provided evidence that olefins react with saturated hydrocarbon parent ions *via* H- and H_2-transfer reactions

$$C_nH_{2n} + RH_2^+ \longrightarrow C_nH_{2n+1} + RH^+ \quad (1)$$

$$C_nH_{2n} + RH_2^+ \longrightarrow C_nH_{2n+2} + R^+ \quad (2)$$

where C_nH_{2n} and RH_2^+ denote olefin molecule and alkane parent ion, respectively.

Since the yield of the unimolecular hydrogen formed in the gas-phase radiolysis of propane decreased appreciably upon the addition of ethylene, we have also suggested in a previous paper[8] that ethylene may interact with unspecified ionic species. In the present investigation, we intend to elucidate the role of added olefins including ethylene and propylene which may scavenge both hydrogen atoms and ionic species as the precursors of product hydrogen in the gas-phase radiolysis. Since quantitative information on H-transfer reactions is relatively little compared with information on H_2-transfer reactions occurring in the radiolysis of RH_2–C_nH_{2n} mixtures, emphasis is placed on determining the extent to which the H-transfer reaction occurs. The role of oxygen which has been used incidentally to elucidate the role of added olefins is also examined critically.

Experimental Section

The materials, *n*-butane, oxygen, sulfur hexafluoride, and nitrous oxide used in this study are identical with those used in a previous study.[9] Ethylene (>99.99%), propylene (>99.99%), cyclopropane (>99.99%), and hydrogen sulfide (>99%), supplied by Takachiho Trading Co., were used after the usual degassing and trap-to-trap distillations. The samples to be irradiated were contained *in vacuo* at −196° in cylindrical Pyrex vessels with a volume of 140 ml. The pressure of *n*-butane was maintained constant at 900 mm throughout this study. The samples were irradiated by ^{60}Co γ rays at a temperature somewhat higher than room temperature at a dose rate of 4.87×10^{19} eV/(g hr) to a total dose of 4.87×10^{19} eV/g. The energy absorbed was determined by Fricke dosimeter, making appropriate correction for electron density. The analytical methods were identical with those described before,[9] except for those described below. When oxygen was added to *n*-butane, hydrogen, methane, and oxygen, which were noncondensable at −196°, were transferred from Pyrex vessels with a volume of 275 ml to a calibrated gas buret by means of a Toepler pump. After pressure–volume measurement, the gas composition was determined with a gas chromatograph equipped with a 3-m molecular sieve 5A column.

Results

The effects of oxygen, ethylene, and sulfur hexafluoride on the product yields at a total dose of $4.87 \times$

(1) See, for example, R. A. Holroyd, *J. Phys. Chem.*, **70**, 1341 (1966).

(2) F. P. Abramson and J. H. Futrell, *ibid.*, **71**, 1233 (1967).

(3) L. W. Sieck and S. K. Searles, *J. Amer. Chem. Soc.*, **92**, 2937 (1970).

(4) L. W. Sieck, S. K. Searles, and P. Ausloos, *J. Chem. Phys.*, **54**, 91 (1971).

(5) P. Ausloos, *Progr. React. Kinet.*, **5**, 113 (1969), and references cited therein.

(6) P. Ausloos and S. G. Lias, *J. Chem. Phys.*, **45**, 524 (1966).

(7) P. Ausloos, A. A. Scala, and S. G. Lias, *J. Amer. Chem. Soc.*, **89**, 3677 (1967).

(8) N. Fujisaki, S. Shida, and Y. Hatano, *J. Chem. Phys.*, **52**, 556 (1970).

(9) N. Fujisaki, S. Shida, Y. Hatano, and K. Tanno, *J. Phys. Chem.*, **75**, 2854 (1971).

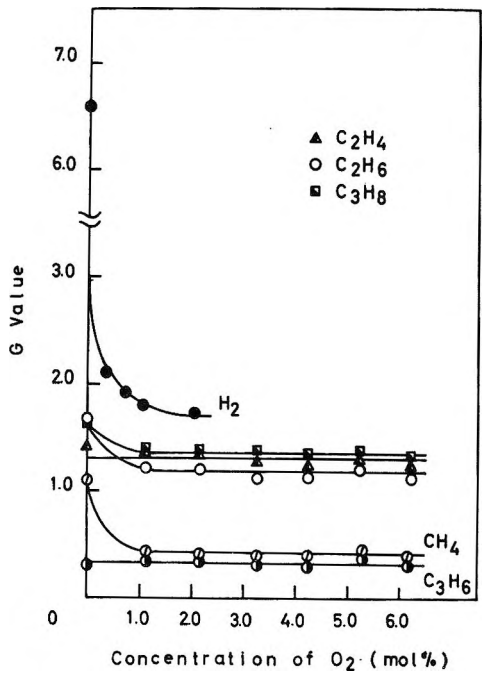

Figure 1. Effect of oxygen on the yield of products from pure *n*-butane at 900 mm.

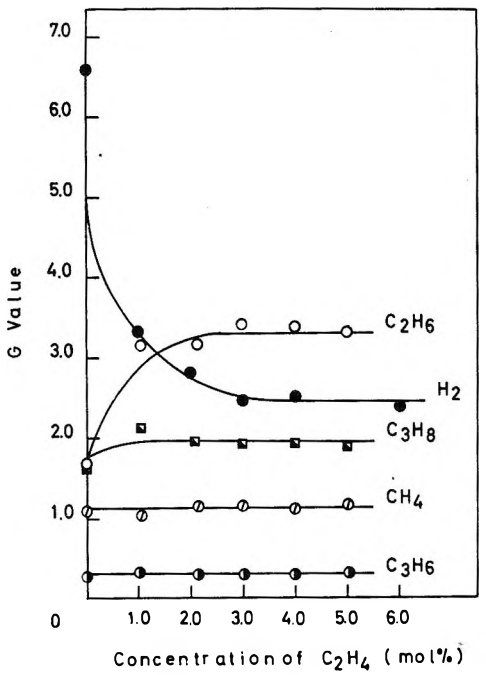

Figure 2. Effect of ethylene on the yield of products from pure *n*-butane at 900 mm.

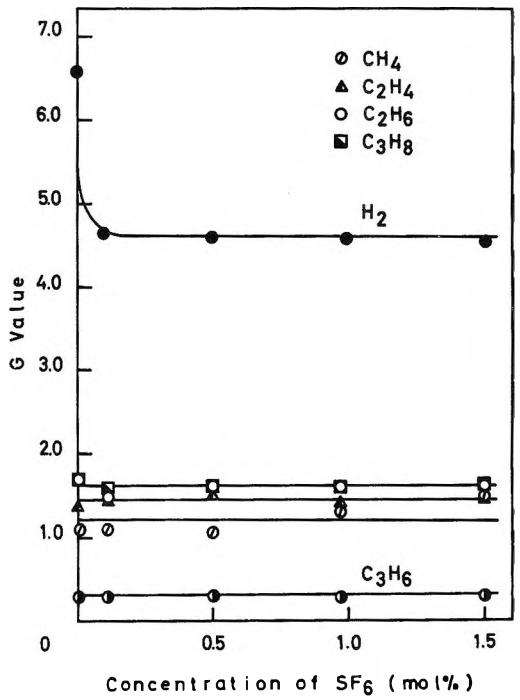

Figure 3. Effect of sulfur hexafluoride on the yield of products from pure *n*-butane at 900 mm.

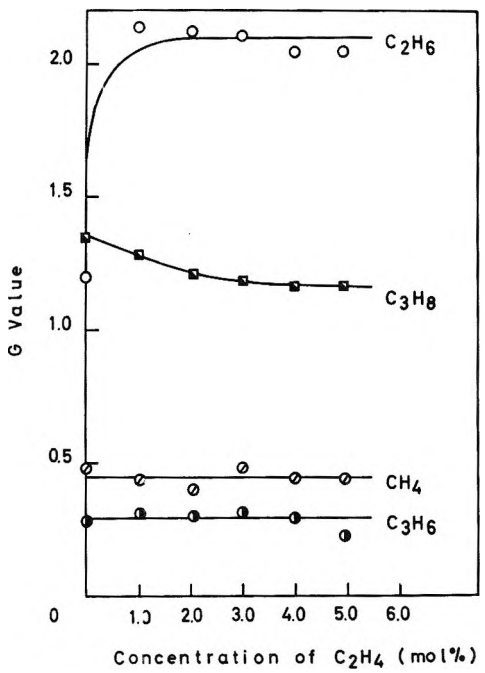

Figure 4. Effect of ethylene on the yield of products from *n*-butane-oxygen (5 mol %) mixtures.

10^{19} eV/g are shown, respectively, in Figures 1, 2, and 3. Figure 2 indicates that an increased yield of ethane upon the addition of ethylene is accompanied by a decreased yield of hydrogen. Comparison of Figures 1 and 2 indicates that the decrease in the hydrogen yield, 4.9 in *G* units, caused by the addition of 2 mol % oxygen is larger than that, 4.2 in *G* units, caused by the addition of 6 mol % ethylene. The yield of hydrogen decreased sharply upon the addition of 0.1 mol % sulfur hexafluoride, while the yield of C_1–C_3 hydrocarbon products remained almost constant upon the addition of SF_6, as shown in Figure 3. Figures 4 and 5 show, respectively, the variation of product yields from *n*-butane containing 5 mol % oxygen as a function of ethylene or propylene concentration. It is

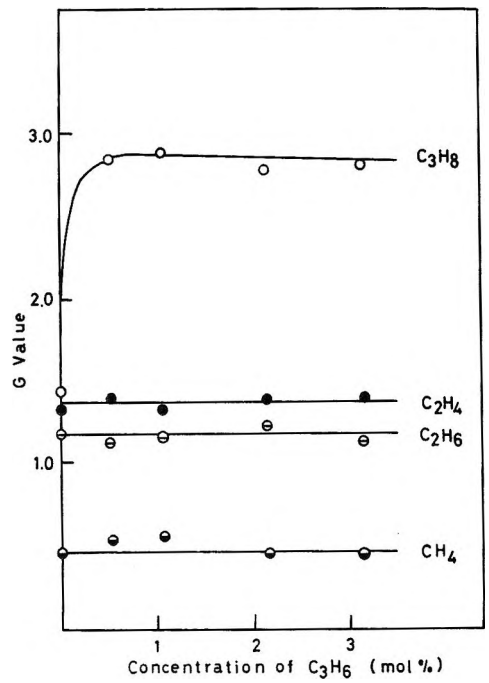

Figure 5. Effect of propylene on the yield of products from *n*-butane-oxygen (5 mol %) mixtures.

seen in Figure 4 that the addition of 5 mol % ethylene increased the G value of ethane by 0.9 and decreased the G value of propane only by 0.2. The addition of 3 mol % propylene increased the G value of propane by 1.5 (Figure 5). The experimental results on the product yields in the presence and absence of scavengers are tabulated in Table I. The results obtained in the gas-phase radiolysis of *n*-C_4H_{10}–5 mol % O_2–c-C_3H_6 mixtures are also included in Table I. In addition to the results presented in the table and figures, the following additional results were obtained. (i) The G value of propane, 2.9, from *n*-C_4H_{10}–O_2 (5 mol %)–C_3H_6 (1.1 mol %) decreased respectively to 1.95 and 1.4 upon the addition of 2.1 and 8.6 mol % hydrogen sulfide. (ii) The G value of nitrogen, 12, from *n*-C_4H_{10}–N_2O (1.1 mol %) decreased respectively to 0.3 and 0 upon the addition of 1.6 and 2.6 mol % oxygen. (iii) The G value of hydrogen, 2.4, from *n*-C_4H_{10}–C_2H_4 (5 mol %) is scarcely affected by the addition of 2 mol % sulfur hexafluoride. The last result is in good agreement with that obtained in the gas-phase radiolysis of propane–ethylene mixtures.[8]

Discussion

The Effect of Added Propylene. As seen in Figure 5, the G value of propane from *n*-C_4H_{10}–O_2 mixtures increased by 1.5 upon the addition of 1 mol % propylene. The increased propane yield is due to the occurrence of H_2-transfer reaction 3 between propylene and the *n*-butane parent ion. In this system, where oxygen is

$$C_3H_6 + n\text{-}C_4H_{10}^+ \longrightarrow C_3H_8 + C_4H_8^+ \quad (3)$$

$$C_3H_6 + n\text{-}C_4H_{10}^+ \longrightarrow C_3H_7 + C_4H_9^+ \quad (4)$$

Table I: The G Values of Products in the Gas-Phase Radiolysis of *n*-Butane[a]

Additive	G value					
	H_2	CH_4	C_2H_6	C_2H_4	C_3H_8	C_3H_6
None	6.6	1.1	1.7	1.4	1.7	0.3
O_2 (6 mol %)	1.7[b]	0.4	1.2	1.3	1.4	0.3
C_2H_4 (5 mol %)	2.4	1.1	3.3	nd	2.0	0.3
C_2H_4 (5 mol %) + O_2 (5 mol %)	nd[c]	0.4	2.1	nd	1.2	0.3
C_3H_6 (3 mol %) + O_2 (5 mol %)	nd	0.4	1.2	1.3	2.9	nd
c-C_3H_6 (2 mol %) + O_2 (5 mol %)	nd	0.4	1.2	1.4	2.0	nd
SF_6 (1.5 mol %)	4.6	1.2	1.6	1.4	1.6	0.3

[a] Pressure of *n*-butane, 900 mm. [b] Concentration of O_2, 2 mol %. [c] nd = not determined.

present, propyl radicals produced by the hydrogen-atom scavenging of propylene or H-transfer reaction 4 may not be responsible for the increase in the propane yield upon the addition of propylene. Evidence for the occurrence of H- and H_2-transfer reactions between an olefin molecule and a saturated hydrocarbon parent ion comes from chemical analysis of the stable end products formed in radiolysis and in photoionization experiments conducted by Ausloos, *et al.*,[5-7] and from recent photoionization mass spectrometric studies.[2-4] From the results obtained by the photoionization of *n*-C_4D_{10}–C_3H_6–O_2 mixtures,[6] the rate constant ratio k_4/k_3 at higher pressures may be derived to be $\sim$0.1.[10] Using 0.1 for k_4/k_3, one can obtain $\sim$0.2 as the G value of the propyl radicals resulting from H-transfer reaction 4. Thus, the G value of the *n*-butane parent ion at 900 mm is estimated to be 1.7, which is the sum of the G values of propane produced *via* reaction 3 and propyl radicals produced *via* reaction 4. A recent mass spectrometric study[11] has provided evidence that the propane parent ion reacts with hydrogen sulfide *via* charge- and proton-transfer reactions. As shown in result i, the G value of propane produced from *n*-C_4H_{10}–O_2–C_3H_6 (1.1 mol %) mixtures decreased by 1.5 upon the addition of 8.6 mol % hydrogen sulfide, which corresponds to an increased yield of propane caused by the addition of propylene to *n*-C_4H_{10}–O_2 mixtures. Similar results have been obtained in the liquid-phase radiolysis of the c-C_6D_{12}–c-C_3H_6–H_2S system.[7] These results may be explainable by the fact that reactions 3 and 4 are interrupted by the addition of hydrogen sulfide.

Recently, however, a mass spectrometric study[4] has demonstrated that propane parent ions undergo to some extent the dimerization reaction 5 prior to the

(10) Assuming that at higher pressures, *e.g.*, 900 mm most of the total propane produced from the above mixture is due to the D_2-transfer reaction between *n*-$C_4D_{10}^+$ and C_3H_6, one can derive the ratio k_4/k_3 to be $\sim$0.1.

(11) L. I. Bone and J. H. Futrell, *J. Chem. Phys.*, **47**, 4366 (1967).

occurrence of an H_2-transfer reaction between the propane parent ion and added ethylene, even at much lower pressures than that in these experiments. There

$$C_3H_8^+ + C_3H_8 \longrightarrow (C_3H_8)_2^+ \quad (5)$$

could thus be some ambiguity in the G value of the *n*-butane parent ion derived directly from the value of k_4/k_3 cited above and the increased yield of propane upon the addition of propylene to n-C_4H_{10}–O_2 mixtures.

The Effect of Added Ethylene. The G value of ethane produced from n-C_4H_{10}–O_2 mixture increased by 0.9 upon the addition of 1 mol % ethylene (Figure 4). The H_2-transfer reaction 6 from the *n*-butane parent ion to ethylene is, as is found in the case of *n*-butane–propylene mixtures, responsible for the increased yield of ethane. Since the G value of the *n*-butane

$$C_2H_4 + n\text{-}C_4H_{10}^+ \longrightarrow C_2H_6 + C_4H_8^+ \quad (6)$$

$$C_2H_4 + n\text{-}C_4H_{10}^+ \longrightarrow C_2H_5 + C_4H_9^+ \quad (7)$$

parent ion has been estimated to be 1.7 from the results on n-C_4H_{10}–C_3H_6 mixtures, the G value of the ethyl radical produced by H-transfer reaction 7 can be derived to be 0.8, with some assumptions that the G value of the *n*-butane parent ion is constant at a constant pressure of *n*-butane and that all parent ions produced react with the added olefin *via* H- or H_2-transfer reactions. Thus, it is shown that k_7/k_6, the relative rate for H and H_2 transfer to an ethylene molecule from an *n*-butane parent ion, is 0.9, much greater than k_4/k_3 for the *n*-butane parent ion–propylene reaction pair. Further, in the case of cyclopropane, k_9/k_8 is estimated to be 1.8 from the increased yield of propane (0.6 in G units) upon the addition of cyclopropane to the n-C_4H_{10}–O_2 mixture (Table I).

$$c\text{-}C_3H_6 + n\text{-}C_4H_{10}^+ \longrightarrow C_3H_8 + C_4H_8^+ \quad (8)$$

$$\searrow\ C_3H_7 + C_4H_9^+ \quad (9)$$

The trend that the importance of the H-transfer reaction relative to the H_2-transfer reaction increases in the order propylene, ethylene, cyclopropane is in agreement with one observed in a recent high-pressure photoionization mass spectrometric study,[3] where the rate constant ratio $k(H)/k(H_2)$ for reactions of cyclohexane parent ion with propylene, ethylene, and the cyclopropane molecule have been measured.

As seen in Figure 4, the G value of propane is decreased slightly by the addition of ethylene to n-C_4H_{10}–O_2 mixtures. It may safely be inferred from the studies[12,13] that propane produced from n-C_4H_{10}–O_2 mixtures is for the most part produced by the hydride-ion-transfer reaction of the propyl ion resulting from the fragmentation of an excited *n*-butane parent ion.

$$C_3H_7^+ + n\text{-}C_4H_{10} \longrightarrow C_3H_8 + C_4H_9^+ \quad (10)$$

Then the decrease in the yield of propane upon the addition of ethylene to n-C_4H_{10}–O_2 mixtures may be due to the condensation reaction 11 and/or proton-transfer reaction 12. However, the slight decrease in

$$C_3H_7^+ + C_2H_4 \longrightarrow C_5H_{11}^+ \quad (11)$$

$$C_3H_7^- + C_2H_4 \longrightarrow C_3H_6 + C_2H_5^+ \quad (12)$$

the yield of propane upon the addition of ethylene indicates that the condensation reaction 11 and/or the proton-transfer reaction 12 is (are) not important compared with the hydride-ion-transfer reaction of the propyl ion in the range of ethylene concentrations used.

The Effect of Added Olefins on Hydrogen Formation. The influence of H- and H_2-transfer reactions occurring in the *n*-butane–olefin mixture on the mechanism of hydrogen formation should be examined here. The *n*-butane parent ion may eventually be neutralized with an electron to give product hydrogen or its precursor in the absence of ethylene.[14]

$$n\text{-}C_4H_{10}^+ + e^- \longrightarrow H,\ H_2 \quad (13)$$

On the other hand, H- and H_2-transfer reactions occurring in the *n*-butane–olefin mixture convert the *n*-butane parent ion into a butene or a butyl ion, which may not give the product hydrogen upon neutralization in the presence of an olefin.[15] Consequently, it may be inferred that the added olefin reduces the hydrogen yield by acting not only as a thermal hydrogen-atom scavenger but also as a parent-ion scavenger. This inference is in coincidence with our previous suggestion[8] that ethylene added to propane reduces not only the bimolecular hydrogen yield but also the unimolecular hydrogen yield by acting as a positive ion scavenger.

Since the yield of propane produced from an n-C_4H_{10}–O_2 mixture is not affected appreciably by the addition of ethylene (Figure 4), the *n*-butane parent ion undergoing H- and H_2-transfer reactions may be different from the parent ion which decomposes to give propyl ion.

In order to elucidate further the eventual fate of the *n*-butane parent ion which reacts with the olefin, the effect of sulfur hexafluoride on the product yields is examined. As shown in Figure 3, the decrease in the yield of hydrogen is not accompanied by any other appreciable changes in the yield of C_1–C_3 products upon addition of sulfur hexafluoride. The effect on the hydrogen yield is explainable by postulating the processes 13 and 14. No appreciable effect of

$$n\text{-}C_4H_{10}^+ + SF_6^- \not\longrightarrow H,\ H_2 \quad (14)$$

(12) R. P. Borkowski and P. Ausloos, *J. Chem. Phys.*, **39**, 818 (1963).

(13) T. Miyazaki and S. Shida, *Bull. Chem. Soc. Jap.*, **38**, 2114 (1965).

(14) Butyl ion which is produced by the hydride-ion transfer reactions of fragment ions will also be neutralized by an electron to give product hydrogen and its precursor in the absence of ethylene.

(15) Y. Hatano and S. Shida, *J. Chem. Phys.*, **46**, 4784 (1967).

sulfur hexafluoride on the yield of C_1–C_3 products indicates that the neutralization of the *n*-butane parent ion with electron leads to C–C bond rupture. The above result in the gas phase differs remarkably from that in the liquid phase, in which not only C–H bond rupture but also C–C bond rupture has been observed in the neutralization of a parent ion by an electron.[8,9,16]

The Role of Added Oxygen. It is rather an unexpected result that the decrease in the hydrogen yield, 4.9 in *G* units, caused by the addition of 2 mol % oxygen is larger than that in the hydrogen yield, 4.2 in *G* units, caused by the addition of 6 mol % ethylene. In the foregoing discussion, we ascribed the decrease in the yield of hydrogen upon the addition of ethylene to thermal hydrogen atom scavenging and parent ion scavenging by ethylene. Thus, the unexpected large decrease in hydrogen yield caused by the addition of oxygen suggests that a certain process including oxygen which corresponds to reactions 6 and 7 in addition to thermal hydrogen atom scavenging by oxygen should at least be invoked to explain the effect of oxygen on the hydrogen yield. The neutralization process (15) is reasonably considered as a process corresponding to reactions 6 and 7. To invoke reaction 15 means that

$$n\text{-}C_4H_{10}^+ + O_2^- \not\longrightarrow H, H_2 \qquad (15)$$

oxygen added as a thermal radical scavenger behaves also as an electron scavenger in the gas phase. In fact, the *G* value of nitrogen from n-C_4H_{10}–N_2O (1.1 mol %) decreased from 12 to 0 upon the addition of 2.6 mol % oxygen. The decrease in the yield of nitrogen from liquid n-C_4H_{10}–N_2O mixtures upon the addition of an appreciable concentration of oxygen has already been observed and ascribed to electron scavenging by oxygen.[9] Although the decomposition mechanism of nitrous oxide added to a saturated hydrocarbon still remains obscure,[17] the decrease in the yield of nitrogen upon the addition of oxygen is explainable by competitive electron scavenging between nitrous oxide and oxygen. In general, the ion–molecule reactions of fragment ions resulting from the decomposition of excited *n*-butane ions are fast compared with the neutralization reaction so that O_2^- cannot intercept the ion–molecule reactions of fragment ions. When, however, the neutralization of n-$C_4H_{10}^+$ and $C_4H_9^+$ in this experiment is concerned, the effect of oxygen as an electron scavenger should be considered. The neutralization process of n-$C_4H_{10}^+$ and $C_4H_9^+$ with electrons which produces the hydrogen or its precursor in the absence of oxygen is changed into the neutralization process 15 by the addition of oxygen.

In the gas-phase radiolysis of propane,[8] we have suggested that hydrogen nonscavengeable by ethylene consists of both bimolecular hydrogen produced by the hydrogen abstraction reaction of hot hydrogen atoms and unimolecular hydrogen produced by the decomposition of excited molecule. The observation that the effect of sulfur hexafluoride and ethylene on the hydrogen yield is almost the same in the radiolysis of *n*-butane as in the radiolysis of propane[8] leads us to assume that the mechanism of hydrogen formation from *n*-butane–ethylene mixtures is essentially the same as that of hydrogen formation from propane–ethylene mixtures. Then the following two observations suggest that oxygen scavenges hydrogen nonscavengeable by both ethylene and sulfur hexafluoride. (i) The *G* value of hydrogen from *n*-butane–oxygen mixtures is smaller than that of hydrogen from *n*-butane–ethylene mixtures (Table I). (ii) The *G* value of hydrogen from *n*-butane–ethylene mixtures is not affected by the addition of sulfur hexafluoride. Further study is needed to elucidate whether a hot hydrogen atom or the precursor of unimolecular hydrogen is scavenged by oxygen. At any rate, it is suggested that in the gas-phase radiolysis of *n*-butane the added oxygen scavenges not only thermal radicals and electrons but also the precursor of hydrogen nonscavengeable by both ethylene and sulfur hexafluoride.

Acknowledgment. The authors wish to thank Professor S. Shida for valuable suggestions.

(16) S. Shida, N. Fujisaki, and Y. Hatano, *J. Chem. Phys.*, **49**, 4571 (1968).

(17) (a) J. M. Warman, *J. Phys. Chem.*, **71**, 4066 (1967); (b) W. J. Holtslander and G. R. Freeman, *ibid.*, **71**, 2562 (1967); (c) K. Takeuchi, K. Shinsaka, S. Takao, Y. Hatano, and S. Shida, *Bull. Chem. Soc. Jap.*, **44**, 2004 (1971); (d) S. Takao, Y. Hatano, and S. Shida, *J. Phys. Chem.*, **75**, 3178 (1971).

Elementary Processes in the Radiolysis of Aqueous Sulfuric Acid Solutions. Determinations of Both G_{OH} and $G_{SO_4^-}$[1,2]

by R. W. Matthews,[3] H. A. Mahlman, and T. J. Sworski*

Chemistry Division, Oak Ridge National Laboratory, Oak Ridge, Tennessee 37830 *(Received October 12, 1971)*

Publication costs assisted by the U. S. Atomic Energy Commission

Kinetic evidence is presented for concurrent production of two oxidizing radicals in the radiolysis of aqueous sulfuric acid solutions: OH and SO_4^- radicals that are presumed to result from direct action of ionizing radiation on water and sulfuric acid anions, respectively. The evidence was obtained from the dependence of $G(Ce^{III})$ on cerium(III) and either formic acid or 2-propanol concentrations in the radiolysis of cerium(IV)–cerium(III)–formic acid mixtures and cerium(IV)–cerium(III)–2-propanol mixtures. Determinations of G_{OH} and $G_{SO_4^-}$ required the use of a computer for least-squares fit of experimental data to complex kinetic equations containing up to 22 dependent variables. Applicability of the kinetic equations is indicated by the excellent agreement for two determinations in 4.0 *M* sulfuric acid: $G_{OH} = 1.76 \pm 0.19$ and $G_{SO_4^-} = 0.95 \pm 0.18$ with 2-propanol solutions; $G_{OH} = 1.78 \pm 0.03$ and $G_{SO_4^-} = 0.94 \pm 0.03$ with formic acid solutions. A small but significant yield of SO_4^- was determined in 0.4 *M* sulfuric acid: $G_{OH} = 2.60 \pm 0.04$ and $G_{SO_4^-} = 0.20 \pm 0.04$. No evidence was obtained for oxidation of sulfuric acid anions by precursors of OH radical such as H_2O^+, since G_{OH} was found to be proportional to electron fraction water.

Introduction

The importance of the SO_4^- radical as an intermediate in the radiolysis of aqueous sulfuric acid solutions has been the subject of numerous investigations. Three different processes have been proposed for the production of SO_4^- radicals: reaction of OH radical with sulfuric acid anions,[4,5] direct action of ionizing radiation on sulfuric acid anions,[6] and reaction of sulfuric acid anions with H_2O^+, a commonly assumed precursor of the OH radical.[7]

The proposal that OH radical reacts with sulfuric acid anions has been substantiated. Rate constant ratios for reaction of OH radical with cerium(III), formic acid, and sulfuric acid anions were determined from the dependence of $G(Ce^{III})$ on cerium(III) and formic acid concentrations in the radiolysis of cerium(IV)–cerium(III)–formic acid mixtures in air-saturated 0.4 *M* sulfuric acid with ^{60}Co γ radiation.[8] More direct evidence for the reaction of OH radical with sulfuric acid anions was obtained by pulse radiolysis techniques.[9]

Boyle[6] proposed the concurrent production of OH and SO_4^- radicals in the radiolysis of aqueous sulfuric acid solutions with G_{OH} proportional to electron fraction water and $G_{SO_4^-}$ proportional to electron fraction sulfuric acid. The evidence, though convincing, was indirect: the formation of hydrogen peroxide, peroxosulfuric acid, and peroxodisulfuric acid in the spur was attributed to combination reactions of some OH and SO_4^- radicals before the remainder escaped by diffusion into the bulk of the solution. No evidence was presented, however, for those SO_4^- radicals that escaped by diffusion into the bulk of the solution.

The energy absorbed by each component in the radiolysis of mixtures is commonly assumed to be proportional to its electron fraction. It has long been recognized, however, that the G values for intermediates that are characteristic of each component may not be proportional to the energy absorbed by each component, owing to either ionization transfer or excitation transfer.[10] The suggestion[7] that SO_4^- radical may result from reaction of sulfuric acid anions with H_2O^+, an example of ionization transfer, has been neither substantiated nor refuted. Our interest in this suggestion is due to the recent model for the radiolysis of water in which hole trapping by anions is postulated to occur.[11]

This paper reports an extension of the previous kinetic study[8] to include the radiolysis of cerium(IV)–cerium(III)–formic acid mixtures in air-saturated 0.04, 0.4, and 4.0 *M* sulfuric acid solutions and cerium(IV)–

(1) Research sponsored by the U. S. Atomic Energy Commission under contract with Union Carbide Corporation.

(2) This paper was presented in part at the 17th annual meeting of the Radiation Research Society, Cincinnati, Ohio, May 18–22, 1969.

(3) Guest Scientist from the Australian Atomic Energy Commission Research Establishment, Lucas Heights, New South Wales.

(4) H. Taube and W. C. Bray, *J. Amer. Chem. Soc.*, **62**, 3357 (1940).

(5) A. O. Allen, C. J. Hochanadel, J. A. Ghormley, and T. W. Davis, *J. Phys. Chem.*, **56**, 575 (1952).

(6) J. W. Boyle, *Radiat. Res.*, **17**, 427 (1962).

(7) A. O. Allen, *ibid.*, **1**, 85 (1954).

(8) T. J. Sworski, *J. Amer. Chem. Soc.*, **78**, 1786 (1956); *Radiat. Res.*, **6**, 645 (1957).

(9) E. Heckel, A. Henglein, and G. Beck, *Ber. Bunsenges. Phys. Chem.*, **70**, 149 (1966).

(10) J. P. Manion and M. Burton, *J. Phys. Chem.*, **56**, 560 (1952).

(11) W. H. Hamill, *ibid.*, **73**, 1341 (1969).

cerium(III)–2-propanol mixtures in air-saturated 0.4 and 4.0 M sulfuric acid solutions. As reported in our preliminary communication,[12] kinetic evidence is presented for the concurrent production of OH and SO_4^- radicals in the radiolysis of aqueous sulfuric acid solutions. The proposal of Boyle[6] is substantiated. The suggestion[7] that sulfuric acid anions react with H_2O^+ to yield SO_4^- is refuted, since G_{OH} is proportional to electron fraction water.

Experimental Section

Materials. Fisher purified ceric ammonium sulfate, G. Frederick Smith Co. reagent cerous sulfate, Matheson Coleman and Bell spectroquality reagent 2-propanol, Baker Analyzed reagent formic acid, Baker and Adamson reagent ferrous ammonium sulfate, and Du Pont reagent sulfuric acid were used without further purification. All solutions were prepared with water from a Barnstead still that was further purified by successive distillations from an acid dichromate solution, from an alkaline permanganate solution, and finally from an all-silica system into silica storage vessels.

Irradiations. Solutions in a 2-cm Pyrocell cylindrical absorption cell were irradiated in ^{60}Co sources of the Ghormley–Hochanadel design.[13] The cell had S18-260 silica windows that did not become colored enough during irradiations to interfere with spectrophotometric analyses of the solutions with a Cary recording spectrophotometer. Dose rates were determined with the ferrous sulfate dosimeter using $G(Fe^{III}) = 15.6$.[14] The energy absorbed in solutions relative to the ferrous sulfate dosimeter was assumed to be in the ratio of electron densities.

Analyses. Changes in cerium(IV) concentration with absorbed dose were determined spectrophotometrically in the irradiation cell. Molar extinction coefficients for cerium(IV) at 320 nm of 5580 in 0.4 M sulfuric acid[14] and 6590 in 4.0 M sulfuric acid[15] were used. The molar extinction coefficient of cerium(IV) at 320 nm in 0.04 M sulfuric acid was markedly affected by the high concentrations of cerium(III) sulfate that we used (ranging from 5099 in its absence to 5446 for 0.058 M) and was determined for each concentration of cerium(III) sulfate. A molar extinction coefficient for iron(III) at 305 nm of 2210 in 0.4 M sulfuric acid[16] was used for ferrous sulfate dosimetry. While all irradiations were made at ambient room temperature, all spectrophotometric analyses were made thermostatically at 25°.

Results

$G(Ce^{III})$ is markedly dependent on both cerium(III) and formic acid concentrations in the radiolysis of cerium(IV)–cerium(III)–formic acid mixtures in air-saturated sulfuric acid solutions.[8] Figure 1 shows the results obtained in 4.0 M sulfuric acid solutions. Similar results were obtained in both 0.4 M and 0.04 M sulfuric acid solutions.

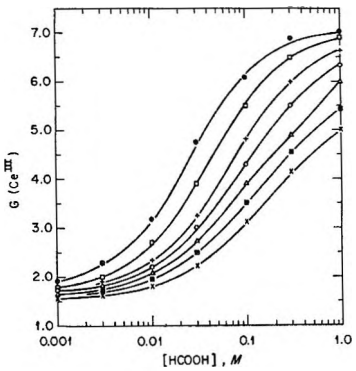

Figure 1. Dependence of $G(Ce^{III})$ on $[Ce^{III}]$ and [HCOOH] in the reduction of cerium(IV) in air-saturated 4.0 M sulfuric acid solutions induced by ^{60}Co γ radiation. Initial $[Ce^{III}]$: (×) 3.0×10^{-2} M, (■) 1.5×10^{-2} M, (△) 6.0×10^{-3} M, (○) 3.0×10^{-3} M, (+) 1.5×10^{-3} M, (□) 6.0×10^{-4} M, (●) 3.0×10^{-4} M. Curves are theoretical and represent least-squares fit of the data to eq III.

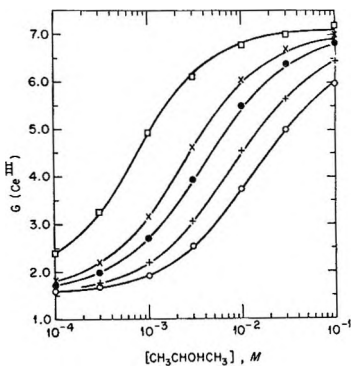

Figure 2. Dependence of $G(Ce^{III})$ on $[Ce^{III}]$ and $[CH_3CHOHCH_3]$ in the reduction of cerium(IV) in air-saturated 4.0 M sulfuric acid solutions induced by ^{60}Co γ radiation. Initial $[Ce^{III}]$: (○) 2.92×10^{-2} M, (+) 1.46×10^{-2} M, (●) 5.86×10^{-3} M, (×) 2.92×10^{-3} M, (□) 6.10×10^{-4} M. Curves are theoretical and represent least-squares fit of the data to eq III.

$G(Ce^{III})$ is also markedly dependent on both cerium(III) and 2-propanol concentrations in the radiolysis of cerium(IV)–cerium(III)–2-propanol mixtures in air-saturated sulfuric acid solutions. Figure 2 shows the results obtained in 4.0 M sulfuric acid solutions. Similar results were obtained in 0.4 M sulfuric acid solutions.

The initial concentration of cerium(IV) in all solutions was about 10^{-4} M. Changes in cerium(IV) concentrations with dose were determined in each solution

(12) R. W. Matthews, H. A. Mahlman, and T. J. Sworski, *J. Phys. Chem.*, 74, 3835 (1970).

(13) J. A. Ghormley and C. J. Hochanadel, *Rev. Sci. Instrum.*, 22, 473 (1951).

(14) C. J. Hochanadel and J. A. Ghormley, *J. Chem. Phys.*, 21, 880 (1953).

(15) R. W. Matthews, H. A. Mahlman, and T. J. Sworski, *J. Phys. Chem.*, 74, 2475 (1970).

(16) T. J. Sworski, *J. Amer. Chem. Soc.*, 77, 4689 (1955); *Radiat. Res.*, 4, 483 (1956).

by five to six successive irradiations. In most cases, the cerium(IV) concentration changed linearly with dose within experimental error. In some cases, the initial rate of reduction was determined by extrapolation from a plot of the rate of cerium(IV) reduction as a function of dose.

There is reportedly[17] no effect of oxygen on $G(Ce^{III})$. The absence of an oxygen effect was attributed to reduction of cerium(IV) by either H atom or the HO_2 radical that results from reaction of H atom with oxygen. A small effect of oxygen on $G(Ce^{III})$ is to be expected, however, owing to the dependence of G_{H_2} on oxygen concentration.[18] We conducted some experiments in deoxygenated 4.0 M sulfuric acid solutions to evaluate the role of oxygen in the radiolysis of cerium(IV)–cerium(III)–formic acid mixtures.

In 0.0015 M cerium(III) solutions, the values for $G(Ce^{III})$ at all formic acid concentrations are slightly higher in initially air-saturated solutions than in initially deoxygenated solutions, as shown in Figure 3. This small effect of oxygen, an increase in $G(Ce^{III})$ of 0.22 ± 0.03 independent of formic acid concentration, is attributed to the reactions of oxygen in the spur that reportedly[18] cause G_{H_2} to decrease.

In 0.03 M cerium(III) solutions, we were surprised to observe net cerium(III) oxidation at low formic acid concentrations in initially deoxygenated solutions as shown in Figure 3. We have established[19,20] that net oxidation of cerium(III) results from reaction of H atom with hydrogen peroxide since reactions of cerium(IV) with both H atom and hydrogen peroxide are slow. Oxygen in air-saturated solutions inhibits reaction of H atom with hydrogen peroxide through intermediate formation of HO_2. For this reason, we used air-saturated solutions in this kinetic study. As indicated by the data in Figure 3, formic acid at high concentrations also inhibits reaction of H atom with hydrogen peroxide. This is attributed to reaction of formic acid with H atom,[21] presumably to yield an intermediate that reduces cerium(IV).

Discussion

The reaction mechanism for radiation-induced reduction of cerium(IV) in aqueous sulfuric acid solutions is well established. Allen[7] proposed that cerium(IV) is reduced by both H atom and hydrogen peroxide while cerium(III) is oxidized by OH radical and

$$G(Ce^{III}) = 2G_{H_2O_2} + G_H - G_{OH} \quad (I)$$

His hypothesis was substantiated by Challenger and Masters[22] who observed concomitant oxidation of radioactive cerium(III) during net reduction of cerium(IV). Allen's hypothesis was further substantiated by studies of the enhancement of $G(Ce^{III})$ by formic acid,[23] thallium(I),[16] and 2-propanol[24] through their reaction with OH radical to yield intermediates that reduce cerium(IV).

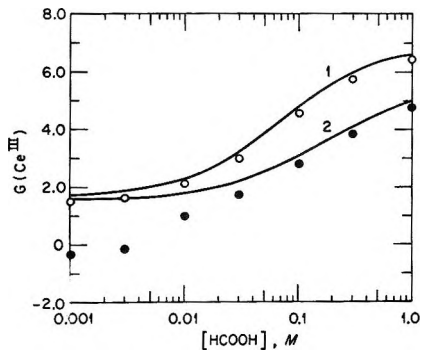

Figure 3. Dependence of $G(Ce^{III})$ on $[Ce^{III}]$ and [HCOOH] in the reduction of cerium(IV) in deoxygenated 4.0 M sulfuric acid solutions induced by ^{60}Co γ radiation. Initial $[Ce^{III}]$: (○) 1.5×10^{-3} M, (●) 3.0×10^{-2} M. The results for air-saturated solutions are indicated by curve 1 for $[Ce^{III}] = 1.5 \times 10^{-3}$ M and by curve 2 for $[Ce^{III}] = 3.0 \times 10^{-2}$ M.

We have considered reactions 1–9 of OH and SO_4^- radicals in order to explain the dependence of $G(Ce^{III})$ on cerium(III), formic acid, and 2-propanol concentrations.

$$OH + HSO_4^- \rightleftharpoons H_2O + SO_4^- \quad (1)$$

$$OH + Ce^{III} \longrightarrow OH^- + Ce^{IV} \quad (2)$$

$$SO_4^- + Ce^{III} \longrightarrow SO_4^{2-} + Ce^{IV} \quad (3)$$

$$OH + HCOOH \longrightarrow H_2O + COOH \quad (4)$$

$$SO_4^- + HCOOH \longrightarrow HSO_4^- + COOH \quad (5)$$

$$COOH + Ce^{IV} \longrightarrow H^+ + CO_2 + Ce^{III} \quad (6)$$

$$OH + CH_3CHOHCH_3 \longrightarrow H_2O + CH_3COHCH_3 \quad (7)$$

$$SO_4^- + CH_3CHOHCH_3 \longrightarrow HSO_4^- + CH_3COHCH_3 \quad (8)$$

$$CH_3COHCH_3 + Ce^{IV} \longrightarrow H^+ + CH_3COCH_3 + Ce^{III} \quad (9)$$

One Primary oxidizing Radical Model: OH. In the radiolysis of cerium(IV)–cerium(III)–formic acid mixtures in air-saturated 0.4 M sulfuric acid solutions, Sworski[8] implicitly assumed that $G_{SO_4^-}$, $k_{-1}[H_2O]/(k_3[Ce^{III}])$, and $k_5[HCOOH]/(k_3[Ce^{III}])$ were negligibly small and obtained

(17) T. J. Hardwick, *Can. J. Chem.*, **30**, 23 (1952).

(18) J. A. Ghormley and C. J. Hochanadel, *Radiat. Res.*, **3**, 227 (1955).

(19) R. W. Matthews, H. A. Mahlman, and T. J. Sworski, *J. Phys. Chem.*, **72**, 3704 (1968).

(20) H. A. Mahlman, R. W. Matthews, and T. J. Sworski, *ibid.*, **75**, 250 (1971).

(21) E. J. Hart, *J. Amer. Chem. Soc.*, **73**, 68 (1951).

(22) G. E. Challenger and B. J. Masters, *ibid.*, **77**, 1063 (1955).

(23) H. E. Spencer and G. K. Rollefson, *ibid.*, **77**, 1938 (1955).

(24) T. J. Sworski, R. W. Matthews, and H. A. Mahlman, *Advan. Chem. Ser.*, **No. 81**, 134 (1968).

$$G(Ce^{III}) = G(Ce^{III})^0 + 2G_{OH}^* \Big/ \left(1 + \frac{k_1[HSO_4^-] + k_2[Ce^{III}]}{k_aS}\right) \quad (II)$$

For cerium(IV)–cerium(III)–formic acid mixtures, k_aS denotes k_4[HCOOH]. For cerium(IV)–cerium(III)–2-propanol mixtures, k_aS denotes k_7[$CH_3CHOHCH_3$]. G_{OH}^*, a function of cerium(III) and sulfuric acid concentrations, denotes the value of G_{OH} that is obtained by the use of eq II. $G(Ce^{III})^0$, also a function of cerium(III) and sulfuric acid concentrations, denotes the value of $G(Ce^{III})$ in the absence of formic acid and 2-propanol.

All of our data adhered well to eq II. The experimental data were fit to eq II by the method of least squares, using the computer program of Lietzke.[25] The data were weighted by assuming that all $G(Ce^{III})$ values had a constant percentage error. Values of $G(Ce^{III})^0$, G_{OH}^*, and the kinetic parameter $(k_1[HSO_4^-] + k_2[Ce^{III}])/k_a$ were obtained as a function of cerium(III) and sulfuric acid concentrations.

Equation II seems to be a valid approximation for cerium(IV)–cerium(III)–formic acid mixtures in 0.04 and 0.4 M sulfuric acid solutions. As shown in Figure 4, the kinetic parameter $(k_1[HSO_4^-] + k_2[Ce^{III}])/k_4$ is approximately a linear function of cerium(III) concentration and has a finite positive value indicated for $[Ce^{III}] = 0$. Figure 4 also shows that eq II is clearly not valid for cerium(IV)–cerium(III)–formic acid mixtures in 4.0 M sulfuric acid solutions.

Similarly, eq II seems to be a valid approximation for cerium(IV)–cerium(III)–2-propanol mixtures in 0.4 M sulfuric acid solutions. As shown in Figure 5, the kinetic parameter $(k_1[HSO_4^-] + k_2[Ce^{III}])/k_7$ is approximately a linear function of cerium(III) concentration and computer analysis yielded a finite positive value for $[Ce^{III}] = 0$. Figure 5 also shows that eq II is again clearly not valid for 4.0 M sulfuric acid solutions.

G_{OH}^* increases with increase in cerium(III) concentration for cerium(IV)–cerium(III)–formic acid mixtures in 0.04 M sulfuric acid solutions, as shown in Figure 6, and for cerium(IV)–cerium(III)–2-propanol mixtures in 0.4 M sulfuric acid solutions, as shown in Figure 7. This is just what we anticipated for the dependence of G_{OH} on cerium(III) concentration, since $G_{H_2O_2}$ decreases with increase in cerium(III) concentration.[16] It was clearly shown in the radiolysis of cerium(IV)–thallium(I) mixtures in 0.4 M sulfuric acid solutions that G_{OH} increases with increase in thallium(I) concentration by an amount equal to twice the concomitant decrease in $G_{H_2O_2}$ causing $G(Ce^{III})$ to be independent of thallium(I) concentration.[16]

G_{OH}^* seems to be independent of changes in cerium(III) concentration for cerium(IV)–cerium(III)–formic acid mixtures in 0.4 M sulfuric acid solutions as shown in Figure 6. G_{OH}^* decreases markedly with increase in cerium(III) concentration in 4.0 M sulfuric acid solutions both for cerium(IV)–cerium(III)–formic acid mixtures, as shown in Figure 6 and for cerium(IV)–cerium(III)–2-propanol mixtures, as shown in Figure 7. These results were unexpected and indicate that eq II

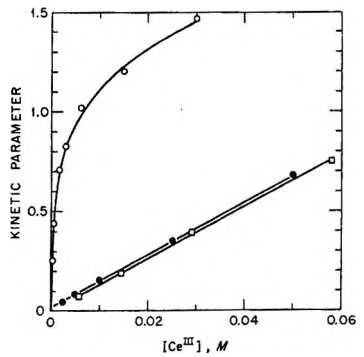

Figure 4. Dependence of the kinetic parameter $(k_1[HSO_4^-] + k_2[Ce^{III}])/k_4$ in eq II on $[Ce^{III}]$. Sulfuric acid concentrations: (○) 4.0 M, (●) 0.4 M, (□) 0.04 M.

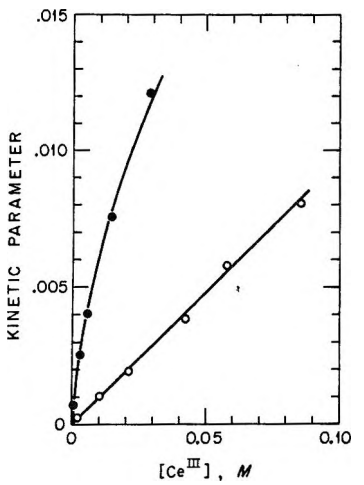

Figure 5. Dependence of the kinetic parameter $(k_1[HSO_4^-] + k_2[Ce^{III}])/k_7$ in eq II on $[Ce^{III}]$. Sulfuric acid concentrations: (●) 4.0 M, (○) 0.4 M.

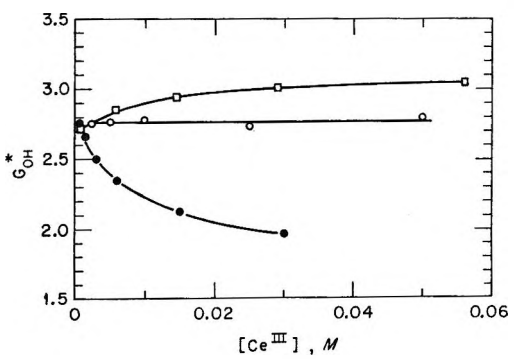

Figure 6. Dependence of G_{OH}^* in eq II on cerium(III) concentration for cerium(IV)–cerium(III)–formic acid mixtures. Sulfuric acid concentrations: (●) 4.0 M, (○) 0.4 M, (□) 0.04 M.

(25) M. H. Lietzke, ORNL-3259, Mar 21, 1962.

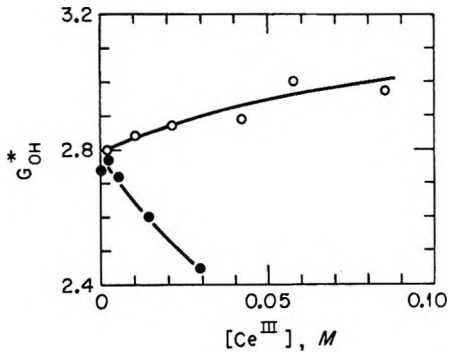

Figure 7. Dependence of G_{OH}^* in eq II on cerium(III) concentration for cerium(IV)–cerium(III)–2-propanol mixtures. Sulfuric acid concentrations: (●) 4.0 M, (○) 0.4 M.

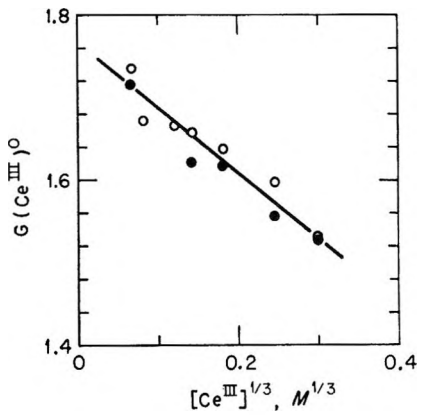

Figure 8. Dependence of $G(Ce^{III})^0$ in eq II on cerium(III) concentration in 4.0 M sulfuric acid solutions containing either (○) formic acid or (●) 2-propanol.

is a poor approximation for 0.4 M sulfuric acid solutions containing cerium(IV)–cerium(III)–formic acid mixtures and not valid for 4.0 M sulfuric acid solutions.

$G(Ce^{III})^0$ in 4.0 M sulfuric acid solutions decreases linearly with the cube root of the cerium(III) concentration as shown in Figure 8. The theoretical significance of this cube-root dependence is its implication that $G_{H_2O_2}$ decreases with increase in cerium(III) concentration, just as previously reported[16] for 0.4 M sulfuric acid solutions.

Two Primary Oxidizing Radicals Models. OH and SO_4^-. Our initial experiments were with cerium(IV)–cerium(III)–formic acid mixtures. The dependence of the kinetic parameter on cerium(III) concentration in 4.0 M sulfuric acid solutions as shown in Figure 4 was found to be quantitatively explicable by postulating that reaction (1) is sensibly reversible. The dependence of G_{OH}^* on cerium(III) concentration in 4.0 M sulfuric acid solutions as shown in Figure 6 was found to be quantitatively explicable by postulating two oxidizing radicals: the OH radical and an unidentified intermediate that either disappears by a first-order process to yield OH radical or reacts with cerium(III) but not with formic acid. The best fit of the experimental data to these postulates was obtained by assuming that the unidentified intermediate was not SO_4^-. This suggested the possibility that the unidentified intermediate may be either H_2O^+ or H_2O^*.

To test the validity of these two postulates, we extended our study to include the cerium(IV)–cerium(III)–2-propanol mixtures. Comparison of Figures 6 and 7 shows that G_{OH}^* in 4.0 M sulfuric acid solutions is not a function of cerium(III) concentration alone. We concluded, therefore, that the unidentified intermediate may also react with formic acid and 2-propanol.

The dependence of $G(Ce^{III})$ on cerium(III) and either formic acid or 2-propanol concentrations in 4.0 M sulfuric acid solutions is quantitatively explicable by the sequence of reactions 1–9 induced by primary yields of both OH and SO_4^-. This reaction mechanism and the stationary-state hypothesis for OH and SO_4^- concentrations require that

$$G(Ce^{III}) = G(Ce^{III})^0 + 2(aG_{OH} + bG_{SO_4^-})/c \quad \text{(III)}$$

in which

$$a = \frac{k_bS}{k_3C} + \frac{k_aS}{k_1A}\left(1 + \frac{k_bS + k_{-1}W}{k_3C}\right)$$

$$b = \frac{k_ak_{-1}SW}{k_3k_1CA} + \frac{k_bS}{k_3C}\left(1 + \frac{k_aS + k_2C}{k_1A}\right)$$

$$c = 1 + \frac{k_bS}{k_3C} + \left(1 + \frac{k_bS + k_{-1}W}{k_3C}\right)\left(\frac{k_aS + k_2C}{k_1A}\right)$$

$C = [Ce^{III}]$, $A = [HSO_4^-]$, and $W = [H_2O]$. For cerium(IV)–cerium(III)–formic acid mixtures, k_bS denotes $k_5[HCOOH]$. For cerium(IV)–cerium(III)–2-propanol mixtures, k_bS denotes $k_8[CH_3CHOHCH_3]$. Equation III was obtained with the assumption that G_{OH} and $G_{SO_4^-}$ are constants, independent of variations in concentrations of cerium(III), formic acid, and 2-propanol.

The experimental data were fit to eq III by the method of least squares. For cerium(IV)–cerium(III)–formic acid mixtures in 4.0 M sulfuric acid solutions, 13 unknowns were determined: the values of G_{OH}, $G_{SO_4^-}$, and four rate constant ratios listed in column 1 of Table I and seven values of $G(Ce^{III})^0$ for the seven different cerium(III) concentrations. For cerium(IV)–cerium(III)–2-propanol mixtures in 4.0 M sulfuric acid solutions, 11 unknowns were determined: the values of G_{OH}, $G_{SO_4^-}$, and four rate constant ratios listed in column 2 of Table I and five values of $G(Ce^{III})^0$ for the five different cerium(III) concentrations.

The experimental data adhere well to eq III, as indicated by the theoretical curves in Figures 1 and 2 that illustrate the least-squares fit of the data to eq III. The excellent agreement between the two sets of values for G_{OH} and $G_{SO_4^-}$ that are listed in columns 1 and 2 of Table I is evidence for the validity of eq III.

Table I: Results from Least-Squares Fit of Experimental Data to Eq III–V

	1[a]	2[b]	3[c]	4[d]
G_{OH}	1.78 ± 0.03	1.76 ± 0.19	1.76 ± 0.03	2.60 ± 0.04
$G_{SO_4^-}$	0.94 ± 0.03	0.95 ± 0.18	0.94 ± 0.03	0.20 ± 0.04
$k_2/(k_1[HSO_4^-])$	30 ± 3	84 ± 17	30 ± 3	(9.3 ± 1.1) × 10^2
$k_{-1}[H_2O]/k_3$	(1.7 ± 0.5) × 10^{-4}	(2.7 ± 3.9) × 10^{-4}	(1.2 ± 0.5) × 10^{-4}	(1.1 ± 0.6) × 10^{-4}
$k_4/(k_1[HSO_4^-])$	14.4 ± 0.5		14.7 ± 0.6	(6.9 ± 0.8) × 10^2
k_5/k_3	(6.0 ± 0.5) × 10^{-3}		(6.5 ± 0.5) × 10^{-3}	(7.2 ± 6.7) × 10^{-3}
$k_7/(k_1[HSO_4^-])$		360 ± 34	202 ± 12	(1.1 ± 0.2) × 10^4
k_8/k_3		0.61 ± 0.11	0.64 ± 0.03	0.71 ± 0.30
$k_{12}[H^+]/k_{11}$			0.35 ± 0.04	
k_{10}/k_7			1.4 ± 0.3	

[a] Cerium(IV)–cerium(III)–formic acid mixtures in 4.0 *M* sulfuric acid; eq III. [b] Cerium(IV)–cerium(III)–2-propanol mixtures in 4.0 *M* sulfuric acid; eq III. [c] All data in 4.0 *M* sulfuric acid; eq IV. [d] All data in 0.4 *M* sulfuric acid; eq V.

Absolute rate constants for reactions of SO_4^- with cerium(III), formic acid, and 2-propanol have been reported:[26] $k_3 = 1.43 \times 10^8\ M^{-1}\ sec^{-1}$, $k_5 = 1.35 \times 10^6\ M^{-1}\ sec^{-1}$, and $k_8 = 4.60 \times 10^7\ M^{-1}\ sec^{-1}$. These values yield $k_5/k_3 = 9.4 \times 10^{-3}$ and $k_8/k_3 = 0.32$, in fair agreement with our determinations listed in Table I.

The large standard errors listed in Table I for $k_{-1}[H_2O]/k_3$ suggest that $k_{-1}[H_2O]/k_3$ is almost negligibly small for most of our solutions, hydrolysis of SO_4^- being significant only for a few of the more dilute cerium(III) solutions. We previously assumed[2] that $k_{-1}[H_2O]/k_3 = 0$ and obtained G_{OH} values of 1.70 ± 0.02 and 1.64 ± 0.08 and $G_{SO_4^-}$ values of 0.97 ± 0.03 and 1.06 ± 0.09 for formic acid and 2-propanol solutions in 4.0 *M* sulfuric acid, respectively. These two sets of values for G_{OH} and $G_{SO_4^-}$ are in agreement within standard errors, but the agreement is not as good as for the values obtained by use of eq III.

The poor agreement between the two values for $k_2/(k_1[HSO_4])$ listed in columns 1 and 2 of Table I is disappointing in view of the excellent agreement between the two sets of values for G_{OH} and $G_{SO_4^-}$. We have speculated on the cause of this poor agreement and suggest that it may be due to reactions 10–12. The net

$$OH + CH_3CHOHCH_3 \longrightarrow H_2O + CH_3CHOCH_3 \quad (10)$$

$$CH_3CHOCH_3 + CH_3CHOHCH_3 \longrightarrow CH_3CHOHCH_3 + CH_3COHCH_3 \quad (11)$$

$$H^+ + CH_3CHOCH_3 + Ce^{III} \longrightarrow CH_3CHOHCH_3 + Ce^{IV} \quad (12)$$

effect for the sequence of reactions (10) and (12) is the oxidation of cerium(III) by OH, thus causing a higher value of $k_2/(k_1[HSO_4^-])$ for 2-propanol solutions.

This suggestion was substantiated by a least-squares fit of the combined data from formic acid and 2-propanol solutions in 4.0 *M* sulfuric acid to

$$G(Ce^{III}) = G(Ce^{III})^0 + 2(aG_{OH} + bG_{SO_4^-})/c + 2(dG_{OH} + eG_{SO_4^-})/f \quad (IV)$$

in which

$$d = \frac{k_8P}{k_3C} + \frac{k_7P}{k_1A}\left[1 + \frac{k_{10}}{k_7}\Big/\left(1 + \frac{k_{12}[H^+]C}{k_{11}P}\right)\right]\left(1 + \frac{k_8P + k_{-1}W}{k_3C}\right)$$

$$e = \frac{k_7k_{-1}PW}{k_3k_1CA}\left[1 + \frac{k_{10}}{k_7}\Big/\left(1 + \frac{k_{12}[H^+]C}{k_{11}P}\right)\right] + \frac{k_8P}{k_3C}\left(1 + \frac{k_7P + k_{10}P + k_2C}{k_1A}\right)$$

$$f = 1 + \frac{k_8P}{k_3C} + \left(1 + \frac{k_8P + k_{-1}W}{k_3C}\right) \times \left(\frac{k_7P + k_{10}P + k_2C}{k_1A}\right)$$

P denotes $[CH_3CHOHCH_3]$ so that d, e, and f are used for cerium(IV)–cerium(III)–2-propanol mixtures. In eq IV, k_aS and k_bS only denote $k_4[HCOOH]$ and $k_5[HCOOH]$ so that a, b, and c, are used for cerium(IV)–cerium(III)–formic acid mixtures.

Twenty-two unknowns were determined: the values of G_{OH}, $G_{SO_4^-}$, and 8 rate constant ratios listed in column 3 of Table I and 12 values of $G(Ce^{III})^0$ for the 12 different cerium(III) concentrations. There are two major effects of assuming the sequence of reactions 10–12 and using eq IV: the value for $k_2/(k_1[HSO_4^-])$ becomes identical with that listed in column 1 of Table I for formic acid solutions and $k_7/(k_1[HSO_4^-])$ decreases significantly.

The difference in the dependence of G_{OH}* on cerium(III) concentration between formic acid and 2-propanol solutions in 0.4 *M* sulfuric acid, shown in Figures 4 and 5, may be evidence for a significant value of $G_{SO_4^-}$. Therefore, a least-squares analysis of the combined data from formic acid and 2-propanol solutions in 0.4 *M* sulfuric acid was made with the constraint that the dependence of G_{OH} on cerium(III) concentration be iden-

(26) L. Dogliotti and E. Hayon, *J. Phys. Chem.*, 71, 3802 (1967).

tical for formic acid and 2-propanol solutions. G_{OH} was assumed to increase linearly with increase in the cube root of the cerium(III) concentration.

The experimental data were fit by the method of least squares to

$$G(Ce^{III}) = G(Ce^{III})^0 + 2[a(G_{OH} + A[Ce^{III}]^{1/3}) + bG_{SO_4^-}]/c \quad (V)$$

Twenty-one unknowns were determined: the values of G_{OH}, $G_{SO_4^-}$, and 6 rate constant ratios listed in column 4 of Table I, 12 values of $G(Ce^{III})^0$ for the 12 different cerium(III) concentrations, and $A = 0.57 \pm 0.08$.

The agreement between the values of $k_{-1}[H_2O]/k_3$, k_5/k_3, and k_8/k_3 for 4.0 and 0.4 M sulfuric acid solutions listed in columns 3 and 4 of Table I is surprisingly excellent and is further evidence for the validity of our two primary oxidizing radicals model. The larger standard errors indicated in the values for 0.4 M sulfuric acid solutions listed in column 4 of Table I are attributable to the role of SO_4^- in 0.4 M sulfuric acid solutions being less important than in 4.0 M sulfuric acid solutions, though still significant. The present determination of $k_2:k_4:k_1[HSO_4^-] = 930:690:1$ for 0.4 M sulfuric acid solutions supersedes the previous determination of $k_2:k_4:k_1[HSO_4^-] = 1600:950:1$ that was obtained by approximation.[8]

In view of the low electron fraction sulfuric acid in 0.04 M sulfuric acid solutions, no attempt was made to determine $G_{SO_4^-}$. The experimental data for cerium(IV)–cerium(III)–formic acid mixtures in 0.04 M sulfuric acid solutions were fit by the method of least squares to eq V with the previous approximations that $G_{SO_4^-}$, $k_{-1}[H_2O]/(k_3[Ce^{III}])$, and $k_5[HCOOH]/(k_3[Ce^{III}])$ were negligibly small. Ten unknowns were determined: $G_{OH} = 2.67 \pm 0.04$, $A = 1.05 \pm 0.13$, $k_2/(k_1[HSO_4^-]) = (1.2 \pm 0.2) \times 10^4$, $k_4/(k_1[HSO_4^-]) = (9.2 \pm 0.9) \times 10^3$, and six values of $G(Ce^{III})^0$ for the six different cerium(III) concentrations.

G_{OH} increases with increase in cerium(III) concentration in both 0.04 M and 0.4 M sulfuric acid solutions. As stated above, this is just what we expected. Our assumption that both G_{OH} and $G_{SO_4^-}$ are constants, independent of variations in cerium(III) concentration, in 4.0 M sulfuric acid solutions may be unjustified. Therefore, we determined the effects of assuming that both G_{OH} and $G_{SO_4^-}$ in eq IV vary linearly with the cube root of the cerium(III) concentration. We also determined, at the same time, the effect of assuming that $G(Ce^{III})^0$ in eq IV and V varies linearly with the cube root of the cerium(III) concentration. The dependence of G_{OH} on cerium(III) concentration is given in Table II. The dependence of $G(Ce^{III})^0$ on cerium(III) concentration is given in Table III. $G_{SO_4^-}$ in 4.0 M sulfuric acid solutions was found to be $(0.95 \pm 0.14) - (0.35 \pm 0.45)[Ce^{III}]^{1/3}$.

The assumption that G_{OH} and $G(Ce^{III})^0$ vary linearly with the cube root of the cerium(III) concentration is a good approximation, except for the dependence of G_{OH} on cerium(III) concentration in 4.0 M sulfuric acid solutions, as evidenced by the low standard errors for the coefficients of $[Ce^{III}]^{1/3}$. In 4.0 M sulfuric acid solutions, it is apparently a gross oversimplification to assume that G_{OH} would vary linearly with $[Ce^{III}]^{1/3}$. The value of 30 ± 3 for $k_2/(k_1[HSO_4^-])$ indicates that the sulfuric acid anions are as reactive with OH radical as 0.033 M cerium(III). We assume, therefore, that sulfuric acid anions in 4.0 M sulfuric acid solutions inhibit significantly the formation of hydrogen peroxide in the spur and enhance the formation of peroxosulfuric and peroxodisulfuric acids. The negligibly small dependence of G_{OH} on $[Ce^{III}]^{1/3}$ in 4.0 M sulfuric acid solutions is attributed to inhibition of reactions of OH with cerium(III) in the spur by sulfuric acid anions.

Table II: Dependence of G_{OH} on Cerium(III) Concentration

$[H_2SO_4]$, M	G_{OH}
4.0	$(1.78 \pm 0.14) + (0.02 \pm 0.42)[Ce^{III}]^{1/3}$
0.4	$(2.57 \pm 0.05) + (0.60 \pm 0.09)[Ce^{III}]^{1/3}$
0.04	$(2.60 \pm 0.04) + (1.29 \pm 0.14)[Ce^{III}]^{1/3}$

Table III: Dependence of $G(Ce^{III})^0$ on Cerium(III) Concentration

$[H_2SO_4]$, M	$G(Ce^{III})^0$
4.0	$(1.76 \pm 0.01) - (0.72 \pm 0.04)[Ce^{III}]^{1/3}$
0.4	$(2.40 \pm 0.02) - (0.74 \pm 0.06)[Ce^{III}]^{1/3}$
0.04	$(2.48 \pm 0.02) - (1.30 \pm 0.09)[Ce^{III}]^{1/3}$

If the only effect of cerium(III) on reactions of OH radical in the spur were to inhibit the formation of hydrogen peroxide, then the decrease in $G(Ce^{III})^0$ by any particular concentration of cerium(III) should be equal to twice the concomitant increase in G_{OH}. Tables II and III show that $2\Delta G_{OH}$ is much larger than $-\Delta G(Ce^{III})^0$ for 0.04 M and 0.4 M sulfuric acid solutions and suggest that cerium(III) is also inhibiting re-formation of water in the spur.

We previously reported that $G(Ce^{III})^0 = 1.66 \pm 0.03$[15] in air-saturated 4.0 M sulfuric acid solutions containing 3.0×10^{-3} M cerium(III) and $G(Ce^{III})^0 = 2.39$[16] in air-saturated 0.4 M sulfuric acid solutions containing no initial cerium(III). These values are in agreement with the results listed in Table III.

Let E_W denote electron fraction water and G_{OH}^0 denote the G value for OH production that results from energy absorption by water. Then $G_{OH}^0 = G_{OH}/E_W$, provided that energy absorption by water is proportional to electron fraction water, neither ionization transfer nor excitation transfer occurs between water

and sulfuric acid anions, and the fraction of OH radicals escaping from the spur by diffusion into the bulk of the solution is independent of sulfuric acid concentration. The dependence of G_{OH}, E_W, and G_{OH}^0 on sulfuric acid concentration is given in Table IV.

Table IV: Dependence of G_{OH} on Electron Fraction Water

$[H_2SO_4]$, M	G_{OH}	E_W	G_{OH}^0
4.0	1.76 ± 0.03	0.700	2.51 ± 0.05
0.4	2.60 ± 0.04	0.963	2.70 ± 0.04
0.04	2.67 ± 0.04	0.997	2.68 ± 0.04
0	2.59 ± 0.09[a]	1.000	2.59 ± 0.09

[a] From ref 27.

The values of G_{OH}^0 for 0.04, 0.4, and 4.0 M sulfuric acid solutions are all equal within standard errors to $G_{OH} = 2.59 \pm 0.09$, the most recent value of G_{OH} for pure water that has been determined in our laboratory.[27] These results substantiate the proposal of Boyle[6] that G_{OH} is proportional to electron fraction water in the radiolysis of aqueous sulfuric acid solutions. They refute the suggestion of Allen[7] that SO_4^- may result from reaction of HSO_4^- with H_2O^+, a commonly assumed precursor of the OH radical.

Evidence has been reported[28] for the dry charge pair[11] in the radiolysis of water: a decrease in $G(H_2O_2)$ by chloride ion in neutral aqueous solutions containing oxygen has been attributed to trapping of the dry hole, H_2O^+, by chloride ion at high concentrations. Our evidence that G_{OH} is proportional to electron fraction water in 4.0 M sulfuric acid solutions and in 4.0 M nitric acid solutions[12] indicates that hole trapping by anions, if it occurs at all, is not a general phenomenon. Definitive evidence for hole trapping would be a dependence of G_{OH} on both electron fraction water and anion concentration.

Under our experimental conditions, equilibrium between OH and SO_4^- is not established. If equilibrium were established, it can be easily shown that a one oxidizing radical model would be applicable even though there were primary yields of both OH and SO_4^-. We can, however, evaluate $[SO_4^-]/[OH]$ for equilibrium conditions by noting that $[SO_4^-]/[OH] = k_1[HSO_4^-]/(k_1[H_2O])$ at equilibrium. Using the reported values of $1.43 \times 10^8\ M^{-1}\ sec^{-1}$ for k_3[26] and $2.2 \times 10^8\ M^{-1}\ sec^{-1}$ for k_2,[29] our values for $k_2/(k_1[HSO_4^-])$ of 30 and 930 and for $k_{-1}[H_2O]/k_3$ of 1.7×10^{-4} and 1.1×10^{-4} yield values for $[SO_4^-]/[OH]$ of 302 and 15.0 for 4.0 and 0.4 M sulfuric acid solutions, respectively. At these sulfuric acid concentrations, $[HSO_4^-]$ is approximately equal[30] to seven-tenths of the sulfuric acid molarity, and the equilibrium concentration quotient $[SO_4^-]/([OH][HSO_4^-])$ for reaction 1 is approximately equal to 100 and 50 for 4.0 and 0.4 M sulfuric acid solutions, respectively. The high concentrations of sulfuric acid in our solutions preclude the calculations of equilibrium values for $[SO_4^-]/[OH]$ using the equilibrium constant evaluated by Wilmarth and Haim.[31]

(27) C. J. Hochanadel and R. Casey, *Radiat. Res.*, **25**, 198 (1965).

(28) T. Sawai and W. H. Hamill, *J. Chem. Phys.*, **52**, 3843 (1970); *J. Phys. Chem.*, **74**, 3914 (1970).

(29) M. Anbar and P. Neta, *Int. J. Appl. Radiat. Isotopes*, **18**, 493 (1967).

(30) T. F. Young, L. F. Maranville, and H. M. Smith, "The Structure of Electrolytic Solutions," Wiley, New York, N. Y., 1959, p 35.

(31) W. K. Wilmarth and A. Haim, "Peroxide Reaction Mechanisms," Interscience, New York, N. Y., 1961, p 175.

The Effect of Temperature on the γ Radiolysis of Aqueous Solutions

by I. Balakrishnan and M. P. Reddy*

Communication No. 1578 from the National Chemical Laboratory, Poona, India *(Received August 2, 1971)*

Publication costs borne completely by The Journal of Physical Chemistry

$G(-Ce^{4+})$ in the aqueous ceric sulfate system is constant in the region 0–30° and thereafter drops steadily, whereas $G(Fe^{3+})$ in the deaerated ferrous sulfate system remains strictly constant at 8.1 ± 0.05 from 0 to 120°. From this it follows rigorously that $G(OH)$ is constant at least from 0 to 30°. This fact makes it possible to identify the formation, in addition to phenol, of two aldehydes in the γ radiolysis of the aerated neutral aqueous benzene system and to characterize them as the α and β isomers of hydroxymucondialdehyde (HMD). The sum of the yields of the three products is equal to $G(OH)$. From 40° upward G(phenol) rises sharply and reaches a value of ~5 at 220°. At 60° and above the HMD appears to be replaced by ketonic products from fragmentation of the benzene ring. An analysis of the temperature coefficient of $G(Fe^{3+})$ of the aerated Fricke system suggests that it is in the main due to a competition between two reactions, $H + O_2 \rightarrow HO_2$ and $H_2^+ + Fe^{2+} \rightarrow H_2 + Fe^{3+}$. The anomaly noticed at the higher temperatures in the ceric and aqueous benzene systems is interpreted as evidence of onset of oxidizing action of HO_2. Adverse consequences of this study for the diffusion theory of radiolysis are discussed.

Introduction

High yields of 10 and 33.7 at 200 and 220°, respectively, reported[1,2] for phenol formation in the γ radiolysis of the aqueous benzene system indicate a possible temperature dependence for the primary yield of hydroxyl radicals. In continuation of earlier work,[3,4] temperature effects in the radiolysis of the aqueous benzene, ferrous, and ceric systems have been studied in this context. The work reveals complexities of mechanism in all of the three systems and attempts to explain them.

Experimental Section

Materials. In addition to the reagents and solvents described earlier,[4] a sample of spectroscopically pure ceric oxide supplied by the Chemistry Division of the Bhabha Atomic Research Center, Bombay, was used to make solutions of ceric sulfate by leaching with hot concentrated sulfuric acid. The 10^{-3} M ceric solutions were preirradiated to a dose which reduced half the ceric ion into cerous.

Procedures. A ^{60}Co γ source of 500 Ci was used, at 3×10^{16} eV g^{-1} min^{-1}, for the irradiations. In the range 0–70° the samples were irradiated in test tubes dipping in water held at the required temperature in a thermosflask closed with a plastic cap. At 70° the cooling in 1 hr was 3–5°. In long irradiations with the aqueous benzene system the temperature of the water was restored every 50 min when the sample was taken out to shake to make up for depletion of oxygen. For irradiations in the range 80–225° a furnace was used. The 4-cm^3 samples of solution were sealed in Pyrex tubes of 1-cm diameter and positioned reproducibly inside the furnace. When the samples attained the temperature of the furnace the chamber was lowered into the source. The variation of temperature in these runs was within 3°. The sample tubes were sufficiently small to hold the pressure of 25 atm developed at 225°. Details of the analytical procedures used have been described earlier.[4]

Results and Discussion

The Hydroxyl Yield as a Function of Temperature. The aerated ferrous sulfate and the ceric sulfate dosimetric systems are known to show a small temperature coefficient, positive and negative, respectively, in their yields over the range 0–60°.[5–8] These observations were repeated here. The results are described in Figure 1. They were obtained by comparing groups of spectrophotometric curves representing runs at different temperatures conducted using an identical experimental setup and obtained within a period of 3 hr. By this procedure the error in G values was reduced to less than ±1%. Samples irradiated at temperatures above 27° need to be run against blank solution heated identically. In particular, we observed thermal oxidation of aerated ferrous ammonium sulfate solutions (10^{-3} M in 0.8 N H_2SO_4) even at 50°. Correction for this effect reduces the G in many cases. For the ceric sulfate system a zero-order heterogeneous reduction

(1) M. A. Proskurnin and Y. M. Kolotyrkin, *Proc. Int. Conf. Peaceful Uses At. Energy*, **29**, 58 (1958).

(2) H. C. Christensen, *Aktiebolaget Atomenergi Stockholm, AE* **193**, 10 (1965); *Chem. Abstr.*, **63**, 10896g (1965).

(3) T. K. K. Srinivasan, I. Balakrishnan, and M. P. Reddy, *J. Phys. Chem.*, **73**, 2071 (1969).

(4) I. Balakrishnan and M. P. Reddy, *ibid.*, **74**, 850 (1970).

(5) T. J. Hardwick, *Can. J. Chem.*, **30**, 33 (1952); **31**, 881 (1953).

(6) H. A. Schwarz, *J. Amer. Chem. Soc.*, **76**, 1587 (1954).

(7) H. A. Dewhurst, Ph.D. Thesis, McGill University, Montreal, Quebec, 1949.

(8) C. J. Hochanadel and J. A. Ghormley, *Radiat. Res.*, **16**, 653 (1962).

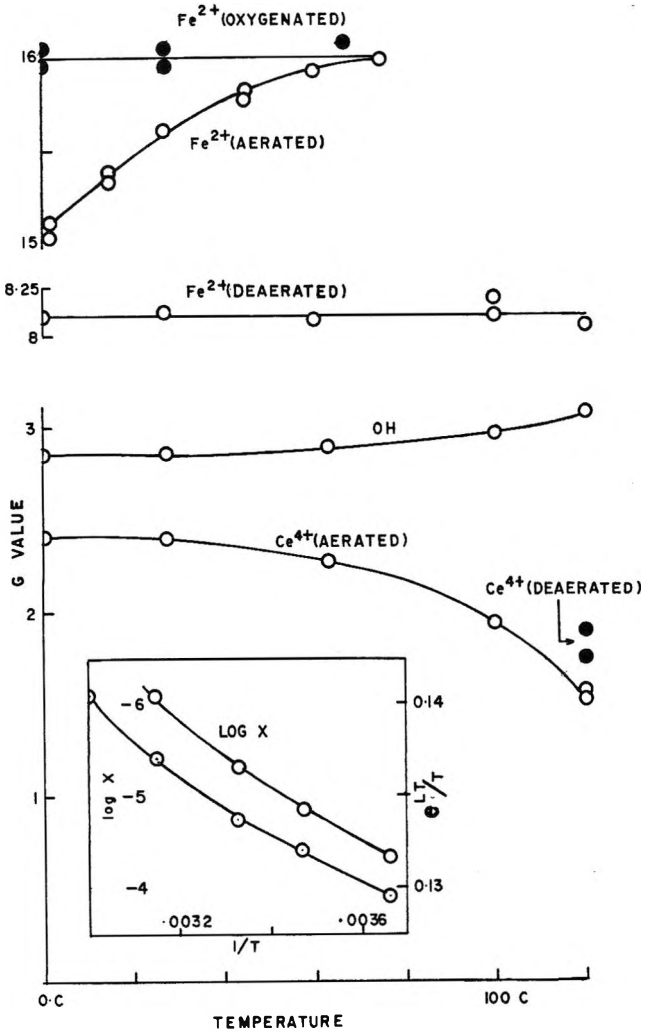

Figure 1. Temperature effect in three aqueous inorganic systems; 10^{-3} M $FeSO_4$, chloride excluded; 3×10^{-4} M $Ce(SO_4)_2$. Compare G(OH) curve here (0.8 N H_2SO_4) with the one in Figure 4 (neutral aqueous solution).

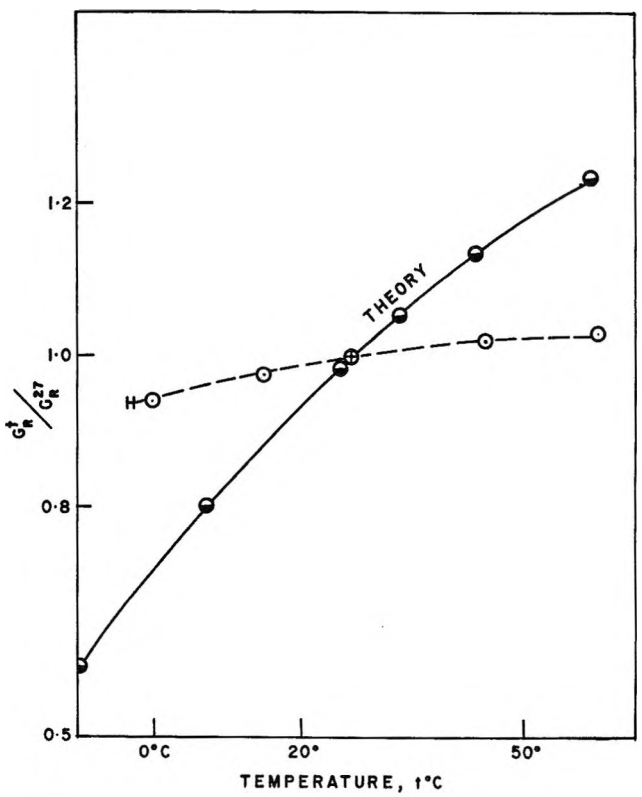

Figure 2. Variation in G_R with temperature expected on the basis of the prescribed diffusion model.[9] Companion curve describes "supposed" variation in G(H) calculated from the aerated ferrous system (Figure 1).

reaction with a rate proportional to the area of glass surface in contact with the solution was observed above 60° and an appropriate correction was applied.

There appears to be a possibility of explaining these temperature coefficients, positive and negative, in terms of an increase in the primary yields of radicals caused by an increase in the diffusion coefficient with temperature. This requirement as predicted by the one radical prescribed diffusion model of Samuel and Magee[9] is described in Figure 2. The companion curve in the figure is what one gets for a supposed variation of G(H) with temperature on this model if the temperature effect in the Fricke system is attributed to enhanced diffusion of the hydrogen atoms from the spurs. Clearly the effect is far too little. One naturally looks for other plausible causes, one of which is considered in detail in the last section of this discussion, but first the question of the possible validity of this idea for the hydroxyl radical is considered. If the G(H) is essentially independent of temperature, any increase in G(OH) at the expense of $G(H_2O_2)$ ought to decrease the $G(-Ce^{4+})$ in the ceric system. This is qualitatively the behavior of the system as described by earlier workers.[5-8] However, in this case again the observed effect is much smaller than what is required by Figure 2. Impurities in the ceric system reacting with hydroxyl radicals could account for the low temperature coefficient. Acting on this supposition we purified several samples of ceric salts by repeated precipitation with ammonia as well as by hydrolysis with triply distilled water and heating the precipitate with sulfuric acid. In all cases purification resulted in a decrease of $G(-Ce^{4+})$ from ~2.6 to ~2.5 and a perceptible diminution of the temperature coefficient. Ultimately a sample of spectroscopically pure ceric oxide was tried and gave the distinct result that $G(-Ce^{4+})$ is actually constant from 0 to 30°, at 2.40 ± 0.05. There is no systematic decrease in G with temperature in this theoretically crucial region.

The deaerated ferrous system was the next to be studied. The $G(Fe^{3+})$ here was found to be constant at 8.1 ± 0.05 from 0 to 120°. (Careful degassing, after thawing and freezing the solution four times, is absolutely essential.) From these two results it follows rigorously that G(OH) in the radiolysis of water is in-

(9) A. H. Samuel and J. L. Magee, *J. Chem. Phys.*, 21, 1080 (1953).

dependent of temperature from 0 to 30° at least. Results for the higher temperature region are discussed in the last section.

The Effect of Temperature on the γ Radiolysis of Aqueous Benzene. An earlier study of this system[4] reported formation of phenol and β-hydroxymucondialdehyde (β-HMD) from an attack of the hydroxyl radical upon benzene. The appearance, in neutral solutions, of an absorption peak at 345 mμ was taken as a measure of the aldehyde. On the assumption of an extinction coefficient of 4080 for this peak the yields of phenol and the aldehyde together gave a value of 2.45, which is the G(OH) for neutral water at room temperature.

In the present study neutral aqueous benzene was first irradiated at 0° and the 345-mμ absorption was found to be only a fourth of its value in the room temperature radiolysis while the G(phenol) of 1.62 was only slightly less than the room temperature value of 1.77. With the knowledge that the G(OH) is independent of temperature at least from 0 to 30° it became evident that there must be a third compound formed from the reaction of OH with benzene. The spectrum of the aqueous layer from the radiolysis at 0° does show an abnormally large absorption at 270 mμ. Upon adjusting pH to 7 by adding alkali, a peak appears at 270 mμ which grows considerably upon further increase in pH while the peak at 345 mμ remains small and tends to become a shoulder on the 270-mμ peak (see Figure 3). The precipitate of dinitrophenylhydrazone yields a G(aldehyde) of 0.84 on a molecular weight of 666 (hydroxymucondialdehyde), as against a value of 0.68 for the radiolysis at 27°. The sum of the yields of phenol and aldehyde, 2.46 (= 1.62 + 0.84), is again clearly equal to G(OH). The infrared spectrum[3] of the 0° hydrazone has no OH absorption. Thus it is clear that the two aldehydes are the α and β isomers of hydroxymucondialdehyde. They are not interconvertible by heat in acid or alkaline solution. As the temperature of the radiolysis is raised the total yield of aldehyde drops but the proportion of the isomer with the 345 mμ increases. The G(aldehyde) is 0.68 at 60° and the alkali sensitivity of the 270-mμ peak is greatly reduced, indicating a drop in the proportion of the second isomer. Figure 3 describes all of these features.

The Identity of the Two Isomeric Aldehydes. The hydrazone method gives accurate values for the total aldehyde yield. Using these and the spectrum of the aqueous layers from a large number of irradiations at 0, 27, and 60° the identity of the two isomers could be determined. If the yield of 0.84 at 0° were to be attributed entirely to one isomer it can be deduced that $\epsilon_{270\ m\mu}$ of this compound cannot be greater than 4600. Likewise, if the total yield of 0.68 at 60° is entirely due to the other isomer it can be shown from the spectra that the $\epsilon_{345\ m\mu}$ cannot be less than 12,000. Thus there is the required difference of one order of magnitude between the two values. In accordance with observation and theoretical requirement (described in item 9 of ref 3 and Figure 5 of ref 4) it is now evident that the 345-mμ peak belongs to the α isomer and the 270-mμ one to β-HMD. An equation in the two unknown extinction coefficients could be set up and solved using the G values and the absorbance values at 270 and 345 mμ for the radiolyses at 0 and 27°. The limits quoted above act as a check and help to determine the extent to which the α compound contributes to the absorption at 270 mμ. The conclusions from these calculations are as follows.

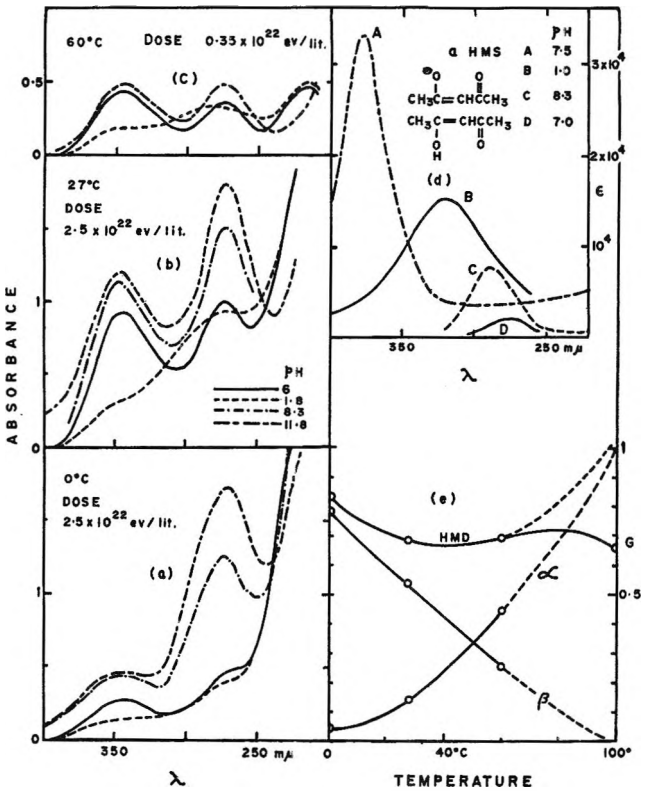

Figure 3. a, b, and c, Uv spectra of aqueous layer from irradiated benzene solutions. ~2×10^{-2} M C_6H_6, neutral water, air saturated. (Spectra for irradiations above 60° are highly erratic; above 150° the 345-mμ peak is replaced by a broad band at 250 mμ, obtainable also by heating to 150° solutions irradiated at room temperature. Oxidation of HMD by H_2O_2 is indicated.) d, A, B, α-hydroxymuconic semialdehyde;[4] C, D, acetyl acetone.[10] e, Variation of α and β isomers with temperature of radiolysis.

1. $\epsilon_{270\ m\mu}$ of β-HMD at a pH of 12 is 4200 ± 100. $\epsilon_{345\ m\mu}$ of α-HMD is 19,000 ± 1000; pH 11–13 is a buffer range for both peaks. It is best to secure this with sodium hydroxide solutions made with carbonate-free water. The $\epsilon_{345\ m\mu}$ value of 4080 submitted in ref 4 is hereby withdrawn. The PNDC method of estimating the aldehyde described there is valid, but the $\epsilon_{370\ m\mu}$ of 7850 applies only to the dye of the particular mixture of α- and β-HMD which is formed at room temperature. Also valid is the ratio of ~5 for the G values in the presence and absence of 1 mM ferrous ion obtained for

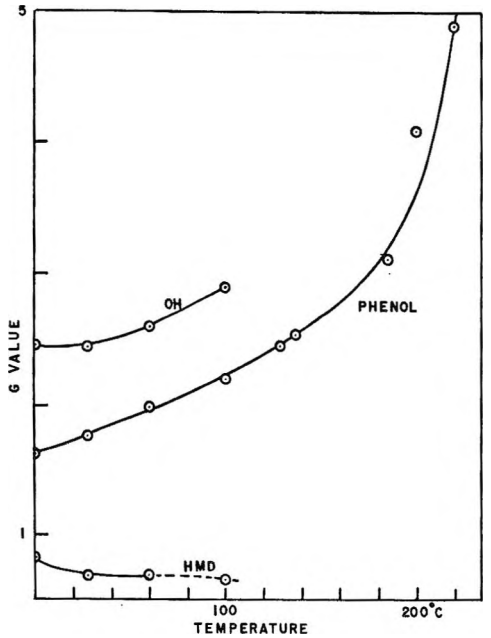

Figure 4. Variation of phenol and HMD in the radiolysis of aqueous benzene at different temperatures. (G(phenol) at 220° is ~5. Thus Proskurnin's[1] value of 33.7 for 220° must come largely from reactions other than the radiation chemistry of water, perhaps peroxide chain mechanisms operative in the gas phase at the high oxygen pressure used by him.)

phenol as well as the aldehyde. Study of the ferrous ion effect repeated for the 0° case yields the same result.

2. α-HMD has a second absorption maximum at 270 mμ of the same intensity as the first at 345 mμ in alkaline solutions. β-HMD has no maximum at 345 mμ but a tail significant only at high concentrations.

3. The enolization of α-HMD appears to be complete at pH ~5 as shown by the appearance of the two-peak spectrum in near full strength. The β-HMD in contrast appears to enolize over the broad range of pH from 7 to 11. The latter is similar to acetyl acetone[10] in this behavior as well as in its extinction coefficient (see part d of Figure 3).

4. In neutral solutions of benzene linearity of yields of phenol and aldehyde is obtained up to a very high dose. Accurate estimates of the extinction coefficients were possible only with solutions irradiated to a dose superior to 10^{22} eV/l. The pH behavior of the spectrum for low doses is anomalous, perhaps because of a relatively larger proportion of hydrogen peroxide among the products.

Mechanism. The fact of formation of the two isomers of HMD can be deduced without doing violence to the mechanism presented earlier.[3,4] In the reaction scheme drawn up in ref 4 the ortho isomer of the hydroxy peroxy radical was depicted as giving phenol exclusively. If an attack of the peroxide radical on the adjacent double bond is visualized for this entity, α-HMD would result exactly like the β isomer and Scheme I would become symmetric.

Scheme I

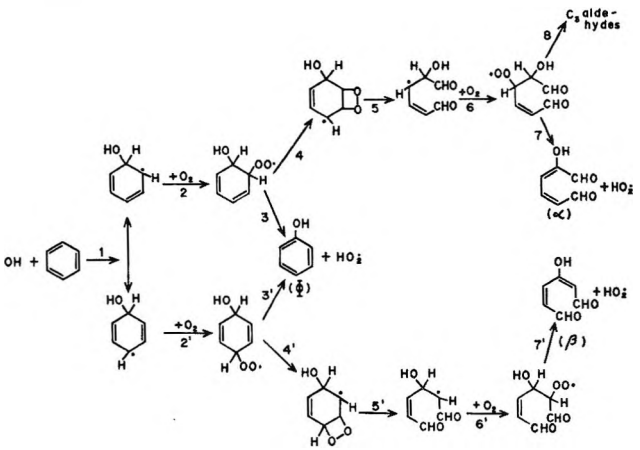

Scheme I yields a convincing explanation for the observed effect of temperature upon the ratio of the products ϕ, α and β (see part e of Figure 3). Speculation regarding the activation energy of the reactions of Scheme I indicates the following trends: reaction 4 involves disturbance of conjugated unsaturation. Hence it is easy to see that $E_4 > E_3$, whereas $E_{3'}$ is likely to be larger than $E_{4'}$ because of the large amount of steric energy required in reaction 3′ in reaching across the ring to the para position. Hence at low temperature one would expect phenol and β-HMD to be the major products. As the temperature is raised, reactions 3′ and 4 are favored with consequent replacement of β-HMD by phenol and the latter in turn by α-HMD. Thus there is no direct competition between α and β but through phenol. This is in agreement with the observations (see part e of Figure 3). In reaction 5 a shift in the radical site has been indicated. Conjugation between the carbonyl and the adjacent double bond would require such a shift.

At the high-temperature end, reaction 8 leading to fragmentation of the carbon skeleton should set in and reduce the yield of HMD. This again accords with observation. At 100° G(aldehyde) is 0.66 by the hydrazone method (see Figure 4) but the behavior of the uv spectrum of the aqueous layer for runs above 60° is erratic, indicating likely presence of several aldehydes which are products of such fragmentation.

Photolysis of the aqueous benzene–hydrogen peroxide system reveals the formation of hydroxy mucondialdehyde and phenol in a ratio similar to that in the radiolysis, providing support for the mechanism of reaction of OH with benzene advanced here. Details of this study will appear in a later publication.

The Higher Temperature Range. Even from ~50° there is a large increase in the yield of phenol while the aldehyde yield is nearly constant (Figure 4). This is not due to any secondary reactions between the first products, brought about by the high temperature. Samples irradiated at room temperature and subse-

(10) F. Cramer, *Chem. Ber.*, 86, 1577 (1953).

quently kept at 120° for 2 hr show the same G(phenol). Also, the effect is not due to any thermal reaction between benzene and hydrogen peroxide decomposing slowly at 120°. Solutions of hydrogen peroxide containing benzene yield no phenol or aldehyde when heated at 120° for several hours. It is clear from this that hydrogen peroxide decomposing at 120° does not yield hydroxyl radicals or atomic oxygen. A plausible explanation for the increase in G(phenol) in the radiolyses above ~50° is the possible onset of the reaction well known in high-temperature chemistry,[11] $H + O_2 \rightarrow OH + O$, which would also explain the disproportionately large increase in the yield of phenol. Oxygen atoms are known to react with benzene to give phenol.[12] Evidence for the possible occurrence of the above reaction obtained in the ceric system will be discussed in the last section where we return to a consideration of the inorganic systems again. More probably, in both cases what is causing the abnormality (which one does not see in the deaerated ferrous system) is not a change in the nature of the reaction between H atoms and O_2 but the onset of the oxidizing tendency of HO_2; thus

$$C_6H_6 + HO_2 \longrightarrow C_6H_5OH + OH$$

$$Ce^{3+} + HO_2 \longrightarrow Ce^{4+} + OH^- + O$$

However, at this stage, no definite choice between these alternatives is possible.

Temperature Coefficient of the Fricke and Ceric Systems. If, as shown above, G(OH) is independent of temperature from 0 to 30° and so is $G(Fe^{3+})$ in the deaerated ferrous system, it is highly unlikely that G(H) is temperature dependent. Thus the small temperature coefficient observed in the Fricke system must be due to other reagents in the system competing with oxygen for the hydrogen atoms. The two obvious candidates, Fe^{2+} and Fe^{3+}, have been proved to be incapable of producing any measurable direct competition in 10^{-3} M ferrous solutions in 0.8 N H_2SO_4 containing only traces of ferric at the start,[13-15] even up to a dose of ~4×10^{21} eV/l. The first of these three studies[13] revealed that a sudden jump in $G(Fe^{3+})$ from 8.2 to 14.8 occurs even when an extremely low concentration (~1.2×10^{-5} M) of oxygen is introduced into deaerated 10^{-3} M ferrous sulfate solution in 0.8 N H_2SO_4, and it appeared as if the normal $G(Fe^{3+})$ of 15.6 represents a plateau value corresponding to complete supression by oxygen of all other reactions that could involve H atoms.

Being obliged to find an explanation for the temperature coefficient in terms of yet another entity competing for H, we worked on the assumption that the rate constant for the reaction forming the hydrogen molecule ion might, after all, be high enough to enable protons to compete with oxygen for the H atoms and that the resulting hydrogen molecule ion might conceivably react slower with oxygen molecules than does the H atom, thus giving a fair chance to the ferrous ion to compete. With this idea in mind, we extended Allen's study[16] by oxygenating the Fricke system at 10^{-3} M ferrous concentration in 0.8 N H_2SO_4, thus raising the oxygen concentration by a factor of ~5. Two striking results ensued (see Figure 1). The $G(Fe^{3+})$ shot up and the temperature coefficient vanished, an identical value of ~16 being obtained at 0, 27, and 60°. Evidently, therefore, the competition for H atoms is twofold. The first, Allen's reaction 5 in the scheme given below, is largely suppressed by oxygen even at 10^{-5} M. The second is an indirect ferrous ion effect acting through H_2^+ which needs a significantly higher concentration of oxygen for its suppression and occurs appreciably even in the air-saturated system. Equation (h) of Allen's study[13] deals only with the first of these and is hence incomplete. We believe the following scheme, retaining Allen's numbering,[13,14] is a genuine description of these complications.

$$H_2O \rightsquigarrow H, OH, H_2, H_2O_2 \qquad (0)$$

$$2Fe^{2+} + H_2O_2 \longrightarrow 2Fe^{3+} + 2OH^- \qquad (1)$$

$$OH + Fe^{2+} \longrightarrow Fe^{3+} + OH^- \qquad (2)$$

$$H + O_2 \longrightarrow HO_2 \qquad (3)$$

$$HO_2 + H^+ + Fe^{2+} \longrightarrow Fe^{3+} + H_2O_2 \qquad (4)$$

$$H^+ + H + Fe^{2+} \longrightarrow Fe^{3+} + H_2 \qquad (5)$$

$$H + Fe^{3+} \longrightarrow Fe^{2+} + H^+ \qquad (6)$$

$$H + H^+ \longrightarrow H_2^+ \qquad (4')$$

$$H_2^+ + O_2 \longrightarrow HO_2 + H^+ \qquad (3')$$

$$H_2^+ + Fe^{2+} \longrightarrow H_2 + Fe^{3+} \qquad (5')$$

Reactions 3′ and 5′ are given without numbers and are recognized as highly plausible in the third[15] of the Allen–Rothschild papers. Ignoring reactions 5 and 6 completely, the stationary-state treatment applied to this scheme can be made to yield, with some algebraic manipulation, the equivalent of Allen's expression (h)

$$G(Fe^{3+}) = 2G(H_2O_2) + G(OH) + G(H) + 2G(H) \times \left\{ \frac{1}{1 + \frac{k_{4'}(H^+)}{k_3(O_2)}} + \frac{1}{\left(1 + \frac{k_3(O_2)}{k_{4'}(H^+)}\right)\left(1 + \frac{k_{5'}(Fe^{2+})}{k_{3'}(O_2)}\right)} \right\}$$

or

(11) M. Venugcpalan and R. A. Jones, "Chemistry of Dissociated Water Vapor and Related Systems," Interscience, New York, N. Y., 1968, pp 350–352, 371, 372.

(12) L. I. Avramenko, I. I. Ioffe, and R. V. Lorentso, *Dokl. Akad. Nauk SSSR*, 66, 1111 (1949).

(13) A. O. Allen and W. G. Rothschild, *Radiat. Res.*, 7, 591 (1957).

(14) A. O. Allen, V. D. Hogan, and W. G. Rothschild, *ibid.*, 7, 603 (1957).

(15) A. O. Allen and W. G. Rothschild, *ibid.*, 8, 101 (1958).

$$G(Fe^{3+}) = G_d + 2G(H) \times \left\{ \frac{1}{1 + \frac{k_{4'}(H^+)}{k_3(O_2)}} + \frac{1}{\left(1 + \frac{k_3(O_2)}{k_{4'}(H^+)}\right)\left(1 + \frac{k_{5'}(Fe^{2+})}{k_{3'}(O_2)}\right)} \right\} \quad (I)$$

or

$$G(Fe^{3+}) = G_d + 2G(H) \times \left\{ 1 - \frac{1}{1 + \frac{k_3(O_2)}{k_{4'}(H^+)} + \frac{k_{3'}(O_2)}{k_{5'}(Fe^{2+})} + \frac{k_3 k_{3'}(O_2)^2}{k_{4'}k_{5'}(H^+)(Fe^{2+})}} \right\} \quad (II)$$

where G_d is the ferric yield in the deaerated ferrous system.

Putting $k_{4'}(H^+)/k_3(O_2) = x$, dealing with expression I, it is easy to see that as (O_2) increases the first term in parentheses rapidly shoots up from zero and tends to $1 - x$, while the second, very much smaller in magnitude, gradually rises from zero and tends to x (with x itself decreasing in the process), so that the value of the factor in parentheses tends from zero to a limit equal to unity. Most regrettably, we are obliged to stop on this qualitative note because no reliable values for the rate constants $k_{3'}$, $k_{4'}$, or $k_{5'}$ are available. Nevertheless, the following conclusions appear to be reasonable.

1. The highest value of $k_{4'}$ reported so far,[16,17] $\sim 10^5$, is too small, at least to one order of magnitude. The value of 10^5 for air-saturated solutions makes the first term in parentheses in expression I differ from unity only in the third decimal place whereas the experimental saturation value of ~ 16 requires this difference to be about five times as much; 10^6 to 5×10^6 would be an acceptable value for $k_{4'}$.

2. The $G(H)$ of 3.7 accepted now for 0.8 N H_2SO_4 solutions is low by at least 0.2. The oxygenated ferrous system gives $G(H) = (16 - 8.1)/2 = 3.95$. The value, of course, is temperature independent.

3. The second factor of the second term in parentheses in expression I represents the competition between reactions 3′ and 5′ and is responsible for the temperature coefficient. It prevents the second term in parentheses from attaining the limiting value of x. Thus the value of the factor in parentheses falls short of the limit of unity. As the radiolysis temperature is raised $k_{5'}$ is exclusively lowered because of the decrease in the dielectric constant of water with temperature ((5′) is a reaction between two species carrying like charges whereas in (3′) only one carries a charge). The following qualitative demonstration of this phenomenon is possible.

It is easy to see that in expression II the last term in the denominator within the factor in large brackets is larger than any of the others by one or possibly two orders of magnitude. So, to a crude approximation, (II) reduces to

$$\frac{(H^+)(Fe^{2+})}{(O_2)^2}\left\{\frac{G(Fe^{3+}) - G_d}{G_d + 2G(H) - G(Fe^{3+})}\right\} \approx \frac{k_3 k_{3'}}{k_{4'}k_{5'}} \quad (III)$$

Using the symbol X for the left-hand expression one may write

$$\log X \approx \log \frac{k_3 k_{3'}}{k_{4'}} - \log Z_{5'} + \frac{E_{5'}}{2.3RT} + \frac{2\epsilon^2}{2.3rDkT} \quad (IV)$$

in which one recognizes at once the application of Moelwyn-Hughes' treatment.[18] The dielectric constant D itself can be expressed as an exponential function of the temperature

$$D = Ce^{-LT} \quad (V)$$

so that $\log X$ values plotted against $1/T$ ought to give not the customary straight line but a graph with an exponential curvature to it. This can be briefly seen in the inset in Figure 1, which includes a plot of the function e^{LT}/T against $1/T$ taking the L value to be 0.00463, *i.e.*, the value for water, in expression V for the dielectric constant. The similarity of form of the two curves clearly shows that there is negligible contribution to $\log X$ from the third term, which would require it to be a straight line with a positive slope. We may conclude that the conventional nonelectrostatic activation energy $E_{5'}$ is negligible for reaction 5′. Perhaps $E_{3'} \approx E_{4'}$, and since E_3 is negligible, the fourth term determines the dependence of $\log X$ on $1/T$.

4. If we set the first three terms in expression IV to be equal to zero (this amounts to the pretence that $k_{3'}$ and $k_{4'}$ are identical and so also k_3 and $k_{5'}$ except for the $P_{5'}$ factor represented by the fourth term), then the room temperature value of X yields a "respectable" figure of 1.2 Å for the critical interionic separation, r. (See ref 18, p 94, Table 2.)

5. For room temperature values, for a $G(H)$ of 3.9 expression III yields an approximate value of 1.64×10^5 for the ratio $k_3 k_{3'}/k_{4'}k_{5'}$. Assuming the numerator to be $\sim 2 \times 10^{20}$ one concludes that $k_{4'}$ $k_{5'}$ could be as high as 10^{15} in conformity with what was said in item 1 of the conclusions.

The Ceric System at High Temperatures. By far the most surprising result obtained in this study is the fact that $G(-Ce^{4+})$ distinctly constant from 0 to 30° drops by a measurable amount even at 45° and at 120° reaches a value as low as 1.5. A limited number of runs with the deaerated system gave measurably higher values. This may be taken to indicate possible onset

(16) J. Jortner and G. Stein, *J. Phys. Chem.*, 66, 1264 (1962).

(17) K. L. Huang and L. T. Bugaenko, *Russ. J. Inorg. Chem.*, 10, 401 (1965).

(18) E. A. Moelwyn-Hughes, "Kinetics of Reactions in Solution," Oxford University Press, London, 1947, p 106 and Chapter IV.

of an oxidizing action of HO_2 upon the cerous ion. O_2 being a product of the radiolysis in this system, one cannot hope to restore the normal value of 2.4 by working with deaerated solutions. As described earlier, there is evidence of disturbance of a similar nature in the aqueous benzene system as well, even at ~50°.

The Temperature Effect in Relation to the Spur Diffusion Model. Figure 2, describing the variation expected in the radical yield in water on the basis of the one radical "prescribed diffusion" model, was obtained using Tables I and II of the Magee–Samuel paper[9] after calculating values at various temperatures for their parameter x which contains the diffusion coefficient for the radical in water. The variation of the latter with temperature is obtained from Einstein's formula, $D = kT/6\pi\eta r$. Actually, only ratios of diffusion coefficients are required so that the effective radius of the radical, r, gets canceled.

The variation expected in G_R in the crucial region 0–30° is quite large, whereas we can now say with certainty that all the primary yields are independent of temperature at least in this region and most probably even beyond 100°. We are at a loss to find any procedure whereby such a diffusion model can be retained in spite of this result.

There appears to be a remote possibility that a decrease in dielectric constant of the medium has the consequence of lowering r_0' as the temperature is increased. If this is able to compensate for the rise in L (*cf.* eq 5 and 6 of ref 9), then x, and hence the yields, could still be insensitive to variation of temperature. Equation 29 of ref 9 may be examined. It is more likely, however, that the primary molecular products are actually the result of separate molecular reactions involving excited or ionized water molecules.

Acknowledgment. The authors are grateful to Dr. G. S. Murthy, who was their colleague here during the period of this investigation, for many useful suggestions and to Dr. H. B. Mathur for procuring a sample of spectroscopically pure ceric oxide without which this work could not be completed.

Pulse Radiolysis of Dioxane and Dioxane + Water Mixtures. The Yield of Free Solvated Electrons and Kinetics of the Radical Reactions

by Shamim A. Chaudhri[1]

Hahn-Meitner-Institut für Kernforschung Berlin GmbH, Sektor Strahlenchemie, 1 Berlin 39, Germany
(Received July 14, 1971)

Publication costs assisted by the Hahn-Meitner-Institut für Kernforschung

The yield of the solvated electrons in pure dioxane which escape geminate recombination with the positive ions has been determined to be 0.19. The dioxane radical reduces tetranitromethane to nitroform anion, $C(NO_2)_3^-$, through an electron transfer process. The kinetic data support a reaction mechanism involving an "intermediate complex" in equilibrium with the reactants. Both the equilibrium constant K and first-order rate constant k of decomposition of the complex were calculated. K and k were found to decrease with decreasing water contents of dioxane–water mixtures. The equivalent conductivity of the ion pair, $C(NO_2)_3^- + H_{solv}^+$ over a whole range of dioxane–water compositions has been measured. From extrapolations a value of 5 ohm^{-1} cm^2 equiv^{-1} for $\Lambda_{(C(NO_3)_2^- + H_{solv}^+}$ in pure dioxane was obtained.

Introduction

The γ radiolysis of dioxane and of dioxane–water mixtures has been extensively studied,[2-5] particularly with regard to the yield of hydrogen and the influence of scavengers on this yield. The reported values for the yield of the solvated electron are at a great variance with one another. Baxendale, *et al.*,[4] measured $G(H_2)$ in pure dioxane and in that containing 2.2 M water plus 20 mM HCl. They found an increase in $G(H_2)$ from 1.26 to 3.5 and derived from this a yield for e_{solv}^- of 2.2/100 eV. However, in their later work[6] on excited states produced in dioxane, they concluded that

(1) Postdoctoral fellow from the Pakistan Atomic Energy Commission, Karachi, with a grant from the Alexander von Humboldt-Stiftung, Bad Godesberg, Germany.

(2) Y. Llabador and J. P. Adolff, *J. Chim. Phys.*, **61**, 681 (1964).

(3) (a) E. A. Rojo and R. R. Hentz, *J. Phys. Chem.*, **69**, 3024 (1965); (b) R. R. Hentz, F. W. Mellows, and W. V. Sherman, *ibid.*, **71**, 3365 (1967).

1.05 H_2 molecules/100 eV might arise from a reaction of HCl with excited dioxane molecules. Hentz, *et al.*,[3b,5] estimated a "limiting" value of the yield of solvated electrons of 3.1–3.4. Since they used relatively high scavenger concentrations, a strong interference with geminate recombination processes occurred which is evidenced by the fact that the G value still increased at N_2O concentrations above 10^{-2} M.

Several experiments led to a G value of the free solvated electron which is much lower than unity. From pulse radiolysis studies[6,7] using electron scavengers such as anthracene and benzophenone, Baxendale, *et al.*, found G(anion) $\approx$ 0.1. The measurement by the clearing field technique gave a value of 0.04.[8]

Tetranitromethane (TNM) is an efficient scavenger of solvated electrons and produces the anion $C(NO_2)_3^-$ according to

$$C(NO_2)_4 + e_{sol}^- \longrightarrow C(NO_2)_3^- + NO_2 \qquad (1)$$

The yield of this anion which is stable and has a strong absorption near 350 mμ can readily be measured. It is the base form of nitroform

$$C(NO_2)_3H \rightleftharpoons C(NO_2)_3^- + H^+ \qquad (2)$$

which is fairly dissociated even in polar organic solvents. As has been shown earlier, the rate of neutralization (*i.e.*, of the back reaction of eq 2) can be measured in organic solvents.[9] While the solvated electron generally reacts very fast with tetranitromethane, the electron transfer from organic radicals to TNM is slower. The present work was carried out in order to determine the yield of the free solvated electron in dioxane, to obtain information about electrical conductivities of ions in dioxane, and to investigate the dependence of the rate of the electron transfer reaction between a dioxane radical and TNM on the composition of dioxane–water mixture.

Experimental Section

Materials. Dioxane (Merck "pro analysis") was treated with activated alumina (Al_2O_3W 200, Woelm, Germany) and then refluxed with Na for 15 hr under a constant flow of very pure dry argon (Linde "reinst"). It was then distilled twice under argon, the middle fraction collected each time.

For experiments on the dioxane mixtures with water no significant difference in the results was found when dioxane "pro analysis" grade was used directly without further distillation. Triply distilled water was used for these experiments.

Tetranitromethane (Fluka purissimum p.a.) was washed repeatedly with triply distilled water immediately before use. The samples (0.5–1 l.) were bubbled with pure argon for about 1 hr before the addition of solutes. The experiments were carried out at 18°.

Equipment. The pulse irradiation was done with a 1.5-MeV Van de Graaff (10 mA) accelerator. The optical setup, the conductivity cell, the flow system, and the associated electronic equipment have been described elsewhere.[10,11]

Dosimetry. The deaerated solutions were irradiated with pulses of 0.3–2 μsec duration and the absorbed dose (0.2–2 krads) was monitored with a secondary emission foil. Absolute dosimetry was based on the simultaneous optical and conductivity measurements of $(C(NO_2)_3^-$ ions, (ϵ_{350nm} = 1.5 $\times$ 10^4 M^{-1} cm^{-1}) in pulse-irradiated aqueous solutions of 10^{-3} M $C(NO_2)_4$ and 10^{-1} M 2-propanol,[12] ($G(C(NO_2)_3^-) = G_{e_{aq}^-} + G_H + G_{OH} = 6$). Appropriate corrections were made for the difference in electron density of the solutions. To minimize photolysis a filter, BG 12, Schott, was used which cut off light below 300 nm.

Spectrum and Extinction Coefficient of $C(NO_2)_3^-$ in Dioxane and Dioxane + Water Mixtures. Solutions of $C(NO_2)_3K$ in dioxane and dioxane + water mixtures showed an absorption maximum at 350 $\pm$ 2 nm, similar to that in water. The ratio of the extinction coefficients of $C(NO_2)_3^-$ in these media to that in water was very close to unity, and ϵ was estimated to be 1.48 $\pm$ 0.04 $\times$ 10^4 M^{-1} cm^{-1}. This agrees with our earlier results in alcohols[9a] and acetone[9b] which showed that medium has virtually no effect on the absorption spectrum and the extinction coefficient of the nitroform anion.

Results and Discussion

Pure Dioxane. Figure 1a shows the optical absorption at 350 mμ as a function of time for a pulsed 10^{-3} M TNM solution in pure dioxane. Since reaction 1 occurs during the pulse, the absorption of $C(NO_2)_3^-$ formed appears immediately after the pulse. The absorption decreases by about 20% after the pulse with $\tau_{1/2}$ = 20 μsec which is due to the partial neutralization of $C(NO_2)_3^-$ ions until the equilibrium of eq 2 is reached. Figure 1b shows an oscilloscope trace for a solution containing 8 $\times$ 10^{-5} M NaOH. No decay of the absorption occurs after the pulse which indicates that the equilibrium of eq 2 is completely shifted toward the right-hand side. $G(C(NO_2)_3^-)$ was found to be 0.19 $\pm$ 0.01 from the absorption increase immediately after the pulse (average of 80 measurements). Curve d in

(4) J. H. Baxendale and M. A. J. Rodgers, *Trans. Faraday Soc.*, **63**, 2004 (1967).

(5) R. R. Hentz and W. V. Sherman, *J. Phys. Chem.*, **72**, 2635 (1968).

(6) J. H. Baxendale and M. A. J. Rodgers, *ibid.*, **72**, 3849 (1968).

(7) J. H. Baxendale, E. M. Fielden, and J. P. Keene, *Science*, **148**, 637 (1965).

(8) W. F. Schmidt and A. O. Allen, *J. Phys. Chem.*, **72**, 3730 (1968).

(9) (a) K.-D. Asmus, S. A. Chaudhri, N. B. Nazhat, and W. F. Schmidt, *Trans. Faraday Soc.*, **67**, 2607 (1971); (b) S. A. Chaudhri, and K.-D. Asmus, *J. Phys. Chem.*, **76**, 26 (1972).

(10) A. Henglein, *Allg. Prakt. Chem.*, **17**, 296 (1966).

(11) G. Beck, *Int. J. Radiat. Phys. Chem.*, **1**, 361 (1969).

(12) K.-D. Asmus and A. Henglein, *Ber. Bunsenges. Phys. Chem.*, **68**, 348 (1964).

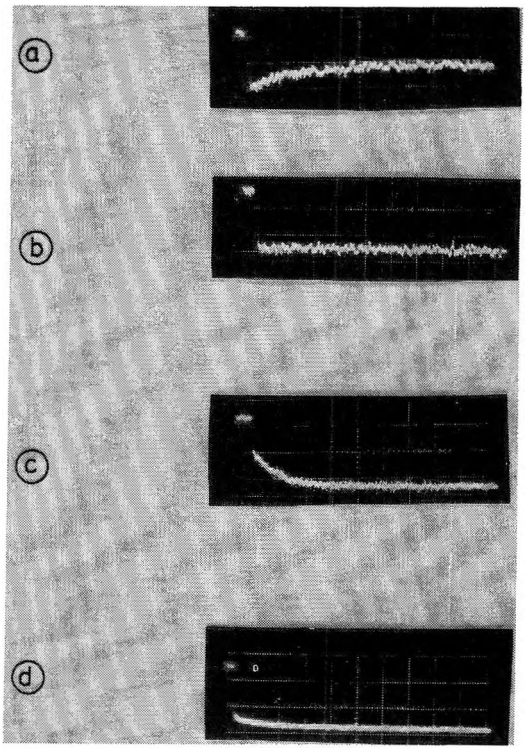

Figure 1. Changes in optical density at 350 nm in pulse-irradiated dioxane and dioxane–water mixtures: a, dioxane; [TNM] = 10^{-3} *M*; pulse dose = *ca.* 2.0 krads, time scale = 20 μsec/div. b, dioxane; [TNM] = 10^{-3} *M*, [NaOH] = 8×10^{-5} *M*; pulse dose = 1.7 krads, time scale = 20 μsec/div; c, dioxane + water (34 mol %); [TNM] = 3.8×10^{-4} *M*; pulse dose = 0.55 krad, time scale = 50 μsec/div; d, dioxane + water (82.5 mol %); [TNM] = 3.4×10^{-4} *M*; pulse dose = 0.24 krad, time scale = 100 μsec/div.

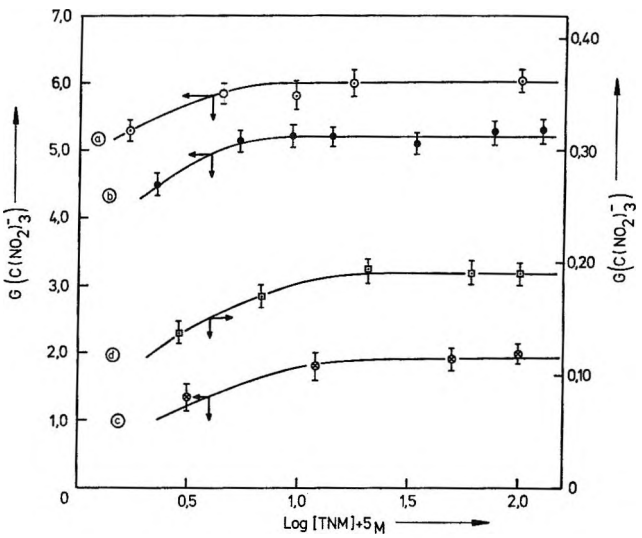

Figure 2. The effect of [TNM] on the total $G(C(NO_2)_3^-)$: a, water containing 10^{-1} *M* dioxane; b, 83 mol % H_2O; c, 34 mol % H_2O in the mixture; d, dioxane.

Figure 2 shows the dependence of $G(C(NO_2)_3^-)$ on the concentration of TNM. $G = 0.19$ is the limiting value reached at TNM concentrations above 10^{-4} *M*. Scavenging of electrons in spurs is not expected to occur in a significant amount at the low concentrations of TNM used in these experiments. The G value of 0.19 is believed to be the yield of the free solvated electron in dioxane. As will be shown later, the reaction of the dioxane radical with TNM is very slow in dioxane solution. It is therefore not expected that any other transient of radiolysis with the exception of e_{aq}^- contributes to the formation of $C(NO_2)_3^-$ during the pulse.

Dioxane–Water Mixtures. Figures 1c and d show oscilloscope traces for the absorption in mixtures of dioxane and water at different time scales. The absorption which is present immediately after the pulse is again attributed to $C(NO_2)_3^-$ resulting from the reaction of eq 1. A second step of $C(NO_2)_3^-$ formation which corresponds to a first-order reaction can be recognized from Figure 1c. This reaction is complete in about 50 μsec. Finally, a slight additional buildup of absorption occurs within several hundred microseconds according to Figure 1d.

The second step is attributed to the reaction of a dioxane radical with TNM. In order to prove that the dioxane radical can transfer an electron to TNM to form $C(NO_2)_3^-$, experiments were carried out with dilute aqueous solutions of dioxane which were saturated with N_2O. In such solutions, e_{aq}^- is converted into OH: $N_2O + e_{aq}^- \xrightarrow{H_2O} N_2 + OH + OH^-$. The OH radicals attack the dioxane (10^{-1} *M*), and the resulting radicals react with TNM. Under these conditions the final absorption amounted to $G(C(NO_2)_3^-) = 6.0$.

The overall yield of $C(NO_2)_3^-$ increased with increasing TNM concentration and rapidly reached a plateau value at [TNM] $\geq 10^{-4}$ *M*. Figure 2 shows the variation of $G(C(NO_2)_3^-)$ with [TNM] for dioxane, for two representative mixtures and for water containing 10^{-1} *M* dioxane. The overall yield decreases with increasing dioxane contents due to the diminishing contribution from the relatively higher yield of reducing species from water.

The kinetics of the reaction between dioxane radical and TNM were studied in detail. The observed first-order rate constant for the second step of $C(NO_2)_3^-$ formation in Figure 1c was less than proportional to the TNM concentration.

The plot of $\tau_{1/2}$ against 1/[TNM] yields a straight line with a positive intercept on the ordinate axis. Figure 3 shows such plots for four dioxane–water mixtures.

A similar kinetic behavior has been observed by Karmann and Henglein[13] for the abstraction of hydrogen atom from H_2S by alcohol radicals. The results were explained by the formation of an intermediate complex in equilibrium with the reactants which then further decomposed into the products.[14] A similar

(13) A. Karmann and A. Henglein, *Ber. Bunsenges. Phys. Chem.*, 4, 421 (1967).

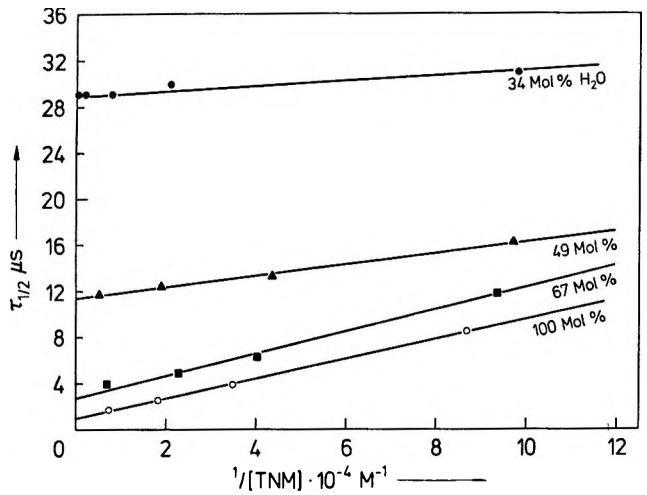

Figure 3. $\tau_{1/2}$ against 1/[TNM] for different dioxane–water mixtures.

mechanism is suggested for the electron transfer reaction between a dioxane radical and TNM

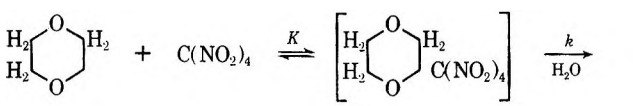

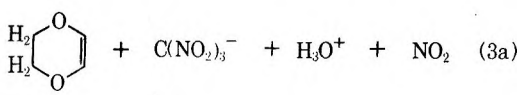

The kinetic treatment[13] leads to the equation

$$\tau_{1/2} = \frac{\ln 2}{k}\left(1 + \frac{K}{[\mathrm{TNM}]}\right) \qquad (3b)$$

where $\tau_{1/2}$ is the observed half-life for the formation of $C(NO_2)_3^-$, K is the equilibrium constant, and k is the first-order rate constant for the decomposition of the intermediate complex into the products. It is assumed that the equilibrium in eq 3a is rapidly established (K is defined as the product of the equilibrium concentrations of the radical and TNM divided by that of the "complex"). The values for k and K were calculated from the intercepts and slopes in Figure 3 using eq 3b. Figure 4 shows a plot of K and k *vs.* the mole % of water in the mixtures.

It can be seen that both the equilibrium constant and the rate constant decrease rapidly with decreasing water contents in the mixture. At lower water contents the equilibrium lies more to the side of the "intermediate complex" but its subsequent decomposition into products is slower. The lower value of k can be explained, if the first step of the decomposition of the complex is the transfer of a proton from the complex to a water molecule.

The third and the slowest step of the buildup of $C(NO_2)_3^-$ absorption in Figure 1d has a half-life ranging from 90 μsec at 85 mole % water to 150 μsec at 45 mole % water. The observed first-order rate constant of this process is independent of TNM concentration and was determined to be (5–8) × 10^3 sec^{-1}. Its order of magnitude agrees with what has been observed for the unimolecular decomposition of nitroform to form $C(NO_2)_3^- + H^+$ according to eq 2 in different polar and nonpolar media.[9] The decrease in half-life with increasing water concentration is explained by the fact that the dissociation constant in water is higher than in organic solvents.

The small amount of $C(NO_2)_3H$, whose slow decay into $C(NO_2)_3^-$ constitutes the third step shown in Figure 1d, could possibly originate as one of the decomposition products from the "intermediate complex" through a reaction path parallel to that shown in (3a).

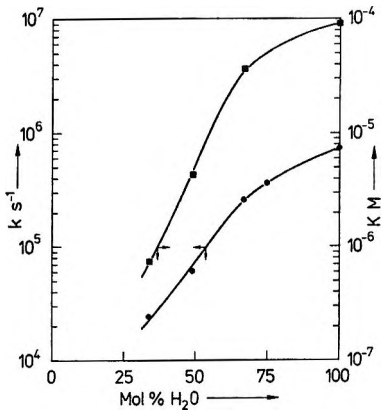

Figure 4. Variation of the equilibrium constant K and the rate constant k with mol % H_2O in the mixture.

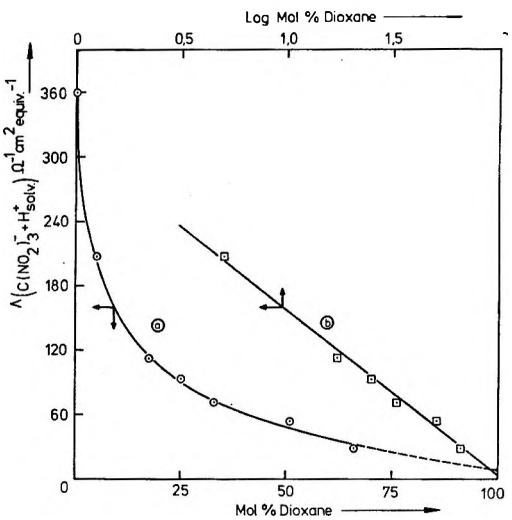

Figure 5. Dependence of the equivalent conductivity Λ on the mol % dioxane in the mixture: a, linear plot; b, semilog plot.

(14) No spectral evidence was obtained for a charge-transfer complex between dioxane molecule and TNM prior to irradiation. TNM spectra are essentially similar both in water and in dioxane, with the difference that a small shoulder at 275 nm is a little broader in dioxane than in H_2O. The spectrum below 248 nm in dioxane was not measured due to strong absorption by the solvent itself.

Conductivity Results. Knowing the concentration of $C(NO_2)_3^-$ from the optical absorption and also of its positive counterion which probably is a solvated proton, the equivalent conductivity of the ion pair can be calculated from the measured conductivity increase of the solutions. It turned out that the conductivity increase in pure dioxane is very low indicating a small equivalent conductivity of the ion pair in this solvent. In water–dioxane mixtures containing more than 35 mole % water, the conductivity signals were large enough to be accurately measured. Figure 5a shows a plot of the calculated equivalent conductivity *vs.* dioxane contents of the mixtures. The curve is similar in shape to the curve giving the dependence of the dielectric constant.[15] Extrapolation to 100% dioxane yields a very low value of the equivalent conductivity of less than 10 ohm^{-1} cm^2 $equiv^{-1}$. A plot of $\Lambda_{(C(NO_2)_3^- + H^+)}$ *vs.* log mole % dioxane is also shown in Figure 5b. The plot yields a straight line. The intercept of 5 ohm^{-1} cm^2 $equiv^{-1}$ on the ordinate axis at 100% dioxane is taken as the equivalent conductivity of the ion pair in this solvent. It may be pointed out that the decomposition of NO_2, produced by the reduction of TNM, to form ions is too slow ($\tau_{1/2}$ for $(NO_2)_2 \rightarrow NO_2^- + NO_3^-$ = 700 μsec[16] in water and *ca.* 10 sec in 2-propanol[9]) to affect our results.

Acknowledgment. The author wishes to express his thanks to Professor A. Henglein for many helpful discussions and for his criticism of this work.

(15) Calculated from the data in J E. Linde, Jr., and R. Fuoss, *J. Phys. Chem.*, **65**, 999 (1961).

(16) M. Grätzel, A. Henglein, J. Lilie, and G. Beck, *Ber. Bunsenges. Phys. Chem.*, **73**, 646 (1969).

The Reactions of Acetone and Hydrogen Peroxide. II. Higher Adducts[1]

by M. C. V. Sauer and John O. Edwards*

Metcalf Chemical Laboratory, Brown University, Providence, Rhode Island 02912 *(Received August 2, 1971)*

Publication costs assisted by U. S. Air Force Office of Scientific Research

The formation of several peroxides derived from acetone and hydrogen peroxide has been investigated by proton magnetic resonance spectroscopy. The kinetics of formation of 2,2-bis(hydroperoxy)propane have been investigated in detail. The slow step was found to exhibit general acid catalysis. Values of rate constants and activation parameters are reported. A general mechanistic scheme for formation of the adducts is proposed.

Introduction

Organic peroxides derived from acetone and hydrogen peroxide have been extensively studied.[1-3] The 1:1 adduct (2-hydroxy-2-hydroperoxypropane, compound I) has recently been shown to be present in the liquid mixtures.[1,4] The following three higher adducts

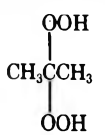

II, 2,2-bis(hydroperoxy) propane

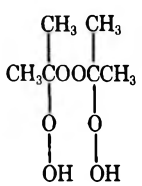

III, α,α′-bis(hydroperoxy)diisopropyl peroxide

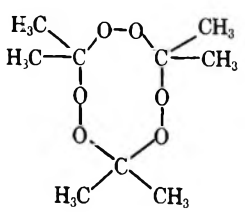

IV, 1,1,4,4,7,7-hexamethyl-1,4,7-cyclononatriperoxane

have been identified.[2,3] Adduct II was isolated[3] (in about 12% yield) when 50% H_2O_2 was reacted with acetone at 0° and a mole ratio of 1:1 in the absence of added hydrogen ion; in the presence of hydrogen ion,

(1) (a) Abstracted from part of the Ph.D. thesis of Maria C. V. Sauer at Brown University, June 1970; (b) Paper I, M. C. V. Sauer and J. O. Edwards, *J. Phys. Chem.*, **75**, 3004 (1971).

(2) A. Rieche, *Angew. Chem.*, **70**, 251 (1958).

(3) N. A. Milas and A. Golubovic, *J. Amer. Chem. Soc.*, **81**, 6461 (1959).

(4) J. Hine and R. W. Redding, *J. Org. Chem.*, **35**, 2769 (1970), and references listed therein.

all three adducts above have been isolated with the cyclic trimer being the predominant product in concentrated solutions.

The mechanisms of formation of these different peroxides derived from acetone and hydrogen peroxide have not been investigated. Further, little is known about the equilibria between the several species. We have studied the different stages of the hydrogen peroxide–acetone interaction in (necessarily) concentrated solution by means of nmr spectroscopy. The data on primary adduct I are published elsewhere.[1b] The mechanism of formation of the higher adducts (II, III, and IV) must be different, as in these three cases replacement of OH by OOR obtains whereas formation of I occurs as an addition across the carbonyl double bond. Data on the higher adducts are presented here.

Experimental Section

General. All reagents, buffers, and equipment were the same as those reported earlier.[1] The evaluation of the equilibrium constants was also carried out as before.

Kinetics. The kinetics of formation of II were investigated as follows. The pH of the peroxide solutions was adjusted with HCl (1 *M*) in cases where buffers were not employed. The pH values were corrected for the influence of hydrogen peroxide on the glass electrode reading.[5] The ionic strength was adjusted in appropriate cases with KCl. All kinetic runs were started by adding the acetone to a known volume of peroxide solution. This operation was carried out in a separate test tube to facilitate mixing, and a small amount of the reaction mixture then was transferred to an nmr tube. A period of 10 min was allowed for temperature equilibration before points were taken.

The rate of disappearance of acetone was measured by nmr peak areas. The peak areas for both acetone and product were evaluated by the automatic integrator on the A-60A spectrometer. The concentration of acetone at any time, t, is given by the equation

$$[\text{acetone}]_t = \left(\frac{I_{Ac}}{I_{Ac} + I_p}\right)_t [\text{acetone}]_0$$

where I_{Ac} is the integrated area of the acetone peak and I_p is the area of the product peak. Brackets are used to denote concentrations, and the subscripts 0 and t refer to initial state and state at time of measurement, respectively. Values of log $[\text{acetone}]_t$ were plotted against time; from the slopes of the resultant lines, values of observed rate constants k_{obsd} were found using the equation

$$k_{obsd} = 2.303\left(\frac{\Delta(\log [\text{acetone}])_t}{\Delta t}\right)$$

Results

Stoichiometries. Each adduct exhibits a characteristic line in the methyl proton region of the nmr spectra, and identification of the lines was made by evaluation of equilibrium constants at different initial concentrations of peroxide and acetone. Adduct I, which is the 1:1 addition product, is formed very rapidly (albeit in low concentration), and it has a known nmr spectrum.[1b,4a] The spectra of freshly prepared solutions of acetone (from 3 to 10 *M*) and hydrogen peroxide (5 to 13 *M*) consist of two low-field signals at 2.23 and 1.43 δ; the 2.23 δ resonance corresponds to the methyl protons of acetone and the 1.43 δ resonance has been assigned[1,4] to adduct I.

The spectra of these same solutions taken over the course of an hour after mixing show a slow decrease in the intensity of the two signals mentioned above and the appearance of a new signal which has a resonance 1 cps upfield from that of I and which quickly becomes larger than that of I. The reaction under investigation was found to be

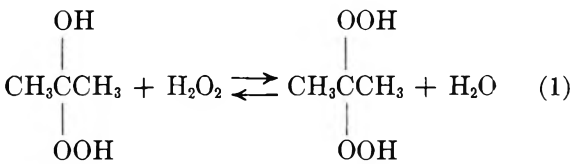

$$CH_3CCH_3 + H_2O_2 \rightleftharpoons CH_3CCH_3 + H_2O \quad (1)$$

(OH, OOH on the left; OOH, OOH on the right)

and the product can be identified (see below) as compound II previously isolated.[2,3]

Over and above the fact that a compound of this nature having the appropriate properties and analysis has been isolated and identified,[3] our assignment of the nmr line to II is based on considerable evidence. First, we observed the compound under the same conditions as it had been isolated by Milas and Golubovic.[3] The position of the methyl proton nmr line is 0.80 δ lower than that of acetone itself; this agrees with the result of Hine and Redding[4] and with the general size of the methyl proton shift observed[4] for all reactions of the type

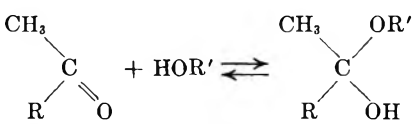

$$\text{CH}_3\text{C(R)=O} + \text{HOR}' \rightleftharpoons \text{CH}_3\text{C(R)(OR')(OH)}$$

The equilibrium constants K_{II} based on a stoichiometry of one acetone and two hydrogen peroxides are constant, and no reasonable alternative structure for this composition presents itself. The values of ΔH and ΔS given below are consistent with a replacement process rather than an addition or elimination reaction. Finally, the kinetic data (rates, acid catalysis, and activation parameters) are analogous to those observed for acetal formation, and compound II may indeed be considered as a modified ketal.

Compound II is the dominant product (as indicated by the size of the nmr signal) when the ratio $[\text{acetone}]/[H_2O_2]$ is equal to or less than 0.07. In those experiments where this ratio is greater than 0.07, a third ad-

(5) J. R. Kolczinski, E. M. Roth, and E. S. Shanley, *J. Amer. Chem. Soc.*, 79, 531 (1957).

duct which is apparently the reaction product derived from condensation of adducts I and II is formed.

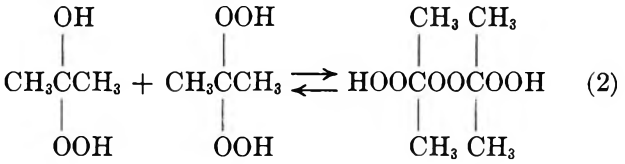

(2)

This product, denoted III, is α,α'-bis(hydroperoxy)diisopropyl peroxide and is observed in the nmr spectra as a signal at 3 cps lower field from that of II.

On further increasing the acetone concentration, ([acetone]/[H_2O_2]) > $^1/_6$, a fourth resonance which we assign to cyclic adduct IV is observed after several days. In solutions where the ratio [acetone]/[H_2O_2] is about unity, the spectra taken 24 hr after the mixing of the reactants indicate the presence of all four products with the 2-hydroxy-2-hydroperoxypropane resonance as a shoulder on the 2,2-bis(hydroperoxy)propane resonance.

Equilibrium Constants. To prove the stoichiometry of the reactions that lead to the formation of 2,2-bis(hydroperoxy)propane and α,α'-bis(hydroperoxy)diisopropyl peroxide, the spectra of several solutions were taken at equilibrium over a range of acetone concentrations from 0.5 to 6 M, of hydrogen peroxide concentration from 9 to 15 M, and of water concentration from 20 to 40 M. The resonances were integrable by planimeter or, in some cases of very good resolution, with the automatic integrator of the spectrometer. The equilibrium constants K_{II} and K_{III} were calculated using the relationships

$$K_{II} = \frac{[II][H_2O]}{[I][H_2O_2]} \qquad K_{III} = \frac{[III][H_2O]}{[I][II]}$$

$$[I]_e = K_I[\text{acetone}]_e[H_2O_2]_e$$

$$[H_2O_2]_e = [H_2O_2]_0 - [I] - 2[II] - 3[III]$$

$$[H_2O]_e = [H_2O]_0 + [II] + 2[III]$$

Values for the equilibrium constants K_{II} and K_{III} at several temperatures are given in Table I. Every constant therein reported represents an average of at least four determinations; at 40°, each K_{II} value represents an average of five runs in the absence of compound III and five runs in the presence of compound III. Table II shows the thermodynamic parameters obtained for each reaction.

Table I: Equilibrium Constants[a] for the Formation of 2,2-Bis(hydroperoxy)propane and α,α'-Bis(hydroperoxy)diisopropyl Peroxide

Temp, °C	K_{II}	K_{III}
5	114 ± 8	44 ± 4
25	170 ± 8	62 ± 8
32	180 ± 8	67 ± 6
40	218 ± 12	78 ± 6

[a] For the definitions of K_{II} and K_{III}, see text.

Table II: Thermodynamic Parameters[a] for the Formation of 2,2-Bis(hydroperoxy)propane and α,α'-Bis(hydroperoxy)diisopropyl Peroxide at 25°

Adduct	$\Delta H°$	$\Delta S°$	$\Delta G°$	$T\Delta S°$
2,2-Bis(hydroperoxy)propane	3.2	21	−3.0	6.2
α,α'-Bis(hydroperoxy)diisopropyl peroxide	2.9	18	−2.4	5.3

[a] The units for $\Delta H°$, $\Delta G°$, and $T\Delta S°$ are kcal mol^{-1} and for $\Delta S°$ are cal mol^{-1} deg^{-1}. The standard deviations are estimated to be about 0.3 for $\Delta H°$, $\Delta G°$, and $T\Delta S°$ and about 1 for $\Delta S°$.

Kinetics of Adduct II Formation. To explain the formation of the 2,2-bis(hydroperoxy)propane, the following mechanism was initially hypothesized.

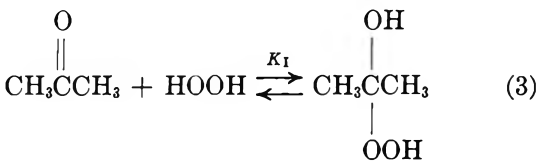

(3)

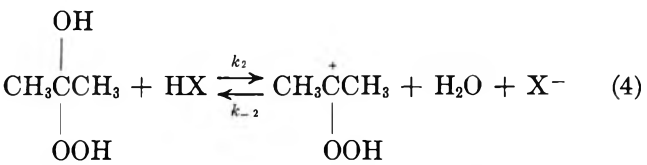

(4)

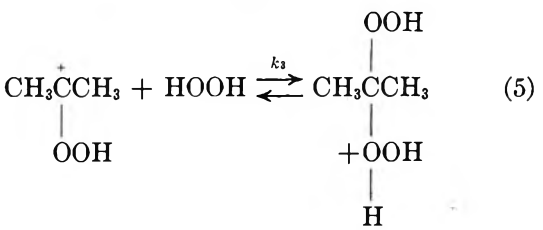

(5)

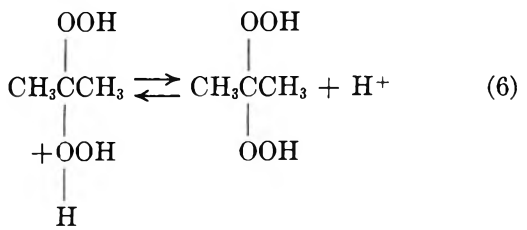

(6)

Different rate laws were derived assuming first step 4 and then step 5 to be the rate-determining step of the reaction. When step 4 is rate determining, the rate law should be

$$\frac{-d[\text{acetone}]}{dt} = \frac{k_2K_I[\text{acetone}][H_2O_2][HX]}{1 + K_I[H_2O_2]} \quad (7)$$

with the denominator having a value near to unity. When step 5 is rate determining, the rate law should be

$$\frac{-d[\text{acetone}]}{dt} = \left(\frac{k_2}{k_{-2}}\right)\left(\frac{k_3K_I[\text{acetone}][H_2O_2]^2[H^+]}{1 + K_I[H_2O_2]}\right) \quad (8)$$

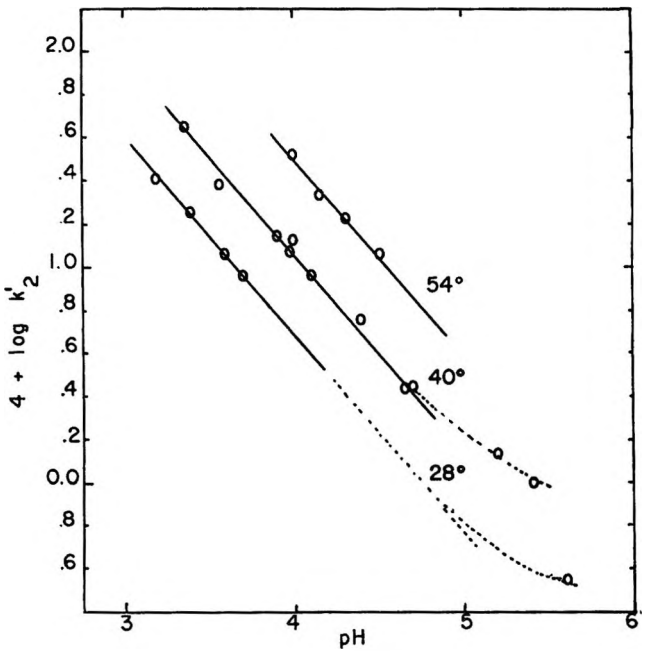

Figure 1. Dependence of rate constant k_2' (as defined in text) on pH at three temperatures.

A significant difference lies in the nature of catalysis by acid: for the first mechanism general acid catalysis is predicted, whereas for the second specific acid catalysis is predicted.

The dependence of the reaction on hydrogen peroxide concentration was studied at 24°, at constant pH and in the absence of any other acid. It was found that the rate law followed by the reaction is the same as the law derived assuming step 4 as the rate-determining step, that is

$$k_{obsd}(1 + K_I[H_2O_2]) = k_2'K_I[H_2O_2]$$

where k_{obsd} is the first-order-pseudo constant for decrease in acetone concentration. The reaction was found to be catalyzed by both H^+ and undissociated acids, and eq 9 shows the observed dependence

$$k_2' = k_0 + k_H[H^+] + k_a[HX] \quad (9)$$

Dependence of the rate constant k_2' on pH at three different temperatures is shown in Figure 1.

At low pH and in the absence of any molecular acid the reaction proceeds largely *via* the path involving catalysis by the solvated proton. Thus, for these data, $k_2' = k_H[H^+]$, and the slope of -1 is observed as expected at pH values lower than 5. A "spontaneous" reaction was observed in the region where the amount of proton catalysis becomes unimportant (pH >5). This spontaneous reaction can be attributed to catalysis by hydrogen peroxide and water. The rate constants k_H and k_0 can be obtained by plotting k_2' against $[H^+]$ (Figure 2) according to the equation

$$k_2' = k_0 + k_H[H^+] \quad (10)$$

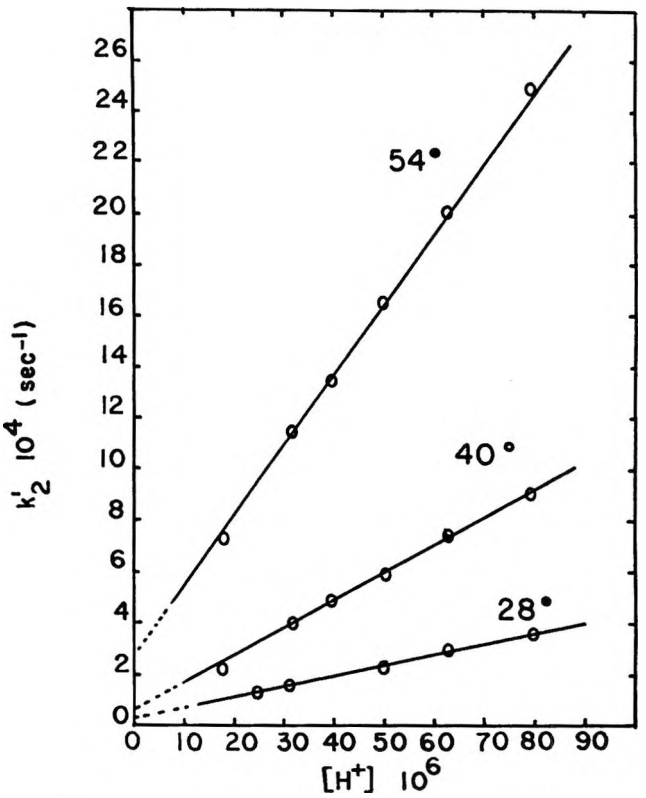

Figure 2. Separation of rate constant k_2' into k_0 and k_H terms (see eq 9) at three temperatures.

The slope of the line is equal to k_H, and the constant k_0 is obtained from the intercept by extrapolation to $[H^+] = 0$. Values of k_H and k_0 at three different temperatures are listed in Table III.

Table III: Proton-Catalyzed and Spontaneous Rate Constants of Formation of 2,2-Bis(hydroperoxy)propane at Three Temperatures

Temp, °C	k_H, M^{-1} sec^{-1}	$k_0 \times 10^4$, sec^{-1}
28	4.25	0.30
41	10.5	0.85
54	27.6	2.70

Table IV: Acid Catalytic Rate Constants at 40° and $\mu = 1$ for the Formation of 2,2-Bis(hydroperoxy)propane

Acid	p^a	q^a	pK_a	k_a, M^{-1} sec^{-1}
H_3O^+	3	1	−1.74	10.5
Cl_3CCOOH	1	2	+0.66	2.00
$Cl_2CHCOOH$	1	2	+1.31	4.5×10^{-1}
HSO_4^-	1	2	+1.52	35×10^{-2}
H_3PO_4	3	2	+1.78	13.9×10^{-2}
$ClCH_2COOH$	1	2	+2.76	2.1×10^{-2}

[a] These are the statistical corrections in the Brönsted equation $k_a/p = G_a((q/p)K_a)^\alpha$.

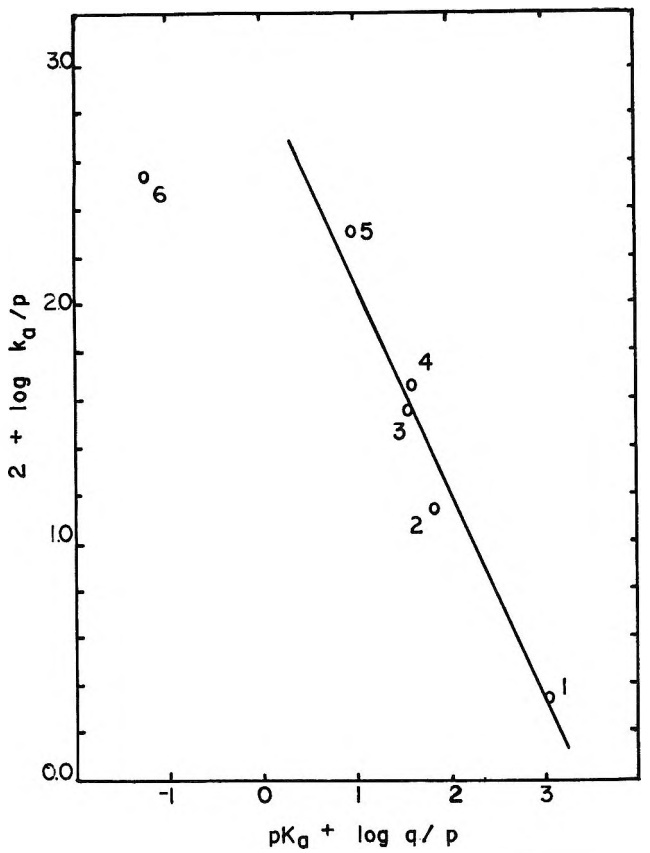

Figure 3. Variation of acid-catalyzed rate constant k_a with pK_a of the corresponding general acid. This Brönsted plot has data for (1) $ClCH_2COOH$, (2) H_3PO_4, (3) HSO_4^-, (4) $Cl_2CHCOOH$, (5) Cl_3CCOOH, and (6) H_3O^+.

At constant pH and working with increasing concentrations of XH, it is possible to obtain the corresponding acid catalytic constant k_a by use of eq 9. Values of k_a for five different acids are listed in Table IV. A Brönsted plot of the system is shown in Figure 3.

Activation parameters of the reaction were calculated for both types of reactions and are listed in Table V. In this case the overall entropies of activation are equal to

$$\Delta S_1^{\pm} = \Delta S_1^{\circ} + \Delta S_H^{\pm} \text{ (H}^+\text{-catalyzed reaction)}$$

and

$$\Delta S_2^{\pm} = \Delta S_1^{\circ} + S_0^{\pm} \text{ (spontaneous reaction)}$$

where ΔS_1° is the change in entropy of the rapid equilibrium step (eq 3) prior to the rate step.

Discussion

General Pathway. The formation reactions of adduct II and adduct III are similar to each other as may be visualized from the general equation

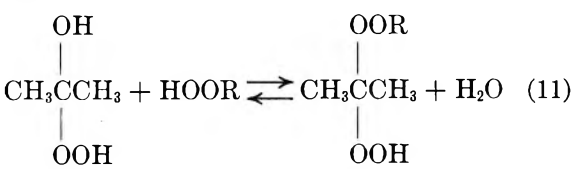

Table V: Activation Parameters[a] at 25° for the Formation of 2,2-Bis(hydroperoxy)propane

	E_a	$\Delta H^{\pm}$	$\Delta S^{\pm}$	$\Delta S^{\pm} - \Delta S_1^{\circ}$
"Spontaneous" reaction	17.5	16.9	−22	6
H^+-catalyzed reaction	13.8	13.2	−10	18

[a] Units for E_a and $\Delta H^{\pm}$ are kcal mol^{-1}, and for $\Delta S^{\pm}$ and $\Delta S^{\pm} - \Delta S_1^{\circ}$ are cal mol^{-1} deg^{-1} The standard deviations for E_a and $\Delta H^{\pm}$ are estimated as 0.3, whereas for $\Delta S^{\pm}$ and $\Delta S^{\pm} - \Delta S_1^{\circ}$ they are 1.

Both reactions involve the replacement of an OH group by an OOR group with concurrent formation of water. For adduct II, HOOR represents hydrogen peroxide; for adduct III, HOOR represents adduct II itself. The similarity in the chemistry of these two reactions is reflected in the similarity of the thermodynamic parameters.

All of the products from the reaction of acetone and hydrogen peroxide can be formed by the steps of eq 1, 2, 3 plus the following

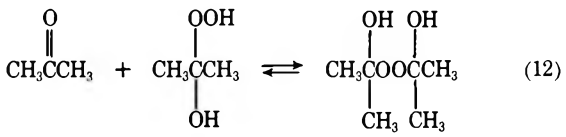

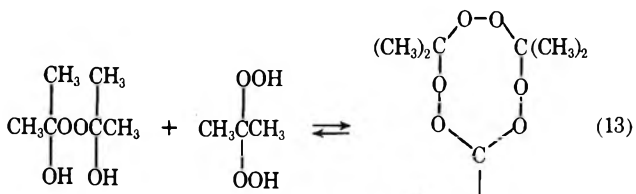

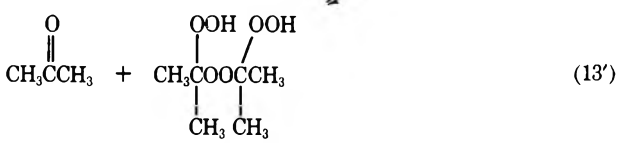

Only two general types of stoichiometry are necessary for the description of products from the reactions of hydroperoxides ROOH and carbonyl compounds R′C(=O)R″. These two types are addition of ROOH across the double bond (such as in eq 3) and conversion of COR‴ to COOR as in eq 11. Although the details vary from adduct to adduct, the general pathways should be related.

Stage 12 was not observed by the nmr technique. The product of this reaction should be present in smaller quantity than adduct I as the acetone concentration is small. The equilibrium constants obtained for formation of adduct I would have shown deviations from constancy if the process were important; no such deviations were observed.

Cyclic adduct IV could result from either of the two steps proposed (eq 13 and 13′) or from some related process. The complexity of the stoichiometry coupled with the fact that adduct IV can under some circumstances be the predominant product (90%) strongly suggests that the other adducts are intermediates in the formation of this stable cyclic peroxide.

Mechanism of Formation of 2,2-Bis(hydroperoxy)propane. According to the results obtained for (a) dependence of rate on peroxide concentration, (b) pH dependence of the rate, (c) general acid catalysis of the rate, and (d) activation parameters, it can be concluded that the mechanism of formation of 2,2-bis(hydroperoxy)-propane is indeed that described in the Results section. The probable steps are (3), (4), (5), and (6) with (4) being the rate-determining step.

The Brönsted law applied to our system is represented in Figure 3. The slope of the line is 0.8, with a negative deviation for H_3O^+. The observed spontaneous reaction is mainly attributed to catalysis by hydrogen peroxide ($pK_a = 11.4$)[6] which is present in a considerable concentration; this cannot, however, be considered as proved.

The activation parameters reflect the changes from ground state to transition state. The entropy of adduct I formation is -28 cal mol^{-1} deg^{-1}, and the observed activation entropies $\Delta S^{\ddagger}_{obsd}$ must be corrected for this contribution. The remnant values $\Delta S_H{}^{\ddagger}$ and $\Delta S_0{}^{\ddagger}$ are $+18$ and $+6$ cal mol^{-1} deg^{-1}, respectively. These are for the processes

$$I + H_3O^+ \longrightarrow CH_3\overset{+}{C}(OOH)CH_3 + 2H_2O$$

and

$$I + H_2O_2 \longrightarrow CH_3\overset{+}{C}(OOH)CH_3 + H_2O + OOH^-$$

These activation entropies, although most certainly complicated as to contributing influences,[7,8] seem to be dominated by the entropy increase resulting from the increase in number of particles.

The reaction of eq 1 is analogous to the formation of an acetal from a hemiacetal, which process is known to be catalyzed by acid. Both general acid catalysis and specific acid catalysis[9-13] have been reported. Therefore, the general acid catalysis found here is unusual, albeit unexceptional.

Acknowledgments. This study was supported by the U. S. Air Force Office of Scientific Research under Grant No. 70-1839; their continuing support is appreciated. Miss Kathleen Edwards is acknowledged for her assistance in calculations and graphing of the kinetic data.

(6) W. G. Evans and N. Uri, *Trans. Faraday Soc.*, **45**, 224 (1949).

(7) F. A. Long, J. G. Pritchard, and F. E. Stafford, *J. Amer. Chem. Soc.*, **79**, 2362 (1957).

(8) M. M. Kreevoy, "Rates and Mechanism of Reactions," part II, A. Weissberger, Ed., Wiley-Interscience, New York, N. Y., 1963, Chapter XXIII.

(9) A. Kanbaanpera and L. Markker, *Acta Chem. Scand.*, **23**, 2465 (1969).

(10) M. M. Kreevoy and R. W. Taft, *J. Amer. Chem. Soc.*, **77**, 3146 (1955), and references therein.

(11) J. Koskikallio and E. Whalley, *Trans. Faraday Soc.*, **55**, 809 (1959).

(12) P. M. Heininger and W. J. Kilpatrick, *J. Amer. Chem. Soc.*, **61**, 2510 (1939).

(13) C. Armour, C. A. Bunton, S. Patai, L. Selman, and C. A. Vernon, *J. Chem. Soc.*, 412 (1961).

Interaction of Sulfur Dioxide and Carbon Dioxide with Clean Silver in Ultrahigh Vacuum

by W. S. Lassiter

NASA Langley Research Center, Hampton, Virginia 23365 *(Received November 12, 1971)*

Publication costs assisted by NASA Langley Research Center

The interaction of sulfur dioxide and carbon dioxide with clean silver in ultrahigh vacuum (UHV) was investigated by Auger electron spectroscopy and work function measurements. Polycrystalline silver, after being cleaned by argon ion bombardment and heating to the extent that no contaminants were observed by Auger spectroscopy, was subjected to sulfur dioxide at a pressure of 10^{-9} Torr. Auger spectra and relative work function measurements were recorded as a function of exposure, revealing that sulfur chemisorbed to the silver surface and that the relative work function increased 0.39 eV during an exposure of 6×10^{-6} Torr sec. Desorbing the sulfur from the silver by heating led to an estimation of a minimum heat of desorption of 59 kcal/mol. The polycrystalline silver was then cleaned again by ion bombardment and heating until no contaminants were observed by Auger spectroscopy. The silver was subjected to carbon dioxide at 10^{-8} Torr. No change in the Auger spectrum or the relative work function of the silver surface occurred during exposure to carbon dioxide, indicating that no adsorption occurred.

Introduction

The understanding of the interaction of various pollutant gases in the atmosphere on silver is important, since silver is not only highly regarded as a decorative metal, but also used in electron emissive devices, highly reflecting surfaces, and photosurfaces.

Two of the most common pollutants in our atmosphere are sulfur dioxide and carbon dioxide. Very little work has been performed relative to the adsorptive characteristics of these two polyatomic gases on silver. Czanderna[1] has shown that no adsorption of carbon dioxide was observed on a reduced silver powder surface, but that after oxygen was preadsorbed, carbon dioxide adsorption occurred. These studies were performed with a vacuum ultramicrobalance at pressures of 10^{-7} to 100 Torr. Czanderna has also studied the adsorption of oxygen on silver.[2] A search of the literature revealed no studies of sulfur dioxide on silver under high-vacuum conditions.

The most efficient way to study adsorption on a metal is to first clean the metal surface in an ultrahigh vacuum (UHV) and then subject the surface to the potential adsorbate of interest. Such an experiment prevents intervention by impurities of adsorption phenomena between adsorbate and adsorbent. It allows interaction of the adsorbate with essentially the virgin adsorbent.

The purpose of the work reported herein was to investigate the adsorptive characteristics of sulfur dioxide and carbon dioxide on clean polycrystalline silver under UHV conditions, which gives rise to a large recontamination time compared with the experiment time. The adsorption was detected by Auger electron spectroscopy, which is reported to be capable of elementally identifying surface constituents to a few hundredths of a monolayer.[3] This technique was complemented by measurements of the work function of the silver surface during exposure. The residual pressure of the vacuum system was 1×10^{-10} Torr. Prior to subjection to each of the gases, the silver surface was cleaned by ion bombardment and heating. The temperature of the silver during Auger and work function measurements was 65–95°.

Experimental Section

The experimentation was performed in a 200-l. UHV system.[4] The silver sample was machined from pure (99.999%) polycrystalline silver and assumed the shape of a cylinder, about 0.25 in. in length. One end of the cylinder was used as the test surface, which was 0.25 in. in diameter and highly polished.

Figure 1 is a schematic of a top view of the apparatus enclosed by the UHV chamber. The sample could be rotated such that it was positioned in front of the Auger analyzer, in front of the work function electron gun, and in front of the cleaning electron gun. The work function electron gun enabled measurement of the work function of the test surface. The cleaning electron gun enabled ion bombardment of the test surface and heating of the sample by electron bombardment.

Surface constituent analysis of the silver test surface was performed with an Auger electron spectrometer utilizing a cylindrical velocity analyzer as a focus-

(1) A. W. Czanderna, *J. Colloid Interface Sci.*, **22**, 482 (1966).
(2) A. W. Czanderna, *J. Phys. Chem.*, **68**, 2765 (1964).
(3) C. C. Chang, *Surface Sci.*, **25**, 53 (1971).
(4) W. S. Lassiter, *J. Vac. Sci. Tech.*, **3**, 418 (1969).

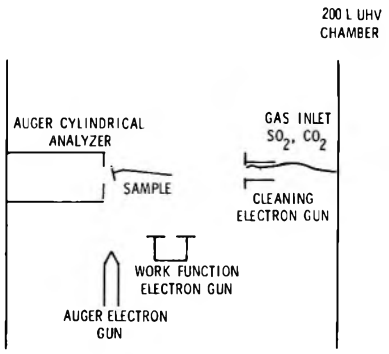

Figure 1. Schematic of apparatus.

ing agent.[5] The cylindrical analyzer was designed according to monochromator design principles, second-order focusing, and for optimum resolving power.[6-10] The spectrometer was operated at an incident beam current and energy of 2 μA and -1500 eV, respectively.

The test surface was cleaned by alternate applications of ion bombardment with 1500-eV argon ions, and heating by electron bombardment to 600°. The sample was cleaned by this technique until no contaminants appeared in the Auger spectra, after which the test surface was subjected to sulfur dioxide.

The retarding-field diode technique[11,12] was used to monitor the relative work function $\Delta\phi$ of the test surface. The relative work function is the difference in the anode and cathode potentials of a diode operating in the retarding-field region. The cathode temperature was held constant sueh that any change in the relative work function was a result of a change in the anode, or test surface, work function. An advantage of this technique is that the relative work function of a surface can be constantly monitored during exposure of the surface to any pollutant, contaminant, and so forth.

Results

Figure 2 shows Auger spectra of the silver surface after the vacuum system had been baked at about 250° for 20 hr and subsequently evacuated to 1×10^{-10} Torr. The ordinate is the derivative of the secondary electron energy distribution, $N(E)$, with respect to energy, and the abscissa is the secondary electron energy, E_a. The data in Figure 2 show that contaminants residing on the silver surface are sulfur, carbon, titanium, and oxygen. All these contaminants, except titanium, exist as large impurities in silver. The titanium was probably deposited on the silver surface during pumpdown of the vacuum chamber, during which time the titanium sublimator attached to the vacuum system was operated frequently.

Figure 3 shows Auger spectra of a clean silver sample after cleaning by ion bombardment and heating. The spectra in Figure 3 were taken after subjecting the sample to an ion bombardment dosage of greater than 500×10^{-4} C and more than 100 hr of heating to 600°.

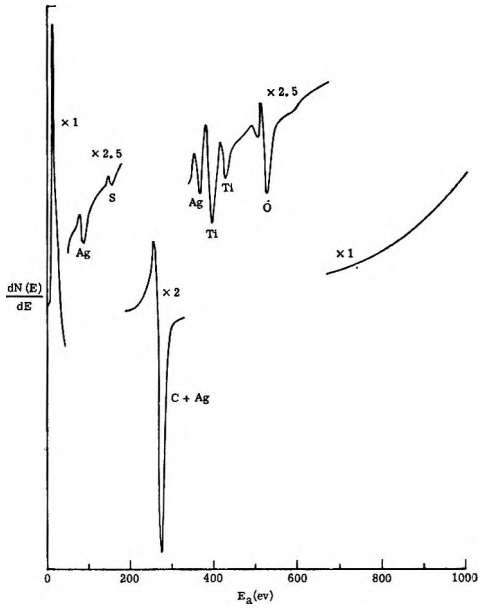

Figure 2. Auger spectra of silver surface prior to ion bombardment or heating.

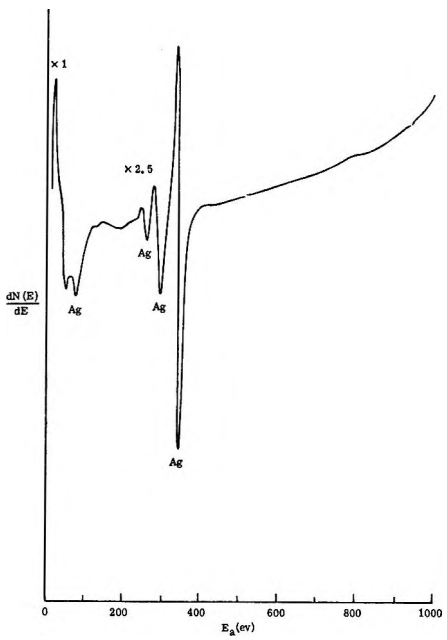

Figure 3. Auger spectra of a clean silver surface.

(5) W. S. Lassiter, Ph.D. Dissertation, N. C. State Univ., Raleigh, N. C., May 1971.

(6) C. E. Kuyatt and J. Arol Simpson, *Rev. Sci. Instrum.*, **38**, 103 (1967).

(7) V. V. Zashkvara, M. I. Korsunskii, and O. S. Kosmachev, *Sov. Phys. Tech. Phys.*, **11**, 96 (1966).

(8) E. Blauth, *Z. Phys.*, **147**, 228 (1957).

(9) H. Z. Sarel, *Rev. Sci. Instrum.*, **38**, 1210 (1967).

(10) H. Hafner, J. Arol Simpson, and C. E. Kuyatt, *ibid.*, **39**, 33 (1968).

(11) C. R. Crowell and R. A. Armstrong, *Phys. Rev.*, **114**, 1500 (1959).

(12) J. M. Bradford, Jr., Ph.D. Dissertation, North Carolina State University, Raleigh, N. C., May 1968.

The long cleaning time was required because of impurities diffusing from the bulk to the surface.

The relative work function of the silver surface showed very little consistent behavior during cleaning. Ion bombardment caused a decrease in the relative work function of as much as 0.8 V, after which heating would increase the relative work function as much as 1 V. The erratic behavior of the relative work function during cleaning is probably due to various changes in structure, surface geometry, and polycrystallinity caused by the cleaning process. Normally, when the silver surface approached a clean state, as indicated by the Auger spectrometer, the variation in the relative work function with further ion bombardment or cleaning was less than 0.25 V. When the sample was clean, no change in relative work function with time was evident.

After the silver sample was clean, as depicted by Figure 3, sulfur dioxide was introduced into the vacuum chamber until the pressure increased from 1×10^{-10} to 1×10^{-9} Torr. The pressure was then held constant at 1×10^{-9} Torr while Auger spectra of the surface were recorded as a function of exposure. Figure 4 shows typical Auger spectra of the silver surface after the surface was exposed to sulfur dioxide The spectra indicate that only sulfur resides on the surface. This condition suggests either of two mechanisms occurring at the surface First, the sulfur dioxide molecule could have been adsorbed and subsequently broken up such that the sulfur was chemisorbed as a sulfide and the oxygen either diffused into the bulk or evaporated from the surface. Second, the sulfur dioxide molecule could have been adsorbed such that the oxygen atoms were bound to the silver atoms and the sulfur atoms were positioned above the silver surface atoms by some distance smaller than the bond length. The primary electron beam would then excite the outermost atoms, the sulfur atoms, but possibly not the oxygen atoms underneath the sulfur atoms. The latter mechanism is highly unlikely, since the bond distances in sulfur dioxide are about 1.43 Å,[13] and because of evidence in the literature[14] of surface penetration by the primary electron beam of up to 10 Å.

A search of the literature revealed no information regarding a reaction between silver and sulfur dioxide at temperatures between 65 and 95°. Further experimental data pertaining to the products of reaction, bonding forces, and surface structure are required to establish the behavior of sulfur dioxide on the silver surface.

Some insight into the mechanism of adsorption can be gained by considering the standard free energies of formation, bond energies, and heats of adsorption. A reaction involving the formation of silver sulfide (Ag_2S), would be more likely than one involving the formation of silver oxide (Ag_2O), since their standard free energies of formation are -9.5 and -2.59 kcal/(mol °K), respectively.[15] The bond energy of sulfur dioxide is 119 kcal/mol. A search of the literature revealed no data on the bond energies of silver sulfide or silver oxide, but revealed a bond energy of 32 kcal/mol for silver monoxide (AgO).[16] Since the bond energy of silver monoxide is not near that of sulfur dioxide, a reaction involving the breaking up of the sulfur dioxide because of attraction of the oxygen to silver is highly unlikely.

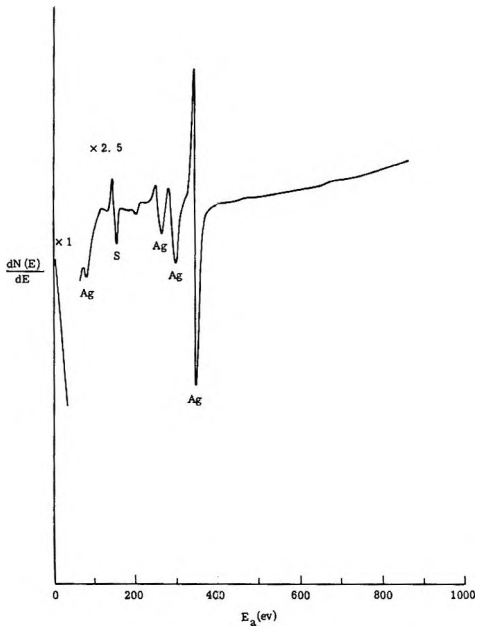

Figure 4. Auger spectra of silver surface during exposure to sulfur dioxide.

Perdereau and Rhead[17] studied the reaction of silver with hydrogen sulfide (H_2S) and found the reaction

$$Ag + H_2S \rightleftarrows (Ag\text{–}S)_{ads} + H_2 \qquad (1)$$

to occur, where the subscript ads means adsorbed sulfur on silver. The results of their study yield a differential heat of adsorption ΔH of 32–34 kcal/mol for the sulfur adsorption on silver, which suggests a rather strong chemisorption. These data indicate that sulfur has a high affinity for silver.

Since heating the silver sample to temperatures above 500° for periods of at least 10 hr was required to completely remove the adsorbed sulfur, the sulfur was probably chemisorbed to the silver. A calculation was made which led to an estimate of the minimum heat of desorption, q_d, of the adsorbed sulfur by the equation for the time of sojourn, τ[18]

(13) P. W. Schenk and R. Steudel, "Inorganic Sulfur Chemistry," Elsevier, New York, N. Y., 1968, pp 367–418.

(14) P. W. Palmberg and T. N. Rhodin, *J. Appl. Phys.*, **39**, 2425 (1968).

(15) N. A. Lange, "Handbook of Chemistry," Handbook Publishers, Sandusky, Ohio, 1946.

(16) T. L. Cottrell, "The Strengths of Chemical Bonds," Butterworths, London, 1958.

(17) J. Perdereau and G. E. Rhead, *Surface Sci.*, **7**, 175 (1967).

(18) J. P. Hobson, *Br., J. Appl. Phys.*, **14**, 544 (1963).

$$\tau = \tau_0 \exp(q_d/RT) \quad (2)$$

where R is the universal gas constant, T the surface temperature, and τ_0 the time of sojourn when zero desorption energy is required to remove the atom. Using $\tau_0 = 10^{-12}$ sec,[19] a time of sojourn τ of the most tightly bound sulfur atom of 10 hr, and a temperature of 500° yields $q_d \sim 59$ kcal/mol, which infers chemisorption of the sulfur to silver.

The same types of tests were performed with carbon dioxide as with sulfur dioxide, except that the carbon dioxide was introduced into the vacuum chamber such that the pressure rose from about 1×10^{-10} to 1×10^{-8} Torr. As before, the silver sample was cleaned such that no contaminants were detected by the Auger spectrometer. Neither carbon nor oxygen was detected on the silver surface with the Auger spectrometer, nor was there any variation in the relative work function of the silver surface with exposure to the carbon dioxide.

Some indication has appeared in the literature that the peak height of Auger peaks can be used to quantitatively describe constituents on a surface. An experiment in which the Auger peak height of a contaminant is used to quantitatively describe the buildup of the contaminant on a surface may be very difficult, since little is known about sticking coefficients of various contaminants to substrates. In this experiment, it was assumed that the Auger peak height of an adsorbed species would increase as adsorption progressed. The sulfur Auger peak height was thus monitored as a function of exposure of the silver sample to sulfur dioxide. The results are shown in Figure 5. The steplike appearance of the data could not be explained, although it suggests that adsorption is proceeding by a nucleation and growth, layer mechanism as suggested by Moazed.[20] Each step would represent the nucleation of a new adsorbed layer of sulfur on the silver surface. The data show that adsorption of sulfur on the silver surface occurred during exposure up to about 6×10^{-6} Torr sec, at which point it appears that the peak height becomes constant.

Following the Auger measurements of sulfur adsorption, the silver sample was cleaned again by ion bombardment and heating to the extent that the Auger spectra indicated no contaminants on the surface. Sulfur dioxide was then inlet into the chamber, as before, and the relative work function of the silver surface was monitored as a function of exposure to sulfur dioxide.

Figure 6 represents the results and shows a plot of the relative work function *vs.* exposure. The relative work function increased about 0.39 V as a result of the

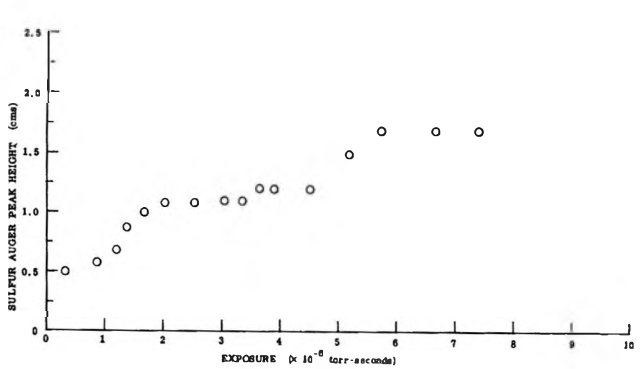

Figure 5. Auger peak height of sulfur as a function of exposure to sulfur dioxide.

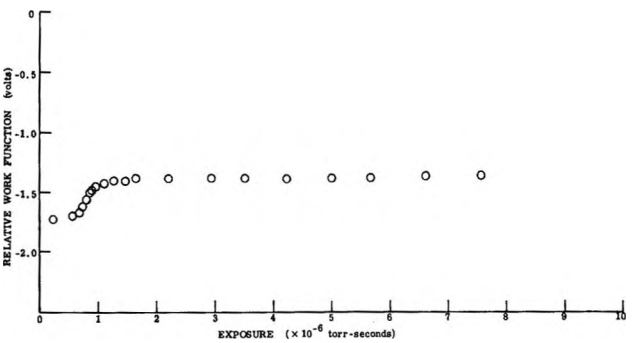

Figure 6. Relative work function as a function of exposure to sulfur dioxide.

adsorption of sulfur on the silver surface. A rapid increase in the relative work function of about 0.29 V occurred between 0.5×10^{-6} and 1.0×10^{-6} Torr sec. Between 1×10^{-6} and 6×10^{-6} Torr sec, a gradual increase in $\Delta\phi$ of 0.10 V occurred, after which no change was observed.

Conclusions

It is shown that when a clean polycrystalline silver surface is subjected to sulfur dioxide at a pressure of 1×10^{-9} Torr, sulfur is chemisorbed to the silver. Heating the contaminated silver leads to an estimation of the minimum heat of desorption of 59 kcal/mol.

Sulfur Auger peak height and relative work function measurements of the surface during exposure show that adsorption occurs during 6×10^{-6} Torr sec exposure at 10^{-9} Torr.

It is also shown that when a clean polycrystalline silver surface is subjected to carbon dioxide at a pressure of 1×10^{-8} Torr, no adsorption occurs.

(19) A. V. Kiselev and B. P. Poshkus, *Trans. Faraday Soc.*, **59**, 176 (1963).

(20) K. L. Moazed, *Ann. N. Y. Acad. Sci.*, **101**, 785 (1963).

Quantum Efficiencies and Radiationless Transitions of Europium(III) in Phosphate Glasses[1a]

by R. Reisfeld, R. A. Velapoldi,* and L. Boehm[1b]

Department of Inorganic and Analytical Chemistry, The Hebrew University of Jerusalem, Jerusalem, Israel
(Received August 23, 1971)

Publication costs borne completely by The Journal of Physical Chemistry

The quantum efficiency of fluorescence from the $^5D_0$ level of Eu^{3+} was obtained by two methods: by lifetime measurements and by comparison with a liquid standard. The quantum efficiency obtained by both methods was 0.95 ± 0.02. The probabilities of populating the $^5D_0$ level *via* excitation to the $^5D_1$, $^5D_2$, $^5D_3$, and $^5L_6$ levels have been calculated. The probability for the $^5D_1 \rightarrow {}^5D_0$ transition of the excited Eu^{3+} in phosphate glasses has been calculated. The interaction of the electronic levels with the glass host is discussed.

Introduction

In a previous paper[2] we suggested that europium-activated glasses can be used as a solid standard for narrow band fluorescence. The objectives of this work are (1) to continue investigations for the development of a solid standard for fluorescence and (2) to study the rate of energy dissipation between various excited levels of europium in glass matrices.

It has been pointed out[3] that a stable standard of fluorescence which can be used interchangeably for standardizing both liquids and solids is needed. While liquid standards have been studied extensively, there are almost no data on transparent solid samples, except for the yield determination developed by Bril,[4] which can be used only for highly reflective phosphors.

In this paper the experimental methods and results of the quantum efficiency determinations are discussed and the probability of nonradiative energy transfer is calculated from the oscillator strengths of the transitions, the fluorescence intensities, and the decay times.

A partial energy level diagram for the levels of the Eu^{3+} ion with a $4f^6$ electron configuration is given in Figure 1. The Eu^{3+} ion in glass fluoresces with measurable intensity from the $^5D_0$ and $^5D_1$ levels[5] to the ^7F multiplet. The fluorescence from the $^5D_0$ level is stronger by two orders of magnitude than the $^5D_1$ fluorescence. The number and types of radiative and nonradiative transfers from these levels are restricted by selection rules. The principal fluorescence emissions from the $^5D_0$ level to the ^7F multiplet are: $^5D_0 \rightarrow {}^7F_0$, $^5D_0 \rightarrow {}^7F_1$, $^5D_0 \rightarrow {}^7F_2$, $^5D_0 \rightarrow {}^7F_3$, and $^5D_0 \rightarrow {}^7F_4$. The fluorescence from the $^5D_0$ to the $^7F_5$ and $^7F_6$ is negligible (less than 1% of the total emission). The $^5D_0 \rightarrow {}^7F_1$ transition is a magnetic dipole transition, while the others are forced electric dipole or quadrupole transitions.[2]

The quantum efficiency of fluorescence from the $^5D_0$ level was determined experimentally using a solution of europium(III) nitrate as a standard having a quantum yield of 0.04.[6] An independent determination of quantum yield was made by calculating the natural radiative lifetime, measuring the experimental decay time, and using eq 2.

Experimental Section

Glasses and Solutions. Glasses were prepared from $NaH_2PO_4 \cdot H_2O$ (analytical reagent, Mallinckrodt, 99.5% purity) and Eu_2O_3 (Molycorp., 99.9% purity). Mixtures containing 0.5, 1.0, 1.5, 2.0, 2.5, 3.0, and 3.5 wt % europium were mixed and melted at 1000° in a platinum crucible. Glass disks 1 mm thick and 12 mm in diameter were obtained by molding the melt on a tile. A glass containing 2 wt % europium in a cuvette form with dimensions 10 × 10 × 40 mm was used for the absorption measurements.

Aqueous solutions of europium(III) nitrate were prepared by dissolving the oxide (American Potash Co., 99.9% purity) in the appropriate amount of nitric acid (Baker Analyzed reagent, 1:1 acid:water). All water was distilled, passed through an ion-exchange resin, and double distilled from a quartz still.

Instrumentation. Fluorescence spectra were taken on a Turner Model 210 spectrofluorometer[7] which gives corrected emission spectra in quanta per unit band-

* Address correspondence to this author at Section 310-04, National Bureau of Standards, Washington, D. C. 20234.

(1) (a) This work was performed under NBS Contract No. (G)-103; (b) this work is a part of an M.Sc. thesis presented by L. Boehm to the Chemistry Department of The Hebrew University.

(2) R. Reisfeld, R. A. Velapoldi, L. Boehm, and M. Ish-Shalom, *J. Phys. Chem.*, **75**, 3981 (1971).

(3) J. N. Demas and G. A. Crosby, *J. Phys. Chem.*, **75**, 991 (1971).

(4) A. Bril, "Luminescence of Organic and Inorganic Materials," Wiley, New York, N. Y., 1962, p 477.

(5) R. A. Velapoldi, R. Reisfeld, and L. Boehm, 9th Rare Earth Conference, Vol. 1, p 123, 1971.

(6) Y. Haas and G. Stein, *J. Phys. Chem.*, **75**, 3668 (1971).

(7) G. K. Turner, *Science*, **146**, 183 (1964).

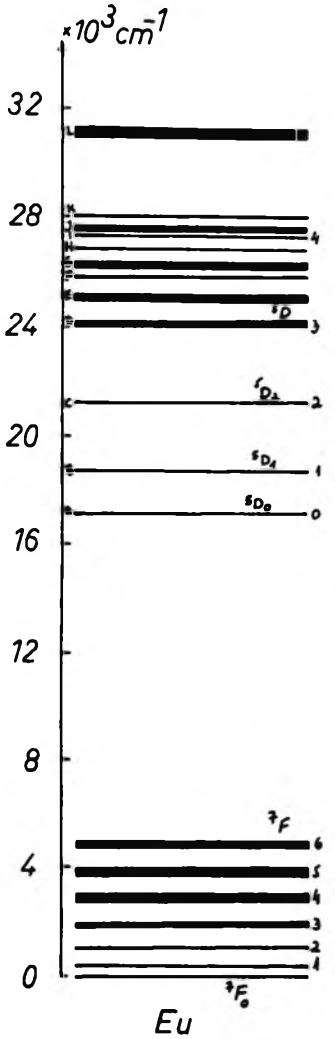

Figure 1. Electronic levels of Eu^{3+} in a crystal.

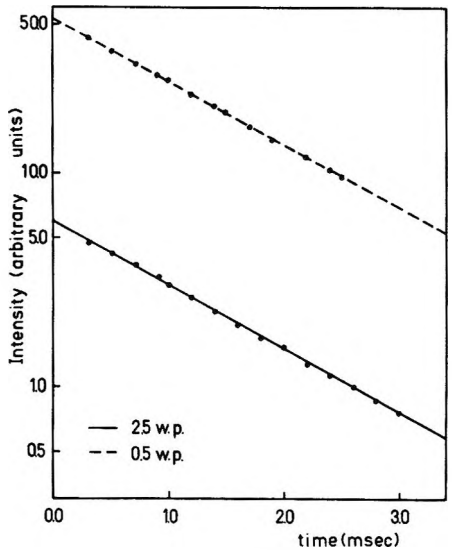

Figure 2. Decay curve of Eu^{3+} in phosphate glass.

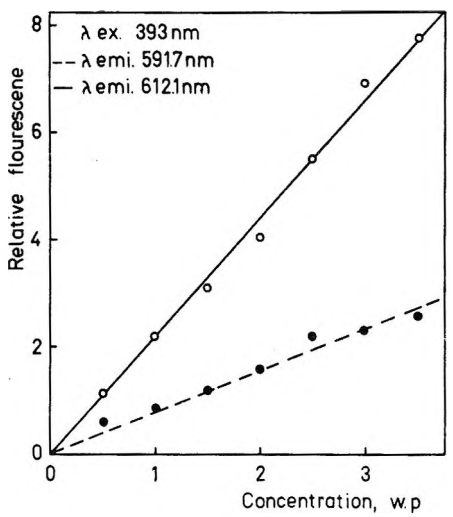

Figure 3. Concentration dependence of $^5D_0 \rightarrow {}^7F_1$ (591.7 nm) and $^5D_0 \rightarrow {}^7F_2$ (612.1 nm) fluorescence of Eu^{3+} in phosphate glass.

width and excitation spectra corrected to constant energy, or on a spectrofluorometer described previously.[8] The latter consists of a 500-W xenon arc lamp (Mazda), excitation monochromator (Bausch and Lomb, 250-mm focal length), sample compartment, emission monochromator (Bausch and Lomb, 500-mm focal length), an EMI 9558 QB photomultiplier connected through a 16-megohm resistor to an EIL Vibron electrometer and Kipp and Zonen recorder. Corrected emission and excitation spectra were obtained from this instrument using spectra obtained from the Turner 210 for corrections.

Decay times were measured using the uncorrected spectrofluorometer by replacing the light source with an EGG FX-6AU flash lamp having an average pulse duration of 3 μsec and an energy of 0.4 J/flash. The photomultiplier was connected directly to a Tektronix type 502 dual-beam oscilloscope with an attached Polaroid camera. All measurements were made at room temperature. Absorption spectra were recorded on a Cary Model 14 spectrophotometer.

Results

Emission intensities from the $^5D_0$ level are tabulated in Table I. They are presented as relative areas under the emission spectrum. The decay of the fluorescence from the $^5D_0$ level is a single exponential for all concentrations measured, with a lifetime of 2.83 msec (Figure 2). The absence of concentration quenching of the fluorescence is also shown in Figure 3.

Fluorescence from the $^5D_1$ level, due to three magnetic dipole transitions, was measured and the results are summarized in Table II. The total intensity of fluorescence emission ratio between the $^5D_0$ level and the $^5D_1$ level was 260 at 2 wt % europium, where the excitation was made *via* the $^5L_6$ level (394 nm). This

(8) R. Reisfeld, A. Honigbaum, G. Michaeli, L. Harel, and M. Ish-Shalom, *Israel J. Chem.*, 7, 613 (1969).

Table I: Relative Transition Probabilities from the $^5D_0$ Level

Transition assignment	Wavelength, nm	Rel area
$^5D_0 \rightarrow {}^7F_0$	579.6	0.012
$^5D_0 \rightarrow {}^7F_1$	591.7	0.333
$^5D_0 \rightarrow {}^7F_2$	612.1	1.000
$^5D_0 \rightarrow {}^7F_3$	653.7	0.073
$^5D_0 \rightarrow {}^7F_4$	695.2	0.342

does not imply that the radiative transition probabilities of the two fluorescences are equal to this ratio, since there exists the possibility of populating the $^5D_0$ level by direct transitions from higher levels without a $^5D_1$ intermediate. Efforts to obtain fluorescence from the $^5D_1$ level by direct excitation to this level were unsuccessful owing to low fluorescence intensities and rapid depopulation to the $^5D_0$ level.

Table II: Relative Fluorescence From the $^5D_1$ Level Compared to the $^5D_0 \rightarrow {}^7F_2$ Transition

Transition assignment	Wavelength, nm	Rel fluorescence
$^5D_0 \rightarrow {}^7F_2$	612.1	1.0000
$^5D_1 \rightarrow {}^7F_0$	526.4	0.0003
$^5D_1 \rightarrow {}^7F_1$	543.7	0.0039
$^5D_1 \rightarrow {}^7F_2$	561.0	0.0022

The concentration dependence of the $^5D_1$ transitions to the ^7F multiplet were not measured in this work. By analogy with the work of Nakazawa and Shionoya,[9] who found a concentration dependence for the fluorescence from the $^5D_3$ level in terbium in phosphate glasses, such a study would be interesting. On the other hand, Weber,[10] in a study of Eu^{3+} in LaF_3, found that the lifetimes of the $^5D_0$ and $^5D_1$ levels exhibit little change with concentration.

Quantum Efficiencies. (1) *By the Comparative Method.* Direct excitation to the $^5D_0$ level in the glass and europium nitrate solution was performed using the $^7F_1 \rightarrow {}^5D_0$ transition at 591 nm. Equation 1[7,11] was

$$Q_u = Q_s \frac{(FA_u)(A_s)(\lambda_{ex})_s(\eta_u^2)}{(FA_s)(A_u)(\lambda_{ex})_u(\eta_s^2)} \quad (1)$$

used to calculate the quantum efficiency of the $^5D_0$ level, where Q is the quantum efficiency, FA is the total area under the emission peaks, A is the absorbance, λ_{ex} is the excitation wavelength, η is the index of refraction, and the subscripts u and s refer to the unknown and standard, respectively ($\eta_s = 1.44$, $\eta_u = 2.14$).

Dawson and Kropp[12] indicated that corrections have to be made if the absorption band of the measured spectrum has a half-width smaller than the half-bandwidth of the excitation monochromator. Because of the relatively wide band of the europium in nitrate solutions and glasses and the narrow spectral band (25 Å) which the excitation monochromator gives, such corrections were not needed in this work.

The quantum efficiency obtained in this manner was 0.95 ± 0.03 for excitation to the $^5D_0$ level.

(2) *From Lifetime Measurements.* The equation for quantum efficiency, Q, is related to the measured lifetime, τ_{measd}, and the natural radiative lifetime, τ_{nat} by

$$Q = \frac{\tau_{measd}}{\tau_{nat}} = \frac{\sum A_r}{\sum A_r + \sum A_{nr}} \quad (2)$$

where τ_{measd} is equal to $1/(\Sigma A_r + \Sigma A_{nr})$. In the case where more than one transition is responsible for the measured lifetime, it is an inverse of the sum of all radiative and nonradiative transition rates.

In the radiative case for Eu^{3+}

$$\sum A_r = k(^5D_0 \longrightarrow {}^7F_0) + k(^5D_0 \longrightarrow {}^7F_1) + k(^5D_0 \longrightarrow {}^7F_2) + k(^5D_0 \longrightarrow {}^7F_3) + k(^5D_0 \longrightarrow {}^7F_4) \quad (3)$$

since $k(^5D_0 \rightarrow {}^7F_5) + k(^5D_0 \rightarrow {}^7F_6) \sim 0$.

The transition probability for the $^5D_0 \rightarrow {}^7F_0$ transition was obtained from the absorption spectrum using eq 4 from Lewis and Kasha,[13] with ϵ corrected for the relative population of the $^7F_0$ level.

$$\frac{1}{\tau_{nat}} = k(^7F_0 \longrightarrow {}^5D_0) = 2.880 \times 10^{-9}(g_l/g_u)\eta^2\nu^2 \int \epsilon(\nu)d\nu \quad (4)$$

where $k(^7F_0 \rightarrow {}^5D_0)$ is the radiative transition probability, g is the degeneracy of the electronic states, η is the index of refraction, ϵ is the molar absorptivity, u and l indicate the upper and lower states, respectively, and ν is the absorption maximum in wavenumbers. By using the calculated value for $k(^7F_0 \rightarrow {}^5D_0)$ and the ratio of the relative fluorescence intensities (in square brackets), we obtain

$$\sum A_r = k(^5D_0 \longrightarrow {}^7F_0) \times \left[1 + \frac{S(^5D_0 \longrightarrow {}^7F_1)}{S(^5D_0 \longrightarrow {}^7F_0)} + \frac{S(^5D_0 \longrightarrow {}^7F_2)}{S(^5D_0 \longrightarrow {}^7F_0)} + \frac{S(^5D_0 \longrightarrow {}^7F_3)}{S(^5D_0 \longrightarrow {}^7F_0)} + \frac{S(^5D_0 \longrightarrow {}^7F_4)}{S(^5D_0 \longrightarrow {}^7F_0)}\right] \quad (5)$$

where S is the area of the relevant transition obtained

(9) E. Nakazawa and S. Shionoya, *J. Phys. Soc. Jap.*, **28**, 1260 (1970).

(10) M. J. Weber in "Optical Properties of Ions in Crystals," H. M. Crosswhite and H. W. Moos, Ed., Interscience, New York, N. Y., 1967, p 467.

(11) A. N. Fletcher, *J. Mol. Spectrosc.*, **23**, 221 (1967).

(12) W. R. Dawson and J. L. Kropp, *J. Opt. Soc. Amer.*, **55**, 822 (1965).

(13) C. N. Lewis and M. Kasha, *J. Amer. Chem. Soc.*, **67**, 994 (1945).

from the emission spectrum and $k(^5D_0 \rightarrow {}^7F_0) = k(^7F_0 \rightarrow {}^5D_0)$.

The value obtained for $1/\Sigma A_r = 2.97$ msec and therefore $Q = 2.83$ msec/2.97 msec = 0.953.

Calculated Results. The quantum efficiency of the $^5D_0$ fluorescence excited to higher selected levels was obtained using formula 1; the $^5D_0$ excitation was used as an internal standard. The results of these measurements are presented in Table III. From this table, the probability of population of $^5D_0$ from upper electronic levels was calculated using formula 6,[12] where

$$Q(A) = p(A)Q(^5D_0) \quad (6)$$

$Q(A)$ is the fluorescence efficiency determined upon excitation of level A, $Q(^5D_0)$ is the fluorescence efficiency calculated when the $^5D_0$ level is excited, and $p(A)$ is the probability that an excited ion initially in state A will convert to the $^5D_0$ level. Values of $p(A)$ are also presented in Table III.

Table III: Quantum Efficiency of $^5D_0$ Fluorescence and Probabilities of Populating the $^5D_0$ Level *via* Excitation to Upper Selected Levels

Excited level	Wavelength, nm	Quantum efficiency	Population probabilities $P(^5D_0)$
$^5D_0$	579.6	0.953	
$^5D_1$	526.4	0.822	0.863
$^5D_2$	466.3	0.693	0.727
$^5D_3$	416.5	0.612	0.642
$^5L_6$	394.0	0.581	0.610

Comparison of Quantum Efficiencies in Glasses and Solutions. It was of interest to compare the quantum efficiencies of Eu^{3+} fluorescence in solution with those in glasses. The results are presented in Table IV.

Table IV: Percentage Quantum Yields of $^5D_0$ Emission of Eu(III) upon Excitation to Selected Levels in Various Media

Excited level	$Eu(ClO_4)_3$ in water[a]	$Eu(NO_3)_3$ in water[a]	Eu(III) in phosphate glass	Eu(III) in[b] silicate glass
$^5D_0$	0.019	0.04	0.95	0.93
$^5D_1$	0.011	0.0185	0.822	0.855
$^5D_2$			0.693	0.764
$^5D_3$			0.612	0.661
$^5L_6$, $^5G_2$	0.0057	0.0073	0.581	0.598
$P(^5D_1 \rightarrow {}^5D_0)$	0.57	0.46	0.86	0.91

[a] Reference 6. [b] R. Velapoldi, R. Reisfeld, and L. Boehm, in preparation.

As is well known (see for instance ref 14), the larger the energy difference between two electronic states, the smaller is the nonradiative transition probability between them. In these cases, the energy difference is measured in units of the particular vibrational quanta (phonons) responsible for the nonradiative transfer.[15]

In this particular case, the energy difference between the $^5D_0$ and ^7F multiplet of Eu^{3+} is approximately 16,000 cm^{-1} the energy of the phonon in the phosphate glass (P–O stretching frequency) is 1100–1300 cm^{-1},[16] while the phonon energy of the O–H bond is 3600–3700 cm^{-1}. Hence, the energy difference in glass corresponds to 14 phonons, whereas in aqueous solution it corresponds to only 4–5 phonons. From this we see that the nonradiative loss in glass should be much smaller than in liquids, as observed experimentally in this work.

Radiative and Nonradiative Rate Constants in Various Media. Using the relation between the quantum efficiency, Q, the radiative rate constant, k_r, and the nonradiative rate constant, k_{g0}

$$Q(^5D_0) = k_r/(k_r + k_{g0}) \quad (7)$$

and the relation between the measured lifetime and quantum efficiency (eq 2), we have calculated the radiative and nonradiative rates for various media. These rates are summarized in Table V.

Table V: Rate Constants of Radiative (k_r) and Nonradiative (k_{g0}) Transitions of the $^5D_0$ Level in Various Media

Quantity	$Eu(ClO_4)_3$ in water[a]	$Eu(NO_3)_3$ in water[a]	Eu(III) in phosphate glass	Eu(III) in[b] silicate glass
Q, %	0.019	0.040	0.953	0.93
k_r, sec^{-1}	183	325	337	336
k_{g0}, sec^{-1}	9800	7800	17	25

[a] See ref 6. [b] See the reference of footnote *b*, Table IV.

These data show that the radiative rates are approximately the same for the Eu^{3+} in solution and in phosphate and silicate glasses, which indicates that in all three media, forced electric dipole transitions become more allowed due to the low symmetry (probably C_s).[2] The symmetry of the europium site must be higher in perchlorate solution, a fact explained by the coordinating ability of the nitrate anion. The Eu^{3+} will be surrounded by only coordinated water molecules in the perchlorate solution and thus have high symmetry. In the nitrate solution, coordination will be shared by the nitrate anions and water molecules, resulting in decreased symmetry.[17] Hence in per-

(14) A. Heller, *J. Mol. Spectrosc.*, **28**, 208 (1968).

(15) B. Barnett and R. Englman, *J. Luminescence*, **3**, 55 (1970).

(16) R. Reisfeld, E. Greenberg, L. Kirshenbaum Boehm, and G. Michaeli, 8th Rare Earth Conference, 1970, Vol. 2, p 743.

(17) J. C. Bailar, Jr., and D. H. Busch in "Chemistry of the Coordination Compounds," J. C. Bailer, Jr., Ed., Reinhold, Princeton, N. J., 1956.

chlorate the main transitions will be those allowed by the selection rules of magnetic dipole and quadrupole transitions resulting in the lower radiative transition probabilities. In contrast to the invariancy of the radiative rate constant, we observe a large difference between the high nonradiative rate constant in solution and the very low rate constant in glass. This fact is again in agreement with the different phonon energies of the O–H bonds in solution and the P–O bonds in glasses.

Rate Constants of the Transitions from the $^5D_1$ Level. The rate constant of depopulation of the $^5D_1$ to $^5D_0$ transition can be calculated from

$$P(^5D_1) = k_{10}/(k_{10} + k_{1g}^{r} + k_{1g}^{nr}) \quad (8)$$

where $P(^5D_1)$ is the probability that an excited Eu^{3+} ion initially in state $^5D_1$ will convert to state $^5D_0$, k_{10} is the rate constant of transfer from the $^5D_1$ level to the $^5D_0$ level, and k_{1g}^{r} and k_{1g}^{nr} are the radiative and nonradiative rates, respectively, of transitions from $^5D_1$ to the ground ^7F manifold.

We can assume that the $^5D_1 \rightarrow {}^7F$ manifold is almostly entirely radiative because of the large energy difference between the two manifolds. This difference is larger than that between the $^5D_0$ level and the ^7F manifold, where we found, as shown in Table V, that k(radiative) = 337 sec^{-1} compared to a k(nonradiative) of 17 sec^{-1}. We can thus assume that $k_{1g}^{r} + k_{1g}^{nr}$ in eq 8 equals k_{1g}^{r} and therefore

$$k_{10} = \left[\frac{P(^5D_1)}{1 - P(^5D_1)}\right](k_{1g}^{r}) \quad (9)$$

We notice also that

$$k_{1g}^{r} = k_{^5D_1 \rightarrow {}^7F_0} + k_{^5D_1 \rightarrow {}^7F_1} + k_{^5D_1 \rightarrow {}^7F_2} \quad (10)$$

The value for $k_{^5D_1 \rightarrow {}^7F_0}$ can be obtained from the oscillator strength, f, of the $^7F_0 \rightarrow {}^5D_1$ transition obtained previously.[2] Using eq 4 of the present paper, we obtain for this case

$$k_{^5D_1 \rightarrow {}^7F_0} = (2.880 \times 10^{-9})\eta^2\nu^2(g_1/g_u)\left(\frac{f}{4.32 \times 10^{-9}}\right) \quad (11)$$

where the constants and terms have the same meanings as in equation 4.

In similar fashion

$$k_{1g}^{r} = k(^5D_1 \longrightarrow {}^7F_0) \times \left[1 + \frac{k(^5D_1 \longrightarrow {}^7F_1)}{k(^5D_1 \longrightarrow {}^7F_0)} + \frac{k(^5D_1 \longrightarrow {}^7F_2)}{k(^5D_1 \longrightarrow {}^7F_0)}\right]$$

By using the value for $k(^7F_0 \rightarrow {}^5D_1)$ obtained from the absorption spectrum and the ratios of the relative fluorescence intensities obtained from the emission spectrum (data in Table II), we obtain $k(^5D_1 \rightarrow {}^7F_0) = 1.1 \times 10^3$ sec^{-1} and $k_{1g}^{r} = 2.2 \times 10^4$ sec^{-1}. The rate of transition from $^5D_1 \rightarrow {}^5D_0$ calculated from eq 9 is $k_{10} = 1.4 \times 10^5$ sec^{-1}. This rate is much higher than the rate of the $^5D_0 \rightarrow {}^7F$ transitions because (a) the radiative transitions are allowed by magnetic dipole selection rules and (b) the nonradiative transitions are likely to occur because of the 2000 cm^{-1} energy difference between the $^5D_1$ and $^5D_0$ levels which corresponds to only two phonons.

Acknowledgment. The authors are grateful to Dr. B. Barnett, Soreq Nuclear Research Center, Yavne, Israel, for his most interesting and helpful discussions.

Structural Investigations of Calcium Binding Molecules. I. The Crystal and Molecular Structures of Ethane-1-hydroxy-1,1-diphosphonic Acid Monohydrate, $C(CH_3)(OH)(PO_3H_2)_2 \cdot H_2O$

by V. A. Uchtman* and R. A. Gloss

Miami Valley Laboratories, The Procter & Gamble Company, Cincinnati, Ohio 45239 *(Received August 18, 1971)*

Publication costs assisted by The Procter & Gamble Company

The crystal and molecular structures of ethane-1-hydroxy-1,1-diphosphonic acid monohydrate have been determined by single crystal X-ray diffraction techniques using the symbolic addition procedure. $C(CH_3)(OH)(PO_3H_2)_2 \cdot H_2O$ ($H_4EHDP \cdot H_2O$) crystallizes in monoclinic space group $P2_1/c$ with unit cell dimensions $a = 7.011 \pm 0.003$ Å, $b = 17.613 \pm 0.007$ Å, $c = 7.143 \pm 0.003$ Å, $\beta = 108° 34' \pm 04'$, $\rho_{calcd} = 1.78$, $\rho_{obsd} = 1.80$, four formula units per unit cell. Full-matrix least-squares refinement resulted in $R_1 = 5.1\%$ and $R_2 = 3.6\%$ for 1757 observed reflections measured by counter techniques. The crystal structure consists of H_4EHDP and water molecules connected by hydrogen bonds in an infinite network. A comparison of the detailed molecular features of H_4EHDP with those of methylene diphosphonic acid (H_4MDP) indicates that considerable flexibility, depending on the nature of R_1 and R_2, exists in the $O_3P-CR_1R_2-PO_3$ framework. The relative aqueous acidities of these compounds are explained in part on the basis of the molecular configurations resulting from steric interactions between the R groups and the phosphonyl oxygens. A description of the hydrogen-bonding network in the crystal is given, and an interesting correlation between hydrogen bond strength and phosphorus–oxygen bond length is described. This correlation is explained as being due to a delocalization and buildup of negative charge density on the phosphonyl oxygens due to attraction of the phosphonic acid protons to the hydrogen bond acceptor.

Introduction

Properties of efficient and effective alkaline earth metal ion sequestration have caused considerable attention to be focused on *gem*-diphosphonates, particularly ethane-1-hydroxy-1,1-diphosphonate, $C(CH_3)(OH)(PO_3)_2^{4-}$, (EHDP™).[1] Previous fundamental studies on EHDP have described acid dissociation constants and metal–ion complex formation. Grabenstetter, Quimby, and Flautt[2] and Carroll and Irani[3] used pH titration techniques to determine the acid dissociation constants of a series of substituted methylene diphosphonic acids, $[R_1R_2C(PO_3H_2)_2]$, and demonstrated a linear correlation of acid properties with the electron-donating power of the substituents. The former study revealed an additional correlation with P^{31} nmr chemical shifts. The investigations of Carroll and Irani also included the determination of complex formation constants for EHDP and alkali metal, calcium, and magnesium ions. In these studies anomalies were found for EHDP when it was compared to other effective complexers. Thus, based on correlations with electron-donating ability, EHDP was found to be a weaker acid than expected; it was similarly found that EHDP interacts to a greater extent with highly electropositive metal ions than would be predicted from results obtained with other members of the series studied. It was suggested that intramolecular hydrogen bonding involving the hydroxyl group and binding of this group to the metal ions might be responsible for these phenomena. Closely related to this work are the physical chemical studies of Grabenstetter, Cilley, and Wiers[4,5] which demonstrated the uncommon and unexplained ability of calcium ion–EHDP solutions to form discrete, polynuclear complexes. Also, Francis and coworkers have demonstrated the ability of certain *gem*-diphosphonates to inhibit calcium hydroxyapatite growth *in vitro*, as well as pathological calcification *in vivo*.[6,7]

Because of this considerable interest in EHDP and in calcium binding in general, it was felt that a single crystal X-ray diffraction study of EHDP and its calcium complexes would be desirable in order to provide definitive molecular structural information. Herein are reported the results of the first part of this study:

(1) C. F. Callis, A. F. Kerst, and J. W. Lyons, "Coordination Chemistry," S. Kirschner, Ed., Plenum Publishing Co., New York, N. Y., 1969, pp 223–247.

(2) R. J. Grabenstetter, O. T. Quimby, and T. J. Flautt, *J. Phys. Chem.*, **71**, 4194 (1967).

(3) (a) R. L. Carroll and R. R. Irani, *Inorg. Chem.*, **6**, 1994 (1967); (b) R. L. Carroll and R. R. Irani, *J. Inorg. Nucl. Chem.*, **30**, 2971 (1968).

(4) R. J. Grabenstetter and W. A. Cilley, *J. Phys. Chem.*, **75**, 676 (1971).

(5) B. H. Wiers, *ibid.*, **75**, 682 (1971).

(6) M. D. Francis, *Calif. Tissue Res.*, **3**, 151 (1969).

(7) M. D. Francis, R. G. G. Russell, and H. Fleisch, *Science*, **169**, 1264 (1969).

the crystal and molecular structures of $H_4EHDP \cdot H_2O$. A report on the crystal and molecular structures of one of the calcium complexes of EHDP, $CaH_2EHDP \cdot 2H_2O$, follows.[8] These reports represent the first part of an extensive study directed at examining the molecular structure characteristics important in effective and efficient calcium binding.

Experimental Section

A suitable single crystal of $H_4EHDP \cdot H_2O$ was obtained by slow evaporation of an aqueous solution of a sample supplied by Monsanto. A regular-shaped crystal of dimensions 0.75 (rotation (b) axis) × 0.25 × 0.35 mm was mounted on a glass fiber with epoxy cement. To prevent adsorption of moisture by the hygroscopic crystal it was coated with a thin film of the cement. Preliminary oscillation, Weissenberg and precession photographs exhibited Laue C_{2h}-$2/m$ symmetry characteristic of the monoclinic system. The crystal was optically aligned about the rotation axis (crystallographic b axis) on a Siemens automated single crystal diffractometer, and 55 diffraction maxima were manually centered. The lattice constants were obtained at 25° by a least-squares refinement of the measured θ angle settings of these 55 reflections. These lattice constants were then used to generate the diffractometer angle settings for all data reflections.

All intensity data were collected at a take-off angle of 2° by the θ–2θ scan technique using Zr-filtered Mo Kα radiation and a scintillation counter followed by pulse height analyzer. The pulse height analyzer window was set to accept 90% of the diffracted radiation. A counter aperture 3 mm in diameter was placed 68 mm from the crystal. The data were collected using "five-values measurement."[9] As a check on crystal and instrument stability one of three standard reflections was measured every 25 reflections. No significant fluctuations in these standards were observed during the course of data collection. A given reflection was considered "unobserved" and assigned a value of $3\sigma_B$ if the net intensity was less than $3\sigma_B$, where σ_B is the standard deviation of the background count.

A total of 1757 observed and 695 unobserved reflections (hkl, $\bar{h}kl$) for which $2\theta \leq 60°$ was collected and treated by the above procedure. Lorentz and polarization corrections were applied. No absorption or extinction corrections were applied. The linear absorption coefficient (μ) of 5.36 cm^{-1} for Mo Kα radiation results in a $\mu R_{max} < 0.22$ for which the change of absorption correction factors with θ is negligible.[10] The effects of absorption result in extremes for the I/I_0 ratio of 0.803 and 0.878. Thus a reflection of measured intensity 1.00 could vary in intensity from 1.14 to 1.25 after correction, *i.e.*, a variation of 4.5% about the mean value. The relatively small values of the real and imaginary dispersion corrections for Mo Kα radiation (*i.e.*, $\Delta f' = 0.1$ and $\Delta f'' = 0.2$ for phosphorus)[11] were assumed not to have any significant effect on the atomic coordinates of this centrosymmetric crystal.[12] The scattering factors used for all atoms were those based on Hartree–Fock–Slater calculations as compiled by Hanson, *et al.*[13]

Results

Unit Cell and Space Group. Lattice constants and their estimated standard deviations for this crystal of $C(CH_3)(OH)(PO_3H_2)_2 \cdot H_2O$ are $a = 7.011 \pm 0.003$ Å, $b = 17.613 \pm 0.007$ Å, $c = 7.143 \pm 0.003$ Å, $\beta = 108° 34' \pm 04'$; unit cell volume = 836.2 Å^3. The experimental density of 1.80 ± 0.02 g/cm^3 (flotation in mixtures of dichloromethane and dibromomethane) agrees well with the value of 1.78 g/cm^3 calculated on the basis of four of the above formula species per unit cell. The total number of electrons per unit cell, $F(000)$, is 464. Systematic absences of $\{h0l\}$ for l odd and $\{0k0\}$ for k odd uniquely define the probable space group as $P2_1/c$ (C_{2h}^5, no. 14). Solution of the structure required the location of two phosphorus, eight oxygen, two carbon, and ideally ten hydrogen atoms corresponding to one $C(CH_3)(OH)(PO_3H_2)_2$ molecule and one H_2O molecule of solvation per asymmetric unit. The crystallographically independent atoms were each found from the structural analysis to occupy the general fourfold set of positions: $\pm (x, y, z;\ x, {}^1/_2 - y, {}^1/_2 + z)$.

Determination of the Structure. Application of the Hauptman–Karle[14] symbolic addition method, using the computer programs FAME, MAGIC, and LINK,[15] led to the successful solution of the atomic arrangement of the crystal. A Wilson plot[16] generated from a total of 2452 observed and unobserved reflections provided an initial scale factor and an overall isotropic temperature factor from which the observed structure amplitudes were placed on an absolute scale and normalized structure factor magnitudes $E|$ were obtained. Statistical analysis[17] of the $|E|$ values so generated provided fur-

(8) V. A. Uchtman, *J. Phys. Chem.*, **76**, 1304 (1972).

(9) "Siemens Automatic Single Crystal Diffractometer AED According to W. Hoppe," March, 1967.

(10) "International Tables for X-Ray Crystallography," Vol. II, The Kynoch Press, Birmingham, England, 1959, p 295.

(11) D. H. Templeton in "International Tables for X-Ray Crystallography," Vol. III, The Kynoch Press, Birmingham, England, 1962, p 215.

(12) D. H. Templeton, *Acta Crystallogr.*, **8**, 842 (1955).

(13) H. P. Hanson, F. Herman, J. D. Lea, and S. Skillman, *ibid.*, **17**, 1040 (1964).

(14) (a) H. Hauptman and J. Karle, "Solution of the Phase Problem I. The Centrosymmetric Crystal," American Crystallographic Association Monograph No. 3, Polycrystal Book Service, Pittsburgh, Pa., 1953. (b) *Cf.* I. L. Karle and J. Karle, *Acta Crystallogr.*, **16**, 969 (1963).

(15) R. B. K. Dewar and A. L. Stone, "FAME and MAGIC, Fortran Computer Programs for Use in the Symbolic Addition Method," University of Chicago, 1966. *Cf.* E. B. Fleischer, R. B. K. Dewar, and A. L. Stone, Abstracts of the American Crystallographic Association Meeting, Winter 1967.

(16) M. J. Bueger, "Crystal Structure Analysis," Wiley, New York, N. Y., 1960, p 234.

ther verification of the centrosymmetric nature of the crystal. Seven reflections of large $|E|$ were assigned symbolic phases A thru G and utilized to initiate the symbolic addition procedure. Approximately 800 reflections for which $E \geq 0.97$ were used in the application of the Hauptman–Karle σ-2 relationship.[14,15] Only those signs with a probability level $p \geq 0.995$ were accepted. After four iterations 496 symbolic signs were determined. The three reflections given symbolic phases E, F, and G were chosen as origin-specifying reflections (*i.e.*, these symbols were given plus signs); the assignment of symbols A, B, and C as minus and D as plus gave the least number of inconsistencies among the symbol equivalences. A three-dimensional Fourier synthesis was computed which used the 496 reflections with phases calculated on the basis of the above symbol assignments. This map indicated the initial coordinates for eleven of the 12 nonhydrogen atoms. A subsequent difference-Fourier map which utilized all observed data revealed the position of the additional nonhydrogen atom which was the oxygen atom of the water molecule.

Several cycles of full-matrix least-squares refinement of these C, P, and O atomic positions with individual isotropic temperature factors gave an unweighted discrepancy factor of

$$R_1 = [\sum||F_o| - |F_c||/\sum|F_o|] \times 100 = 8.2\%$$

Further cycles of refinement utilizing anisotropic temperature factors resulted in $R_1 = 6.6\%$. A difference-Fourier map calculated from the parameters of this last refinement cycle revealed 12 peaks of intensity between 0.7 and 0.5 ϵ Å^{-3}. Ten of these positions corresponded to chemically reasonable hydrogen atom locations, and they were assigned as such; of the other two peaks one (0.63 ϵ Å^{-3}) was less than 1 Å from the methylene carbon and the other (0.55 ϵ Å^{-3}) was less than 0.6 Å from a phosphonyl oxygen. These two peaks were assumed to be the result of anisotropic motion not corrected for in this incompletely refined model, or artifacts of the data. The inclusion of the ten hydrogen atom positions, with isotropic thermal parameters of 6.0, in a structure factor calculation reduced R_1 to 6.0%. Two additional cycles of refinement in which the hydrogen parameters were held constant resulted in final discrepancy factors of

$$R_1 = 5.1\%$$

$$R_2 = [\sum\omega||F_o| - |F_c||^2/\sum\omega|F_o|^2]^{1/2} \times 100 = 3.6\%$$

Refinement was based on the minimization of $\Sigma\omega_i\Delta F_i^2$ and weights were determined according to the relationship $\omega_i = 1/\sigma_i^2(F_o)$. The last cycle of refinement resulted in no significant positional parameter shifts greater than 0.3 of the standard deviation of the parameter. A final difference map calculated from these parameters revealed only two peaks >0.5 ϵ Å^{-3} (0.63 and 0.60) and only one peak <-0.5 ϵ Å^{-3} (−0.56). These were all close enough to nonhydrogen atoms to be ascribable to uncorrected anisotropic motion.

Final atomic positional and anisotropic thermal parameters are given in Tables I and II; Table III lists interatomic distances and angles.[18] The X-ray 67 system of programs, modified for use on the Control Data Corp. 6600 computer, was used for the majority of computing operations. Data reduction was carried out on a local IBM 1800 computer using local programs written by M. R. Becker and N. C. Webb of these laboratories.

Table I: Final Atomic Positional Parameters with Their Standard Deviations for $C(CH_3)(OH)(PO_3H_2)_2 \cdot H_2O$

	$x(10^4\sigma x)$	$y(10^4\sigma y)$	$z(10^4\sigma z)$
P1	0.6218(1)	0.3665(1)	0.2870(1)
P2	0.8023(1)	0.4089(1)	−0.0425(1)
O1	0.4494(3)	0.3272(1)	0.1264(3)
O2	0.5695(4)	0.4511(1)	0.3064(3)
O3	0.6763(3)	0.3277(1)	0.4848(3)
O4	1.0020(3)	0.3978(1)	−0.0914(3)
O5	0.6432(3)	0.3591(1)	−0.1887(3)
O6	0.7436(3)	0.4910(1)	−0.0381(3)
O7	0.8988(3)	0.2872(1)	0.1934(3)
O8	0.2615(3)	0.2260(1)	0.2255(4)
C1	0.8416(5)	0.3653(2)	0.2010(5)
C2	1.0170(5)	0.4063(2)	0.3525(5)
H1[a]	1.000	0.456	0.400
H2	1.050	0.381	0.467
H3	1.132	0.400	0.313
H4	0.805	0.260	0.120
H5	0.137	0.234	0.223
H6	0.335	0.195	0.330
H7	0.363	0.276	0.187
H8	0.467	0.483	0.225
H9	0.920	0.554	0.055
H10	0.630	0.356	−0.325

[a] These hydrogen positional parameters were obtained from a difference Fourier map, and no refinement of them was attempted. They were given isotropic temperature factors of 6.0.

Discussion

The crystal structure of ethane-1-hydroxy-1,1-diphosphonic acid monohydrate ($H_4EHDP \cdot H_2O$) consists of columns of symmetry related H_4EHDP molecules linked together by a complex hydrogen-bonding network which utilizes both hydroxyl and phosphonic

(17) (a) *Cf.* G. H. Stout and L. H. Jensen, "X-Ray Structure Determination," Macmillan, New York, N. Y., 1968, p 321; (b) I. L. Karle, K. S. Dragonette, and S. A. Brenner, *Acta Crystallogr.*, 19, 713 (1965).

(18) A listing of the observed and calculated structure factors will appear immediately following this article in the microfilm edition of this volume of the journal. Single copies may be obtained from the Business Operations Office, Books and Journals Division, American Chemical Society, 1155 Sixteenth Street, N.W., Washington, D. C. 20036, by referring to code number JPC-72-1298. Remit check or money order for $3.00 for photocopy or $2.00 for microfiche.

Table II: Final Anisotropic Temperature Factors[a] and Their Standard Deviations for $C(CH_3)(OH)(PO_3H_2)_2 \cdot H_2O$

	$\beta 11(10^4\sigma)$	$\beta 22(10^4\sigma)$	$\beta 33(10^4\sigma)$	$\beta 12(10^4\sigma)$	$\beta 13(10^4\sigma)$	$\beta 23(10^4\sigma)$
P1	0.0096(2)	0.0014(1)	0.0069(2)	0.0007(1)	0.0017(2)	0.0001(1)
P2	0.0086(2)	0.0012(1)	0.0079(2)	0.004(1)	0.0023(2)	0.0000(1)
O1	0.0101(1)	0.0028(1)	0.0090(1)	−0.0011(2)	0.0004(5)	−0.0003(2)
O2	0.0173(7)	0.0019(1)	0.0153(7)	0.0023(2)	0.0034(6)	−0.0001(2)
O3	0.0171(7)	0.0018(1)	0.0083(5)	0.0010(2)	0.0037(5)	0.0006(2)
O4	0.0118(6)	0.0018(1)	0.0175(7)	0.0005(2)	0.0065(5)	0.0005(2)
O5	0.0114(6)	0.0024(1)	0.0088(5)	0.0017(2)	0.0026(5)	0.0009(2)
O6	0.0117(6)	0.0013(1)	0.0137(6)	0.0000(2)	0.0009(5)	−0.0007(2)
O7	0.0113(6)	0.0013(1)	0.0151(6)	0.0007(2)	0.0010(5)	−0.0001(2)
O8	0.0105(6)	0.0022(1)	0.0190(7)	0.0003(2)	0.0031(5)	0.0010(2)
C1	0.0101(3)	0.0011(1)	0.0083(7)	−0.0001(3)	0.0018(6)	−0.0001(2)
C2	0.0128(9)	0.0023(1)	0.0111(8)	−0.0012(3)	−0.0010(7)	−0.0010(3)

[a] Anisotropic temperature factors are expressed as $\exp\{-(h^2\beta_{11} + k^2\beta_{22} + l^2\beta_{33} + 2hk\beta_{12} + 2hl\beta_{13} + 2kl\beta_{23})\}$.

acid groups. These columns lie along the *c* lattice direction; columns of symmetry related water molecules which act as both hydrogen bond donors and acceptors lie parallel to and bridge the H_4EHDP columns. This arrangement in the monoclinic unit cell is illustrated in Figure 1. Table IIIC lists the hydrogen bond distances and angles, all but one (*vide infra*) of which are not unusual (within the error limits of the hydrogen positional parameters which were not varied in the least-squares refinement). All hydrogen bonding is intermolecular, with no evidence of intramolecular hydrogen bonding. The one unusual hydrogen bond involves a phosphonic acid hydrogen (H7) as donor and the water molecule as acceptor. This hydrogen position was found on the difference map midway between the two oxygen atoms (O1···O8 distance is 2.450 Å). However, this cannot be termed significant due to the relatively large errors in the unrefined hydrogen atom positions.

The molecular parameters of H_4EHDP (Figure 2) are in general not significantly different from expected values. The phosphorus–oxygen distances fall into two classes. Distances corresponding to P–OH (1.541, 1.550; and 1.559, 1.537; average 1.547 Å) fall well within the range of average values previously observed for phosphonyl groups: *e.g.*, 1.53 Å in nitrilotrimethylene triphosphonic acid (I),[19] 1.57 Å in 2-aminoethylene phosphonic acid (II),[20] 1.54 Å in methylene diphosphonic acid (III),[21] and 1.57 Å in CaH_2EHDP (IV).[8] The second class of phosphorus–oxygen distances corresponds to P=O (1.505 and 1.507 Å); these are somewhat longer than those found in I (1.48 Å) and III (1.47 Å), and in fact they are closer to the average values of 1.50, 1.51, and 1.51 Å found for the P–O distances in the ionized phosphonate groups of I, II, and IV, respectively, where the oxygen atoms carry a partial negative charge. All four of the phosphonic acid hydrogens are involved in hydrogen bonds and an interesting correlation between the strength of these hydrogen bonds and the P–O distances has been observed (see Table IV). One of the P–OH···O hydrogen bonds

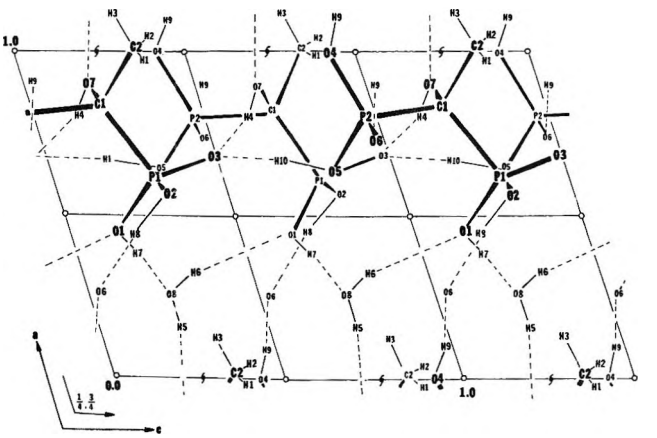

Figure 1. [010] projection of the monoclinic unit cell of $C(CH_3)(OH)(PO_3H_2)_2 \cdot H_2O$.

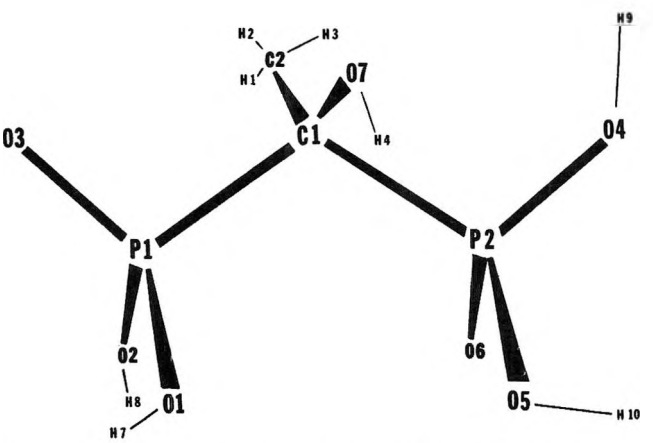

Figure 2. Molecular configuration of $C(CH_3)(OH)(PO_3H_2)_2$.

of each phosphonyl group is quite strong (O1···O8, 2.450; and O5···O3′, 2.479 Å) while the other is some-

(19) J. J. Daly and P. J. Wheatley, *J. Chem. Soc. A*, 212 (1967).

(20) Y. Okaya, *Acta Crystallogr.*, **20**, 712 (1966).

(21) F. M. Lovell, Abstracts of the American Crystallographic Association Meeting, July 1964, and private communication from F. M. L.

Table III: Interatomic Distances and Angles and Their Standard Deviations for $C(CH_3)(OH)(PO_3H_2)_2 \cdot H_2O$[a]

A. Bonding Distances

P1–O1	1.541(2)	O1–H7	1.24
P1–O2	1.550(3)	O2–H8	0.95
P1–O3	1.505(2)	O4–H9	1.00
P2–O4	1.559(3)	O5–H10	0.95
P2–O5	1.537(2)	O7–H4	0.85
P2–O6	1.507(3)	C2–H1	0.96
C1–P1	1.832(4)	C2–H2	0.89
C1–P2	1.840(4)	C2–H3	0.94
C1–C2	1.534(4)	O8–H5	0.88
C1–O7	1.440(4)	O8–H6	0.94

B. Bonding Angles

O1–P1–O2	110.29(13)	H1–C2–H2	99
O1–P1–O3	113.53(14)	H1–C2–H3	115
O2–P1–O3	110.42(14)	H2–C2–H3	103
O1–P1–C1	106.81(15)	H1–C2–H2	121
O2–P1–C1	106.80(16)	H2–C2–C1	109
O3–P1–C1	108.69(14)	H3–C2–C1	108
O4–P2–O5	106.56(14)	H4–O7–C1	113
O4–P2–O6	113.37(14)	H5–O8–H6	114
O5–P2–O6	114.71(13)	H7–O1–P1	115
O4–P2–C1	106.51(14)	H8–O2–P1	132
O5–P2–C1	105.17(15)	H9–O4–P2	107
O6–P2–C1	109.90(16)	H10–O5–P2	123
O7–C1–C2	107.80(24)		
O7–C1–P1	107.30(23)		
O7–C1–P2	108.86(23)		
P1–C1–P2	115.07(16)		
P1–C1–C2	109.19(25)		
P2–C1–C2	108.41(25)		

C. Hydrogen Bond Distances and Angles[b]

O1- - -O8	2.450(4)	O5- - -O3′	2.479(4)
O8- - -H7	1.22	O3′- - -H10	1.57
O1–H7- - -O8	173	O5–H10- - -O3′	157
O2- - -O6′	2.618(3)	O7- - -O3′	2.696(3)
O6′- - -H8	1.71	O3′- - -H4	1.89
O2–H8- - -O6′	159	O7–H4- - -O3′	158
O4- - -O6″	2.612(3)	O8- - -O1′	2.900(4)
O6″- - -H9	1.64	O1′- - -H6	2.05
O4–H9- - -O6″	164	O8–H6- - -O1′	151
		O8- - -O7′	2.703(4)
		O7′- - -H5	1.87
		O8–H5- - -O7′	158

D. Some Significant Nonbonding Distances Less than 3.2 Å[c]

P1···P2	3.098(2)	H1···H2	1.41
O1···O2	2.537(4)	H1···H3	1.61
O1···O3	2.547(3)	H2···H3	1.44
O2···O3	2.509(3)	H5···H6	1.51
O5···O6	2.563(3)		
O5···O4	2.482(3)		
O6···O4	2.562(4)		

[a] Distances are in angstroms and angles in degrees; standard deviations of the last significant figure, where available, are given in parentheses. [b] Primed symbols denote positions symmetry related to those in Table I. [c] All nonbonding distances not listed involving hydrogens were greater than 1.8 Å.

what weaker (O2···O6′, 2.618; and O4···O6″, 2.612 Å). The P–OH groups involved in strong hydrogen bonds have phosphorus–oxygen distances considerably shorter than those involved in weaker hydrogen bonds (1.541 *vs.* 1.550 and 1.537 *vs.* 1.559 Å); at the same time the P=O bond lengths are significantly longer than expected and as mentioned above are approaching the average P–O distance of 1.50 Å found in ionized phosphonates, as are the shorter P–OH bond lengths. These observations can be explained on the basis of a delocalization and buildup of negative charge density on the phosphonyl oxygens due to attraction of the phosphonic acid protons to their hydrogen bond acceptor. Such a correlation between hydrogen bond strength and phosphorus–oxygen bond length is also found to hold true for other phosphonic acids where the coordinates are known with sufficient precision, *e.g.*, nitrilotrimethylene triphosphonic acid (see Table IV).

Attempts have been made to explain the variations in acid dissociation constant of a series of methylene diphosphonic acids ($R_1R_2C(PO_3H_2)_2$) on the basis of the effects of the substituents R_1 and R_2.[2,3] In particular, the acidity of H_4EHDP was weaker than predicted on the basis of just substituent electron-withdrawing effects.[3] Insofar as steric effects may also be important in this respect, a comparison of the structures of methylene diphosphonic acid (H_4MDP, $R_1 = R_2 = H$) and H_4EHDP ($R_1 = CH_3$, $R_2 = OH$) is of interest On replacing the methylene hydrogens of H_4MDP with the more sterically active OH and CH_3 groups several changes to relieve steric strain might be possible: (1) an increase in the C–P–O angles with a concurrent decrease in the O–P–O angles; (2) a decrease in the P–C–P angle with a concurrent decrease in the P···P distance; (3) a rotation about the P–C bonds; and/or (4) a lengthening of the P–C bonds. The first of these effects is not observed, as average values for these angles are quite similar in both molecules. Although the expected directional change is observed in the P–C–P angle (115° in EHDP *vs.* 117° in H_4MDP) the P···P distance is not decreased, as expected, but rather increases from 3.00 to 3.10 Å due to the lengthening of the P–C bonds from 1.79 Å in H_4MDP to 1.83 and 1.84 Å in H_4EHDP. These latter values are also close to the observed P–C distances of 1.85 and 1.82 Å found for the partially ionized H_2EHDP^{2-} anion in $CaH_2EHDP \cdot 2H_2O$, but significantly less than the value of 1.874 Å found in the completely ionized carbonyldiphosphonate anion in $Na_4CO(PO_3)_2 \cdot 2H_2O$.[22]

The most significant difference between H_4MDP and H_4EHDP is the relative positions of the phosphonyl oxygens with respect to rotation about the P–C bond (Figure 3). In H_4MDP the two PO_3 groups are about 35° staggered with respect to each other when viewed along the P–P axis. For this molecule the intramolec-

(22) V. A. Uchtman and R. J. Jandacek, to be reported.

Table IV: Correlation of Phosphorus–Oxygen Bond Lengths and Hydrogen Bond Lengths[a]

			$C(CH_3)(OH)(PO_3H_2)_2$				
P1–O1H	1.541	O1H···O8	2.450				
P1–O2H	1.550	O2H···O6	2.618	Av	2.534	P1=O3	1.505
P2–O5H	1.537	O5H···O3	2.479				
P2–O4H	1.559	O4H···O6	2.612	Av	2.546	P2=O6	1.507
			$NH^+(CH_2PO_3H_2)_2(CH_2PO_3H)^-$ [b]				
P1–O2H	1.519	O3H···O4	2.458				
P1–O3H	1.537	O2H···O1	2.532	Av	2.495	P1=O1	1.489
P3–O9H	1.534	O9H···O6	2.524				
P3–O7H	1.543	O7H···O6	2.602	Av	2.563	P3=O8	1.465
			$CH_2(PO_3H_2)_2$[c]				
P2–O6H	1.52	O6H···O3	2.57				
P2–O4H	1.55	O4H···O5	2.52	Av	2.55	P2=O5	1.47
P1–O1H	1.54	O1H···O3	2.53				
P1–O2H	1.55	O2H···O5	2.66	Av	2.59	P1=O3	1.47

[a] Distances are given in angstroms; standard deviations for both P–O and O···O distances are at least 0.004 Å for NTP and H_4EHDP, but are not known for H_4MDP. [b] Reference 19. [c] Reference 21.

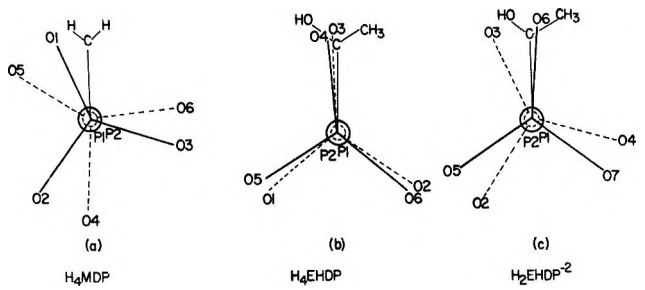

Figure 3. Relative orientations of phosphonyl groups in (a) H_4MDP,[21] (b) H_4EHDP, (c) CaH_2EHDP,[8] viewed along the P–C–P plane.

ular repulsive interactions between the phosphonyl group and the methylene hydrogens must be relatively insignificant, allowing the molecule to achieve, by rotation about the P–C bonds, a configuration which minimizes interactions between phosphonyl oxygen atoms. However, in H_4EHDP the PO_3 groups are nearly eclipsed, with an approximately planar W (or "cis") configuration for the O–P–C–P–O chain of atoms. Equally disposed on either side of this plane are the two pairs of phosphonyl oxygens and the OH and CH_3 groups. From an examination of models it can be seen that such an arrangement provides a minimum of repulsion between the OH and CH_3 groups, particularly the hydrogen atoms of the latter, and the phosphonyl oxygens. This interaction must now become more important, with respect to the most stable molecular configuration, than that between oxygen atoms of the phosphonyl groups. Thus, assuming no gross molecular configurational differences between the most stable species in solution and the species in the hydrated crystal, the weakness of H_4EHDP acidity in aqueous solution, relative to H_4MDP, may be a consequence of a preferred eclipsed configuration imposed by the OH and CH_3 groups; this would result in an ionized species which is less stable, due to an inability to achieve a configuration which more completely minimizes repulsion of negatively charged oxygens, than an anion which could assume a more staggered configuration, *e.g.*, MDP. Partial ionization of H_4EHDP, as in CaH_2-EHDP,[8] results, in the crystalline phase, in a slight deviation from the eclipsed configuration (Figure 3). This occurs primarily by a rotation of one phosphonyl group. However, this group is strongly complexed by Ca^{2+}, and the effects of this complexation on the ligand configuration cannot be estimated without an examination of the structure of the uncomplexed anion.

The work of Grabenstetter, Quimby, and Flautt[2] provides a further indication that steric effects, as well as electronic effects, of the methylene carbon substituents should be considered when attempting to explain the relative acidities of *gem*-diphosphonic acids. In their work it was observed that in the correlation of $pK_4°$ with Taft σ^* values, one group of compounds had pK_4 values larger than predicted by the correlation equation, and the other compounds had pK_4 values lower than predicted. The former group consisted of compounds with more sterically active methylene substituents which, according to the above argument, would force the molecule into an eclipsed configuration, resulting in weakened acid dissociation constants. This group consisted of the $R_1R_2C(PO_3H_2)_2$ acids where R_1, R_2 = CH_3, H; CH_3, CH_3; CH_3, OH; and Cl, Cl. The second group, which has substituents less sterically active and which we would predict to have staggered configurations, consists of compounds with R_1, R_2 = H, H; H, OH; and H, Br.

The above comparison of H_4MDP and H_4EHDP in-

dicates that a considerable degree of flexibility exists in the $O_3P-CR_1R_2-PO_3$ unit, depending on the nature of R_1 and R_2. Such flexibility is important not only in achieving minimum intramolecular steric repulsion, especially important for the ionized anions, but also in achieving effective metal–ligand interaction. This latter point is demonstrated in the structure of CaH_2EHDP and will be covered in more detail in a subsequent report on the crystal structure of $CaH_2EHDP \cdot 2H_2O$.[8]

Acknowledgments. We would like to thank Professor James M. Stewart and the personnel of the Control Data Corporation for their assistance in the use of the X-ray 67 system. Also we acknowledge Dr. F. M. Lovell for sending us results prior to publication.

Structural Investigations of Calcium Binding Molecules. II. The Crystal and Molecular Structures of Calcium Dihydrogen Ethane-1-hydroxy-1,1-diphosphonate Dihydrate, $CaC(CH_3)(OH)(PO_3H)_2 \cdot 2H_2O$; Implications for Polynuclear Complex Formation

by V. A. Uchtman

Miami Valley Laboratories, The Procter & Gamble Company, Cincinnati, Ohio 45239 *(Received August 18, 1971)*

Publication costs assisted by The Procter & Gamble Company

The crystal and molecular structures of a calcium complex of ethane-1-hydroxy-1,1-diphosphonate, $CaC(CH_3)(OH)(PO_3H)_2 \cdot 2H_2O$, have been determined by single crystal X-ray diffraction techniques, using standard heavy-atom techniques. To our knowledge, this represents the first reported X-ray structural investigation of a metal *gem*-diphosphonate complex. $CaH_2EHDP \cdot 2H_2O$ crystallizes in a triclinic unit cell, space group $P\bar{1}$; reduced cell parameters are $a' = 6.961(3)$, $b' = 7.625(4)$, $c' = 9.729(4)$ Å, $\alpha' = 92.52(7)°$, $\beta' = 106.08(7)°$, $\gamma' = 112.85(5)°$, $\rho_{calcd} = 2.06$ g cm^{-3}, $\rho_{exptl} = 2.05$ g cm^{-3}, two formula units per unit cell. Full-matrix least-squares refinement resulted in $R_1 = 4.9\%$ and $R_2 = 4.0\%$ for 2218 observed reflections measured by counter techniques. The crystal structure of $CaH_2EHDP \cdot H_2O$ consists of an infinite array of H_2EHDP^{2-} and water molecules and Ca^{2+} ions linked together by hydrogen bonding and calcium coordination of oxygens from both H_2EHDP^{2-} and water molecules. The H_2EHDP^{2-} anion exists in the crystal with one hydrogen on each phosphonyl group. The calcium ion has eight oxygen atoms in its primary coordination sphere: five from three symmetry-related H_2EHDP^{2-} ligands and three from water molecules. The CaH_2EHDP structure represents the first reported example of a metal chelate ring involving the un-ionized hydroxyl group of a hydroxyphosphonic acid. A hypothetical model has been constructed for the formation and structure of Ca–EHDP polynuclear aggregates. In this model the importance of the presence of multiple metal-binding sites (*i.e.*, more than two potentially stable chelating positions) is stressed. It is predicted that only those *gem*-diphosphonates, $R_1R_2C(PO_3)_2$, where either R_1 or R_2 is a potential binding site should be capable of significant polynuclear aggregate formation.

Introduction

Francis and coworkers have recently demonstrated that *gem*-diphosphonates, containing P–C–P bonds, have the capability of affecting calcium hydroxyapatite crystal growth both *in vitro* and *in vivo*.[1-3] They have discussed the possible usefulness of these materials in the treatment of human diseases involving calcium and phosphate metabolisms.[4] One such material that has received considerable attention is ethane-1-hydroxy - 1,1 - diphosphonate, $C(CH_3)(OH)(PO_3)_2^{4-}$, ($EHDP^{TM}$).

(1) M. D. Francis, *Calcif. Tissue Res.*, **3**, 151 (1969).

(2) H. Fleisch, R. G. G. Russell, and M. D. Francis, *Science*, **165**, 1262 (1969).

(3) M. D. Francis, R. G. G. Russell, and H. Fleisch, *ibid.*, **165**, 1264 (1969).

(4) W. R. King, M. D. Francis, and W. R. Michael, *Clin. Orthop. Relat. Res.*, **78**, 251 (1971).

In addition to the biochemical studies mentioned above, several studies have been conducted on the physical chemistry of aqueous solutions of EHDP;[5-9] some of this work has been briefly summarized in a previous report.[10] Results of these studies show that substituted methylene diphosphonic acids [$R_1R_2C(PO_3H_2)_2$] are effective complexers of alkaline earth metal ions in high pH solutions. Carroll and Irani[6,7] found that EHDP interacts with highly electropositive metal ions to a greater extent than was predicted from results with other members of the series. Closely related to this work are the investigations of Grabenstetter, Cilley, and Wiers[11] which demonstrated the unexpected ability of calcium ion–EHDP solutions to form discrete, polynuclear complexes. These complexes, formed in solutions as dilute as 2×10^{-3} *M* Ca^{2+}, had Ca/EHDP ligand ratios approaching, but not equal to, 2:1. Binding of the hydroxyl group to the metal ions has been suggested as being important in complexing between Ca^{2+} and EHDP.

The importance of ligand and metal–complex geometries to these properties prompted this present study: a single crystal X-ray diffraction examination of a calcium EHDP complex, $CaC(CH_3)(OH)(PO_3H)_2 \cdot 2H_2O$. Continuing attempts to prepare suitable single crystals of Ca_2EHDP have been unsuccessful, possibly due to complications arising from polynuclear complex formation. This report is the second in a series of investigations aimed at examining the structural factors (*e.g.*, spacing of functional groups and donor atoms in the ligand molecule and geometry of resulting complexes) which influence calcium ion binding by organic ligands. A previous report[10] on the crystal and molecular structures of $H_4EHDP \cdot H_2O$ has preceded this one. A report on the parent diphosphonic acid, methane-1,1-diphosphonic acid, H_4MDP has also appeared.[12]

To our knowledge this present report represents the first X-ray structural examination of a metal *gem*-diphosphonate complex.

Experimental Section

Single crystals of $CaH_2EHDP \cdot 2H_2O$ were obtained in the following manner by R. A. Gloss of these laboratories. A powdered sample of $CaH_2EHDP \cdot xH_2O$, prepared from calcium monohydrogen phosphate and disodium dihydrogen EHDP, was placed in an excess of water in a stoppered vial. After approximately 1 week at 60° the original powder sample completely converted into large well-shaped crystals of $CaH_2EHDP \cdot 2H_2O$. The elemental composition of this material was substantiated by the successful crystal structure determination.

A suitable single crystal of dimensions 0.20 × 0.25 × 0.35 (rotation (*b*) axis) mm was mounted on a glass fiber with epoxy cement. Preliminary oscillation, Weissenberg, and precession photographs indicated triclinic symmetry. The crystal was optically aligned on a Siemens automated single crystal diffractometer, and 50 diffraction maxima were manually centered. Lattice constants were obtained at 25° by least-squares refinement of the measured θ angle settings of these 50 reflections. These lattice constants were then used to generate diffractometer angle settings for all data reflections. The method of data collection was identical with a procedure previously reported.[10] A total of 2218 observed reflections and 434 unobserved reflections (*i.e.*, net intensity less than three times the standard deviation of the background counts) for which $2\theta \leq 60°$ (Mo Kα radiation) was collected from the *hkl*, $\bar{h}kl$, $h\bar{k}l$, and $\bar{h}\bar{k}l$ octants. No absorption or extinction corrections were applied. The linear absorption coefficient (μ) of 10.49 cm^{-1} for Mo Kα radiation results in a $\mu R_{max} < 0.315$ for which the change of absorption correction factors with θ is negligible.[13] The effects of absorption result in extremes for the I/I_0 ratio of 0.730 and 0.810. Thus a reflection of measured intensity 1.0 could vary in intensity from 1.24 to 1.37 after correction, *i.e.*, a variation of 5% about the mean value. The relatively small values of the real and imaginary dispersion corrections for Mo Kα radiation (*i.e.*, $\Delta f' = 0.1$ and 0.2, and $\Delta f'' = 0.2$ and 0.4 for phosphorus and calcium, respectively)[14] were assumed not to have any significant effect on this centrosymmetric crystal.[15] The scattering factors used for all atoms except Ca^{2+} were those compiled by Hanson, *et al.*[16] Ca^{2+} scattering factors were obtained from the International Tables.[17]

Results

Unit Cell and Space Group. Lattice constants (25°) and their estimated standard deviations for this crystal

(5) R. J. Grabenstetter, O. T. Quimby, and T. J. Flautt, *J. Phys. Chem.*, **71**, 4194 (1967).

(6) R. L. Carroll and R. R. Irani, *Inorg. Chem.*, **6**, 1994 (1967); and references therein.

(7) R. L. Carroll and R. R. Irani, *J. Inorg. Nucl. Chem.*, **30**, 2971 (1968).

(8) M. I. Kabachnik, R. P. Lastovskii, T. Ya. Medved', V. V. Medyntsev, I. D. Kolpakova, and N. M. Dyatlova, *Dokl. Akad. Nauk SSSR*, **177**, 582 (1967).

(9) C. F. Callis, A. F. Kerst, and J. W. Lyons in "Coordination Chemistry," S. Kirschner, Ed., Plenum Publishing Co., New York, N. Y., 1969, p 223.

(10) V. A. Uchtman and R. A. Gloss, *J. Phys. Chem.*, **76**, 1298 (1972).

(11) (a) R. J. Grabenstetter and W. A. Cilley, *ibid.*, **75**, 676 (1971); (b) B. H. Wiers, *ibid.*, **75**, 682 (1971); (c) B. H. Wiers, *Inorg. Chem.*, **10**, 2581 (1971).

(12) F. M. Lovell, Abstracts of the American Crystallographic Association Meeting, July 1964; private communication from F. M. L.

(13) "International Tables for X-Ray Crystallography," Vol. II, the Kynoch Press, Birmingham, England, 1959, p 295.

(14) Reference 13, Vol. III, 1962, p 215.

(15) D. H. Templeton, *Acta Crystallogr.*, **8**, 842 (1955).

(16) H. P. Hanson, F. Herman, J. D. Lea, and S. Skillman, *ibid.*, **17**, 1040 (1964).

(17) Reference 13, Vol. III, 1962, p 201.

of $CaC(CH_3)(OH)(PO_3H)_2 \cdot 2H_2O$ are $a = 6.961(3)$, $b = 8.085(4)$, $c = 9.729(4)$ Å, $\alpha = 106.26(7)°$, $\beta = 106.08(7)°$, $\gamma = 60.33(5)°$; unit cell volume = 450.4 Å^3. These values were used in all calculations; however, the reduced triclinic cell parameters are $a' = 6.961$, $b' = 7.625$, $c' = 9.729$ Å, $\alpha' = 92.52°$, $\beta' = 106.08°$, $\gamma' = 112.85°$. The experimental density of 2.05 ± 0.02 g cm^{-3} (determined by flotation in mixtures of bromoform and methylene chloride) agrees with the value of 2.06 g cm^{-3} calculated on the basis of two of the above formula species per unit cell. The total number of electrons per unit cell, $F(000)$, is 288. The assignment of $P\bar{1}$ (C_i^1, no. 2) as the space group was verified by the successful refinement of the structure in this space group.[18,19] Solution of the structure in space group $P\bar{1}$ required the location of one calcium, two phosphorus, nine oxygen, two carbon, and, ideally, ten hydrogen atoms, corresponding to one formula unit per asymmetric unit. The crystallographically independent atoms were each found from the structural analysis to occupy the general twofold set of positions $\pm(x, y, z)$.

Determination of the Structure. Consideration of the peaks on a three-dimensional Patterson interatomic vector map, calculated using all observed reflections, led to approximate positions for the one calcium and two phosphorus atoms. A three-dimensional Fourier synthesis, calculated using these positions, revealed the approximate positions of the remaining nonhydrogen atoms. A structure factor calculation using these positions and all observed reflections resulted in the following discrepancy factors

$$R_1 = [\sum||F_o| - |F_c||/\sum|F_o|] \times 100 = 39\%$$

$$R_2 = [\sum\omega||F_o| - |F_c||^2/\sum\omega|F_o|^2]^{1/2} \times 100 = 30\%$$

No peaks greater than 1.6 e/Å^3 were observed on a difference electron density map calculated at this point. Several cycles of least-squares refinement, initially with individual isotropic temperature factors and later with anisotropic factors, resulted in $R_1 = 5.1\%$. A difference electron density map using all data revealed reasonable positions for ten hydrogen atoms. One of these positions (H6) was only 0.35 Å from a center of symmetry, resulting in a separation of only 0.7 Å between it and its symmetry related position. It was assumed[18,19] that the proton associated with the P1 phosphonyl group was disordered. After an additional cycle of least-squares refinement, in which the hydrogen positions, with isotropic temperature factors of 6.0, were included but not varied, another difference map was calculated. All peaks on this map were < 0.5 e/Å^3. All peaks > 0.35 e/Å^3 could be accounted for as being due to uncorrected anisotropic thermal motion of phosphorus and oxygen atoms. A peak of intensity 0.4 e/Å^3 was in a position (H7) which would correspond to a proton bonding to another oxygen of the P1 phosphonyl group. A consideration of P–O bond distances (*vide infra*) indicated that it is reasonable to assume that there is a disorder of the proton belonging to this phosphonyl group such that half the molecules have the proton bonded to O6 (at position H7) and the other half to O7 (at position H6) (see Figure 3). Two additional cycles of anisotropic least-squares refinement, in which all hydrogen positions were held constant and

Table I: Final Atomic Positional Parameters with Their Standard Deviations for $CaC(CH_3)(OH)(PO_3H)_2 \cdot 2H_2O$

	$x(10^5\sigma x)$	$y(10^5\sigma y)$	$z(10^5\sigma z)$
Ca	0.20267(13)	0.20507(12)	0.98631(9)
P1	0.15803(19)	0.20256(17)	0.34431(12)
P2	0.27368(18)	0.74334(16)	0.87527(12)
O1	0.00302(50)	0.94457(41)	0.23868(33)
O2	0.14018(44)	0.75136(40)	0.97606(30)
O3	0.41091(43)	0.85239(37)	0.93418(29)
O4	0.44119(46)	0.52581(40)	0.81808(32)
O5	0.28954(42)	0.11389(37)	0.22089(28)
O6	0.29222(46)	0.11941(42)	0.48336(30)
O7	0.05588(50)	0.42593(40)	0.37600(31)
O8	0.11997(44)	0.52324(39)	0.14694(30)
O9	0.34196(45)	0.23047(39)	0.78632(30)
C1	0.08201(68)	0.84759(58)	0.71298(44)
C2	0.21645(75)	0.78782(66)	0.59190(47)
H1[a]	0.166	0.886	0.230
H2	0.332	0.840	0.652
H3	0.130	0.814	0.504
H4	0.270	0.660	0.578
H5	0.390	0.428	0.814
H6[b]	0.036	0.472	0.476
H7[b]	0.455	0.020	0.500
H8	0.120	0.510	0.236
H9	0.270	0.500	0.164
H10	0.486	0.128	0.794
H11	0.310	0.194	0.692

[a] These hydrogen positional parameters were obtained from difference-Fourier maps and were not refined. They were given isotropic temperature factors of 6.0. [b] These are the two probable positions for the disordered proton (see Results) of one of the phosphonyl groups.

(18) The disordering assumed for one of the phosphonyl groups (see section on Determination of the Structure) can also be explained on the basis of an incorrect choice of space group. However, the expenses of carrying out additional least-squares refinements in space group $P1$, which would require two independent formula units per unit cell and thus double the number of parameters, did not permit such attempts. The results of a statistical analysis[19] on normalized structure factor magnitudes, $|E|$ (scaled such that the average of $|E^2|$'s was 1.0), are given below.

	Calcd	Theor (centric)	Theor (acentric)
$\langle\|E\|\rangle$	0.819	0.798	0.886
$\langle\|E^2 - 1\|\rangle$	0.953	0.968	0.736

For the purpose of discussion, in the remainder of this report the structure will be referred to as disordered.

(19) (a) *Cf.* G. H. Stout and L. H. Jensen, "X-Ray Structure Determination," Macmillan, New York, N. Y., 1968, p 321; (b) I. L. Karle, K. S. Dragonette, and S. A. Brenner, *Acta Crystallogr.*, 19, 713 (1965).

Table II: Final Anisotropic Temperature Factors[a] with Their Standard Deviations for $CaC(CH_3)(OH)(PO_3H)_2 \cdot 2H_2O$

	$\beta_{11}(10^4\sigma)$	$\beta_{22}(10^4\sigma)$	$\beta_{33}(10^4\sigma)$	$\beta_{12}(10^4\sigma)$	$\beta_{13}(10^4\sigma)$	$\beta_{23}(10^4\sigma)$
Ca	0.0053(2)	0.0041(2)	0.0035(1)	−0.0017(2)	0.0014(1)	0.0006(1)
P1	0.0093(3)	0.0076(2)	0.0036(1)	−0.0037(2)	0.0016(1)	0.0004(1)
P2	0.0067(3)	0.0058(2)	0.0037(1)	−0.0030(2)	0.0010(1)	0.0008(1)
O1	0.0167(10)	0.0073(7)	0.0080(5)	−0.0047(7)	0.0019(5)	0.0011(4)
O2	0.0106(9)	0.0107(7)	0.0055(4)	−0.0057(6)	0.0026(5)	0.0015(4)
O3	0.0089(8)	0.0062(6)	0.0056(4)	−0.0041(6)	0.0021(4)	−0.0006(4)
O4	0.0112(9)	0.0063(6)	0.0089(5)	−0.0027(6)	0.0041(5)	−0.0000(4)
O5	0.0085(8)	0.0065(6)	0.0037(3)	−0.0018(6)	0.0025(4)	0.0001(4)
O6	0.0132(9)	0.0122(7)	0.0040(4)	−0.0036(7)	0.0001(5)	0.0024(4)
O7	0.0202(10)	0.0060(6)	0.0057(4)	−0.0050(7)	0.0037(5)	0.0001(4)
O8	0.0087(8)	0.0072(6)	0.0056(4)	−0.0020(6)	0.0020(4)	0.0012(4)
O9	0.0113(9)	0.0082(7)	0.0053(4)	−0.0016(6)	0.0025(5)	0.0007(4)
C1	0.0122(12)	0.0069(9)	0.0043(5)	−0.0040(9)	0.0021(6)	0.0005(5)
C2	0.0164(14)	0.0141(12)	0.0048(6)	−0.0064(11)	0.0031(7)	0.0011(6)

[a] Anisotropic temperature factors are expressed as $\exp\{-(h^2\beta_{11} + k^2\beta_{22} + l^2\beta_{33} + 2hk\beta_{12} + 2hl\beta_{13} + 2kl\beta_{23})\}$.

Table III: Interatomic Distances and Angles and Their Standard Deviations for $CaC(CH_3)(OH)(PO_3H)_2 \cdot 2H_2O$[a,b]

A. Calcium Coordination

Ca...O9	2.497(4)	Ca...O3''	2.421(3)
Ca...O8'	2.484(3)	Ca...O2'	2.352(4)
Ca...O5'	2.420(3)	Ca...O1'	2.608(3)
Ca...O3'	2.448(3)	Ca...O8''	2.578(3)

B. Bonding Distances for Ligands

P1–C1	1.815(6)	O1–H1	1.01
P1–O5	1.507(3)	O4–H5	1.00
P1–O6	1.530(3)	O6–H7	1.01
P1–O7	1.549(3)	O7–H6	0.96
P2–C1	1.857(4)	C2–H2	1.05
P2–O2	1.496(4)	C2–H3	0.91
P2–O3	1.505(4)	C2–H4	0.89
P2–O4	1.595(3)	O8–H8	0.90
C1–C2	1.530(7)	O8–H9	0.94
C1–O1	1.457(5)	O9–H10	0.93

C. Bond Angles for Ligands

O2–P2–O3	116.58(18)	C1'–O1–H1	109
O2–P2–O4	111.22(20)	C1–C2–H2	97
O3–P2–O4	106.87(17)	C1–C2–H3	114
O2–P2–C1	109.58(20)	C1–C2–H4	100
O3–P2–C1	105.27(22)	H2–C2–H3	127
O4–P2–C1	106.75(16)	H2–C2–H4	115
O5–P1–O6	113.25(15)	H3–C2–H4	101
O5–P1–O7	112.43(21)	P2–O4–H5	115
O6–P1–O7	110.46(16)	P1–O7–H6'	116
O5–P1–C1'	107.51(19)	P1–O6–H7'	123
O6–P1–C1'	107.92(23)	H8–O8–H9	96
O7–P1–C1'	104.78(19)	H10–O9–H11	93
P2–C1–P1'	113.68(31)		
P2–C1–O1'	103.98(25)		
P2–C1–C2	109.58(26)		
P1'–C1–O1	107.24(26)		
P1'–C1–C2	113.53(30)		
O1'–C1–C2	108.23(45)		

D. Hydrogen Bond Distances and Angles

O5...O9	2.694(4)	O7...O8	2.768(5)
O5...H10	1.80	O7...H8	1.92
O9–H10...O5	161	O8–H8...O7	157
O4...O8	2.812(5)	O7...O7'[c]	2.522(4)
O4...H9	1.88	O7...H6'	1.58
O8–H9...O4	173	O7'–H6'...O7	167
O9...O4	2.716(5)		
O9...H5	1.72		
O4–H5...O9	169		
O6...O9	2.806(4)		
O6...H11	1.94		
O9–H11...O6	168		
O6...O6'[c]	2.550(4)		
O6...H7'	1.54		
O6'–H7'...O6	174		

E. Some Nonbonding Distances

P1...P2'	3.074(2)	H2...H4	1.64
O2...O3	2.554(6)	H3...H4	1.82
O2...O4	2.551(4)	H2...H3	1.76
O4...O3	2.491(4)	H8...H9	1.37
O5...O6	2.536(4)	H10...H11	1.32
O5...O7	2.540(4)		
O6...O7	2.530(5)		

[a] Distances are in angstroms and angles in degrees; standard deviations of the last significant figure, where available, are given in parentheses. [b] Primed symbols denote positions symmetry-related to those in Table I. [c] It is assumed that the disordered protons are involved in the indicated hydrogen bonds.

H6 and H7 were assigned multiplicities of 0.5, resulted in final discrepancy factors of $R_1 = 4.9\%$ and $R_2 = 4.0\%$; there were no parameter shifts greater than 0.1 of the standard deviation of the parameter. Refinement was based on the minimization of $\Sigma\omega_i\Delta F_i^2$ and weights were determined according to $\omega_i = 1/\sigma_i^2(F_o)$.

Final atomic positional and temperature parameters are given in Tables I and II, respectively.[20] Table III lists interatomic distances and angles. The X-ray 63 and X-ray 67 systems of programs,[21] modified for use on CDC 3600 and 6600 computers were used for the majority of computing operations. In the later stages of refinement use was made of local IBM 360-44 versions of ORFLS[22] and FOURIER[23] programs. Data reduction was carried out on a local IBM 1800 computer using local programs written by N. C. Webb and M. R. Becker.

Discussion

The crystal structure (Figure 1) of calcium dihydrogen ethane-1-hydroxy-1,1-diphosphonate dihydrate, $CaH_2EHDP \cdot 2H_2O$, consists of an infinite array of H_2EHDP^{2-} and water molecules and Ca^{2+} ions linked together by hydrogen bonding and calcium coordination of oxygens from both H_2EHDP^{2-} and water molecules. Calcium ions lie in zigzag chains close to the 001 plane, and they are connected such that alternating four-membered rings are formed with, in one case, two symmetry-related water oxygens bridging two calciums (Ca...Ca 4.119 Å) and, in the other case, two symmetry-related phosphonyl oxygens bridging two calciums (Ca...Ca 3.825 Å). These Ca...Ca separations are the shortest in the crystal. Hydrogen bonding is completely intermolecular and occurs between phosphonyl groups and between water molecules and phosphonyl groups. There is no evidence of hydrogen bonding involving the EHDP hydroxyl group. The diphosphonate molecules are linked in zigzag chains by what appears to be strong hydrogen bonding (O6...O6′, 2.550 Å; O7...O7′, 2.522 Å) of symmetry-related P1 phosphonyl groups across a plane parallel to the *ab* plane at $c = 0.5$.

The calcium ion contains eight oxygen atoms in its primary coordination sphere; Ca...O distances range from 2.352 to 2.608 Å and all other Ca...O distances are greater than 3.2 Å. The observed irregular eightfold coordination geometry (Figure 2) is not unusual for calcium ion. Of the eight coordinated oxygens five are from three different but symmetry-related H_2EHDP^{2-} molecules and three are from water molecules. Conversely, associated with each H_2EHDP^{2-} molecule are three symmetry-related Ca^{2+} ions (Figure 3). The most strongly bound calcium ion is involved in a six-membered chelate ring involving oxygens of geminal phosphonyl groups (Ca...O2, 2.352; Ca...O5, 2.420). A second calcium ion is bound in a five-membered chelate ring involving the methylene hydroxyl group

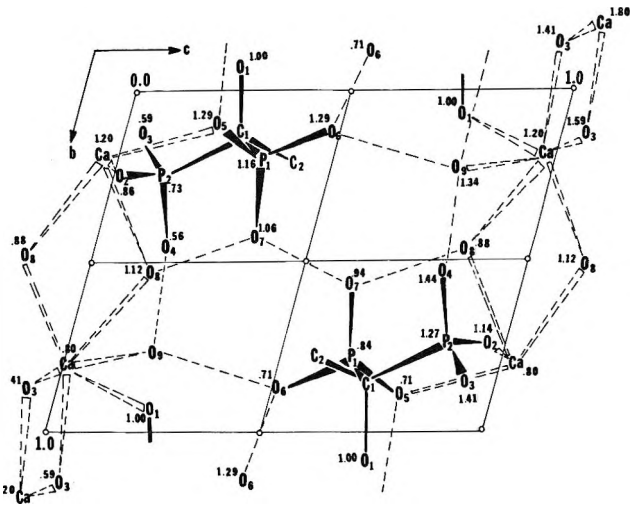

Figure 1. [100] Projection of the triclinic unit cell of $CaC(CH_3)(OH)(PO_3H)_2 \cdot 2H_2O$. The approximate x coordinate of several atoms is indicated. Hydrogen positions are not indicated for clarity. Only some of the calcium coordination is indicated.

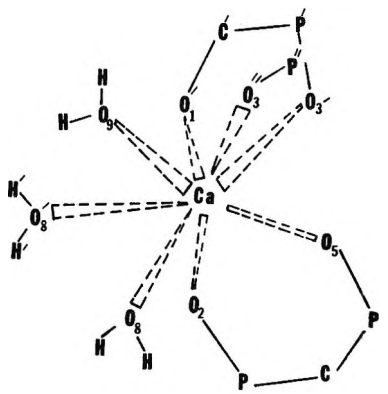

Figure 2. The coordination about the calcium ion of CaH_2EHDP.

(Ca...O1, 2.608) and a phosphonyl oxygen (Ca...O3, 2.448); this same phosphonyl oxygen terminally binds the third calcium ion to the H_2EHDP^{2-} ligand (Ca...O3, 2.421). Coordination of un-ionized hydroxyl groups *via* chelate rings has been previously observed in the structures of the calcium salts of such hydroxycarboxylic acids as tartaric,[24] arabonic,[25] 5-keto-D-glu-

(20) A listing of the observed and calculated structure factors will appear immediately following this article in the microfilm edition of this volume of the journal. Single copies may be obtained from the Business Operations Office, Books and Journals Division, American Chemical Society, 1155 Sixteenth Street, N.W., Washington, D. C. 20036, by referring to code number JPC-72-1304. Remit $3.00 for photocopy or $2.00 for microfiche.

(21) J. M. Stewart, Technical Report 67-58, Dec 1967, Computer Science Center, University of Maryland.

(22) W. R. Busing, K. O. Martin, and H. A. Levy, "OR FLS, A Fortran Crystallographic Least-Squares Program," ORNL-TM-305, Oak Ridge National Laboratory, 1962.

(23) J. F. Blount, Ph.D. Thesis (Appendix), University of Wisconsin, 1965.

(24) G. K. Ambady, *Acta Crystallogr., Sect. B*, **24**, 1548 (1968).

(25) S. Furberg and S. Helland, *Acta Chem. Scand.*, **16**, 2373 (1962).

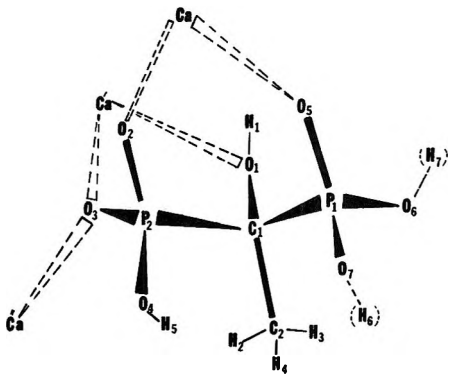

Figure 3. The H_2EHDP^{2-} ligand of CaH_2EHDP, with calcium coordination indicated.

conic,[26] and α-D-glucoisosaccharinic,[27] all of which contain eight-coordinate calcium ions. CaH_2EHDP, however, represents the first reported example of a metal chelate ring involving the un-ionized hydroxyl group of a hydroxyphosphonic acid.

The molecular parameters of the H_2EHDP^{2-} anion in CaH_2EHDP do not differ greatly from those of H_4EHDP. The expected effects of partial ionization on the P–O bond lengths are observed; these P–O distances are all within the ranges of previously observed and expected values (see ref 10). From a consideration of the P–O bond lengths and the probable hydrogen atom positions it is apparent that in the crystal the H_2EHDP^{2-} anion exists with one proton on each phosphonyl group. This is consistent with pH titrations which exhibit two strong, indistinguishable protons during neutralization. In the crystal a disordering of the P1 phosphonyl group (see Results), such that in half of the molecules the proton is bound to O6 and in the other half to O7, results in two irregular P1–O bond lengths for this group. The P1–O5 bond length of 1.507 Å is not unexpected for an ionized phosphonate group (see ref 10); however, the P1–O6 and P1–O7 bond lengths of 1.530 and 1.549 Å, respectively, are close to a value of 1.55 Å obtained from averaging a normal P–OH bond length (*e.g.*, 1.595 Å for the P2–O4 length of the other phosphonyl group) and a normal P–O$^-$ bond length (*e.g.*, 1.505 and 1.496 Å for P2–O3 and P2–O2). Significant effects of this disordering are not apparent in other molecular parameters.

In a previous report[10] we referred to the steric effects of the methylene carbon substituents on the configuration and, consequently, the relative acid strengths of *gem*-diphosphonic acids, particularly H_4EHDP. It was postulated that to minimize steric interactions between the methyl hydrogen atoms and phosphonyl oxygens, rotation about the P–C bonds was restricted such that, in the crystal, the H_4EHDP molecule was observed to have a planar "W" arrangement for the O–P–C–P–O chain of atoms and eclipsed PO_3 groups. However, in H_4MDP, where there exist no such steric restrictions to rotation about the P–C bonds, the molecule assumes a more staggered configuration, presumably to minimize interactions between oxygens of the *gem*-phosphonyl groups. In the structure of CaH_2EHDP small distortions from the eclipsed "W" configuration do occur.

The PO_3 groups, which are nearly eclipsed in H_4EHDP, are less so in CaH_2EHDP: 25° staggered (when viewed in projection along the P...P axis) for the latter *vs.* 4° for the former, compared to 60° if the PO_3 groups were exactly staggered (Figure 4). This distortion is primarily a result of rotation about the P2–C1 bond in a direction such that O3 moves out of the P–C–P plane and away from the methyl group. The P2 phosphonyl group oxygens are bound to three symmetry-related Ca^{2+} ions, which may account for the distortion away from an eclipsed configuration.

In those aqueous calcium ion–EHDP solutions where only 1:1 complexes are present, the six-membered chelate ring formation involving the two phosphonyl oxygens is probably the preferred and most significant configuration. Grabenstetter and Cilley[11a] have demonstrated, however, that in aqueous solutions (pH ≈ 11) of Ca^{2+} and EHDP, where the concentration ratio Ca^{2+}/EHDP ≈ 1.5, complexes with more than one bound Ca^{2+} per $EHDP^{4-}$ ligand definitely occur. They found that their potentiometric titration data could best be fit by assuming, in addition to the expected CaEHDP complex, an aggregate of stoichiometry Ca_7EHDP_4. Moreover, Wiers[11b] characterized by light scattering and sedimentation much larger aggregates having molecular weights of the order of 10^4 g/mol, radii of 26 Å and charges of *ca.* −20 esu. A hypothetical model for the formation and structure of such aggregates can be constructed by making some assumptions which are not unreasonable based on the structural features observed for CaH_2EHDP.

At a concentration ratio close to unity the predominant complex is probably CaEHDP in which the Ca^{2+} is bound in a six-membered chelate ring utilizing two phosphonyl oxygens (I, Figure 5). As the Ca/EHDP concentration ratio is increased and approaches 2, a second Ca^{2+} can bind to a CaEHDP complex *via* either a five-membered ring using a phosphonyl oxygen (at a terminus of the "W," *vide supra*) and the hydroxyl oxygen (II, Figure 5), or a six-membered ring using two suitably positioned phosphonyl oxygens (which are not part of the "W" chain of atoms) (III, Figure 5). Wiers has shown[11c] that at a concentration ratio of ~2 an immediate precipitate forms of stoichiometry $Ca_2EHDP \cdot xH_2O$. However, at concentration ratios between 1 and 2, Grabenstetter and Cilley could best fit their potentiometric titration data by assuming that only the complexes CaEHDP, Ca_3EHDP_2, Ca_4EHDP_3,

(26) A. A. Balchin and C. H. Carlisle, *Acta Crystallogr.*, 19, 103 (1965).

(27) R. Norrestam, P. Werner, and M. Von Glehn, *Acta Chem. Scand.*, 22, 1395 (1968).

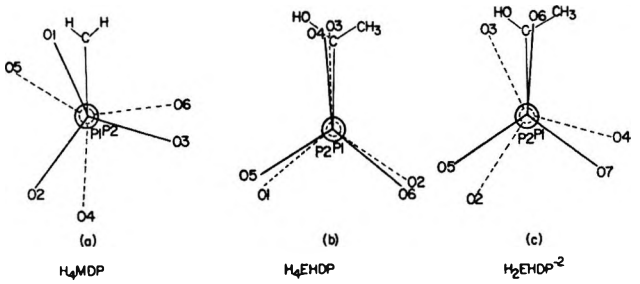

Figure 4. Relative orientations of phosphonyl groups in (a) H_4MDP,[12] (b) H_4EHDP,[10] and (c) CaH_2EHDP, viewed along the P–C–P plane.

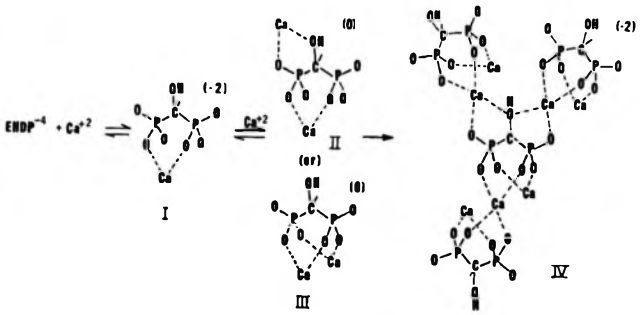

Figure 5. A schematic structural model for formation of a Ca_7EHDP_4 aggregate.

and $(Ca_7EHDP_4)_n$ were present. Therefore in this range of concentration ratios Ca_2EHDP complexes must be unstable with respect to aggregation with other Ca_2EHDP and/or CaEHDP complexes to form polynuclear complexes, ultimately of stoichiometry $(Ca_7EHDP_4)_n$ (IV, Figure 5). Formation of such an aggregate could occur by stepwise addition of three formally uncharged Ca_2EHDP complexes to a negatively charged $CaEHDP^{2-}$ complex. Such aggregation does not seem unreasonable in view of the two additional chelation sites on a $CaEHDP^{2-}$ complex and the one additional chelation site on a formally uncharged Ca_2EHDP complex. Also, all such sites are in positions where binding of a calcium ion or complex would not impose significant electrostatic repulsions between metal ions or ligands. Grabenstetter and Cilley found it necessary to include an aggregation constant, K_o, representing the hypothetical reaction $Ca_7EHDP_4 + (Ca_7EHDP_4)_n \rightleftharpoons (Ca_7EHDP_4)_{n+1}$; this was also consistent with the observations of Wiers indicating the presence of very large aggregates with molecular weights around 10^4 g/mol. Individual 7:4 aggregates (IV, Figure 5) might combine *via* Ca^{2+} bridging between EHDP ligands of different 7:4 aggregates. This growth would continue until the negative charge buildup on a large aggregate ($n \approx 10$) prevents addition of more negatively charged 7:4 aggregates. These large aggregates should be in equilibrium with simple CaEHDP mononuclear complexes since the presence of both was necessary to explain the titration results. At a very slow rate these large aggregates must convert to crystal nuclei of $(Ca_2EHDP)_m$ stoichiometry, since Wiers observed[11c] that at Ca/EHDP concentration ratios between 1 and 2 a precipitate of this composition did form after long periods of time.

Although this model is certainly not a unique solution, it does demonstrate a conceivable structure for such aggregates based on available data. Furthermore we can predict that other ligands, which have available suitable, sufficiently separated chelating sites for more than two metal ions, should be capable of exhibiting polynuclear aggregate formation in certain concentration regions. Thus, an important feature of the model for Ca–EHDP aggregate formation is the ability of EHDP to bind Ca^{2+} ions *via* not only two chelate rings using only phosphonyl oxygens but also *via* a relatively stable five-membered chelate ring which includes the hydroxyl group. We would therefore expect *gem*-diphosphonates $R_1R_2C(PO_3)_2$, where R_1 and R_2 were not potential donor groups to Ca^{2+} coordination, not to exhibit stable polynuclear aggregate formation. In this group are compounds such as MDP ($R_1 = R_2 = H$), Cl_2MDP ($R_1 = R_2 = Cl$), ethane-1,1-diphosphonate (ETP; $R_1 = CH_3$, $R_2 = H$), etc. However, compounds such as methanehydroxydiphosphonate (MHDP; $R_1 = H$, $R_2 = OH$), ethane-1-hydroxy-1,1,2-triphosphonate (EHTP, $R_1 = OH$, $R_2 = CH_2PO_3$), etc., should exhibit polynuclear aggregate formation. Unpublished results from these laboratories are not inconsistent with these statements.[28] Precipitation boundary experiments indicate that EHTP and propane-1-hydroxy-1,1,3-triphosphonate ($R_1 = OH$, $R_2 = CH_2CH_2PO_3$) are capable of forming polynuclear calcium complexes; results for ETP, MDP, and MHDP were inconclusive because of insolubility of mixed sodium salts.

Acknowledgments. The preparation of crystalline $CaH_2EHDP \cdot 2H_2O$ by R. A. Gloss of these laboratories, the assistance of personnel of the Cincinnati Data Center, Control Data Corporation, and the assistance of Mrs. Gayle Kloss and Dr. R. J. Herbold of The Procter & Gamble Company, Mathematical Services Department, are appreciatively acknowledged. I would also like to acknowledge valuable conversations with Drs. W. A. Cilley (Miami Valley Laboratories) and B. H. Wiers (Winton Hill Technical Center) of The Procter & Gamble Company, and Professor R. A. Plane of Cornell University.

(28) P. Vanden Eynden and W. A. Cilley, unpublished results.

X-Ray Diffraction Study of Possible Clustering in Cesium Salt of Ethylene–Acrylic Acid Copolymer

by Ryong-Joon Roe

Bell Laboratories, Murray Hill, New Jersey 07974 *(Received June 21, 1971)*

Publication costs assisted by Bell Laboratories

Possible clustering of ions in olefin–carboxylic acid copolymers and their salts has been postulated in the past by many to explain various properties observed with these materials. A detailed study in this work by a wide-angle X-ray diffraction technique, however, has given us results which do not support the existence of such clusters. X-Ray intensities (Mo Kα) scattered from an ethylene–acrylic acid copolymer (containing 12.6 wt % of the latter comonomer) and its cesium salt (78% neutralization) were measured at diffraction angles ranging from 3.9 to 129.6°. The Fourier transform of the interference intensity data was computed to obtain the radial distribution functions of atom pairs. When the difference is taken of the radial distribution functions obtained with the copolymer acid and salt samples, the contributions from pairs of light atoms are largely canceled out and, in the resulting difference plot, the peaks corresponding to Cs–Cs pairs are heavily weighted because of the much higher atomic number of Cs. The examination of such a plot, however, did not give any indication of cluster formation, but showed strong evidence for dimer complex formation.

I. Introduction

The structure and properties of ionic polymers, such as the copolymers of olefin and carboxylic acid and their salts, have been the subject of study in recent years by a number of workers.[1] An important point of controversy with regard to the structure of such polymers is the possibility of clustering of ionic groups. Aggregation of the latter into clusters or microdomains has been postulated to explain varieties of phenomena observable with these ionic polymers: X-ray diffraction pattern,[2-4] electron microscope observation,[2,5] dynamic mechanical data,[6-9] and melt rheology.[10] Thermodynamic calculations, presented by Eisenberg,[11] also seem to suggest the formation of clusters. Such a view is, however, not universally accepted, and evidence indicating more uniform distribution of ionic groups throughout the copolymer was presented from dynamic mechanical studies[12] and from nmr line-width studies.[13]

In this work we reexamine the question of cluster formation in cesium salt of ethylene–acrylic acid copolymer by a wide-angle X-ray diffraction technique. It is well known[14] that the X-ray diffraction data from amorphous liquids or glass can be processed (through Fourier transformation) to derive the radial distribution function (RDF) or the probability distribution of occurrence of atomic pairs as a function of interatomic separation. By comparing the RDF of the Cs salt with that obtained from the unneutralized ethylene–acrylic acid copolymer, one can derive information concerning the distribution of Cs atoms in space. Such a procedure is possible because of the much higher scattering power of X-ray by Cs atoms as compared to other light atoms in the polymer.

II. Experimental Section

The ethylene–acrylic acid copolymer, containing 12.6 wt % of acrylic acid, was supplied by Union Carbide. The Cs salt of the copolymer was prepared and kindly made available to the present study by E. P. Otocka. The amount of Cs contained in the sample, as analyzed by X-ray fluorescence and atomic emission spectroscopy, is 15.5 wt %, which corresponds to 78% neutralization of the acid groups. Hereafter we refer to the original acid copolymer and its Cs salt simply as acid and salt for brevity.

Diffraction data were obtained with an X-ray dif-

(1) E. P. Otocka, *J. Macromol. Sci., Rev. Macromol. Sci.*, **5**, 275 (1971).

(2) R. Longworth and D. J. Vaughan, *Nature (London)*, **218**, 85 (1968).

(3) F. C. Wilson, R. Longworth, and D. J. Vaughan, *Polym. Prepr., Amer. Chem. Soc., Div. Polym. Chem.*, **9**, 505 (1968).

(4) B. W. Delf and W. J. MacKnight, *Macromolecules*, **2**, 309 (1969).

(5) H. A. Davis, R. Longworth, and D. J. Vaughan, *Polym. Prepr., Amer. Chem. Soc., Div. Polym. Chem.*, **9**, 515 (1968).

(6) R. Longworth and D. J. Vaughan, *ibid.*, **9**, 525 (1968).

(7) W. J. MacKnight, T. Kajiyama, and L. McKenna, *Polym. Eng. Sci.*, **8**, 267 (1968).

(8) B. E. Read, E. A. Carter, T. M. Conner, and W. J. MacKnight, *Brit. Polym. J.*, **1**, 123 (1969).

(9) A. V. Tobolsky, P. F. Lyons, and N. Hata, *Macromolecules*, **1**, 515 (1968).

(10) S. Bonotto and E. F. Bonner, *ibid.*, **1**, 510 (1968).

(11) A. Eisenberg, *ibid.*, **3**, 147 (1970).

(12) E. P. Otocka and T. K. Kwei, *ibid.*, **1**, 244, 401 (1968).

(13) E. P. Otocka and D. D. Davis, *ibid.*, **2**, 437 (1969).

(14) B. E. Warren, "X-ray Diffraction," Addison-Wesley, Reading, Mass., 1969; R. W. James, "The Optical Principles of the Diffraction of X-rays," Cornell University Press, Ithaca, N. Y., 1965.

fractometer manufactured by Picker Nuclear Corp. The primary beam from a Mo target filtered through Zr foils was scattered from the sample, of size 2 × 6 × 0.1 cm, held in parafocusing reflection geometry. No special precaution was taken to control the humidity of the sample during the measurements. The diffracted intensity was measured with a scintillation counter through a pulse-height analyzer. The range of diffraction angles 2θ covered extended from θ = 1.95 to 64.81°, or s = 0.6 to 16.0, where $s = 4\pi \sin\theta/\lambda$, λ being the wavelength of the radiation (0.7107 Å). In order to facilitate later computation, the measurements were carried out at 78 diffraction angles spaced at equal intervals of s (Δs = 0.2). The resolution in the RDF to be obtained is related to the density and range of data points in s through the Nyquist relation[15,16]

$$n = 2r_{max}s_{max}/(2\pi) \quad (1)$$

where n is the number of data points. Thus, the sets of data collected in this work enabled us to determine the RDF to r_{max} = 16 Å at the resolution of Δr = 0.2 Å. The total range of s covered was divided into two overlapping sections, s = 0.6–5.0 and s = 3.4–16.0. The slit openings were adjusted to limit the horizontal divergence of the scattered beam to 0.2 and 2.0° in the first and second section, respectively, and the vertical divergence (by Soller slits) to 2.0 and 3.8°, respectively. Each section was scanned from the beginning to the end repeatedly to accumulate counts in order to minimize the effect of variation in the primary beam intensity. After absorption, polarization, and background corrections, the intensity data from the two sections were combined together. The total numbers of counts accumulated at each s were varied to keep the statistical error in $si(s)$ (defined by eq 5 in section III) approximately constant and ranged from 40,000 at s = 0.6 to 5,000,000 at s = 16.0. Automatic, unattended operation of the diffractometer for the collection of data was achieved through the data acquisition system, manufactured by Cambera Industries, which took its instructions from a previously prepared punched paper tape.

III. Analysis of Intensity Data

We define a structural unit, for convenience, as the average composition of a unit containing one backbone carbon atom, and let n_i represent the number of i-type atoms in a structural unit ($i = 1 \ldots m$). The values of n_i's calculated from the chemical composition are C (1.027), O (0.053), H (2.000) for the acid, and C (1.027), O (0.053), H (1.979), and Cs (0.0209) for the salt.

The intensity I (in electron units) of X-ray scattered coherently by the sample is related, as given by eq 2 below, to the radial distribution functions $\rho_{ij}(r)$, which specify the number of j-type atoms per unit volume at a distance r from a given i-type atom.

$$I(s) = N\sum_{i=1}^{m} n_i f_i^2 + (4\pi N/s)\int_0^\infty r \sin sr \times \sum_{i=1}^{m}\sum_{j=1}^{m} n_i f_i f_j[\rho_{ij}(r) - \rho_j^0]dr \quad (2)$$

where N = the total number of structural units contributing to the scattered intensity, f_i = the atomic scattering factor of i-type atoms, $\rho_j^0 = \rho_{ij}(\infty)$ = the average number of j-type atoms per unit volume. The first term in (2) represents the sum of scattering contributed independently by all the atoms present, and the second term arises from the interference effect between the scattered amplitudes by a pair of atoms.

In the present work m = 4, since there are four different kinds of atoms, C, O, H, and Cs, present. Hereafter, we denote Cs atoms by the subscript i or j equal to 1 and C, O, and H atoms by the subscript equal to 2, 3, and 4, respectively. The information we are seeking, in particular, is therefore $\rho_{11}(r)$.

The atomic scattering factors f_i are continuously decreasing functions of s, and their precise shapes for different atoms are similar but vary somewhat from one to another. If we define the normalized atomic scattering factor of Cs atoms, f_e, by

$$f_1 = Z_1 f_e \quad (3)$$

where Z_i is the number of electrons in an i-type atom, it is then possible to represent the scattering factors of other atoms by the following approximate relation

$$f_i \approx Z_i f_e \qquad i = 2, 3, 4 \quad (4)$$

The consequence of approximation 4 is that in the final result the shape of $\rho_{11}(r)$ is correctly represented, but the shapes of all other $\rho_{ij}(r)$'s will be somewhat smeared, an effect that is advantageous for our purpose. In a term more familiar to crystal structure analysis, our procedure is analogous to sharpening the Patterson function with respect to Cs atoms.

Combining (2), (3), and (4), one can then write

$$i(s) \equiv [I(s)/N - \sum_{i=1}^{m} n_i f_i^2]/f_e^2 \quad (5)$$

$$= (4\pi/s)\int_0^\infty r \sin sr \times \sum_{i=1}^{m}\sum_{j=1}^{m} n_i Z_i Z_j[\rho_{ij}(r) - \rho_j^0]dr \quad (6)$$

The quantity $i(s)$, defined by (5), is called the reduced or interference intensity function and contains all the experimental information concerning the arrangement of atoms in the sample. By application of the Fourier inverse theorem, from (6), one obtains

(15) J. W. Cooley, P. A. W. Lewis, and P. D. Welch, *IEEE Audio*, 15, 79 (1967).

(16) G. D. Bergland, *IEEE Spectrum*, 6, 41 (1969).

$$4\pi r[D(r) - D_0] = (2/\pi) \int_0^\infty si(s) \sin sr \, ds \quad (7)$$

where

$$D(r) \equiv \sum_{i=1}^{m} \sum_{j=1}^{m} n_i Z_i Z_j \rho_{ij}(r) \quad (8)$$

and D_0, which is the average of $D(r)$ throughout the sample, is related to the sum of ρ_j^0 in a similar way.

In Figure 1 the filled circles represent the observed intensity (I/N) per structural unit after they have been corrected for background, absorption, polarization, multiple scattering, and Compton scattering, and then normalized. (The open circles at $s = 0.2$ and 0.4 were obtained from separate low-angle diffraction measurements and are subject to a much larger error than others.) Also drawn in Figure 1 are solid curves representing the independent scattering. The information on the spacial arrangement of atoms is contained in the pattern of deviation of the observed intensity from the latter. In Figure 2 such useful information is displayed in a more apparent manner. Here s times the interference intensity function $i(s)$ defined by (5) is plotted against s. The patterns of variation of intensity, at high s, is now greatly amplified because of the multiplicative factors s and $1/f_e^2$, both of which increase greatly with increasing s.

The correction for multiple scattering was made following the procedure described by Warren and Mozzi,[17] but a new set of correction factors appropriate to the limited thickness of our samples was calculated in this work[18] and used. The intensity of Compton scattering was calculated from the theoretical scattering factors for free atoms recently computed and tabulated by Cromer and Mann.[19] The normalization of the experimental intensity to an absolute scale in electron units was accomplished by matching the observed intensity at high s values to the independent scattering intensity. Besides, in order to correct for a possible small error in normalization, and also to eliminate spurious long-wavelength components in the observed $si(s)$ function, we made use[20,21] of the physical fact that $\rho_{ij}(r)$ is zero when $r < 0.8$ Å and also $\rho_{ij}(r)$ is zero when $r < 2.3$ Å.

Fourier transform of the $si(s)$ function according to eq 7 then gives the function $4\pi r[D(r) - D_0]$. However, the integration limit in (7) extends to infinity while our data are available only to $s = 16$. Truncation of integration to a finite limit of s usually gives rise to false peaks in the resulting $D(r)$ function. One way of overcoming such a difficulty is to multiply $si(s)$ with a modification function, which diminishes smoothly to zero at the maximum s. The effect of such a modification function is, in general, to broaden the peaks in the final $D(r)$ somewhat.[22] A Gaussian function is commonly used for this purpose. In this work, instead, we employ one termed "ideal" by Starshak and Larsen,[23] which broadens the peaks in $D(r)$ somewhat less than a

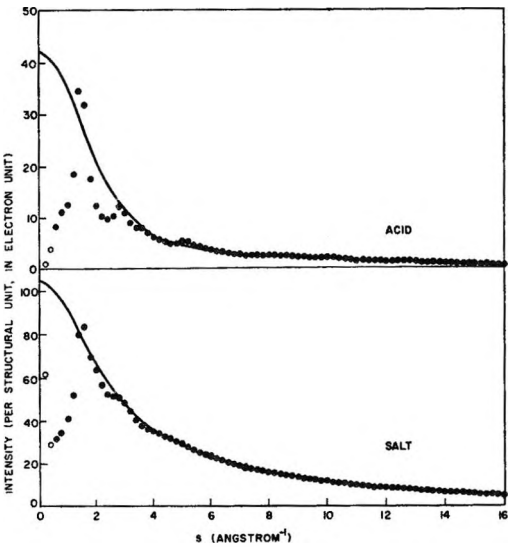

Figure 1. Observed X-ray intensity, corrected for background, absorption, polarization, multiple scattering, and Compton scattering, is plotted against $s = 4\pi \sin \theta/\lambda$. The solid curve represents the independent scattering by collection of atoms. The top plot is for the ionomer acid sample and the bottom for the salt sample.

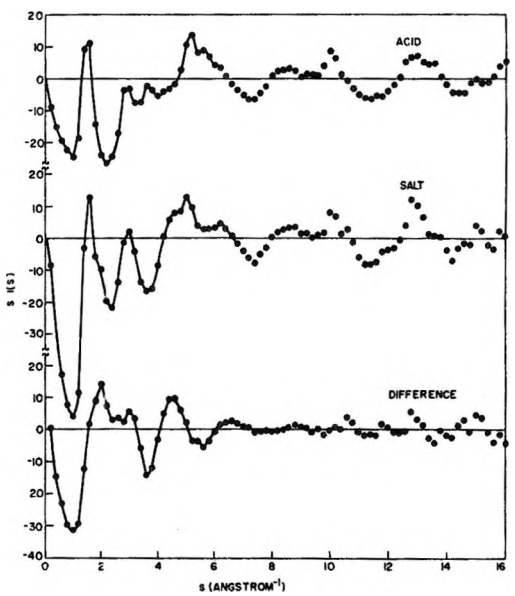

Figure 2. The interference intensity function $i(s)$, (defined by eq 5), multiplied by s, is plotted against $s = 4\pi \sin \theta/\lambda$. The top plot is for the acid sample, the middle for the salt, and the bottom is the difference of the above two.

(17) B. E. Warren and R. L. Mozzi, *Acta Crystallogr.*, **21**, 459 (1966).

(18) R.-J. Roe, manuscript in preparation.

(19) D. T. Cromer and J. B. Mann, *J. Chem. Phys.*, **47**, 1892 (1967); D. T. Cromer, *ibid.*, **50**, 4857 (1969).

(20) H. A. Levy, M. D. Danford, and A. H. Narten, Oak Ridge National Laboratory Report ORNL-3960, May 1966.

(21) R. Kaplow, S. L. Strong, and B. L. Averbach, *Phys. Rev. A*, **138**, 1336 (1965).

(22) J. Waser and V. Schomaker, *Rev. Mod. Phys.*, **25**, 671 (1953).

(23) A. J. Starshak and R. D. Larsen, manuscript in preparation; presented at the 160th National Meeting of the American Chemical Society, Chicago, Ill., Sept 1970.

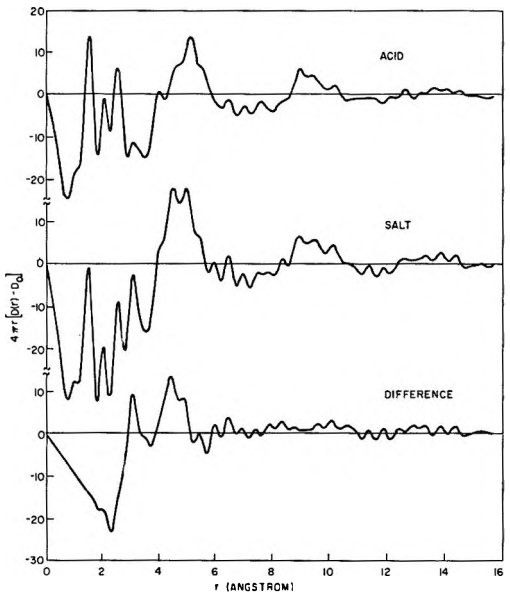

Figure 3. Results of Fourier transformation of $si(s)$ functions shown in Figure 2, plotted against the distance of atomic separation r. $D(r)$ is the sum of the radial distribution functions of atom pairs weighted by the products of their atomic numbers.

Gaussian does. This is a function which is equal to unity from $s = 0$ to $(3/4)s_{max}$ and then thereafter decreases sinusoidally to zero at s_{max}. The values of $4\pi r[D(r) - D_0]$ obtained by Fourier transformation of the product of the observed $si(s)$ data with such a modification function are plotted in Figure 3 against the radial distance r. The Fourier transform was evaluated with a digital computer using the "fast Fourier transform" subroutine.[16,24]

IV. Results and Discussion

The densities of the acid and salt samples are 0.946 and 1.107 g/cm^3, respectively. The molar volume per structural unit (containing one backbone carbon atom) is therefore 16.06 cm^3 for the acid and 16.22 cm^3 for the salt. The difference, 0.16 cm^3/mol, can be accounted for largely as the difference between the molar volumes of H^+ and Cs^+ ions. (A Cs^+ ion has a crystalline ionic radius of 1.67 Å, or occupies a spherical volume of 11.8 cm^3/mole. There is 0.0209 Cs atom per structural unit, and thus the average volume occupied by Cs^+ ions per structural unit would be 0.25 cm^3 if in a crystalline environment, and somewhat larger if in an amorphous state, while the volume occupied by H^+ ions would be much smaller.) In other words, there is very little difference in the actual volume occupied by the part of the polymers excluding the cations, whether it is in the acid or in the salt sample. A similar inference can be made from the fact that the difference in the glass transition temperature T_g between the acid and the corresponding salt is, in general, minor,[12] and therefore the fractional free volume at room temperature would not be too different. Again, the apparent heat of fusion measured with DSC is 254 cal/mol of structural unit with the acid sample and 228 cal with the salt sample, indicating almost insignificant difference in the degree of crystallinity between the two.

From these data we infer that the mutual spacial arrangement of light atoms (C, O, H) in the salt sample is not greatly disturbed by replacement of H with Cs atoms in neutralizing the acid. Thus, if we take the difference of $D(r)$ functions obtained with the acid ($D^A(r)$) and salt samples ($D^S(r)$), the contribution of $\rho_{ij}(r)$ for pairs of light atoms will be almost completely canceled out. In other words, the following relationship holds approximately

$$\Delta D(r) \equiv D^S(r) - D^A(r) \approx n_1 Z_1 \left[Z_1 \rho_{11}(r) + 2 \sum_{j=2}^{4} Z_j \rho_{1j}(r) \right] \quad (9)$$

(where we made use of the fact that $n_1\rho_{1j} = n_j\rho_{j1}$). If Cs ions are distributed more or less uniformly throughout the sample, the ratio of ρ_{11} to ρ_{1j} ($j = 2, 3, 4$) would be about the same as n_1/n_j on the average, and the contribution of the term $Z_1\rho_{11}$ would still be much smaller than that of the second term in eq 9, despite the much larger value of $Z_1(=55)$ as compared to Z_j ($j = 2, 3, 4$). However, if there exist clusters of Cs ions so that ρ_{11} becomes comparable to ρ_{12}, etc., within a certain range of r, then the contribution of $Z_1\rho_{11}$ will become very prominent and the values of $\Delta D(r)$ will be much higher than the average $\Delta D_0 = D_0^S - D_0^A$ within that range. The method we employ here is essentially the application of the technique of isomorphic replacement of heavy atoms, well known in crystal structure determination.

The difference of $si(s)$ functions observed for the acid and salt samples is plotted at the bottom of Figure 2. At the bottom of Figure 3 is shown the difference of the $4\pi r[D(r) - D_0]$ values obtained with the acid and salt samples. (Because of the linearity of the Fourier transform operator, the difference of Fourier transforms is equal to the Fourier transform of the difference.) A pattern that is noted immediately in Figure 3 is that the $\Delta D(r)$ function is almost featureless beyond $r \approx 6$ Å. In the plot for the acid sample, the three prominent peaks below 3 Å arise from C–C pairs (first, second, and third neighbors) within a single polymer chain. The broad peak centered around 5 Å is contributed mainly by the C–C pairs belonging to neighboring chains. Deviation of $D^A(r)$ from the average D_0^A persists even at around 14 Å and probably beyond, indicating the presence of some long-range order corresponding to the partly crystalline nature of the sample. In contrast, the lack of features in the difference plot can be interpreted as implying the following two things. First, Cs ions are located in amorphous regions so that a given Cs ion, looking out into

(24) A. J. Starshak and R. D. Larsen, *Phys. Chem. Liquids*, **2**, 45 (1970).

the surrounding region of carbon atoms, cannot discern any long- or medium-range order. This conclusion is in accord with our expectation from other considerations. Secondly, the difference plot does not give any indication of the existence of clustering. If there existed clusters of diameter, say, 10 Å, in which the concentration of Cs ions is much higher than the average, the values of $\Delta D(r)$ below 10 Å would have been much higher than the average ΔD_0. Further, inside these clusters one would have expected a certain short-range order in the disposition of Cs ions, which would have led to a few prominent peaks superimposed on the generally high level of $\Delta D(r)$. But none of these features are present in our results.

In order to substantiate the conclusion that the result given in Figure 3 indicates a lack of clustering, we have made a calculation to show the kind of RDF that we would have obtained if there actually existed clusters of ions. The calculation, as given in the Appendix, is based on a simple model consisting of a mixture of two types of particles, light and heavy. The relative numbers of light and heavy particles were so chosen to make the model correspond to the salt sample. The degree of clustering is characterized by two parameters: R, the radius of a spherical domain in which heavy particles are concentrated, and M, the number of heavy particles in a cluster. The values of $4\pi r[\Delta D(r) - \Delta D_0]$ calculated for three different sets of these parameters are plotted in Figure 4, and are compared with the experimental results. The values of the parameters R and M used and the average intercluster distances $\bar{d}$ calculated therefrom (see Appendix) are

curve 1: $R = 4$ Å, $M = 8$, $\bar{d} = 21.9$ Å

curve 2: $R = 4$ Å, $M = 6$, $\bar{d} = 19.9$ Å

curve 3: $R = 6$ Å, $M = 12$, $\bar{d} = 25.0$ Å

(In calculating $\bar{d}$, the value of V/N taken is that appropriate for the salt, that is, 16.22 cm³/mol or 26.93 Å³/structural unit.) According to Eisenberg,[11] the maximum number of cations that can be allowed in a cluster is 8, because of a steric requirement to accommodate the polymeric anions. Curve 1 represents a "tight" cluster containing the maximum allowable number of cations in a sphere of a smallest possible radius. Curve 2 represents a more loose cluster containing less than the maximum number of cations in a sphere of the same small size. Curve 3 is for a much larger cluster which contains 12 cations, more than the possible maximum, but the density of cations is less than half of that in the "tight" cluster. In the three calculated curves shown in Figure 4, the discontinuities at 2.8 and 4 Å are the consequence of our model, in which the closest approach allowed between a light and heavy particle is 2.8 Å and that between two heavy particles is 4 Å. In all the calculated curves the values of $[\Delta D(r) - \Delta D_0]$ are much higher than the experimental result at the radial distances r between 4 Å and *ca.* $1.5R$. In clusters consisting of real atoms and ions there would have been peaks and valleys, indicative of a short-range order, superimposed on the smooth calculated curves. In any case, the difference between the observed and calculated curves would have been unmistakable. At distances r larger than $2R$, the calculated values of $[\Delta D(r) - \Delta D_0]$ are all negative, indicating the absence of pairs of heavy particles separated by a distance larger than the cluster diameter, and this feature is again lacking in the experimental result. (At still larger distances, there would be contributions to $[\Delta D(r) - \Delta D_0]$ from heavy particle pairs belonging to different clusters, which would result in a shallow, broad peak centered around the intercluster distance $\bar{d}$.) In all the calculated curves considered here, the heavy particles present in the system were assumed to be concentrated all in the clusters. If, on the other hand, only half of the total number of heavy particles had participated in clusters, while the rest were distributed uniformly throughout, the absolute values of the calculated $[\Delta D(r) - \Delta D_0]$ beyond 4 Å would have been halved approximately. Even in such cases, the difference from the experimental result would have been unmistakable.

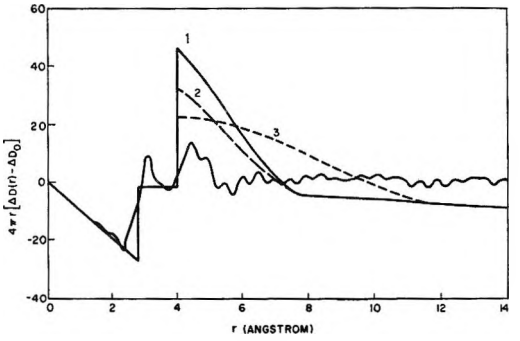

Figure 4. The experimental values of $4\pi r^2[\Delta D(r) - \Delta D_0]$, as given by the bottom plot of Figure 3, are compared with three hypothetical curves calculated for a simple model in which ions are aggregated into clusters. The values of the cluster radius R, the number of ions per cluster M, and the average intercluster distance $\bar{d}$ are: (1) $R = 4$ Å, $M = 8$, $\bar{d} = 21.9$ Å; (2) $R = 4$ Å, $M = 6$, $\bar{d} = 19.9$ Å; (3) $R = 6$ Å, $M = 12$, $\bar{d} = 25.0$ Å.

We now turn to the consideration of the features shown between 3 and 6 Å in the observed $[\Delta D(r) - \Delta D_0]$ plot. This, of course, reflects the short-range order which invariably exists around any atoms. The first shell at around 3 Å arises almost certainly from the Cs–O pair, while the density of $\Delta D(r)$, higher than normal around 4.5 Å, suggests the possibility of contributions by Cs–Cs ion pairs. In Figure 5 is shown the plot of $4\pi r^2 \Delta D(r)$ against r. In such a plot of $4\pi r^2 D(r)$, in general, the area under a peak is equal to the total number of atom pairs at a distance r (weighted by the product of Z_i's). In order to calculate the areas under the peaks in Figure 5, we have attempted to fit

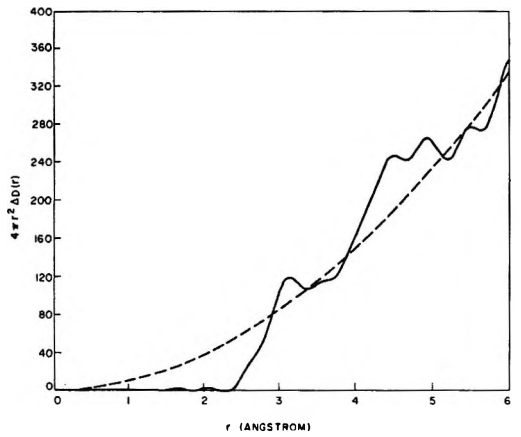

Figure 5. The plot of $4\pi r^2\Delta D(r)$ against r, where $\Delta D(r)$ is as given by the bottom plot of Figure 3. The curve with a broken line is the plot of $4\pi r^2\Delta D_0$ corresponding to a material having no structure.

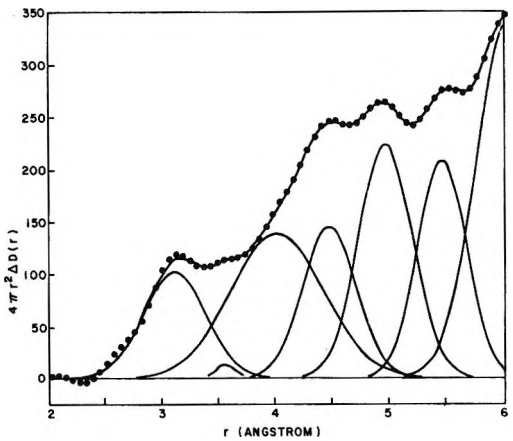

Figure 6. Attempt is made to estimate the areas under each peak in the result shown in Figure 5 by fitting a superposition of Gaussian curves by a nonlinear least-squares program. The solid circles are experimental results and the heavy line passing through these points is the sum of the Gaussian curves drawn with thin lines.

the curve with a superposition of seven Gaussian functions. Actually, such a Gaussian fit is never unique, except for the very first peak, nor is it justified theoretically. Nevertheless, we adopt it as a useful, practical way of obtaining approximate areas under each peak, and the result, obtained by a nonlinear least-squares computer program, is shown in Figure 6. From the area of the first peak centered around 3.11 Å we obtain the value of 3.7 for ρ_{13} for Cs–O pairs, which indicates that there are approximately four oxygen atoms coordinated around each Cs ion at an average distance of 3.1 Å. Among the remaining peaks we assign the one at 4.5 Å as arising from Cs–Cs pairs. This assignment is consistent with the known distances of Cs–Cs closest approach in crystals[25] of elemental Cs (body-centered cubic, 5.25 Å), CsF (NaCl structure, 4.24 Å), CsCl (NaCl structure, 4.96 Å), CsCl (simple cubic, 7.14 Å), Cs acid tartrate (4.11 Å), and Rb gluconate (Rb–Rb = 4.14 Å). The value of ρ_{11} calculated from the area is equal to 1.3. The coordination of approximately one Cs ion and four O atoms around a given Cs ion can be interpreted as a strong indication of formation of a salt pair complex. Evidence for such a complex formation was obtained earlier by Otocka, Hellman, and Blyler[26] on the basis of a rheological study of an ionomer salt material.

In summary, we conclude that the result of the present X-ray diffraction study fails to give any evidence of formation of clusters of ionic groups of around 15 Å or smaller in size, but shows a strong indication for dimer formation. Our result cannot discount unequivocally the possibility of formation of clusters much larger than 15 Å or of clusters of a smaller size in which ionic groups are only weakly concentrated. But the latter two possibilities appear remote on thermodynamic grounds, since, as Eisenberg[11] has shown, the unfavorable entropic effect accompanying cluster formation can be compensated for only by release of sufficient electrostatic energy through interactions of ionic groups.

Acknowledgment. I wish to thank E. P. Otocka for providing the ionomer salt sample and for useful discussions, T. Y. Kometani and S. M. Vincent for the Cs analysis, and C. Gieniewski for density and dsc measurements and for assistance in X-ray measurements.

Appendix

We want to calculate the RDF that we would have obtained if there were clusters of cations, in order to compare it with the experimental RDF. We perform the calculation for a model structure which incorporates only the features essential for our purpose. Our model is an assembly of N structural units in volume V, each structural unit consisting of two types of particles, heavy (H) and light (L). The average number of particles n_H and n_L in a structural unit, and the number of electrons in a particle, Z_H and Z_L, are chosen as follows to make our model correspond to the ionomer salt sample.

$$n_H = 0.0209; \quad n_L = 1$$

$$Z_H = 55; \quad Z_L = 8.5636$$

The heavy particles are situated only in isolated spheres (clusters) of radius R and of volume $v = (4/3)\pi R^3$, each sphere containing M heavy particles, while the light particles are distributed uniformly throughout the sample (both inside and outside the clusters). The total number of clusters in the sample is equal to $n_H N/M$, and therefore the average distance $\bar{d}$ between clusters is given by

$$\bar{d} \approx (MV/n_H N)^{1/3} \qquad \text{(A1)}$$

(25) R. W. G. Wyckoff, "Crystal Structures," Vol. 1 and 5, 2nd ed, Interscience, New York, N. Y., 1966.

(26) E. P. Otocka, M. Y. Hellman, and L. L. Blyler, *J. Appl. Phys.*, 40, 4221 (1969).

The quantity we are going to calculate is the one analogous to eq 9, and is defined by

$$\Delta D(r) = n_H Z_H^2 \rho_{HH}(r) + 2n_H Z_H Z_L \rho_{HL}(r) \quad (A2)$$

where $\rho_{HL}(r)$ is the probability of finding a light particle in a unit volume separated by a distance r from a heavy particle. Because of the finite sizes of our particles, we assume that a pair of particles cannot approach closer than a certain minimum distance, r_{HL}^0 and r_{HH}^0. Beyond these limiting distances of approach, the particles are assumed to be distributed uniformly. In this respect our model is only a crude approximation to an assembly of hard spheres. For $\rho_{HL}(r)$, we have

$$\rho_{HL}(r) = 0, r \leq r_{HL}^0 \quad (A3)$$
$$\approx \rho_L^0, r > r_{HL}^0$$

where ρ_L^0 is the average density of light particles throughout the sample. For $\rho_{HH}(r)$, we have

$$\rho_{HH}(r) = 0, r \leq r_{HH}$$
$$= [(M - 1)/v\beta]\alpha(r/R), r_{HH}^0 < r < 2R \quad (A4)$$
$$= 0, 2R < r \ll \bar{d}$$

In the second equality in (A4), the factor in brackets refers to the fact that inside the cluster there are $(M - 1)$ heavy particles (excluding the first particle from which the distance r is measured) within the available volume $v\beta$, where β allows for the volume occupied by the first particle.

The second factor $\alpha(r/R)$ is the probability that the end of a vector of length r starting from any point inside the sphere is still within the sphere, and is given by[27]

$$\alpha(r/R) = 1 - (3/4)(r/R) + (1/16)(r/R)^3 \quad (A5)$$

Using (A5), the volume correction factor β is obtained by

$$v\beta = \int_{r_{HH}^0}^{2R} 4\pi r^2 \alpha(r/R) dr \quad (A6)$$

or

$$\beta = 1 - (r_{HH}^0/R)^3 + 9/16(r_{HH}^0/R)^4 - (1/32)(r_{HH}^0/R)^6 \quad (A7)$$

The last equality in (A4) states the fact that there are no pairs of heavy atoms which are separated by distance r larger than the diameter of the cluster but far smaller than the intercluster distances. For r comparable to $\bar{d}$ or larger, there will be increasing contributions of $\rho_{HH}(r)$ from pairs belonging to different clusters, but we are not concerned with the RDF at large r and therefore accept (A4) as approximately valid throughout the range of our interest.

(27) H. H. Paalman and C. J. Pings, *Rev. Mod. Phys.*, **35**, 389 (1963).

Ion and Isotopic Exchange among Solids

by H. Gaus, H. W. Levi, and W. Lutze*

Nuclear Chemistry Division, Hahn-Meitner-Institut für Kernforschung, Berlin, Germany
(Received December 1, 1970)

Publication costs assisted by Hahn-Meitner-Institut

Some ion-exchange and isotopic exchange processes have been performed between sodalite and inorganic salts. These results show the various ions to behave as they do in the case of solid–liquid exchange processes. The quantitative evaluation of such processes has been demonstrated in the case of Na^+ isotopic exchange. A new mathematical solution of Fick's law was necessary. This is described in an appendix.

Clearfield and Troup[1] have reported observations on an ion-exchange process involving two solid phases, suggesting that such processes might be typical of ion exchangers in the hydrogen form because of the volatility of the hydrogen compound formed. We have observed solid-phase exchange processes between sodalite in the sodium form and various salts. The results, mentioned very briefly earlier,[2] are described here in more detail.

The chemical formula of sodalite is $Na_8[Al_6Si_6O_{24}]Cl_2$. The material used in this study originated in Bancroft, Canada; its characteristics were checked by X-ray, optical, and activation analysis. The cubic lattice had a lattice constant of $a = 8.9$ Å and the refractive index was 1.485. Both values agree with those reported in

(1) A. Clearfield and J. M. Troup, *J. Phys. Chem.*, **74**, 2578 (1970).
(2) H. W. Levi and W. Lutze, *Angew. Chem.*, **79**, 1003 (1967).

the literature. Determination of Na and Cl gave a deficiency of 4.9 ± 0.5% owing to impurities that could not be separated from the sodalite crystals—rutile, hornblende, carbonates, pyrite, and others.

The technique of the exchange experiments was to use small spheres (0.2-mm diameter) prepared from sodalite crystals. After the spheres had been treated with Na-22 as a tracer, which was distributed homogeneously within the sodalite by thermal diffusion, they were pressed into tablets together with a salt under a pressure of 14,000 kg/cm². This arrangement was chosen to permit quantitative analysis of the exchange kinetics if that should be desired. The tablets were tempered by heating to temperatures between 400 and 700°. For each run, the temperature was maintained to an accuracy of ±5°. The period of tempering varied from 2 to 24 hr. After tempering, the tablets were dissolved in water and the residual radioactivity in the sodalite was measured. The degree of exchange was calculated from the difference in radioactivity before and after tempering.

To make sure that exchange does not result merely from pressurizing the tablet or from dissolving the alkali halide away from the sodalite, we ran control experiments with unheated tablets. In these experiments, radioactive release from the sodalite samples appeared negligible—say, 1% or less.

Table I shows the results of various ion-exchange reactions performed at 400°. The Li exchange was completed in a relatively short time. The other exchange processes ceased before completion—evidently the result of an ion-sieve effect. Such an effect was to be expected from the crystal structure of sodalite and had been observed earlier by Orr[3] when he investigated ion-exchange processes between sodalite and salt melts. Additional evidence of the Na–Li exchange was found from X-ray patterns indicating a contraction of the cubic lattice from $a = 8.95$ Å in the pure Na form to $a = 8.72$ Å in the Li form. The degree of exchange could be followed as a function of time by estimating the ratio of the respective peaks.

Table I: Results of Ion-Exchange Reactions at 400°

Salt	Tempering period, hr	Fraction of Na exchanged
LiCl	2	0.98
KCl	2	0.20
	24	0.20
RbCl	2	0.05
	24	0.05
CsCl	2	0.05
	24	0.05

Besides the ion-exchange experiments, we ran isotopic exchange experiments with NaCl tablets to measure the self-diffusion coefficients for Na. The purpose was to find out whether solid–solid exchange measurements were suitable for quantitative as well as qualitative evaluation. From isotopic exchange between sodalite spheres and Na salt melts[4] and from diffusion experiments with NaCl single crystals,[5] the self-diffusion coefficients of Na are known; they imply that the diffusion coefficient for Na should be less in NaCl than in sodalite.

For the mathematical description of an exchange process under the conditions maintained in this study, we consider an initially homogeneous tracer concentration within a sphere of radius r_0 surrounded by an infinitely large medium, into which the tracer diffuses. One may distinguish three cases with respect to the relative velocities of diffusion inside and outside the sphere. The diffusion coefficient inside the sphere may be (i) much greater than that outside, (ii) approximately equal to that outside, or (iii) much less than that outside.

Formulas and numerical values for $g(t)$, the fraction of tracer particles remaining within the sphere after time t, are available for case iii.[6,7] For cases i and ii, however, we found no appropriate formulas in the literature; we proceed, therefore, to derive them here.

For case i, we assume that inside the sphere, the tracer concentration does not depend on space but only on time; outside the sphere, the tracer concentration $c(r, t)$ follows Fick's second law

$$\frac{\partial}{\partial t}c(r, t) = D\frac{1}{r}\frac{\partial^2}{\partial r^2}[rc(r, t)] \tag{1}$$

As boundary conditions we take (with appropriate units for c)

$$c(r_0, t) = g(t) \tag{2}$$

and the relation between $g(t)$ and $c(r, t)$ due to conservation of the tracer particles. Then one may obtain the following equation for $g(t)$ (see Appendix)

$$g(\tau) = \frac{2\sqrt{3}}{\pi}\int_0^\infty \frac{e^{-x^2\tau}x^2dx}{1 + x^2 + x^4} \tag{3}$$

with

$$\tau = 3Dt/r_0^2 \tag{4}$$

where D is the diffusion coefficient outside the sphere and t is time. If τ is not too large, the numerical calculation may be performed by using the following development (see Appendix)

(3) W. C. Orr and R. Ward, USAEC-Report No. NYO-6653.

(4) H. W Levi and W. Lutze, *Phys. Status Solidi A*, **5**, K159 (1971).

(5) D. Mapother, H. N. Crooks, and R. Maurer, *J. Chem. Phys.*, **18**, 1232 (1950).

(6) H. Gaus, *Z. Naturforsch. A*, **16**, 1130 (1961).

(7) K. E. Zimen, HMI-B 16, May 1961; T. Lagerwall and K. E. Zimen, HMI-B 25, June 1963.

$$g(\tau) = a_0 + a_1\tau^{1/2} + a_2\tau^{2/2} + a_3\tau^{3/2} + \ldots \quad (5)$$

with

$$a_0 = 1 \qquad a_1 = -2\sqrt{3/\pi} \qquad a_2 = 2$$
$$a_3 = -(4/3)\sqrt{3/\pi} \qquad a_4 = 1/2 \qquad a_5 = 0 \quad (6)$$

where the coefficients a_ν for $\nu \geq 4$ are given by

$$a_\nu = \frac{2}{\nu}a_{\nu-2} - \frac{4}{\nu(\nu-2)}a_{\nu-4} \quad (7)$$

For large values of τ, one may derive an asymptotic form of eq 3. We introduce $x' = x\sqrt{\tau}$ as a new variable, which brings τ into the denominator of eq 3. Then we retain only the largest power of τ in the denominator and integrate. Subtracting the result from eq 3 and repeating the procedure, we get further terms. After two steps we have

$$g(\tau) = \frac{1}{2}\sqrt{\frac{3}{\pi}}\left(\tau^{-3/2} - \frac{3}{2}\tau^{-5/2}\right) \quad (8)$$

For $\tau > 6$, the error is less than 0.5%.

In case ii, the concentration $c(r, t)$ is obtained by well-known methods.[8] The fraction of tracer particles in the sphere at time τ is given by

$$g(\tau) = \frac{2}{\sqrt{\pi}}\int_0^\xi \exp(-x^2)dx - \frac{1}{\sqrt{\pi}}\left[\frac{2}{\xi^3}(\exp(-\xi^2) - 1) - \frac{1}{\xi}\exp(-\xi^2) + \frac{3}{\xi}\right] \quad (9)$$

with $\xi = \sqrt{3/\tau}$ and τ as given by (4). Numerical evaluations of eq 5 and 9 were performed by means of a computer. The results are plotted in Figure 1. This diagram may be used to calculate self-diffusion coefficients from fractional releases. The condition $D^{Na}_{sodalite} \gg D^{Na}_{NaCl}$, presumably valid in this study, calls for use of curve 1.

However, the two curves demonstrate that there is not much difference in results when $D_{inside}/D_{outside}$ is approximately equal to unity (case ii) or when $D_{inside}/D_{outside}$ greatly exceeds unity.

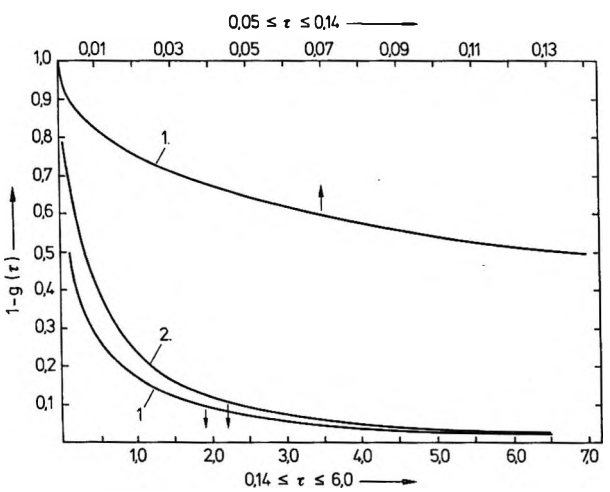

Figure 1. Computed curves for the evaluation of self-diffusion coefficients (after eq 5 and 9).

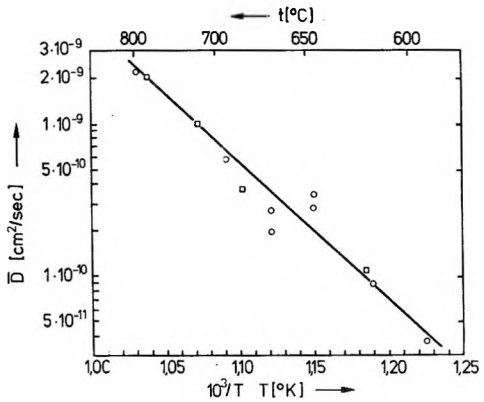

Figure 2. Arrhenius plot of self-diffusion coefficients in NaCl: (□) this investigation, (○) Mapother (ref 5).

The self-diffusion coefficients of sodium in NaCl obtained in this investigation and those obtained by Mapother[5] in diffusion experiments with single crystals of NaCl are plotted against $1/T$ in Figure 2. The diagram shows that solid–solid exchange performed under proper experimental conditions is, in principle, suitable for determining diffusion coefficients in one of the solid phases.

Appendix

For a derivation of eq 3, we start with the following solution of (1) and (2).

$$c(r, t) = \int_{-\infty}^{+\infty} dt' \int_{-\infty}^{+\infty} d\alpha \frac{r_0}{2\pi r} g(t') \exp[i\alpha(t - t')] \times \exp\left[-\frac{1}{\sqrt{2}}\left(1 + i\frac{\alpha}{|\alpha|}\right)\sqrt{\frac{|\alpha|}{D}}(r - r_0)\right] \quad (A1)$$

For $r = r_0$, the second exponential is unity and the first exponential leads to the δ function $\delta(t - t')$; thus (2) is fulfilled. Further, the operations of both sides of eq 1 give a factor $i\alpha$ under the integrals; thus (1) is satisfied. Concerning the relation between $g(t)$ and $c(r, t)$, it is convenient to treat the problem from a more general point of view. We allow creation of particles inside the sphere at an arbitrary rate $f(t)$ per cubic centimeter and per second, and we assume no particles throughout at $t = -\infty$. Then we have

$$\frac{4\pi}{3}r_0^3 f(t) = \frac{4\pi}{3}r_0^3\frac{\partial}{\partial t}g(t) - 4\pi r_0^2 D\left(\frac{\partial c(r, t)}{\partial r}\right)_{r=r_0} \quad (A2)$$

By using (2) and (A1), this becomes

$$f(t) = \frac{1}{2\pi}\int dt' \int d\alpha g(t') e^{i\alpha(t-t')}\varphi(\alpha) \quad (A3)$$

with

(8) Ph. Frank and R. v. Mises, "Die Differential- und Integralgleichungen der Mechanik und Physik," Vol. II, Braunschweig, 1935, XIII, eq 49.

$$\varphi(\alpha) = i\alpha + \frac{3D}{r_0^2} + \frac{3}{r_0}\sqrt{\frac{D}{2}}\left(1 + i\frac{\alpha}{|\alpha|}\right)\sqrt{|\alpha|} \quad \text{(A4)}$$

Equation A3 can be solved for $g(t')$

$$g(t') = \frac{1}{2\pi}\int dt''\int d\beta f(t'')e^{i\beta(t'-t'')}[\varphi(\beta)]^{-1} \quad \text{(A5)}$$

as one may verify easily by inserting (A5) into (A3) and integrating first over t'.

Now we consider the special case

$$f(t) = \delta(t) \quad \text{(A6)}$$

which corresponds to the initial condition mentioned in the text

$$g(0) = 1 \qquad c(r, 0) = 0 \quad \text{(A7)}$$

Then (A5) becomes

$$g(t) = \int_{-\infty}^{+\infty} \frac{1}{2\pi}e^{i\beta t}[\varphi(\beta)]^{-1}d\beta \quad \text{(A8)}$$

$$= \int_0^{\infty} d\beta + \text{conjugate} \quad \text{(A9)}$$

In (A9) within the expression (A6) for $\varphi(\beta)$ we may replace $|\beta|$ by β. Then for $\tau > 0$ we may continue $\varphi(\beta)$ into the first quadrant of the complex β plane, without a zero of $\varphi(\beta)$ in the first quadrant. By integrating over the closed contour: positive real axis—quarter of a large circle into first quadrant—positive imaginary axis, it follows that

$$0 = \int_0^{\infty} d\beta + 0 + \int_{i\infty}^{0} d\beta$$

Substituting new variables in the second integral according to

$$\beta = is\frac{3D}{r_0^2} \qquad t = \tau\frac{r_0^2}{3D} \quad \text{(A10)}$$

and expressing the first integral by the second one, we get finally

$$\bar{g}(\tau) \equiv g(t) = \int_0^{\infty} \frac{1}{2\pi}\frac{e^{-s\tau}ids}{1 - s + i\sqrt{3s}} + \text{conjugate} \quad \text{(A11)}$$

For convinience, we omit the bar over $g(\tau)$. With an obvious substitution, we arrive at eq 3 of the text.

In order to get a development for numerical calculation of $g(\tau)$, we note that according to (3), $g(\tau)$ satisfies the following equation for $\tau > 0$

$$-\frac{d}{d\tau}g(\tau) + g(\tau) + \int_{\tau}^{\infty} g(\tau')d\tau' = \sqrt{\frac{3}{\pi\tau}} \quad \text{(A12)}$$

Furthermore, one may calculate from (A11), as required by the initial condition

$$g(0) = 1 \quad \text{(A13a)}$$

and also

$$\int_0^{\infty} g(\tau')d\tau' = 1 \quad \text{(A13b)}$$

Therefore, we may put in (A12)

$$\int_{\tau}^{\infty} g(\tau')d\tau' = b_0 + b_2\tau^{2/2} + b_3\tau^{3/2} + \ldots + b_\nu\tau^{\nu/2} + \ldots \quad \text{(A14)}$$

where from (A12) and (A13a,b)

$$b_0 = 1 \qquad b_1 = 0 \qquad b_2 = -1 \qquad b_3 = \frac{4}{3}\sqrt{\frac{3}{\pi}} \quad \text{(A15)}$$

and for $\nu \geq 4$

$$b_\nu = \frac{2}{\nu}b_{\nu-2} - \frac{4}{\nu(\nu-2)}b_{\nu-4} \quad \text{(A16)}$$

By applying $(-d/d\tau)$ to (A14) and using (A15) and (A16), we get the development (5) with eq 6 and with the same recurrence formula (7) as (A16).

An Average Value of the Cross Section for H + HBr → H_2 + Br over the 0.35–1.7-eV Collision Energy Range[1]

by R. G. Gann and J. Dubrin*

Department of Chemistry, Massachusetts Institute of Technology, Cambridge, Massachusetts 02139
(Received November 16, 1971)

Publication costs assisted by the U. S. Atomic Energy Commission

An average cross section for the title reaction has been computed from certain previously reported hot atom (photochemical-recoil) data. The cross section is equal to 1.6 ± 0.3 Å^2, and it is defined as $S_R(E)_{HBr} = \int_{0.35}^{1.7} h'(E)S_R(E)dE$, where $S_R(E)$ is the corresponding microscopic quantity and $h'(E)$ is a *known* normalized distribution function of energies.

Introduction

We have recently employed a photolytic bulb method to determine the excitation function or translational energy dependence of the cross section for reaction 1 from threshold (~0.35 eV) to ~2 eV.[2] Hydrogen

$$H^* + n\text{-}C_4D_{10} \longrightarrow HD + C_4D_9 \qquad (1)$$

atoms of different well known initial kinetic energies between 0.3 and 2.1 eV were generated for reaction by the selective photodissociation of either HI or HBr in the presence of the reactant.[3] Those hydrogen atoms having a kinetic energy greater than the threshold energy for (1) are termed "hot" atoms and are designated H*. In addition to reaction 1, the hot hydrogens also react with the HBr(HI)

$$H^* + HBr \longrightarrow H_2 + Br \qquad (2)$$

Unreacted hydrogen atoms that have been translationally relaxed or moderated below the threshold energy for abstraction from butane

$$H^* + n\text{-}C_4D_{10} \longrightarrow H + C_4D_9 \qquad (3)$$

$$H^* + HBr \longrightarrow H + HBr \qquad (4)$$

are preferentially removed or scavenged by reaction with the HBr

$$H + HBr \longrightarrow H_2 + Br \qquad (5)$$

The activation energy for reaction 2 is ~0.1 eV.[4] In the limit of zero HBr, the steady-state H_2/HD product ratio is a measure of the competition between moderating (3) and reactive (1) encounters in pure butane. A knowledge of the nonreactive differential scattering cross sections for (3), together with the H_2/HD product ratio as a function of initial H atom energy, allows one to calculate the excitation function for (1) over the energy range sampled experimentally. However, since very little is known about the magnitude and energy dependence of the nonreactive inelastic cross sections for (3), yields were also measured in systems highly diluted with a rare gas, xenon. Then by suitable extrapolation of the yield data, the competition between translational energy degradation and chemical reaction could be referenced effectively to an "elastic scattering" medium.[2,5] Thus the computation of the excitation function only requires a knowledge of the H–Xe potential.

Here, we calculate from some of the moderator data an average or phenomenological cross section for reaction 2. The yield data[2] from the reaction of H atoms of 1.7 eV initial energy are employed, and thus this cross section represents an average of the microscopic quantity over the 0.35–1.7-eV collision energy range.

Method and Calculations[2,5,6]

A quantity of special interest in a three-component HBr–C_4D_{10}–Xe system is the limiting integral reaction probability. It is experimentally defined at a particular (′) source kinetic energy as

$$IRP_0'(H^*\text{-}C_4D_{10}) \equiv \lim_{X_{C_4D_{10}} \to 0} \frac{Y_0'(X_{C_4D_{10}})}{X_{C_4D_{10}}} \qquad (6)$$

$Y_0'(X_{C_4D_{10}})$ is the HD yield as a function of butane mole fraction, $X_{C_4D_{10}}$. Since the $X_{HBr}/X_{C_4D_{10}}$ is normally maintained constant, both X_{HBr} and $X_{C_4D_{10}}$ tend to zero with increasing Xe content. Expression 7 relates this experimental quantity to the excitation function $S_R(E)_{C_4D_{10}}$ for (1).

(1) This work was supported in part by the U. S. Atomic Energy Commission through funds provided under Contract AT(30-1)-905.

(2) R. G. Gann, W. M. Ollison, and J. Dubrin, *J. Chem. Phys.*, **54**, 2304 (1971). References to other photochemical-recoil studies are contained in this reference.

(3) A. Kuppermann, J. Stevenson, and P. O'Keefe, *Discuss. Faraday Soc.*, **44**, 46 (1967); R. N. Porter, *J. Chem. Phys.*, **45**, 2284 (1966).

(4) I. Amdur and G. G. Hammes, "Chemical Kinetics: Principles and Selected Topics," McGraw-Hill, New York, N. Y., 1966.

(5) R. G. Gann, W. M. Ollison, and J. Dubrin, *J. Amer. Chem. Soc.*, **92**, 450 (1970).

(6) C. Rebick and J. Dubrin, *J. Chem. Phys.*, **53**, 2079 (1970).

$$IRP_0'(\text{H*–}C_4D_{10}) = \int_{E_0}^{\infty} S_R(E)_{C_4D_{10}} \int_0^{\infty} \frac{n_0'(E_L)_{Xe}}{S(E_L)_{Xe}} G(E_L,E)dE_L dE \quad (7)$$

E_0 is the threshold energy, 0.35 eV, for (1). The quantity $n_0'(E_L)_{Xe}$ is the H–Xe collision density function evaluated in the limit of zero butane, and $S(E_L)$ is the H–Xe total scattering cross section. $G(E_L,E)$ is a known, normalized distribution function of relative kinetic energies E between an atom of laboratory energy E_L and a target gas having a Maxwellian velocity distribution. Since the source energy used here is substantially greater than E_0 and since the masses of C_4D_{10} and Xe are much greater than that of H, we can simplify (7) with negligible error[6]

$$IRP_0'(\text{H*–}C_4D_{10}) = \int_{0.35}^{1.7} \frac{n_0'(E)_{Xe}}{S(E)_{Xe}} S_R(E)_{C_4D_{10}} dE \quad (8)$$

In these moderator studies, the H_2/HD product ratio was also determined as a function of the [HBr]/[C_4D_{10}] composition ratio at *fixed* moderator content,[2] *i.e.*, [Xe]/([C_4D_{10}] + [HBr]) = constant. The measurements were conducted at Xe mole fractions of 0, 0.94, 0.96, 0.98, and 0.985. The H_2/HD ratio was linearly dependent on the [HBr]/[RD] ratio and within experimental error the slopes m' of such plots were equal to one another. The finding that m' is independent of Xe content suggests the energy dependence of the collision density is about the same for the moderated and unmoderated media. In any event, it is very reasonable to identify the slope measured at very high moderation with that in the limit of pure rare gas.

$$m' = m_0'; \quad m_0' \equiv \left.\frac{d\left(\frac{H_2}{HD}\right)}{d\left(\frac{HBr}{C_4D_{10}}\right)}\right|_{X_{Xe}\to 1} \quad (9)$$

The limiting slope m_0' is equal to the ratio of the limiting integral reaction probabilities for reactions 1 and 2

$$m_0' = \frac{IRP_0'(\text{H*–HBr})}{IRP_0'(\text{H*–}C_4D_{10})} \quad (10)$$

and by analogy to (8), we may write

$$IRP_0'(\text{H*–HBr}) = \int_{0.35}^{1.7} \frac{S_R(E)_{HBr}}{S(E)_{Xe}} n_0'(E)_{Xe} dE \quad (11)$$

where $S_R(E)_{HBr}$ is the excitation function for (2). At the initial energy 1.7 eV, the slope m' ($\equiv m_0'$) is 3.4 ± 0.6 and the corresponding $IRP_0'(\text{H*–}C_4D_{10})$ is 3.45 ± 0.10.[2] Using (10), we then find

$$IRP_0'(\text{H*–HBr}) = 11.7 \pm 2.3 \quad (12)$$

As discussed at length elsewhere,[6,7] little error is involved in representing $n_0'(E)_{Xe}$ in (11) by the asymptotic form given by

$$n_0'(E)_{Xe} = \frac{M}{2\mu} S(E)_{Xe}[Q(E)_{Xe}E - {}^3/_2 kTQ(E)_{Xe}]^{-1} \quad (13)$$

and thus expression 11 is given by

$$IRP_0'(\text{H*–HBr}) = \frac{M}{2\mu}\int_{0.35}^{1.7} S_R(E)_{HBr}[Q(E)_{Xe}E - {}^3/_2 kTQ(E)_{Xe}]^{-1}dE \quad (14)$$

The mass M is the sum of the H and Xe masses; μ is the reduced mass of this pair; $Q(E)_{Xe}$ is the H–Xe momentum transport cross section and is calculated from the H–Xe repulsive potential. The average cross section for reaction 2 then follows from (14)

$$\overline{S_R(E)}_{HBr} = \frac{\int_{0.35}^{1.7} S_R(E)_{HBr}[Q(E)_{Xe}E - {}^3/_2 kTQ(E)_{Xe}]^{-1}dE}{\int_{0.35}^{1.7}[Q(E)_{Xe}E - {}^3/_2 kTQ(E)_{Xe}]^{-1}dE} \quad (15a)$$

$$= \frac{IRP_0'(\text{H*–HBr})}{\left(\frac{M}{2\mu}\right)\int_{0.35}^{1.7}[Q(E)_{Xe}E - {}^3/_2 kTQ(E)_{Xe}]^{-1}dE} \quad (15b)$$

$Q(E)_{Xe}$ is computed from the potential measured by Fink and given in ref 2.

$$Q(E)_{Xe} = 13.4E^{-0.37}\ \text{Å}^2 \quad (16)$$

Using (16) along with (12), we find from (15b)

$$\overline{S_R(E)}_{HBr} = 1.6 \pm 0.3\ \text{Å}^2 \quad (17)$$

(The bath temperature, T, is 296°K.[2])

For convenience, expression 15 is written in terms of a normalized distribution function of energies, $h'(E)$

$$\overline{S_R(E)}_{HBr} = \int_{0.35}^{1.7} S_R(E)_{HBr} h'(E)dE \quad (18)$$

$$h'(E) = \frac{[Q(E)_{Xe}E - {}^3/_2 kTQ(E)_{Xe}]^{-1}}{\int_{0.35}^{1.7}[Q(E)_{Xe}E - {}^3/_2 kTQ(E)_{Xe}]^{-1}dE} \quad (19)$$

$$= 0.65E^{0.37}[E - 0.04]^{-1}$$

The distribution function is shown in Figure 1.

Discussion

Martin and Willard (MW)[8] have measured the relative amounts of H_2 and HD from reaction of 2.9-eV H atoms with HBr–D_2 mixtures (H + D_2 → HD + D). From an estimate of the average number of moderating collisions a hot hydrogen undergoes with D_2 in the 0.4–2.9 eV interval, they determined an average reaction

(7) The rapid approach to asymptotic behavior is a result of the very small fractional energy loss in an H–Xe collision. A more exact form which gives the functional dependence of the "high energy tail" ($n_0'(E)_{Xe}$ above 1.7 eV) is found in the thesis of R. Gann (also see ref 6).

(8) R. M. Martin and J. E. Willard, *J. Chem. Phys.*, **40**, 3007 (1964).

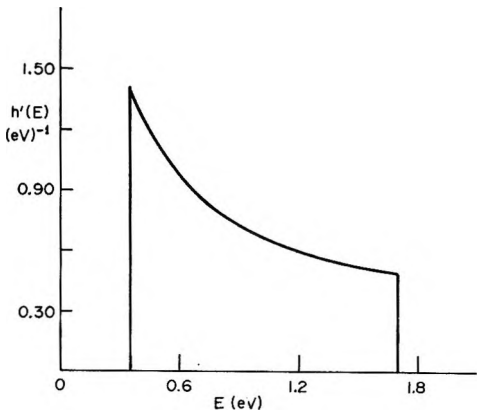

Figure 1. The distribution function $h'(e)$ given by expression 19 in the text.

probability, $\overline{p(E)}$, for (2) over the same energy interval. When $p(E)$ is multiplied by the H–HBr collision cross section employed by the authors in their calculation, one obtains an average reaction cross section of 7.5 Å². A direct comparison of our cross section with MW's is not possible since the initial energies are substantially different. However, we strongly believe that their value is too large. In the MW analysis, a hard-sphere (elastic) potential was used to compute the average fractional energy loss that a hot hydrogen atom suffers in a moderating collision with D_2. In actual fact, the H–D_2 repulsive potential[9] is much "softer," and in the potential energy range of interest it can be represented adequately by an inverse power form

$$V(r)_{H-D_2} = \frac{C}{r^4}; \qquad C = 1.7 \text{ eV Å}^4 \qquad (20)$$

With the above potential, we find the average fractional energy loss $\bar{\epsilon}$ to be substantially less than predicted by a hard-sphere potential, *e.g.*, at $E = 1.5$ eV, $\bar{\epsilon} \sim 0.07$ as opposed to the hard-sphere value of 0.32. Since the number of moderating collisions is inversely dependent on $\bar{\epsilon}$, it can be reasoned that the MW calculation overestimates $\overline{p(E)}$ and thus $\overline{S_R(E)}$. Moreover, as calculated in their manner, these values are not that meaningful—the *actual* distribution of collision energies in the H–D_2 system is essentially unspecified.[10] The calculation of the steady-state collision density requires a prior knowledge of the excitation function for H + D_2 → HD + D. On the other hand, the average or phenomenological cross section derived here (0.35–1.7 eV), is defined in terms of a known distribution function $h'(E)$. It is of interest to note that if an $\bar{\epsilon}$ of 0.07 for the H–D_2 system is used instead of the hard-sphere value, the MW treatment results in an average cross section of 1.5 Å² for (2). This is essentially equal to the value found here for 1.7-eV H atoms. This close agreement suggests that the cross section for (2) (on the average) does not rise in passing from 1.7 to 2.9 eV. Obviously this and any further interpretations require assumptions about the relative steady-state collision densities and excitation functions (see previous paragraph).

It certainly would be desirable to determine $S_R(E)_{HBr}$, using the photochemical recoil method. For this purpose, one needs to measure the limiting slope, defined by (9), at various initial energies. The subsequent analysis is quite straightforward. Although we have reported measurements for 1.2 and 2.1 eV initial energy,[2] the experimental errors are such that little can be reached conclusively about the energy dependence of (2) in this interval. More accurate measurements are planned.

(9) K. T. Tang and M. Karplus, *J. Chem. Phys.*, **49**, 1676 (1968); R. Nelson, Ph.D. Thesis, Massachusetts Institute of Technology, Cambridge, Mass., 1968.

(10) Given the average fractional energy loss, one may easily calculate the average number of moderating collisions a hot atom makes over a specified energy interval. However, the collision density is desired, if one wishes to compute the average cross section from a prior knowledge of $S_R(E)_{HBr}$; *i.e.*, no meaningful comparison of experiment with theory is possible without this information.

Radical Concentration Growth in Irradiated Solid Systems. A Simple Model Involving Competitive Radical Production, Thermal Decay, and Radiation-Induced Decay

by Paul J. Ogren[1]

Department of Chemistry, Maryville College, Maryville, Tennessee 37801 *(Received October 7, 1971)*

Publication costs assisted by Maryville College and the National Center for Atmospheric Research

A model for the growth of radical concentrations in solids undergoing irradiation is developed assuming three processes known to be important in several systems: (1) a constant radical production rate, (2) nonexponential first-order thermal decay of radicals formed at a particular time, and (3) radiation-induced decay proportional both to the dose rate and the number of radicals present at a particular time. The model is then applied with satisfactory results to the growth of ethyl radicals in γ- or β-irradiated ethyl iodide glass at 77°K.

The production and decay of radicals produced in solids by radiation is a highly complex process in many situations, although in a few cases radical disappearance following irradiation appears to follow simple first- or second-order kinetic laws.[2,3] In several other cases, complex first-order thermal decay has been observed, *i.e.*, decay is nonexponential in character, but the fractional decay rate at a given time after radiation has ceased is the same for systems with widely varying initial concentrations.[3-5]

While study of decay rates of radicals following irradiation provides information on thermal processes for removal, additional removal mechanisms can occur during irradiation, so-called "radiation-catalyzed" decay processes.[4-8] The nature of these can be inferred from studies of growth curves of the radicals under various conditions, and, in the absence of thermal decay, the mathematical description of such curves is well understood in many cases.[6]

An analysis of such growth curves in the presence of thermal decay is presented here assuming (1) a constant rate of radical production, (2) complex first-order decay of radicals formed at a particular time, and (3) radiation-induced decay which occurs only during irradiation and which is proportional to the dose rate and to the number of radicals present at a given time t. Also discussed is the application of this model to a particular system, that of ethyl radicals produced by γ or β irradiation of glassy ethyl iodide at 77°K.

Development of the Model

Assuming complex first-order thermal decay, we let the decay of the set of radicals produced by irradiation during a given short time interval Δt be given by

$$N = N_0 f(\tau) \tag{1}$$

or, in differential form

$$dN/d\tau = N_0 f'(\tau) \tag{2}$$

where $\tau = 0$ is the time of formation of the set. Often, $f(\tau)$ can be evaluated experimentally from the decay of radicals produced by a sufficiently short period of irradiation. In cases where radiation-induced decay is unimportant, the net rate of production of radicals during irradiation then becomes

$$d\eta/dt = R + \sum_{\substack{\text{all}\\ \text{sets}}} N_0 f'(\tau) = R + \sum_{j=1}^{t/\Delta t} (R\Delta t) f'(j\Delta t) \tag{3}$$

where η = the total number of radicals, R = the radical production rate, and t = the time from the start of irradiation. As Δt approaches 0, the summation may be replaced by integration and eq 3 reduces to

$$d\eta/dt = R + \int_0^t f'(t) R dt = Rf(t) \tag{4}$$

The integrated form showing the change in total radicals as a function of time is then

$$\eta = \int_0^t Rf(t) dt \tag{5}$$

To include a simple model for radiation-induced decay in this analysis, we first assume that the popula-

(1) Address correspondence to the author at the Advanced Study Program, National Center for Atmospheric Research, Boulder, Colo. 80302.

(2) R. F. C. Claridge and J. E. Willard, *J. Amer. Chem. Soc.*, **87**, 4992 (1965).

(3) W. G. French and J. E. Willard, *J. Phys. Chem.*, **72**, 4604 (1968).

(4) M. Shirom and J. E. Willard, *ibid.*, **72**, 1702 (1968).

(5) H. W. Fenrick, N. B. Nazhat, P. J. Ogren, and J. E. Willard, *ibid.*, **75**, 472 (1971).

(6) W. Snipes and P. K. Horan, *Radiat. Res.*, **30**, 307 (1967).

(7) V. K. Ermolaev and V. V. Voevodsky, *Proc. Tihany Symp. Radiat. Chem. 2nd*, 2, (1967).

(8) P. J. Ogren and J. E. Willard, *J. Phys. Chem.*, **75**, 3359 (1971).

tion in set N, decaying by a complex first-order thermal process, consists of subsets n_i decaying according to simple first-order laws

$$N(\tau) = \sum_i n_i = \sum_i n_{0,i} e^{-\lambda_i \tau} = N_0 f(\tau) \quad (6)$$

If one now includes radiation-induced removal in each subset which is proportional to the dose rate and to the number of radicals n_i present at a given time, then the decay rate in a subset becomes

$$dn_i/d\tau = -\lambda n_i - \alpha R n_i = -(\lambda_i + \alpha R) n_i \quad (7)$$

and (6) becomes

$$N = \sum_i n_{0,i} e^{-(\lambda_i + \alpha R)\tau} = e^{-\alpha R \tau} \sum_i n_{0,i} e^{-\lambda_i \tau} = N_0 f(\tau) e^{-\alpha R \tau} \quad (8)$$

The assumption of a constant α for all subsets here is equivalent to the assumption that radiation-induced decay is proportional to the total number of radicals present. The latter assumption, in the absence of thermal decay, leads to growth curve analyses summarized by Snipes and Moran.[6]

Since (8) is now of the same general form as (1), a comparison of (8) with (1) and (5) shows that, for radical growth accompanied by radiation-induced decay

$$\eta(t) = R \int_0^t e^{-\alpha R t} f(t) dt \quad (9)$$

The assumption leading to eq 6 is physically reasonable for some systems, where radical decay is thought to proceed by geminate recombination of reacting partners, with small variations in the relative location of the partners accounting for complex first-order decay.[3-5] For other models of first-order decay, such as recombination of radicals in isolated spurs,[9] the assumption is not physically reasonable. Mathematically, however, eq 6 is still valid for many such cases. To illustrate for the continuous case, if we write

$$N = N_0 f(\tau) = N_0 \int_0^\infty P(x) e^{-x\tau} dx \quad (10)$$

we then have an equation which claims to represent $f(\tau)$ as a continuous sum of exponential terms ($P(x)$ is a normalized probability distribution function). However, $P(x)$ is now seen to be the function whose Laplace transform is $f(\tau)$, with the existence of $P(x)$ being a sufficient condition for the validity of the treatment leading to (9). Reference to a standard table of such transforms indicates that $P(x)$ is defined for a wide range of functions $f(\tau)$ of potential interest in the present problem.[10] If P is defined, it is automatically normalized, since $f(0) = 1$.

Application of the Model to Ethyl Iodide Glass at 77°K

Ethyl radicals in ethyl iodide glass at 77°K decay thermally following γ irradiation according to a complex first-order law.[5] An empirical equation satisfying the decay is[11]

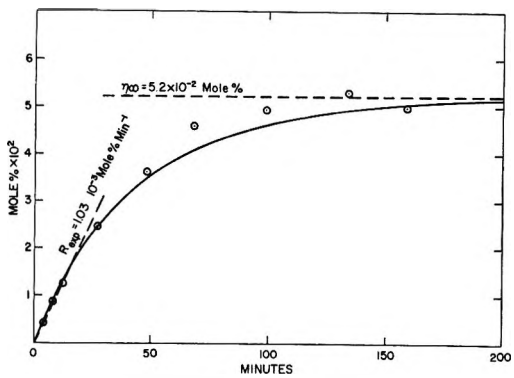

Figure 1. Calculated and experimental growth of ethyl radicals in glassy ethyl iodide at 77°K; 2×10^{18} eV g^{-1} min^{-1} γ dose rate; $G = 2$; $R = 1.3 \times 10^{-3}$ mol % min^{-1}; $\alpha = 14.5$ mol % $^{-1}$.

$$N = N_0 f(\tau) = N_0 \left[\frac{0.37}{(1 + 3.0 \times 10^{-2})\tau} + \frac{0.63}{(1 + 2.3 \times 10^{-3})\tau} \right] \quad (11)$$

where τ is in minutes. During the cobalt-60 γ irradiation at 2×10^{18} eV g^{-1} min^{-1}, the growth of ethyl radicals reaches a plateau rather quickly, as seen in Figure 1.[12] The fact that this plateau is reached much more rapidly than would be predicted from eq 5 and 11 suggests the operation of radiation catalysis, a suggestion supported by other more direct evidence as well.[5] Since (10) is defined for this empirical decay equation, eq 9 can be applied. Equations 9 and 11 have been used to compute the solid line shown, using parameters of $R = 1.3 \times 10^{-3}$ mol % min^{-1}, $\alpha = 14.5$ mol %$^{-1}$. Computations were carried out using a Hewlett-Packard 2114B computer.

It should be noted that the experimental initial growth rate of Figure 1 is only about 1.03×10^{-3} mol % min^{-1}. This discrepancy with the R value used results principally from the radiation catalysis, with a smaller contribution from the fast-decaying first term in eq 11. This factor can significantly affect G values measured from experimental initial growth rates in this system.[5,8,13] It should also be noted that, at sufficiently high dose rates (and hence radical concentrations), radiation catalysis is the limiting factor for radical growth, as is observed for many systems in the absence of thermal decay.[6] For $\alpha = 14.5$ mol %$^{-1}$,

(9) A. H. Samuel and J. L. Magee, *J. Chem. Phys.*, **21**, 1080 (1953).

(10) For a more general discussion of some conditions under which $P(x)$ is defined, see W. R. LePage, "Complex Variables and the Laplace Transform for Engineers," McGraw-Hill, New York, N. Y., 1961, Chapter 10.

(11) For further details, see P. J. Ogren, Ph.D. Thesis, University of Wisconsin, 1968.

(12) Experimental data from ref 5, 8, and 11.

(13) P. B. Ayscough and C. Thompson, *Trans. Faraday Soc.*, **58**, 1477 (1962).

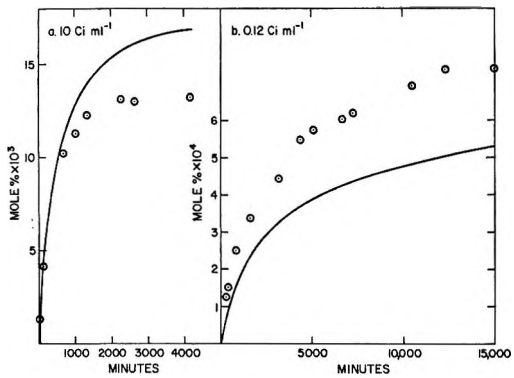

Figure 2. Calculated and experimental ethyl radical growth in tritiated ethyl iodide glass at 77°K: (a) 10 Ci ml^{-1}; (b) 0.12 Ci ml^{-1}.

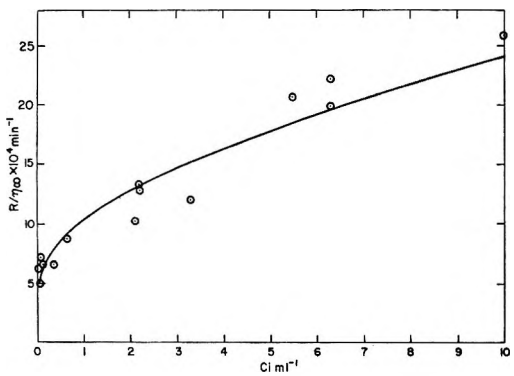

Figure 3. Calculated and experimental values of R/η_∞ as a function of dose rate; 10 Ci ml^{-1} = 6.6 × 10^{16} eV g^{-1} min^{-1}. For γ irradiation at 2 × 10^{18} eV g^{-1} min^{-1}, calculated R/η_∞ = 0.0216 min^{-1}, experimental R/η_∞ = 0.0198 min^{-1}.

the limiting concentration of radicals even in the absence of thermal decay would be about 6.9 × 10^{-2} mol %, a value nearly reached in the present example.

The growth of ethyl radicals using tritium β radiation has also been studied in this system.[8,11] Assuming that complex first-order thermal decay competes with growth, one would predict that the shapes of the growth curves would be independent of dose rate, but dose rate dependence is in fact observed implying additional radiation-induced decay. Figure 2 illustrates this point for growth curves of 10 Ci ml^{-1} (6.6 × 10^{16} eV g^{-1} min^{-1}) and 0.12 Ci ml^{-1} trititated ethyl iodide samples. The solid lines are computed using (11), the α value found for the γ-irradiated system, and the appropriate R value assuming G(ethyl radicals) = 2. Although the agreement between experimental and calculated curves is satisfactory only in a qualitative sense, there are several sources of uncertainty both in the experimental data and in the matching procedure. Comparison with directly determined experimental concentrations, as in Figure 2a, must allow for fairly large uncertainties in esr intensity and calibration measurements. In the case of Figure 2b, the experimental concentrations were assigned by assuming that the slope of the computed curve at 10 min matched the experimental initial growth rate of the esr signal. Owing to the very low dose rate, however, the "initial" experimental growth rate could be determined only after about 100 min.[8] If, as computer calculations suggest, the growth rate at 10 min is about 25% higher than that measured at 100 min, then matching of the computed and experimental data at 100 min would lower the experimental points of Figure 2b by about 20%. The directly measured concentrations, with still higher inherent errors due to very low esr signal levels, are about 50% lower than the points of Figure 2b.

Finally, the values of R/η_∞ for ethyl radicals in several tritiated samples are plotted as a function of dose rate in Figure 3 together with the calculated curve. The calculated curve, again based on (9) and (11), approaches zero at R values much less than those used experimentally. For values of $\alpha R > 10^{-3}$ min^{-1}, numerical integration of (9) could be efficiently employed to calculate η_∞. For much lower values of αR, however, convergence of this integral is very slow, and numerical evaluation using the standard formula

$$\int_\infty^1 \frac{e^{-ax}}{x}\,dx = \gamma + \log a + \sum_1^\infty (-1)^n \frac{a^n}{n \cdot n!} \quad (12)$$

was employed. The computed R value was based on the calculated radical concentration at 10 min, to correspond with the earliest times of experimental evaluation of initial radical growth. This compensates somewhat for the discrepancy between theoretical R values and the early initial slopes mentioned above. Figure 3 gives a realistic idea of the scatter to be expected for these particular experimental data.

In summary, the parameters chosen empirically to account for the growth curves of ethyl radicals in the γ-irradiated ethyl iodide system also serve reasonably well to predict the behavior of the β-irradiated system at dose rates which are as much as four orders of magnitude lower. This indicates that the mathematical model used for this system is reasonable and also suggests that for this system there is little difference in the effects of γ and β irradiation. The actual mechanism of radiation-induced decay in the system remains uncertain, although several possibilities have been discussed elsewhere.[8]

Acknowledgment. I am grateful to Professor John E. Willard for useful discussions regarding this work.

Proton-Transfer Kinetics in the Aminobenzoic Acids

by R. D. White and L. J. Slutsky*

Department of Chemistry, University of Washington, Seattle, Washington 98195 *(Received November 11, 1971)*

Publication costs borne completely by The Journal of Physical Chemistry

Ultrasonic attenuation in solutions of the isomeric aminobenzoic acids in methanol, water, acetone, and methanol–water mixtures has been measured as a function of frequency, temperature, and pH. Relaxation spectra calculated from Eyring and Eigen's values of the rate constants for dissociation and recombination in the aminobenzoic acids, and related bimolecular rate constants estimated from the Debye–Smoluchowsky theory, give a satisfactory account of the frequency and pH dependence of acoustic absorption in aqueous solution. Only in the case of *o*-aminobenzoic acid in nonaqueous solvents is it found necessary to postulate a direct unimolecular mechanism of internal proton transfer. For *o*-aminobenzoic acid in methanol and acetone the principal source of excess acoustic absorption appears to be perturbation of the classical $\rightleftharpoons$ zwitterion equilibrium. Our results imply a forward rate constant $k_f = 1 \times 10^7$ sec^{-1}, a reverse rate constant $k_b = 1.4 \times 10^8$ sec^{-1} and an activation energy derived from the temperature dependence of k_b of 8 kcal/mol. The standard volume change in methanol for formation of the zwitterion from the classical form of *o*-aminobenzoic acid is found to be -32.4 cm^3/mol.

I. Introduction

The kinetics of the diffusion-controlled proton-transfer reactions of amino acids and simple polypeptides have been fairly extensively investigated.[1-3] There is not a comparably large body of data on the rates of internal charge-transfer reactions

$$\mathrm{RH} \underset{k_b}{\overset{k_f}{\rightleftharpoons}} \mathrm{ZH} \qquad (1)$$

where ZH represents the zwitterionic and RH the classical form of an amino acid or simple peptide.

Of course it is always possible that the reaction represented by eq 1 proceeds by a diffusion-controlled dissociation followed by a diffusion-controlled recombination or by a pure bimolecular mechanism and thus that the rate constants which appear in eq 1 are implicit in the kinetics of a series of related bimolecular reactions

$$\mathrm{Z^- + H^+} \underset{k_{2b}}{\overset{k_{2f}}{\rightleftharpoons}} \mathrm{RH} \qquad (2)$$

$$\mathrm{Z^- + H^+} \underset{k_{3b}}{\overset{k_{3f}}{\rightleftharpoons}} \mathrm{ZH} \qquad (3)$$

$$\mathrm{RH + H^+} \underset{k_{4b}}{\overset{k_{4f}}{\rightleftharpoons}} \mathrm{HRH^+} \qquad (4)$$

$$\mathrm{H^+ + OH^-} \underset{k_{5b}}{\overset{k_{5f}}{\rightleftharpoons}} \mathrm{H_2O} \qquad (5)$$

$$\mathrm{ZH + H^+} \underset{k_{6b}}{\overset{k_{6f}}{\rightleftharpoons}} \mathrm{HRH^+} \qquad (6)$$

$$\mathrm{HRH^+ + Z^-} \underset{k_{7b}}{\overset{k_{7f}}{\rightleftharpoons}} \mathrm{2RH} \qquad (7)$$

$$\mathrm{HRH^+ + Z^-} \underset{k_{8b}}{\overset{k_{8f}}{\rightleftharpoons}} \mathrm{2ZH} \qquad (8)$$

$$\mathrm{HRH^+ + RH} \underset{k_{9b}}{\overset{k_{9f}}{\rightleftharpoons}} \mathrm{ZH + HRH^+} \qquad (9)$$

$$\mathrm{Z^- + RH} \underset{k_{10b}}{\overset{k_{10f}}{\rightleftharpoons}} \mathrm{ZH + Z^-} \qquad (10)$$

However, there remains the possibility of more direct transfer through intramolecular hydrogen bonds or solvent bridges, particularly in nonaqueous solvents and in amino acids and proteins near physiological pH where the concentrations of H^+ and OH^- are low and the processes represented by eq 2–10 are of necessity slow.

We have attempted to measure the rates of the proton-transfer reactions of the isomeric aminobenzoic acids in water, methanol, acetone, and water–methanol mixtures as a function of pH and temperature. Only in the case of *o*-aminobenzoic acid dissolved in acetone and methanol is it necessary to postulate a direct internal proton-transfer mechanism to account for our results.

II. Experimental Section and Results

A. General. In the absence of significant dispersion the excess acoustic absorption, α, due to a single process with relaxation time, τ, may be expressed as a function of the frequency (f) by[4]

(1) M. Eigen and L. de Maeyer, "Technique of Organic Chemistry," Vol. VIII, part II, A. Weissberger, Jr., Ed., Wiley, New York, N. Y., 1961.

(2) M. Eigen and E. Eyring, *J. Amer. Chem. Soc.*, **84**, 3254 (1962).

(3) K. Applegate, L. J. Slutsky, and R. C. Parker, *ibid.*, **90**, 6909 (1968); R. D. White, L. J. Slutsky, and S. Pattison, *J. Phys. Chem.*, **75**, 161 (1971).

$$\frac{\alpha}{f^2} = \frac{C\tau}{1 + (2\pi\tau f)^2} \tag{11}$$

For the process represented by eq 1

$$C = 2\pi^2\rho C_0\bar{V}^2RT\Gamma_M[(\beta\Delta H/C_pRT) - (\Delta V/\bar{V}RT)]^2$$
$$\Gamma_M = M_0K_z/(1 + K_z) \tag{12}$$

where ρ is the density, C_0 the velocity of sound, $\bar{V}$ the volume per mole of solution, β the coefficient of thermal expansion, C_p the molar heat capacity at constant pressure, M_0 the total molar concentration of the amino acid, and ΔH and ΔV the enthalpy and volume changes for the process in question,[4] and $K_z = k_f/k_b$ is the equilibrium constant for eq 1. The relaxation time in terms of the rate constants of eq 1 is given by[4]

$$\tau = \frac{1}{k_f + k_b} \tag{13}$$

For a complex series of equilibria such as that represented by eq 2–10, the total absorption will be the sum of a number of terms of the form of eq 11.

The experimental technique used here has been described previously.[3] The only significant alteration has been to increase the diameter of the active portion of the transducers to 2 in. with a consequent considerable improvement in the accuracy of measurement in the 3–7-MHz range. However, to determine τ accurately even for a single relaxation it is still necessary to obtain data both at frequencies well above and well below the relaxation frequency ($1/2\pi\tau$). In the range of frequencies accessible to us (3–100 MHz) we are able to meet this condition only for *o*-aminobenzoic acid.

B. Results in Methanol and Acetone. Plots of α/f^2 *vs.* f for *o*-, *m*-, and *p*-aminobenzoic acids in methanol at room temperature are given in Figures 1 and 2. Results for *o*-aminobenzoic acid in methanol at room temperature and 0° are given in Figure 3 as are room temperature results for acetone. Equation 11 gives a satisfactory account of the data obtained in pure methanol and acetone, and there is no reason to believe that more than one process makes a large contribution to the absorption. The identification of this one process is the first and principal interpretative problem.

Values of C and τ deduced from a least-squares adjustment of the constants of eq 11 are given in Table I as are concentrations, temperatures, measured values of the velocity of sound, and values of the other thermodynamic parameters which appear in eq 12. The standard volume changes listed in Table III are deduced from the measured values of C and eq 12 assuming that $|\Delta V/\bar{V}| > |\beta\Delta H/C_p|$ to resolve the ambiguity in the sign of the square root. This assumption will be justified in the Discussion.

C. Results in Water. Owing to the low solubilities of the aminobenzoic acids in water and the consequent low value of the excess absorption at low frequency we

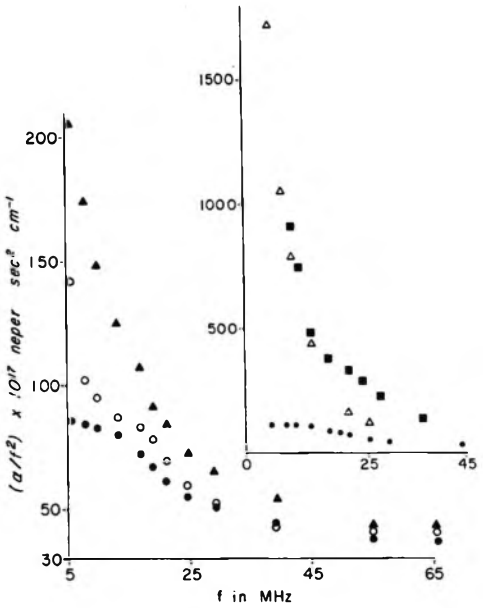

Figure 1. Frequency dependence of the acoustic absorption at 25° for 0.5 *M* *o*-aminobenzoic acid in water, methanol, and water–methanol solutions. In the lower panel: ●, methanol; ○, 0.125 volume fraction H_2O; ▲, 0.250 H_2O. Results for △, 0.50 H_2O, and ■, water, are given in the upper panel in the form of a plot of the excess absorption divided by the molar concentration *vs.* f. The data for methanol are reproduced in the upper panel to facilitate comparison of the scales.

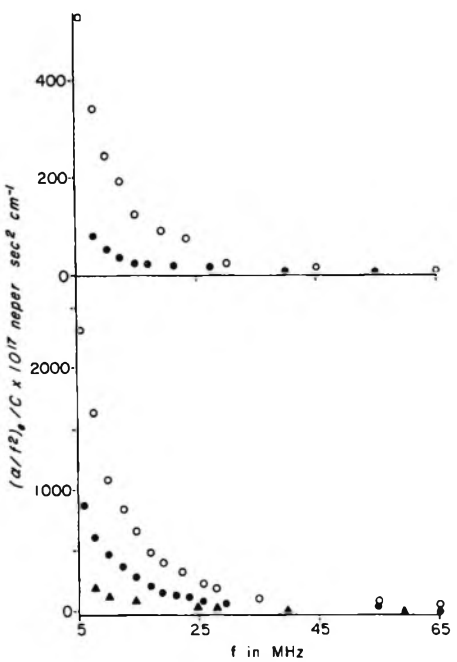

Figure 2. Frequency dependence of the excess acoustic absorption per mole at 25° for para (upper panel) and meta (lower panel) aminobenzoic acids in methanol and water–methanol solutions. Upper panel: ▲, methanol; ○, 0.50 H_2O; lower panel: △, methanol; ●, 0.25 H_2O; ○, 0.417 H_2O.

(4) K. F. Herzfeld and T. A. Litovitz, "Absorption and Dispersion of Ultrasonic Waves," Academic Press, New York, N. Y., 1959.

Table I: Kinetic and Thermodynamic Parameters for *o*-Aminobenzoic Acid

Solvent	T, °C	M_0, mol/l.	$\tau \times 10^8$, sec	$C \times 10^8$, nepersec/cm	$C_0 \times 10^{-5}$, cm/sec	$\bar{V}$,[a] cm³	$\beta \times 10^3$, °K⁻¹	$\bar{C}_p$,[a] cal/(mol °K)	ρ,[a] g/cm³
Methanol	25	0.25	0.76	3.9	1.140	40.7	1.20	19.5	0.787
Methanol	25	0.5	0.69	8.6	1.156	40.7	1.20	19.5	0.787
Methanol	0	0.5	1.8	3.3	1.240	39.5	1.15	19.5	0.810
Acetone	25	1.0	0.77	8.5	1.235	73	1.49	29.9	0.792

[a] See D. E. Gray, "American Institute of Physics Handbook," McGraw-Hill, New York, N. Y., 1951.

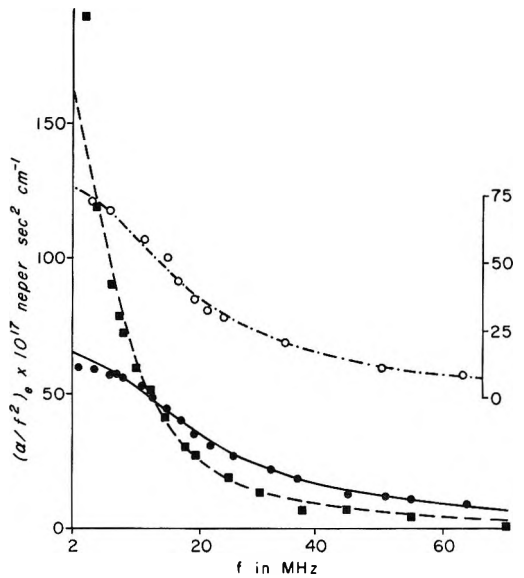

Figure 3. Frequency dependence of the excess acoustic absorption in 0.5 *M* solutions of *o*-aminobenzoic acid in methanol at 25° (solid circles) and 0° (squares). The open circles and right-hand scale give the experimental results for *o*-aminobenzoic acid 1 *M* in acetone at 25°. The continuous curves are generated from eq 11 using the parameters in Table I.

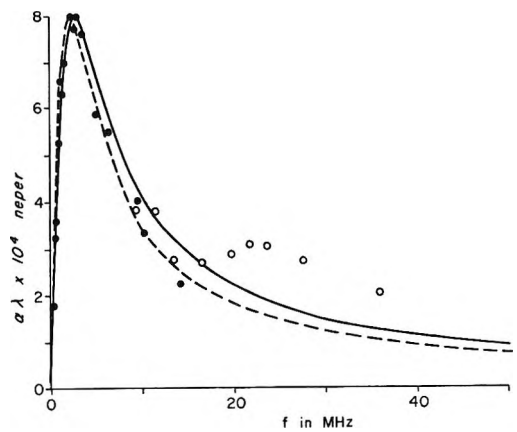

Figure 4. Excess acoustic absorption per wavelength for 0.03 *M* aqueous solutions of *o*-aminobenzoic acid at 25° and pH 3.5 as a function of frequency. Open circles represent the results of this work; solid circles are the results obtained by Eggers.[5] The broken curve is calculated using reactions 2–6 as the basis set with the thermodynamic and kinetic parameters set forth in Tables III and IV. The solid curve includes reactions 2–10 in the basis set.

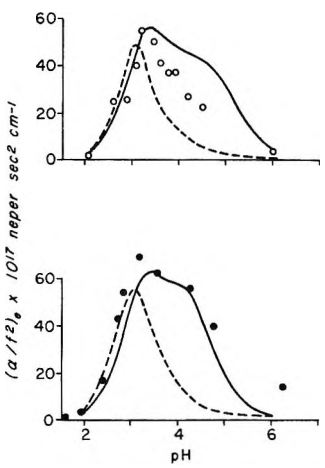

Figure 5. Excess acoustic absorption in 0.02188 *M* aqueous solutions of *m*-aminobenzoic acid (upper panel) and 0.0248 *M* *p*-aminobenzoic acid (lower panel) at 25° and 5.4 MHz as a function of pH.

can determine neither C nor τ with any accuracy. However, the velocity of sound and hence the apparent acoustic losses due to diffraction are relatively independent of pH, and the variation of the absorption with pH at a fixed frequency can be determined far more accurately than the frequency dependence of the absorption. In the case of *o*-aminobenzoic acid Eggers,[5] in an apparatus designed primarily for work at low frequencies, has determined the attenuation in 0.03 *M* aqueous solutions between 0.4 and 16 MHz. His results and the results of this work (9–41 MHz) are displayed in Figure 4. The experimentally determined pH dependence of the absorption at 5.4 MHz in solutions of the meta and para isomers is given in Figure 5, and α/f^2 *vs.* f for *m*- and *p*-aminobenzoic acid is plotted in Figure 6.

D. Results in Methanol–Water. Figures 1 and 2 display the excess acoustic absorption as a function of frequency and solvent composition for *o*-, *m*-, and *p*-aminobenzoic acids. Values of C and τ deduced from a least-squares fit of eq 11 to the data are given in Table II.

(5) F. Eggers, *Acustica*, 19, 323 (1967/68).

Table II: Kinetic and Thermodynamic Parameters for the Aminobenzoic Acids in Methanol–Water Solutions at 25°

Isomer	M_0, mol/l.	Solvent composition	$\tau \times 10^8$, sec	$C \times 10^8$, nepersec/(mol cm)	$C_0 \times 10^{-5}$, cm/sec	ρ,[a] g/cm³	$\bar{V}$,[a] cm³/mol	$\beta \times 10^3$,[a] °K	$\bar{C}_p$,[b] cal/mol
o	0.5	0.125 H_2O–0.875 MeOH	0.9 + slow	20	1.273	0.838	35.5	1.2	19.4
o	0.5	0.25 H_2O–0.75 MeOH	1.4	13	1.350	0.870	31.4	0.99	19.4
o	0.15	0.50 H_2O–0.50 MeOH	3.8	120	1.513	0.929	25.3	0.81	19.8
m	0.125	0.25 H_2O–0.75 MeOH	2.3	17	1.362	0.870	31.4	0.99	19.4
m	0.083	0.417 H_2O–0.583 MeOH	2.6	40	1.478	0.912	27.0	0.94	19.7
p	0.222	0.50 H_2O–0.50 MeOH	2.9	8	1.513	0.929	25.3	0.81	19.8

[a] Landolt-Börnstein, "Zalenwerte und Funktionen 6 Auf," II. 1, 851, Springer-Verlag, New York, N. Y., 1971. [b] J. Timmermans, "Physico Chemical Constants of Binary Systems," Vol. 4, Interscience, New York, N. Y., 1960, p 169.

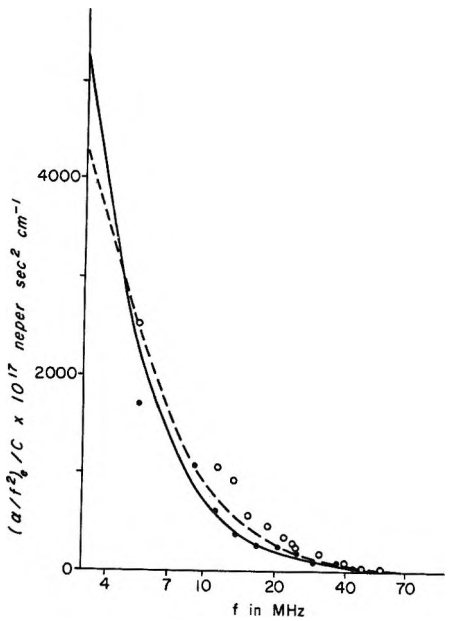

Figure 6. Frequency dependence of the excess acoustic absorption divided by the molar concentration for 0.0248 *M* aqueous *p*-aminobenzoic acid at pH 3.56 (open circles) and 0.02188 *M* *m*-aminobenzoic acid at pH 3.85 (solid circles). The broken curve is calculated for the para isomer from the parameters in Tables III and IV using the complete basis set (eq 2–10). The solid curve represents the result of an equivalent calculation for the meta isomer.

A single Debye relaxation will not give a satisfactory account of the frequency dependence of the excess attenuation in solutions of *o*-aminobenzoic acid in 12.5:87.5 water–methanol. A high-frequency relaxation at 18 MHz (presumably corresponding to the process responsible for the 21 MHz relaxation frequency in pure methanol) and a second relaxation at an ill-defined frequency below the lowest measuring frequency will describe the data within experimental accuracy. As the percentage of water is increased, the lower frequency process becomes more prominent, obscuring the rather weak absorption associated with the high-frequency relaxation. For the meta and para isomers the weak low-frequency absorption process in pure methanol is enhanced and shifted to higher frequencies by the addition of water.

III. Discussion

A. Thermodynamics. From a study of the frequency dependence of α/f^2 it is possible in favorable cases to evaluate C and τ directly. To proceed to the evaluation of individual rate constants and standard volume changes it is necessary to know the equilibrium constants and standard enthalpy changes. Values of ionization constant (K_I) and heat of ionization (ΔH_I) for the isomeric aminobenzoic acids in aqueous solution are known.[6-8] Cohn and Edsall[8a] have discussed the calculation of the equilibrium constants for the reactions represented by eq 1, 2, and 3 from the observed ionization constants of the acids and their esters. Their results for K_z are given in Table III. The equilibrium constant for the ionization reaction as determined directly by titration may be expressed in terms of the equilibrium constants for eq 2 and 3 as[8a] $(1/K_I) = K_2 + K_3$ and the value of ΔH_I obtained from the temperature dependence of K_I is $\Delta H_I = -(\Delta H_2 + \Delta H_3) + K_I(K_2\Delta H_3 + K_3\Delta H_2)$. To estimate ΔH_2 and ΔH_z it is necessary to further assume that the effect of a substituent on the pK_a of a substituted benzoic acid is primarily an effect on the enthalpy of ionization.[8b] With this assumption ΔH_2 can be deduced from K_2 and the heat of ionization of benzoic acid and ΔH_3 calculated from ΔH_I. The heat of formation of the zwitterion from the classical form is then given by $\Delta H_z = \Delta H_3 - \Delta H_2$. Values of ΔH_z so calculated are given in Table III. The ΔH for ionization of the ethyl ester of the acid should be very close to $-\Delta H_4$. The values of K_z and ΔH_z in nonaqueous systems have been estimated with the aid of the expression developed by Scatchard and

(6) R. A. Robinson and A. I. Biggs, *Aust. J. Chem.*, **10**, 128 (1957).

(7) H. C. Saraswat and U. D. Tripathi, *Bull. Chem. Soc. Jap.*, **38**, 1555 (1965).

(8) (a) E. J. Cohn and J. T. Edsall, "Proteins, Amino Acids, and Peptides as Ions and Dipolar Ions," Reinhold, New York, N. Y., 1943, p 97; (b) J. Christensen, D. Wrathall, R. Izatt, and D. Tolman, *J. Phys. Chem.*, **71**, 3001 (1967).

Table III: $\Delta H°$ and $\Delta V°$ of Ionization and Zwitterion Formation for the Aminobenzoic Acids at 25°

Isomer	Solvent	ΔH_1[a]	ΔH_2[a]	ΔH_3[a]	ΔH_z[a]	ΔV_z[b]	ΔV_1[b]	ΔV_3[b]	ΔV_4[b]	pK_1	pK_z	pK_2	pK_3	pK_4
Ortho	Aqueous	6.091	−1.48	−12.8	−11.3	−12.6	9.5	−3.1	9.5	5.125	0.70	−4.92	−4.22	−2.79
Meta	Aqueous	9.665	−0.59	−12.3	−11.7	−11.0	10	−1.0	10	4.90	−0.36	−4.27	−4.63	−3.20
Para	Aqueous	3.938	−1.40	−14.5	−13.1	−11.4	9.4	−2.0	9.4	4.95	0.83	−4.86	−4.03	−3.21
Ortho	Methanol	...	...	...	−10.7	−32.4	...	...	...	...	1.2	...	...	...

[a] Units: kcal/mol. [b] Units: cm³/mol.

Kirkwood[9] for the change in electrostatic energy ($\Delta\Phi$) when a dipolar ion is transferred from water to a medium of dielectric constant D_0.

$$\Delta\Phi = Ne^2\left[\frac{1}{b} - \frac{1}{R}\right]\left[\frac{1}{D_0} - \frac{1}{D_w}\right] \qquad (14)$$

The Scatchard–Kirkwood model of the zwitterion consists of two spheres of radius b with centers separated by a distance R. We have calculated R from the known molecular geometry assuming that the center of charge of the carboxyl group resides halfway between the two oxygens and that the center of charge of the $-NH_3$ group lies in the center of the triangle formed by the three hydrogen atoms. A distance appropriate to an N–H--O hydrogen bond (2.7 Å) was used for b. N is Avogadro's number and e is the electronic charge.

B. Water. The low solubility of the aminobenzoic acids and consequent low absorption in water makes it impracticable to determine the relaxation time as a function of concentration and thus to conclusively distinguish between unimolecular and more complex mechanisms. Thus, the identification of the process or processes which lead to the observed frequency and pH dependence of the acoustic absorption is difficult to accomplish. It is, however, possible to demonstrate that, by using known or assuming plausible values for the constants in eq 2–10 and 11, it is unnecessary to postulate an intramolecular proton-transfer mechanism as a means of rationalizing the observed data.

The reactions 2–5 form a sufficient basis set to describe the deviation from the equilibrium composition of an aminobenzoic acid solution; hence ΔH, ΔV, and K for the remaining reactions may be deduced from the values of these functions for the basis reactions. Reaction 5 is known to have a volume change of 21 cm³/mol.[10] The volume changes for reactions 2–4 are not known. Reactions 2 and 4 correspond to the neutralization of a carboxylic acid which, in general, has a volume change of about 10 cm³/mol.[11] Reaction 3 corresponds to the attachment of a proton to an amine group. The volume changes for the neutralization of protonated amine groups by hydroxide ions are known to range from 22 to 27 cm³/mol.[3] Combining this neutralization reaction with reaction 5 (the ionization of water) gives a volume change for protonation of the amine group of −1 to −6 cm³/mol. The enthalpy changes account for only a small percentage of the acoustic absorption in water where β/C_p is very small and are significant only in organic and mixed solvents. The volume changes and equilibrium constants for reactions 1 and 6–10 may be easily deduced from those of reactions 2–5. Equilibrium constants for reactions 1–4 are given in Table III. The volume changes in Table III give both good agreement with experiment and are consistent with the known ΔV's of analogous reactions.

Eigen and Eyring[2] have measured rate constants for eq 2. Their measurements include contributions from reaction 4, and we have used their rate constants for both reactions 2 and 4. For reactions 3 and 6 we have taken the average values of k_f and k_b for the attachment of a proton to a primary amine group.[1] For reactions 7–10 rates are estimated from the Debye–Smoluchowski equation[12]

$$k_f = 4\pi\sigma N_A Z_A Z_B e_0^2 (G_A + G_B)/ \\ (DkT(\exp(Z_A Z_B e_0^2/Dr_D kT) - 1)) \qquad (15)$$

where N_A is Avogadro's number, Z_A and Z_B the signed valences of species A and B, D the dielectric constant, e_0 the electronic charge, T the temperature in °K, r_D the reaction radius, G_A and G_B the diffusion coefficients of species A and B, k is Boltzmann's constant, and σ the steric factor. The dielectric constant was taken to be 78.5, and the reaction radius was assumed to be the length of a hydrogen bond, about 2.7 Å. These parameters have successfully accounted for the observed rates of the diffusion controlled bimolecular proton-transfer reactions of a number of amino acids and simple peptides.[3] Diffusion coefficients for *o*-, *m*-, and *p*-aminobenzoic acid are 0.840, 0.774, and 0.843 × 10^{-5} mol cm^{-2} sec^{-1},[13] respectively. The steric factor, σ, for reactions 7–10 may be estimated on the basis of simple geometrical considerations. Since each participant in a reaction must have its reactive site oriented toward its partner, the maximum fraction of collisions with the proper orientation will be about one-

(9) G. Scatchard and J. G. Kirkwood, *Phys. Z.*, **33**, 297 (1932).

(10) P. Drude and W. Nernst, *Z. Phys. Chem.* (*Leipzig*), **15**, 79 (1894).

(11) Reference 8, p 158.

(12) P. Debye, *Trans. Electrochem. Soc.*, **82**, 265 (1942); M. V. Smoluchowski, *Z. Phys. Chem.* (*Leipzig*), **92**, 129 (1917).

(13) R. C. Weast, Ed., "Handbook of Chemistry and Physics," The Chemical Rubber Co., Cleveland, Ohio, 1966, p F-43.

fourth. The solid angle in which effective encounters can occur will be reduced even further when substituent groups are near the reactive site. The steric factor for *o*-aminobenzoic acid should suffer the greatest reduction and was assigned values of 0.125 for reactions 8–10 and 0.25 for reaction 7. For the meta and para isomers σ was given its maximum value of 0.25 for reactions 7–10. The resulting forward rate constants for reactions 2–10 are summarized in Table IV.

Table IV: Forward Rate Constants

	$k_f \times 10^{-10}$, l. mol^{-1} sec^{-1}		
Reaction	Ortho	Meta	Para
2	5.8[a]	4.6[a]	3.7[a]
3	1.5[b]	1.5[b]	1.5[b]
4	5.8[a]	4.6[a]	3.7[a]
5	14.0[b]	14.0[b]	14.0[b]
6	1.5[b]	1.5[b]	1.5[b]
7	0.245	0.225	0.245
8	0.0425	0.080	0.085
9	0.0425	0.080	0.085
10	0.0425	0.080	0.085

[a] Reference 2. [b] Reference 1.

The relaxation equations were set up in terms of the degrees of advancement of either reactions 2–6 or reactions 2–10, and the relaxation times and normal modes obtained with the aid of a standard matrix diagonalization program. As there are only four linearly independent reactions (2–5) a number of zero eigenvalues (infinite relaxation times) are found for both the five and nine reaction basis sets. The contributions of these eigenvalues to the acoustic absorption can be shown to be zero. The C_i's were computed from the eigenvectors,[14] proper cognizance being taken of the linear dependencies in the basis set[15] and the absorption calculated according to eq 11. The results of the calculations are shown in Figure 5, where the broken lines represent the absorption due to reactions 2–6 and the solid lines show the results for the more complete basis set, and in Figure 6 where only the values for the larger basis set are given. The agreement between the calculated and experimental curves is quite good, and an essentially quantitative fit may be achieved by *ad hoc* adjustment of the imperfectly known volume changes and steric factors. In particular, it seems likely that reactions 8–10 will proceed at rates significantly lower than the diffusion limit.

From a pH of about 2.75–6 the principal contribution to the excess acoustic absorption arises from the perturbation of the equilibrium between the classical and zwitterionic forms. Expansion of the basis set to include reactions 7–10 causes a reduction in the relaxation times of two of the modes, while having only a small effect on the nature of the normal reactions. Thus, although the important normal reactions are, as suggested by Eggers[5] and Eigen,[1] intramolecular proton transfers, these intramolecular transfers proceed almost exclusively by bimolecular mechanisms even in these rather dilute solutions.

C. Methanol and Acetone. Comparison of the results for 0.25 and 0.5 *M* *o*-aminobenzoic acid in methanol indicate that C is proportional to the concentration and τ, within experimental accuracy, is independent of the concentration as would be expected if the perturbation of the equilibrium represented by eq 1, or any other unimolecular or effectively unimolecular process is the source of the excess absorption.

The fact that the absorption is small for the para isomer and that the relaxation time is significantly slower for the meta than for the ortho isomer would tend to nominate internal ionization rather than solvation or vibrational heat capacity relaxation as the process responsible for acoustic absorption as would the similarity in relaxation times observed in acetone and methanol. There is thus a fair amount of circumstantial evidence for our conclusion that τ represents the relaxation time for the classical zwitterion equilibrium. Accepting this premise the rate constants which appear in eq 1 for *o*-aminobenzoic acid in methanol at 25° are $k_f = 1 \times 10^7$ sec^{-1} and $k_b = 1.4 \times 10^8$ sec^{-1}. The activation energy deduced from the temperature dependence of k_b is about 8 kcal/mol.

There are two possible choices (−22.5 and −32.4 cm^3/mol) of $\Delta V°$ for eq 1 based on positive and negative values of the quantity in square brackets in eq 12. The Drude–Nernst equation which approximately relates the electrostrictive volume change associated with dissolution of an ion of charge q and radius r in a solvent of dielectric constant D to the pressure derivative of the dielectric constant[10] ($\Delta V = -(q^2/2r)\ (dD^{-1}/dP)$) would suggest that the volume change for an internal ionization reaction in methanol ($dD^{-1}/dP = -1.71 \times 10^{-6}$ atm^{-1})[16] should be more than three times greater than the volume change of the same reaction in water ($dD^{-1}/dP = -0.55 \times 10^{-6}$ atm^{-1}). The volume change in water is about −12.6, and thus the higher value of the volume change is in good agreement with that which would be predicted from ΔV in water and the Drude–Nernst equation.

The equilibrium constants for the ionization of simple acids are generally reduced by about two orders of magnitude in passing from aqueous to alcoholic solution.[17] When such reductions in the equilibrium constants are made assuming, for want of more detailed information, that the diffusion coefficients are unchanged, the important normal reactions are a conversion of the clas-

(14) P. R. Schimmel, *J. Chem. Phys.*, **54**, 4136 (1971).

(15) R. D. White, to be published.

(16) B. B. Owen and S. R. Brinkley, *Phys. Rev.*, **64**, 32 (1943).

(17) L. Michaelis and M. Mizutani, *Z. Phys. Chem.* (*Leipzig*), **116**, 135 (1925).

sical into zwitterionic form with a predicted relaxation frequency of about 0.6 MHz and anion + cation = 2 neutral (classical) with a predicted relaxation frequency of about 1.7 MHz. Thus, the weak absorption with a low apparent relaxation frequency which we observe in methanolic solutions of the meta and para isomers is the predicted result in the absence of a direct internal proton-transfer mechanism even in these rather concentrated solutions.

D. Methanol–Water. As the fraction of water in the solvent mixture is increased the larger values of the equilibrium constants imply larger values of Γ and thus increased absorption due to both of the low-frequency modes. As one passes from water to methanol, the solubility of the acids is much increased, and in inspecting the results in Table II it should be noted that the low values of the relaxation time in methanol–water reflect the higher concentrations rather than solvent properties.

IV. Conclusions

Perturbation of the internal charge-transfer equilibrium is the principal contributor to the acoustic relaxation spectrum of aqueous solutions of the isomeric aminobenzoic acids at low pH. However, it is possible to give a satisfactory account of the rate of internal transfer from the known rates of ionization and recombination reactions, and there is no need to adduce a direct unimolecular internal transfer reaction. Volume changes for zwitterion formation and related ionic reactions have been deduced from the acoustic data. In methanol the relaxation frequency (or frequencies) which characterize the acoustic absorption due to the meta and para isomers are too low to be accurately determined. In the case of the ortho isomer in methanol a discrete relaxation at 23 MHz is found at 25°. It is argued that this corresponds to internal proton transfer in a cyclic hydrogen-bonded system.

The Temperature Dependence of the Apparent and Partial Molal Volumes of Concentrated Aqueous Electrolyte Solutions of Tetraalkylammonium Bromides, Cetyltrimethylammonium Bromide, and Ammonium and Lithium Bromides

by Antonio LoSurdo* and Henry E. Wirth

Department of Chemistry, Syracuse University, Syracuse, New York 13210 *(Received July 23, 1971)*

Publication costs assisted by Syracuse University

The apparent molal volume, ϕ_{2t}, and partial molal volume, $\bar{V}_2$, of concentrated (1 *m* to saturation) aqueous solutions of tetraalkylammonium bromides, R_4NBr (R = methyl, ethyl, *n*-propyl, and *n*-butyl), cetyltrimethylammonium bromide, and ammonium and lithium bromides have been determined from density measurements in the temperature range between 5 and 65°. A modified Young's rule for mixtures of electrolytes, $\phi_{obsd} = (\phi_1)_\mu(1 - \beta) + (\phi_2)_\mu\beta/2$, has been used to explain the concentration dependences of ϕ_{2t} and $\bar{V}_2$. The results indicate that there are strong coulombic–hydrophobic cation–cation interactions which may give rise to multiply charged aggregates in quaternary ammonium bromide systems.

Introduction

Current interest in the influence of tetraalkylammonium halides on the structure of water,[1-10] cation–cation pairing,[11-13] and micelle[14-17] formation suggests further experimental studies of these phenomena. For this reason the behavior of concentrated aqueous electrolyte solutions of quaternary ammonium bromides, cetyltrimethylammonium bromide, and ammonium and lithium bromides has been investigated in

(1) W. Y. Wen and S. Saito, *J. Phys. Chem.*, **68**, 2639 (1964); *ibid.*, **69**, 3569 (1965).

(2) B. J. Levien, *Aust. J. Chem.*, **18**, 1161 (1965).

(3) L. B. Hepler, J. M. Stokes, and R. H. Stokes, *Trans. Faraday Soc.*, **61**, 20 (1965).

the temperature range 5–65°. Evidence[18-20] from light scattering, X-rays, and conductivity experiments indicate that there are spherical micelles present at low concentrations (0.05 *m*) of cetyltrimethylammonium bromide solutions. These micelles transform into rod-shaped aggregates at higher concentrations.[19]

Some preliminary results[16,17] suggest that there are strong coulombic–hydrophobic cation–cation interactions which may give rise to multiply charged aggregates in aqueous solutions of tetraalkylammonium bromides. These interactions are greatest for molecules with long hydrophobic chains. In view of this, attention has been given to the possible existence of aggregates in tetraalkylammonium bromide solutions.

Experimental Section

Materials. Tetramethylammonium bromide, tetraethylammonium bromide, tetra-*n*-propylammonium bromide, and tetra-*n*-butylammonium bromide (Eastman) and cetyltrimethylammonium bromide (Pfaltz and Bauer) were recrystallized once from suitable organic liquid mixtures using a modified procedure of Conway, *et al.*,[4] and were dried under vacuum at 70–80° for at least 48 hr. The weight volumetric analyses for bromide using a modified Volhard's method[21] indicated their purities to be better than 99.9%. Ammonium bromide (Fisher purified) was used without further purification. Stock solutions were prepared by dissolving the recrystallized salts in doubly distilled water, and the concentrations were determined by Volhard's method. Solutions of known molality were prepared by weight dilutions of the stock solutions.

Procedure. The densities were determined using the method described elsewhere.[22] The dilatometer was constructed of Vycor by Corning Glass Co. and had an internal volume of approximately 66 ml. Each experimental run used a combination of mercury (about 67 g) and solution. The thermostated bath system[22] was controlled to ±0.005° or better at each of the temperatures used.

The coefficient of thermal expansion of the dilatometer was 2.7×10^{-6} ml/°C as compared with 2.2×10^{-6} found by the authors[22] for a larger Vycor dilatometer, and 2.4×10^{-6} as calculated from the linear coefficient of expansion for Vycor.[23]

Results

The densities of concentrated aqueous solutions (1 *m* to saturation) of $(Me)_4NBr$, $(Et)_4NBr$, $(n\text{-}Pr)_4NBr$, $(n\text{-}Bu)_4NBr$, cetyl-$(Me)_3NBr$, and NH_4Br have been determined[24] at 10° intervals between 5 and 65° and represented by the equation

$$d_t = d_0 + \alpha t + \beta t^2 + \gamma t^3 \qquad (1)$$

The values of d_0, α, β, and γ given in Table II[25] are those evaluated from the experimental data by the method of least squares. The densities obtained from these equations at 5° intervals between 5 and 65° were used to calculate the apparent molal volumes, ϕ_{2t}, of the above electrolytes. The absolute densities are reliable to $\pm 5 \times 10^{-5}$ g/ml.

The apparent molal volumes, ϕ_{2t}, given in Table I,[25] were calculated using the equation

$$\phi_{2t} = \frac{1000 + m_2M}{m_2d_2} - \frac{1000}{m_2d_1} \qquad (2)$$

where M denotes the molecular weight of the solute, d_1 is the density of water, and d_2 is the density of the solution of molal concentration m_2. The values of ϕ_{2t} are reliable to ±0.05 ml/mol and are in excellent agreement with those of Wen and Saito[1] at 25°.

The temperature variation of apparent molal volumes at constant molality computed from eq 2 was represented by

$$(\phi_{2t} - \phi_0) = at + bt^2 + ct^3 \qquad (3)$$

and the variation in apparent molal volume with molality at constant temperature by

$$\phi_m = \phi_0' + a'm^{1/2} + b'm + c'm^{3/2} + d'm^2 \qquad (4)$$

The coefficients of these equations, tabulated in Tables III, IV, and V,[25] were obtained from least-squares and

(4) B. E. Conway, R. E. Verrall, and J. E. Desnoyers, *Trans. Faraday Soc.*, **62**, 2738 (1966).

(5) B. E. Conway and R. E. Verrall, *J. Phys. Chem.*, **70**, 1473 (1966); **70**, 3952 (1966).

(6) R. E. Verrall and B. E. Conway, *ibid.*, **70**, 3961 (1966).

(7) J. Padova and I. Abrahamer, *ibid.*, **71**, 2112 (1967).

(8) J. F. Millero and W. D. Hansen, *ibid.*, **72**, 1758 (1968).

(9) R. Gopal and M. A. Siddiqi, *ibid.*, **72**, 1814 (1968).

(10) H. Ruterjans, F. Schreiner, U. Sage, and Th. Ackermann, *ibid.*, **73**, 986 (1969).

(11) F. Franks and T. H. Smith, *Trans. Faraday Soc.*, **63**, 2586, (1967).

(12) W. Y. Wen and K. Nara, *J. Phys. Chem.*, **71**, 3907 (1967).

(13) T. L. Broadwater and D. F. Evans, *ibid.*, **73**, 164 (1969).

(14) S. Lindenbaum and G. E. Boyd, *ibid.*, **68**, 911 (1964).

(15) H. E. Wirth, *ibid.*, **71**, 2922 (1967).

(16) H. E. Wirth and A. LoSurdo, *ibid.*, **72**, 751 (1968).

(17) A. LoSurdo and H. E. Wirth, *ibid.*, **76**, 130 (1972).

(18) G. S. Hartley, B. Collie, and C. S. Sarnis, *Trans. Faraday Soc.*, **32**, 795 (1936); C. S. Sarnis and G. S. Hartley, *ibid.*, **34**, 1288 (1938).

(19) F. Reiss-Husson and V. Luzzati, *J. Phys. Chem.*, **68**, 3505 (1964).

(20) M. Czerniawski, *Rocz. Chem.*, **40**, 1935 (1966); **41**, 119 (1967).

(21) N. H. Furman, "Standard Methods of Chemical Analysis," Vol. 1, Van Nostrand, Princeton, N. J., 1966, pp 242, 329, 330.

(22) H. E. Wirth and A. LoSurdo, *J. Chem. Eng. Data*, **13**, 226 (1968).

(23) E. L. Wheeler, "Scientific Glass Blowing," Interscience, New York, N. Y., 1958, p 18.

(24) A. LoSurdo, Ph.D. Dissertation, Syracuse University, Syracuse, N. Y., 1970.

(25) Listings of the coefficients for eq 1, 2, 3, and 4 given in Tables I–V will appear immediately following this article in the microfilm edition of this volume of the journal. Single copies may be obtained from the Business Operations Office, Books and Journals Division, American Chemical Society, 1155 Sixteenth Street, N.W., Washington, D. C. 20036 by referring to code number JPC-72-1333. Remit check or money order for $3.00 for photocopy or $2.00 for microfiche.

have been used to calculate the partial molal volumes, $\bar{V}_2$, and partial molal expansibilities, ϕ_E', of the electrolyte solutions.

The partial molal volumes, $\bar{V}_2$, have been evaluated using the relation

$$\bar{V}_2 = \phi_{2t} + \frac{m^{1/2}}{2}\left(\frac{\partial \phi_m}{\partial m^{1/2}}\right) \quad (5)$$

The values of $\bar{V}_2$ are reliable to ±0.8 ml/mol at the highest concentrations. For the lowest concentrations the uncertainty in $\bar{V}_2$, $\epsilon(\bar{V}_2)$, is approximately ±0.1 ml/mol. For the intermediate concentrations $\pm 0.1 < \epsilon(\bar{V}_2) < \pm 0.8$ ml/mol.

The partial molal expansibilities, ϕ_E', were calculated from eq 6 and the results are discussed below.

$$\phi_E' = \frac{\partial \phi_{2t}}{\partial t} = a + 2bt + 3ct^2 \quad (6)$$

Discussion of Results

The concentration dependences of the apparent and partial molal volumes of $(n\text{-Bu})_4$NBr and $(n\text{-Pr})_4$NBr are presented graphically for various temperatures in Figures 1 and 2. At low concentrations negative derivations from the Debye–Hückel limiting law (DHLL) are observed at all temperatures for cetyltrimethylammonium bromide and tetraalkylammonium bromide solutions. In contrast to the plots for simple salts, *e.g.*, NH_4Br and LiBr,[26] plots of ϕ_{2t} and $\bar{V}_2$ *vs.* $m^{1/2}$ for $(n\text{-Bu})_4$NBr, $(n\text{-Pr})_4$NBr, and cetyl-$(Me)_3$NBr show minima which become more pronounced as the temperature is lowered. The observation of similar minima for $(Me)_4$NBr and $(Et)_4$NBr is prevented by the onset of saturation.

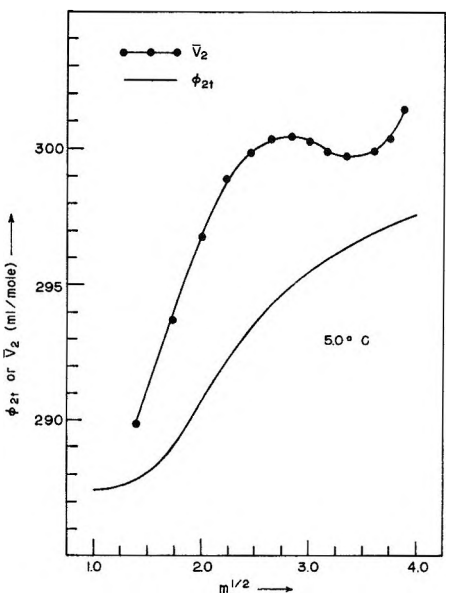

Figure 1. Experimental values for the apparent ϕ_{2t}, and partial, $\bar{V}_2$, molal volumes *vs.* the square root of the molality for $(n\text{-Bu})_4$NBr at 5°. Values of ϕ_{2t} and $\bar{V}_2$ are in milliliters per mole.

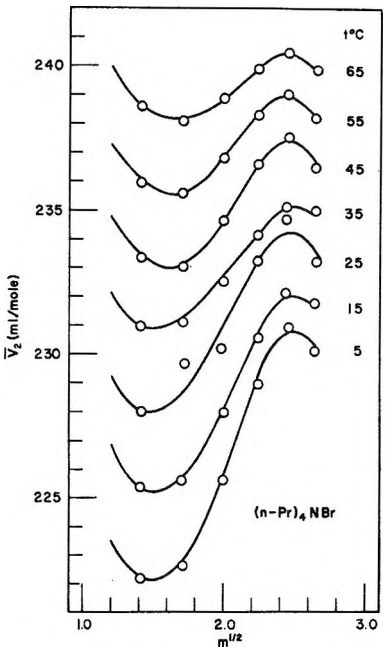

Figure 2. Experimental values for the partial molal volumes, $\bar{V}_2$, *vs.* the square root of the molality for $(n\text{-Pr})_4$NBr at the specified temperatures in degrees centigrade. Values of $\bar{V}_2$ are in milliliters per mole.

Deviations from the Debye–Hückel limiting law have been generally rationalized in terms of water structure promoting influence of the hydrophobic groups of the cations,[1] cation–cation pairing,[11–13] and micelle[15,16] formation. It has been further suggested[13] that the increasing concentration of the larger R_4N^+ ions eventually leads to cooperative networks in which the cations are compelled to share "water clusters" similar to the crystalline clathrate–hydrate "cages" studied by Jeffrey and coworkers.[27] The sharing of these water cages would force cations closer together with coulombic repulsions being reduced, presumably, by the participation of some anions[28] in the structure. Increasing concentrations would break the open hydrogen-bonded water structure, thus qualitatively attributing the decrease in ϕ_{2t} and $\bar{V}_2$ to cation association.

Equilibria in Aqueous Solutions of Tetraalkylammonium Bromides. Recent nmr data show evidence for cation–cation association[29] and multiply charged aggregates[17] in aqueous solutions of tetraalkylammonium halides. If one assumes an equilibrium between simple cations and cation dimers (or multiply charged ag-

(26) For LiBr the apparent and partial molal volumes were calculated from the density data obtained from C. J. West, Ed., "International Critical Tables," McGraw-Hill, New York, N. Y., 1933.

(27) D. Feil and G. A. Jeffrey, *J. Chem. Phys.*, **35**, 1863 (1961); M. Bonamico, R. K. McMullan, and G. A. Jeffrey, *ibid.*, **37**, 2219 (1962); R. K. McMullan, B. Bonamico, and G. A. Jeffrey, *ibid.*, **39**, 3295 (1963).

(28) R. H. Diamond, *J. Phys. Chem.*, **67**, 2513 (1963).

(29) H. G. Hertz, B. Lindman, and V. Siepe, *Ber. Bunsenges. Phys. Chem.*, **73**, 542 (1969).

gregates) in which the formation of the dimer (or these aggregates) is accompanied by a decrease in volume, then the general shape of the ϕ_{2t} *vs.* $m^{1/2}$ curves can be explained for the quaternary ammonium halides.

Using $(n\text{-Bu})_4\text{NBr}$ as an example, it is suggested that n $(n\text{-Bu})_4\text{N}^+$ cations may undergo coulombic–hydrophobic interactions to form aggregated species arranged in a three-dimensional quasicrystalline lattice. To reduce the repulsive coulombic interactions between the cations, hydrated Br^- ions may be trapped within the aggregates or on their surface.[17] Hydrophobic interactions from the overlapping nonpolar side chains of $(n\text{-Bu})_4\text{N}^+$ ions hold the aggregate together.[30] In general, an aggregate may have $(n - m)$ Br^- ions $(n \geq m)$ and, therefore, $(n - m)$ positive charges. The values of n and m vary with salt concentration, the greatest values being probably at the critical aggregate concentration (cac), *i.e.*, the concentration corresponding to a break in the curves of moles of benzene *vs.* molality,[16] and the minima in the ϕ_{2t} *vs.* $m^{1/2}$ curves.

The proposed model is difficult to treat quantitatively due to lack of data. However, as an illustrative example, suppose the equilibrium

$$2(n\text{-Bu})_4\text{N}^+ \rightleftarrows (n\text{-Bu}_4\text{N})_2^{2+} \qquad (7)$$

exists in aqueous solutions of tetra-*n*-butylammonium bromide.[31] The equilibrium constant, K, for this reaction is given by

$$K = \frac{m_2\gamma_2}{m_1^2\gamma_1^2} = \frac{\beta\gamma_2}{2m(1 - \beta)^2\gamma_1^2} \qquad (8)$$

Here γ_1 and γ_2 represent the mean ionic activity coefficients of the monomer $(n\text{-Bu})_4\text{N}^+$ and dimer $(n\text{-Bu}_4\text{N})_2^{2+}$ respectively, β is the degree of association, and $m_1 = m\,(1 - \beta)$ and $m_2 = m(\beta/2)$ are the molalities of the ionic species 1 and 2 in a solution of total molality m.

If Young's rule[32] is applied to this system (reaction 7), it becomes

$$\phi_{\text{obsd}} = \frac{(\phi_1)_\mu m_1 + (\phi_2)_\mu m_2}{m_1 + m_2} = (\phi_1)_\mu(1 - \beta) + (\phi_2)_\mu(\beta/2) \qquad (9)$$

where ϕ_{obsd} is the experimental apparent molal volume of $(n\text{-Bu})_4\text{NBr}$ solution, and $(\phi_1)_\mu$ and $(\phi_2)_\mu$ are the respective apparent molal volumes of the monomer and dimer in solutions containing only water and these electrolytes at an ionic strength $\mu = m_1 + 3m_2$. It is assumed that

$$(\phi_1)_\mu = \phi_1^\circ + 1.86\mu^{1/2} \qquad (10)$$

and

$$(\phi_2)_\mu = \phi_2^\circ + 5.58\mu^{1/2} \qquad (11)$$

where the ionic strength μ is given by

$$\mu = m\left(1 + \frac{\beta}{2}\right) \qquad (12)$$

and ϕ_1° and ϕ_2° are the limiting apparent molal volumes of $(n\text{-Bu})_4\text{NBr}$ and $(n\text{-Bu}_4\text{N})_2\text{Br}_2$ at $m = 0$, respectively.

As a crude approximation K, γ_1, and γ_2 are assigned values of unity.[33] Then β can be calculated from eq 8. Using $\phi_1^\circ = 302.9$[1] and $\phi_2^\circ = 577.9$ ml/mol[13,34] at 25° the apparent molal volumes, ϕ_{obsd}, of $(n\text{-Bu})_4\text{NBr}$ were calculated (Figure 3) for several concentrations of m using eq 9 through 12, and the results were contrasted with the experimental curves of Wen and Saito[1] and this investigation. The calculated points reproduce the general behavior of the experimental curves (Figure 3).

Similarities in behavior are observed between the other quaternary ammonium bromides and $(n\text{-Bu})_4\text{NBr}$. Conceivably, the formation of highly charged species, if they exist, is dependent on the nature of the alkyl groups and electrolyte concentration. Increasing the salt concentration would increase the size and number of aggregated species through a critical concentration beyond which additional salt increases the concentration of the higher charged species. Increasing the temperature would disrupt the aggregates,

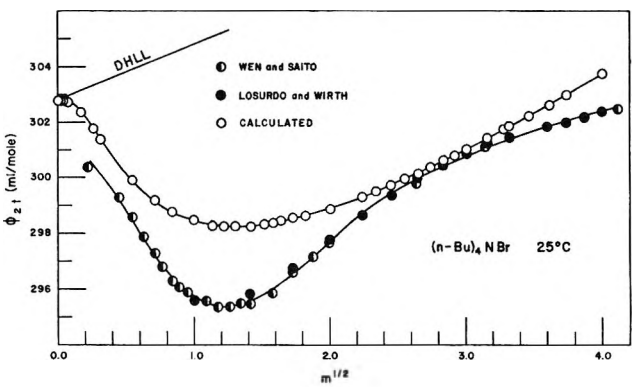

Figure 3. Contrast between calculated and experimental apparent molal volumes, ϕ_{2t}, *vs.* $m^{1/2}$ for $(n\text{-Bu})_4\text{NBr}$ at 25°. The calculated ϕ_{2t} were computed from $\phi_{\text{obsd}} = \phi_{2t} = (\phi_1)_\mu(1 - \beta) + (\phi_2)_\mu(\beta/2)$.

(30) W. Kauzman, *Advan. Protein Chem.*, **14**, 1 (1959).

(31) The argument presented here is similar to that proposed by Wirth.[16] The new method postulates an equilibrium between multiply charged species.[17] Wirth's method[16] proposed an equilibrium between uncharged monomers, dimers, trimers, etc.

(32) T. F. Young and M. B. Smith, *J. Phys. Chem.*, **58**, 716 (1954).

(33) In principle γ_1 and γ_2 could be obtained from the modified Debye–Hückel relation

$$-\log \gamma_i = \frac{Am_i^{1/2}}{1 + B\mathring{a}m_i^{1/2}} + Cm_i$$

through an iterative procedure.

(34) Broadwater and Evans[13] have published data on the apparent molal volume of $(n\text{-Bu})_3\text{N}(\text{CH}_2)_8\text{N}(n\text{-Bu})_3\text{Br}_2$ to serve as a model for the $(n\text{-Bu})_4\text{N}^+$ cation–cation pair. This octane-1,8-bis(tri-*n*-butylammonium)dibromide has the attributes of a 2:1 electrolyte and its extrapolated value of ϕ° may serve as the limiting value of ϕ_2° at $m = 0$ since the dimer proposed by eq 7, if it exists, is expected to have a ϕ_2° less than twice the value of ϕ_1° for $(n\text{-Bu})_4\text{NBu}$.

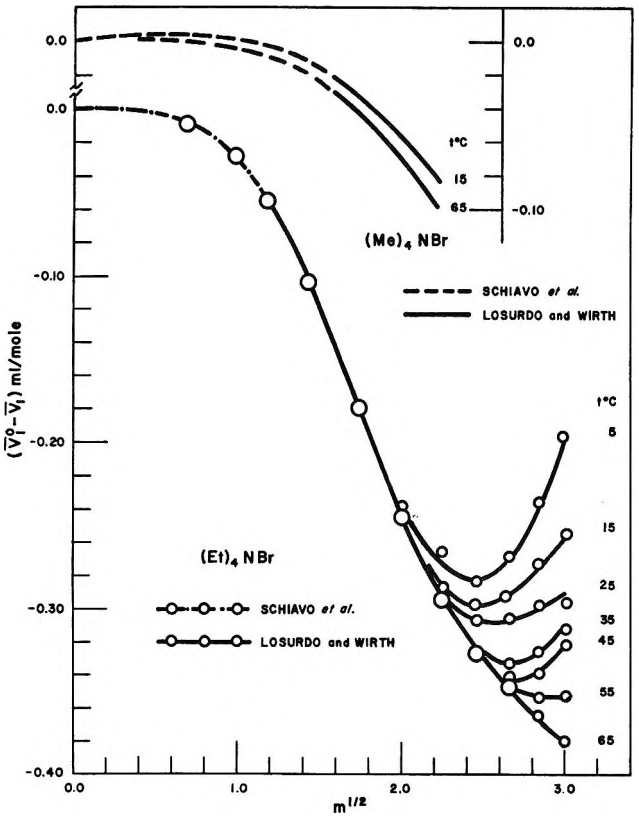

Figure 4. Partial molal volumes of water ($\bar{V}_1^0 - \bar{V}_1$) *vs.* the square root of the molality for $(Me)_4NBr$ and $(Et)_4NBr$ calculated from eq 13 on the assumption that these salts are completely ionized. Values of ($\bar{V}_1^0 - \bar{V}_1$) are in milliliters per mole.

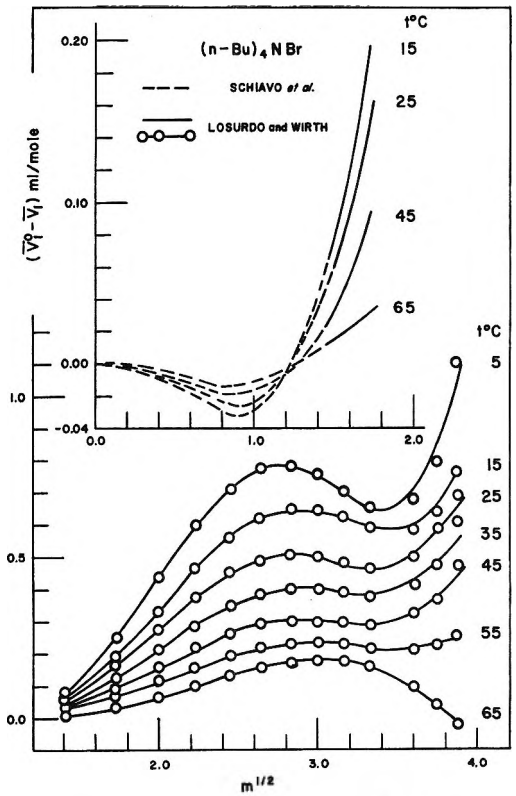

Figure 5. Partial molal volumes of water ($\bar{V}_1^0 - \bar{V}_1$) *vs.* the square root of the molality for $(n\text{-}Bu)_4NBr$ calculated from eq 13 on the assumption that this salt is completely ionized. Values of ($\bar{V}_1^0 - \bar{V}_1$) are in milliliters per mole.

thus decreasing their concentration. This viewpoint is in agreement with observations and is consistent with the solubility,[16] nmr,[17,29] and conductivity and viscosity[35] data.

Plots of ϕ_{2t} *vs.* $m^{1/2}$ for R_4NBr show a minimum which is a function of R. As expected, the observed relative shift of the minimum increases as cetyl-$(Me)_3NBr$ (0.7 *m*) < $(n\text{-}Bu)_4NBr$ (1.2 *m*) < $(n\text{-}Pr)_4NBr$ (4.0 *m*) < $(Et)_4NBr$ (above 5 *m*) < $(Me)_4NBr$ (above saturation).

In contrast, both NH_4Br and LiBr show a gradual increase in ϕ_{2t} with concentration at all temperatures. This is expected since these salts are probably completely dissociated electrolytes.

The apparent molal expansibilities of R_4NBr and NH_4Br were calculated from eq 6. Plots of ϕ_E' *vs.* $m^{1/2}$ are mirror images of the ϕ_{2t} *vs.* $m^{1/2}$ graphs. The curves for $(n\text{-}Bu)_4NBr$, $(n\text{-}Pr)_4NBr$, and $(Et)_4NBr$ are positive, go through a maximum, and then decrease. The maximum occurs at concentrations where the ϕ_{2t} data pass through a minimum. Tetramethylammonium bromide decreases to a minimum.

"Water Structure" Inferences from Apparent Molal Volumes of Solute and Partial Molal Volumes of Solvent. If the solutions of tetraalkylammonium bromides are considered to be completely ionized, it can be shown[15,24] that the partial molal volume of water, $\bar{V}_1$, in these solutions is given by

$$\bar{V}_1 = \bar{V}_1^0 + \frac{m(\phi_2 - \bar{V}_2)}{55.51} = \bar{V}_1^0 - \frac{m^{3/2}}{111.02}\left(\frac{\partial\phi_2}{\partial m^{1/2}}\right) \quad (13)$$

where $\bar{V}_1^0$ is the molar volume of pure water, *m* is the molal concentration, and ϕ_2 and $\bar{V}_2$ are the apparent and partial molal volumes of the solute. Since for most "normal" electrolytes $\bar{V}_2 > \phi_2$ (the slope $\partial\phi_2/\partial m^{1/2}$ is positive), $\bar{V}_1 < \bar{V}_1^0$. This decrease in volume could be attributed to water structure breaking by the electrolyte.[15,24] With the quaternary ammonium halides usually[1,11,13,15] $\bar{V}_2 < \phi_2$ (the slope $\partial\phi_2/\partial m^{1/2}$ is negative); hence $\bar{V}_1 > \bar{V}_1^0$ and water structure making[1,15,24] is implied. Values of $\bar{V}_1$ in $(Me)_4NBr$, $(Et)_4NBr$, and $(n\text{-}Bu)_4NBr$ solutions were calculated (Figures 4 and 5) from eq 13. The results are in excellent agreement with those of Schiavo and coworkers.[36]

If, however, the solutions of tetraalkylammonium bromides contain other species, as postulated here, then

(35) A. LoSurdo and H. E. Wirth, to be published.

(36) S. Schiavo, B. Scrosati, and A. Tommasini, *Ric. Sci.*, **37**, 211 (1967).

$$\bar{V}_1 = \bar{V}_1^0 + \frac{\sum_{i=1}^{n} m_i(\phi_i - \bar{v}_i)_\mu}{55.51} \quad (14)$$

For an equilibrium between simple cations and cation dimers (reaction 7), eq 14 reduces to

$$\bar{V}_1 = \bar{V}_1^0 + \frac{m_T}{55.51}\left[(1-\beta) \times (\phi_1 - \bar{v}_1)_\mu + \frac{\beta}{2}(\phi_2 - \bar{v}_2)_\mu\right] \quad (15)$$

where ϕ_1 and $\bar{v}_1$ and ϕ_2 and $\bar{v}_2$ are the respective apparent and partial molal volumes of the monomer and dimer in solutions containing only water and these electrolytes at an ionic strength $\mu = m_1 + 3m_2$; β is the degree of association.

From this viewpoint, the effects of R_4NBr on the partial molal volume of water, $\bar{V}_1$, would be that of a mixture of "normal" electrolytes and increased water structuring would not occur.[15]

In summary, the results presented here suggest that the structure of concentrated aqueous solutions of tetraalkylammonium bromides is different from that of dilute solutions and that of normal electrolytes. This structure difference can be described as due to coulombic–hydrophobic cation–cation interactions leading to multiply charged aggregates arranged in a quasi-crystalline lattice.

Acknowledgment. This work was supported by the Office of Saline Water, Grant No. 14-01-0001-623.

Volumetric Properties of Aqueous Solutions of Organic Compounds.

I. Cyclic Ethers and Cyclic Amines

by S. Cabani,* G. Conti, and L. Lepori

Istituto di Chimica Fisica, Università di Pisa, Pisa, Italy *(Received October 12, 1971)*

Publication costs assisted by Consiglio Nazionale delle Ricerche

Measurements of apparent molal volumes Φ_v in water of some cyclic monoethers, diethers, and amines have been carried out at 25° with a differential buoyancy balance at concentrations varying from 0.02 to 0.4 *M*. The values of Φ_v of monoethers and amines decrease linearly with increasing concentration at a rate which increases with growing size of the hydrocarbon part of the molecule. On the contrary, Φ_v values of diethers are found to be independent of concentration. The volume and entropy changes associated with the transfer from the pure liquid state to aqueous dilute solution are compared. The observed phenomenology is justified in terms of local changes of solvent structure around the solute molecules.

Introduction

In recent papers,[1,2] data for free energy, enthalpy, and entropy changes associated with the transfer of cyclic ethers and cyclic amines from the liquid or the gas state to dilute aqueous solution were reported. In this paper the volumetric properties of the aqueous solutions of these classes of compounds at 25° will be considered.

Measurements of partial molal volumes $\bar{V}_2$ in aqueous solutions of some of the ethers examined here were previously made by Franks, *et al.*[3] Laliberté and Conway[4] reported values of partial molal volumes for piperidine and 1-methylpiperidine in 0.1 *N* KOH at 25°. The excess partial molar volume $\bar{V}^E$ of pyrrolidine at 26.5° and in the 0.01–0.02 mole fraction range was reported by Brower, *et al.*[5]

The interest for the volumetric behavior of aqueous solutions as a useful tool for elucidating local changes of solvent structure brought about by neutral or charged solute molecules has already been illustrated (see, *e.g.*, ref 6–11).

(1) S. Cabani, G. Conti, and L. Lepori, *Trans. Faraday Soc.*, **67**, 1933 (1971).

(2) S. Cabani, G. Conti, and L. Lepori, *ibid.*, **67**, 1943 (1971).

(3) F. Franks, M. A. Quickenden, D. S. Reid, and B. Watson, *ibid.*, **66**, 582 (1970).

(4) L. H. Laliberté and B. E. Conway, *J. Phys. Chem.*, **74**, 4116 (1970).

(5) K. R. Brower, J. Peslak, and J. Elrod, *ibid.*, **73**, 207 (1969).

(6) F. Franks and D. J. G. Ives, *Quart. Rev., Chem. Soc.*, **20**, 1 (1966).

(7) M. E. Friedman and H. A. Sheraga, *J. Phys. Chem.*, **69**, 3795 (1965).

Experimental Section

Materials. The examined ethers (tetrahydrofuran (THF), tetrahydropyran (THP), 2-methyltetrahydrofuran (2-MeTHF), 2,5-dimethyltetrahydrofuran (2,5-Me_2THF), 1,3-dioxolane and 1,4-dioxane) and amines (aziridine, pyrrolidine, piperidine, hexamethylenimine, heptamethylenimine, 1-methylpyrrolidine, and 1-methylpiperidine) were commercial products; azetidine was prepared in our laboratory following Wadsworth's method.[12] All the products were rectified on metallic sodium and their purity was controlled by glc analysis. Water used in all the experiments was deionized and further distilled from an alkaline potassium permanganate solution.

Apparatus. Solution densities were measured with a hydrostatic differential balance similar to that described by Conway.[13] Floats having a volume of about 180 ml were used. An automatic electronic device employing two phototransistors as transducers and a solenoid acting on a small permanent magnet maintained the balance practically always in its equilibrium position. Wetting of the tungsten wires (0.05-mm diameter) holding the floats was thus avoided. The buoyancy value was read out as a voltage signal on a digital voltmeter and subsequently checked by switching off the magnetic device and equilibrating the balance with known weights. Temperature oscillations inside the test vessel, checked with a Hewlett-Packard digital quartz thermometer, were within ±0.001°. No significant temperature differences were found across the thermostat.

Density values were reproducible to the sixth decimal place, and the absolute accuracy of the measurements was determined with test runs on KCl aqueous solutions at 25° in the concentration range 0.01–0.5 *M*. By means of a weighted rigorous least-squares adjustment,[14] the data obtained were fitted to the equation

$$\Phi_v - 1.868\sqrt{c} = \Phi_v^0 + hc \qquad (1)$$

Values of $\Phi_v^0 = 26.81 \pm 0.01$ ml mol^{-1} and $h = 0.05 \pm 0.04$ ml l. mol^{-2}, in close agreement with other authors' data,[15-18] were found.

Measurements. The solutions to be studied were made up by adding, with a syringe, weighed amounts of the pure compound to the test vessel containing a known amount of water. Up to seven successive additions were generally made. No systematic error was apparently made with such a procedure. The solutions of heptamethylenimine, which is slightly soluble, were separately prepared and subsequently added to the cylinder. In the case of aziridine and azetidine, only two successive additions were made owing to the relatively low stability of these compounds in water solution. Piperidine was also investigated in 0.1 *N* KOH.

The apparent molal volumes Φ_v at the molar concentration c of a solute with molecular weight M were calculated by

$$\Phi_v = \frac{M}{d^0} + \frac{1000\Delta P}{cG_W} \qquad (2)$$

where d^0 is water density at 25° ($d^0 = 0.9970482$ g/cm^3), ΔP is the buoyancy value expressed as a mass difference, and G_W is the water mass displaced by the test float.

The Φ_v values of the ethers, in the concentration range considered, were best described in terms of the equation

$$\Phi_v = \Phi_v^0 + hc \qquad (3)$$

In the case of the amines (B) fictitious values of the apparent molal volumes Φ_v^{obsd} were first calculated by introducing in eq 2 the molecular weight of the hypothetical species $B \cdot H_2O$. A correction for hydrolysis was then applied in the hypothesis that Φ_v^{obsd} can be expressed as a sum of the contributions of the apparent molal volumes $\Phi_{B\cdot H_2O}$ and $\Phi_{BH^+OH^-}$ of the hypothetical neutral species $B \cdot H_2O$ and of an electrolyte of the type BH^+OH^-. This correction was performed through the equation

$$\frac{\Phi^*}{(1-\alpha)} = \Phi^0_{B\cdot H_2O} + (1-\alpha)c_B{}^0 h + \frac{\alpha^2 c_B{}^0}{(1-\alpha)}h^+ \qquad (4)$$

obtained assuming for $\Phi_{B\cdot H_2O}$ and $\Phi_{BH^+OH^-}$ (the latter corrected for the Debye term) a linear dependence on concentration with slope h and h^+, respectively. The Φ^* function is calculated as

$$\Phi^* = \Phi_v^{obsd} - \alpha 1.868\sqrt{\alpha c_B{}^0} - \alpha\Phi^0_{BH^+OH^-} \qquad (5)$$

once the degree of hydrolysis α and the limiting molal volume of the BH^+OH^- species are known.

The α values at the actual ionic strength were calculated by an iterative procedure using the known values of the thermodynamic hydrolysis constant $K_h{}^T$ and molal activity coefficient values given by the Debye–Hückel limiting law. The term $\Phi^0_{BH^+OH^-}$ was calculated employing the values $\Phi^0_{Na^+Cl^-} = 16.61$ ml mol^{-1} and $\Phi^0_{Na^+OH^-} = -4.60$ ml mol^{-1} taken from

(8) F. Franks and H. T. Smith, *Trans. Faraday Soc.*, **64**, 2962 (1968).
(9) F. Franks and H. T. Smith, *ibid.*, **63**, 2586 (1967).
(10) W. Y. Wen and S. Saito, *J. Phys. Chem.*, **68**, 2639 (1964).
(11) B. E. Conway, *Annu. Rev. Phys. Chem.*, **17**, 481 (1966).
(12) J. H. Wadsworth, *J. Org. Chem.*, **32**, 1184 (1967).
(13) B. E. Conway, R. E. Verrall, and J. E. Desnoyers, *Trans. Faraday Soc.*, **62**, 2738 (1966).
(14) W. E. Wentworth, *J. Chem. Educ.*, **42**, 96 (1965); **42**, 162 (1965).
(15) O. Redlich and D. M. Meyer, *Chem. Rev.*, **64**, 221 (1964).
(16) F. H. Spedding, M. J. Pikal, and D. O. Ayers, *J. Phys. Chem.*, **70**, 2440 (1966).
(17) F. Vaslow, *ibid.*, **70**, 2286 (1966).
(18) L. I. Dunn, *Trans. Faraday Soc.*, **64**, 1898 (1968).

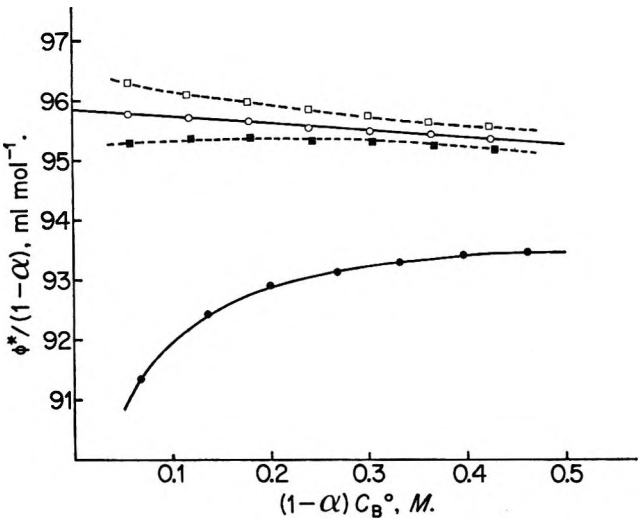

Figure 1. Apparent molal volumes of pyrrolidine in aqueous solution at 25°: (●) data uncorrected for hydrolysis ($\alpha = 0$); data corrected for hydrolysis (○) $pK_h^T = 2.695$, (□) $pK_h^T = 2.6$, (■) $pK_h^T = 2.8$.

Redlich and Meyer[15] and Bodanszky and Kauzmann,[19] respectively, while the values of $\Phi^0_{BH^+Cl^-}$ were experimentally determined (refer to the following paper[20]). For each of the amines here considered and for each c_B^0 value, the term $\alpha^2 c_B^0/(1 - \alpha)$ was nearly constant. Equation 4, therefore, practically reduces to a straight line with slope h and intercept

$$N = \Phi^0_{B\cdot H_2O} + K_h^T h^+ \qquad (6)$$

On the other hand, the values of the thermodynamic hydrolysis constant range from 10^{-6} to 2×10^{-3}, and the values of h^+ for uniunivalent electrolytes are generally lower than 1; the term $K_h^T h^+$ is, consequently, at the worst, of the order of magnitude of the experimental errors. The limiting partial molal volume of the free amine ($\bar{V}_B^0$) is thus calculated with a very good approximation by subtracting from N the molar volume of water ($V_W = 18.069$ ml mol^{-1} at 25°).

As an example, Figure 1 shows the function $\Phi^*/(1 - \alpha)$ *vs.* $(1 - \alpha)c_B^0$ for pyrrolidine, either uncorrected for hydrolysis or corrected using three different values for the K_h^T constant. Large deviations from linearity are observed, with differences of 0.1 unit of pK_h^T, when the amine concentration is lower than 0.2 M.

Results and Discussion

The Φ_v^0 and h parameters for the ethers and the amines considered here are summarized in Tables I and II, respectively. In these tables are also reported values of the molar volumes V_2 at 25° for the pure substances, as evaluated from density data reported in the literature, and values of the excess molar volume at infinite dilution $\bar{V}^{0E}$ calculated as $\bar{V}^{0E} = \bar{V}_2^0 - V_2$, with $\bar{V}_2^0 = \Phi_v^0$.

Our results for $\bar{V}_2^0$ for THF, THP, and 1,4-dioxane are in good agreement with Franks' data. Good agreement with the Franks data is also observed in the trend of the functions $\Phi_v = f(c)$ except for THP.[21] A remarkably high absolute value of h for this compound, in the 0.01–0.05 concentration range, is in fact evident from the plot reported by Franks.[3] The analogous concentration dependence of THF apparent molal volume in the same concentration range has been, on the other hand, ignored by the author. As far as piperidine and 1-methylpiperidine are concerned, the slight differences between $\bar{V}_2^0$ values (in water) found by us and those of Laliberté and Conway[4] (in 0.1 N KOH) can probably be ascribed to effects of the medium.

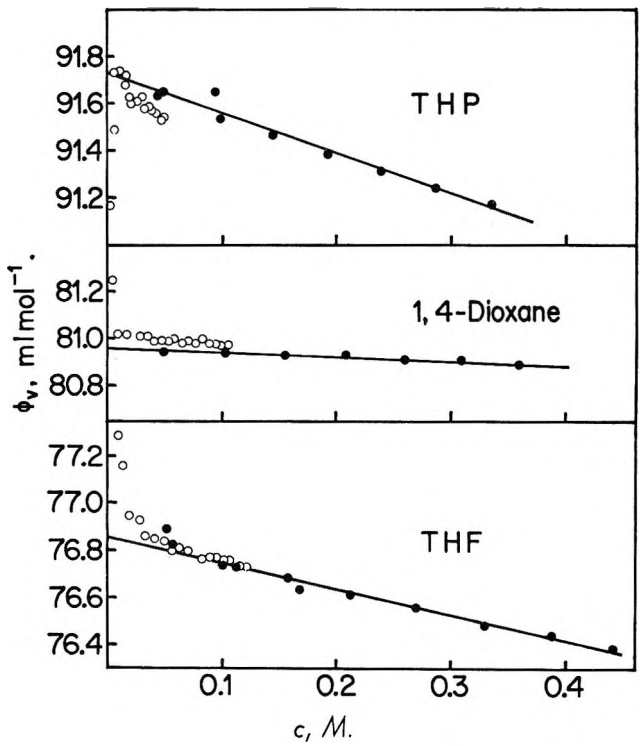

Figure 2. Apparent molal volumes against molar concentration of some cyclic ethers in water at 25°: (●) our data, (○) data deduced from Franks' $\bar{V}_2$ values[3] (see ref 21).

Examination of Tables I and II shows the following. (i) For monofunctional compounds, the transfer from the liquid to aqueous dilute solution produces a strong volume decrease $\bar{V}^{0E}$, while the slope $h/\bar{V}_2^0 = (1/\bar{V}_2^0)$·

(19) A. Bodanszky and W. Kauzmann, *J. Phys. Chem.*, **66**, 177 (1962).

(20) S. Cabani, G. Conti, L. Lepori, and G. Leva, *ibid.*, **76**, 1343 (1972).

(21) Franks did not report actual Φ_v values. These were deduced by us by subtracting from the molar volume of the pure substance the $\bar{V}^E$ values reported in Figure 2 of ref 3. Molalities were converted to molarities, and the function $\bar{V}_2 = \bar{V}_2^0 + 2hc$ was analyzed in order to calculate its slope $2h$. The values of $\bar{V}_2$ were then converted to Φ_v by the relation $\Phi_v = \bar{V}_2 - hc$. In the case of THF, $\bar{V}^{0E}$ was taken equal to 4.85 ml mol^{-1}, as deduced from Figure 2 of ref 3, instead of 4.63 ml mol^{-1} as reported in Table 2 of the same reference. By adding the $\bar{V}^{0E}$ datum to the limiting molal volume ($\bar{V}_2^0 = 76.9$ ml mol^{-1}) a value of 81.75 ml mol^{-1} is obtained for the molar volume (V_2) of THF at 25°, in close agreement with the value interpolated from the data of Cini and Taddei ($V_2 = 81.72$ ml mol^{-1}): R. Cini and G. Taddei, *Nuovo Cimento B*, **63**, 354 (1966).

Table I: Apparent Molal Volume ($\Phi_v = \bar{V}_2^0 + hc$) and Excess Volumes ($\bar{V}^{0E}$) of Cyclic Ethers in Water at 25°

Ether	No. of expt	Concn range, M	$\bar{V}_2^0$, ml mol^{-1}	h, ml l. mol^{-2}	$(h/\bar{V}_2^0) \times 10^2$, M^{-1}	$\bar{V}_2$, ml mol^{-1}	$\bar{V}^{0E}$, ml mol^{-1}	Ref
THF	11	0.05–0.44	76.85 ± 0.01	−1.08 ± 0.03	−1.4	81.72	−4.9	This work
	17	0.005–0.13	76.9				−4.7	3
							−2.9[a]	5
THP	9	0.05–0.34	91.73 ± 0.01	−1.70 ± 0.05	−1.9	98.20	−6.5	This work
	16	0.005–0.05	91.8			98.20	−6.5	3
2-MeTHF	7	0.04–0.27	94.00 ± 0.02	−1.74 ± 0.09	−1.9	101.4	−7.4	This work
2,5-Me$_2$THF	7	0.02–0.17	111.00 ± 0.03	−4.57 ± 0.22	−4.1	120.5	−9.5	This work
THF-2-carbinol	18	0.005–0.1	93.8			97.4	−3.6	3
THP-2-carbinol	17	0.005–0.05	108.1			113.48	−5.4	3
1,3-Dioxolane	7	0.06–0.43	65.37 ± 0.02	+0.17 ± 0.06	+0.3	70.32	−5.0	This work
1,4-Dioxane	7	0.05–0.36	80.96 ± 0.02	−0.17 ± 0.07	−0.2	85.75	−4.8	This work
	17	0.005–0.1	81.1			85.75	−4.7	3
							−5.0[a]	5

[a] Temperature 26.5°.

Table II: Volumetric Properties of Cyclic Amines in Water at 25°

Amine	No. of expt	c_B^0, M	$\bar{V}_2^0$,[a] ml mol^{-1}	h, ml l. mol^{-2}	$h/\bar{V}_2^0 \times 10^2$, M^{-1}	V_2, ml mol^{-1}	$\bar{V}^{0E}$, ml mol^{-1}	Ref
Aziridine	11	0.08–0.55	48.87 ± 0.02	−0.38 ± 0.08	−0.8	52.1	−3.2	This work
Azetidine	17	0.01–0.24	63.71 ± 0.01	−0.85 ± 0.08	−1.3	68.2	−4.5	This work
Pyrrolidine	7	0.05–0.45	77.77 ± 0.01	−1.20 ± 0.03	−1.5	83.3	−5.5	This work
							−7.0[b]	5
Piperidine	7	0.05–0.37	92.53 ± 0.01	−2.43 ± 0.05	−2.6	99.39	−6.9	This work
		0.05–0.25	91.97 ± 0.02[c]	−1.4 ± 0.1	−1.5		−7.4	This work
			91.10[c]					4
			90.2					*d*
Hexamethylenimine	8	0.05–0.37	105.55 ± 0.01	−1.68 ± 0.04	−1.6	113.1	−7.5	This work
Heptamethylenimine	15	0.01–0.16	120.09 ± 0.02	−5.22 ± 0.19	−4.3	126.8	−6.7	This work
1-Methylpyrrolidine	6	0.05–0.31	97.29 ± 0.02	−3.71 ± 0.11	−3.8	104.5	−7.2	This work
1-Methylpiperidine	7	0.05–0.31	110.54 ± 0.02	−3.45 ± 0.10	−3.1	121.6	−11.1	This work
			109.91[c]					4

[a] Values obtained by subtracting the molar volume of water from the intercept of the function $\Phi^*/(1-\alpha) = f[(1-\alpha)c_B^0]$ (see, *e.g.*, Figure 1). The α values were calculated from the pK_a reported in ref 2, except for azetidine for which a pK_a = 11.35 value was used. [b] At 26.5°. [c] From measurements in 0.1 *N* KOH. [d] S. D. Haman and S. C. Lim, *Aust. J. Chem.*, **7**, 329 (1954).

($d\Phi_v/dc$) is always negative. Both quantities $\bar{V}^{0E}$ and $h/\bar{V}_2^0$ increase in absolute value as the number of hydrocarbon residues is increased. (ii) For compounds containing more than one hydrophilic center, the volume decrease is still strong, while $h/\bar{V}_2^0$ is nearly zero.

Negative values of $\bar{V}^{0E}$ are typical for aqueous solutions of nonelectrolytes. The analysis of the limited amount of the available $\bar{V}^{0E}$ data seems to show that these, specifically, depend upon the number and steric position of hydrocarbon residues as well as upon the number, type, and steric position of the functional groups in the molecule. More experimental information is, however, necessary in order to rationalize, if possible, the volumetric behavior of nonelectrolytes in water. One should finally notice that $\bar{V}^{0E}$ values are referred to the molar volume of the pure liquid, and this is not a satisfactory reference state. Though various proposals have been put forward for the choice of the most convenient reference state for the partial molal volume,[3] this question is still unresolved. Such a difficulty is overcome when one considers effects associated with chain lengthening for solutes in very dilute solution, since these effects do not depend on structure properties of the pure compounds in the condensed state.

In spite of the above difficulty, we think that useful information on solute–solvent interactions can be obtained even from the excess molar volumes. Therefore, effects such as those associated with chain length or the number of polar sites will be discussed here by considering the volumetric behavior of pure compounds and of their aqueous solutions.

Cyclic Ethers and Cyclic Amines. Values for the contribution of the methylene group to the molar volume

Table III: Average Increments of V_2, $\bar{V}_2^0$ and $\bar{V}^{0E}$ for Introduction of a Methylene Group[a]

Class of compounds	V_{CH_2}, ml mol^{-1}	$\bar{V}^0_{CH_2}$, ml mol^{-1}	$\bar{V}^0_{CH_2}{}^E$, ml mol^{-1}	Type of process
n-Alkanols[b]	16.6 ± 0.3	15.6 ± 0.2	−1	$CH_3(CH_2)_nOH \rightarrow CH_3(CH_2)_{n+1}OH$ n = 1–3
Cyclic amines	15.7 ± 0.5	14.6 ± 0.3	−1	$(CH_2)_nNH \rightarrow (CH_2)_{n+1}NH$ n = 2–4
	13.7 ± 0.0	13.8 ± 0.8	0	n = 5, 6
N-Methyl cyclic amines	17.1	13.3	−3.8	1-CH_3-pyrrolidine → 1-CH_3-piperidine
Cyclic ethers	16.5	14.9	−1.6	THF → THP
2-Carbinol cyclic ethers[c]	16.1	14.3	−1.8	THFA → THPA

[a] The reported uncertainties were calculated as mean deviations from the average. [b] Reference 8 and D. M. Alexander, *J. Chem. Eng. Data*, **4**, 252 (1959). [c] Reference 3.

V_{CH_2} or to the limiting partial molal volume $\bar{V}^0_{CH_2}$ for some series of compounds are reported in Table III. It is to be noted that V_{CH_2} values for cyclic amines exhibit an alternate trend along the series, with a sharp drop from a value of V_{CH_2} = 16 ml mol^{-1}, passing from pyrrolidine to piperidine, down to V_{CH_2} = 13.7 ml mol^{-1} for the change piperidine → hexamethylenimine. Similar behavior is shown when these compounds are considered in solution. Two series of volume increments per mole of CH_2 are therefore reported for these substances: this in spite of the fact that, for cyclic compounds, additivity rules, which take into account only the chain length, are not in principle applicable owing to the different contributions to the volume from rings of different sizes.

Examination of the data in Table III shows significant differences between cyclic and open-chain compounds. For instance, against V_{CH_2}(alcohols) $\simeq$ V_{CH_2}(cyclic ethers), one observes $\bar{V}^0_{CH_2}$(alcohols) > $\bar{V}^0_{CH_2}$(cyclic ethers). On the other hand, in the transfer from the gas state to aqueous solution the entropy change per CH_2 group is lower for cyclic ethers than for aliphatic hydrocarbons and normal alcohols.[2] Therefore, the larger volume decrease due to the hydrophobic interaction, which is observed in cyclic compounds in comparison with open-chain molecules, can be attributed to the easier introduction of the hydrocarbon part of the ring molecules inside the cluster cavities rather than to their higher ability to promote cluster formation.

It may also be noticed that the CH_2 contribution to the excess molar volumes is larger, in absolute value, for ethers than for alcohols and amines up to six-membered rings (see $\bar{V}^0_{CH_2}{}^E$ of Table III). The excess molar volumes are, on the contrary, practically equal for *n*-butyl alcohol, THF, and pyrrolidine as well as for amyl alcohol, THP, and piperidine (see Table IV). These facts can be explained with the different interactions between water and the functional groups of the solutes. Presumably, in the case of alcohols and cyclic amines, which can act both as donors or acceptors of protons, neither local volume expansions nor contractions take place in the surroundings of the hydrophilic centers. On the contrary, near the ether oxygen, unable to exchange protons with water, a local expansion is observed. Any generalization in this respect is, however, premature owing to the insufficient amount of experimental information available.

Table IV: Limiting Excess Molar Volumes at 25°

Compounds	$\bar{V}^{0E}$, ml mol^{-1}
n-Butyl alcohol[a]	−5.4
THF	−4.9
Pyrrolidine	−5.5
1,3-Dioxolane	−4.9
n-Pentyl alcohol[b]	−6.3
THP	−6.5
Piperidine	−6.9
1,4-Dioxane	−4.8

[a] Reference 8. [b] At 20° (see ref 7).

Cyclic Diethers. The entropy loss in the gas → solution transfer for monoethers is very large and comparable with that observed for hydrocarbons. If the molecule, however, contains two ether functions, the entropy loss is much smaller, probably because the two polar sites prevent cluster formation (see ref 2). As far as volumetric data are concerned (see Table IV), the THF excess molar volume is substantially equal to that of 1,3-dioxolane, while $\bar{V}^{0E}$ of 1,4-dioxane only slightly differs from $\bar{V}^{0E}$ of THP. Contrary to the case of monofunctional ethers, whose volume decrease is attributed to the penetration of the molecule into the cluster cavities, the volume loss occurring in the diethers is interpreted in terms of the prevented formation of clusters. The creation of a dense water region around the diether molecules is thus responsible for the observed volume contraction. Here again, hydration entropy and volume change are strictly related, but the interpretation is opposite to that invoked for structure-promoting solutes (*e.g.*, mono-ethers). Structure promoters therefore show a volume decrease $\bar{V}^{0E}$ increasing with increasing absolute value of ΔS_h, but for structure breakers the decrease becomes smaller with increasing $|\Delta S_h|$.

Dependence of Apparent Molal Volumes on Concentration. The quantity $h/\bar{V}_2^0 = (1/\bar{V}_2^0)(d\Phi_v/dc)$ is always negative for monofunctional compounds (see Tables I and II), its actual value depending upon the size of the hydrocarbon part of the molecule. In the presence of more than one polar group, however, small positive values may also be found. If one agrees to the reasonable hypothesis that the Φ_v dependence on concentration is attributable to solute–solute interactions, negative values of the quantity $h/\bar{V}_2^0$ may originate from icelike water stabilization due to long-range solute–solute interactions through water clusters. Such a process is obviously not operating in diethers: their structure-breaking ability is in fact reflected in nearly zero $h/\bar{V}_2^0$ values.

Justification for negative excess molar volumes in water in terms of alterations of the solvent structure around solute molecules is now commonly accepted.[3,7-9] Other interpretations have been proposed, however, in which negative values for $\bar{V}^{0E}$ of nonelectrolytes are attributed to flexibility loss of the molecule[5] or to the high internal pressure of the water.[22] Comparison between entropy values in the gas and in dilute aqueous solution for open-chain compounds and analogous cyclic compounds allowed the deduction that the former practically retain, in the solution process, their degrees of internal freedom.[2] Therefore, the interpretation of volumetric phenomenology in terms of solvent structural modifications seemed to us at present the most reasonable. It is also supported by data such as those reported in Table IV, which could be hardly justified in terms of loss in flexibility of the molecule.

Acknowledgment. This work has been supported by financial assistance from Consiglio Nazionale delle Ricerche (C.N.R.).

(22) W. L. Masterton, *J. Chem. Phys.*, **22**, 1830 (1954).

Volumetric Properties of Aqueous Solutions of Organic Compounds.

II. Chloride Salts of Cyclic Amines

by S. Cabani,* G. Conti, L. Lepori, and G. Leva

Istituto di Chimica Fisica, Università di Pisa, Pisa, Italy *(Received October 12, 1971)*

Publication costs assisted by C.N.R. (Consiglio Nazionale delle Ricerche)

The apparent molal volume Φ_v in aqueous solution at 25° of a series of cyclic amine salts of the type $(CH_2)_n$-NH_2Cl (n = 2–7), $(CH_2)_nNHCH_3Cl$ (n = 4, 5), and $(CH_2)_nN(CH_3)_2Cl$ (n = 4, 5) have been measured with a differential buoyancy method in the concentration range 0.01–0.3 M. The values of Φ_v show negative deviations from the Debye–Hückel limiting law, which are the larger the larger the hydrocarbon portion of the molecule is. Comparisons are made between cyclic amines and the corresponding acid cations and the results discussed in terms of the additivity of the limiting partial molal volumes in homologous series of compounds. The effects of increasing alkyl coordination to the N center in neutral and charged molecules are also considered. The volume changes in the proton ionization process $\Delta\bar{V}^0_{ion}$ have finally been related to the entropy changes ΔS^0_{ion}.

Introduction

In the preceding paper,[1] the volumetric behavior of aqueous solutions of neutral cyclic amines (B) was examined. In order to calculate the limiting partial molal volume $\bar{V}^0_B$ of these compounds, correction for hydrolysis and therefore knowledge of the $\bar{V}^0_{BH^+}$ values of acid cations (BH^+) was required. The latter data, on the other hand, are of great interest for a clearer understanding of the water–N^+ center interactions in organic molecules[2-6] as well as for a better characterization of the acid dissociation of alkyl aminium ions. We would like to recall, to this purpose, that the thermodynamic studies of the ionization process of cations

(1) S. Cabani, G. Conti, and L. Lepori, *J. Phys. Chem.*, **75**, 1338 (1972).

(2) B. E. Conway, *Annu. Rev. Phys. Chem.*, **17**, 481 (1966).

(3) R. E. Verrall and B. E. Conway, *J. Phys. Chem.*, **70**, 3961 (1966).

(4) B. E. Conway and L. H. Laliberté, "Hydrogen Bonded Solvent Systems," A. K. Covington and P. Jones, Ed., Taylor and Francis, London, 1968, p 139.

(5) L. H. Laliberté and B. E. Conway, *J. Phys. Chem.*, **74**, 4116 (1970).

(6) J. E. Desnoyers and M. Arel, *Can. J. Chem.*, **45**, 359 (1967).

of mono-, bi-, and trisubstituted aliphatic amines in solution emphasized the necessity to take in due consideration the modifications of the solvent structure near the molecules of solute.[7-12]

Volumetric data on salts of the type $(CH_2)_nNH_2Cl$ (n = 2–7) and $(CH_2)_nNHCH_3Cl$ (n = 4, 5) are discussed here. Measurements of the partial molal volumes of the 1,1-dimethylpyrrolidinium and 1,1-dimethylpiperidinium chlorides were also made. Values of the volume changes for the acid dissociation $\Delta\bar{V}^0_{ion}$ of the cations mentioned above were finally computed and compared with the ionization entropies ΔS^0_{ion} previously determined.[13]

Experimental Section

Materials. The salts under study, except for aziridine and azetidine hydrochlorides, were prepared according to the usual procedures. The crude products were recrystallized from pure organic solvents (absolute ethyl alcohol, ether, chloroform, etc.) or from their mixtures and then carefully dried by heating under vacuum.

Stock solutions were prepared by adding a known amount of water to a weighed quantity of compound immediately after drying. The purity of the salts was checked by Cl^- analysis. Deionized water, distilled over $KMnO_4$, was used throughout all the experiments.

Apparatus and Measurements. A differential buoyancy balance previously described[1] was used for density measurements. The solutions to be studied were generally prepared directly in the test vessel by gradual addition, by means of a syringe, of weighed amounts of salt stock solution to a known amount of water. In the case of aziridine and azetidine, on the contrary, the solutions were prepared separately by adding the stoichiometric amount of HCl to the aqueous solution of the amine or *vice versa*. Measurements were performed immediately after preparation of the solutions.

Results

In the concentration range investigated, the apparent molal volumes, once corrected for the Debye's term following the method of Redlich and Mayer,[14] were satisfactorily described by the equation

$$\Phi_v' = \Phi_v^0 + hc \qquad (1)$$

where $\Phi_v' = \Phi_v - 1.868\sqrt{c}$. Values of the limiting partial molal volume $\bar{V}_2^0 = \Phi_v^0$ and of the slope h were calculated from eq 1 through a weighted least square adjustment. These data are given in Table I. As an example, in Figure 1 are reported the experimental data relative to different samples of piperidine hydrochloride; the dashed curves were calculated by assuming an uncertainty in the density measurements of ±2 ppm.

The agreement between our $\bar{V}_2^0$ values for piperidine and 1-methylpiperidine hydrochlorides and those reported by Laliberté and Conway[5] for the same substances is quite satisfactory, even though these authors found a zero slope of the function $\Phi_v = f(c)$ in the low concentration range (see Figures 1 and 2). Actually, the limited number of experiments made by us in very dilute solutions is insufficient to establish unambiguously the trend of the function $\Phi_v = f(c)$ for $c \to 0$. A fine agreement is also found between the values of the limiting partial molal volume of the

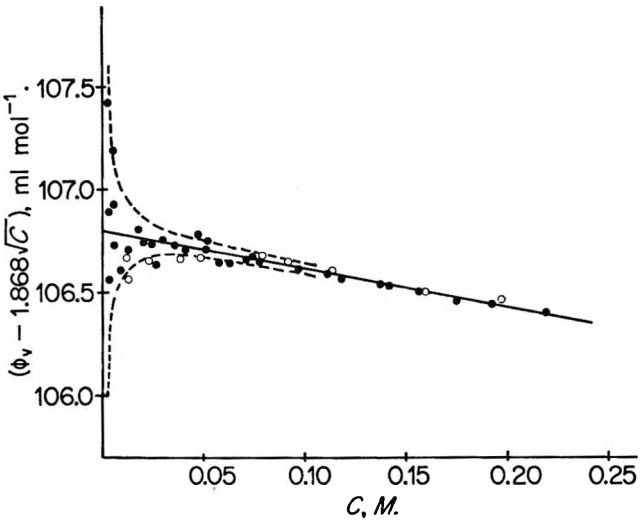

Figure 1. Apparent molal volumes of piperidine hydrochloride in water (25°), corrected for the Debye–Hückel concentration dependence, as a function of concentration: (●) this work, (○) Laliberté and Conway.[5] The dashed curves were drawn by assuming an uncertainty in the density measurements of ±2 ppm.

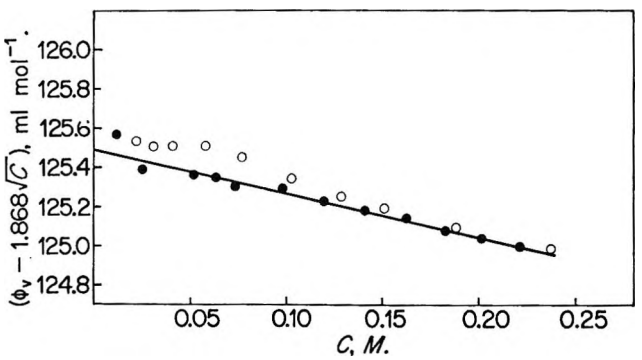

Figure 2. Plot of $\Phi_v - 1.868\sqrt{c}$ against molar concentration for 1-methylpyrrolidine hydrochloride in water at 25°: (●) this work, (○) Laliberté and Conway.[5]

(7) D. H. Everett and W. F. K. Wynne-Jones, *Trans. Faraday Soc.*, **35**, 1380 (1939).
(8) A. G. Evans and S. D. Hamann, *ibid.*, **47**, 34 (1951).
(9) H. S. Frank and M. Evans, *J. Chem. Phys.*, **13**, 507 (1945).
(10) A. F. Trotman-Dickenson, *J. Chem. Soc.*, 1293 (1949).
(11) R. G. Pearson, *J. Amer. Chem. Soc.*, **70**, 204 (1948).
(12) R. G. Pearson and F. V. Williams, *ibid.*, **76**, 258 (1954).
(13) S. Cabani, G. Conti, and L. Lepori, *Ric. Sci.*, **38**, 1039 (1968).
(14) O. Redlich and D. M. Meyer, *Chem. Rev.*, **64**, 221 (1964).

Table I: Apparent Molal Volume, $\Phi_v = \bar{V}_2^0 + 1.868\sqrt{c} + hc$, of Cyclic Amine Salts in Water at 25°

Salt	No. of expt	Concn range, M	$\bar{V}_2^0$, ml mol^{-1}	h, ml l. mol^{-2}	$\bar{V}^0_{BH^+}$,[a] ml mol^{-1}	$(h/\bar{V}_2^0) \times 10^2$, M^{-1}
Aziridine hydrochloride	6	0.09–0.80	61.99 ± 0.14	−0.45 ± 0.47	38.4	−0.7
Azetidine hydrochloride	11	0.01–0.22	76.56 ± 0.06	−0.59 ± 0.52	53.0	−0.8
Pyrrolidine hydrochloride	14	0.01–0.43	91.72 ± 0.02	−1.04 ± 0.08	68.1	−1.1
Piperidine hydrochloride	32	0.003–0.22	106.80 ± 0.01	−1.91 ± 0.12	83.2	−1.8
		0.01–0.20	106.67[b]	0.0 up to c = 0.075[b]	83.1[b]	
Hexamethylenimine hydrochloride	11	0.03–0.26	120.87 ± 0.03	−1.96 ± 0.14	97.3	−1.6
Heptamethylenimine hydrochloride	13	0.01–0.28	134.94 ± 0.02	−3.06 ± 0.12	111.3	−2.3
1-Methylpyrrolidine hydrochloride	12	0.02–0.34	110.64 ± 0.02	−1.51 ± 0.08	87.0	−1.4
1-Methylpiperidine hydrochloride	12	0.01–0.22	125.49 ± 0.02	−2.18 ± 0.12	101.9	−1.7
		0.02–0.25	125.51[b]	0.0 up to c = 0.055[b]	101.9[b]	
1,1-Dimethylpyrrolidinium chloride	13	0.015–0.27	126.11 ± 0.02	−2.46 ± 0.09	102.5	−2.0
1,1-Dimethylpiperidinium chloride	11	0.015–0.26	140.14 ± 0.02	−2.74 ± 0.11	116.5	−2.0
					116.5[b]	

[a] $\bar{V}^0_{BH^+} = \bar{V}_2^0 - \bar{V}^0_{Cl^-}$ with $\bar{V}^0_{Cl^-}$ = 23.6 ml mol^{-1}: B. E. Conway, R. E. Verrall, and J. E. Desnoyers, *Trans. Faraday Soc.*, **62**, 2738 (1966). [b] See ref 5.

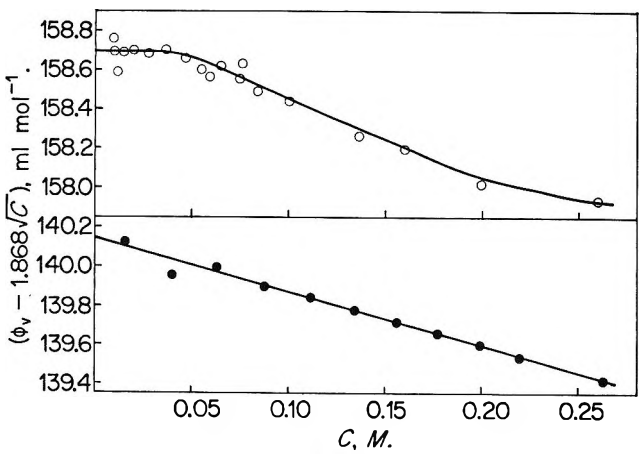

Figure 3. Plots of $\Phi_v - 1.868\sqrt{c}$ as a function of concentration for 1,1-dimethylpiperidinium hydrohalides: (●) this work, (○) Laliberté and Conway.[5]

1,1-dimethylpiperidinium ion, obtained from the Φ_v^0 values of the chloride (this work) and the iodide[5] salts, by assuming $\bar{V}^0_{Cl^-}$ = 23.6 ml (g-ion)$^{-1}$ and $\bar{V}^0_{I^-}$ = 42.2 ml (g-ion)$^{-1}$ at 25°.[15] Apparent molal volumes of the 1,1-dimethylpiperidinium chloride and iodide against the molar concentration are plotted in Figure 3.

Discussion

The volumetric behavior of a great number of N-containing organic compounds with different coordinations on the nitrogen atom has already been widely examined.[3-6,15-19] Nevertheless, we wish to consider this question again in terms of the effects associated with (i) chain lengthening in homologous series and (ii) increasing methyl coordination on the nitrogen atom. Attention will also be given to the volume changes associated with the proton ionization process of saturated aminium ions.

Effect of Chain Length. For both hydrochloride salts (Table I) and neutral amines,[1] the values of $h/\bar{V}_2^0$ are always negative, while their magnitudes increase as the molecular weight grows, showing an alternate trend along the series. An alternate trend is also exhibited by the partial molal volumes of the free bases ($\bar{V}^0_B$) and of their conjugated acids ($\bar{V}^0_{BH^+}$). However, as in the case of neutral amines, also for acid cations it seems correct to distinguish between compounds with 2–5 from those with 5–7 carbon atoms. Two mean values of methylene contribution to the limiting molal volume $\bar{V}^0_{CH_2}$ are thus reported in Table II; they are, in any case, close to those calculated for the corresponding amines.

The analogies between the amines and their acid cations indicate that, in the case of monofunctional compounds, the interactions water–hydrophobic part and water–polar site of solute molecule can be treated almost independently. This statement is also sup-

(15) B. E. Conway, R. E. Verrall, and J. E. Desnoyers, *Trans. Faraday Soc.*, **62**, 2738 (1966).

(16) F. Franks and H. T. Smith, *ibid.*, **63**, 2586 (1967); **64**, 2962 (1968).

(17) W. Y. Wen and S. Saito, *J. Phys. Chem.*, **68**, 2639 (1964); **69**, 3569 (1965).

(18) L. G. Hepler, J. M. Stokes, and R. H. Stokes, *Trans. Faraday Soc.*, **61**, 20 (1965).

(19) L. A. Dunn, *ibid.*, **64**, 2951 (1968).

Table II: Average Contributions per CH_2 Group to the Molar Volume and to the Limiting Partial Molal Volume in Some Homologous Series of N-Containing Organic Compounds[a]

Series	V_{CH_2}, ml mol^{-1}	$\bar{V}^0_{CH_2}$, ml mol^{-1}	Considered compounds		Ref
Secondary cyclic amines	15.7 ± 0.5	14.6 ± 0.3	$(CH_2)_nNH$	n = 2–5	This work
	13.7 ± 0.0	13.8 ± 0.8		n = 5–7	
Secondary cyclic amine salts		14.9 ± 0.3	$(CH_2)_nNH_2Cl$	n = 2–5	This work
		14.1 ± 0.0		n = 5–7	
N-Methyl cyclic amines	17.1	13.3	$(CH_2)_nNCH_3$	n = 4, 5	This work
N-Methyl cyclic amine salts		14.8	$(CH_2)_nNCH_3HCl$	n = 4, 5	This work
Primary *n*-aliphatic amines	16.55 ± 0.2		$C_nH_{2n+1}NH_2$	n = 2–8	*c*
Primary *n*-aliphatic amine salts		16.2 ± 0.3[b]	$C_nH_{2n+1}NH_3Br$	n = 2–5	6
		15.9 ± 0.02		n = 5–8	
Secondary *n*-aliphatic amines	16.26 ± 0.05		$(C_nH_{2n+1})_2NH$	n = 2–5	*c*
Secondary *n*-aliphatic amine salts		16.0 ± 0.0	$(C_nH_{2n+1})_2NH_2Cl$	n = 2–4	5
Tertiary *n*-aliphatic amine salts		16.1	$(C_nH_{2n+1})_3NHCl$	n = 2, 3	3
Tetra-*n*-alkylammonium salts		16.4	$(C_nH_{2n+1})_4NBr$	n = 2, 3	5
		15.3		n = 3, 4	
Tetraalkylammonium salts of cyclic amines		14.0	$(CH_2)_nN(CH_3)_2Cl$	n = 4, 5	This work

[a] The methylene contribution to the volume was calculated from: $V_{CH_2} = \{V_{(C_{n+1}H_{z+2})_mX} - V_{(C_nH_z)_mX}\}/m$, where X is a functional group (NH, NCH_3, NH_2^+, $N^+(CH_3)_2$, etc.) and C_nH_z is a cyclic ($z = 2n$, $m = 1$) or open-chain *n*-alkyl ($z = 2n + 1$; m = 1–4) radical containing a number of carbon atoms $n \geq 2$. The reported uncertainties were calculated as mean deviations from the average. [b] In this series of compounds the $\bar{V}^0_{CH_2}$ values were averaged arbitrarily. In effect, a monotonic decrease is observed from the value $\bar{V}^0_{CH_2}$ = 16.50 ml mol^{-1} ($C_2H_5NH_3Br \rightarrow n$-$C_3H_7NH_3Br$) to the value $\bar{V}^0_{CH_2}$ = 15.95 ml mol^{-1} (n-$C_4H_9NH_3Br \rightarrow n$-$C_5H_{12}NH_3Br$). [c] R. R. Dreisbach, "Physical Properties of Chemical Compounds," Vol. III, American Chemical Society, Washington, D. C., 1967.

ported by data relative to open-chain compounds for which $\bar{V}^0_{CH_2}$ is practically constant for cations of primary, secondary, or tertiary amines as well as for tetraalkylammonium ions (see Table II). In cyclic compounds, however, as shown by other thermodynamic data,[20] the effect of the polar site probably vanishes at two bond lengths distant from the hydrophilic center against at least the four bond lengths distant for open-chain compounds; see, *e.g.*, $\bar{V}^0_{CH_2}$ values for acid cations of primary *n*-aliphatic amines.[6]

Finally, the marked difference observed in the $\bar{V}^0_{CH_2}$ values between open-chain (mean value ≃16.0 ± 0.2 ml mol^{-1}) and cyclic (mean value ≃14.5 ± 0.5 ml mol^{-1}) N-containing compounds is noteworthy. Probably this is due to solute and solvent structure effects: volumetric data on the aqueous solutions of neutral open-chain amines may be useful in order to elucidate this question.

Effects of Methyl Substitution. Some examples of methyl substitution on the nitrogen atom are reported in Table III. The $\bar{V}^0_{CH_3}$ value changes only slightly when passing from primary to secondary and from these to tertiary amines and is sensibly higher than the $\bar{V}^0_{CH_2}$ value (see table II) for either neutral or charged molecules as well as for both cyclic and open-chain amines.

A considerable drop in the volume increment per mole of CH_3 is, however, noticed in passing from trialkyl to tetraalkyl cations. At the same time, cations containing exclusively methyl groups coordinated to an N^+ center are clearly different from cations containing also radicals other than methyl. For instance, a value of $\bar{V}^0_{CH_3}$ = 16.4 ml mol^{-1} is observed passing from $(CH_3)_3NH^+$ to $(CH_3)_4N^+$ against the values of $\bar{V}^0_{CH_3}$ = 15.5 and 14.6 ml mol^{-1} for the changes 1-CH_3-

Table III: Increments of V_2 and $\bar{V}_2^0$ for Introduction of a CH_3 Group on the Nitrogen Center[a]

Type of process	V_{CH_3}, ml mol^{-1}	$\bar{V}^0_{CH_3}$, ml mol^{-1}
$CH_3NH_2 \rightarrow (CH_3)_2NH$	22.0	18.6[b]
$(CH_3)_2NH \rightarrow (CH_3)_3N$	24.9	19.3[b]
Pyrrolidine → 1-CH_3-pyrrolidine	21.2	19.6
Piperidine → 1-CH_3-piperidine	22.2	18.0
$CH_3NH_3^+ \rightarrow (CH_3)_2NH_2^+$		18.7[c]
$(CH_3)_2NH_2^+ \rightarrow (CH_3)_3NH^+$		18.1[c]
$(CH_3)_3NH^+ \rightarrow (CH_3)_4N^+$		16.4[c]
Pyrrolidinium → 1-CH_3-pyrrolidinium		18.9
1-CH_3-Pyrrolidinium → 1,1-$(CH_3)_2$-pyrrolidinium		15.5
Piperidinium → 1-CH_3-piperidinium		18.7
1-CH_3-Piperidinium → 1,1-$(CH_3)_2$-piperidinium		14.6

[a] The methyl contribution to the volume was evaluated as $V_{CH_3} = V_{(CH_3)_mY} - V_{(CH_3)_{m-1}YH}$, where Y is a group of the type NH, NH_2^+, $N(CH_2)_4$, etc. and m = 1–4. This quantity represents the volume change for CH_3 group added on the nitrogen center, including the loss of one H atom. [b] Reference 3. [c] Reference 5.

(20) S. Cabani, G. Conti, and L. Lepori, *Trans. Faraday Soc.*, **67**, 1943 (1971).

pyrrolidinium → 1,1-$(CH_3)_2$-pyrrolidinium and 1-CH_3 piperidinium → 1,1-$(CH_3)_2$-piperidinium, respectively.

The latter two values are of the same order of magnitude of the values of $\bar{V}^0_{CH_2}$ reported in Table II as well as of those obtained for $(C_2H_5)_3NH^+ \rightarrow (C_2H_5)_4N^+$ ($\bar{V}^0_{CH_2}$ = 13.9 ml mol^{-1}) and for $(n\text{-}C_3H_7)_3NH^+ \rightarrow (n\text{-}C_3H_7)_4N^+$ ($\bar{V}^0_{CH_2}$ = 15.1 ml mol^{-1}) using the calculation method and the experimental data given by Verral and Conway.[3]

The sharp drop in the $\bar{V}^0_{CH_3}$ value, which is always observed when we pass from cations containing the nitrogen center tricoordinated at carbon atoms to cations containing tetracoordinated nitrogen, is due to the prevailing effect of water structure promotion, typical of tetraalkylammonium ions,[17] over the electrostriction removal. The lower $\bar{V}^0_{CH_3}$ values which are calculated for the changes 1-CH_3-pyrrolidinium → 1,1-$(CH_3)_2$-pyrrolidinium and 1-CH_3-piperidinium → 1,1-$(CH_3)_2$-piperidinium with respect to the $(CH_3)_3NH^+ \rightarrow (CH_3)_4N^+$ change are, on the other hand, hard to explain: the charge distribution on asymmetrical ions and the electrostriction removal as well as the water–cation interactions should at least be taken into account.

Volume Changes in the Ionization Process. Volume changes associated with the reaction

$$BH^+ \longrightarrow B + H^+ \qquad (2)$$

were calculated through

$$\Delta\bar{V}^0_{ion} = \bar{V}^0_B + \bar{V}^0_{H^+Cl^-} - V^0_{BH^+Cl^-} \qquad (3)$$

assuming for the limiting partial molal volume of HCl the value 17.815 cc mole^{-1}.[21] The results are reported in Table IV with the ionization entropy (ΔS^0_{ion}) values. For comparison, data for other amines are also given. The ionization entropies vary sensibly passing from secondary to tertiary cyclic amines, as already observed for methylamines.[22] On the contrary, $\Delta\bar{V}^0_{ion}$ values are practically independent of the type of amine. A slight decrease of $\Delta\bar{V}^0_{ion}$ is, however, observed along the series of secondary as well as of tertiary cyclic amines. This trend is not in accordance with what is expected on the basis of the packing density concept, proposed by King to account for the effect of the chain length on volume changes associated with the ionization reaction of acid cations.[23]

The small $\Delta\bar{V}^0_{ion}$ changes, compared with the large changes in ΔS^0_{ion} which are observed for N-containing acid cations as the degree of alky substitution is varied, can hardly be interpreted.[3] However, the close analogy in the volumetric behavior of amines and their conjugated acids suggests that the hydrophobic part of both these solutes is inserted in the cluster cavities,

Table IV: Volume and Entropy Changes Associated with the Ionization Process: $BH^+ \rightarrow B + H^+$

Base	$\bar{V}^0_B$, ml mol^{-1}	$\bar{V}^0_{BH^+Cl^-}$, ml mol^{-1}	$\Delta\bar{V}^0_{ion}$, ml mol^{-1}	ΔS^0_{ion}, eu
Aziridine	48.87	61.99	+4.7	−6.8
Azetidine	63.71	76.56	+5.0	−9.4
Pyrrolidine	77.77	91.72	+3.9	−8.7
Piperidine	92.53	106.80	+3.5	−8.3
	90.2	107.3	+0.8[a]	
Hexamethylnimine	105.55	120.87	+2.5	−7.3
Heptamethylenimine	120.09	134.94	+3.0	
1-Methylpyrrolidine	97.29	110.64	+4.5	−15.0
1-Methylpiperidine	110.54	125.49	+2.9	−13.7
Ammonia	24.6	36.0	+6.4[a]	−0.3[b]
Methylamine	40.0	53.8	+4.0[c]	−4.7[d]
	41.6	55.5	+3.9[a]	−4.1[b]
Dimethylamine	58.6	72.5	+3.9[c]	−9.5[d]
	59.1	73.1	+3.8[a]	−8.7[b]
Trimethylamine	77.9	90.6	+5.1[c]	−15.2[d]
	78.4	91.7	+4.5[a]	−15.1[b]

[a] S. D. Hamann and S. C. Lim, *Aust. J. Chem.*, **7**, 329 (1954). [b] J. J. Christensen, R. M. Izatt, D. P. Wrathall, and L. D. Hansen, *J. Chem. Soc. A*, 1212 (1969). [c] Reference 3. [d] D. H. Everett and W. F. K. Wynne-Jones, *Proc. Roy. Soc., Ser. A*, **177**, 499 (1941).

thus lengthening their mean life, independently of the neutral or charged character of the polar site. The volume and entropy changes accompanying the proton dissociation reaction should then be mainly determined by the modification which the functional group undergoes and by the different interactions between this center and water in the free bases and in their acid cations.

The large difference in the ΔS^0_{ion} values between primary, secondary, and tertiary amines have been attributed to the different solvation of the acid cations with respect to the free amines. Therefore, the constancy of $\Delta\bar{V}^0_{ion}$ can be justified assuming that the polar groups capable of forming hydrogen bonds cause no appreciable volume changes when introduced into the solvent. The nearly constant $\Delta\bar{V}^0_{ion}$ value ($\Delta\bar{V}^0_{ion}$ = 3 ± 2 ml mol^{-1}) observed for all the amines should then be almost exclusively due to the loss of the proton from acid cations. More ΔS^0_{ion} and $\Delta\bar{V}^0_{ion}$ data are necessary in order to better clarify the thermodynamics of this process.

Acknowledgment. The authors are indebted to the Consiglio Nazionale delle Ricerche (C.N.R.) which supported this work.

(21) L. A. Dunn, *Trans. Faraday Soc.*, **62**, 2348 (1966).
(22) D. H. Everett and W. F. K. Wynne-Jones, *Proc. Roy. Soc., Ser. A*, **177**, 499 (1941).
(23) E. J. King, *J. Phys. Chem.*, **73**, 1220 (1969).

The Basic Modes of Transport in Molten Salts

by P. L. Spedding

Department of Chemical and Materials Engineering, University of Auckland, Auckland, New Zealand
(Received January 22, 1971)

Publication costs borne completely by The Journal of Physical Chemistry

The difference between the conduction and diffusive transport modes in melts is discussed in terms of the movement of the basic entities of which the melt is composed. Data for the conduction and diffusion in TlCl are used to illustrate a suggested method of separating out the contributions of ions, ionic agglomerates, and molecules to the conductive and diffusive transport modes. Indications are that individual ions are the predominant conductive and diffusive vehicle in a region above the melting point of the salt while ionic agglomerates are the predominant conductive and diffusive entity just above the melting point. About 900° the molecular character of the melt commences to become significant; thereafter it increases in importance up to the critical point where it is predominant.

Klemm[1] has pointed out that the form of the temperature dependence of molten salt conductance as found by Yaffe and Van Artsdalen[2] implied the existence of a conductance maximum at temperatures approaching the critical point. Grantham and Yosim[3,4] have observed these maxima for a variety of melts. Indeed such maxima also occur in aqueous electrolyte solutions. As melts become less molecular and more ionic in character the observed specific conductance maxima in general shift first to higher temperatures and then to lower temperatures as the conductance at the maximum increases. The corresponding diffusion coefficient–temperature relation shows a consistent rise with no maximum.[5] This indicates clearly that there are differences in the basic mechanisms controlling conduction and diffusion in melts. Some idea of the nature of these differences can be gained by a detailed examination of the temperature relations of these two different transport modes. A great deal of discussion about the difference between conductive and diffusive transport in melts has been centered around the Nernst–Einstein relation, and many suggestions have been advanced to explain the positive deviations from its predictions that have been observed for melts.[6-11] However, conduction and diffusion can be interpreted in terms of several complementary effects some of which follow the Nernst–Einstein relation.

Spedding and Mills[11] developed the suggestion that diffusion could be viewed in terms of movement of the two basic entities of which the melt was composed, namely agglomerates of ions and individual particles. The speed of movement of these entities would be expected to depend on their physical size. If this were the case, then the observed increase in diffusion with temperature can occur on two accounts, firstly through increased movement of both the ionic agglomerates and individual particles which make up the melt, but more importantly through the thermal breakdown of the ionic agglomerates into individual ions.[5] Conduction, on the other hand, can be viewed as proceeding through a combination of a Grotthus-type mechanism (or more correctly a Grotthus–Clausius mechanism) of charge transfer operating within and between the ionic agglomerates, and through individual movement of ions. The Grotthus mechanism thus would contribute to conduction but not to diffusion. Increased temperature would raise conduction through greater Grotthus-type charge movement and through faster movement of the individual ions, which increase in number as the ionic agglomerates are thermally broken down. However, the thermal breakdown of ionic agglomerates ultimately leads to a decrease in conduction because the Grotthus mechanism wanes as the agglomerates are thermally destroyed and the melt increases in molecular or "gas-like" character as the critical point is approached. This latter effect has been observed by Grantham and Yosim.[3b]

(1) A. Klemm, Euratom. Report, EUR 2466 e, 1964, p 31.

(2) I. S. Yaffe and E. R. Van Artsdalen, *J. Phys. Chem.*, **60**, 1125 (1956).

(3) (a) L. F. Grantham and S. J. Yosim, *ibid.*, **67**, 2506 (1963); (b) L. F. Grantham and S. J. Yosim, *ibid.*, **72**, 762 (1968); (c) L. F. Grantham and S. J. Yosim, *J. Chem. Phys.*, **38**, 1671 (1963); (d) L. F. Grantham and S. J. Yosim, *ibid.*, **45**, 1192 (1966).

(4) (a) L. F. Grantham, *J. Chem. Phys.*, **43**, 1415 (1965); (b) L. F. Grantham, *ibid.*, **44**, 1509 (1966); (c) L. F. Grantham, *ibid.*, **49**, 3835 (1968).

(5) P. L. Spedding, *Rev. Pure Appl. Chem.*, **21**, 1 (1971).

(6) A. S. Dworkin, R. B. Escue, and E. R. Van Artsdalen, *J. Phys. Chem.*, **64**, 872 (1960).

(7) A. Z. Borucka, J. O'M. Bockris, and J. A. Kitchener, *Proc. Roy. Soc., Ser. A*, **241**, 554 (1957).

(8) J. O'M. Bockris and G. W. Hooper, *Discuss. Faraday Soc.*, **32**, 218 (1961).

(9) F. Lantelme and M. Chemla, *Bull. Soc. Chim. Fr.*, **169**, 969 (1963).

(10) C. A. Angell, *J. Phys. Chem.*, **69**, 399 (1965).

(11) (a) P. L. Spedding and R. Mills, *J. Electrochem. Soc.*, **112**, 594 (1965); (b) P. L. Spedding and R. Mills, *ibid.*, **113**, 599 (1966); (c) R. Mills and P. L. Spedding, *J. Phys. Chem.*, **70**, 4077 (1966).

An initial evaluation of these suggested transport modes arises from an examination of the diffusion and conduction data of TlCl. This salt was chosen because the measured diffusion coefficient of both the cation and anion virtually are the same; thus it avoids any complications of considering two different diffusion coefficients when applying the Nernst–Einstein equation. The conductance data for TlCl, κ_T, are shown as the full line in Figure 1. The data have been extended beyond the experimental range reported by Grantham and Yosim[3d] by using a reduced variable technique which allowed a universal curve to be developed that fitted the majority of the available data.[3,4] Additional experimental work in this laboratory has confirmed the reliability of this extrapolation technique up to 1448°. The apparatus which was used consisted of a simple coaxial alumina cell capable of operating under pressure. It was made from a close fitting rod and tube so that the annular space provided a suitable restrictive conduction path between the electrodes. Strictly, the extended TlCl conductance data beyond 1448° should be checked by experiment. The same applies to the diffusion data, D_T, presented in Figure 2, which has been extended beyond the experimental range by using an Arrhenius-type plot.

In Figure 1 the conduction, κ_T, is shown as being the sum of two different conduction modes: the Grotthus mechanism of conduction associated with ionic agglomerates, κ_A, and individual ionic conduction, κ_I. These two latter curves were obtained in the following manner. Before the melting point the solid salt had a small but definite conductance due to individual ionic transport. At the melting point the total conductance κ_T increased sharply. It was assumed that the sharp rise in conductance was due to the commencement of the Grotthus mechanism and that individual ionic conductance remained at about the same level as that observed in the solid salt before melting. At the other extremity of the conductance curve it was assumed that both the conduction modes reduced to a low value when the critical point was approached, firstly because the ionic agglomerates which allowed the Grotthus mechanism to occur had been destroyed thermally or more correctly reduced to molecular size, and secondly almost all the individual ions had been removed by the liquid increasing in molecular character. Both the conduction modes κ_A and κ_I must maximize, and it was assumed that this was due to the operation of two opposing effects in each case. The Grotthus mechanism, which was assumed to be predominant at the melting point, initially increased with temperature but was opposed by the gradual removal of ions from the agglomerates by thermal energy. Individual ionic conduction initially increased rapidly with temperature because more individual ions were made available from the thermal breakdown of the ionic agglomerates. It will be shown later that at about 900° individual ionic conduction commenced to decrease as the molecular character of the melt started to become significant. The exact nature of the molecular liquid formed in this melt is uncertain, but from the work of Bauer and Porter[12] and Cubicciotti[13] it is most likely composed of the dimer in the region of the critical point. The conduction due to individual ions passed through a maximum value and reduced to some low conductance at the critical point. Since only three points on each of the two conductance curves κ_A and κ_I could be plotted, that is the value at the melting point, the critical point, and their intersection, the intervening regions have been sketched in. It can be argued that distributions other than the two shown in Figure 1 are possible. However, a detailed examination of all pos-

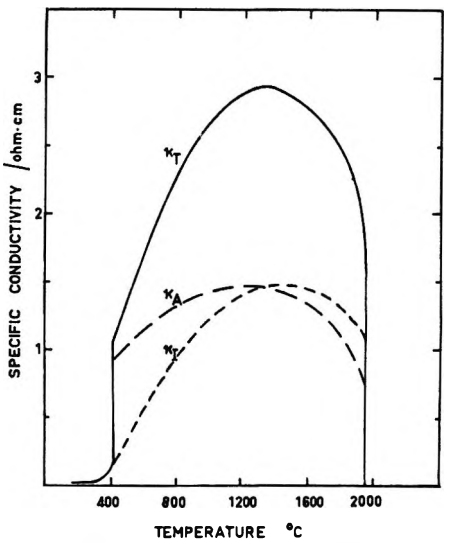

Figure 1. Conductivity of thallium chloride melt, κ_T, shown as the sum of the conductivity due to individual ions, κ_I and that due to the Grotthus mechanism of ionic agglomerates, κ_A.

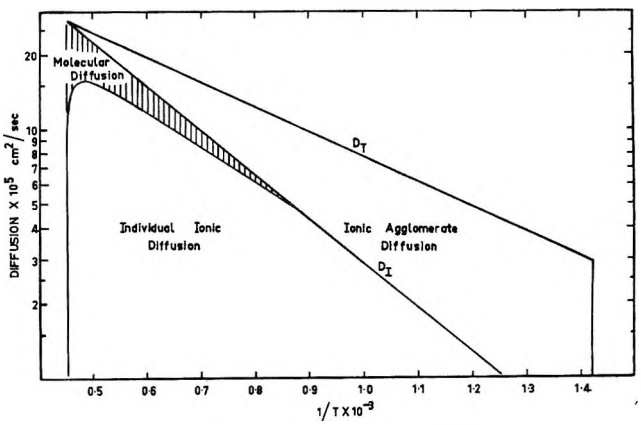

Figure 2. Self-diffusion of thallium chloride melt, D_T, shown as being made up of the diffusion of ionic agglomerates, individual ions, D_I, and molecules.

(12) S. H. Bauer and R. F. Porter, "Molten Salt Chemistry," M. Blander, Ed., Wiley, New York, N. Y., 1964, p 607.

(13) D. Cubicciotti, *J. Phys. Chem.*, 68, 1528 (1964).

sible alternatives has shown that the distributions given in Figure 1 are the most reasonable.

Thus in Figure 1 the overall conductance κ_T was assumed to be the sum of the Grotthus conductance, κ_A, and the individual ionic conductance κ_I, and rose rapidly from the ionic conductance of the solid phase at the melting point[14,15] to a maximum value and then fell away to the conductance of the molecular liquid at the critical point. The individual ionic conductance κ_I followed a similar pattern rising rapidly from the conductance of the solid at the melting point to a maximum value and then falling away to a low value at the critical point. The Grotthus conductance κ_A, on the other hand, had a relatively high value of conductance at the melting point, actually the difference between the observed total conductance and the ionic conductance of the solid, rose slowly to a maximum value, and dropped away to some low value of conductance at the critical point.

The effects of the suggested conductive transport modes on diffusion are detailed in Figure 2, where D_T is the average of the $D_{Tl}{}^+$ and $D_{Cl}{}^-$ data for TlCl,[16-18] and D_I is the diffusion coefficient calculated from the individual ionic conduction data κ_I of Figure 1 using the Nernst–Einstein relation eq 13, while the ionic agglomerate diffusion D_A, is the difference between these two.

$$D_A = D_T - D_I \tag{1}$$

Clearly the ionic agglomerates provide the major contribution to diffusion at the melting point. As the temperature is increased above the melting point, individual ionic movement becomes increasingly more important at the expense of the ionic agglomerates. There is an inflection in the calculated individual ionic transport data D_I at about 900°. If this is ignored and the D_I data are extended, they meet the measured individual ionic diffusion data D_T at the critical point. This may be fortuitous but is nevertheless suggestive that the melt commences to exhibit a significant molecular character about 900° at the expense of the individual ions. The form of the calculated individual ionic diffusion D_I above 900° suggests that the molecular character of the melt increases in importance up to the critical point where it is predominant.

Therefore it can be concluded that only the individual ions contribute to conduction and diffusion in the normal manner and can be expected to obey the Nernst–Einstein relation, equation 13. On the other hand, the Grotthus mechanism contributes to conduction but not to diffusion while any molecular melt character has the opposite effect. In short both the Grotthus mechanism and molecular melt character result in diffusive transport which cannot be expected to follow the Nernst–Einstein relation. The same would be true for the movement of ionic agglomerates because charge masking effects are involved.

Taking a basis of 1 g-mol of TlCl and that A g-mol is present as individual ions, then the amount of salt held as ionic agglomerates is $1 - A$ g-mol. The contribution to the observed diffusion coefficient D_T at temperature T°K by the net movement of individual ions is the product of the number of g-mol of a particular ion and its pure diffusion coefficient when only individual ions are present. However, the measured diffusion coefficients D_T in Figure 2 are shown for one type of ion, either $D_{Tl}{}^+$ or $D_{Cl}{}^-$, in order to better illustrate the molecular nature of the fluid being predominant at the critical point, so that

$$D_I = AC \exp(-E/RT) \tag{2}$$

where C is a constant and E is the activation energy for the pure individual ionic diffusion process in cal/g-mol.

Assuming that the ionic agglomerates thermally break according to an Arrhenius law then for the temperature region between the melting point and the critical point

$$A = A_0 \exp(-B/RT) \tag{3}$$

where A_0 is a constant and B is the activation energy for the agglomerate breaking process. From eq 2

$$D_I = A_0 C \exp[-(B + E)/RT] \tag{4}$$

The conduction of the solid at the melting point has been assumed to be due to individual ions exclusively. From the data given in Figure 1 an estimate of 0.0181 can be made for A at the melting point. From this estimate the agglomerates at the melting point can be shown to consist only of the first and second coordination shells. Ignoring the formation of molecules, and taking $A = 1.0$ at the critical point, then eq 3 leads to

$$A = 6.38 \exp(-8200/RT) \tag{5}$$

Bu substitution in eq 4

$$D_I = 6.38C \exp[(-8200 + E)/RT] \tag{6}$$

From Figure 2 the D_I data which were calculated using the Nernst–Einstein relation allow the following relation to be derived if the inflection point at 900° is ignored

$$D_{I+M} = 17.0 \times 10^{-4} \exp(-8200/RT) \tag{7}$$

Therefore $C = 2.67 \times 10^{-4}$ and $E = 0$. That is, the activation energy for diffusion of the individual ions is virtually zero.

The diffusion coefficient at any temperature due to the net movement of ionic agglomerates is given by

(14) R. J. Friauf, *Phys. Chem. Solids*, **18**, 203 (1961).

(15) A. R. Beljajew, E. A. Sheintschushina, and L. A. Firsanowa, "Physikalische Chemie geschmolzener Salze," VEB Georg Thieme, Leipzig, 1964, p 119.

(16) E. Berne and A. Klemm, *Z. Naturforsch. A*, **8**, 400 (1953).

(17) A. Klemm, *ibid.*, **15**, 173 (1960).

(18) C. A. Angell and J. W. Tomlinson, *Trans. Faraday Soc.*, **61**, 2312 (1965).

$$D_A = (1 - A)G \exp(-I/RT) \quad (8)$$

where G is a constant and I is the activation energy for ionic agglomerate diffusion. By substitution for A in eq 8

$$D_A = [G \exp(-I/RT)] - [6.38 \exp(-8200/RT][G \exp(-I/RT)] \quad (9)$$

From the data of Figure 2

$$D_A = D_T - D_{I+M} \quad (10)$$

and by substitution for D_T and D_{I+M}

$$D_A = [7.6 \times 10^{-4} \exp(-4550/RT)] - [17.0 \times 10^{-4} \exp(-8200/RT)]$$

This is a complex function, as is illustrated in Figure 3, and it is not possible to evaluate fully eq 9 and 10 in terms of an Arrhenius equation above 900° where the melt begins to exhibit appreciable molecular character. The same comments apply to the diffusion of molecules D_M although the Arrhenius plot is followed for a greater temperature range. From Figure 3, the limited relations which can be found in this case are

$$D_A = 2.07 \times 10^{-4} \exp(-2900/RT)$$

from the melting point up to 900° (11)

$$D_M = 3.92 \times 10^{-3} \exp(-16{,}200/RT)$$

between 1000 and 1800° (12)

The Arrhenius coefficients for diffusion in eq 11 and 12 are worth comment. The ionic agglomerate diffusion has an Arrhenius coefficient which is an appreciable fraction of the observed Arrhenius coefficient for diffusion of +4550 cal/g-mol in contrast to the activation energy of the individual ionic diffusion. On the other hand, the molecular diffusion Arrhenius coefficient of

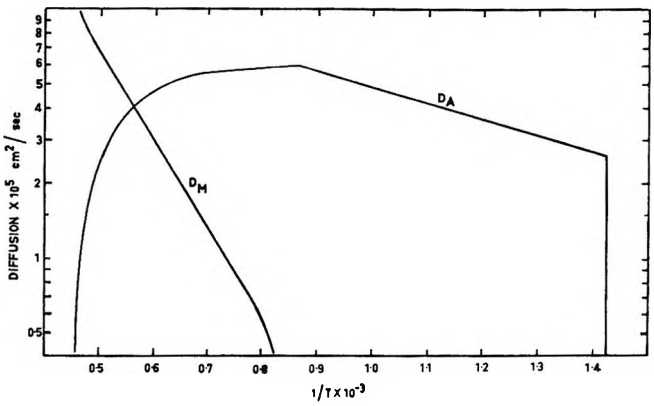

Figure 3. The diffusion coefficients for the movement of ionic agglomerates, D_A, and molecules, D_M, in thallium chloride melt.

+16,200 cal/g-mol is very large. The reason for this is obscure. The Arrhenius coefficient for movement of the ionic agglomerates provides about 65% of the observed Arrhenius coefficient for diffusion up to 900°. The remainder of the observed Arrhenius coefficient arises from the thermal breakup of the agglomerates providing diffusion through individual ions. Above 900° the Arrhenius coefficient is increasingly made up from the Arrhenius coefficient for molecular movement within the melt.

The conduction due to individual ionic movement is given by the simple equation

$$\Lambda_I = F^2 D_I / RT \quad (13)$$

The conduction due to movement of ionic agglomerates and the Grotthus mechanism is more complex

$$\Lambda_A = F^2 D_A / RT + H(1 - A) \exp(-J/RT) \quad (14)$$

where H is a constant and J is the Arrhenius coefficient for conductive movement *via* the Grotthus mode. Equation 14 cannot be evaluated simply in terms of an Arrhenius expression.

The Chemistry of Recoiling Silicon Atoms. V. Product-Forming Reactions in Phosphine–Silane Mixtures[1]

by Peter P. Gaspar,* Peter Markusch, J. Dewey Holten, III, and John J. Frost

Department of Chemistry, Washington University, Saint Louis, Missouri 63130 *(Received August 3, 1971)*

Publication costs assisted by the U. S. Atomic Energy Commission

Product studies on reactions of recoiling silicon atoms in binary mixtures of phosphine, the silicon precursor, and silane, disilane, and trisilane, respectively, support a mechanism for the product-forming steps involving silylene $^{31}SiH_2$ as the principal reactive intermediate which gives rise to the observed products. In each case the major product is a next-higher homolog of the starting silane, the expected product of Si–H insertion by $^{31}SiH_2$. Four other mechanisms are discussed and rejected on the basis of product studies and scavenger experiments. Competition experiments in ternary phosphine–silane–disilane and quaternary phosphine–silane–disilane–nitric oxide mixtures are correlated by a kinetic scheme for the product-determining steps involving a single intermediate. It is suggested that the product-determining steps are the product-forming steps and that the single kinetically important intermediate is $^{31}SiH_2$. Formation of lower homologs of the major products is explained by the unimolecular dissociation of vibrationally excited silylene insertion products.

Introduction

Initial observations on the reactions of silicon atoms recoiling from the nuclear transformation $^{31}P(n,p)^{31}Si$ were presented 3 years ago.[2] Our goal has been to answer the questions: what is the chemistry of recoiling silicon atoms, and how do the reactions of recoiling silicon atoms take place? It is hoped that these studies will provide insight into the nature of primary reaction processes—collisions leading to the formation or rupture of one or several bonds. In this paper we return to the elucidation of the final step of the reaction sequence which converts recoiling silicon atoms into stable tetravalent silicon compounds.[3] In future papers the nature of the primary reactions of the recoiling atoms will be considered.

The small total number of atoms produced in a recoil experiment, typically 10^8 to 10^{10} in the case of ^{31}Si, and the infinitessimal steady-state concentration during the experiment—*less than one ^{31}Si atom per reaction mixture*—preclude direct kinetic measurements at the present state of the art, and compel the use of end-product studies to shed light on reaction mechanisms. This approach to gas-phase hot-atom chemistry was pioneered by Willard,[4] Wolfgang,[5] Wolf,[6] and Rowland[7] in their studies of the reactions of recoiling halogen, tritium and carbon atoms. The reactions of recoiling silicon atoms in the gas phase have been investigated by determining the reaction products from various substrates and measuring the effects on product distributions of changes in such disposable parameters as the structures of substrates, the total pressure of the reaction mixture, and the amounts of moderators and scavengers present.[8] Products have been conveniently identified and their yields determined by a combination of vapor-chromatography and flow counting, a standard technique in hot-atom chemistry.[9]

Because their reactions are more complex, the problem of unravelling the reaction mechanism for recoiling *polyvalent* atoms is unfortunately of considerably greater difficulty than the corresponding investigation of a monovalent or divalent atom.

The well characterized primary reactions of recoiling atoms are shown in Table I.[5,6,8] One or at most two bonds to the recoiling atom are formed in a single step. Abstraction and displacement are processes which can form stable products from a single collision of *univalent* recoiling atoms (i, ii, Table I) and have been thoroughly investigated in the case of tritium and the halogens.[4,5,7] Of course even monovalent atoms can undergo reactions which form reactive species if bond breaking in the target molecule accompanies or follows displacement, or if addition to a π bond occurs (iii, iv, Table

(1) AEC Technical Report No. COO-1713-24. This work has been carried out with financial support under contract from the U. S. Atomic Energy Commission.

(2) P. P. Gaspar, S. A. Bock, and W. C. Eckelman, *J. Amer. Chem. Soc.*, **90**, 6914 (1968). A preliminary communication also appeared: P. P. Gaspar, B. D. Pate, and W. Eckelman, *ibid.*, **88**, 3878 (1966).

(3) A preliminary account of this work has appeared: P. P. Gaspar and P. Markusch, *Chem. Commun.*, 1331 (1970).

(4) J. E. Willard, *Ann. Rev. Nucl. Sci.*, **3**, 193 (1953); J. B. Evans and J. E. Willard, *J. Amer. Chem. Soc.*, **78**, 2908 (1956).

(5) R. Wolfgang, *Progr. React. Kinet.*, **3**, 97 (1965).

(6) A. P. Wolf, *Advan. Phys. Org. Chem.*, **2**, 202 (1964).

(7) F. Schmidt-Bleek and F. S. Rowland, *Angew. Chem. Int. Ed.*, **3**, 769 (1964); E. K. C. Lee, J. W. Root, and F. S. Rowland in "Chemical Effects of Nuclear Transformations," Vol. I, International Atomic Energy Agency, Vienna, 1965, p 55.

(8) For lucid presentations of the principles of gas phase hot-atom chemistry see ref 4 and 5 and also G. Stöcklin, "Chemie heiszer Atome," Verlag Chemie, Weinheim/Bergstrasse, 1969.

(9) R. Wolfgang and F. S. Rowland, *Anal. Chem.*, **30**, 903 (1958).

Table I: Schematic Representation of Primary Reactions of Monovalent and Divalent Recoiling Atoms. A is a monovalent Atom, and B is a Divalent Atom. Stable Products Are Shown in Boldface

i.	Abstraction	A + X—Y—Z → **A—X** + ·Y—Z
ii.	Displacement	A + X—Y—Z → **A—Y—Z** + X·
iii.	Displacement with bond cleavage	A + X—Y—Z → A—Y· + X· + Z·
iv.	Addition	A + W=Y → A—W—Y·
v.	Insertion	B + X—Y—Z → **X—B—Y—Z**
vi.	Addition	B + W=Y → **B** (**W——Y**)
vii.	Abstraction	B + X—Y—Z → ·B—X + ·Y—Z
viii.	Displacement	B + X—Y—Z → ·B—Y—Z + X·
ix.	Insertion with bond cleavage	B + X—Y—Z → X—B—Y· + Z·

I). The valence of a divalent atom can be saturated by insertion into single bonds and addition to π bonds (v, vi, Table I), both processes giving stable products. However, those reactions of a monovalent atom which lead to stable products give, in the case of divalent atoms, reactive intermediates (vii, viii, Table I).

A polyvalent atom generally cannot form a stable molecule by saturating its valence in a single reactive collision. Therefore the end products actually identified in a recoil experiment with a polyvalent atom result from a *sequence* of consecutive reactions. The primary reactions of the recoiling atoms produce intermediates which are the reactants in secondary reactions whose products may themselves be unstable species which must undergo further transformations before stable products are formed. The necessity of characterizing a sequence of consecutive reactions is the cause of the added complexity in the study of polyvalent, in distinction to monovalent, recoil atoms.

Product structures provide important clues for the identification of reactive intermediates in the reactions of polyvalent recoiling atoms. Strictly speaking, of course, product studies can only *preclude* certain intermediates. Thus in the case of recoiling carbon atoms, the *absence* of hexanes as reaction products of recoiling carbon atoms and pentane would have effectively eliminated CH_2 from consideration as an active intermediate, since methylene and pentane are known to yield the three isomeric hexanes *n*-hexane and 2- and 3-methylpentane in ratio 3:2:1.[10] The finding of the hexanes in correct ratio was used as positive evidence for the intermediacy of methylene in recoil carbon reactions.[11,12]

On the basis of a similar analogy it was proposed that $^{31}SiH_2$ is an important intermediate in the reactions of recoiling silicon atoms.[2] Here the analogy was carried one step further since the insertion reaction of silylene has only been firmly established in silane pyrolyses in the past 2 years.[13,14] In 1968 it seemed that the formation of disilane as a major product from recoiling silicon atoms and silane (in the presence of phosphine) could most easily be rationalized by insertion of $^{31}SiH_2$ into an Si–H bond of silane. In the meantime other workers have demonstrated that the insertion reaction indeed occurs.[13-15] It is clear, however, that there are alternative mechanisms. Disilane could also be rationalized by a coupling of radioactive silyl radicals with normal silyl radicals produced from silane by radiation damage.

$$^{31}SiH_2 + SiH_4 \longrightarrow H_3{}^{31}SiSiH_3 \quad (1)$$

$$^{31}SiH_3 + SiH_3 \longrightarrow H_3{}^{31}SiSiH_3 \quad (2)$$

A major motive in extending our product studies to mixtures of phosphine with higher silanes was the desire to make a firm choice between $^{31}SiH_2$ and $^{31}SiH_3$ as necessary product-forming intermediates.

It should be mentioned that product studies from the reaction of recoiling silicon atoms with disilane and trisilane were first reported by Cetini and coworkers.[16] These workers used the $^{30}Si(n,\gamma)^{31}Si$ nuclear transformation to produce recoiling silicon atoms. This nuclear reaction produces a silicon atom with such low recoil energy that neutralization of the initial positive ion before chemical reactions occur cannot be regarded as assured.[2,17] Indeed differences in reactivity have been noted between silicon atoms recoiling from $^{31}P(n,p)^{31}Si$ and $^{30}Si(n,\gamma)^{31}Si$.[17] No products higher than trisilane were reported by Cetini, *et al.*, possibly as noted by the authors, due to radiation damage,[16] but more likely due to limitations in the available chromatographic apparatus.

A model has already been presented for the product-determining steps in the reactions of recoiling silicon atoms in pure phosphine and in phosphine–silane, phosphine–ethylene, and phosphine–silane–ethylene mixtures.[2] The relative reactivity of a single intermediate toward the substrates present was believed to determine the product ratios.

$$X + SiH_4 \xrightarrow{k_1} H_3{}^{31}SiSiH_3 \quad (3)$$

$$X + SiH_4 \xrightarrow{k_2} {}^{31}SiH_4 \quad (4)$$

(10) W. vE. Doering, R. Buttery, R. Laughlin, and N. Chaudhuri, *J. Amer. Chem. Soc.*, **78**, 3224 (1956).

(11) B. Gordon, A. Steinberg, and A. P. Wolf, Brookhaven National Laboratory Annual Report, BNL 523 (AS-12) 51 (1958).

(12) A. Wolf in "Chemical Effects of Nuclear Transformations," Vol. II, International Atomic Energy Agency, Vienna, 1961, p 3.

(13) P. P. Gaspar and B. J. Herold, "Silicon, Germanium and Tin Structural Analogs of Carbenes" in "Carbene Chemistry," 2nd ed, W. Kirmse, Ed., Academic Press, New York, N. Y., 1971.

(14) R. B. Baird, M. D. Sefcik, and M. A. Ring, *Inorg. Chem.*, **10**, 883 (1971).

(15) M. Bowrey and J. H. Purnell, *J. Amer. Chem. Soc.*, **92**, 2594 (1970).

(16) G. Cetini, M. Castiglioni, P. Volpe, and O. Gambino, *Ric. Sci.*, **39**, 3921 (1969).

(17) P. P. Gaspar, S. A. Bock, and C. A. Levy, *Chem. Commun.*, 1317 (1968).

$$X + PH_3 \xrightarrow{k_5} {}^{31}SiH_4 \quad (5)$$

$$X + PH_3 \xrightarrow{k_6} \text{other products and involatile material} \quad (6)$$

The data on the variation of absolute and relative yields of volatile products from phosphine–silane mixtures were adequately correlated by expressions relating product yields to substrate ratios which were derived from this partial kinetic scheme.[2] Phosphine–silane–ethylene mixtures gave results compatible with the same reaction scheme supplemented with steps involving the reactions of ethylene. While any number of more complex reaction schemes *could* lead to the same responses to variations of the substrate ratios as were observed experimentally, it was felt that any scheme involving several product-forming intermediates in varying ratios would lead to deviations from the linear relationships observed.

In the reaction systems previously employed to test the above kinetic scheme the bulk of the volatile products were formed in the reactions of just one of the substrates present. The experiments to test the simple kinetic scheme should become more meaningful when several components whose concentrations in the reaction system are varied lead to high yields of volatile products. Therefore competition experiments have been undertaken in ternary mixtures containing silane and disilane in addition to phosphine.

As stated above, $^{31}SiH_2$ was chosen as the most likely intermediate X in the kinetic scheme shown because of the formation of the "insertion product" disilane. The alternative set of product-forming steps involving coupling reactions of silyl radicals was rendered unlikely by scavenger experiments in which the presence of small quantities of nitric oxide or ethylene caused only a minor decrease in the absolute product yields without perturbing the relative yields.

While $^{31}SiH_2$ is certainly a plausible intermediate in the reactions of recoiling silicon atoms, evidence in its favor was not conclusive. The alternative intermediate $^{31}SiH_3$ was difficult to exclude definitively by means of scavenger experiments because the chemistry of silyl radicals was not and is not well known. Silyl radicals have not been characterized. No electronic spectrum of SiH_3 is contained in Herzberg's great compendium,[18] and only recently has an esr spectrum of SiH_3 in solution become available.[19] Thus the failure of certain molecules to act as scavengers can only be interpreted as precluding the participation of silyl radicals on the basis of *assumptions* about how silyl radicals react.[20]

Reactions of recoiling silicon atoms in mixtures of phosphine with higher silanes have been investigated because the product distributions enable a distinction to be made between silyl radicals and silylene as necessary intermediates, free from much of the ambiguity of the phosphine–silane system. In the latter system both intermediates can give rise to the observed major product disilane by reactions 1 and 2 above. With disilane, however, $^{31}SiH_2$ should give trisilane as major product, while $^{31}SiH_3$ can couple with both types of silyl radicals formed from disilane by radiation damage, giving rise to both disilane and trisilane as major products. An extended set of product-forming steps is considered in the discussion (*vide infra*).

$$H_3SiSiH_3 \xrightarrow[\text{damage}]{\text{radiation}} SiH_3 + H_2SiSiH_3 + \text{other products} \quad (7)$$

$$^{31}SiH_3 + SiH_3 \longrightarrow H_3{}^{31}SiSiH_3 \quad (2)$$

$$^{31}SiH_3 + H_2SiSiH_3 \longrightarrow H_3{}^{31}SiSiH_2SiH_3 \quad (8)$$

This paper is confined to the consideration of the nature of the product-forming steps because the evidence presented for the determination of the reactive intermediates consists of qualitative and quantitative product studies. As one works "backward" along the multi-step reaction sequence which converts a polyvalent atom to stable products, the identification of reactive intermediates by analogy with known species which give the same products becomes progressively more tenuous. We feel ourselves to be on reasonably safe ground in analyzing the product-forming steps. The same arguments cannot be extended simply to earlier steps in the reaction sequence whose products as well as reactants must be ascertained by indirect means.

The arguments of the discussion section will be seen to buttress previous conclusions identifying $^{31}SiH_2$ as the sole important intermediate in product-forming steps. It may be argued that this is gilding the lily. However, careful consideration of the silylene model for the formation of major products is necessary because we shall argue in succeeding papers that certain stable end products of recoil silicon reactions which are not compatible with an SiH_2 intermediate provide important clues both to the nature of other intermediates *and* to the details of primary reactions of recoiling silicon atoms.

Disilane and higher silanes were chosen as reaction substrates for several reasons in addition to the hope that the structures of reaction products would shed light on the intermediates in product-forming steps. (a) The high yields obtained from phosphine–silane mixtures suggested that high yields could be expected from other silanes. (b) The presence of Si–Si bonds

(18) G. Herzberg, "Electronic Spectra of Polyatomic Molecules," D. Van Nostrand, Princeton, N. J., 1966, p 513.

(19) P. J. Krusic and J. K. Kochi, *J. Amer. Chem. Soc.*, **91**, 3938 (1969).

(20) These assumptions are reasonable and are, where possible, being tested. Silyl radicals in solution add to ethylene very rapidly (unpublished work of P. P. Gaspar and K. Y. Choo. See also P. J. Krusic and J. K. Kochi, *J. Amer. Chem. Soc.*, **91**, 6161 (1969)).

provides a structural feature which might influence the reactions of the recoiling atoms. (c) The larger numbers of internal degrees of freedom and the more facile pyrolysis of the higher silanes provide opportunities to study consequences of vibrational excitation in recoil silicon reactions.

Experimental Section

Materials. Phosphine (99.5%) was obtained from the Rocky Mountain Research Co. and was used without purification. No impurities were detected by vapor chromatography. Silane (semiconductor grade) from Matheson Gas Products was used without purification. No impurities were detected by gas chromatography and mass spectroscopy. Disilane and trisilane were prepared by lithium aluminum hydride reduction of the appropriate perchlorosilane.[21] Neon (cp 99.99%) and nitric oxide (cp 99.0%) were obtained from Air Products and Chemicals, Inc., and were used without purification. Higher silanes and silylphosphine were prepared for carrier purpose by conversion of silane in a silent electric discharge.[22] Identification was by mass spectroscopy. Trimethylphosphine was prepared by reaction of a methyl grignard reagent with phosphorus trichloride.[2]

Reaction Mixtures. Reaction mixtures were prepared on a conventional high-vacuum line equipped with greaseless Teflon and Viton stopcocks. Vacua of less than 10^{-5} Torr pressure were attained for outgassing purposes using a mercury diffusion pump. Reaction mixtures were prepared by freezing condensable gases into quartz ampoules from a 182-cm^3 section of the vacuum line followed by any noncondensable components. Pressures were measured with a Statham Model PA-731-350-TC absolute pressure transducer (0 to 1 psi range) frequently calibrated against mercury and butyl phthalate manometers. The transducer was used with a Statham Model SC-1100 bridge amplifier whose output was read on a digital voltmeter. The 0 to 50 Torr capacity of the transducer gives a 0 to 5 V readout with less than 0.5% nonlinearity. All reaction mixtures were prepared and irradiated in 6 mm i.d. × 9-cm quartz ampoules. Recoil loss was determined by comparison of absolute yields of volatile products with those extrapolated from high pressures in larger (14 mm i.d.) ampoules. Recoil losses for 1:1 phosphine–silane mixtures are: zero at 1000 Torr, 9 ± 1% at 500 Torr, and 41 ± 4% at 200 Torr.

Fast-Neutron Irradiations. As many as 18 ampoules could be irradiated together strapped to a thin-walled polyethylene spindle rotated continuously during the *ca.* 45 min irradiation period to ensure equal integrated neutron fluxes for all ampoules. The ampoules were shielded from thermal neutrons by a cadmium sheet. No detectable ^{31}Si activity is produced from 3000 Torr of pure gaseous silane. Fast neutrons were produced by a *ca.* 20-μA current of 13-MeV deuterons produced by the Washington University Cyclotron impinging on a beryllium target. The ^{9}Be(d,n)^{10}Be nuclear transformation produced a flux of *ca.* 10^8 neutrons/cm^2 sec at the reaction mixtures.

Analysis of Reaction Mixtures. Radioactive products were detected and their yields were determined by conventional radio-gas chromatographic procedures previously described.[2] For most of the present experiments a windowless flow counter was used (Nuclear Chicago Model 4997 digital gas radiochromatography system) in which counter gas is mixed with the effluent carrier gas stream of the vapor chromatograph before it enters the counter.

Ampoules containing reaction mixtures were broken directly in the inlet manifold of the vapor chromatograph without aliquots being taken. The heated breaking chamber and heated connecting tubes to the vapor chromatograph are of stainless steel. The breaking chamber has its own vacuum pump and helium supply for repeated evacuation and purging prior to breaking the ampoules.

Chromatographic columns are 0.25-in. o.d. aluminum tubing 18 ft in length. All product yields were determined on a stationary phase consisting of 60 g of diethyl phthalate plus 20 g of DC 555 silicone oil/100 g of 40–50 mesh diatomaceous earth solid support (Anakrom ABS, acid- and base-washed and silanized). Authentic carrier silane, disilane, and trisilane were coinjected with the irradiated reaction mixtures for yield determinations. Reaction products were identified by comparison of retention times with authentic materials injected serially and consecutively. Trisilane was identified by comparison of reaction product and authentic trisilane on three stationary phases: diethyl phthalate–silicone oil, tricresyl phosphate, and neopentylglycol sebacate.

Quantitative analyses of reaction mixtures were carried out with catherometer (hot wire) detector, chromatographic column, breaker, and connecting lines at 50° and counter at 100°. The helium carrier gas flow rate was 80 ml/min. Propane was used as counter gas (Matheson instrument grade 99.5% passed through a pyrogallol deoxygenating tower and several drying towers) at 100 ml/min. The counter plateau was at *ca.* 2100 to 2600 V. When methane was used as counter gas, difficulty was encountered with both quenching and spurious count enhancement due to silanes in the windowless counter. With propane counter gas there was no quenching nor enhancement so long as a reaction mixture contained less than *ca.* 2000 ml Torr of silane or less than *ca.* 1400 ml Torr of disilane. Even smaller quantities of higher silanes cause quenching or enhancement.

(21) P. P. Gaspar, C. A. Levy, and G. M. Adair, *Inorg. Chem.*, 9, 1272 (1970).

(22) E. J. Spanier and A. G. MacDiarmid, *ibid.*, 1, 432 (1962).

Absolute yield measurements were carried out as previously described.[2] Improved accuracy was obtained when radioactive products were trapped on glass wool in Pyrex ampoules and the radioactivity measured in a liquid scintillation counter. The ampoules containing individual products trapped after chromatographic separation were broken directly in the counting vials under scintillator fluid. The activity of each product was compared to the total activity induced in a reaction mixture. The total activity was obtained by breaking a complete reaction ampoule in a counting vial. An error analysis has also been published.[2]

Dose. The total dose in these experiments was less than 10^{-2} eV per molecule as determined by acetylene dosimetry.[23]

Results

Product yields have been determined from the fast-neutron irradiation of the following reaction mixtures: (a) phosphine–silane, (b) phosphine–disilane, (c) phosphine–trisilane, (d) phosphine–silane–disilane, (e) phosphine–silane–disilane–nitric oxide, and (f) trimethylphosphine–trimethylsilane. In addition, experiments were carried out with 1:1 phosphine–silane mixtures varying the total pressure and the duration of fast-neutron irradiation.

Phosphine–Silane. Silane and disilane were the only radioactive products originally reported from phosphine–silane mixtures.[2] Trisilane has now been established as an additional product formed in yields of less than 10% of the total volatile activity (TVA).[3] No higher product has been found under conditions where 1% of the TVA was readily visible and authentic carriers tetrasilanes and pentasilanes were added after neutron irradiation. Figure 1 shows the variation of product yields as a function of the composition of the reaction mixture at constant total pressure. Yields of all volatile products increase with increasing silane concentration. Figure 2 shows the trisilane yield plotted against the square of the silane concentration. A second-order dependence is indicated (see Discussion).

The identity of trisilane was confirmed by comparison of retention times with authentic trisilane on three different columns. A decay analysis on trapped purified product gave a half-life of 2.69 hr in good agreement with the literature value of 2.65 hr.[24]

A fourth, very minor, product is silylphosphine $H_3{}^{31}SiPH_2$, formed in *ca.* 4% of TVA (2% absolute) from 1:1 phosphine–silane mixture. Silylphosphine is *only* observed as a radioactive product when nonradioactive silylphosphine is present *during neutron bombardment.* That the nonradioactive silylphosphine is acting as a carrier only is indicated by the yield of *radioactive* silylphosphine remaining constant over a hundredfold change of silylphosphine concentration (mole fraction 0.001 to 0.1). Apparently silylphosphine in unstable

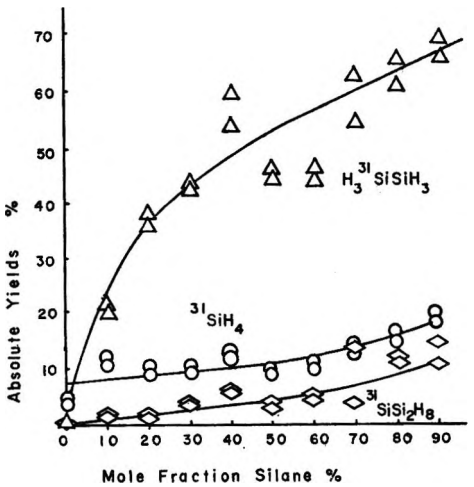

Figure 1. Variation of absolute product yields from phosphine–silane mixtures with composition at constant total pressure (1000 Torr). If error bars were shown they would extend 0.15 of each yield above and below each point.

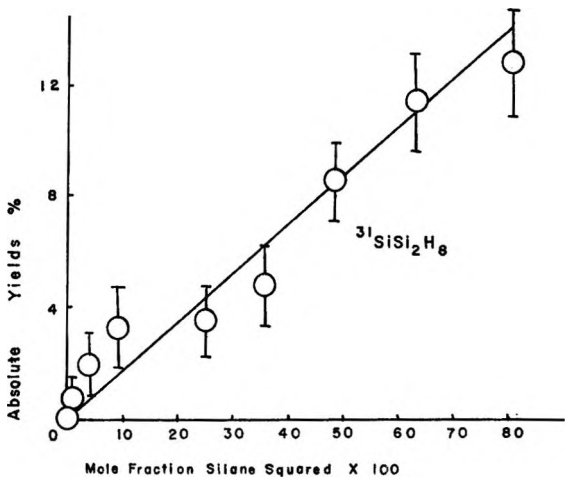

Figure 2. Variation of trisilane yield from phosphine–silane mixtures at constant total pressure (1000 Torr) with the square of the silane concentration.

under the reaction conditions. The radioactive product was identified by comparison of retention times with authentic silylphosphine on three different columns. A decay analysis on the isolated product indicated that the activity is due to ^{31}Si.

Phosphine–Disilane. Trisilane is the major radioactive product from phosphine–disilane mixtures,[3] comprising *ca.* 70% of the volatile products. Silane, disilane, tetrasilanes, and pentasilanes are also formed in low yields as shown in Table II. Figure 3 shows the variation of product yields with composition of the reaction mixture at constant total pressure. Again all yields increase with silane concentration, the yield

(23) L. M. Dorfman and F. J. Shipko, *J. Amer. Chem. Soc.*, 77, 4723 (1955).

(24) C. M. Lederer, J. M. Hollander, and I. Perlman, "Table of Isotopes," 6th ed, Wiley, New York, N. Y., 1967, p 10.

Table II: Relative Yields of Volatile Radioactive Products from 1:1 Mixtures of Phosphine with Various Silanes at a Total Pressure of 1000 Torr[a]

Reaction mixture	Yields as % of total volatile activity[a]					
	$^{31}SiH_4$	$H_3{}^{31}SiSiH_3$	$^{31}SiSi_2H_6$	$i\text{-}^{31}SiSi_3H_{10}$	$n\text{-}^{31}SiSi_3H_{10}$	$^{31}SiSi_4H_{12}$[c]
1:1 PH_3–SiH_4	13.8 ± 1.4	76.4 ± 7.6	9.8 ± 1.0	0[b]	0[b]	0[b]
1:1 PH_3–Si_2H_6	8.5 ± 0.9	5.5 ± 0.6	69.2 ± 7.0	4.2 ± 0.4	10.5 ± 1.1	*d*
1:1 Ph_3–Si_3H_8	8.1 ± 0.8	6.0 ± 0.6	1.1 ± 0.1	19.7 ± 2.0	59.2 ± 5.9	3.9 ± 0.4

[a] In all cases combined absolute product yields total *ca.* 50 ± 10%. [b] None observed under conditions where 1% would have been detected. [c] Isomers not identified. [d] Product detected, but quantitative data not available.

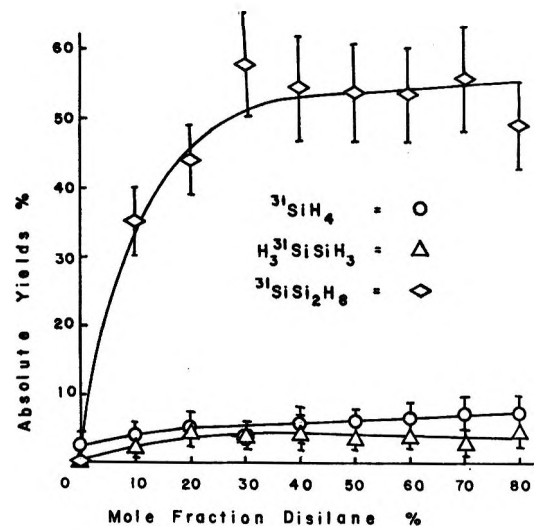

Figure 3. Variation of absolute product yields from phosphine–disilane mixtures with composition at constant total pressure (1000 Torr).

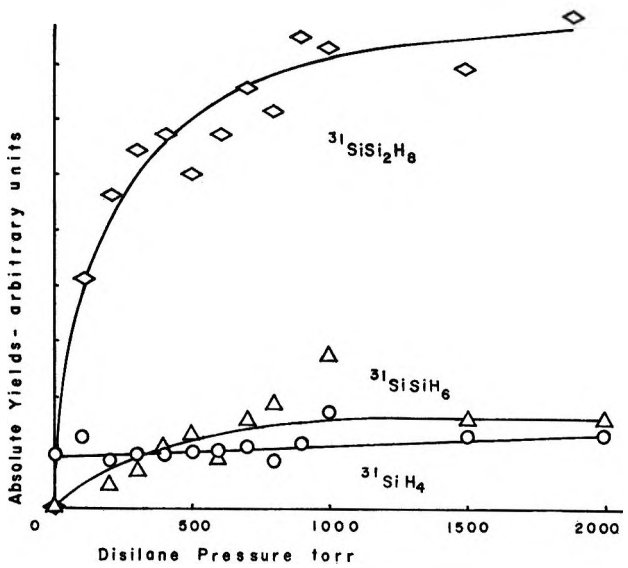

Figure 4. Variation of absolute product yields from phosphine–disilane mixtures at constant phosphine pressure and varying disilane pressure. Arbitrary units can be converted to percentage units using combined total yields of 60 ± 20% at high disilane pressures.

of $^{31}SiH_4$ being least affected. Figure 4 shows product yields as a function of disilane pressure, holding the phosphine pressure constant. Above 1000 Torr of disilane (90.9%) product yields approach a constant value, as expected when recoil loss is negligible, the composition of the reaction mixtures is essentially constant, and the sum of volatile product yields approaches a constant value.

Phosphine–Trisilane. Tetrasilanes are the major radioactive products from a 1:1 phosphine–trisilane mixture accounting for three-fourths of the observed volatile products as shown in Table II. A small amount of pentasilane (4% TVA) of unknown structure was detected. Hexasilanes and still higher silanes would not have been detected under the chromatographic conditions employed. The ratio of *normal-* to *iso*-tetrasilane is 3.1 ± 0.3.

Phosphine–Silane–Disilane. Figures 5 and 6 indicate the product yields as a function of composition at constant total pressure and constant concentration of phosphine. The data for Figure 5 were taken at 1000 Torr total pressure, 500 Torr of PH_3. The data for Figure 6 were taken at 600 Torr total pressure, 100 Torr of PH_3. The combined absolute yields remain constant independent of the silane–disilane ratio. Yields of radioactive disilane and trisilane change monotonically, trisilane increasing and disilane decreasing with increasing disilane concentration, as expected from the results of experiments in binary mixtures (*vide supra*).

Phosphine–Silane–Disilane–Nitric Oxide. Figure 7 gives product yields as a function of composition at constant total pressure and constant concentrations of phosphine and nitric oxide scavenger. The similarity of Figures 5, 6, and 7 is striking. While the absolute yields of all products decrease *ca.* 45% in the presence of 1 to 5% nitric oxide scavenger, the relative yields are unaffected. Table III gives the variation of $^{31}SiH_4$ and $^{31}SiSiH_6$ yields from 1:1 phosphine–silane mixtures with nitric oxide concentration.

Trimethylphosphine–Trimethylsilane. Fast neutron irradiation of a mixture of 200 Torr of $(CH_3)_3P$ and 800 Torr of $(CH_3)_3SiH$ yielded products identified as $^{31}SiH_4$, $(CH_3)_3Si^{31}SiH_3$ and $(CH_3)_3Si^{31}SiH_2Si(CH_3)_3$ in ratio 1:4:2 as well as several unidentified peaks com-

Table III: Variation of Silane and Disilane Yields from 1:1 Phosphine–Silane Mixtures with Nitric Oxide Concentrations[a,b,c]

% Added nitric oxide	Yields $^{31}SiH_4$ counts	Yields $^{31}SiSiH_6$ counts	Yields $^{31}SiSiH_6/^{31}SiH_4$
0	5008	19,269	3.85
	5709	21,160	3.71
1	3003	10,276	3.42
	3305	11,589	3.51
2	3043	10,638	3.50
	3128	11,030	3.53
5	3559	9,742	2.74
	3094	10,441	3.37

[a] All samples irradiated simultaneously at equal flux. All reaction mixtures contained 500 Torr each of phosphine and silane. [b] Number of counts extrapolated to end of irradiation for each sample. [c] Probable errors are ±10% for all data in this table.

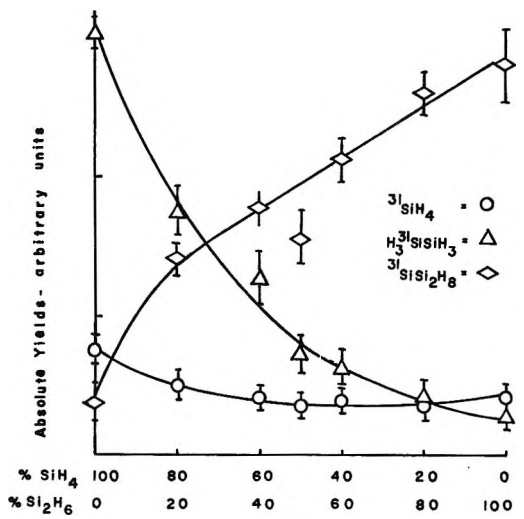

Figure 5. Variation of absolute product yields from phosphine–silane–disilane mixtures with composition at constant total pressure (1000 Torr) and constant phosphine pressure (500 Torr). Combined absolute yields total 40 ± 10% at all compositions.

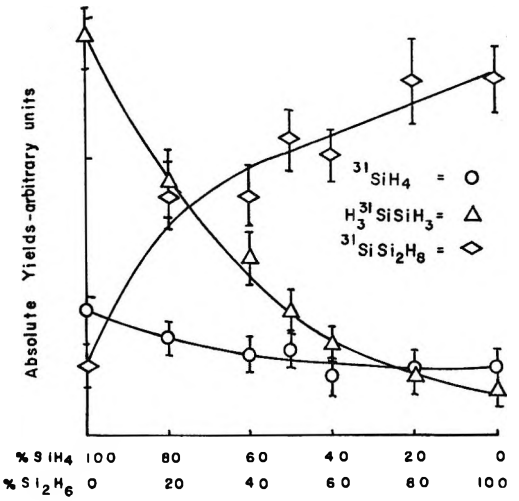

Figure 6. Variation of absolute product yields from phosphine–silane–disilane mixtures with composition at constant total pressure (600 Torr) and constant phosphine pressure (100 Torr). Combined absolute yields total 70 ± 15% at all compositions.

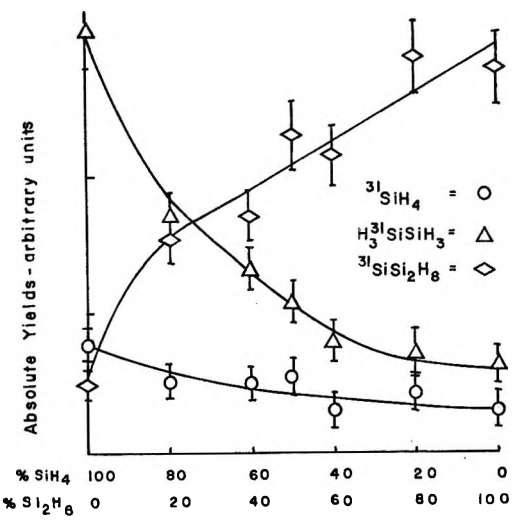

Figure 7. Variation of absolute product yields from phosphine–silane–disilane–nitric oxide mixtures at constant total pressure (1020 Torr) and constant phosphine (200 Torr) and nitric oxide (20 Torr) pressures. Combined absolute yields total 40 ± 10% at all compositions.

prising *ca.* 40% of the TVA. Combined absolute yields of *ca.* 20% were obtained.

Pressure Dependence. A series of 1:1 mixtures of phosphine and silane at total pressure 200 to 2000 Torr was irradiated simultaneously with fast neutrons. The absolute yields of disilane and trisilane decrease with total pressure while the silane yield increases slightly. When corrected for recoil loss the silane yield increases with decreasing pressure, the disilane yield decreases slightly, and the trisilane yield decreases. The data are shown in Figure 8.

Effect of Duration of Irradiation. A series of 1:1 phosphine–silane mixtures at constant total pressure of 1000 Torr was subjected to fast neutron irradiation of constant flux but varying duration. The results are presented in Table IV. For irradiation times of 1.6 to 16 μA-hr all yields are constant within experimental error. At 32 μA-hr there is a decrease in the yield of the major radioactive product, disilane, of *ca.* 30%. Over the tenfold range 1.6 to 16 μA-hr there appears to be little effect of radiation damage on absolute or relative product yields. At a longer irradiation time, 32 mA-hr, decreased yields are apparent.

Discussion

Possible Product-Forming Steps and the Relevance of Scavenger Experiments. The major volatile radioactive products from reactions of recoiling silicon atoms in mixtures of phosphine with various silanes always contain one more silicon atom than the reactant silane.

Table IV: Variation of Product Yields from 1:1 Phosphine–Silane Mixtures with Neutron Irradiation Time[a,b,c]

Microampere hours, t, μA-hr	Total volatile activity		Yields								
			$^{31}SiH_4$			$^{31}SiSiH_6$			$^{31}SiSi_2H_8$		
	Counts	Counts/t	Counts	% TVA	Counts/t	Counts	% TVA	Counts/t	Counts	% TVA	Counts/t
1.6	14,450	9031	1,343	9.6	871	11,632	80.4	7270	1,426	9.8	891
4	36,550	9138	3,368	9.2	842	31,808	87.0	7952	1,374	3.7	344
8	70,720	8802	8,774	12.4	1097	58,236	82.6	7280	3,416	4.8	427
16	158,571	9911	15,056	9.6	942	135,594	85.5	8475	7,912	4.9	495
32	217,331	6791	34,349	15.8	1073	168,486	77.5	5265	14,496	6.6	453

[a] All samples irradiated at equal flux from constant deuteron current 20 μA/hr. [b] Number of counts extrapolated to end of irradiation for each sample. [c] Probable errors are ±10% for all data in this table except errors for trisilane, which are ±20%.

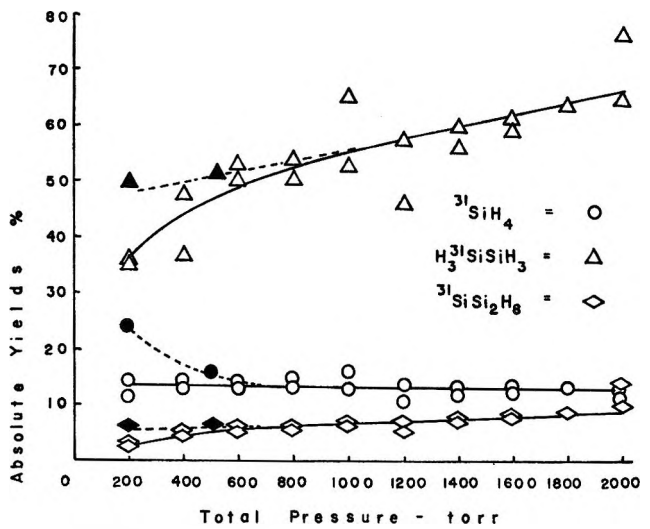

Figure 8. Variation of absolute product yields from 1:1 phosphine–silane mixtures with pressure. Yields detected are shown as normal "white" points. "Black" points show typical corrections for recoil loss below 1000 Torr. Dashed lines are yield curves corrected for recoil loss. Recoil loss is negligible above 600 Torr.

Several mechanisms must be considered as *a priori* possibilities for the product-forming steps.

a. Abstraction of Single Hydrogen Atom by Trivalent Silicon.

$$SiH_3(SiH_2)_n{}^{31}SiH_2\cdot + H\text{–}Z \longrightarrow SiH_3(SiH_2)_n{}^{31}SiH_3 + Z \quad (n = 0, 1, 2;\ H\text{–}Z = SiH_4, Si_2H_6, Si_3H_8, PH_3) \quad (9)$$

b. Abstraction of Two Hydrogens by Divalent Silicon.

$$SiH_3(SiH_2)_n{}^{31}SiH\colon + H_2Z \longrightarrow SiH_3(SiH_2)_n{}^{31}SiH_3 + Z \quad (n = 0, 1, 2;\ H_2Z = SiH_4, Si_2H_6, Si_3H_8, PH_3) \quad (10)$$

c. Insertion by Silylene.

$$^{31}SiH_2 + H\text{–}(SiH_2)_nSiH_3 \longrightarrow H_3{}^{31}Si(SiH_2)_nSiH_3 \quad (n = 0, 1, 2) \quad (11)$$

d. Coupling of Silyl Radicals.

$$^{31}SiH_3 + \cdot(SiH_2)_nSiH_3 \longrightarrow H_3{}^{31}Si(SiH_2)_nSiH_3 \quad (n = 0, 1, 2) \quad (12)$$

Of the four mechanisms above, two (a and d) involve trivalent silicon free radicals. If scavengers were available which could divert silyl radicals in competition with silanes themselves, then the two free radical paths could be distinguished from the two mechanisms involving divalent silicon intermediates, but only if there is a significant *difference in reactivity* between the trivalent and divalent species.

Scavenger experiments have been reported previously and did not lead to a change in the product spectrum other than a slight diminution of all yields.[2] These observations were taken as evidence against the occurrence of the "radical paths" a and d. Unfortunately, the reaction efficiencies of the scavengers employed toward silyl radicals are still unknown. In most cases where small amounts of scavengers have been reported to alter the reaction products significantly, the reactive silicon intermediate was not identified. For instance, Gunning and coworkers have found that the presence of 6% nitric oxide in silane completely suppressed the formation of disilane upon mercury-sensitized decomposition of silane.[25] The reactive intermediate in disilane formation from silane could not be positively identified as SiH_3. Although SiH_3 was considered the most likely reactive species present, quantum yield measurements required the participation of processes other than simple scission of single Si–H bonds of SiH_4.[25] That NO might indeed be a suitable scavenger for differentiating reactions of SiH_2 and SiH_3 was indicated by the lack of scavenger action by NO in a photochemical experiment believed to produce a divalent silicon species. Gunning and coworkers relied heavily on scavenger evidence to indicate that the vacuum ultraviolet photolysis of methylsilane yields methylsilylene.[26]

(25) M. A. Nay, G. N. C. Woodall, O. P. Strausz, and H. E. Gunning, *J. Amer. Chem. Soc.*, 87, 179 (1965).

(26) K. Obi, A. Clement, H. E. Gunning, and O. P. Strauss, *ibid.*, 91, 1622 (1969).

$$CH_3SiH_3 \xrightarrow[\substack{1236\ \text{Å}\\1470\ \text{Å}}]{h\nu} CH_3SiH + H_2 \text{ and } 2H \quad (13)$$

The presence of scavenger quantities of NO led to only a slight decrease in the yield of the major product which was attributed to insertion by the silylene intermediate

$$CH_3SiH + H\text{–}SiH_2CH_3 \longrightarrow CH_3SiH_2SiH_2CH_3 \quad (14)$$

The small decrease in yield of the 1,2-dimethyldisilane, similar to that found by us in the recoiling silicon experiments, was believed due to the low reactivity of divalent silicon species toward nitric oxide,[26] the same *postulate* previously made by us.[2] Gunning had previously demonstrated that alkylsilyl radicals CH_3SiH_2, $(CH_3)_2SiH$, and $(CH_3)_3Si$ *are* efficiently scavenged by nitric oxide.[25]

Kamaratos and Lampe have studied the mercury-photosensitized reactions of silane with nitric oxide.[27] The induction period for the formation of disilane was was ascribed to the efficient scavenging of silyl radicals by nitric oxide. However, the production of silyl radicals was *assumed* rather than demonstrated. The involvement of silyl radicals in disilane formation was inferred from the scavenger effect of nitric oxide and from the formation of SiH_3ONNO during the induction period.

Our previously reported scavenger experiments taken by themselves indicate that silyl radicals are not important precursors to the major products from recoiling silicon atom reactions. The uniform decrease in *all* product yields (*ca.* 45%) in the presence of 1 to 5% NO indicates that all the major products are derived from intermediates weakly scavenged by NO. This argument remains questionable until independent evidence is presented for the occurence of divalent and absence of trivalent silicon species in systems employed in the scavenger experiments. It is hoped that such independent evidence is furnished by the product studies and competition experiments reported in this paper.

Path d above requires an encounter between two radicals for product formation to occur. The infinitesimal concentration of recoil species (*vide supra*) renders very unlikely the coupling of two *radioactive* silyl radicals, even if $^{31}SiH_3$ is an important intermediate. Therefore path d requires the participation of *nonradioactive* silyl radicals which could be produced from silane and higher silanes by radiation damage. Ando and Oae have reported the formation of *ca.* 1% disilane from the ^{60}Co γ radiolysis of silane with total energy deposited (dose) of *ca.* 3×10^{-2} eV/molecule.[28] This dose is at least an order of magnitude greater than that which is received in our recoiling silicon experiments. Nevertheless, sufficient concentrations of nonradioactive silyl radicals may be generated by radiation damage to make path d a practical possibility.

Schmidt and Lampe have also studied the γ radiolysis of silane.[29] Disilane formation was believed to be due to ionic as well as radical reactions, with the latter predominating.

Product Studies as Indicators for the Mechanism of Product Formation. In the phosphine–silane system path d cannot be distinguished from path c on the basis of the product spectrum. Both paths lead to disilane as the major product

$$\text{path c: } {}^{31}SiH_2 + SiH_4 \longrightarrow H_3{}^{31}SiSiH_3 \quad (1)$$

$$\text{path d: } {}^{31}SiH_3 + SiH_3 \longrightarrow H_3{}^{31}SiSiH_3 \quad (2)$$

In the case of higher silanes, the two paths can be distinguished by the products formed. Radiation damage to disilane should give rise to silyl *and* disilanyl radicals[30] and path d is expected to give rise to both radioactive disilane *and* trisilane, while path c leads to trisilane as the major product.

$$\text{path c: } {}^{31}SiH_2 + H_3SiSiH_3 \longrightarrow H_3{}^{31}SiSiH_2SiH_3 \quad (15)$$

$$\text{path d: } H_3SiSiH_3 \xrightarrow[\text{damage}]{\text{radiation}} SiH_3 \text{ and } SiH_2SiH_3 \quad (16)$$

$$^{31}SiH_3 + SiH_3 \longrightarrow H_3{}^{31}SiSiH_3 \quad (2)$$

$$^{31}SiH_3 + SiH_2SiH_3 \longrightarrow H_3{}^{31}SiSiH_2SiH_3 \quad (17)$$

The experiments have indicated that disilane and trisilane as well as silane give single predominant products (counting both isomers of tetrasilane together, see Table II). Thus the product spectrum favors path c. While the relative concentrations of various silyl radicals produced by radiation damage to a given silane are not known, the production of "silylene insertion products" in yields greater than ten times those of next lower homologs argues strongly against the operation of mechanism d. The insensitivity of product yields to the duration of irradiation found over a tenfold range from $^1/_{10}$ the normal irradiation time also indicates a minimal role for radiation damage in product formation. The formation of radioactive silane is discussed below.

Another mechanism for the formation of higher silanes from silyl radicals has been proposed recently which consists of a simultaneous insertion into a SiH bond and detachment of a hydrogen atom by a silyl radical.[31]

(27) E. Kamaratos and F. W. Lampe, *J. Phys. Chem.*, **74**, 2267 (1970).

(28) W. Ando and S. Oae, *Ann. Rept. Rad. Center Osaka Pref.*, **2**, 95 (1961); *Bull. Chem. Soc. Jap.*, **35**, 1540 (1962).

(29) J. F. Schmidt and F. W. Lampe, *J. Phys. Chem.*, **73**, 2706 (1969).

(30) There is no report of the radiolysis of disilane. The radiolysis of hydrocarbons does lead to both C–C and C–H bond rupture. See S. C. Lind, "Radiation Chemistry of Gases," Reinhold, New York, N. Y., 1961, pp 103, 174; also A. V. Topchiev, Ed., "Radiolysis of Hydrocarbons," Elsevier, Amsterdam, 1964. Silanes tend to suffer both SiH *and* Si–Si bond rupture more than hydrocarbons under electron impact. See J. D. Pupezin and K. F. Zmbov, *Bull. Inst. Nucl. Sci. "Boris Kidrich" (Belgrade)*, **8**, 89 (1958).

(31) M. A. Ring, M. J. Puentes, and H. E. O'Neal, *J. Amer. Chem. Soc.*, **92**, 4845 (1970).

path e: $H'\text{–}SiH_2 + H''\text{–}SiH_3'' \longrightarrow H''H_2SiSiH_3'' + H'$ (18)

This is an extraordinary reaction for which no analogy exists. Ring and coworkers have calculated an extremely long chain length $10^{11.5}$ for the sequence including path e above and another chain-carrying step

$$H + H\text{–}SiH_3 \longrightarrow H_2 + SiH_3 \quad (19)$$

Since path e is first order in silyl radical it does not require the formation of radicals by radiation damage to operate in the recoiling silicon systems. We regard it, however, as a highly improbable mechanism until additional evidence is presented in its favor. In accord with this mechanism, Ring and coworkers found that the hydrogen produced from the pyrolysis of silane–perdeuteriosilane mixtures consisted largely of HD.[31] This suggested that the primary step in silane pyrolysis is the cleavage of a single Si–H bond, rather than the loss of molecular hydrogen.

$$SiH_4 \xrightarrow{\Delta} SiH_3 + H \quad (20)$$

$$SiD_4 \xrightarrow{\Delta} SiD_3 + D \quad (21)$$

$$H + SiH_4 \longrightarrow H_2 + SiH_3 \quad (19)$$

$$D + SiD_4 \longrightarrow D_2 + SiD_3 \quad (22)$$

$$H + SiD_4 \longrightarrow HD + SiD_3 \quad (23)$$

$$D + SiH_4 \longrightarrow HD + SiH_3 \quad (24)$$

$$SiH_4 \xrightarrow[\Delta]{X} SiH_2 + H_2 \quad (25)$$

$$SiD_4 \xrightarrow[\Delta]{X} SiD_2 + D_2 \quad (26)$$

On the other hand the major product, disilane, contained virtually no SiH_3SiD_3, but it did contain significant amounts of SiH_2DSiD_3 and $SiHD_2SiH_3$. This precluded simple radical coupling and direct displacement by silyl radicals as paths for the formation of disilane and left as an alternate possibility path e. The kinetic analysis, however, required the competing reaction, the simple coupling of silyl radicals, to have an unusually low preexponential factor of 10^6 l. mol^{-1} sec^{-1}, some four orders of magnitude below that for methyl radicals.[31] It has been recently shown that trimethylsilyl radicals $(CH_3)_3Si$ undergo dimerization at a normal rate in liquid solution[32] and we have found that silyl radicals themselves undergo dimerization at $-120°$ slightly more rapidly than trimethylsilyl radicals.[33] It should also be pointed out that in the mercury-photosensitized decomposition of silane, in which silyl radicals are probable reaction intermediates, the quantum yield of hydrogen formation is less than 10, which is incompatible with the long chain length calculated by Ring and coworkers.[31]

Path b has been rendered unlikely by experiments in the system $(CH_3)_3P\text{–}HSi(CH_3)_3$, where the silane offers the only labile hydrogen atom, and neither substrate has two labile hydrogens.[34] Thus path b cannot operate in this system. Nevertheless, 1,1,1-trimethyldisilane is formed in reasonable yield as is 1,1,1,3,3,3-hexamethyltrisilane. The former product has been obtained (corresponding to path c) under conditions where SiH_2 is believed to be the active intermediate[35] and the latter has been obtained from the thermal evaporation of silicon and cocondensation with trimethylsilane.[36]

$$SiH_2 + H\text{–}Si(CH_3)_3 \longrightarrow H_3SiSi(CH_3)_3 \quad (27)$$

$$Si + H\text{–}Si(CH_3)_3 \longrightarrow H\text{–}Si\text{–}Si(CH_3)_3 \quad (28)$$

$$H\text{–}Si\text{–}Si(CH_3)_3 + H\text{–}Si(CH_3)_3 \longrightarrow (CH_3)_3SiSiH_2Si(CH_3)_3 \quad (29)$$

Thus the *major products* from the reactions of recoiling silicon atoms with mixtures of phosphine with disilane, trisilane, respectively, and of trimethylphosphine with trimethylsilane are in accord with the proposal (path c) that insertion by silylene is the major product-forming reaction. While paths a and e are not excluded by product studies, they are rendered unlikely by the scavenger experiments. Paths b and d are excluded by the product studies.

Competition Experiments. In order to test whether the product-determining steps in the reactions of recoiling silicon atoms can be described by a simple kinetic scheme, competition experiments were undertaken in ternary mixtures. The phrase "product-determining" is used rather than "product-forming" in order to beg the question whether the products are formed directly in these elementary reactions or whether instead the product-determining steps are simply branch points in the overall mechanism. In the ternary (and quaternary) mixtures investigated, phosphine–silane–disilane and phosphine–silane–disilane–nitric oxide, the components whose concentrations were varied in a series of experiments both give rise to high yields of volatile products. Thus a clearer test was undertaken

(32) P. T. Frangopol and K. U. Ingold, *J. Organometal. Chem.*, **25**, 69 (1970).

(33) P. P. Gaspar and K. Y. Choo, unpublished work.

(34) It has been shown (P. P. Gaspar and P. Markusch, unpublished work) that C–H bonds do not participate in the product-determining reactions of recoiling silicon atoms. From phosphine–alkane (methane, ethane, propane, isobutane) and phosphine–silane–alkane mixtures covering a wide range of compositions and pressures, no volatile radioactive alkyl silanes have been detected. Added alkanes are *less* effective at reducing the yield of radioactive silanes than is neon although alkanes should be better moderators than neon and have less effect on product ratios. Therefore it is inferred that alkanes do participate in the reaction sequence which produces the observed products, but not in the product-determining steps.

(35) M. Bowrey and J. H. Purnell, *J. Amer. Chem. Soc.*, **92**, 2594 (1970).

(36) P. S. Skell and P. W. Owen, *ibid.*, **89**, 3933 (1967).

of the kinetic scheme than the previously reported competition experiments in phosphine–silane mixtures in which only silane gave reasonable yields of volatile products.

The specific question which we have attempted to answer is: does a minimum mechanism involving one intermediate in the product-determining steps suffice to describe the reactions of recoiling silicon atoms in phosphine–silane–disilane systems?[37]

The minimum kinetic scheme for PH_3–SiH_4–Si_2H_6 mixtures (ignoring the steps which produce involatile products) is

$$X + SiH_4 \xrightarrow{k_1} a^{31}SiH_4 + b^{31}SiSiH_6 + c^{31}SiSi_2H_8 \quad (30)$$

$$X + Si_2H_6 \xrightarrow{k_2} d^{31}SiH_4 + e^{31}SiSiH_6 + f^{31}SiSi_2H_8 + g^{31}SiSi_{>2}H_{>8} \quad (31)$$

The stoichiometric constants a through g may be regarded as the ratios of the individual rate constants for reaction of species X with a substrate molecule to give a particular product to the sum of the individual rate constants for reactions of species X with the substrate.

$$X + SiH_4 \xrightarrow{k_a} {}^{31}SiH_4 \quad (30a)$$

$$X + SiH_4 \xrightarrow{k_b} {}^{31}SiSiH_6 \quad (30b)$$

$$X + SiH_4 \xrightarrow{k_c} {}^{31}SiSi_2H_8 \quad (30c)$$

$$k_1 = k_a + k_b + k_c \quad (32)$$

$$a = k_a/k_1 \quad (33)$$

$$b = k_b/k_1 \quad (34)$$

$$c = k_c/k_1 \quad (35)$$

These constants a through g are equal to the relative product yields from *binary* phosphine–silane and phosphine–disilane mixtures.

From this scheme the following function is derived relating the product ratio $^{31}SiSi_2H_8/^{31}SiSiH_6$ to the substrate ratio Si_2H_6/SiH_4.

$$\frac{d[^{31}SiSiH_6]}{dt} = \{bk_1[SiH_4] + ek_2[Si_2H_6]\}[X] \quad (36)$$

$$\frac{d[^{31}SiSi_2H_8]}{dt} = \{ck_1[SiH_4] + fk_2[SiH_6]\}[X] \quad (37)$$

Then

$$\frac{^{31}SiSi_2H_8}{^{31}SiSiH_6} = \frac{ck_1[SiH_4] + fk_2[Si_2H_6]}{bk_1[SiH_4] + ek_2[Si_2H_6]} \quad (38)$$

Rearrangement of eq 38 gives

$$\frac{b(^{31}SiSi_2H_8/^{31}SiSiH_6) - c}{f - e(^{31}SiSi_2H_8/^{31}SiSiH_6)} = \frac{k_2}{k_1}\frac{[Si_2H_6]}{[SiH_4]} \quad (39)$$

Figure 9 shows the data from two series of experiments

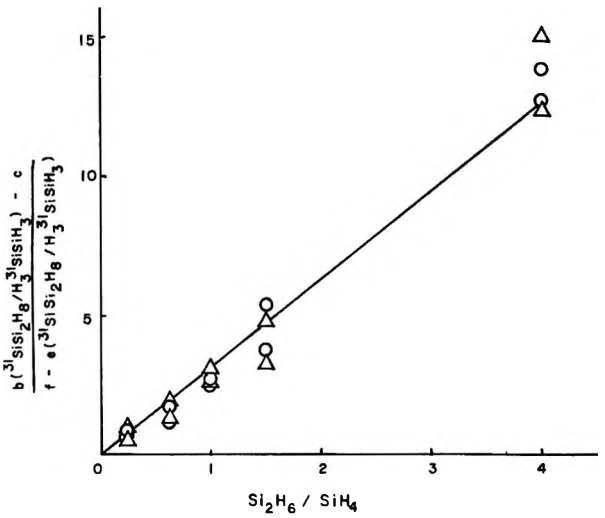

Figure 9. Variation of product ratio function (left-hand side of eq 39) as a function of substrate ratio. Circles represent data from Figure 5 and triangles represent data from Figure 6.

plotted according to eq 39 above. The constants b, c, e, and f are obtained from binary phosphine and phosphine–disilane mixtures. In the first series of experiments there was 100 Torr of PH_3 present and 500 Torr of a mixture of SiH_4 and Si_2H_6. The yield data are given in Figure 5. In the second series reaction mixtures, whose results are given in Figure 6, consisted of 500 Torr of PH_3 and 500 Torr of mixed silanes. The following conclusions seem warrented by Figure 9.

(a) The plot is linear within experimental error indicating that the kinetic scheme is compatible with the available data.

(b) Neither the change in total pressure from 600 to 1000 Torr nor the change in the amount of phosphine present from 17% to 50% affects the function plotted in Figure 9, even though the absolute yields of volatile products drop from *ca.* 80% to *ca.* 50% as the phosphine increases from 17 to 50%. Thus the formation of involatile products may be regarded as a reaction which competes for intermediate X or for a precursor to intermediate X.

(c) It is therefore suggested that a kinetic scheme involving a single intermediate X or a set of intermediates formed in constant ratio is responsible for the determination of product ratios. However, since a single rate-constant ratio suffices to describe the phosphine–silane–disilane system over a wide range of concentrations; it seems likely that only a single intermediate is involved in the product-determining steps.[37]

(d) The slope of the plot in Figure 9 gives the reactivity ratio of disilane to silane which is 2.8 ± 0.5. The ratio of hydrogens in the two molecules is 1.5, so disilane is apparently twice as reactive as silane

(37) It can easily be shown that if to a second intermediate Y is ascribed all the reactions of X, but with different relative rate constants, then product yields, relative and absolute, will depend on the relative amounts of X and Y formed.

on a perhydrogen basis. Two explanations seem possible:[3] (1) Si–H bonds of disilane may be weaker than those of silane[38] thus facilitating Si–H insertion by $^{31}SiH_2$; and (2) $^{31}SiH_2$ might insert into the Si–Si bond of disilane as well as into the Si–H bonds.[3,35] Only a degradation experiment to locate the ^{31}Si in the radioactive trisilane product will directly indicate whether Si–Si insertion occurs.

$$^{31}SiH_2 + Si_2H_6 \xrightarrow[\text{insertion}]{\text{Si–H}} H_3{}^{31}SiSiH_2SiH_3 \quad (40)$$

$$^{31}SiH_2 + Si_2H_6 \xrightarrow[\text{insertion}]{\text{Si–Si}} H_3Si^{31}SiH_2SiH_3 \quad (41)$$

The minimum kinetic scheme can be corrected by taking into account the fact that the formation of radioactive trisilane from silane is second order in silane concentrations, as shown by Figure 2.

$$X + SiH_4 \xrightarrow{k_1} a^{31}SiH_4 + b^{31}SiSiH_6 \quad (42)$$

$$Y + 2SiH_4 \xrightarrow{k_3} {}^{31}SiSi_2H_8 \quad (43)$$

$$X + SiH_6 \xrightarrow{k_2} d^{31}SiH_4 + e^{31}SiSiH_6 + f^{31}SiSi_2H_8 + g^{31}SiSi_{>2}H_{>8} \quad (44)$$

Let us introduce the simplifying assumption that Y and X are produced in constant ratio, that is

$$[Y] = m[X] \quad (45)$$

Then it can be shown that in the absence of disilane the following product ratio should be obtained

$$\frac{^{31}SiSi_2H_8}{^{31}SiSiH_6} = \frac{mk_3}{k_1}[SiH_4] \quad (46)$$

Data from phosphine–silane mixtures at constant total pressure are given in Figure 10 plotted according to the equation above. The plot appears linear with zero intercept and the slope gives an experimental value for the quantity mk_3/k_1. Then for phosphine–silane–disilane mixtures the following new function can be derived relating the product ratio to the substrate ratio

$$\frac{d[^{31}SiSiH_6]}{dt} = \{bk_1[SiH_4] + ek_2[Si_2H_6]\}[X] \quad (47)$$

$$\frac{d[^{31}SiSi_2H_8]}{dt} = k_3[Y][SiH_4]^2 + fk_2[X][Si_2H_6] \quad (48)$$

Introducing eq 45 as an assumption one obtains by integration of eq 47 and 48 the product ratio

$$\frac{^{31}SiSi_2H_8}{^{31}SiSiH_6} = \frac{mk_3[SiH_4]^2 + fk_2[Si_2H_6]}{bk_1[SiH_4] + ek_2[Si_2H_4]} \quad (49)$$

Rearrangement of eq 49 gives

$$\frac{b(^{31}SiSi_2H_8/^{31}SiSiH_6) - (mk_3/k_1)[SiH_4]}{f - e(^{31}SiSi_2H_8/^{31}SiSiH_6)} = \frac{k_2[Si_2H_6]}{k_1[SiH_4]} \quad (50)$$

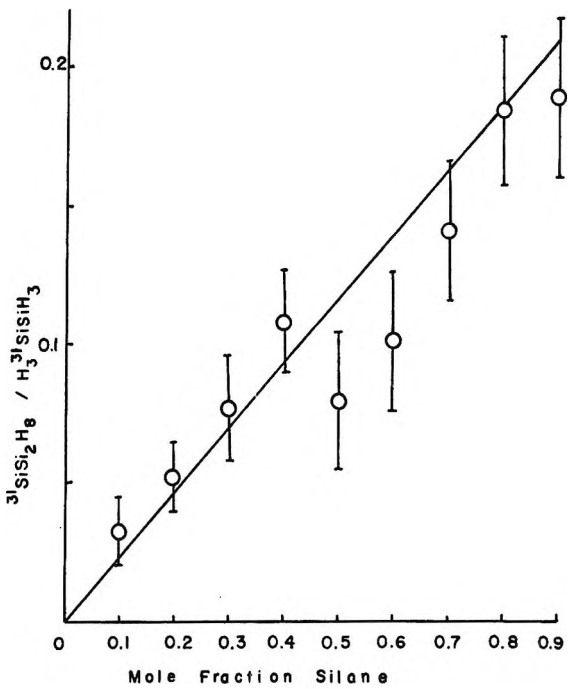

Figure 10. Variation of trisilane to disilane product yield ratio from phosphine–silane mixtures with composition at constant total pressure (1000 Torr). Product yields shown in Figure 1.

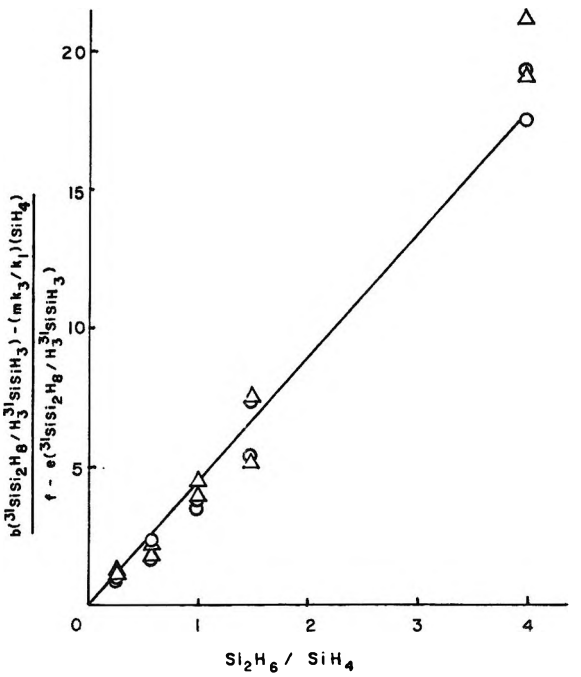

Figure 11. Variation of product ratio function (left-hand side of eq 50) as a function of substrate ratio. Data from Figure 5 are represented by circles, from Figure 6 by triangles. Figure 10 provides the quantity mk_3/k_1.

The plot of this function is shown in Figure 11, use having been made of the quantity mk_3/k_1, the slope of the line in Figure 10, and of the constants b and f

(38) R. P. Hollandsworth and M. A. Ring, *Inorg. Chem.*, 7, 1635 (1968).

derived from binary mixtures. The product ratios are taken from the data of Figures 5 and 6.

While this plot is also linear there is no obvious improvement over the plot of eq 39 shown in Figure 9. It is probable that the experimental error is larger than the possible correction. It is clear that the correction due to the inclusion of eq 43 in the kinetic scheme is small since the ratio of $^{31}SiSi_2H_8/^{31}SiSiH_6$ from the phosphine–silane mixtures is less than 0.2 even at 90% silane.

Having seen that phosphine–silane–disilane mixtures give product yields which are in agreement with the simple kinetic scheme given by eq 42, 43, and 44, it was thought desirable to determine whether the same kinetic scheme would rationalize product yields from mixtures containing scavenger. In binary phosphine–silane systems the presence of a few % nitric oxide has been shown to decrease yields of volatile products by *ca.* 40% without changing product ratios.[2]

The yield *vs.* composition curves (Figure 7) for the series of experiments on mixtures containing 200 Torr (19.6%) of PH_3 and 800 Torr (78.4%) of silane and disilane and 20 Torr (1%) of NO are similar in form to those obtained in the absence of NO (Figures 5 and 6). Thus even in ternary mixtures of phosphine, silane, and disilane, nitric oxide decreases absolute yields without affecting relative product yields. This is underlined by subjecting the data of Figure 7 to kinetic analysis by plotting the product ratio *vs.* substrate ratio function, eq 39. The result, shown in Figure 12 is a straight line with slope 2.5 ± 0.5, identical within experimental error to that found in the absence of NO. That the relative reactivity of SiH_4 and Si_2H_6 does not change in the presence of scavenger even though absolute product yields decrease suggests that at the point in the reaction sequence at which scavenging occurs, a single intermediate is involved rather than several intermediates.

Formation of Silane and Other Lower Homologs of Major Products. The present model for the formation of major products in the reactions of recoiling silicon atoms in mixtures of phosphine and silane, disilane, and trisilane consists of insertion of $^{31}SiH_2$ into silicon–hydrogen bonds. Previously the formation of radioactive silane caused embarrassment, since silane is obviously not a direct product of a silylene reaction unless path b is operative. Since radioactive silyl radicals are believed to be unimportant as reaction intermediates, mechanism a is also excluded as a source of radioactive silane. The same intermediate is believed to be the precursor of radioactive silane and disilane in the phosphine–silane system. This is confirmed by scavenger experiments in which the silane–disilane ratio stays the same even though the total yields decrease by *ca.* 45%. If the common precursor of radioactive silane and disilane is $^{31}SiH_2$, then what is suggested is the conversion of $^{31}SiH_2$ to $^{31}SiH_4$ without the intervention of $^{31}SiH_3$. This had been recognized before the details of such a reaction were known.[2]

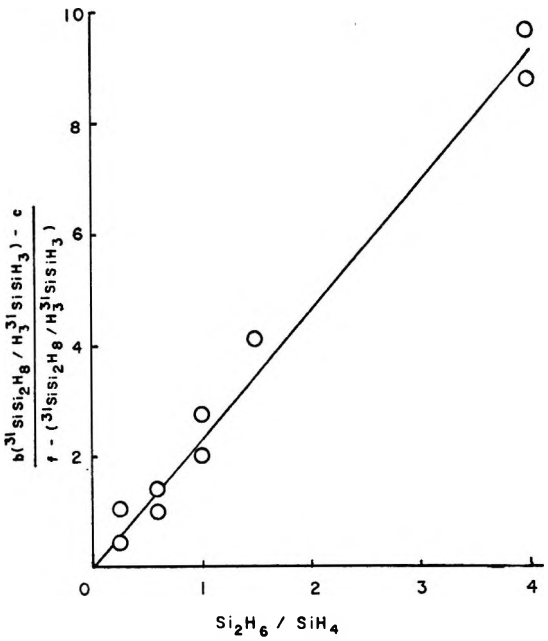

Figure 12. Variation of product function ratio (left-hand side of eq 39) as a function of substrate ratio from phosphine–silane–disilane–nitric oxide mixtures. The product yield data for the same experiments are shown in Figure 7.

The most plausible explanation for the formation of silane from the reactions of recoiling silicon atoms in phosphine–silane mixtures comes from the finding by several groups that disilane suffers pyrolysis to silane and silylene.[33,39,40]

$$Si_2H_6 \longrightarrow SiH_2 + SiH_4 \qquad (51)$$

This suggests a reasonable mechanism for the formation of radioactive silane from $^{31}SiH_2$ and SiH_4 without the intervention of $^{31}SiH_3$. The insertion of $^{31}SiH_2$ into an Si–H bond of SiH_4 to form disilane is exothermic, and the initially vibrationally "hot" disilane must be collisionally deactivated or it will dissociate. If the unsymmetrical cleavage yields $^{31}SiH_2$ then the insertion has simply undergone reversal. If nonradioactive silylene is produced, then radioactive silane has also been formed

$$^{31}SiH_2 + SiH_4 \rightleftharpoons (H_3{}^{31}SiSiH_3)^* \longrightarrow SiH_2 + {}^{31}SiH_4$$
$$\xrightarrow[\text{stabilization}]{} H_3{}^{31}SiSiH_3 \qquad (52)$$

Evidence for this mechanism is found in the pressure dependence of product yields from 1:1 phosphine–silane mixtures, Figure 8. When corrected for recoil loss, the absolute yield of radioactive silane *increases* with decreasing pressure, while the disilane yield (and

(39) E. M. Tebben and M. A. Ring, *Inorg. Chem.*, 8, 1787 (1969).
(40) P. Estacio, M. D. Sefcik, E. K. Chan, and M. A. Ring, *ibid.*, 9, 1068 (1970).

the trisilane yield) decreases. A similar mechanism explains the formation of radioactive silane *and* disilane from phosphine–disilane mixtures and silane, disilane, and trisilane from phosphine–trisilane mixtures.

Summary

We have presented the results of product studies and competition experiments on the reactions of recoiling silicon atoms with mixtures of phosphine and various silanes. In terms of these results we have discussed five possible mechanisms for the formation of the major products, which are the next higher homologs of the silane substrate. The products formed are in accord with the insertion by $^{31}SiH_2$ being the predominant product forming step (path c). This insertion reaction was initially suggested by us on the basis of preliminary experiments, but has in the intervening 5 years become well established in pyrolysis and photolysis experiments by other workers. While a coupling mechanism involving $^{31}SiH_3$ (path d) can be ruled out by the combined evidence of product studies and the earlier scavenger experiments, other mechanisms have also been considered and rejected. A reaction sequence whose last step is abstraction of a single hydrogen atom (path a) is rejected on the basis of the scavenger experiments. Another mechanism involving abstraction of two hydrogens as the last step (path b) is ruled out by the formation of the silylene insertion product from substrates without two labile hydrogens. The mechanism requiring pseudo-insertion by a silyl radical (path e) is precluded by the scavenger experiments. Competition experiments between silane and disilane indicate that a kinetic scheme including a single intermediate in product-determining steps suffices to describe the phosphine–silane–disilane system. That intermediate may be safely regarded as $^{31}SiH_2$.

In a future paper the question of the primary steps in recoiling silicon reactions will be taken up. We will provide evidence for a primary mechanism consisting largely of insertion reactions. Thus the formation of trisilane in silane–phosphine mixtures, reported in this paper but not explained, is believed to be due to two consecutive insertion reactions

$$^{31}Si + SiH_4 \longrightarrow (H\text{-}^{31}Si\text{-}SiH_3)^* \xrightarrow{\text{stabilization}} H\text{-}^{31}Si\text{-}SiH_4$$

$$\downarrow$$

$$H\text{-}^{31}Si \longrightarrow \longrightarrow {}^{31}SiH_2 \qquad (53)$$

$$\uparrow$$

$$^{31}Si + PH_3 \longrightarrow (H\text{-}^{31}Si\text{-}PH_2)^* \xrightarrow{\text{stabilization}} H\text{-}^{31}Si\text{-}PH_3$$

$$H\text{-}^{31}Si\text{-}SiH_3 + SiH_4 \longrightarrow H_3Si^{31}SiH_2SiH_3 \qquad (54)$$

Acknowledgments. Without the influence of the late Professor Richard Wolfgang, this work would never have been undertaken and without his ideas the work could not have been carried out. His intellectual and material assistance and most of all his enthusiasm leave us greatly in his debt. Encouragement from and valuable discussions with Dr. Alfred Wolf and Professor Michael J. Welch are much appreciated, as is the continued interest by Dr. William C. Eckelman, who began these experiments. Mr. John Hood designed the fast-neutron target assembly and has supervised the irradiations. Dr. Gerald W. Stewart assisted in the determination of absolute yields.

Thermodynamics of Transfer of Tetrabutylammonium Bromide from Water to Aqueous Urea Solutions and the Effects on the Water Structure

by T. S. Sarma and J. C. Ahluwalia*

Department of Chemistry, Indian Institute of Technology, Kanpur-16, India *(Received March 22, 1971)*

Publication costs borne completely by The Journal of Physical Chemistry

The enthalpies (at 25 and 35°) and the partial molal heat capacities (at 30°) of transfer of Bu_4NBr from water to aqueous urea solutions (up to 10 *m*) have been determined calorimetrically. The entropies of transfer are obtained by combining the enthalpies of transfer with the free energies of transfer reported in the literature. The results show that transfer of Bu_4NBr from water to aqueous urea solutions is accompanied by a negative free energy change, positive enthalpy and entropy changes, and a decrease in partial molal heat capacity. The results are consistent with the view that solutes containing nonpolar groups find aqueous urea less structured than pure water. The effect of urea breaking down water structure, which seems to be significant only at higher concentrations of urea, increases with the increase in concentration reaching saturation effect around 10 *m*. The implication of the results on the role of urea causing denaturation of proteins has been discussed.

Introduction

The role of urea in affecting the structure of water has been critically analyzed recently by Holtzer and Emerson.[1] The pertinent references on the various studies on the urea–water binary system have been listed in our previous papers.[2,3] Our studies[2,3] on the nmr and the excess partial molal heat capacities of the urea class of protein denaturants have led us to suggest that urea does not appear to alter water structure significantly, and if the water structural changes play an important role in the denaturation of proteins by urea, then it is more likely that urea modifies the water structure in the presence of proteins. It would then seem more relevant and fruitful to study the transfer behavior of model compounds containing large nonpolar groups (structure-making solutes) from water to aqueous urea solutions containing large concentration of urea. A number of studies in this direction[4-9] support the contention that urea behaves as a structure breaker. The studies[10,11] on the transfer behavior of structure-breaking solutes like common electrolytes from water to concentrated urea solutions also lead to the same conclusion that urea breaks water structure. Recent studies on the activity coefficients of the water–urea–Bu_4NBr ternary system by Wen and Chen[12] have led them to suggest that the lowering of the activity coefficients of urea and Bu_4NBr in the urea–water–Bu_4NBr ternary system may be due to either the water-structure-breaking effect of urea or to the formation of some complexlike aggregates between urea and R_4N^+ salts in aqueous solution.

In this paper, we have reported the results on the enthalpies, entropies, and heat capacities of transfer of Bu_4NBr from water to aqueous urea solutions (up to 10.2 *m*), and we find that urea does behave as a structure breaker (the structure-breaking effect of urea increasing with concentration) in the ternary system of urea–water–Bu_4NBr. The implication of this is discussed in the denaturation of proteins by urea.

Experimental Section

The submarine calorimeter and the operational procedure used for the measurements of the integral heats of solution have been described previously.[13,14] The temperature of the thermostat was maintained to ±0.002°. Electronic amplification was used with a thermistor as the temperature-sensing device. With this calorimeter a temperature difference of the order of 2×10^{-5}° could be detected. The calorimeter was calibrated by measuring heats of solution of KCl

(1) A. Holtzer and M. F. Emerson, *J. Phys. Chem.*, **73**, 26 (1969).

(2) S. Subramanian, D. Balasubramanian, and J. C. Ahluwalia, *ibid.*, **73**, 266 (1969).

(3) S. Subramanian, T. S. Sarma, D. Balasubramanian, and J. C. Ahluwalia, *ibid.*, **75**, 815 (1971).

(4) P. L. Whitney and C. Tanford, *J. Biol. Chem.*, **237**, PC 1735 (1962); Y. Nozaki and C. Tanford, *ibid.*, **238**, 4074 (1963).

(5) D. B. Wetlaufer, S. K. Malik, L. Stoller, and R. L. Coffin, *J. Amer. Chem. Soc.*, **86**, 508 (1964).

(6) G. C. Kresheck and L. Benjamin, *J. Phys. Chem.*, **68**, 2476 (1964).

(7) W. A. Hargraves and G. C. Kresheck, *ibid.*, **73**, 3249 (1969).

(8) F. Franks and D. L. Clarke, *ibid.*, **71**, 1155 (1967).

(9) H. S. Frank and F. Franks, *J. Chem. Phys.*, **48**, 4746 (1968).

(10) J. H. Stern and D. J. Kulluck, *J. Phys. Chem.*, **73**, 2795 (1969).

(11) G. A. Vidulich, J. R. Andrade, P. P. Blanchette, and T. J. Gilligan, III, *ibid.*, **73**, 1621 (1969).

(12) W. Y. Wen and C. L. Chen, *ibid.*, **73**, 2895 (1969).

(13) S. Subramanian and J. C. Ahluwalia, *ibid.*, **72**, 2525 (1968).

(14) T. S. Sarma, R. K. Mohanty, and J. C. Ahluwalia, *Trans. Faraday Soc.*, **65**, 2333 (1969).

Table I: Enthalpies and Heat Capacities of Transfer of Bu_4NBr from Water to Aqueous Urea

Urea, m	25.0° $\Delta\bar{H}_s°$, cal mol^{-1}	25.0° ΔH_{tr}, cal mol^{-1}	35.0° $\Delta\bar{H}_s°$, cal mol^{-1}	35.0° ΔH_{tr}, cal mol^{-1}	30.0° $\Delta C_{p_{tr}}$, cal deg^{-1} mol^{-1}
0	-2050 ± 15[a]		-260 ± 15[a]		0
2.20	-1319 ± 29	731 ± 19[b]	246 ± 18	506 ± 23	-22 ± 3
4.89	-815 ± 19	1235 ± 25	593 ± 10	855 ± 18	-38 ± 3
8.01	-427 ± 23	1623 ± 20	761 ± 25	1021 ± 30	-60 ± 4
10.20	-343 ± 24	1707 ± 28	796 ± 18	1056 ± 24	-65 ± 4

[a] Values in pure water taken from ref 14. [b] Uncertainty (std dev) in ΔH_{tr} was calculated as $e\Delta\bar{H}_{tr} = [(e\Delta\bar{H}_s°)^2 + (e\Delta H_s°)^2]^{1/2}$.

in water and of THAM (tris(hydroxymethyl)aminomethane) in 0.1 *N* HCl. The values obtained were in good agreement (within 0.2%) with those reported by Gunn.[15]

Bu_4NBr was obtained from Eastman Organic Chemicals. It was recrystallized by the method reported in the literature.[16] The recrystallized salt was dried *in vacuo* at 60–80°. Urea was obtained from BDH Ltd. (AR grade, assay >99.5%) and was used as such. Calorimetric measurements were made with freshly prepared urea solutions.

Results

The partial molal heats of solution $\Delta\bar{H}_s$ of Bu_4NBr in 2.20, 4.89, 8.01, and 10.2 *m* aqueous urea solutions at 25 and 35° are given as supplementary material.[17] Since the concentration of Bu_4NBr in aqueous urea solution (0.0007–0.0035 *m*) was close to infinite dilution, any small concentration dependence of heats of solution $\Delta\bar{H}_s$ being within the experimental error, the partial molal heat of solution at infinite dilution, $\Delta\bar{H}_s°$, was taken to be the average of a number of $\Delta\bar{H}_s$ measurements. The $\Delta\bar{H}_s°$ values of Bu_4NBr in 2.2, 4.89, 8.01, and 10.2 *m* aqueous urea solutions at 25 and 35° are listed in Table I along with the values in pure water reported earlier from this laboratory.[14] The uncertainty in the $\Delta\bar{H}_s°$ values is expressed as standard deviation from the mean value. The $\Delta\bar{H}_s°$ values of Bu_4NBr in aqueous urea solutions at 25° are in fairly good agreement with those reported by Cassel and Wen.[18] The enthalpies of transfer, ΔH_{tr} (at 25 and 35°), and partial molal heat capacities of transfer, $\Delta C_{p_{tr}}$ at 30° from water to aqueous urea solutions were derived from these data and are listed in Table I. The recently reported[12] free energies of transfer of Bu_4NBr from water to aqueous urea solutions (up to 5 *m*) at 25° are plotted as a function of molality of urea in Figure 1 and extrapolated to 8 *m* urea. The values of free energies of transfer, ΔG_{tr}, thus obtained (up to 8 *m* urea) are listed in column 2 of Table II. In Figure 1 are also plotted the enthalpies of transfer, ΔH_{tr}, at 25 and 35° given in Table I as a function of concentration of urea up to 10.2 *m*, and the interpolated values at 25° are given in column 3 of Table II. By combining these enthalpies of transfer, ΔH_{tr}, at 25°, with free energies of transfer, ΔG_{tr}, at 25°, the entropies of transfer at 25° were derived and are listed in column 4 of Table II. The values of the partial molal heat capacity transfer, $\Delta C_{p_{tr}}$ (up to 10.2 *m*) at 30° are plotted as a function of molality of urea in Figure 2, and the smoothed and interpolated values are given in column 5 of Table II.

Table II: Thermodynamics of Transfer of Bu_4NBr from Water to Aqueous Urea

Urea, m	ΔG_{tr}[a](25°), cal mol^{-1}	ΔH_{tr}[b](25°), cal mol^{-1}	ΔS_{tr}[c](25°), cal deg^{-1} mol^{-1}	$\Delta C_{p_{tr}}$[d](30°), cal deg^{-1} mol^{-1}
1	-133	396	1.8	-10.5
2	-247	680	3.1	-19.5
3	-345	910	4.2	-27
4	-430	1095	5.1	-34
5	-507	1235	5.8	-40.5
6	-575	1300	6.3	-46.5
8	-704	1600	7.7	-57.5
10		1715		-66.5

[a] ΔG_{tr} values were obtained by plotting the ΔG_{tr} values reported in ref 12 as a function of molality and extrapolating to 8 *m* urea. [b] ΔH_{tr} values given in Table I were plotted as a function of molality of urea (see Figure 1), and smoothed out values are given here. The estimated uncertainty (standard deviation) in ΔH_{tr} values is ±25 cal mol^{-1}. [c] Derived from ΔG_{tr} and ΔH_{tr} values given in columns 1 and 2. The estimated uncertainty (standard deviation) in ΔS_{tr} values is ±0.1 eu. [d] Smoothed-out values from Figure 2. The estimated uncertainty (standard deviation) in $\Delta C_{p_{tr}}$ values is ±3 cal deg^{-1} mol^{-1}.

Discussion

The results given in Table II and Figures 1 and 2 show that the transfer of the highly structure-making solute Bu_4NBr[13] from water to aqueous urea is accom-

(15) S. R. Gunn, *J. Phys. Chem.*, **69**, 2902 (1965)

(16) A. K. R. Unni, L. Elias, and H. I. Schiff, *ibid.*, **67**, 1216 (1963).

(17) The detailed listing of the values of partial molal heats of solution $\Delta\bar{H}_s$ will appear immediately following these pages in the microfilm edition of this volume of the journal. Single copies may be obtained from the Business Operations Office, Books and Journals Division, American Chemical Society, 1155 Sixteenth St., N.W., Washington, D. C. 20036, by referring to code number JPC-72-1366. Remit check or money order for $3.00 for photo copy or $2.00 for microfiche.

(18) R. B. Cassel and W. Y. Wen, *J. Phys. Chem.*, **76**, 1369 (1972).

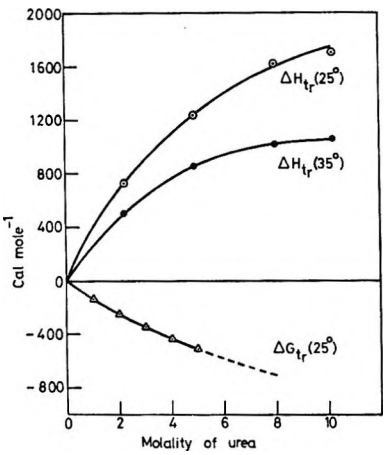

Figure 1. The free energies and enthalpies of transfer of Bu_4NBr from water to aqueous urea solutions as a function of molality of urea: (△) ΔG_{tr} at 25°, (○) ΔH_{tr} at 25°, (●) ΔH_{tr} at 35°.

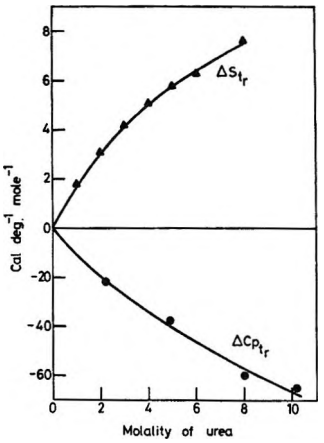

Figure 2. The partial molal heat capacity and entropies of transfer of Bu_4NBr from water to aqueous urea solutions as a function of molality of urea: (▲) ΔS_{tr} at 25°, (●) $\Delta C_{p_{tr}}$ at 30°.

panied by a negative free energy change, positive enthalpy and entropy changes, and a decrease in partial molal heat capacity. The effect on these transfer thermodynamic functions increases with the increase in the urea concentration, reaching almost maximum effect around 10 *m* urea. The enthalpies of transfer of Bu_4NI and Am_4NI from water to 7 *M* aqueous urea as obtained from solubility studies by Franks and Clarke[8] are also positive, though less in numerical value, but are of the same order of magnitude as our calorimetric values.

The positive entropy change and negative partial molal heat capacity change (see Figure 2) of Bu_4NBr from water to aqueous urea solutions indicate that Bu_4NBr finds aqueous urea as less structured than pure water. The $\Delta C_{p_{tr}}$ values (see Table II and Figure 2) indicate that with increasing concentration of urea the structure of aqueous urea solution decreases appreciably, reaching the saturation effect around 10 *m*. In 10 *m* aqueous urea solution, the excess partial molal heat capacity and therefore the structure-making capacity of Bu_4NBr is reduced by about one-third its capacity in pure water.

Recently Wen and Chen[12] have reported that their activity coefficient results of water–urea–Bu_4NBr and water–urea–Me_4NBr could be explained on the basis of either (i) that urea breaks water structure or (ii) that urea forms complexes with R_4N^+ salts in aqueous solutions. Assuming that complex formation is accompanied by a decrease in entropy, the positive enthalpies of transfer of Bu_4NBr from water to aqueous urea rule out the complex formation of urea with Bu_4NBr in aqueous urea, thus favoring the other possibility that urea breaks water structure.

The results of this study are also consistent with those of earlier studies[4-8] on calorimetry, solubility and partial molal volume of solutes containing nonpolar groups such as hydrocarbons, amino acids, as well as studies on calorimetry and viscosity of common electrolytes.[10,11] The calorimetric investigations on the transfer of amino acids from water to 6 *M* urea by Kresheck and Benjamin[6] show that the transfer (except in the case of glycine which is a structure-breaking solute) is accompanied by decrease in free energy, enthalpy, and partial molal heat capacity and increase in entropy. However, the increase in nonpolar side chain of the amino acids was found to increase the enthalpy (less negative) and entropy of transfer while further decreasing the partial molal heat capacity.[6] It was shown by these workers that the effect of an increase in the nonpolar side chain in an amino acid by an isobutyl group was to increase the enthalpy of transfer by 833 cal mol^{-1}, increase the entropy of transfer by 3.5 eu, and decrease the partial molal heat capacity by 37 cal deg^{-1} mol^{-1}. This is the same trend as found for an R_4NBr salt, indicating that the effect of the transfer of the nonpolar groups in different aliphatic compounds from water to aqueous urea solutions may be comparable and possibly involve the same mechanism.

Wetlaufer, *et al.*,[5] from their solubility studies of hydrocarbons showed that the transfer of hydrocarbons from water to 7 *M* urea is accompanied by a negative change in free energy and a positive change in enthalpy, which is consistent with our results and supports the contention that R_4N^+ salts behave as soluble hydrocarbons. Frank and Franks[9] have recently proposed a model to account quantitatively for the results of Wetlaufer, *et al.*, on the solubilities of hydrocarbons in water and 7 *M* aqueous urea solutions. They have suggested that the effect of urea on the water structure is rather subtle in the sense that it acts as a statistical structure breaker, unlike the structure-breaking action by ions of common electrolytes. They have given the details in their model as to how this is brought about.[9]

The statistical structure-breaking effect of urea on water seems to be consistent with our previous studies[2,3] in the water–urea binary system, where it was shown that addition of small amounts of urea did not alter the water structure, as well as being consistent with the present study in the ternary system of water–urea–Bu_4NBr, which shows that the structure-breaking effect of urea increases appreciably with increasing concentration until reaching almost saturation limit around 10 m ($\sim$7 M), where the water to urea ratio is about 6 to 1.

If a concentrated aqueous urea solution is less structured than pure water, then the addition of structure-breaking solutes such as common electrolytes should be accompanied by a decrease in their structure-breaking capacity. In other words, the transfer of structure-breaking solutes from water to aqueous urea solutions should be accompanied by a positive standard free energy change and negative standard enthalpy and entropy changes and an increase in standard partial molal heat capacity. One indeed finds evidence in support of this in the limited studies in this direction.[10]

The importance of the role of the effect of urea on the water structure in the denaturation of proteins cannot be stated with certainty at this stage. It may be, as has been suggested earlier by many workers, that as a consequence of the weakening of hydrophobic forces the solvation of the denatured form of the protein is favored in aqueous urea solution. If the structure-breaking effect of urea plays an important part in denaturation, then the mechanism of its structure breaking, as has been suggested earlier in this paper, should be different from that of ions of common electrolytes. The idea of urea acting as statistical structure breaker, suggested by Frank and Franks,[9] which is supported by our observation, needs to be verified by further calorimetric and other investigations on the effect of the transfer of solutes, from water to concentrated aqueous urea solutions, as well from water to concentrated aqueous solutions of structure-breaking solutes such as common electrolytes.

Acknowledgment. We are thankful to the Council of Scientific and Industrial Research, India, for part of the financial support.

Thermodynamics of Transfer of Three Tetraalkylammonium Bromides from Water to Aqueous Urea Solutions at 25° [1]

by R. Bruce Cassel and Wen-Yang Wen*

Jeppson Laboratory, Chemistry Department, Clark University, Worcester, Massachusetts 01610 *(Received April 21, 1971)*

Publication costs assisted by the National Science Foundation

The heats of solution of tetramethyl-, tetraethyl-, and tetrabutylammonium bromides have been measured in water and in aqueous urea solutions of different concentrations. The measurements were carried out over a salt concentration range of 0.001–0.1 m in order to observe the effect of urea on the apparent molal heat content and to aid in the extrapolation to infinite dilution. The enthalpies of transfer from water to aqueous urea were calculated and were combined with free energies of transfer of the tetramethyl- and tetrabutylammonium salts to give entropies of transfer. While the free energies of transfer for the two salts are both small negative, the enthalpy and entropy of transfer of tetramethylammonium bromide were found to be large negative, and those of tetrabutylammonium bromide large positive. These contrasting results are discussed in terms of changes in water structure induced by urea and by the tetraalkylammonium ions. Our results support models of urea as a water-structure breaker.

Introduction

The investigation of the changes in the conformational structure of proteins induced by added solute in solution has stimulated interest in studies of electrolytes and nonelectrolytes in water.[2] In order to acquire a meaningful model for the structural changes taking place at the protein–solvent interface and in the regions surrounding ions, it has been useful to study simple two-component systems. From studies of the tetra-

(1) Abstracted in part from Ph.D. thesis of R. B. Cassel, Clark University, 1971.

(2) W. Kauzmann, *Advan. Protein Chem.*, **14**, 1 (1959).

alkylammonium salts, for instance, have come many interesting insights into the complex structural changes taking place in water as a result of the presence of various ions.[3]

As a necessary link between the basic two-component systems and the much more complex biological systems, the investigation of multicomponent systems has begun to net information about solute–solute interactions.[4,5] In particular, the effects of aqueous urea on various solutes containing nonpolar groups have been a stimulating subject of investigations.[6-10] Despite a large amount of experimental data available on the simpler urea–water system,[11] there exist divergent views on the effect of urea upon the structure of water.[10,12-14]

In our previous study, urea has been found to lower the activity coefficients of tetraalkylammonium salts in aqueous solution.[15] The lowering of the activity coefficients of both urea and salts could be due either to the water-structure breaking effect of urea or to the formation of some complexlike aggregates. Since a test to choose between these two explanations may lie in the enthalpy of transfer from water to aqueous urea, we explore in this paper the effect of urea on the heats of solution and heats of dilution of three contrasting tetrallkylammonium bromides.

Experimental Section

Materials. Tetraalkylammonium halides were obtained from Eastman Kodak Co. and were recrystallized twice from the following solvent systems before use: ethanol–methanol for $(CH_3)_4NBr$ and acetone–ether for $(C_2H_5)_4NBr$ and $(C_4H_9)_4NBr$. Water used was distilled and deionized, having a specific conductance of less than 1×10^{-6} ohm^{-1} cm^{-1}. Reagent grade urea was obtained from Fisher Scientific Co. and was recrystallized twice from methanol. Urea solutions were prepared fresh each day, except for the 8.3 and 10.9 *m* urea solutions, which were used for two days.

The Calorimeter. This single-cell calorimeter, which has been described in detail elsewhere,[1] was designed to measure heats of solution and dilution or mixing. The calorimeter vessel consists of a 250-ml dewar attached at the top to a cyclindrical brass housing and brass tubes which extend above the surface of the bath. These contain the shaft of the stirring propellor, mechanical linkages for opening bulbs or pipets, and wiring (see Figure 1). A Peltier cooling device, powered by a precision power supply, is used to maintain the calorimeter a few thousandths of a degree below the bath temperature, thus counterbalancing the steady heat of stirring. The use of this cooler eliminates condensation effects in the chamber above the calorimeter, allows rapid temperature restoration after exothermic events, and facilitates the establishment of thermal equilibrium in preparation for calorimetric measurement. The temperature of the calorimeter solution

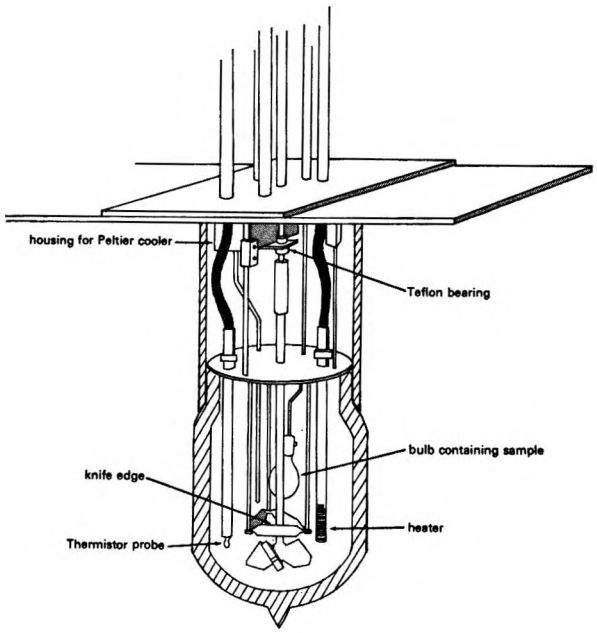

Figure 1. A schematic diagram showing a cross section of the submarine calorimeter.

is measured using a thermistor in a Wheatstone bridge circuit, the offbalance of which is amplified by a nanovolt null detector,[16] filtered, and recorded. The thermistor probe,[17] which consists of a 1000-ohm thermistor bead encased in a thin film of Teflon, has a heat dissipation constant of 8 mW/deg; this results in an internal heating of not more than a few ten thousandths of a degree.

The Wheatstone bridge employs resistance standards having a drift of less than 1 ppm/deg. All bridge connections are gold to gold and bolted in good thermal contact to a mutual heat sink. The bridge is temperature lagged, well shielded, and kept at low humidity. Under ideal conditions and complete ther-

(3) For a summary of references, see W. Y. Wen and J. H. Hung, *J. Phys. Chem.*, **74**, 170 (1970).

(4) For a summary of references, see R. H. Wood and P. J. Reilly, *Annu. Rev. Phys. Chem.*, **21**, 387 (1970).

(5) J. H. Stern and J. T. Swearingen, *J. Phys. Chem.*, **74**, 167 (1970).

(6) Y. Nozaki and C. Tanford, *J. Biol. Chem.*, **238**, 4074 (1963).

(7) G. C. Kresheck and L. Benjamin, *J. Phys. Chem.*, **68**, 2476 (1964).

(8) M. J. Schick and A. H. Gilbert, *J. Colloid Sci.*, **20**, 464 (1965).

(9) D. B. Wetlaufer, S. K. Malik, L. Stoller, and R. L. Coffin, *J. Amer. Chem. Soc.*, **86**, 508 (1964).

(10) H. S. Frank and F. Franks, *J. Chem. Phys.*, **48**, 4746 (1968).

(11) For a summary of references, see R. H. Stokes, *Aust. J. Chem.*, **20**, 2087 (1967).

(12) M. J. Schick, *J. Phys. Chem.*, **68**, 3585 (1964).

(13) M. Abu-Hamdiyyah, *ibid.*, **69**, 2720 (1965).

(14) A. Holtzer and M. F. Emerson, *ibid.*, **73**, 26 (1969).

(15) W. Y. Wen and C. M. L. Chen, *ibid.*, **73**, 2895 (1965).

(16) Keithley Nanovolt Null Detector, Model 147, Keithley Instruments, Inc., Cleveland, Ohio.

(17) Thermistor probe, Model 44103, Yellow Springs Instruments, Yellow Springs, Ohio.

mal equilibrium, the noise level corresponds to a temperature fluctuation of $\pm 2.5 \times 10^{-6}$°. For 13 duplicate heat capacity measurements, each resulting in a temperature change of 0.0225°, the heat capacity was obtained with a standard deviation of 0.074%, indicating a temperature resolution of 1.7×10^{-5}°. For smaller heat changes, this resolution approaches 2.5×10^{-6}°.

Standardization of Calorimeter. The calorimeter was standardized by measuring the heat of solution and neutralization of tris(hydroxymethyl)aminomethane (THAM) in excess 0.1 *M* hydrochloric acid. The hydrochloric acid was prepared by direct dilution of concentrated HCl solution. Fisher primary standard THAM was screened using 60- and 100-mesh screens. The crystals passing through the former and resting on the latter were dried at 80° for 48 hr *in vacuo* and loaded into thin-walled glass bulbs and sealed using epoxy.

The heat of reaction was obtained for seven samples and the results were corrected to 25.000° using the temperature derivatives ascertained by Irving and Wadso.[18] The average heat of neutralization at 25° was observed to be −7109 cal/mol, with a calculated 95% confidence level of ±8 cal/mol. This agrees well with other literature values of −7117,[19] −7107,[20] and −7104 cal/mol.[18]

Treatment of Data

The following diagram illustrates the thermodynamic processes under consideration.

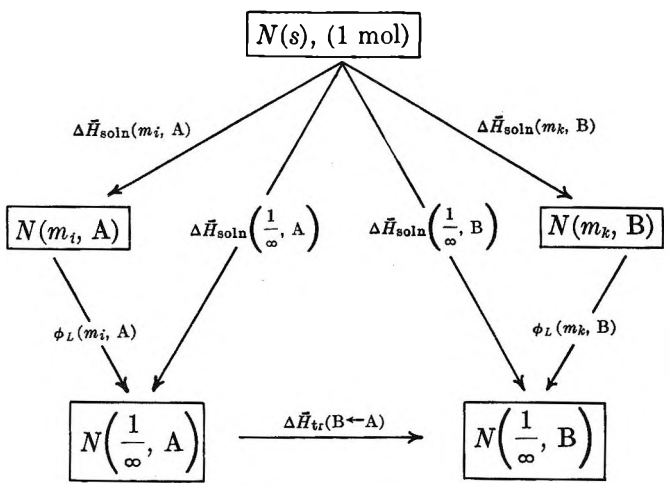

The molar heats of solution of a salt in a solution of m_i mol of salt per kilogram of solvent A, $\Delta\bar{H}_s(m_i, \text{A})$, is obtained directly from the i consecutive heats of solution by

$$\Delta\bar{H}_s(m_i, \text{A}) = \left(\sum_{j=1}^{i} Q_j\right) \Big/ \left(\sum_{j=1}^{i} N_j\right)$$

where Q_j is the experimental heat of solution, resulting from dissolving N_j mol of salt. $\Delta\bar{H}_s(1/\infty, \text{A})$, the molar heat of solution at infinite dilution, is obtained by fitting the $\Delta\bar{H}_s(m_i, \text{A})$ data to a smooth curve and extrapolating this curve to infinite dilution using a limiting law. Taking the value of $\bar{H}_s(1/\infty, \text{A})$ as zero on the heat scale gives $\phi_L(m_i, \text{A})$ directly.

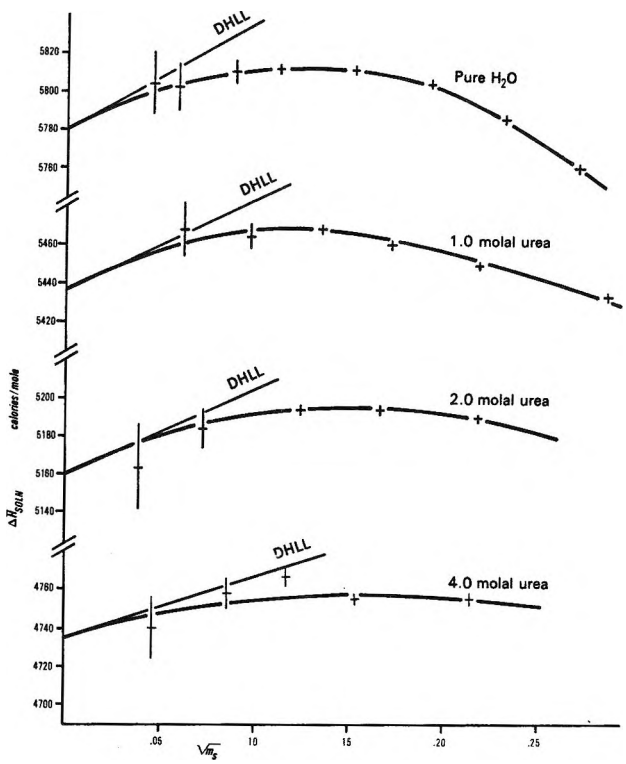

Figure 2. Enthalpy of solution of Me_4NBr in aqueous urea solutions plotted against the square root of salt molality at 25°.

From a correlative series of measurements, dissolving the salt in solvent B (also possibly a mixed solvent), $\Delta\bar{H}_s(1/\infty, \text{B})$ and $\phi_L(m_i, \text{B})$ are obtained. The enthalpy of transfer at infinite dilution to solvent B from solvent A can then be seen to be

$$\Delta\bar{H}_{tr}(\text{B} \longleftarrow \text{A}) = \Delta\bar{H}_s(1/\infty, \text{B}) - \Delta\bar{H}_s(1/\infty, \text{A})$$

Results

The calorimetric results obtained have been tabulated[21] and are shown in Figures 2–7. The uncertainty in the heat of solution for the ith consecutive sample bulb is given as

$$\delta_i = \left\{\sum_{j=1}^{i}\left[\left(0.001 + \frac{0.003}{Q_j}\right)\Delta\bar{H}_s(m_j)\right]^2\right\}^{1/2}$$

(18) R. J. Irving and I. Wadso, *Acta Chem. Scand.*, 18, 195 (1964).

(19) R. H. Wood, H. L. Anderson, J. D. Beck, J. R. France, W. E. deVry, and J. L. Soltzberg, *J. Phys. Chem.*, 71, 2149 (1967).

(20) S. R. Gunn, *ibid.*, 69, 2902 (1965).

(21) Experimental data on enthalpies of solution of tetraalkylammonium bromides in water and enthalpies of transfer of these salts from water to aqueous urea solutions at 25° will appear following these pages in the microfilm edition of this volume of the journal. Single copies may be obtained from the Business Operations Office, Books and Journals Division, American Chemical Society, 1155 Sixteenth Street, N.W., Washington, D. C. 20036, by referring to code number JPC-72-1369. Remit check or money order for $3.00 for photocopy or $2.00 for microfiche.

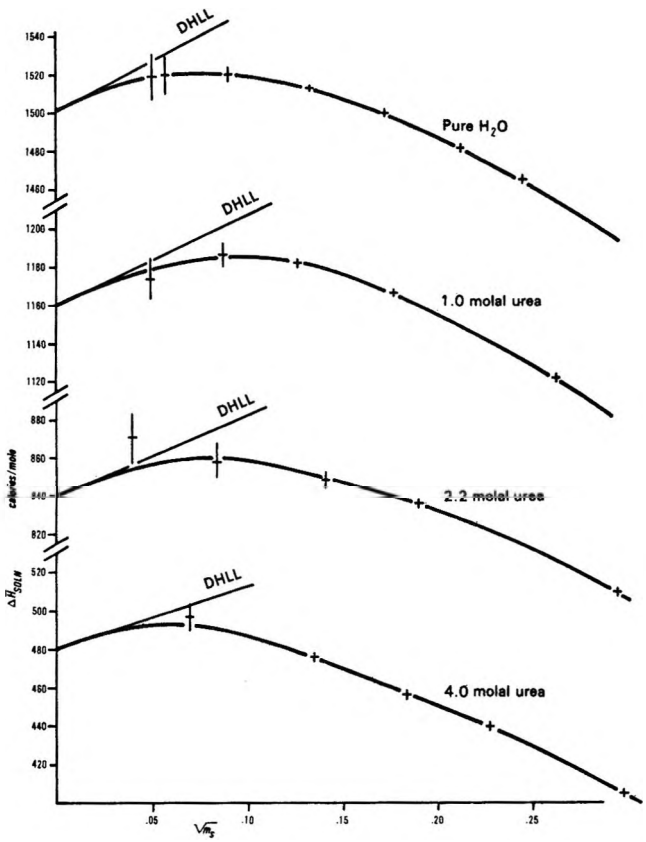

Figure 3. Enthalpy of solution of Et_4NBr in aqueous urea solutions plotted against the square root of salt molality at 25°.

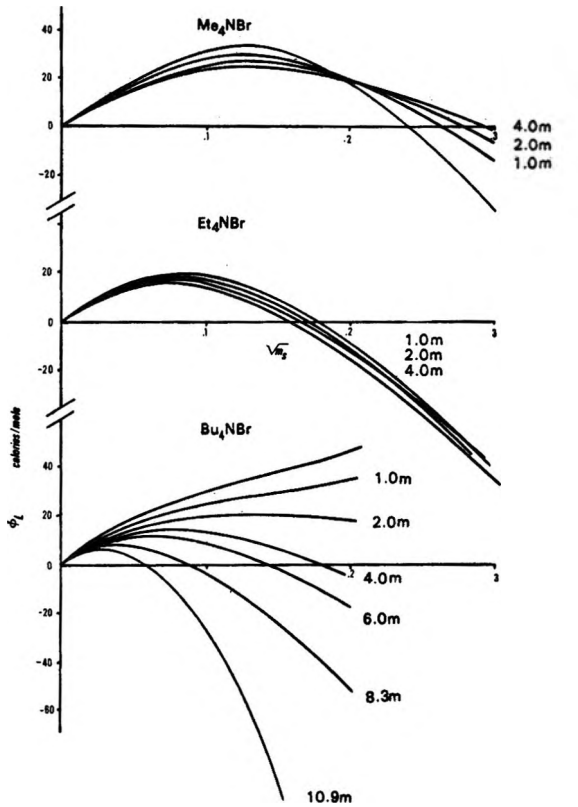

Figure 5. Apparent molal heat contents of tetraalkylammonium bromides in water and in aqueous urea solutions plotted against the square root of salt molality at 25°.

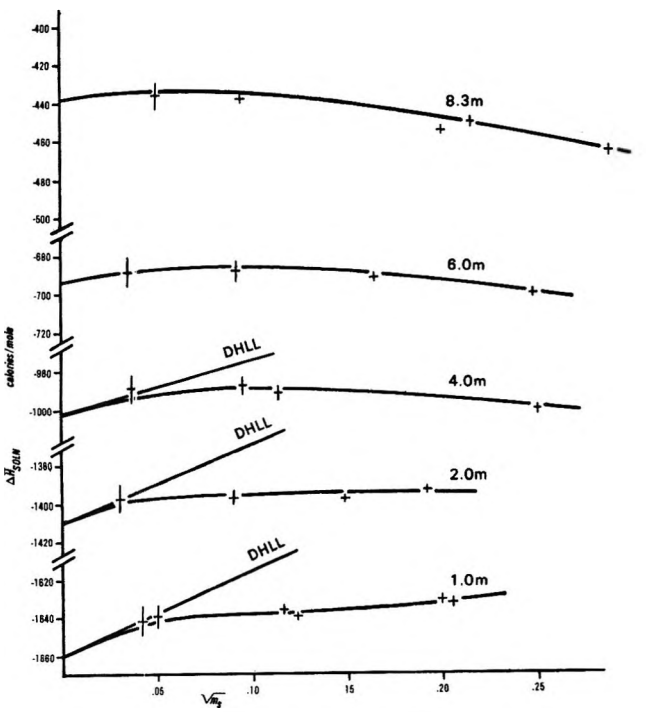

Figure 4. Enthalpy of solution of Bu_4NBr in aqueous solutions plotted against the square root of salt molality at 25°.

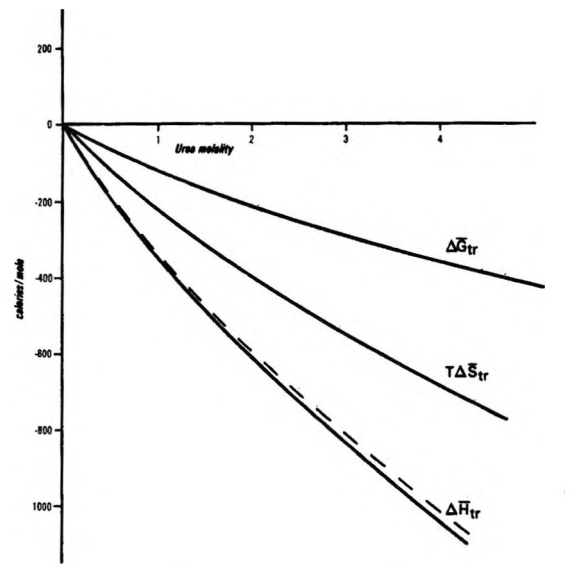

Figure 6. Thermodynamic transfer functions for Me_4NBr transferring from pure water to aqueous urea solutions plotted against urea molality at 25° (at infinite dilution of the salt); (- - - - -) Et_4NBr.

where Q_j is the experimental heat change on dissolution and $\Delta\bar{H}_s(m_j)$ is the enthalpy of solution per mole of salt. The first term arises from the uncertainty of temperature measurement (0.1%) and the second from the uncertainty (0.003 cal) in the heat of glass bulb opening. This uncertainty is indicated in Fig-

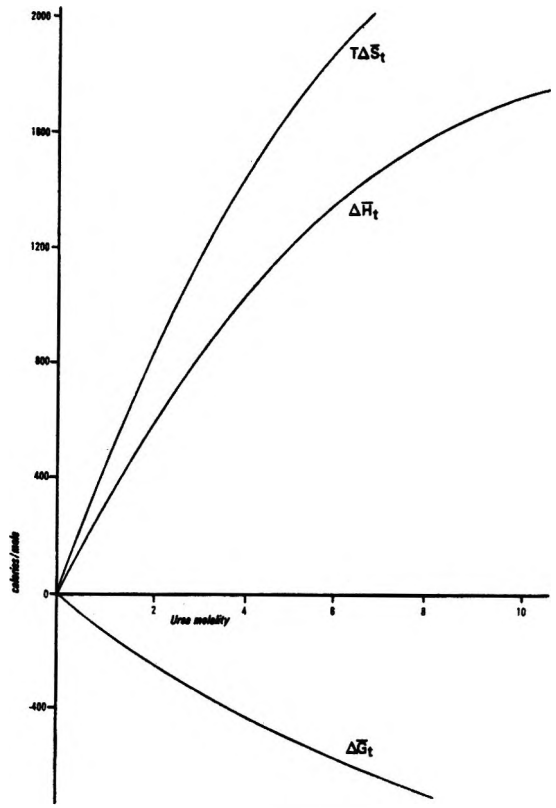

Figure 7. Thermodynamic transfer functions for Bu_4NBr transferring from pure water to aqueous urea solutions plotted against urea molality at 25° (at infinite dilution of the salt).

Table I: Enthalpies of Solution in and Enthalpies of Transfer to Aqueous Urea for Tetraalkylammonium Bromides at Infinite Dilution of Salt at 25°

	Urea, m[a]	$\bar{H}_{soln}(1/\infty)$, cal/mol	$\bar{H}_{tr}(1/\infty)$, cal/mol
Me_4NBr	0	5780 ± 8	
	1.0	5437 ± 12	−343 ± 14
	2.0	5167 ± 12	−613 ± 14
	4.0	4736 ± 12	−1044 ± 14
Et_4NBr	0	1500 ± 10	
	1.0	1165 ± 12	−335 ± 16
	2.2	840 ± 12	−660 ± 16
	4.0	465 ± 18	−1035 ± 20
Bu_4NBr	0	−2036 ± 7	
	1.0	−1663 ± 10	373 ± 12
	2.0	−1412 ± 10	624 ± 12
	4.0	−1002 ± 10	1034 ± 12
	6.0	−694 ± 10	1342 ± 12
	8.3	−440 ± 15	1596 ± 16
	10.9	−260 ± 20	

[a] Moles per kilogram of H_2O.

ures 2, 3, and 4 by the length of the error bars.[22] Greater errors were incurred in the dissolution in 8.3 and 10.9 m urea solutions because of the high viscosity and because of transient complex formation.

The low-concentration calorimetric results have been extrapolated to infinite dilution using the Debye–Hückel limiting law. The parameters essential for the calculation of the limiting slope were taken from the work of Wyman[23] and of Stokes.[11] The enthalpies of solution at infinite dilution of salt and the enthalpies of transfer from pure water to aqueous urea are tabulated in Table I. The apparent molal heat contents are given in Table II.

Table II: Apparent Molal Heat Contents of Tetraalkylammonium Bromides in Urea Solutions at 25°

		Molality of urea						
	$\sqrt{m_s}$[a]	0	1	2	4	6	8.3	10.9
Me_4NBr	0.05	19	17	16	15			
	0.10	31	28	26	23			
	0.15	32	28	26	23			
	0.20	20	19	18	17			
	0.25	−3	4	7	9			
	0.30	−33	−12	−5	0			
Et_4NBr	0.05	18	17	16	14			
	0.10	17	18	17	15			
	0.15	9	7	6	4			
	0.20	−8	−10	−12	−16			
	0.25	−32	−35	−35	−38			
Bu_4NBr	0.05	18	17	15	13	9	6	2
	0.10	30	24	20	13	7	−5	−26
	0.15	35	29	21	5	−4	−24	
	0.20	44	34			−16	−46	

[a] The square root of the molality of the tetraalkylammonium bromides.

The enthalpies of transfer for Me_4NBr and Bu_4NBr to aqueous urea solutions have been combined with previously reported free energy data[15] to obtain the entropies of transfer.

Discussion

(1) *Apparent Molal Heat Contents of R_4NBr in Pure Water.* The changes in various thermodynamic functions which accompany the dissolution of tetraalkylammonium halides in water have been interpreted in terms of changes in the structure of the solvent. It has been postulated that Pr_4N^+ and Bu_4N^+ ions promote the water structure within their cospheres and Me_4N^+ ion disrupts it.[3] Observed thermodynamic excess functions for these salts in water give strong support to the above contention.[19,24-26] The present

(22) In response to differing data from another laboratory for the Bu_4NBr–urea–H_2O system, a check was made on these data. Urea and Bu_4NBr were obtained from the same sources as above, but different lots, recrystallized from different solvents, and thoroughly dried. The calorimetry was carried out on a modified version of the above apparatus. The heats of solution thus obtained reproduced the earlier work within 15 cal/mol.

(23) J. Wyman, Jr., *J. Amer. Chem. Soc.*, 55, 4116 (1933).

work extends the previous heat content measurements[24] to another order of magnitude of high dilution. It reveals no crossing of the enthalpy curves of Me_4NBr, Et_4NBr, and Bu_4NBr at low concentrations.[27] It is noteworthy, however, that all the bromides studied approach the Debye–Hückel limiting law from the bottom.[28]

(2) *Apparent Molal Heat Contents of R_4NBr in Urea Solutions.* As shown in Table II and Figure 5, the effect of urea is such as to reduce the absolute value of the heat content relative to that in pure water. To the extent that changes in enthalpy on dilution reflect changes in solvent structural equilibrium within solute co-spheres, then this behavior can be interpreted as indicating that urea diminishes the structural characteristics of water. It is noted that the water-structure-promoting effect of Bu_4NBr has been weakened. This is because $\phi_L - \phi_L^0$ is large negative for Bu_4NBr, while the corresponding values are small for both Me_4NBr and Et_4NBr. At high concentrations of urea, ϕ_L of Bu_4NBr is seen to change signs and drop rapidly. This dropping of enthalpy curve reflects the partial ordering of salt and urea incipient to complex formation. At very high concentrations of either the salt or urea, complex formation was observed to occur as has been previously reported.[29] It should be emphasized, however, that the large positive enthalpy of transfer from pure water to aqueous urea (see next section) effectively rules out the possibility that the negative free energy of transfer ($\Delta G_{tr} < 0$) of this salt to urea solutions *at low salt concentrations* is due to complexlike aggregate formation.[15]

(3) *Enthalpy of Transfer.* The thermodynamic functions for the transfer of a salt at infinite dilution from one solvent to another reflect differences in solvation, work of cavity formation, dipole interaction, and so forth. One term which contributes significantly to the enthalpy of solvation in a highly structured solvent is that due to changes in the solvent structure due to the presence of the solute species. For a transfer process between two aqueous media differing primarily by the degree of structuredness, such as $D_2O \leftarrow H_2O$,[30] this effect may be the primary contribution to the heat of transfer. To the extent that this approximation is correct, the heats of transfer from H_2O to dilute urea solutions may be interpreted as indicating the structural changes taking place in the cospheres of the salt ions being transferred. Since the transfer process was carried out for three cations having the same anion, the differences in thermodynamic behavior are to be attributed to the effects of the cations. As can be seen from Figures 6 and 7, these differences are considerable and are consistent with the picture previously developed for these solutes in aqueous solution.

For Me_4NBr, the values of $\Delta\bar{G}_{tr}$, $\Delta\bar{H}_{tr}$, and $\Delta\bar{S}_{tr}$ are negative. The transfer of Me_4Br from pure water to aqueous urea is spontaneous because the energy decrease accompanying the process is greater than the corresponding decrease in entropy. If both urea and Me_4NBr have the effect of breaking the water structure, Me_4NBr in aqueous urea will have less structure to break than in pure water and result in both negative $\Delta\bar{H}_{tr}$ and $\Delta\bar{S}_{tr}$.

The transfer of Bu_4NBr from pure water to aqueous urea is spontaneous in spite of the unfavorable increase in enthalpy, since this is more than compensated by a greater increase in entropy accompanying this process. These results can be qualitatively accounted for when one again assumes urea to act as a structure breaker and Bu_4NBr as a structure maker. Apparently, the large structure-promoting effect of Bu_4N^+ ion in water is greatly diminished by the presence of urea molecules in its surroundings. Wetlaufer, *et al.*,[9] reached a similar conclusion on the basis of their study on the hydrocarbon gas solubilities in aqueous solutions.

Different mechanisms have been proposed to explain the structure-breaking effect of urea,[10,12] but the most reasonable one to date is that of Frank and Franks.[10] They used a mixture model for water consisting of bulky and dense species to explain the effect of urea on the hydrocarbon solubilities. Hydrocarbon molecules were considered to dissolve separately in the two kinds of water, as if they were distributed between two phases. Added urea was pictured as only being able to enter into the dense water, thereby causing the equilibrium shift to water from the bulky to dense species with a net effect of structure breaking.

Recently, Stern and Kulluk[31] have reported the enthalpies of transfer of sodium chloride from pure water to aqueous urea. They evaluated the entropies of transfer of the same process by combining their data with the corresponding free energy data obtained by Bower and Robinson.[32] For NaCl, the values of $\Delta\bar{G}_{tr}$ are positive, while both values of $\Delta\bar{H}_{tr}$ and $\Delta\bar{S}_{tr}$ are negative; these signs are just opposite to the corresponding ones for Bu_4NBr. The effect of urea on inorganic salts seems to contrast strikingly to that on organic salts containing large nonpolar groups.

The detailed mechanisms of denaturation of proteins by added urea are very complex and far from being

(24) S. Lindenbaum, *J. Phys. Chem.*, **70**, 814 (1966).

(25) H. S. Frank and W. Y. Wen, *Discuss. Faraday Soc.*, **24**, 133 (1957).

(26) H. Ruterjans, F. Schreiner, U. Sage, and Th. Ackerman, *J. Phys. Chem.*, **73**, 986 (1969).

(27) The plots of log $\gamma_\pm$ *vs.* $m^{1/2}$ for Et_4NCl and Bu_4NCl at 25° are found to cross each other at $m^{1/2} = 0.39$ by Frank and Rupert; see J. P. Rupert, Ph.D. Thesis, University of Pittsburgh, 1969.

(28) This subject will be treated in a later paper which will include low concentration data for other halides in detail.

(29) S. Saito, M. Lee, and W. Y. Wen, *J. Amer. Chem. Soc.*, **88**, 5107 (1966).

(30) C. V. Krishnan and H. L. Friedman, *J. Phys. Chem.*, **74**, 2356 (1970).

(31) J. H. Stern and J. D. Kulluk, *ibid.*, **73**, 2795 (1969).

(32) V. E. Bower and R. A. Robinson, *ibid.*, **67**, 1524 (1963).

well understood. In view of this, further investigations on the interaction of urea with simple model compounds will be of considerable interest.

Acknowledgments. The authors wish to acknowledge the financial support of the National Science Foundation.

Reaction of the Excited Oxygen Atoms $O(^1D_2)$ with Cyclopentane[1a]

by P. Michaud[1b] and R. J. Cvetanović*

Division of Chemistry, National Research Council of Canada, Ottawa, Canada K1A OR9 *(Received December 8, 1971)*

Publication costs assisted by the National Research Council of Canada

Reaction of excited singlet oxygen atoms $O(^1D_2)$ with cyclopentane in the gas phase has been studied at room temperature. The reaction conforms to the general pattern established previously for acyclic paraffins. The main reaction path is the insertion of $O(^1D_2)$ into a CH bond of cyclopentane to form a highly vibrationally excited molecule of cyclopentanol. The mean lifetime of the "hot" cyclopentanol is 1.7×10^{-9} sec. Another distinct reaction path, representing about 20% of the total reaction, is the abstraction of H atoms from cyclopentane by $O(^1D_2)$ atoms. Molecular elimination of H_2, representing about 10% of the total reaction, is the third distinct reaction path observed.

Introduction

Previous studies[2,3] in this laboratory have shown that $O(^1D_2)$ atoms interact with paraffins mainly in two ways: (1) by insertion into the CH bonds of the paraffin to form vibrationally excited alcohols, which undergo fragmentation if not stabilized by collisions, and (2) by abstraction of H atoms to form OH and alkyl radicals. A third reaction path, molecular elimination of H_2 after the interaction of $O(^1D_2)$ with the paraffin, generally takes place to a much smaller extent. The insertion occurs indiscriminately regardless of the CH bond strength, giving, for example, the statistical ratios of 3:1 *n*-propyl alcohol to isopropyl alcohol from propane[2] and 9:1 iso- to *tert*-butyl alcohol from isobutane.[3a] The lifetimes of the "hot" alcohols depend on the number of degrees of freedom in the molecule and increase from about 10^{-11} sec for the "hot" propyl alcohols to about 4×10^{-9} sec for the hot neopentyl alcohol. The pressures required for the stabilization of the hot alcohols decrease correspondingly from several thousand Torr for propyl alcohols to about 1000 Torr for butyl alcohols and to only 150 Torr for neopentyl alcohol.

A question of importance is whether the insertion of $O(^1D_2)$ and the abstraction by it occur as two distinct processes, or the abstraction is only a part of the unimolecular decomposition of the "hot" alcohols. An answer to this question has to be obtained from studies of pressure effects on the yields of the products from the two types of reaction. The study of the reaction of isobutane[3a] indicated that the two reactions are probably independent, and that of neopentane[3b] provided conclusive proof that they are indeed two distinct processes. The reaction of neopentane has been particularly suitable for this type of study because of the very simple composition of the reaction products as a result of the symmetry of neopentane and the relatively low and thus experimentally convenient pressure at which the "hot" insertion product is stabilized. In this reaction, insertion forms only neopentyl alcohol and abstraction only neopentyl radicals. Neopentyl radicals do not disproportionate but only combine to form 2,2,5,5-tetramethylhexane. This "abstraction" product was found to persist at pressures well in excess of the pressure of 150 Torr at which the hot neopentyl alcohol is completely stabilized. Abstraction is thus shown to be a distinct process.

To further confirm these results and obtain additional information on the intriguing diversity of $O(^1D_2)$ interaction with paraffins, another symmetrical C_5 paraffin, cyclopentane, has been selected for the present study. This paraffin is also expected to give a single insertion product, cyclopentanol, and, in the abstraction reaction, only one hydrocarbon free radical, cyclopentyl. Cyclopentyl radicals can recombine, to form cyclopentylcyclopentane, and, unlike neopentyl radicals, they can

(1) (a) Issued as N.R.C.C. No. 12574. (b) National Research Council of Canada Postdoctorate Fellow, 1969–1971.

(2) H. Yamazaki and R. J. Cvetanović, *J. Chem. Phys.*, **41**, 3703 (1964).

(3) (a) G. Paraskevopoulos and R. J. Cvetanović, *ibid.*, **50**, 590 (1969); (b) *ibid.*, **52**, 5821 (1970).

also disproportionate, to form cyclopentane and cyclopentene.[4]

The choice of cyclopentane for the present study has also been motivated by the desire to obtain information on the nature of interaction of $O(^1D_2)$ atoms with cycloparaffins, since such information is at present not available.

Experimental Section

The excited oxygen atoms, $O(^1D_2)$, were generated by direct photolysis of N_2O, using the 2139-Å line from two Phillips 93106E zinc lamps. Although the emission from these lamps did not show any mercury lines[2,3a] a mercury-free system was nevertheless used for the purification and storage of the reactants. The cylindrical reaction cell was 10 cm long, *ca.* 5 cm i.d., had a total volume of 190.0 ± 0.5 ml, and was provided with Suprasil quartz end windows. The light from the two lamps was focused by means of two ultrasil lenses.

The materials used were Matheson nitrous oxide (98% minimum purity) and American Petroleum Institute (API) cyclopentane (stated purity 99.970 ± 0.009%). Nitrous oxide was subjected to degassing at −196° and to several trap-to-trap distillations *in vacuo*, the last from a Dry Ice–acetone bath. Only traces of cyclopentene (0.020 ± 0.005%) could be detected by gas chromatography on a 20-ft 2% squalane modified activated alumina column. Before each run, nitrous oxide was degassed at −196°. Cyclopentane was subjected to several freeze–thaw cycles and was also degassed at −196°.

The noncondensable gases (H_2, N_2, CH_4, and CO) were collected by a Toepler pump through two spiral traps at −196°. To prevent loss by occlusion, the contents of the first trap were frozen over into the second trap under continuous pumping during which the reaction cell and the first trap were heated to 180°. The collected noncondensables were measured in a gas buret and analyzed on an 18-ft 13X Molecular Sieve column with helium as the carrier gas. Occasional concurrent determinations were made by mass spectrometry and by combustion over granular copper oxide in a tube at 250°. The three types of determinations showed good mutual agreement. The estimated chromatographic errors were, for N_2, 2–3% and, for H_2, because of its low detector response in helium, 10–12% and even larger for very small samples. The determinations were based on the gc peak height measurements with appropriate calibrations.

The condensable products and excess of the reactants were collected in a 2-l. mixing bulb at −196°. The reaction cell and the traps were finally heated to 180° to assure quantitative transfer. To prevent loss by absorption in stopcock grease, only greaseless stopcocks and mercury cutoffs were used in the analytical system. Several aliquots of the collected condensable products were analyzed by gas chromatography. Oxygenated products were analyzed on a 300-ft 0.015-in. i.d. stainless-steel capillary column coated with β,β′-thiodipropionitrile (β,β′-TDPN) and on a 0.35% di-*n*-decyl phthalate (DDPH) 20-ft $^3/_{16}$ in.-i.d. 120–140 mesh glass beads column. Both columns were used at room temperature with helium as the carrier gas. The quantitative determinations were based on the gc peak areas, with benzene as an internal standard. Cyclopentanol, cyclopentanone, and *n*-pentanal (*n*-valeraldehyde) were identified on both columns by seeding with authentic samples. The identifications were confirmed by similar treatment on a 300-ft 0.015-in. i.d. stainless-steel capillary column coated with dinonyl phthalate and, for cyclopentanol and cyclopentanone, by direct mass spectrometric analysis of the peaks eluted from the β,β′-TDPN capillary column. With the use of the β,β′-TDPN capillary column, a minor peak was identified as 4-pentenal, a known product of the photolysis of cyclopentanone.[5] Initial additions of small amounts of cyclopentanone to the reactants largely increased this peak. Qualitatively similar behavior was observed on the di-*n*-decyl phthalate packed column on which 4-pentenal was not well separated from *n*-pentanal.

The heavier hydrocarbon products, cyclopentylcyclopentane (bp = 190°) and *n*-butylcyclopentane (bp = 153°), were retained sufficiently long on the β,β′-TDPN column to be well separated from the huge peak of the unreacted cyclopentane and the more strongly retained oxygenated compounds. The identity of the two hydrocarbons was confirmed by seeding with authentic compounds (API samples) on the β,β′-TDPN column and on a 300-ft 0.015-in. i.d. stainless-steel capillary column coated with squalane. Cyclopentylcyclopentane was also prepared by the mercury-photosensitized reaction of cyclopentane[4] and was identified by mass spectrometry. Ethylcyclopentane has been identified and analyzed on the di-*n*-decyl phthalate packed column. The lighter hydrocarbons (C_2H_4, *n*-butane, and cyclopentene) were analyzed on a 20-ft 2% squalane modified activated alumina column at room temperature with a flame ionization detector. The determinations were based on the peak areas, and cyclopentane served as an internal standard. The reported values are averages from two to three chromatograms.

Cyclopentanol, the main reaction product, was usually measured on the β,β′-TDPN capillary column and on the DDPH packed column. The two measurements were in excellent agreement, and their estimated precision was 3–5%. The precision for the minor products was about 5–10%. The following flame ionization detector molar responses relative to benzene taken as unity were used: cyclopentanol, 0.63; cyclopent-

(4) R. L. Stock and H. E. Gunning, *Can. J. Chem.*, **38**, 2295 (1960).
(5) R. Srinivasan, *J. Amer. Chem. Soc.*, **81**, 1546 (1959).

anone, 0.67; *n*-pentanal, 0.63; 4-pentenal, 0.63 (taken the same as for *n*-pentanal); cyclopentylcyclopentane, 1.52; *n*-butylcyclopentane, 1.41; ethylcyclopentane, 1.12. The corresponding molar responses for the lighter hydrocarbons (C_2H_4, *n*-butane, cyclopentane, and cyclopentene) were taken to be directly proportional to the number of carbon atoms.[6] In some experiments water was also measured; a 12-ft Porapak R column at 100° was used and cyclopentane served as internal standard.

After a number of runs, a brownish polymer deposit was observed on the windows of the reaction cell. Between experiments, therefore, the cell was filled with oxygen and flamed to burn off the polymer. Another way to remove the polymer was to expose the cell filled with oxygen to uv light for at least 12 hr.

Results

The reaction was studied at room temperature, 24 ± 2°. Nitrous oxide absorbs[7] only weakly the 2139-Å line, and long exposure times (100–2000 min) were therefore required. The percentage conversion of cyclopentane was usually kept below 1%.

Reaction Products and Their Yields. At not too low a pressure, for example at 450 Torr, the major reaction products were cyclopentanol, hydrogen, water, cyclopentylcyclopentane, and cyclopentene. Other oxygen-containing products, carbon monoxide, cyclopentanone, *n*-pentanal, and 4-pentenal, were also formed, but in much smaller amounts. Cyclopentanol is the expected "insertion" product, while water, cyclopentylcyclopentane, and cyclopentene are the expected "abstraction" products, the last two resulting from combination and disproportionation of two cyclopentyl radicals.[4] In addition, small quantities of *n*-butylcyclopentane, ethylcyclopentane, *n*-butane, and ethylene were detected and measured. Ethane and butene-1 were also detected, but they were present only in trace amounts and were not measured.

The yields of the products expressed relative to the nitrogen formed are shown in Figures 1 and 2. Use of 15/1 cyclopentane/N_2O ratios was apparently sufficient to prevent an appreciable $O(^1D_2)$ reaction with N_2O. This is in agreement with the data in the literature[8] and unpublished results from this laboratory which show that at a 15/1 cyclopentane/N_2O ratio essentially all $O(^1D_2)$ atoms react with cyclopentane. Under such conditions, N_2 provides a measure of $O(^1D_2)$ atoms generated. On the other hand, if an appreciable $O(^1D_2)$ attack on N_2O were to occur, it would produce additional N_2 and some O_2 and NO. The effect of O_2 and NO would be to scavenge some of the free radicals produced in the $O(^1D_2)$–cyclopentane reaction.

The most interesting result evident from Figure 1 is that the yield of cyclopentanol decreases and that of H_2 increases with the extent of reaction (as measured by the amount of N_2 produced). Such behavior was

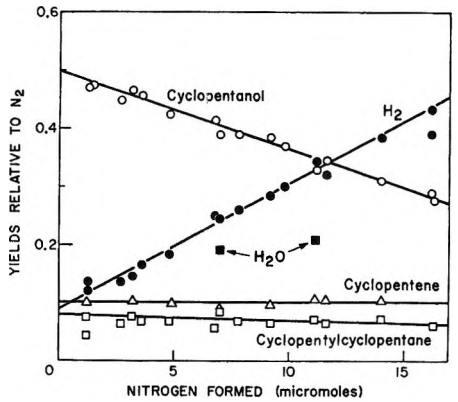

Figure 1. Dependence of the yields of the major products on the extent of reaction (cyclopentane/N_2O = 15/1, SF_6 added 340 Torr, total pressure 450 Torr, temperature 24 ± 2°).

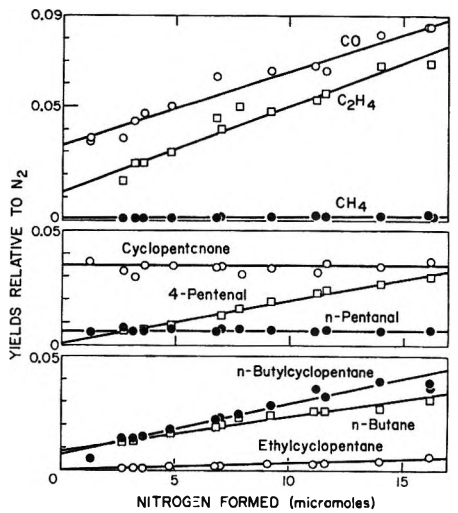

Figure 2. Dependence of the yields of the minor products on the extent of reaction (conditions are the same as stated in the caption to Figure 1).

unexpected, since in the previous work with isobutane[3a] and neopentane[3b] the alcohol yields remained approximately constant. In the present case it appears, therefore, that as cyclopentanol accumulates in the course of the reaction some of it might be photolyzed and leads to a secondary production of H_2. The uv absorption spectrum of cyclopentanol is not known, but the absorption spectra of methanol, ethanol, and 1- and 2-propanol show in the wavelength range studied

(6) H. Purnell, "Gas Chromatography," Wiley, New York, N. Y., 1962, p 302.

(7) K. Watanabe, M. Zelikoff, and E. C. Y. Inn, Geophysical Research Papers, No. 21, Geophysics Research Directorate, Air Force Cambridge Research Center, Cambridge, Mass., June 1953.

(8) The reactions involved are: $O(^1D_2)$ + cyclopentane → products (2), $O(^1D_2) + N_2O \rightarrow N_2 + O_2$ (a), and $O(^1D_2) + N_2O \rightarrow 2NO$ (b), where $k_a = k_b$: P. M. Scott, K. F. Preston, R. J. Andersen, and L. M. Quick, *Can. J. Chem.*, **49**, 11 (1971). Unpublished determinations in this laboratory gave $k_2/k_{neopentane} = 0.93 \pm 0.03$. From the data in the literature (K. F. Preston and R. J. Cvetanović, *J. Chem. Phys.*, **45**, 2888 (1966); G. Paraskevopoulos and R. J. Cvetanović, *J. Amer. Chem. Soc.*, **91**, 7572 (1969)), $k_{neopentane}/(k_a + k_b) = 7.75$. It is therefore calculated that $k_2/(k_a + k_b) = 7.2$.

(1500–2000 Å) the first absorption bands, with maxima at about 1818 Å, completely devoid of structure.[9] The intensity of absorption increases in the order methanol < 1-propanol < ethanol < 2-propanol. Photolysis of normal alcohols has been studied[10] using a hydrogen discharge lamp (λ >1520 Å), but no results have been reported for the wavelength used in the present study (2139 Å).

Secondary Photolysis of Cyclopentanol. Several experiments were carried out to test whether cyclopentanol may undergo some photolysis at 2139 Å. In the first series of experiments, small amounts of cyclopentanol (Matheson Coleman and Bell, stated purity 99%+) were added to a 15/1 cyclopentane–N_2O mixture. Gc analyses of the cyclopentanol on the β,β'-TDPN capillary column and on the DDPH packed column did not show any impurity. The amount of cyclopentanol added was varied, but the extent of reaction was kept approximately constant (10 ± 1 μmol of N_2). The results are summarized in Table I. Figure 3 shows that H_2 yield increases linearly with the amount of cyclopentanol initially added while the net cyclopentanol formed (*i.e.*, cyclopentanol found by gc less cyclopentanol initially added) decreases in a corresponding manner. As shown in Figure 3, the absolute values of the slopes of the two linear plots are the same within the experimental error.

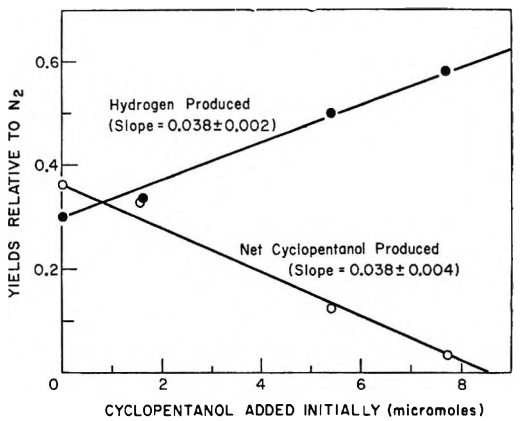

Figure 3. Effect of cyclopentanol additions on the yields of hydrogen and of the net cyclopentanol produced (reaction conditions are given in Table I).

Table I: Effect of Cyclopentanol Additions on the Yields of Products in the Reaction of $O(^1D_2)$ Atoms with Cyclopentane[a]

Total pressure, Torr	445	453	456	453
Cyclopentanol added, Torr		0.16	0.53	0.75
SF_6 added, Torr	342	350	350	347
N_2 formed, μmol	9.80	10.46	9.81	8.83
Rates of Product Formation Relative to $r_{N_2} = 1$				
Cyclopentanol (net)[b]	0.362	0.338	0.122	0.033
Cyclopentanone	0.034	0.035	0.050	nm
4-Pentenal	0.019	0.018	nm[c]	nm
H_2	0.299	0.336	0.500	0.581
CO	0.066	0.089	0.143	0.166
C_2H_4	0.048	0.074	0.103	nm
n-Butane	0.024	0.025	0.025	nm
Cyclopentylcyclopentane	0.066	0.070	0.063	nm
n-Butylcyclopentane	0.028	0.046	0.081	nm
Ethylcyclopentane	0.003	0.003	0.004	nm
n-Pentanal	0.007	0.004	nm	nm

[a] Cyclopentane/N_2O = 15/1, temperature 24 ± 2°. The first column gives composite data from two runs. [b] Cyclopentanol found in the products less the initially added amount. [c] nm = not measured.

In a second series of experiments, cyclopentanol was directly photolyzed at 2139 Å. The main reaction products are shown in Table II. H_2 is the principal product and CO and cyclopentanone are also formed in substantial amounts. Of the hydrocarbons detected, *n*-butane, C_2H_4, and cyclobutane are the most important. The H_2 yield is greatly decreased in the presence of 10 Torr of C_2H_4, showing that most of the hydrogen is formed from H atoms.

An attempt was made to determine the absorption coefficient (ϵ) of cyclopentanol at 2139 Å using a DU2 Beckman uv spectrophotometer. A liquid-phase determination with uv spectrograde cyclopentane as solvent gave ϵ 0.29 ± 0.02 atm^{-1} cm^{-1}, while gas-phase measurements in a quartz absorption cell gave ϵ 0.24 ± 0.04 atm^{-1} cm^{-1}. The uncertainties were higher in the gas-phase determinations because of difficulties with

Table II: Products of the Photolysis of Cyclopentanol at 2139 Å[a]

Cyclopentanol, Torr	2.11	2.09	2.41
SF_6 added, Torr		448	410
C_2H_4 added, Torr			10.0
Total pressure, Torr	2.11	450.1	422.4
Exposure time, min	960	1075	960
Cyclopentanol used, μmol	6.01	nm	nm
Products Formed			
H_2, μmol	8.13	8.08	0.84
CO, μmol	3.53	3.76	4.30
Cyclopentanone, μmol	1.52	nm	nm
C_2H_6 (rel yield[b])	0.091	0.043	nm
C_2H_4 (rel yield[b])	0.364	0.180	nm
C_3H_8 (rel yield[b])	0.055	0.030	nm
C_3H_6 (rel yield[b])	0.061	0.032	nm
n-Butane (rel yield[b])	1.000	1.000	nm
Cyclobutane (rel yield[b])	0.127	0.043	nm

[a] Temperature 24 ± 2°. nm = not measured. [b] Yields relative to *n*-butane taken as unity.

(9) A. T. Harrison, B. J. Cederholm, and M. A. Terwilliger, *J. Chem. Phys.*, **30**, 355 (1959).

(10) J. G. Calvert and J. N. Pitts, Jr., "Photochemistry," Wiley, New York, N. Y., 1966, p 441.

the measurement and transfer into the absorption cell of small amounts of cyclopentanol. Nevertheless, the gas-phase ϵ value seems to be of the right order of magnitude.

From the results of the above two series of experiments and the values obtained for the extinction coefficient of cyclopentanol at 2139 Å, it can be safely assumed that cyclopentanol formed in the reaction of $O(^1D_2)$ atoms with cyclopentane undergoes some secondary photolysis as its amount increases in the course of the reaction.

Other Secondary Reactions. Among the other products which may undergo secondary photolysis or reactions are cyclopentene and cyclopentanone. Their yields have been measured and that of cyclopentene has been corrected for the small amount initially present as impurity in cyclopentane.

Cyclopentene absorbs[11] to some extent at 2139 Å and is thus likely to undergo some secondary photolysis. In agreement with this, there is a strong increase in the yield of H_2 when small amounts of cyclopentene (about 80 times the amount present initially as impurity) are added to a 15/1 cyclopentane–N_2O reaction mixture. This is shown by the comparative results without and with cyclopentene added given in Table III. Cyclopentene additions are also seen not to affect appreciably the yields of the oxygenated products, cyclopentanol, cyclopentanone, and CO. This result shows that cyclopentanone is *not* formed in this reaction system by addition of $O(^3P)$ atoms to cyclopentene, although cyclopentanone is known to be a major product of that reaction.[12] Indirectly it thus also shows an absence of appreciable concentrations of $O(^3P)$, as will be discussed in greater detail later. It also rules against any appreciable attack of $O(^1D_2)$ on cyclopentene.

Cyclopentanone, which accounts for about 3.5% of the $O(^1D_2)$ atoms, absorbs the 2139-Å line to some extent.[13] The products of its direct photolysis are C_2H_4, cyclobutane, and CO, with small amounts of 4-pentenal.[13] Ethylene, CO, and 4-pentenal have been found in the reaction products, but at best only trace amounts of cyclobutane were detected. The data in the last column of Table III show that small initial additions of cyclopentanone to a cyclopentane–N_2O reaction mixture increase the yields of C_2H_4, CO, 4-pentenal, and cyclobutane.

The other products that may undergo secondary photolysis are the two aldehydes, *n*-pentanal and 4-pentenal. *n*-Pentanal accounts only for 0.6% of the $O(^1D_2)$ atoms and 4-pentenal becomes appreciable only at larger conversions. Their effects on the reaction were not investigated.

The Effect of Pressure. The effect of pressure variations between 15 and 750 Torr on the yields of the products is shown in Figures 4 and 5. The yield of cyclopentanol, the insertion product, increases and levels off at pressures higher than about 200 Torr. The yields of the abstraction products, cyclopentylcyclopentane and cyclopentene, remain approximately constant at high pressures and decrease slightly at lower pressures. The yields of the fragmentation products, H_2, CO, C_2H_4, and ethylcyclopentane, decrease as the pressure is increased and level off again at a pressure in excess of about 200 Torr. To allow for the secondary photolysis, the yields of cyclopentanol plotted in Figure 4 were obtained by extrapolating to zero time (*i.e.*, to zero N_2) determinations at three different extents of

Table III: Effect of Cyclopentene and Cyclopentanone Additions on the Yields of Products in the Reaction of $O(^1D_2)$ Atoms with Cyclopentane[a]

Total pressure, Torr	452	453	443
Cyclopentene added, Torr		1.97	
Cyclopentanone added, Torr			1.58
SF_6 added, Torr	354	344	335
N_2 formed, μmol	6.83	9.44	4.80
Rates of Product Formation Relative to $r_{N_2} = 1$			
Cyclopentanol	0.414	0.402	0.423
Cyclopentanone	0.035	0.048	nm
4-Pentenal	0.007	0.009	0.388
H_2	0.252	0.432	0.230
CO	0.063	0.091	0.127
C_2H_4	0.045	nm	0.390
n-Butane	0.020	nm	0.015
Cyclobutane	Trace	nm	0.238
Cyclopentylcyclopentane	0.057	0.073	0.073
n-Butylcyclopentane	0.023	0.027	0.016
Ethylcyclopentane	0.002	nm	0.008
Cyclopentene	0.101	nm	0.114

[a] Cyclopentane/N_2O = 15/1; temperature 24 ± 2°. nm = not measured.

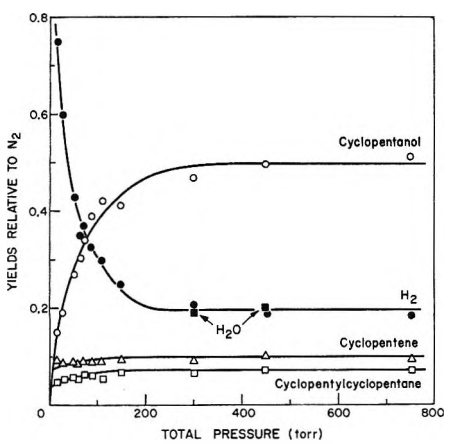

Figure 4. Pressure dependence of the initial yields of the major products relative to N_2.

(11) Ultra Violet Spectral Data, American Petroleum Institute, Research Project 44, No. 570.

(12) R. J. Cvetanović, D. F. Ring, and L. C. Doyle, *J. Phys. Chem.*, 75, 8056 (1971).

(13) A. T. Blades, *Can. J. Chem.*, 48, 2269 (1970).

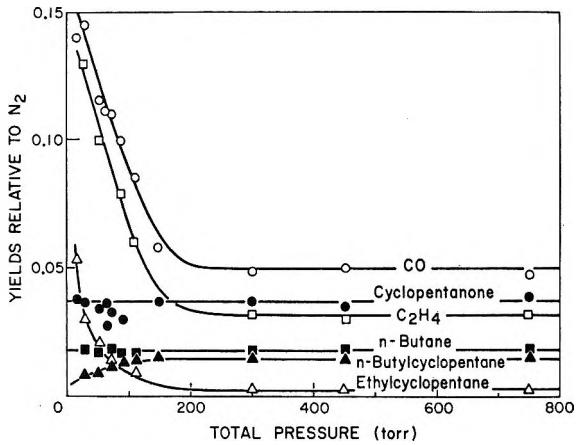

Figure 5. Pressure dependence of the yields of the minor products relative to N_2.

reaction. For the other products in Figures 4 and 5 the conversions were kept as low as possible, between 0.4 and 0.6%. The yields of N_2 ranged from 1 to 6 μmol, with the smaller values at lower pressures.

Discussion

The discussion and interpretation of the results may be based on the following reaction scheme.

$$N_2O + h\nu \longrightarrow N_2 + O(^1D_2) \quad (1a)$$

$$\longrightarrow N_2 + O(^3P) \quad (1b)$$

$$O(^1D_2) + RH \longrightarrow ROH^* \quad (2a)$$

$$\longrightarrow R + OH \quad (2b)$$

$$\longrightarrow H_2 + \text{products} \quad (2c)$$

$$\longrightarrow RH + O(^3P) \quad (2d)$$

$$ROH^* \longrightarrow \text{fragmentation products} \quad (3)$$

$$ROH^* + M \longrightarrow ROH + M \quad (4)$$

$$ROH + h\nu \longrightarrow \phi(H_2) + \text{products} \quad (5)$$

RH stands for cyclopentane, ROH for cyclopentanol, ROH* for vibrationally excited cyclopentanol. M is any molecule in the gas mixture which removes excess vibrational energy from ROH*, *i.e.* cyclopentane, N_2O, and SF_6 when added. (SF_6 acts only as a deactivator of ROH* but does not[2] deactivate $O(^1D_2)$ atoms.) Reaction 5, the secondary photolysis of cyclopentanol, is formally written as giving H_2 directly, although it proceeds mainly with H atoms as the intermediates which abstract from cyclopentane to form H_2.[14] ϕ is the quantum yield (*i.e.*, the stoichiometric number) of the H_2 which results from the photolysis of cyclopentanol.

Insertion of $O(^1D_2)$ Atoms into CH Bonds. It has been established in earlier work with propane,[2] isobutane,[3a] and neopentane[3b] that $O(^1D_2)$ atoms insert into the CH bonds of paraffins to form vibrationally excited (hot) alcohols. The reaction with cyclopentane follows the same pattern. The hot cyclopentanol is stabilized at about 200 Torr, *i.e.*, at a slightly higher pressure than the hot neopentanol (150 Torr). Below 200 Torr, the yield of cyclopentanol decreases and that of the fragmentation products increases (Figures 4 and 5) as a result of the incomplete collisional stabilization of the hot cyclopentanol molecules. As will be shown later, a least-squares analysis shows that in the limit of infinite pressure the stabilized cyclopentanol, *i.e.*, the "insertion" reaction, corresponds to about 55% of the $O(^1D_2)$ atoms reacting with cyclopentane.

Abstraction by $O^1(D_2)$ Atoms. Abstraction of H atoms from cyclopentane, reaction 2b, will be followed in the present system by the rapid abstraction by OH from cyclopentane (RH) to form water and cyclopentyl radicals (R), *i.e.*

$$RH + OH \longrightarrow H_2O + R$$

Cyclopentyl radicals subsequently recombine to give cyclopentylcyclopentane, and disproportionate to give cyclopentane and cyclopentene. The ratio of the two reactions is close to unity.[4] Figure 4 shows that the measured abstraction products, H_2O, cyclopentylcyclopentane, and cyclopentene, persist at pressures well above 200 Torr, *i.e.*, at pressures at which the insertion product had reached its plateau value. True abstraction from cyclopentane by $O(^1D_2)$ therefore occurs. The high-pressure yields of cyclopentene and of cyclopentylcyclopentane are similar, as expected, and their sum approximately equals the yield of water. These yields indicate that the "abstraction" represents about 20% of the total reaction of $O(^1D_2)$ atoms with cyclopentane. At lower pressures there is an increased consumption of cyclopentyl radicals in reactions with radicals formed by fragmentation, particularly ethyl radicals, and the yields of cyclopentene and cyclopentylcyclopentane slightly decrease.

Molecular Elimination. In the studies of the reactions of $O(^1D_2)$ with isobutane[3a] and neopentane,[3b] it was concluded that molecular elimination of H_2 and aldehydes, first proposed by DeMore and Raper[15] for the reaction of $O(^1D_2)$ with CH_4, may occur to a small extent. In the present case, the expected products of molecular elimination, reaction 2c, are H_2 and cyclopentanone, and both are formed. To test whether this molecular elimination does indeed occur, experiments were carried out at total pressures of about 450 Torr,

(14) At larger conversions, a small fraction of H atoms will be scavenged by the cyclopentene formed in the reaction, since H atoms add to cyclopentene about 175 times more rapidly than they abstract from cyclopentane.[4] In the experiments carried out, cyclopentane was always present in large excess, and it can be calculated that only about 11% of H atoms were scavenged by cyclopentene at the largest conversions used and none in the limit of zero conversion. To a good approximation, therefore, the addition of H atoms to cyclopentene can be disregarded for the purpose of the present discussion.

(15) W. B. DeMore and O. F. Raper, *J. Chem. Phys.*, **46**, 2500 (1967).

adding O_2 or C_2H_4 to 15/1 cyclopentane–N_2O reaction mixtures. The results are shown in the last three columns of Table IV. O_2 completely suppresses the yields of the free-radical products (cyclopentylcyclopentane, *n*-butylcyclopentane, and ethylcyclopentane), does not seem to affect the yield of cyclopentanol, and increases significantly the yields of cyclopentanone, CO, and 4-pentenal. The yield of H_2 is not inhibited completely either by O_2 or C_2H_4, indicating that molecular

Table IV: Effect of O_2 and C_2H_4 Additions on the Yields of Products in the Reaction of $O(^1D_2)$ Atoms with Cyclopentane[a]

Total pressure, Torr	452	459	458	446
O_2 added, Torr		1.28	4.32	
C_2H_4 added, Torr				10.39
SF_6 added, Torr	354	351	347	327
N_2 formed, μmol	6.83	8.36	7.71	5.35
O_2 consumed, μmol		12.01	10.76	
Rates of Product Formation Relative to $r_{N_2} = 1$				
Cyclopentanol	0.414	0.398	0.428	0.382
Cyclopentanone	0.035	0.132	0.151	0.053
4-Pentenal	0.007	0.016	0.020	0.004
H_2	0.252	0.135	0.118	0.088
CO	0.063	0.105	0.096	0.093
Cyclopentylcyclopentane	0.057	None	None	0.052
n-Butylcyclopentane	0.023	None	None	0.013
Ethylcyclopentane	0.002	None	None	0.038
n-Pentanal	0.007	0.012	0.010	0.013

[a] Cyclopentane/N_2O = 15/1, temperature 24 ± 2°.

elimination of H_2, reaction 2c, does occur. The ethylene-scavenging results indicate a 9% yield of molecular H_2, which would then represent the extent of molecular elimination. Perhaps a better measure of the extent of reaction 2c, extrapolation of the H_2 yield in Figure 1 to zero reaction time (*i.e.*, to zero N_2), gives a value of 9.1%. The two values agree very well, but are both considerably larger than the yield of cyclopentanone. The difference could be due to photolysis of cyclopentanone, to some formation of other products in reaction 2c, and also to some error in the extrapolation of the H_2 yields to zero time. The value of 9% is also considerably larger than the extents of molecular elimination in the case of isobutane[3a] (3%) and neopentane[3b] (2%).

As mentioned, O_2 addition does not seem to affect the yield of cyclopentanol. At the same time, Table IV shows that a large amount of oxygen is consumed in the process. Also, new products, mainly formaldehyde and acetaldehyde, have been identified but not measured. Oxygen consumption (11–12 μmol) in these experiments has been much in excess of the calculated yield of cyclopentyl radicals (1.6–1.7 μmol). These results indicate that a chain reaction is involved, although its nature has not been further investigated. However, formation of aldehydes, mainly formaldehyde and acetaldehyde, in the attack of O_2 on cyclopentyl radicals has been reported in the literature.[16]

Secondary Reactions. Secondary Photolysis of Cyclopentanol. As shown above, the decrease in the yield of cyclopentanol with reaction time (Figure 1) may be ascribed to secondary photolysis of cyclopentanol. From a steady-state treatment of reactions 1–5, the following expression is obtained for the rate of production of cyclopentanol relative to the rate of production of nitrogen

$$d[ROH]/d[N_2] = \alpha - \beta[ROH]$$

with

$$\alpha = \frac{k_{2a}}{k_2}\frac{k_4[M]}{k_3 + k_4[M]}$$

$$\beta = \frac{\epsilon_5}{\epsilon_1[N_2O]}$$

and $k_2 = k_{2a} + k_{2b} + k_{2c} + k_{2d}$.

ϵ_1 and ϵ_5 are, respectively, the absorption coefficients of N_2O and cyclopentanol. Since both ϵ_1 and ϵ_5 are very small, it was assumed here that the ratio of the light absorbed by cyclopentanol and N_2O is

$$Ia(5)/Ia(1) = \epsilon_5[ROH]/\epsilon_1[N_2O]$$

Integration of the rate expression gives, for the concentrations of ROH and N_2 at a time t

$$\ln\frac{\alpha - \beta[ROH]_t}{\alpha - \beta[ROH]_0} = -\beta[N_2]$$

where $[ROH]_0$ is the initial concentration of cyclopentanol. If no cyclopentanol is initially added, *i.e.*, $[ROH]_0 = 0$

$$[ROH]_t = (\alpha/\beta)\{1 - \exp(-\beta[N_2])\}$$

or, expanding the exponential

$$\left(\frac{[ROH]}{[N_2]}\right)_t = \alpha\left\{1 - \frac{\beta}{2}[N_2] + \frac{\beta^2}{6}[N_2]^2 - \frac{\beta^3}{24}[N_2]^3 + (-1)^n\frac{\beta^n}{(n+1)!}[N_2]^n + \ldots\right\} \quad (I)$$

$[ROH]/[N_2]$ is therefore a decreasing function of $[N_2]$, as found experimentally. A least-squares analysis of the cyclopentanol plot in Figure 1 gives for the intercept $\alpha = 0.495 \pm 0.005$ and for the slope $(\alpha\beta/2) = 0.0133 \pm 0.0005$ μmol^{-1}. The indicated error limits are standard deviations. Therefore, $\beta = 0.0537$ μmol^{-1} and, since $\beta = \epsilon_5/\epsilon_1[N_2O]$, a value for ϵ_5, the absorption coefficient of cyclopentanol, can be derived. The average amount of N_2O in these experiments has been 68 μmol, and taking[7] $\epsilon_1 = 0.092$ atm^{-1} cm^{-1}, it is found that $\epsilon_5 = 0.34$ atm^{-1} cm^{-1}. Considering the indirect nature of

(16) I. R. McGowan and C. F. H. Tipper, *Proc. Roy. Soc., Ser. A*, **246**, 64 (1958).

this derivation, the value obtained is in satisfactory agreement with the experimental determinations of 0.29 ± 0.02 and 0.24 ± 0.04 atm^{-1} cm^{-1} in liquid and vapor phase, respectively.

An analogous steady-state treatment gives for the rate of production of hydrogen

$$d[H_2]/d[N_2] = (k_{2c}/k_2) + \phi\beta[ROH]_t$$

and therefore, when cyclopentanol is not initially added

$$d[H_2]/d[N_2] = (k_{2c}/k_2) + \phi\alpha\{1 - \exp(-\beta[N_2])\}$$

so that, after integration and expansion of the exponential

$$\left(\frac{[H_2]}{[N_2]}\right)_t = \frac{k_{2c}}{k_2} + \phi\alpha\left\{\frac{\beta}{2}[N_2] - \frac{\beta^2}{6}[N_2]^2 + \frac{\beta^3}{24}[N_2]^3 - \ldots\right\} \quad (II)$$

It is clear that if all H_2 is formed in reaction 2c and in the secondary photolysis of cyclopentanol and if, as may be expected, one molecule of H_2 is produced for each molecule of cyclopentanol photolyzed (*i.e.*, $\phi = 1$), the theoretical value of the linear H_2 plot in Figure 1 should be $\alpha\beta/2$. The slope should therefore be of opposite sign but numerically the same as for cyclopentanol. However, the least-squares value of the slope for H_2 in Figure 1 is 0.0212 ± 0.0007 μmol^{-1}, which is much larger than 0.0133 ± 0.0005 μmol^{-1}, the absolute value of the slope of the cyclopentanol plot. The difference is too large to be attributed to experimental errors and shows that some hydrogen is formed in secondary reactions other than reaction 5, perhaps in the secondary photolysis of cyclopentene and of the aldehydic products, all of which absorb the 2139-Å line.

More direct evidence for hydrogen formation in the secondary photolysis of cyclopentanol is provided by the results of the experiments with various amounts of cyclopentanol initially added to a 15/1 cyclopentane–N_2O reaction mixture diluted with SF_6, shown in Table I and Figure 3. In this case the integrated (and expanded) equations for H_2/N_2 and $(ROH_t - ROH_0)/N_2$ become

$$\left(\frac{[H_2]}{[N_2]}\right)_t = \left(\frac{[H_2]}{[N_2]}\right)_{t,[ROH]_0=0} + \phi\beta[ROH]_0\left\{1 - \frac{\beta}{2}[N_2] + \frac{\beta^2}{6}[N_2]^2 - \ldots\right\} \quad (III)$$

$$\frac{[ROH]_t - [ROH]_0}{[N_2]} = \left(\frac{[ROH]}{[N_2]}\right)_{t,[ROH]_0=0} - \beta[ROH]_0\left\{1 - \frac{\beta}{2}[N_2] + \frac{\beta^2}{6}[N_2]^2 - \ldots\right\} \quad (IV)$$

$([H_2]/[N_2])_{t,[ROH]_0=0}$ and $([ROH]/[N_2])_{t,[ROH]_0=0}$ are, respectively, the relative yields at time t of H_2 and cyclopentanol when no cyclopentanol is initially added. When a series of experiments is carried out at constant N_2, as in Figure 3, these quantities remain constant and expressions III and IV show that H_2/N_2 should increase and the net cyclopentanol decrease linearly with increasing $[ROH]_0$. The absolute values of the initial slopes should be the same, as is actually found in Figure 3. This identity shows that ϕ in reaction 5 is unity. The calculated theoretical value of the slope, *i.e.*, of $\beta\{1 - (\beta[N_2]/2) + (\beta^2[N_2]^2/6) - \ldots\}$, taking $\beta = 0.0537$ μmol^{-1} and $N_2 = 9.8$ μmol (the average amount of N_2 formed in the four experiments listed in Table I), is 0.042 μmol^{-1}, which is very close to the experimental values of 0.038 ± 0.004 μmol^{-1}.

The results obtained in the photolysis of cyclopentanol vapor, summarized in Table II, are also consistent with the trends shown in Table I. The increase in the yields of H_2, CO, cyclopentanone, C_2H_4 and *n*-butylcyclopentane with increasing $[ROH]_0$ demonstrate that photolysis of cyclopentanol plays an important role in the experiments listed in Table I.

Side Reactions of Cylopentene. As mentioned earlier, cyclopentene formed in the course of the reaction by disproportionation of cyclopentyl radicals and present initially as a small impurity in cyclopentane does not react with $O(^1D_2)$ (or with $O(^3P)$ if present). This is evident from the fact that a small cyclopentene addition to a cyclopentane–N_2O reaction mixture leaves the yields of the oxygenated products virtually unaltered (Table III), and such typical major products of the $O(^3P)$ reaction with cyclopentene as cyclopentene oxide and cyclobutylcarboxaldehyde[12] are not detected. At the cyclopentane/cyclopentene ratio of 50 used, any $O(^3P)$ atoms present in the system would be efficiently scavenged by the much more reactive cyclopentene. It is evident therefore that reaction 2c, deactivation of $O(^1D_2)$ to $O(^3P)$ by cyclopentane, is negligible, in agreement with the similar earlier findings with isobutane and neopentane.

Cyclopentanone is also a major product of the $O(^3P)$ reaction with cyclopentene.[12] It is observed as a minor product in the present study, but its yield is affected little by cyclopentene addition and it must therefore be formed in some other way rather than by $O(^3P)$ addition to cyclopentene.

Cyclopentene additions strongly increase the yield of hydrogen and also increase slightly the yields of C_2H_4 and ethylcyclopentane (Table III). A brownish polymer deposit is simultaneously formed on the walls of the reaction cell. It is very likely that these results are due to photolysis of cyclopentene. Although there is some information on the mercury-photosensitized decomposition of cyclopentene,[17] nothing appears to be

(17) W. A. Gibbons, W. F. Allen, and H. E. Gunning, *Can. J. Chem.*, **40**, 568 (1962).

known about the products of its direct photolysis. By analogy with related reactions,[18] it is likely that H atoms are a major primary product. The larger slope in Figure 1 of the plot of the yield of hydrogen than of cyclopentanol, discussed earlier, may then be ascribed at least partly to secondary photolysis of cyclopentene. Such an explanation would require an extinction coefficient (ϵ) for cyclopentene of about 1 atm^{-1} cm^{-1}, which is a reasonable value, since for cyclohexene[11] $\epsilon = 3$ atm^{-1} cm^{-1}.

The approximate constancy of the rate of production of cyclopentene shown in Figure 1 may appear inconsistent with the assumption that it is partly consumed in secondary photolysis. However, the photolysis generates free radicals and H atoms, and the latter abstract from cyclopentane to produce cyclopentyl radicals. Disproportionation reactions of these radicals then provide an additional source of cyclopentene. Additional free radicals result also from the photolysis of cyclopentanol and, to a smaller extent, from other oxygenated reaction products. The various secondary processes which occur are complex and not well understood. A quantitative treatment is therefore not possible, but it can be seen qualitatively that the loss of cyclopentene through photolysis may be offset by the increased rate of its formation at larger conversions. A somewhat similar explanation may be applicable to cyclopentanone, which shows an approximately constant rate of formation (Figure 2), although, as will be discussed, it probably also undergoes some secondary photolysis.

Secondary Photolysis of Cyclopentanone. Cyclopentanone absorbs the 2139-Å light and undergoes photolysis, for which the following primary steps have been suggested[5]

$$\text{cyclopentanone} + h\nu \longrightarrow \begin{matrix} 2C_2H_4 + CO \\ \text{cyclobutane} + CO \\ \text{4-pentenal} \end{matrix}$$

The results obtained with cyclopentanone added to a cyclopentane–N_2O reaction mixture (last column of Table III) show indeed a large increase in the yields of C_2H_4, CO, cyclobutane, and 4-pentenal and suggest that in normal experiments these products may at least partly result from the photolysis of cyclopentanone.

Material Balance. An accurate material balance is difficult to obtain because of the complex character of the minor products and the analytical difficulties in the determinations of water. Nevertheless, the material balance for oxygen atoms approaches 85% at total pressures above 200 Torr. In view of the nature of the products, potential difficulty with their quantitative recoveries, and the overall experimental uncertainties, for example in the gc response factors, this result is reasonable and shows that no major features of the reaction have been overlooked. At lower pressures, fragmentation is extensive and it would appear that not all the "fragmentation" products have been recovered and measured. In these experiments no attempt was made to determine quantitatively the yields of water. The material balance of oxygen atoms in the experiments at lower pressures is thus considerably poorer.

Fragmentation and Lifetimes of the Hot Cyclopentanol. Several estimates of the thermochemical quantities of interest for the present work are listed in Table V.

Table V: Estimates of the Relevant Thermochemical Quantities (kcal/mol) at 298.2°K

Species	$\Delta H_f°$	Species	$\Delta H_f°$
$O(^1D_2)$	104.9[a]	c-C_5H_9	24.3 ± 1.1[b]
c-C_5H_{10}	−18.5[b]	OH	9.3[b]
c-C_5H_9·OH	−60.1[b]	H	52.1[b]

Bond broken	$\Delta H°$	Bond broken	$\Delta H°$
c-C_5H_9–H	94.9 ± 1.0[c]	·O–H	102[b]
C–C in c-C_5H_{10}	~75.5[d]	α-C–C in c-C_5H_9·OH	~72[d]
c-C_5H_9–OH	93.7[c]	α-C–H in c-C_5H_9·OH	~90[d]
c-C_5H_9·O–H	102[b]		

Reaction	Exothermicity
$O(^1D_2)$ + c-C_5H_{10} → c-C_5H_9·OH	146.5
$O(^1D_2)$ + c-C_5H_{10} → c-C_5H_9 + OH	52.8

[a] D. R. Stull, Ed., "JANAF Thermochemical Tables," The Dow Chemical Co., Midland, Mich., 1963. [b] J. G. Calvert and J. N. Pitts, Jr., "Photochemistry," Wiley, New York, N. Y., 1966, pp 815–826. [c] Estimated using the $\Delta H_f°$ values for c-C_5H_{10}, c-C_5H_9·, H, and OH listed in this table. [d] Estimated using the rules for the additivity of group properties: S. W. Benson, "Thermochemical Kinetics: Methods for the Estimation of Thermochemical Data and Rate Parameters," Wiley, New York, N. Y., 1968.

The insertion of $O(^1D_2)$ atoms into a CH bond of cyclopentane is about 146.5 kcal/mol exothermic if the cyclopentanol formed is in the ground electronic state, as expected and in agreement with the observed pressure effects.

At low pressures the hot cyclopentanol molecules formed in the reaction undergo fragmentation. If the excess energy is randomized, the weakest bond in the molecule, the α-CC bond, would be expected to fragment preferentially to form the biradical A. If the

$$\cdot CH_2CH_2CH_2CH_2\dot{C}H\cdot OH$$
A

biradical A were stabilized, some formation of *n*-pentanal and 4-pentenol would be expected as a result of isomerization through H-atom migration. The former is a very minor product, but its yield does not increase at lower pressures. The latter has not been detected. The same is true for *n*-butanol, another po-

(18) C. D. Poole, Jr., and R. S. Anderson, *J. Chem. Phys.*, **31**, 346 (1959).

tential product of a stabilized biradical A. It would appear, therefore, that biradical A, which has about 71 kcal/mol excess energy when formed, undergoes rapidly further fragmentation, probably into C_2H_4, CO, and H atoms. Since the main fragmentation products, C_2H_4 and CO, are also formed in side reactions, a quantitative treatment of their yields would be difficult and the mechanism of fragmentation remains uncertain. However, extrapolations to zero reaction time of the C_2H_4 and CO yields at higher pressures approach values close to zero (0.012 and 0.032, respectively), indicating that fragmentation is at best small under these conditions.

The lifetime of the hot cyclopentanol formed in reaction 2a can be determined from the effect of pressure on the ROH/N_2 ratios at zero reaction time, since, in view of the expressions derived earlier

$$(\mathrm{ROH/N_2})_{\mathrm{N_2}=0} = \alpha$$

where

$$\alpha = \frac{k_{2a}}{k_2}\frac{k_4[\mathrm{M}]}{k_3 + k_4[\mathrm{M}]}$$

or

$$\alpha^{-1} = (k_2/k_{2a})\{1 + (k_3/k_4)/[\mathrm{M}]\}$$

The plot of $1/\alpha$ *vs.* $1/[\mathrm{M}]$ is linear, as shown in Figure 6, indicating "strong" deactivation of the hot alcohol, *i.e.*, taking place essentially in one step. A stepwise ("weak") deactivation would lead to deviation from linearity.[3a]

The least-squares values and the standard deviations of the intercept and slope of the plot in Figure 6 are, respectively, $k_2/k_{2a} = 1.83 \pm 0.10$ and $(k_2/k_{2a})(k_3/k_4) = (0.046 \pm 0.002) \times 10^{-4}$ mol/cm^3 so that $k_4/k_3 = 4.0 \times 10^5$ cm^3/mol. Assuming $k_4 = 2.4 \times 10^{14}$ cm^3 mol^{-1} sec^{-1}, which is the calculated collision frequency, the mean lifetime of the hot cyclopentanol is $1/k_3 = 1.7 \times 10^{-9}$ sec. This value should be compared with the following other lifetimes of the hot alcohols formed by insertion of $O(^1D_2)$ atoms into CH bonds of paraffins: about 10^{-11} sec for *n*- and isopropyl alcohols,[2] 4.5×10^{-10} sec for isobutyl alcohol,[3a] 2.6×10^{-10} sec for *tert*-butyl alcohol,[3a] and 4.2×10^{-9} sec for neopentyl alcohol.[3b] Cyclopentanol has six degrees of freedom fewer than neopentyl alcohol, and its somewhat shorter lifetime agrees with the qualitative expectation.

Kassel's expression[19]

$$k_3 = A_3(1 - E_0/E)^{s-1}$$

can be used to calculate approximately the value of the preexponential factor A_3. Taking from Table V the values $E = 146.5$ kcal/mol and $E_0 = 72$ kcal/mol and adopting empirically that $(n/2) < s < (2n/3)$, where n is the total number of oscillators in the molecule, it is found that A_3 is between the limits of $10^{14.6}$ and $10^{16.6}$ sec^{-1}. A value in this range is consistent with the pre-

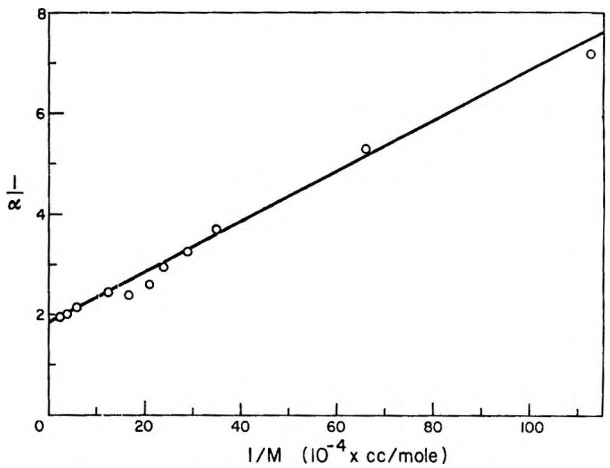

Figure 6. Plot of the reciprocal rate (extrapolated to zero reaction time) of stabilization of cyclopentanol.

exponential factors observed for the ring opening of small-ring compounds.[20]

The preexponential factor is related to the entropy of activation, $\Delta S_3^{\ddagger}$, by the expression

$$A_3 = (ekT/h)\exp(\Delta S_3^{\ddagger}/R)$$

so that the above limits for A_3 give 6.1 eu $< \Delta S_3^{\ddagger} <$ 15.4 eu. If the rate of the unimolecular decomposition is controlled by the opening of the ring, it can be assumed that the structure of the activated complex is very close to that of the biradical A. It can then be taken approximately that

$$\Delta S_3^{\ddagger} \approx S^\circ_{298}(\text{biradical A}) - S^\circ_{298}(\text{cyclopentanol})$$

The entropy of the biradical A may itself be approximately equated to the entropy of *n*-pentyl alcohol, so that

$$\Delta S_3^{\ddagger} \approx S^\circ_{298}(n\text{-pentyl alcohol}) - S^\circ_{298}(\text{cyclopentanol})$$

i.e.,[10] $\Delta S_3^{\ddagger} \approx 95 - 83 = 12$ eu, which is in the range 6.1–15.4 eu calculated above. More precise calculations of k_3 using the RRKM unimolecular reaction rate theory would not be possible without an experimental value of A_3 (or of an assumed structure of the activated complex).[21] The approximate calculations nevertheless show that the observed pressure effects on the yields of cyclopentanol are consistent with unimolecular decomposition of highly vibrationally excited cyclopentanol molecules in their ground electronic state. In this connection it is interesting to mention that the calculated A_3 is one to two orders of magnitude smaller than the calculated A factor for the unimolecular de-

(19) L. S. Kassel, "The Kinetics of Homogeneous Gas Reactions," Chemical Catalogue, New York, N. Y., 1932.

(20) S. W. Benson, "Thermochemical Kinetics: Methods for the Estimation of Thermochemical Data and Rate Parameters," Wiley, New York, N. Y., 1968.

(21) G. M. Wieder and R. A. Marcus, *J. Chem. Phys.*, **37**, 1835 (1962).

composition of the hot neopentyl alcohol into two fragments.[3b] Thus, although in the case of cyclopentanol a weaker bond is being broken, entropy gain in the ring opening is smaller than in the fragmentation into two detached entities in the case of neopentyl alcohol, and the two rate constants differ relatively little.

The k_2/k_{2a} value of 1.83 ± 0.10 obtained from the intercept of the plot in Figure 6 gives $k_{2a}/k_2 = 0.55 \pm 0.03$, *i.e.*, 55% of the $O(^1D_2)$ atoms insert into the CH bonds of cyclopentane.

Acknowledgment. The authors are grateful to Dr. R. F. Pottie for the mass spectrometric analyses.

COMMUNICATIONS TO THE EDITOR

On the Question of Alkylperoxy Radical Stabilization by Cobalt Ions

Publication costs borne completely by The Journal of Physical Chemistry

Sir: In 1967, Brandon and Elliott[1] suggested that the stability of alkylperoxy radicals was greatly increased by "association" with certain heavy metal ions. Their principal evidence consisted of the observation that the addition of *tert*-butyl hydroperoxide or cumyl hydroperoxide to a benzene solution of manganese, cobalt, or vanadium (as naphthenates, soaps, or acetylacetonates) yielded the esr signal characteristic of peroxy radicals and that these signals decayed slowly over the course of hours rather than seconds as would be the case if the peroxy radicals had been generated photochemically. This general result has recently been confirmed by Tkáč, Veselý, and Omelka,[2] who have described in some detail the behavior of "long-lived complex-bonded" radicals produced by reacting *tert*-butyl hydroperoxide with cobalt(II) acetylacetonate. However, neither group of workers appears to have made certain that hydroperoxide was absent from their reaction mixtures *while they were observing the "stabilized" peroxy radicals.*[3] If hydroperoxide were indeed present then quite high concentrations of peroxy radicals could persist for long periods. Thus, the rate constant for the reaction

$$\textit{tert}\text{-BuOO}\cdot + \textit{tert}\text{-BuOO}\cdot \xrightarrow{2k_t} \text{nonradical products}$$

is $\sim 1 \times 10^3\ M^{-1}\ \text{sec}^{-1}$ at room temperature.[4] If *tert*-butylperoxy radicals are being generated from the hydroperoxide at a rate R_i their steady-state concentration is given by

$$[\textit{tert}\text{-BuOO}\cdot]_{ss} = (R_i/10^3)^{1/2}\ M$$

A value of $R_i = 10^{-5}\ M\ \text{sec}^{-1}$ would yield $[\textit{tert}\text{-BuOO}\cdot]_{ss} = 10^{-4}\ M$. With a 1 M solution of *tert*-butyl hydroperoxide in benzene it is clear that the peroxy radical concentration could remain unchanged for many hours.[5,6]

Our interest in peroxy radicals[7] and in the reactions of radicals at metals atoms[8] prompted the present experiments which were designed to distinguish between the "continuous-creation" theory and the "complex-bonded" theory of peroxy radical stability. The general experimental conditions which were found by Tkáč, *et al.*,[2] to yield high radical concentrations were followed. That is, 2% of dried cobalt(II) acetonylacetonate dissolved in benzene or toluene was mixed with 50% of its volume of *tert*-butyl hydroperoxide (1 M in the same solvent, or neat); initial concentrations were $Co(acac)_2$ $\sim 5 \times 10^{-2}\ M$ and *tert*-BuOOH ~ 0.33 or $\sim 3.3\ M$. The solution turns green immediately (Co^{III} formation) and there is initially a rapid evolution of oxygen. The rate of oxygen evolution decreases after a few seconds, and, with the 3.3 M hydroperoxide, then continues at a low rate for several hours. The radical concentration depends somewhat on the experimental conditions (temperature, dryness of the $Co(acac)_2$, etc.[9]). At room temperature both 0.33 and 3.3 M hydroperoxide

(1) R. W. Brandon and C. S. Elliott, *Tetrahedron Lett.*, 4375 (1967).

(2) A. Tkáč, K. Veselý, and L. Omelka, *J. Phys. Chem.*, 75, 2575, 2580 (1971).

(3) The Tkáč, *et al.*,[2] statement that "nmr analysis of the reaction mixture revealed that even when *tert*-BuOOH was present in considerable excess over $Co(acac)_2$ it completely decomposed. . ." is ambiguous since it is not clear whether the radicals had also disappeared at this time.

(4) J. A. Howard, *Advan. Free Radical Chem.*, 4, 49 (1972).

(5) Under these free-radical conditions the actual rate of hydroperoxide decomposition would be $\sim 10R_i$ because there is an induced decomposition with a chain length of ~10 in this solvent.[6]

(6) R. Hiatt, J. Clipsham, and T. Visser, *Can. J. Chem.*, 42, 2754 (1964); A. Factor, C. A. Russell, and T. G. Traylor, *J. Amer. Chem. Soc.*, 87, 3692 (1965); J. R. Thomas, *ibid.*, 87, 3935 (1965); R. Hiatt, T. Mill, K. C. Irwin, and J. K. Castleman, *J. Org. Chem.*, 33, 1421 (1968); J. A. Howard and K. U. Ingold, *Can. J. Chem.*, 47, 3797 (1969).

(7) K. U. Ingold, *Accounts Chem. Res.*, 2, 1 (1969).

(8) K. U. Ingold and B. P. Roberts, "Free Radical Substitution Reactions" Wiley, New York, N.Y., 1971.

gave, in typical experiments, radical concentrations of $\sim 2 \times 10^{-4}$ M about 1–2 min after mixing of the reagents. The concentration decreased over the next 5–10 min to $\sim 8 \times 10^{-5}$ M but then changed very slowly, dropping to about 6×10^{-5} M after 60 min. With 3.3 M hydroperoxide the radical concentration was still $\sim 4 \times 10^{-5}$ M after 5 hr but with 0.33 M hydroperoxide there was little or no radical left after 2 or 3 hr. The g value of the radical was identical with that of a *tert*-butylperoxy radical generated by photolysis of *tert*-butyl hydroperoxide in benzene (which certainly argues against complex formation).

Tkáč, *et al.*,[2] observed and we have confirmed that the esr signal disappears on cooling the reactants (in toluene) to below $-20°$. The signal can be completely regenerated by warming the solution back to room temperature. This was attributed[2] to the reversible formation of a diamagnetic "complex-bonded" radical dimer. However, it can equally well be explained as a decrease in R_i with temperature provided $E_i > E_t$.

In toluene at $\sim -100°$ photolysis of the $Co(acac)_2$–hydroperoxide reaction mixture yielded peroxy radicals which decayed over the course of 5–15 min when the light was cut off. The rate of this decay was the same as in experiments in which the radicals had been generated (in equal concentration) by photolysis of the hydroperoxide in toluene in the absence of $Co(acac)_2$. Therefore, *tert*-BuOO· radicals cannot form a cobalt stabilized species at any significant rate at $-100°$.

tert-Butylperoxy radicals were also generated by photolysis of azoisobutane in oxygen-saturated toluene. At $-100°$ radical decay in the dark was sufficiently slow[10] that the effect on the concentration of *tert*-butylperoxy radicals of adding the $Co(acac)_2$–*tert*-BuOOH mixture could be observed. In small amounts (*e.g.*, 5% by volume) a precooled $Co(acac)_2$–*tert*-BuOOH mixture produced a sharp decrease in the *tert*-BuOO· concentration after which the radicals continued to decay at the usual rate. The sharp drop in the peroxy radical concentration is apparently due to the presence of a small amount of Co^{II} in equilibrium with the Co^{III} in the $Co(acac)_2$–*tert*-BuOOH mixture. This conclusion was reached since, in a similar experiment, in which a precooled solution of $Co^{II}(acac)_2$ was added in an amount such that the Co^{II} concentration was only slightly greater than the peroxy radical concentration, the peroxy radicals were immediately and completely destroyed. The trapping of peroxy radicals by $Co^{II}(acac)_2$ is known to be rapid.[11]

$$ROO\cdot + Co^{II}(acac)_2 \longrightarrow RO\text{-}Co^{III}(acac)_2$$

Finally, the concentration of *tert*-butyl hydroperoxide was monitored during the course of two reactions carried out at room temperature. The benzene and hydroperoxide were removed from the catalyst by vacuum distillation at room temperature and the hydroperoxide was analyzed by gas chromatography (15% diisodecyl phthalate on Chromosorb P in a glass column). With an initial concentration of hydroperoxide of 3.3 M the concentration after 30 min was ~ 3.15 M and after 90 min it was ~ 2.95 M. In the 30–90-min period $d[tert\text{-}BuOOH]/dt \approx 0.2$ M $hr^{-1} = 5.5 \times 10^{-5}$ M sec^{-1}. In this period $[tert\text{-}BuOO\cdot]_{ss}$ was $\sim 8 \times 10^{-5}$ M and hence $R_i \approx 6.4 \times 10^{-6}$ M sec^{-1} which is about $^1/_{10}$ of the rate of hydroperoxide destruction as we would expect.[5,6] In a similar experiment, the hydroperoxide concentration decreased from an initial 0.33 M to 0.18 M after 5 min and then to 0.13 M after 35 min,[12] corresponding to $d[ROOH]/dt \approx 3 \times 10^{-5}$ M sec^{-1}. Since $[tert\text{-}BuOO\cdot]_{ss}$ was again $\sim 8 \times 10^{-5}$ M, R_i is about $^1/_5$ of the rate of hydroperoxide decomposition. The shorter chain length for the induced decomposition in the second experiment may be due to the lower hydroperoxide concentration.

In summary, there is no experimental evidence in support of the view that the "long-lived" peroxy radicals produced in the *tert*-butyl hydroperoxide–cobalt acetylacetonate system owe their longevity to the formation of a complex with the $Co(acac)_2$ or any of its oxidation products. The present results do not rule out such complexes particularly in other solvents, or with other heavy metals,[13] or with other radicals.[14–22] However, radical–metal complexes should not be proposed solely on the basis of radical lifetimes *unless* the radical

(9) The line width of the esr signal was rather variable, depending apparently on the ease with which the oxygen could escape from solution. Normally the signal broadened with time if the reaction was carried out in the esr tube. However, a constant width signal could be obtained if samples were withdrawn from a reaction carried out in a more open vessel.

(10) The decay rate was similar or perhaps slightly smaller than when the radicals were generated by photolysis of *tert*-butyl hydroperoxide in toluene at $-100°$.

(11) E. T. Denisov, *Russ. Chem. Rev.*, **40**, 24 (1971).

(12) The presence of *tert*-BuOOH in this reaction mixture 15 min after mixing was confirmed by nmr.

(13) An eight-line esr spectrum is produced by mixing *tert*-BuOOH with vanadium naphthenate or acetylacetonate in *ethanol* (a = 5 G, g = 2.0116) which is not inconsistent with a coupling of the peroxy radical with the vanadium[1] (nuclear spin $^7/_2$). The radical involved might, however, be the HOO· radical (produced by oxidation of the ethanol) rather than the *tert*-BuOO· radical (*cf.* ref 20–22). In benzene, vanadium produced the usual broad single line characteristic of peroxy radicals.[1]

(14) There is a wealth of esr spectral evidence indicating that in *aqueous* systems the hydroperoxy radical can complex with the ions of a number of heavy metals, *e.g.* Ti,[15–17] Ce,[16,18,19] V,[20–22] Zr,[22] Hf,[22] Th,[22] and U.[22]

(15) M. S. Bains, J. C. Arthur, Jr., and O. Hinojosa, *J. Phys. Chem.*, **72**, 2250 (1968).

(16) G. Czapski, H. Levanon, and A. Samuni, *Isr. J. Chem.*, **7**, 375 (1969).

(17) Y. Shimizu, T. Shiga, and K. Kuwata, *J. Phys. Chem.*, **74**, 2929 (1970).

(18) G. Czapski and A. Samuni, *Isr. J. Chem.*, **7**, 362 (1969).

(19) A. Samuni and G. Czapski, *ibid.*, **8**, 551 (1970).

(20) M. S. Bains, J. C. Arthur, Jr., and O. Hinojosa, *J. Amer. Chem. Soc.*, **91**, 4673 (1969).

(21) M. Seteka, Y. Kirino, T. Ozawa, and T. Kwan, *J. Catal.*, **15**, 209 (1969).

(22) M. S. Bains, J. C. Arthur, Jr., and O. Hinojosa, *Inorg. Chem.*, **9**, 1570 (1970).

generating reactions are complete before the lifetime is measured.

CHRISTOPHER INGOLD LABORATORIES
UNIVERSITY COLLEGE LONDON
LONDON WC1H OAJ, ENGLAND

K. U. INGOLD

RECEIVED OCTOBER 22, 1971

Photochemistry of the Copper(II)–Malonate System. A "Sensitized" Reaction

Publication costs borne completely by The Journal of Physical Chemistry

Sir: The photochemical decomposition of monocarboxylate complexes of several transition metal ions in aqueous solution has been reported.[1] The photochemistry is characteristically an electron transfer which results in irreversible reduction of the metal ion center and formation of a carboxyloxy radical, RCOO·. Previous studies suggest that this radical loses CO_2 rapidly.[2]

Recently, studies on the photochemistry of malonato complexes of cobalt(III),[3] manganese(III),[4] and iron(III)[5] have been reported. Based on product studies, the photochemistry of these complexes is that predicted from studies on monocarboxylate complexes. The photochemistry of uranyl malonate has also been reported[6] and unlike that of the first row transition metals is a "sensitized" decomposition of the ligand giving carbon dioxide and acetate as final products.

As part of our studies on the photochemistry of labile complexes, we are exploring the photochemistry of the copper(II)–malonate (Mal = malonate) system using both conventional and flash photochemical techniques. Copper(II) forms two labile complexes with malonate, the second of which is formed only with a large excess of ligand ($\sim 3 \times 10^{-2}$ M excess for $CuMal_2^{2-}/CuMal \simeq 10$). The complexes have d–d absorption bands in the red (λ_{max} ~700 nm, $\epsilon \simeq 40$ M^{-1} cm^{-1})[7] and charge-transfer bands in the ultraviolet (CuMal, λ_{max} ~240 nm, $\epsilon \simeq 3100$ M^{-1} cm^{-1}; $CuMal_2^{2-}$, λ_{max} ~250 nm, $\epsilon \simeq 6400$ M^{-1} cm^{-1}).

The photolysis (λ 253.7 nm) of degassed solutions of *bis*-malonatocuprate(II) resulted in the production of acetate ion and CO_2 in equimolar amounts: $\phi(CO_2) \simeq 0.07$, $\phi(OAc^-)/\phi(CO_2) \simeq 0.94$; for copper(II)–malonate, $\phi(CO_2) \simeq 0.08$. After mass spectral identification, P–V–T measurements were used to determine the CO_2 yields. No Tyndall effect due to metallic copper was observed nor was cuprous ion, analyzed by adding 1,10-phenanthroline,[8] detected ($[Cu^+]/[Cu^{2+}] < 0.3\%$ for $[CO_2]/[Cu^{2+}] = 7400\%$). The acid anions (malonate, succinate, and acetate) were analyzed by nmr spectroscopy after the solutions were passed through a cation-exchange resin (Dowex 50w-X8) column to remove the copper. Since succinate ion was not detected in the early runs, a known amount of sodium succinate was added as an internal standard. In a typical experiment with a hundredfold excess of malonate, photolysis was carried to ~50% decomposition (*e.g.*, $[Cu^{2+}] = 10^{-4}$ M, $[Mal^{2-}]_0 = 10^{-2}$ M, $[OAc^-]_{formed} \simeq 5 \times 10^{-3}$ $M = 50 \times [Cu^{2+}]$). Direct photolysis of the excess ligand could be ruled out. These results indicate that the photochemistry of the copper(II)–malonate system is, like that of uranyl oxalate and malonate, a "sensitized" decomposition to the extent that the metal ion does not undergo an irreversible reduction.

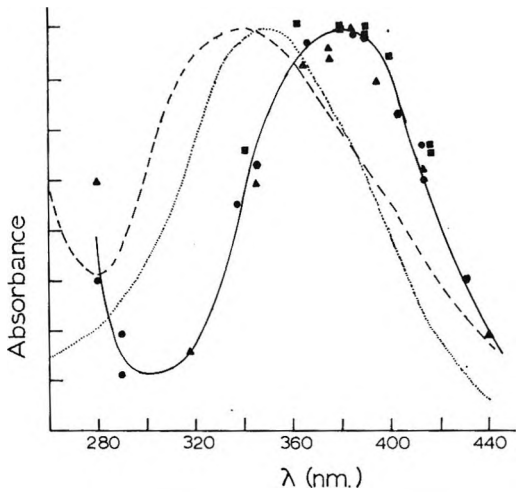

Figure 1. Normalized absorption spectra for $\cdot CH_2COO^-$, ..., ref 10; $\cdot CH(COO^-)_2$, - - - -, ref 11; transient observed on flashing solution 1.0×10^{-4} M $CuSO_4$, 1.0×10^{-3} M Na_2Mal, 20-cm cell, ●; 1.0×10^{-4} M $CuSO_4$, 1.0×10^{-2} M Na_2Mal, 10-cm cell, ▲; 1.0×10^{-4} M $CuSO_4$, 1.0×10^{-2} M Na_2Mal, 35-cm cell, ■; 1.0×10^{-3} M $CuSO_4$, 1.00×10^{-4} M Na_2Mal, 13-cm cell, ⬢.

Isotope experiments with malonate-d_2 resulted in the formation of only acetate-d_2, which indicates that acetate is not formed by an acetate radical abstracting a hydrogen atom from the methylene group of malonate.

Flash experiments[9] performed on argon-purged solutions of *bis*-malonatocuprate(II) revealed a strongly absorbing intermediate formed entirely during the

(1) See V. Balzani and V. Carassiti, "Photochemistry of Coordination Compounds," Academic Press, London, 1970.

(2) L. Herk, M. Feld, and M. Seward, *J. Amer. Chem. Soc.*, **83**, 2998 (1961); E. R. Kantrowitz, M. Z. Hoffman, and J. F. Endicott, *J. Phys. Chem.*, **75**, 1914 (1971).

(3) R. Van Eldik and J. A. Van den Berg, *J. S. Afr. Chem. Inst.*, **22**, 175 (1969); *Chem. Abstr.*, **72**, 125452*s* (1970).

(4) R. Van Eldik and J. A. Van den Berg, *J. S. Afr. Chem. Inst.*, **23**' 85 (1970); *Chem. Abstr.*, **73**, 102419*t* (1970).

(5) R. Van Eldik and J. A. Van den Berg, *J. S. Afr. Chem. Inst.*' **23**, 96 (1970); *Chem. Abstr.*, **73**, 104257*n* (1970).

(6) G. E. Heckler, A. E. Taylor, C. Jenson, D. Percival, R. Jensen, and P. Fung, *J. Phys. Chem.*, **67**, 1 (1963).

(7) D. P. Graddon, *J. Inorg. Nucl. Chem.*, **7**, 73 (1958).

(8) D. H. Wilkins and G. F. Smith, *Anal. Chim. Acta*, **9**, 538 (1953).

(9) G. D. Cooper and B. A. DeGraff, *J. Phys. Chem.*, **75**, 2897 (1971).

flash with maximum absorption at ~380 nm; for copper(II) malonate, λ_{max} ~370 nm. The spectrum of the transient obtained using the point-by-point method at 100 μsec after the flash under a variety of conditions for *bis*-malonatocuprate(II) is shown in Figure 1 along with the spectra reported for the acetate[10] and malonate[11] radicals. From the λ_{max} values it is apparent that the intermediate is neither the free acetate nor the free malonate radical.

First-order plots of the decay of the intermediate(s) formed by flashing solutions of predominantly bis complex are slightly curved in most cases and appear to be the superposition of at least two straight lines. The decay cannot be fitted to second-order kinetics. A log–log plot of rate constants obtained from the initial slopes *vs.* $HMal^-$ was linear over some six decades with a slope of 0.5. There was no dependence of the decay on either pH or $[Mal^{2-}]$ except insofar as $[HMal^-] = k[H^+][Mal^{2-}]$.

Under conditions in which CuMal is the only complex present, the decay kinetics of the intermediate are simpler and fit a rate expression of the form $-d[\text{intermediate}]/dt = (k_1[HMal^-] + k_2[H_2Mal])[\text{intermediate}]$ where $k_2 \simeq 50k_1$. The present data point to a model such as shown schematically here for copper(II) malonate.

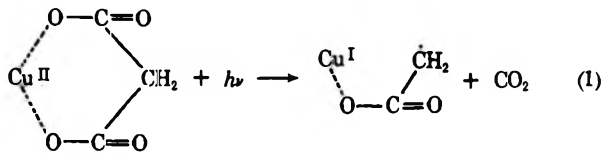

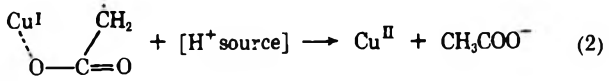

where [H+ source] = $HMal^-$, H_2Mal, and perhaps H_3O^+. This tentative mechanism reflects two significant points strongly suggested by our data. First, in marked contrast to the usual charge-transfer photochemistry of the first-row transition metal and Cu(II) in particular, the ligand is oxidized without permanent reduction of the metal ion. Second, the flash experiments strongly suggest that the oxidized ligand (malonoxy radical, or more likely since CO_2 is probably rapidly lost, acetate radical) remains bound to the reduced metal center until the radical is reduced to the acetate ion by Cu(I). Further work on the mechanism is in progress.

(10) P. Neta, M. Simic, and E. Hayon, *J. Phys. Chem.*, **73**, 4207 (1969).
(11) M. Simic, P. Neta, and E. Hayon, *ibid.*, **73**, 4214 (1969).

DEPARTMENT OF CHEMISTRY
UNIVERSITY OF VIRGINIA
CHARLOTTESVILLE, VIRGINIA 22901

JOHN Y. MORIMOTO
B. A. DEGRAFF*

RECEIVED FEBRUARY 3, 1972

There when you need them...

are the annual 700 pages of data published quarterly in the

Journal of Chemical & Engineering Data

This American Chemical Society journal is especially valuable in light of today's new instrumentation.

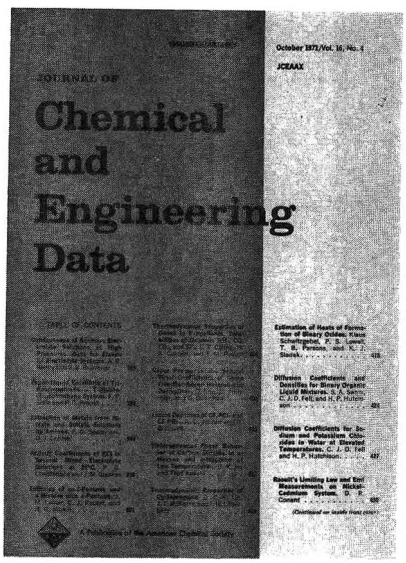

You'll find *four* clearly defined areas in JC & ED. They are:

☐ Experimental data relating to pure compounds of mixtures covering a range of states.

☐ Manuscripts based on published experimental information, which make tangible contributions through the reorganization or systematic presentation of such data . . . or which set forth a well documented method of prediction of properties as a function of state.

☐ Experimental data which aid in the identification or utilization of new organic or inorganic compounds.

☐ Papers relating primarily to newly developed or novel synthesis of organic compounds and their properties.

Sending for a subscription to the JOURNAL OF CHEMICAL & ENGINEERING DATA is so much easier than searching for data deposited in archives. Just fill in and return the form below. We'll do the rest.

American Chemical Society / 1155 Sixteenth Street, N.W., Washington, D.C. 20036

Please enter my subscription to **The Journal of Chemical & Engineering Data** at the rates checked below.

ACS Members: ☐ U.S. $15.00 ☐ Canada, PUAS $18.00 ☐ Other Nations $18.50

Nonmembers: ☐ U.S. $45.00 ☐ Canada, PUAS $48.00 ☐ Other Nations $48.50

☐ Bill me ☐ Bill employer ☐ Payment enclosed (Payable to American Chemica Society)

Name _____ Title _____

Employer _____

Address: ☐ Home ☐ Business _____

City _____ State/Country _____ Zip _____

Nature of employer's business? ☐ Manufacturing or processing ☐ Academic ☐ Government ☐ Other _____ (Please indicate)

Note: Subscriptions at ACS Member Rates are for personal use only.

☐ I am an ACS member ☐ I am not an ACS member

Payment must be made in U.S. currency, by international money order, UNESCO coupons, U.S. bank draft; or order through your book dealer.

T3A